

# 'Analytical Chemistry in Near Space: Exploring the Stratosphere, threats to the Ozone Layer, and the Ongoing Challenges to Ozone Recovery'

by

Elinor Catherine Tuffnell

Submitted: September 2024

A thesis submitted to the School of Environmental Sciences of the University of East Anglia,  
in partial fulfilment of the requirements for the degree of Doctor of Philosophy

"This copy of the thesis has been supplied on condition that anyone who consults it is understood to recognise that its copyright rests with the author and that use of any information derived there-from must be in accordance with current UK Copyright Law. In addition, any quotation or extract must include full attribution."

## Abstract

Under the international agreement that formed the Montréal Protocol on Substances that Deplete the Ozone Layer, the production and consumption of ozone-depleting substances was phased out, in order to limit their contribution to stratospheric ozone depletion. Ongoing monitoring is necessary in order to ensure compliance with the Montréal Protocol, to identify and respond to new threats to the ozone layer and verify that the atmospheric abundance of ozone-depleting substances continues to fall.

Here I utilise a number of different techniques to investigate ozone-depleting substances, this includes model data but primarily focuses on measurements taken using in-situ sample collection from large balloon flights, high-altitude research aircraft flights, and the novel 'AirCore' technique which collected samples using smaller balloons. Firstly, this thesis investigates four comparatively longer-lived CFCs (CFC-13, CFC-114, CFC-114a and CFC-115), and derives (sometimes for the first time) observation-based policy relevant metrics for these under-studied compounds. Model data is used to investigate how changes to stratospheric circulation or chemistry could affect these metrics for these compounds, and a sensitivity study of the model is conducted.

Next this thesis explores the feasibility of deriving stratospheric concentrations of seven atmospheric trace gases through sampling via the AirCore technique. These compounds are: PFC-116, HFC-125, CFC-113, CFC-115, methyl chloride, HCFC-141b, and HCFC-142b. In addition to testing a range of factors in order to refine a set of 'best practices' for the technique, the thesis explores the effect of seasonality and location on key metrics (FRFs and ODPs), the rates at which they dissociate in the stratosphere and their potential for ozone depletion. The thesis investigates previously held assumptions regarding how fractional release (the rate at which a compound dissociates in the stratosphere) is calculated and the impact of seasonality and latitude on these.

Having explored a number of compounds that are of interest in ozone depletion chemistry, this thesis investigates ways to monitor their impact on the ozone layer, identifying multiple challenges to accurate monitoring and testing solutions to them. Alongside deriving new estimates of policy relevant metrics which are important tools in accurately assessing and combating threats to the ozone layer, and deriving new emissions estimates for some compounds, this thesis has a few overall conclusions. Firstly, that CFC-13

did not have a previous estimate for stratospheric lifetime, but had a total atmospheric lifetime of 650 years, while CFC-115 had a previous stratospheric lifetime estimate of 664. These lifetime estimates are revised here to 315 years and 369 years respectively, and in order to account for current abundance greater emissions are required (and estimated here). Secondly that the assumptions underlying the calculation of fractional release leave a broad margin for uncertainty, with FRFs varying significantly (e.g.  $\pm 12\%$  for CFC-113 and  $\pm 19\%$  for CFC-115) over different seasons and geographical areas. Finally, that in the absence of reliable in-situ data (methods for which this thesis explores), model simulations and lab-based kinetics experiments cannot tell the whole story, which is something this research seeks to address.

## **Access Condition and Agreement**

Each deposit in UEA Digital Repository is protected by copyright and other intellectual property rights, and duplication or sale of all or part of any of the Data Collections is not permitted, except that material may be duplicated by you for your research use or for educational purposes in electronic or print form. You must obtain permission from the copyright holder, usually the author, for any other use. Exceptions only apply where a deposit may be explicitly provided under a stated licence, such as a Creative Commons licence or Open Government licence.

Electronic or print copies may not be offered, whether for sale or otherwise to anyone, unless explicitly stated under a Creative Commons or Open Government license. Unauthorised reproduction, editing or reformatting for resale purposes is explicitly prohibited (except where approved by the copyright holder themselves) and UEA reserves the right to take immediate 'take down' action on behalf of the copyright and/or rights holder if this Access condition of the UEA Digital Repository is breached. Any material in this database has been supplied on the understanding that it is copyright material and that no quotation from the material may be published without proper acknowledgement.

## Acknowledgements

I want to thank first my supervisory team, without whom none of this would have been possible. Johannes Laube, whose enthusiasm and knowledge made the great challenge of doing a PhD in this field actually feel achievable. Harald Boenisch who helped me make sense of the incredibly complex world of modeling. Bill Sturges whose style of helpful and constructive feedback helped me stay motivated and enthused about my work. Emma Leedham-Elvidge, who in addition to academic support, helped me navigate the labyrinthine world of university bureaucracy. I faced many challenges during my years working on this PhD; thank you all for never giving up on me.

I want to thank my family. My parents Vivienne and Nigel, whose love and endless support made all of this a reality, and without whom I could never have got this far. Robin, Lewis and Vibrissa, who kept my morale high even when I was really struggling. Graham Edge, whose technical expertise and emotional support helped me through so many crises. My Gran Jean who has always been very proud of my hard work. And finally, to my maternal grandparents, Mavis and Geoffrey Booth who sadly did not live to see me complete this PhD, but were immensely proud of me for it, particularly as my Granddad was himself a chemist and knew how difficult this path would be.

## Statement of Work Attribution

The Geophysica flight campaigns that produced the samples analysed in Chapter 3 were conducted before I began this PhD, and thus I was not a participant. Most of the samples from these flights were analysed (using the GC-MS techniques described in section 2.3) before I joined the team, primarily by Dr Laube, Dr Leedham-Elvidge, and Dr Adcock. I assisted in a small number of these (as this was very early in my PhD, I was not yet trained to work independently in the lab). The data produced by the GC-MS system was then analysed, and from this mixing ratios and mean ages were derived (see sections 2.3), this process was initially done by either Dr Laube, Dr Leedham-Elvidge, or Dr Adcock. Once I had been trained in how to do this, I took over the task. Occasions arose during research where it was necessary to go back to this GC-MS data and check certain things (for example instrument precision, was a sample's mixing ratio erroneously high in the data, had any copy-paste errors occurred? Etc...), and so I personally reanalysed this data. From this point on all analysis, discussion, and results (unless otherwise stated in the text) were my own work.

In regard to data collection in Chapter 4, from 2018 onwards I was involved in varying capacities with AirCore flights. Some flights I was present for personally, during which my role was primarily logistics and coordination, in addition to hands-on assistance during launches. Outside of this I assisted in planning and preparations for flights. AirCore samples were primarily analysed on the GC-MS by Dr Laube, though I assisted with some of them where possible. I worked on the automated inlet system for the GC-MS extensively, writing a user guide and the code to automate the system (both of which, in updated forms, are still used). The stability tests took place during COVID lockdown, and restrictions meant I could not be present for these tests. GC-MS Data from both AirCore flights and stability tests, was analysed primarily by me. All further analysis, discourse and results are my own work (unless otherwise stated in the text).

As with most people graduating at this time (and for some years to come), my research was impacted heavily by the pandemic. Restrictions meant that planned lab or field work either needed to be delayed, abandoned, or could only be done in a much-reduced manner. This should be taken into account when evaluating the hands-on work I was able to do.

To my knowledge, with one small caveat, none of the results in this thesis are published elsewhere. That caveat is that Laube et al., (2025) used my analysis of the stability tests for methyl chloride, as well as my analysis for other compounds not covered in this thesis, to verify the stability of those compounds during AirCore sampling. The findings of Chapter 3, minus the modeling section, have been written up in paper format, and will hopefully be accepted for publication in the near future.

# Table of Contents

Abstract .....	2
Acknowledgements.....	4
Statement of Work Attribution .....	5
Table of Contents .....	7
List of Figures .....	9
List of Tables .....	13
List of Equations.....	14
Chapter 1 Introduction .....	15
1.1 The creation and destruction of ozone in the Stratosphere .....	15
1.2 Ozone-Depleting Substances and their replacements.....	20
1.3 Atmospheric circulation and the Brewer-Dobson circulation .....	23
1.4 Key Concepts and Policy Relevant Metrics.....	29
1.5 Aims and rationale.....	33
Chapter 2 Methodology.....	35
2.1 Sample collection overview.....	35
2.1.1 Research Aircraft Flights .....	35
2.1.2 Large Balloon Flights .....	35
2.1.3 AirCore Flights .....	37
2.1.4 Satellites.....	40
2.2 Atmospheric Chemistry Transport Models .....	41
2.3 Gas Chromatography/Mass Spectroscopy .....	42
2.4 Bivariate Data .....	47
2.5 Bootstrapping and statistical analysis.....	48
2.6 Fractional Release Factors: Background, Context, and Calculation .....	49
Chapter 3 Long Lived CFCs.....	54
3.1 Introduction .....	54
3.1.1 Why the focus on long lived CFCs? .....	54
3.1.2 Long lived CFCs: Sinks, Sources, Abundance and Emission trends .....	55
3.1.3 Archived Air Introduction.....	58
3.2 Methodology.....	59
3.2.1 Flight dates and other details.....	60
3.2.2 Details specific to the processing of these samples.....	61
3.2.3 A sensitivity study of the Model.....	62
3.2.4 FRFs and how they were derived for this Chapter.....	64
3.2.5 FRF and lifetime correlation: lifetime estimation .....	69
3.2.6 Archived Air Methods .....	75
3.3 Results.....	76
3.3.1 FRF results .....	76
3.3.2 Stratospheric Lifetime Results.....	78
3.3.3 Ozone Depletion Potentials.....	81
3.3.4 Model results.....	82
3.3.4.a Mean Age-Tracer correlation .....	82
3.3.4.b Chemistry and Circulation scenarios.....	93
3.3.4.c Model Lifetimes.....	101
3.3.4.d Fractional Release Factors from the GSFC .....	107
3.3.4.e Stratospheric tracer transport in CLaMS and GSFC. ....	119
3.3.4.f Summary of Model Results .....	123
3.3.5 Archived Air Results .....	124
3.3.5.a Archived Air Samples of CFC-13 – Results.....	126
3.3.5.b Archived Air Samples of CFC-115 -Results.....	128

3.3.5.c	Archived Air Samples of CFC-114 - Results.....	131
3.3.5.d	Archived Air Samples of CFC-114a – Results .....	134
3.4	Discussion.....	136
3.4.1	Archived Air Discussion.....	143
3.5	Conclusion.....	144
Chapter 4	Exploring the Stratosphere with AirCores.....	147
4.1	Introduction .....	147
4.1.1	Exploring the stratosphere with AirCores .....	147
4.1.2	Introducing the Compounds.....	148
4.1.2.a	A short introduction to PFC-116.....	149
4.1.2.b	A short introduction to HFC-125.....	150
4.1.2.c	A short introduction to CFC-113.....	151
4.1.2.d	A short introduction to CFC-115.....	152
4.1.2.e	A short introduction to Methyl Chloride.....	153
4.1.2.f	A short introduction to HCFC-141b .....	154
4.1.2.g	A short introduction to HCFC-142b .....	155
4.2	Methodology.....	155
4.2.1	AirCores.....	156
4.2.2	Sub-sampling.....	161
4.2.3	Stability Tests.....	165
4.2.4	Analysis of Samples.....	167
4.2.5	Mean Ages derived from AirCores Measurements.....	167
4.3	Results.....	171
4.3.1	PFC-116 .....	171
4.3.2	HFC-125.....	176
4.3.3	CFC-113 .....	178
4.3.4	CFC-115 .....	185
4.3.5	Methyl Chloride .....	188
4.3.6	HCFC-141b.....	192
4.3.7	HCFC-142b.....	195
4.3.8	Mean Ages.....	199
4.3.9	FRFs.....	202
4.3.10	ODPs .....	212
4.4	Discussion.....	216
4.4.1	Idiosyncrasies of technique.....	216
4.4.2	Seasonality and Latitude .....	217
4.4.3	ODPs .....	221
4.5	Conclusion.....	223
4.5.1	AirCore and sampling techniques.....	223
4.5.2	Mean Ages.....	224
4.5.3	FRFs.....	225
4.5.4	ODPs .....	225
Chapter 5	Summary, conclusions, future work.....	227
5.1	Overview of major research findings.....	227
5.1.1	Overview from ‘Chapter 3: Long Lived CFCs’ .....	227
5.1.2	Overview from ‘Chapter 4: AirCores’ .....	234
5.2	Suggestions for future work/policy implications.....	238
Glossary	.....	241
Appendix A	– Background trends and Flights.....	243
Appendix B	– Stability Test Results.....	250
Appendix C	– Additional Figures.....	261
Appendix D	Statistical techniques – technical details.....	280
Bibliography	.....	289

## List of Figures

Figure 1.1. Taken from (Bönisch et al., 2011).....	25
Figure 2.1. A photograph of an AirCore .....	38
Figure 2.2. The stages of sample preparation.....	43
Figure 3.1. Mixing ratio (ppt) of (a) CFC-13, (b) CFC-115, (c) CFC-114, and (d) CFC-114a,.....	67
Figure 3.2. Fractional Release Factors (FRF) plotted against Mean Age (yr).....	69
Figure 3.3. Plotting FRF at 3 years mean ages against Lifetime (yr) for mid latitude, .....	72
Figure 3.4. Plotting FRF at 3 years mean ages against Lifetime (yr) for mid latitude, FRFs and lifetimes from Burkholder et al. (2022).....	73
Figure 3.5. A comparison estimated stratospheric lifetimes (generated using the ‘power’ trendline), using either FRFs at 3 or 5 years mean age.....	75
Figure 3.6. FRF at 3 years mean age, plotted against Stratospheric lifetime (yr). .....	77
Figure 3.7. Newly estimated stratospheric lifetimes for each compound, .....	79
Figure 3.8. OB09. Comparison between GSFC baseline scenario (GSFC_O), CLaMS .....	85
Figure 3.9. KIR10. Comparison between GSFC baseline scenario (GSFC_O), CLaMS.....	86
Figure 3.10. KIR11. Comparison between GSFC baseline scenario (GSFC_O), CLaMS.....	87
Figure 3.11. Potential temperature (K) plotted against Mean Age (yr) for all three campaigns, .....	89
Figure 3.12. Mixing ratios (ppt) for all compounds, plotted against mean age (yr). .....	90
Figure 3.13. The correlation between CFC-11 mixing ratio (ppt) and mean age (yr) from GSFC_0 for OB09 campaign. Trendline is a second order polynomial. ....	93
Figure 3.14. The difference (in yr) (average residuals) between the mean age-mean age correlations and a 1,1 line CFC-11. ....	94
Figure 3.15. The difference (in yr) (average residuals) between the mean age-mean age correlations and a 1,1 line for (a) CFC-13, (b) CFC-115, (c) CFC-114, and (d) CFC-114a.....	95
Figure 3.16. Steady-state stratospheric lifetime (yr) from the GSFC baseline scenario, for CFC-13, CFC-114, CFC-114a, and CFC-115, plotted against date.....	102
Figure 3.17. Shows the % difference in stratospheric lifetime for each scenario, .....	103
Figure 3.18. Percentage difference in lifetime for the scenario (or Chapter 3), .....	106
Figure 3.19. The FRF for each compound, for each campaign, plotted against Mean Age (yr).....	109
Figure 3.20. FRFs at (a) 3 years and (b) 5 years mean age, for CFC-115 .....	112
Figure 3.21. FRFs at (a) 3 years and (b) 5 years mean age for CFC-13 .....	113
Figure 3.22 FRFs at (a) 3 years and (b) 5 years mean age for CFC-114 .....	114
Figure 3.23 FRFs at (a) 3 years and (b) 5 years mean age for CFC-114a .....	115
Figure 3.24. The steady-state stratospheric lifetimes (yr) of (a) CFC-13, (b) CFC-115, (c) CFC-114, and (d) CFC-114a, generated using different methods .....	117
Figure 3.25. CFC-11 MR (ppt) plotted against mean age for the OB09 campaign.....	120
Figure 3.26. CFC-11 MR (ppt) plotted against mean age for the KIR10 campaign. ....	121
Figure 3.27. CFC-11 MR (ppt) plotted against mean age for the KIR10 campaign. ....	122
Figure 3.28. Mixing ratios (ppt) for CFC-13, plotted against date. ....	126
Figure 3.29. For CFC-13, the FRF at (a) 3 and (b) 5 years mean age .....	127
Figure 3.30. Mixing ratios (ppt) for CFC-115, plotted against date. ....	129
Figure 3.31. For CFC-115, the FRF at (a) 3 and (b) 5 years mean age .....	130
Figure 3.32. Mixing ratios (ppt) for CFC-114, plotted against date. ....	132
Figure 3.33. For CFC-114, the FRF at (a) 3 and (b) 5 years mean age .....	133
Figure 3.34. Mixing ratios (ppt) for CFC-114a, plotted against date.....	134
Figure 3.35. For CFC-114a, the FRF at (a) 3 and (b) 5 years mean age .....	135
Figure 3.36. Showing emissions calculated for all four compounds,.....	138
Figure 3.37. The emissions estimates for all four compounds, .....	140
Figure 4.1. The AirCore ‘Hester’. .....	157
Figure 4.2. Preparing for launch:.....	160
Figure 4.3. The simple sub-sampler ‘Luna’.....	162
Figure 4.4. Complex sub-sampler ‘Ed’. Note each copper-coloured loop connected to the stainless-steel rotary valve in the centre. Ed is here supported by a wooden scaffold, and there is a flow-meter attached to the valve. ....	163

Figure 4.5. The mean slope for the correlation between the SF <sub>6</sub> derived mean ages and the PFC-116 or HFC-125.....	169
Figure 4.6. Showing factors potentially affecting PFC-116 (C <sub>2</sub> F <sub>6</sub> ) mixing ratio (ppt) plotted against CFC-11 mixing ratio (ppt),.....	173
Figure 4.7. 'Selected' Flights only. The mixing ratio of PFC-116 (ppt) in the tropospheric background trend....	175
Figure 4.8. Showing Factors affecting HFC-125 mixing ratio (ppt) plotted against CFC-11 mixing ratio (ppt), ..	177
Figure 4.9. Mixing ratio for HFC-125 (ppt), plotted against date, for the tropospheric background trend .....	178
Figure 4.10. Factors affecting CFC-113 mixing ratio (ppt) plotted against CFC-11 mixing ratio (ppt), .....	180
Figure 4.11. Mixing ratio of CFC-113 (ppt) plotted against date (yr), for the NOAA global background trend, the 5 Geophysica flights explored in section 3.2.1, and the AirCore flights explored here. ....	183
Figure 4.12. FRFs for CFC-113 plotted against mean age (yr) for 4 Geophysica flights, and all AirCore flights..	184
Figure 4.13. Factors affecting CFC-115 mixing ratio (ppt) plotted against CFC-11 mixing ratio (ppt), .....	186
Figure 4.14. Mixing Ratio for CFC-115 (ppt) plotted against date (yr).....	187
Figure 4.15. FRFs v Mean Age for CFC-115. This includes most AirCore flights examined here (the 25.04.2020 flight is excluded due to excessive outliers which obscured the data), and four of the Geophysica flights. ....	188
Figure 4.16. Factors affecting Methyl Chloride mixing ratio (ppt) plotted against CFC-11 mixing ratio (ppt), ..	189
Figure 4.17. Selected flights only. Methyl chloride (CH <sub>3</sub> Cl) Mixing Ratio (ppt) plotted against date .....	191
Figure 4.18. FRFs plotted against Mean Age (yr) for Methyl Chloride. Including the KAL16 Geophysica flight for reference, and the 13.10.2020, 14.05.2018 and 01.05.2018 AirCore flights. ....	192
Figure 4.19. Factors affecting HCFC-141b mixing ratio (ppt) plotted against CFC-11 mixing ratio (ppt), .....	193
Figure 4.20. Mixing Ratio for HCFC-141b plotted against date (yr), .....	194
Figure 4.21. FRFs plotted against Mean Age for HCFC-141b, for the AirCore flights.....	195
Figure 4.22. Factors affecting HCFC-142b mixing ratio (ppt) plotted against CFC-11 mixing ratio (ppt), .....	197
Figure 4.23. 'Good' flights only. Mixing Ratio for HCFC-141b plotted against date, .....	198
Figure 4.24. FRFs plotted against Mean Age for HCFC-142b, for the AirCore flights.....	199
Figure 4.25. SF <sub>6</sub> derived mean ages (yr) plotted against C <sub>2</sub> F <sub>6</sub> derived mean ages (yr), for the 2018 flights .....	200
Figure 4.26. SF <sub>6</sub> derived mean ages (yr) plotted against HFC-125 derived mean ages (yr), for the 2018 flights	200
Figure 4.27. The FRF at 3 years mean age of different compounds, calculated for each flight. ....	205
Figure 4.28. The FRF at 3 years mean age of different compounds, calculated for each flight, plotted against latitude. ....	208
Figure 4.29. The FRF at 3 years mean age of different compounds, calculated for each flight, plotted against fraction of year.....	210
Figure 4.30. A plot of Table 4-8, showing ODPs derived from Chapter 4, FRF results, .....	214
Figure 4.31. The FRF at 3 years mean age for CFC-113, plotted against Fraction of year.....	219
Figure 4.32. FRF at 3 years mean age for HCFC-141b plotted against fraction of year. ....	220

## List of Appendix Figures

Figure A.1 Mixing ratio (ppt) for CFC-13, plotted against date. ....	243
Figure A.2 Mixing ratio (ppt) for CFC-114, plotted against date. ....	244
Figure A.3. Mixing ratio (ppt) for CFC-114a, plotted against date.....	244
Figure A.4. CFC-115 mixing ratio (ppt) plotted against date. ....	245
Figure A.5. CH <sub>3</sub> Cl mixing ratio (ppt) plotted against date (All Flights). ....	245
Figure A.6. CH <sub>3</sub> Cl mixing ratio (ppt) plotted against date (yr) (selected flights).....	246
Figure A.7. CFC-113 mixing ratio (ppt) plotted against date. ....	246
Figure A.8. HFC-125 mixing ratio (ppt) plotted against date (All available flights).....	247
Figure A.9. HFC-125 mixing ratio (ppt) plotted against date (selected flights). ....	247
Figure A.10. HCFC-141b mixing ratio (ppt) plotted against date.....	248
Figure A.11. HCFC-142b mixing ratio (ppt) plotted against date (selected flights). ....	248
Figure A.12. C <sub>2</sub> F <sub>6</sub> mixing ratio (ppt) plotted against date (All Flights).....	249
Figure A.13. C <sub>2</sub> F <sub>6</sub> mixing ratio (ppt) plotted against date (Selected Flights). ....	249

Figure B.1. Time since fill (days), plotted against percentage difference from the standard. (a). CFC-11. (b). CFC-113. (c) CFC-115. (d) HCFC-141b. (e) HCFC-142b. (f) HFC-125. (g) C <sub>2</sub> F <sub>6</sub> . (h) CH <sub>3</sub> Cl. Error range is instrument precision. ....	251
Figure B.2. Percentage difference from standard for all compounds, when sampling lab-air introduced via valve 9. ....	253
Figure B.3. Dilution series for the standard SX3591, for each compound, compared to (in percentage difference) the SX3600 standard.....	255
Figure B.4. Percentage difference from standard when stored in either the Lyra AirCore, or the Shaun sub-sampler. ....	256
Figure B.5. The effect on each compound from being passed through a Picarro G2401. ....	258
Figure B.6. Effect of temperature on each compound. ....	259
Figure C.1. Comparison between Laube et al (2016) and Vollmer et al (2018). ....	261
Figure C.2. FRFs at 3 years mean age from Archived Air Data (section 3.3.5), plotted against Fraction of Year, ....	262
Figure C.3 CFC-13 mixing ratio (ppt) for OB09, KIR10, and KIR11 campaigns, ....	263
Figure C.4. CFC-115 mixing ratio (ppt) for OB09, KIR10, and KIR11 campaigns, ....	264
Figure C.5. CFC-114 mixing ratio (ppt) for OB09, KIR10, and KIR11 campaigns, ....	265
Figure C.6. CFC-114a mixing ratio (ppt) for OB09, KIR10, and KIR11 campaigns, ....	266
Figure C.7. PFC-116 (C <sub>2</sub> F <sub>6</sub> ) mixing ratio (MR, ppt) plotted against CFC-11 mixing ratio (MR, ppt), for all AirCore flights listed in section 4.2, and two Geophysica flights (KAL16, and KAT17). Errors derived using instrument precision, to 1 sigma uncertainty. ....	267
Figure C.8. 'Selected' Flights only. PFC-116 (C <sub>2</sub> F <sub>6</sub> ) mixing ratio (ppt) plotted against CFC-11 mixing ratio (ppt), for all AirCore flights listed in section 4.2,( excluding 25.04.2020 and the two flights which used the 'Luna' sub-sampler) and two Geophysica flights (KAL16, and KAT17). Errors derived using instrument precision, to 1 sigma uncertainty.....	267
Figure C.9. HFC-125 mixing ratio (ppt) plotted against CFC-11 mixing ratio (ppt), ....	268
Figure C.10. 'Selected' Flights only. HFC-125 mixing ratio (ppt) plotted against CFC-11 mixing ratio (ppt), .....	268
Figure C.11. CFC-113 mixing ratio (ppt) plotted against CFC-11 mixing ratio (ppt),.....	269
Figure C.12. CFC-115 mixing ratio (ppt) plotted against CFC-11 mixing ratio (ppt),.....	269
Figure C.13. 'Selected' flights only. CFC-115 mixing ratio (ppt) plotted against CFC-11 mixing ratio (ppt), ....	270
Figure C.14. Methyl Chloride mixing ratio (ppt) plotted against CFC-11 mixing ratio (ppt),.....	270
Figure C.15. 'Selected' flights only. Methyl Chloride mixing ratio (ppt) plotted against CFC-11 mixing ratio (ppt), ....	271
Figure C.16. HCFC-141b mixing ratio (ppt) plotted against CFC-11 mixing ratio (ppt), ....	271
Figure C.17. All Flights. HCFC-142b mixing ratio (ppt) plotted against CFC-11 mixing ratio (ppt),.....	272
Figure C.18. 'Selected' flights only. HCFC-142b mixing ratio (ppt) plotted against CFC-11 mixing ratio (ppt), ..	273
Figure C.19 Mixing ratio (ppt) of (a) CFC-13 and (b) CFC-115, plotted against mean age (yr). ....	274
Figure C.20. Mixing ratio (ppt) of (a) CFC-13, (b) CFC-115, (c) CFC-114, and CFC-114a, plotted against mean age (yr). ....	275
Figure C.21. Mixing ratio (ppt) of (a) CFC-13, (b) CFC-115, (c) CFC-114, and CFC-114a, plotted against mean age (yr). ....	276
Figure C.22. Displays the 6 chemistry scenarios from the GSFC-2D model for the OB09 campaign, .....	277
Figure C.23. Displays the 6 chemistry scenarios from the GSFC-2D model for the KIR10 campaign,.....	278
Figure C.24 Displays the 6 chemistry scenarios from the GSFC-2D model for the KIR11 Campaign, this also includes.....	279
Figure D.1. Slopes predicted by Barreto & Howland (2010) and Cantrell (2008), compared to the original data. ....	281
Figure D.2. Intercepts predicted by Barreto & Howland (2010) and Cantrell (2008), compared to original data. ....	282
Figure D.3. The 'original' data plotted with a linear trendline. ....	284
Figure D.4. The resampled data, with a linear trendline through the data points. ....	285
Figure D.5. The initial layout of the bootstrap excel sheet, using CFC-115 FRF and Mean Age data from the 2009 Oberpfaffenhofen campaign.....	286
Figure D.6. A plot of the relative distribution of FRFs at 3 and 5 years mean age, these are the results from resampling of the original data. ....	287



## List of Tables

Table 1-1. All Compounds examined in detail in this thesis.....	22
Table 3-1. The Location (including latitude and longitude) of each flight, the date, and the Code used to identify them in this text. ....	59
Table 3-2 The campaigns, .....	61
Table 3-3. Mean ages, FRF at 3 and 5 years mean ages, for ten compounds from Leedham-Elvidge et al., (2018) for both high and mid latitudes, compared to Burkholder et al. (2022). Lifetime here refers to stratospheric lifetime. ....	71
Table 3-4. Fractional Release factors for this chapter’s compounds of interest. ....	76
Table 3-5. The previous estimates (P) for stratospheric lifetime Burkholder et al. (2022) and the newly estimated lifetimes depending on which correlation was used. ....	80
Table 3-6. Ozone Depletion Potentials (ODPs) predicted using FRFs at 3 and 5 years mean age, compared to those listed in WMO 2022 .....	81
Table 3-7. Table showing emission estimates and ODP-weighted emissions estimates calculated for all four compounds. All emissions estimates are the global mean for the period of 2009-2017. ‘Original’ refers to data from.....	141
Table 4-1. The locations of each launch, the dates of launches, .....	156
Table 4-2. The precision for the compounds examined in Chapter 4, from Adcock et al., (2021), and from AirCore measurements.....	171
Table 4-3. The minimum temperatures experienced by the AirCores, and the length of time they were below zero degrees C.....	181
Table 4-4. The slope and intercept values for the correlation between SF <sub>6</sub> derived mean ages and C <sub>2</sub> F <sub>6</sub> or HFC-125 derived mean age averages with their respective uncertainties. Includes both the original sample range (1n) and the expanded 5n dataset (as described in sections 3.2.4 and 4.2.2). ....	201
Table 4-5. The slope and intercept of C <sub>2</sub> F <sub>6</sub> and SF <sub>6</sub> derived mean ages from archived air data.....	202
Table 4-6. FRF results for each compound, compared to the previously estimated FRFs. ....	211
Table 4-7. ODPs derived from Table 4-6 FRF results, using either FRFs from AirCore flights only, or a combination of AirCore and Geophysica derived FRFs.....	212
Table 4-8. The compounds explored in this chapter, the potential factors that might have affected them, and whether or not this was found to be the case in section 4.3 or the stability tests (Appendix B). ....	216
Table 5-1. Shows the newly derived metrics as well as their previous estimates.....	230
Table 5-2. (A repeat of Table 4-8, as it serves as a useful summary of which factors affected which compounds). ....	236

## List of Equations

Equation 1-1. Step 1 in stratospheric ozone creation .....	15
Equation 1-2. Step 2 in stratospheric ozone creation .....	15
Equation 1-3. CFC bond to one Chlorine atom split. ....	17
Equation 1-4. Chlorine radical reacts with ozone.....	17
Equation 1-5. Odd oxygen reacts with ClO* .....	17
Equation 1-6. Net result of ozone depletion.....	17
Equation 1-7. Reaction of ClONO <sub>2</sub> with HCl .....	18
Equation 1-8. Reaction of ClONO <sub>2</sub> with H <sub>2</sub> O .....	18
Equation 1-9. Reaction of HOCl with HCl.....	18
Equation 1-10. Reaction of N <sub>2</sub> O <sub>5</sub> with H <sub>2</sub> O .....	18
Equation 1-11. Simplified equation for calculation of Ozone Depletion Potential.....	32
Equation 1-12. The full equation for calculation of ODPs.....	32
Equation 1-13. The 'new' formula for deriving EESC, .....	32
Equation 2-1. Equation for obtaining a blank corrected relative response. ....	47
Equation 2-2. The formulation used to derive FRFs .....	50
Equation 2-3. The summary of Equation 2-3, in simplified terms. ....	51
Equation 2-4. The time-independent equation for entry mixing ratios,.....	52
Equation 2-5. Formula for the new loss weighted distribution function G* .....	53
Equation 3-1. Deviation against reference .....	96
Equation 3-2. Equation relating the time evolution of the atmospheric burden.....	137
Equation 3-3. Equation relating Global Atmospheric lifetimes τ(t), to Atmospheric burden.....	137
Equation 3-4. Equation relating the steady state lifetime (T <sub>ss</sub> ) to globally integrated loss/removal processes	137
Equation 4-1. Equation for the conversion between the AGAGE dataset and the NOAA dataset. ....	170

## Chapter 1 Introduction

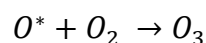
### 1.1 The creation and destruction of ozone in the Stratosphere

The atmosphere can be divided into a number of 'layers', the first layer is the troposphere which extends from the Earth's surface to approximately 8 km above at the poles and approximately 15 km above the equator. The precise location of the transition region at which the troposphere ends and the stratosphere begins, called the tropopause, varies seasonally and does not always fit neatly within the above-mentioned boundaries. The stratosphere extends from the tropopause to a height of roughly 50 km ending in another boundary layer the stratopause, above which extends the mesosphere.

In the troposphere temperature decreases with increasing altitude, however after the tropopause there is a temperature inversion: we see an increase in temperature with increased altitude. This is due to the 'ozone layer' which is the stratospheric region with the highest concentration of ozone (between ~15 and 35 km altitude). Ozone itself absorbs heat, and the reaction between a single oxygen radical, and a dioxygen molecule:  $O^* + O_2$  (a key reaction in the formation of ozone) is strongly exothermic. While in the troposphere, ozone is formed by chemical reactions involving both naturally occurring gasses and those with anthropogenic origin, in the stratosphere ozone is created when the bonds within oxygen molecules ( $O_2$ ) are broken by UV radiation from the sun, resulting in two oxygen radicals (Equation 1-1). These radicals are then available to react with  $O_2$  molecules, resulting in the creation of ozone (Equation 1-2).



*Equation 1-1. Step 1 in stratospheric ozone creation*



*Equation 1-2. Step 2 in stratospheric ozone creation*

As UV radiation is required for these reactions, ozone creation is greatest in the tropics, and least in the polar regions. While the bulk of ozone creation occurs at the tropics, due to atmospheric circulation the ozone layer is generally thinnest near the equator, and thickest near the poles, thickness also varies by season. Thickness here refers to how much ozone is present in the column over a given area, columns of ozone are measured in Dobson

units (DU), with one Dobson unit representing the number of molecules of ozone required to create a layer of pure ozone 0.01mm thick, while at a temperature of 0° celcius and with a pressure of 1 atmosphere. So 3 mm of ozone would be 300 DU. This distribution of stratospheric ozone (Dobson *et al.*, 1927; Dobson, 1956) and water vapour (Brewer, 1949) is explained by the 'Brewer-Dobson Circulation' (BDC). In the BDC, tropospheric air enters the stratosphere in the tropics, where ozone creation is at its maxima. It then moves upward and poleward, before descending in the middle and high latitudes.

The ozone layer forms a protective layer over the earth, absorbing UV solar radiation which would be harmful or even deadly to organic life. A decrease in stratospheric ozone would allow more ultraviolet (UV) radiation from the Sun to reach the Earth's surface. Of the three types of UV radiation emitted by the sun UV-C is particularly dangerous to life as its shorter wavelength (100-280 nanometres (nm)) means a higher energy radiation which is very strongly absorbed by organic materials (Lucas *et al.*, 2006). The ozone layer absorbs all UV-C radiation, most UV-B (280-315 nm), and some UV-A (315-400 nm). Increased exposure to UV-B radiation leads to many negative health effects. Skin erythema, which leads to sunburn, being the most common. Excess exposure increases the risk of skin cancer and eye cataracts and can suppress the immune system. However, exposure to UV-B radiation is vital to the production of Vitamin D (in humans and many animals), which is necessary for bone metabolism and the immune system. Maintaining healthy levels of exposure to UV-B is a delicate balance, which would be jeopardised by decreased protection from the ozone layer (Salawitch *et al.*, 2023).

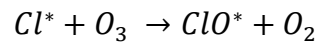
It is for this reason that the discovery of the Ozone Hole in 1985 by (Farman *et al.*, 1985) was so alarming. Anthropogenic emissions of Ozone-Depleting Substances (ODSs), notably halogenated compounds such as chlorofluorocarbons (CFCs), hydrochlorofluorocarbons (HCFCs) and the brominated halons, had led to the destruction of ozone in sufficient quantities to form the Ozone Hole over the Antarctic, and to a lesser extent, the Arctic. Among other effects, this has led to an increase of harmful UV radiation, with the greatest increase in the polar regions, and the smallest increase in the tropics. This has seen a corresponding increase in adverse effects on human health (notably skin cancers and cataracts) (Salawitch *et al.*, 2023).

A number of substances are active in ozone depletion, notably: hydroxyl radicals (OH·), nitric oxide radicals (NO·), chlorine radicals (Cl·) and bromine radicals (Br·). These

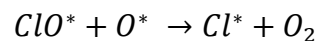
have both natural and anthropogenic sources. One source of chlorine radicals are CFCs, which are inert in the troposphere, but when they enter the stratosphere UV radiation is capable of breaking the halogen – carbon bonds producing a chlorine radical (Equation 1-3) which can then react with ozone, producing an O<sub>2</sub> molecule and a chlorine monoxide (ClO\*) radical (Equation 1-4). The ClO\* molecule can then react with odd oxygen (e.g. an excited oxygen atom O\*), resulting in an O<sub>2</sub> molecule and the chlorine radical is then released to continue the catalytic cycle (Equation 1-5).



*Equation 1-3. CFC bond to one Chlorine atom split.*



*Equation 1-4. Chlorine radical reacts with ozone.*



*Equation 1-5. Odd oxygen reacts with ClO\*.*



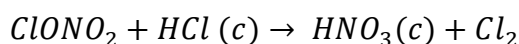
*Equation 1-6. Net result of ozone depletion.*

As Equation 1-6 results in a net decrease of ozone, if left unchecked these reactions would result in massive, and eventually total loss of ozone in the stratosphere. However, this is only one part of a larger process of ozone creation and destruction. The balance between creation and destruction of ozone is determined by both the amounts of reactive gases, and how the effectiveness of different reactions changes with the intensity of sunlight, position in the stratosphere, and temperature. The catalytic destruction cycle terminates when the radical (and its reservoir) involved in the reaction is removed or destroyed, or when the catalyst or conditions for the reaction are removed.

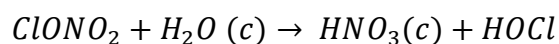
Ozone is created primarily in the tropics, then transported by stratospheric circulation polewards. There, a unique set of conditions create the perfect conditions for ozone destruction. Aerosols and Polar Stratospheric Clouds (PSCs) can provide reaction surfaces on which the reactions described in Equation 1-3 can occur, the active chlorine created then reacts with ozone, destroying it in the process (Equation 1-4), or reacts with

odd oxygen, thereby preventing it from reacting with O<sub>2</sub> to form ozone (Equation 1-5). Ozone-depleting substances are present in the stratosphere as trace gases, usually within the parts per trillion (ppt) range. Ozone is present in the low parts per million (ppm) range. As PSCs occur at altitudes (typically between 15 and 25 km) which comprise the bulk of the ozone layer (roughly between 15 km and 30 km), the highly reactive chlorine created in Equation 1-3 is created in a region with abundant ozone which it can then deplete. The presence of PSCs facilitates reactions between ozone-depleting substances and ozone. The formation of PSCs also results in denoxification (conversion of NO<sub>x</sub> to HNO<sub>3</sub>) and denitrification (removal of HNO<sub>3</sub> via gravitational settling of hydrate particles). This removal of nitric acid (HNO<sub>3</sub>) means it is not available for reaction with NO<sub>2</sub> (Tritscher *et al.*, 2021).

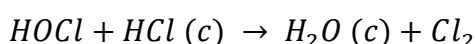
Inorganic chlorine (Cly) in the lower stratosphere during the polar vortices has two reservoir species: HCl and ClONO<sub>2</sub>, neither of these compounds is reactive towards O<sub>3</sub>. (Solomon, 1988; Wilmouth *et al.*, 2006; Tritscher *et al.*, 2021). Chlorine from these compounds can be converted into a reactive form via heterogeneous reactions such as (condensed phase, indicated by (c)):



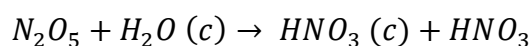
*Equation 1-7. Reaction of ClONO<sub>2</sub> with HCl*



*Equation 1-8. Reaction of ClONO<sub>2</sub> with H<sub>2</sub>O*



*Equation 1-9. Reaction of HOCl with HCl*



*Equation 1-10. Reaction of N<sub>2</sub>O<sub>5</sub> with H<sub>2</sub>O*

In Equation 1-7, Equation 1-8 and Equation 1-9 the chlorine bearing products are photolabile (i.e. they are susceptible to photolysis), which releases chlorine radicals which take part in the destruction of ozone (Equation 1-4 and Equation 1-5). In Equation 1-10 the HNO<sub>3</sub> and H<sub>2</sub>O remain in their condensed phase (c), and can then be used in Equation 1-7,

Equation 1-8 and Equation 1-9 (Crutzen *et al.*, 1986; McElroy *et al.*, 1986; Solomon *et al.*, 1986; Solomon, 1988; Abbatt *et al.*, 1992b, 1992a; Tritscher *et al.*, 2021).

Stratospheric ozone is naturally created and destroyed in seasonal cycles, but the addition of man-made ozone-depleting substances has disrupted this equilibrium, resulting in net ozone depletion. However, this is not uniform; when conditions favour reactions which create ozone, ozone abundances increase, while when conditions favour ozone destructive processes, ozone abundance decreases.

## 1.2 Ozone-Depleting Substances and their replacements.

The Montréal Protocol is a global agreement that was developed to protect stratospheric ozone by phasing out both the production and the use of ODSs. The Montréal Protocol was finalised in 1987; it banned the production and use of CFCs in developed countries from 1996, and developing countries since 2010 (Mäder *et al.*, 2010). Our knowledge about the ozone layer and threats to it, is constantly evolving.

New ODSs can be discovered, or new emissions of known ones, and for this reason the Montréal Protocol is regularly updated (6 times so far) in order keep pace with new research that improves our understanding of ozone-depleting substances and their emissions. Because of this the Montréal Protocol should not be seen as static, but as something dynamic which adapts to developing scientific research. The better we understand ODSs and the processes surrounding ozone-depletion, the better we can protect the ozone layer.

Chlorofluorocarbons (CFCs) were first synthesised by Thomas Midgley, Jr in 1928 as safe, nontoxic, non-flammable gas to replace the toxic gases used by early refrigerators, such as ammonia (NH<sub>3</sub>), methyl chloride (CH<sub>3</sub>Cl), and sulphur dioxide (SO<sub>2</sub>), which had led to fatal accidents. Their apparent safety meant CFCs were adapted for a wide number of uses, from propellants to air conditioning. Unfortunately, when the role of CFCs in ozone depletion was discovered, their extensive use meant that it was necessary to phase out their production and consumption in stages. This has allowed for short- and long-term replacements to be developed and deployed.

While the abundance of most CFCs is in decline, Montzka *et al.*, (2018) reported a slowdown in that rate of decline for CFC-11 after 2012. A number of papers which used observation-based data found unusually high abundances of several CFCs (in particular CFC-11 and CFC-12) between 2009 and 2019 in areas of China (Lin *et al.*, 2019; Zeng *et al.*, 2020; Benish *et al.*, 2021; Huang *et al.*, 2021; Yang *et al.*, 2021). Emissions from eastern China (Rigby *et al.*, 2019; Adcock *et al.*, 2020) were a major contributor, and in addition satellite-based evidence suggest CFC-11 sources around India and the Arabian peninsula (Chen *et al.*, 2020). During this time period it is believed that illegal production and trade of CFCs was conducted, with Chinese authorities seizing small quantities (tens of tonnes) of ODSs including CFC-11 during inspections of industrial facilities (UNEP, 2018, 2019; Girschikofsky

*et al.*, 2019; Park *et al.*, 2021). Since 2019 however the slowdown in the decline of CFC-11's abundance has reversed seeing an increase in the rate of decline equivalent to a return to pre-2012 values (Montzka *et al.*, 2021; Park *et al.*, 2021)

When evaluating ozone-depleting substances, it is helpful to have some way to quantify their potential effect on stratospheric ozone. Ozone Depletion Potentials (ODPs) are indices which are used to compare the capacity of compounds to destroy stratospheric ozone, relative to CFC-11. ODPs take into account how quickly the compound dissociates in the stratosphere, how many chlorine (or where present, bromine) atoms are in a molecule of the compound, and the lifetime of the compound. How this is calculated, including the formulae used, is covered in more depth in section 1.4.

The first wave of replacements for CFCs were the hydrochlorofluorocarbons (HCFCs), which the Montréal Protocol allowed for the use of HCFCs as transitional, short-term substitutes for compounds with higher ODPs. HCFCs are used in a number of applications, including as solvents, refrigerants and insulating foams. Compared to CFCs, HCFCs are generally less effective at destroying stratospheric ozone because unlike CFCs they are reactive in the troposphere due to containing hydrogen (H), and thus substantial chemical removal has occurred before the compound reaches the stratosphere. Another reason is that their primary sink is through reaction with the OH radical, which is comparatively rare in the stratosphere, therefore a larger concentration of HCFCs survive their transport through the stratosphere and back into the troposphere, intact. As part of the 2007 Adjustment to the Montréal Protocol HCFC phaseout was accelerated with production to cease by 2020 for 'developed' countries and by 2030 for 'developing' countries (Graziosi *et al.*, 2015).

Hydrofluorocarbons (HFCs) are also a transitional, short-term substitute for ODSs such as CFCs and HCFCs. As HFCs contain no chlorine or bromine they do not contribute to ozone depletion. However, HFCs (like most ODSs) are Greenhouse Gases (GHGs) with (mostly) long stratospheric lifetimes, thus contributing to human-induced climate change. HFC-125 (examined in Chapter 4) has a Global Warming Potential (GWP) of 3820, GWPs are a metric used to determine the relative contribution of a substance to climate warming, and is defined as 'the ratio of the radiative forcing for a given mass emission of a substance, relative to the same mass emission of CO<sub>2</sub>, summed over a given period of time (typically 20 or 100 years' (Burkholder *et al.*, 2022).

The stratospheric lifetimes of HFCs vary extensively, with some as low as 20 year (e.g. HFC-152) and others as high as 3636 years (e.g. HFC-23), but usually number over 100 years (Fang *et al.*, 2016). HFC-125 which is examined in Chapter 4 has a stratospheric lifetime of 665 years (Table 1-1).

Table 1-1. All Compounds examined in detail in this thesis. This includes the compounds' names, formulae, atmospheric abundance, stratospheric lifetime, total lifetime, ozone depletion potential, global warming potential, and fractional release factor (at 3 years mean age). Unless otherwise stated, all data was taken from Burkholder *et al.* (2022)

Compound	Formulae	Atmospheric abundance, 2020, ppt	Stratospheric Lifetime, yr	Total Lifetime, yr	Ozone depletion potential (ODP)	Global Warming Potentials (direct) (GWP), 100-yr <sup>1</sup>	Fractional Release Factor (FRF)
CFC-11	CCl <sub>3</sub> F	224	55	52	1	6410	0.47
CFC-12	CF <sub>2</sub> Cl <sub>2</sub>	497.2	103	101	0.75	12500	0.24
CFC-113	CClCF <sub>3</sub>	68.9	94.5	93	0.82	6530	0.3
CFC-13	CClF <sub>3</sub>	3.32	-	650	0.3	16300	-
CFC-114	C <sub>2</sub> Cl <sub>2</sub> F <sub>4</sub>	16.3	191	189	0.53	9450	0.13
CFC-114a	C <sub>2</sub> Cl <sub>2</sub> F <sub>4</sub>	1.11	106.7	105	0.72	7410	-
CFC-115	CF <sub>3</sub> CClF <sub>2</sub>	8.7	664	540	0.45	9630	0.07
PFC-116	C <sub>2</sub> F <sub>6</sub>	4.94	-	10000	0	12600	-
Methyl Chloride	CH <sub>3</sub> Cl	549.4	30.4	0.9	0.015	6	0.44
HFC-125	CF <sub>3</sub> CHF <sub>2</sub>	32.6	665	30.7	0	3820	-
HCFC-141b	CH <sub>3</sub> CCl <sub>2</sub> F	24.5	49.4 <sup>1</sup> or 101 <sup>2</sup> (64–221)	8.81	0.095 <sup>1</sup> or 0.083 <sup>2</sup> (0.069 – 0.102)	808	0.34 <sup>1</sup> or 0.31 <sup>2</sup> (0.27-0.36)
HCFC-142b	CH <sub>3</sub> CClF <sub>2</sub>	21.7	148 <sup>1</sup> or 178 <sup>2</sup> (103–459)	18	0.054 <sup>1</sup> or 0.037 <sup>2</sup> (0.023 - 0.057)	2190	0.17 <sup>1</sup> or 0.13 <sup>2</sup> (0.11-0.15)

<sup>1</sup>.(Burkholder & Hodnebrog, 2022)

<sup>2</sup>.(Leedham-Elvidge *et al.*, 2018)

The 2016 Kigali Amendment to the Montréal Protocol placed limits on future growth of the emission of HFCs which have high Global Warming Potentials (GWPs) (Fang *et al.*, 2016). GWPs are a metric which measures the radiative forcing for a given greenhouse gas, compared to the same mass of CO<sub>2</sub>, summed over a given period of time (typically 20 or 100 years). Radiative forcing is a measure of the contribution to climate change from a given factor, in this case a long-lived trace gas. This allows an easily parsed comparison between

the relative strengths of different greenhouse gases. CO<sub>2</sub> by definition has a GWP of 1, and the larger the GWP of a gas, the more it has the potential to warm the atmosphere, compared to the same quantity of CO<sub>2</sub> over the same time period (Laube *et al.*, 2022). The GWPs discussed in this thesis are ‘direct’ GWPs. These capture only the direct radiative effects of the ODSs themselves, but does not include radiative effects of ozone responses, smaller effects of methane and water vapour or changes in ODS mixing ratios (this would be reflected in ‘indirect GWPs’ which are not as relevant to this thesis).

Another class of greenhouse gas examined here are the PFCs (PFC-116 is examined in Chapter 4), and these are among the longest-lived (PFC-116 has a total lifetime of 10,000 years, Table 1-1) and most potent greenhouse gas (PFC-116 has a GWP-100 of 12600, Table 1-1). PFCs have had a number of uses, such as in semiconductor and other electronics manufacture for cleaning, chemical vapour deposition and plasma etching (Mühle *et al.*, 2010). Due to their high potential for global warming, effective monitoring of emissions and abundance of these compounds is vital to efforts to mitigate climate change. In addition, PFC-116 is useful as an ‘age tracer’ in the stratosphere, due to its very long lifetime, and the fact that it is largely inert in the stratosphere and has a monotonically changing tropospheric concentration (Leedham-Elvidge *et al.*, 2018).

In addition to the above discussed families of compounds, this thesis also examines a chlorinated non-CFC gas: methyl chloride (CH<sub>3</sub>Cl). CH<sub>3</sub>Cl has some anthropogenic sources such as feedstock and coal combustion (Li *et al.*, 2017) and from biomass burning (Mead *et al.*, 2008). However, CH<sub>3</sub>Cl’s origin is predominantly natural, and thus it is not controlled under the Montréal Protocol (Burkholder *et al.*, 2022). Methyl chloride is explored in Chapter 4 because it is the second most abundant ODS, and the only one examined here with primarily natural sources. This thesis will examine a range of compounds, including CFCs, HCFCs, HFCs and PFCs. All compounds examined in depth in this thesis are included in Table 1-1.

### **1.3 Atmospheric circulation and the Brewer-Dobson circulation**

The Brewer-Dobson circulation (BDC) refers to the net transport of tracers, mass, and heat within the stratosphere. Aside from chemical processes, stratospheric circulation is the main driver of trace gas distribution. The BDCs importance to the transport chemistry of

ozone and trace gases, means that a solid understanding of it is essential to predicting both short and long-term impacts of CFC emissions and ozone depletion. However, as will be discussed, different studies have given contradictory results regarding the speed and transport pathways of the BDC. Chapter 3 performs a model sensitivity study which (among other things) investigates how well the Goddard Space Flight Centre (GSFC) 2D model is able to simulate changes to the strength of the BDC. In addition to ozone, the BDC is also responsible for the transport of air and trace gases within the stratosphere (Plumb, 2002; Shepherd, 2007; Butchart, 2014; Abalos *et al.*, 2020), and these trace gases are used in Chapter 3 to explore possible changes to the BDC.

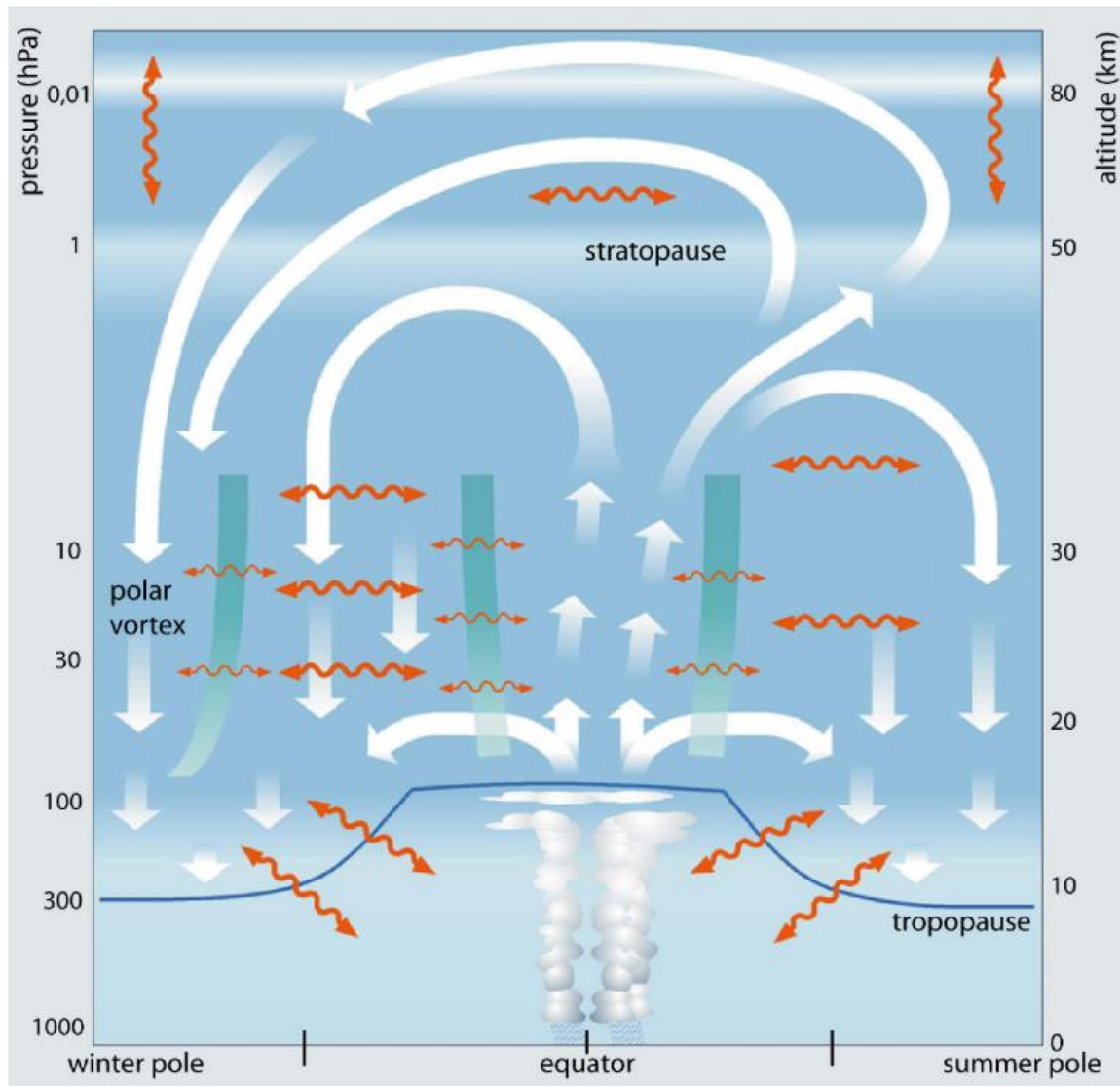


Figure 1.1. Taken from (Bönisch et al., 2011). "Fig. 1. Schematic of the BDC as the combined effect of residual circulation and mixing in the stratosphere and mesosphere. The thick white arrows depict the [Transformed Eulerian Mean] (TEM) mass stream function as representation of the residual circulation whereas the wavy orange arrows indicate two-way mixing processes. Both, circulation and mixing are mainly induced by wave activity on different scales (planetary to gravity waves). The thick green lines represent stratospheric transport and mixing barriers. The Figure is by courtesy of Dr. U. Schmidt and it is adapted from a non peer-reviewed research report of our institute"

The BDC is generally separated into two facets; the first being two-way mixing (the wavy orange arrows in Figure 1.1) which is the stirring of air masses as a result of wave dissipation, resulting in irreversible tracer transport (Plumb, 2002; Abalos *et al.*, 2020). The other facet of the BDC is the mean meridional mass circulation or residual circulation, and this is represented by thick white arrows in Figure 1.1. Age of air (AoA) includes transport effects from both these facets (Hall, 2000; Douglass *et al.*, 2008; Reithmeier *et al.*, 2008; Birner *et al.*, 2011).

The residual circulation is itself divided into two branches; the deep and shallow branches. The shallow branch transports air within the ‘tropically controlled transition region’ (Rosenlof, 1997), and is roughly limited to latitudes below 50° N/S and levels below 50 hPa, and has average overturning timescales under 1 year (Birner *et al.*, 2011). The deep branch extends into the upper stratosphere and mesosphere (the white arrows at the very top of Figure 1.1). The deep branch enters the stratosphere almost entirely within 5° of the equator, while the shallow branch enters closer to the poleward edges of the tropics (Birner *et al.*, 2011).

In Figure 1.1 we see upwelling in the tropics, and downwelling in the extratropics, and these regions are separated from each other by transport barriers (green lines in the centre). The region where mixing is suppressed by transport barriers is the ‘tropical pipe’ (Neu *et al.*, 1999). The age spectra of air in the tropics and extratropic differs even when air parcels share a mean age value, as different transport processes (such as advection, eddy-mixing, and turbulent diffusion) will result in different age spectra (Garny *et al.*, 2024a).

Between the tropical tropopause and around 20-22 km altitude (the ‘tropically controlled transition region’), the subtropical transport barrier (which is at the edge of the ‘tropical pipe’), can be described as ‘weak’ (Volk *et al.*, 1996) or ‘leaky’ (Neu *et al.*, 1999). Here the quasi-horizontal two-way mixing is far more intense than that occurring at higher stratospheric levels (Bönisch *et al.*, 2011).

The mechanism for the persistent air mass flow poleward in the middle and upper winter stratosphere is known as the ‘extratropical pump’ (Holton *et al.*, 1995) or the ‘Rossby-wave pump’ (Plumb, 2002). As the planetary-scale Rossby waves can only be westward, the pumping action is one way, and the air proceeds in a poleward direction in order to conserve angular momentum (Holton *et al.*, 1995). This results in tropical air being drawn up, then later pushed down in middle and high latitudes. For it to be otherwise would require the existence of a reverse flow from the pole to the equator, which cannot happen as there is no eastward Rossby-wave drag in order to balance the angular momentum budget (Butchart, 2014).

The transit time varies by seasonality, and by which ‘branch’ of the Brewer-Dobson Circulation is involved. The lower branch, which its associated with the tropically controlled transit region, has considerably shorter transport timescales in summer than in winter, with (on average) mean transit times of 0.5 years during May, and 0.3 years during August

(Bönisch *et al.*, 2009), with the youngest air in the lowermost stratosphere in the extra tropics occurring in autumn, and the oldest air in spring (Birner *et al.*, 2011). This seasonal cycle could be partially explained by seasonal cycles in both branches of the residual circulation, not just effects from two-way mixing (Bönisch *et al.*, 2009). The shallow branch is active during all seasons, but is strongest during winter and spring. The deep branch on the other hand is most active during winter and spring, but is virtually inactive during summer. Transit times in high latitudes are largely controlled by the deep branch. (Birner *et al.*, 2011). Knowing this one can estimate that the age of air in the extratropical lowermost stratosphere would be primarily influenced by the shallow branch during summer and autumn, but that the deep branch may make a stronger contribution during winter and spring (Birner *et al.*, 2011).

The total ozone column over the poles is at its lowest in late winter through to early spring, and was exceptionally low in 2020, which saw the lowest value in the northern polar cap since 1979 (when satellite measurements began) (Lawrence *et al.*, 2020). This low total ozone column was partially caused by the unusually strong, cold, and persistent stratospheric polar vortex, as it provided ideal conditions for ozone destruction as the strong, undisturbed vortex constitutes a strong transport barrier, and the temperatures were sufficiently cold to allow the formation of polar stratospheric clouds for an extended period of time (Bernhard *et al.*, 2020).

While there are many factors influencing the speed of the BDC, the timescales are usually on the order of days-weeks for vertical transport (in the tropics), and months-years for horizontal transport (from tropics to the poles). A robust feature of model climate predictions is an acceleration of the Brewer-Dobson Circulation, due to tropospheric warming as a result of anthropogenic climate change (Olsen *et al.*, 2007; Oman *et al.*, 2009; Oberländer *et al.*, 2013; Butchart, 2014). However, it initially proved difficult to find evidence of changes to the speed of the BDC from observations. This is because indirect estimates of circulation, such as using temperature data and trends via satellites, are consistent with an acceleration of the overturning circulation (Young *et al.*, 2012), but estimates of changes in stratospheric age of air via observational data of chemical tracers were unable to find clear trends, or even indicated a deceleration of the BDC (Engel *et al.*, 2009; Bönisch *et al.*, 2011; Diallo *et al.*, 2012; Seviour *et al.*, 2012; Stiller *et al.*, 2012). However, some later studies (Oberländer-Hayn *et al.*, 2016) have found evidence for an

acceleration of the BDC. Fu et al., (2019) used observational data to show a mean acceleration of the BDC between 1980-1999 but a deceleration between 2000-2018 and speculates that this maybe down to the effects of depletion and healing of ozone. This is likely to be because, as Polvani *et al.*, (2019) found, ODSs have an impact on BDC trends, primarily via the depletion or recovery of stratospheric ozone in polar regions (primarily the south pole). They also found that ODSs result in seasonal and hemispheric asymmetries to these trends.

The transport pathway a tracer is exposed to will determine the rate of disassociation it experiences. Transport pathways that bring a tracer into its sink region will see higher disassociation than transport pathways that do not. For the long-lived CFCs that are examined in Chapter 3 (where atmospheric circulation is explored via models), the sink regions are high up in the stratosphere, as they require the highest actinic flux to break molecular bonds via photolysis, and the flux increases with altitude. This means that these long-lived CFCs will enter their sink region via the deep branch of the BDC. Model simulations find that the greatest contributors to Arctic tracer mass originate in Europe, East Asia, and North America, and the next largest contributions are from the Tibetan Plateau, South Asia and the Middle East (Zheng *et al.*, 2024).

In Chapter 3 the possible impacts of a change in the speed of the BDC is explored, utilising both in-situ based observations and model data (section 3.2.3). However, many multi-model assessments of the BDC focus mostly or entirely on the residual circulation alone, leaving aside two-way mixing (Butchart *et al.*, 2010; Chipperfield *et al.*, 2014; Hardiman *et al.*, 2014). This is changing and papers such as Abalos et al. (2021) have worked to integrate the effect of both residual circulation and mixing. As model results can be evaluated using in-situ derived data, this is one of the goals of the model sensitivity study undertaken in Chapter 3.

Another feature the model evaluated in Chapter 3 is that it can simulate a speeding-up or slowing down of the BDC. However, it does this for the entire residual circulation. One of the questions being explored regarding whether or not the BDC is speeding up, is which branches are affected and to what extent. The compounds explored in Chapter 3 are comparatively long-lived and have their sink regions high up in the deep branch of the BDC. So, if for example, only the shallow branch was speeding up, under true atmospheric conditions we may not see a change in the speed of dissociation for these compounds (and

thus their lifetimes). However, in a model only depicting a uniform change in speed across both branches, this would result in the model predicting changes to the lifetimes that might not reflect actual atmospheric conditions.

#### 1.4 Key Concepts and Policy Relevant Metrics

The atmospheric lifetime of a gas is the length of time after it is emitted it takes to drop to  $1/e$  of its initial abundance. That lifetime is determined by its sinks and reactivity. As CFCs are largely inert in the troposphere, and their sinks are almost exclusively in the stratosphere, the stratospheric and overall atmospheric lifetimes are essentially the same and can therefore be used interchangeably. Of the compound families examined in this thesis, this only applies to the CFCs. Other compounds, such as HFCs and HCFCs often have drastically different total atmospheric lifetimes compared to their stratospheric lifetimes. Nevertheless, knowing how reactive an ozone-depleting substance (ODS) is in the stratosphere is crucial in determining how much ozone it will deplete and for how long this will continue. Chapter 3 derives new estimates of stratospheric lifetimes for four under-researched CFCs: CFC-13, CFC-114, CFC-114a, and CFC-115. These newly estimated lifetimes will have important implications for (among other things) our understanding of the potential rate of ozone recovery and the scope of emissions of these compounds.

There are a number of ways the stratospheric lifetime of a compound can be derived (Ko *et al.*, 2013). These include model simulations (Hartley *et al.*, 1993; Minschwaner *et al.*, 1993; Montzka *et al.*, 1999, 2011; Butchart *et al.*, 2006; Douglass *et al.*, 2008; Bergamaschi *et al.*, 2009; Lee *et al.*, 2011; Patra *et al.*, 2011; John *et al.*, 2012; Rigby *et al.*, 2013), satellite data (Ko *et al.*, 1991; Bergamaschi *et al.*, 2009; Minschwaner *et al.*, 2012; Brown *et al.*, 2013), lab-based kinetics experiments (Burkholder *et al.*, 2020), and by examining the relationship between tracer-tracer or tracer-mean age (Plumb *et al.*, 1992; Plumb, 1996; Kloss *et al.*, 2014). Chapter 3 uses a version of the tracer-mean age method, which will be discussed in more detail in section 3.2.5.

One means of studying the stratospheric circulation, is the use of mean Age of Air (AoA) calculations (Volk *et al.*, 1997; Douglass *et al.*, 2008; Laube *et al.*, 2013). The AoA of an

air parcel is the average transport time since the air parcel entered the stratosphere primarily through the tropical tropopause (Holton, 1990). However, the mixing process is complex, and an individual air parcel will not have a single age; instead it will be composed of the different ages of its components. This results in a 'spectra of ages' (Strunk *et al.*, 2000).

Mean AoA calculations can be used as a proxy; since physically measuring changes to the strength of the BDC is not currently feasible, a derived quantity is necessary. AoA is also used to calculate air mass fluxes between atmospheric regions (e.g. between the stratosphere and the troposphere). AoA can also be used to calculate the state of ozone recovery, as AoA calculations are used in the calculation of effective equivalent stratospheric ozone, stratospheric lifetimes, and Ozone Depletion Potentials (ODP)s (Leedham-Elvidge *et al.*, 2018).

In order to derive mean ages, it is necessary to compare the observed abundance of a 'tracer' species in the stratosphere, to the observed global tropospheric time series of that gas. This assumes that the tracer gas is largely chemically inert in the stratosphere and has a monotonically (neither increasing nor decreasing), ideally linear changing tropospheric concentration. An ideal tracer should not have sinks or sources in the stratosphere and should show an ideally linear tropospheric trend over the past 10—15 years (Engel *et al.*, 2002). Close to these criteria are the most common tracers for this type of calculation: CO<sub>2</sub> and sulfur hexafluoride (SF<sub>6</sub>).

These are frequently used to track large-scale stratospheric transport and transport trends, and to evaluate atmospheric residence times of ozone-depleting substances, and thus their impact on the Ozone Layer. Both of these tracer gases have their limitations; CO<sub>2</sub> has a complicated tropospheric trend and a stratospheric source (oxidation of hydrocarbons). Due to its biogenic sink CO<sub>2</sub> has a seasonal cycle and is therefore neither increasing linearly nor monotonically. This limits its utility as an age tracer to mean ages >~2.5 years. SF<sub>6</sub> is also not ideal as it is influenced by mixing in of depleted mesospheric air into the stratosphere, which biases mean ages derived using this tracer (Leedham-Elvidge *et al.*, 2018).

It should be noted that SF<sub>6</sub>'s chemical sinks introduce a substantial bias to Age of Air (AoA); these sinks are stronger than previously assumed, which becomes particularly relevant with rising concentrations of SF<sub>6</sub> (Stiller *et al.*, 2012; Kovács *et al.*, 2017; Ray *et al.*,

2017; Leedham-Elvidge *et al.*, 2018; Loeffel *et al.*, 2022; Garny *et al.*, 2024b). In particular Loeffel *et al.*, (2022) found that the bias of AoA that was introduced by the chemical sinks of SF<sub>6</sub>, increased with increasing mixing ratios, therefore biases have been increasingly strong since the 2000s. Work has been done to establish reliable means to compensate for this bias, and this thesis primarily makes use of the method described in Leedham-Elvidge *et al.*, (2018) which uses the ratio between SF<sub>6</sub> derived mean ages with those derived using other age tracers. Garny *et al.* (2024b) has also proposed a correction scheme based on fit parameters using models. While ideally these fit parameters would utilise observational data the sparse nature of that data has meant at present observational data is unable to constrain the fit parameters. For this reason, and the fact the paper was published less than 6 months before this thesis is due to be submitted (and thus the time needed to implement the new correction scheme is not practically served by doing so), this correction scheme is not used.

Leedham-Elvidge *et al.*, (2018) tested six potential new tracers, 5 of which proved suitable; including perfluorocarbons (CF<sub>4</sub>, C<sub>2</sub>F<sub>6</sub> and C<sub>3</sub>F<sub>8</sub>) and hydrofluorocarbons (CHF<sub>3</sub>, HFC-23 and HFC-125). Since a high bias in SF<sub>6</sub>-derived mean ages was found, unless otherwise stated, the mean ages used here were derived using a simple correction developed in Leedham-Elvidge *et al.*, (2018).

Using a suitable age tracer (or combination of such) allows the derivation of another important metric for ozone chemistry: Fractional Release Factors (FRFs). FRFs are defined as “the fraction of the halocarbon species *x* injected into the stratosphere that has been dissociated” (Solomon *et al.*, 1992b). This dissociation happens in the reactions shown in Equation 1-3 and Equation 1-4. Calculating and understanding FRFs is important as an ODS with a larger FRF has a greater capacity for ozone destruction. Because of this, calculating FRFs is also a necessary component (alongside calculating their relation to mean ages of air) in the derivation of ‘observation based semi-empirical’ ODPs (Laube *et al.*, 2013). The ODP of a compound is defined as ‘the reduction in total ozone (O<sub>3</sub>) column per unit of mass for that compound divided by the reduction in total O<sub>3</sub> column per unit of mass for the reference compound trichlorofluoromethane [CFC-11]’ (Patten *et al.*, 2010). For this both the FRFs and lifetimes for each compound were needed in order to calculate the loss of global O<sub>3</sub> due to unit mass emissions, divided by the loss of global O<sub>3</sub> due to unit mass emissions of CFC-11 (Patten *et al.*, 2010) (Equation 1-11 and Equation 1-12).

$$ODP_i = \frac{\text{Global } O^3 \text{ loss due to unit mass of emissions of } i}{\text{Global } O^3 \text{ loss due to unit mass emissions of CFC}_{11}}$$

Equation 1-11. Simplified equation for calculation of Ozone Depletion Potential. Where 'i' is the compound of interest.

$$ODP_i = (\alpha n_{Br,i} + n_{Cl,i}) \frac{f_i}{f_{CFC_{11}}} \frac{\tau_i}{\tau_{CFC_{11}}} \frac{M_{CFC_{11}}}{M_i} \frac{1}{3}$$

Equation 1-12. The full equation for calculation of ODPs. Where i is the gas of interest;  $\alpha$  is the bromine efficiency factor, n is the number of chlorine (or bromine) atoms in molecule i; f is the "fractional halogen release factor";  $\tau$  is the atmospheric lifetime (in this case the stratospheric lifetime); and M is the molecular weight.

Both Chapter 3 and Chapter 4 derive FRFs and ODPs for their compounds of interest and explore the implications of these newly derived metrics. This includes an exploration of the robustness of the calculations and assumptions underlying them.

Equivalent Effective Stratospheric Chlorine (EESC) is a parameter used to estimate the total effective quantity of halogens in the stratosphere.

$$\begin{aligned} EESC_{new}(\Gamma, t) &= \Sigma_{Cl} \left( n_i \bar{f}_i(\Gamma) \int_0^\infty \chi_{0,i}(t-t') G_{N,i}^\#(\Gamma^\#, t') dt' \right) \\ &+ \alpha \Sigma_{Br} \left( n_i \bar{f}_i(\Gamma) \int_0^\infty \chi_{0,i}(t-t') G_{N,i}^\#(\Gamma^\#, t') dt' \right) \end{aligned}$$

Equation 1-13. The 'new' formula for deriving EESC, equation 21 in Engel et al., (2018).

It is the sum of chlorine and bromine which is derived from the tropospheric abundances of ozone-depleting substances (ODSs) and weighted in order to reflect their predicted depletion of stratospheric ozone. Equation 1-13 displays the 'new' formula for EESC, derived by Engel et al., (2018). In which  $\Gamma$  stands for mean age,  $\Gamma^\#$  stands for the mean arrival time,  $t'$  for transit time, a specific time t, place r, age spectrum G, the release time distribution  $G^\#$  ('which describes the probability for an inorganic halogen atom released from this source gas to arrive at this place r in the stratosphere, again as a function of transit time' (Newman et al., 2007)), normalized release time distribution  $G_{N,i}^\#$ , tropospheric time series  $\chi_0$  of the tracer,  $n_i$  as the number of chlorine/bromine atoms in species i,  $f_i$  the fractional release factor, with  $\bar{f}_i$  time-independent fractional release factor.  $\alpha$  is a factor

which represents the higher effectivity of bromine to ozone depletion (usually 60 is used for both high and mid latitudes (Newman *et al.*, 2007)).

EESC is used to describe these combined effects of both chlorine and bromine, though it is only a valid proxy for anthropogenic ozone depletion if all other parameters (notably atmospheric transport) remain unchanged (Engel *et al.*, 2018). EESC has been widely used as a proxy to describe the effect on stratospheric ozone of bromine and chlorine, notably in the analysis of time series of ozone, or in the discussion of the effects of geoengineering or volcanoes (Weatherhead *et al.*, 2006; Tilmes *et al.*, 2009; Shepherd *et al.*, 2014; Chipperfield *et al.*, 2017).

The last concept to be covered in this section is that of ‘stratospheric chlorine loading’ which is the percentage of chlorine contained in a compound that is emitted and ultimately released into the stratosphere in the form of reactive chlorine (Kindler *et al.*, 1995). This can be a useful metric in determining the potential of a compound to deplete stratospheric ozone and is helpful when understanding FRFs (section 2.6).

## **1.5 Aims and rationale.**

The Montréal Protocol has been one of, if not the, most successful environmental protection agreements to date. For ozone recovery gains to be maintained and continued, it is vital to continue to monitor potential threats to the ozone layer (both existing and emerging), to accurately describe the chemistry and dynamics of the stratosphere, and to generate the most up-to-date policy relevant metrics which can inform both national and international climate protection policies.

This thesis focuses on threats, both historical and ongoing, to the ozone layer, and has three overarching aims:

- To derive new and improved policy relevant metrics for a range of compounds of relevance to stratospheric chemistry. These metrics include stratospheric steady state lifetimes, fractional release factors, and ozone depletion potentials.
- To investigate a range of techniques for monitoring stratospheric composition and use an interdisciplinary approach to investigate the chemistry and dynamics of the stratosphere.

- To offer refinements of some existing techniques in order to gain a more detailed picture of ODSs, their emissions, abundance, and eventual depletion.

Chapter 2 provides an overview of the techniques used in the research chapters.

Chapter 3 focuses on observational measurements derived from research aircraft flights and uses model data to investigate stratospheric steady-state lifetimes, fractional release factors, and ozone depletion potential of four long-lived CFCs. Samples of stratospheric air were collected during five aircraft campaigns at different latitudes, seasons and atmospheric conditions, allowing a broad investigation. The use of model data gives additional insight into the findings from observational data and ultimately strengthens the conclusions of this chapter. This chapter also includes a short section focused on data from archived air samples, and this is used to enhance and expand upon the findings of other sections.

Chapter 4 focuses on observational measurements derived from several years of balloon-borne “AirCore” flight data. It expands the number of compounds that can be shown to be reliably measured by AirCore, assesses the techniques used for optimum precision, investigates the effects of seasonality and latitude on fractional release factors and ozone depletion potentials, as well as the effect such variation might have had on existing estimates.

Chapter 5 finishes this thesis with a summary of key conclusions and suggestions for further research.

## Chapter 2 Methodology

### 2.1 Sample collection overview

Each chapter used different collection methods and had somewhat different sampling procedures as a result. Chapter 3 uses primarily high altitude research aircraft for collection of samples (section 2.1.1, for details of the flights see Table 3-2). The chapter also includes a section which uses archived air samples collected via large balloon-borne (section 2.1.2) sampling (see Table 3-1 for all flight details). Chapter 4 uses primarily AirCore-borne sample collection (Table 4-1), though does compare this to data collected by the high altitude research aircraft Geophysica (covered in more depth in Chapter 3) and also refers back to archived air data from section 2.1.2.

#### 2.1.1 Research Aircraft Flights

One method of collecting atmospheric samples is the use of research aircraft. The research flight data used in this thesis was collected during multiple flights of the M55 Geophysica high altitude research aircraft, the latest of which (the 2016 and 2017 campaigns) were part of the StratoClim EU project ([www.stratoclim.org](http://www.stratoclim.org)). The M55 Geophysica is a subsonic aircraft, capable of performing long endurance flight at altitudes up to 21 km.

Using a research aircraft has several advantages including that the plane can cover large areas relatively quickly and can potentially carry a significant array of scientific instruments to collect or even analyse samples during the flight. However, aircraft campaigns are very expensive, and due to this they are infrequent. They also cannot cover the full altitude range; the M55 Geophysica reaches altitudes of up to 21 km, while the stratosphere extends (in some areas) up to 50 km. They do however have the advantage of manoeuvrability over balloon-borne research; a research aircraft can target specific regions and altitudes, while a balloon's trajectory is controlled by air currents and buoyancy.

#### 2.1.2 Large Balloon Flights

In section 3.1.3 archived air from historical large balloon flights is analysed. These are flights from 1976, 1981, 1982, 1993 and 1999 (with one flight in 2015 using high-altitude

research aircraft), and samples from these flights have been stored in stainless steel canisters. 'Large' is very relative, but these balloons are often large enough to be described as 'the size of a football stadium', which are on average 100-120 meters long and 64-75 meters wide. Payloads for these large balloons can be 1588kg or more in some cases. The Super-pressure Balloon-borne Imaging Telescope for example used a 1 million cubic metre helium balloon, with a 60-100 m long flight train (Romualdez *et al.*, 2016). Large balloon flights have similar advantages and disadvantages to aircraft flights. Depending on the type of balloon it could be in the air from a few hours to many months, although at present sampling is only possible in shorter flights that last a few hours (Laube, 2008; Ray *et al.*, 2017). Sampling requires storage space which may be in short supply when all available payload allowance is taken up with other scientific instruments. While sampling is currently not practical on longer flights, if suitable space for sample storage were possible this would allow for more detailed studies into spacial distribution of tracers, circulation patterns and air mass mixing, than is currently feasible via sampling.

One side benefit of a large balloon flight is that since it is pushed by air currents, the balloon's trajectory can act as a tracer for movement of air masses. A wide range of payload weights are possible, from a few hundred grams to several tonnes, and depending on the type of balloon used, they can operate from a few hundred meters off the ground, up to around 40 km. This is one key advantage of balloon-borne measurements over research aircraft measurements; the M55 Geophysica research aircraft (section 2.1.1) has a maximum altitude of around 21 km, while high altitude balloons can reach roughly 40 km. While this does not cover the entire range of the stratosphere, balloons can cover a significantly greater altitude range than research aircraft. Safety and environmental concerns may also be a factor in choosing between balloon-borne measurements and research aircraft. Balloons typically have no engine or fuel, nor a pilot or passengers that might be endangered if the flight were to run into difficulties. Research aircraft typically run on fossil fuels, while balloons typically rely on helium. While this does not produce greenhouse gases, helium is becoming increasingly rare and expensive, and although various experiments into hybrid hydrogen-helium lift gases are being investigated, at present large balloons primarily rely on helium. Similar to research aircraft flights, large balloons are also expensive. Launches are limited by aviation authorities in many countries due to safety concerns over payload weight, especially during landing.

### 2.1.3 AirCore Flights

There are many challenges to studying stratospheric gases. Satellites are unable to resolve many trace-gases, and require 'ground truthing' for validation. Research aircraft and large balloon campaigns are expensive, and due to legal restrictions on payload size there are only a limited number of places large balloons can be launched. Legal restrictions vary by country, in the UK for example the payload restriction is a maximum of 4 kg, with no more than 3kg in a single section of the payload (so equipment needs to be spread out along the rope attached to the balloon). This is for safety reasons, and typically only countries with large, open, unpopulated areas (such as remote regions of Canada or Finland) are suitable for balloons with larger payloads.

An alternative is to use 'small' (1.5-3 kg) balloons to carry 'AirCores'; long (~50-150 m) coiled stainless steel tubes used to collect a vertical profile of stratospheric and tropospheric air. The AirCore (Figure 2.1) has a sealed end and an open end, as the balloon rises the pressure of the air outside the AirCore becomes increasingly lower relative to the air within the AirCore, thus causing the air in the AirCore to be evacuated during ascent. During decent the reverse occurs, as the air pressure within the AirCore is lower than the air pressure outside, outside air is drawn passively (without the need for a pump) into the AirCore. This allows the AirCore to collect a continuous sample, the different 'sections' of air (air drawn in at different pressure altitudes) are separated by distance rather than valves. Details of the AirCores used for this thesis can be found in section 4.2.1.



*Figure 2.1. A photograph of an AirCore (polystyrene box in foreground) with an insert showing the AirCore device itself. In the background can be seen the helium balloon being filled.*

Once recovered the AirCore can be analysed immediately upon return to the lab, or transferred into a suitable sub-sampler to maintain separation until the sample can be

analysed (see section 4.2.2 for details on the sub-sampling techniques used in this research). Dr Tans, the inventor of the AirCore at NOAA, Boulder, US, developed an algorithm to relate the section of the AirCore sample to the altitude/pressure at which it was collected. The algorithm uses a fluid dynamics model and flight data, in particular the pressure and temperature of outside air, and the temperature of the tube (there are 3-5 sensors for pressure and temperature, affixed to different sections of the AirCore) (Tans, 2021).

AirCores take their name from ice cores, as the technique allows the collection of a continuous profile rather than discrete samples. The technique was inspired by the findings of ~100 year old air trapped in the deepest layers of firn. Firn, which is the upper layer of unconsolidated snow on top of an ice sheet, is porous and permeable (Battle *et al.*, 1996). However, the air diffuses extremely slowly, thereby preserving the air trapped over the last century. With this observation, the idea of using a long tube in a similar manner was tested, and it was verified that there was very little diffusive mixing (in the order of 1-3 meters after 24 hours) of the sample along the length of the tube (Karion *et al.*, 2010; Moore *et al.*, 2014; Tans, 2021). This allows the AirCore sample to be divided into 'sub-samples' to be analysed separately (see section 4.2.2 for details).

The AirCore technique had great potential for validation of satellite retrievals of column-averaged greenhouse gases, and a regular deployment of AirCores was proposed as a cost-effective means to study and monitor climate change processes and atmospheric circulation (Moore *et al.*, 2014). AirCore measurements have been used as part of the validation process for various satellite-borne instruments including TES (Tropospheric Emission Spectrometer) nadir and MLS (Microwave Limb Sounder) limb measurements from the Aura satellite to estimate atmospheric carbon monoxide (Luo *et al.*, 2013), and has been used for 'ground truthing' satellite measurements (Long *et al.*, 2020) and for validating models (Lan *et al.*, 2017; Gerken *et al.*, 2021).

The AirCore technique have also been used to validate ground-based measurements, for example spectral measurements collected in Sodankylä (67.4°N, 26.6°E), Northern Finland, using the Fourier Transform Spectrometer (FTS) instrument (Tukiainen *et al.*, 2016) and Total Carbon Column Observing Network (TCCON) of ground-based spectrometers (Wunch *et al.*, 2010; Byrne *et al.*, 2020). The AirCore measurements used in this thesis were collected via balloon-borne instruments; however, the AirCore technique is versatile enough that it can be adapted for use on unmanned aerial vehicles (UAVs), for example (Andersen

*et al.*, 2018) used UAVs to carry ‘active’ AirCores; instead of the passive sampling used in this study, sampling used a pump to pull air through the tubing during the flight. This allows for spatially sampling atmospheric air.

AirCores were initially used for trace gases with larger atmospheric concentrations such as CO<sub>2</sub> and CH<sub>4</sub> (Karion *et al.*, 2010; Engel *et al.*, 2017; Membrive *et al.*, 2017), and their isotopic composition (Mrozek *et al.*, 2016; Paul *et al.*, 2016). Their use has since been expanded to the study of several lower abundance trace gases; (Laube *et al.*, 2020) obtained mixing ratios for six gases (CFC-11, CFC-12, HCFC-22, H-1211, H-1301, and SF<sub>6</sub>), and Li *et al.*, (2023) used the technique to examine (N<sub>2</sub>O, SF<sub>6</sub>, CFC-11, CFC-12, H-1211, and CFC-113). Chapter 4 will further expand the number of compounds that can be reliably obtained from AirCore measurements by seven (CFC-115, CFC-113, HCFC-141b, HCFC-142b, HFC-125, SF<sub>6</sub>, and CH<sub>3</sub>Cl). Chapter 4 will also explore and refine the conditions necessary to capture viable samples of these compounds, in particular investigating how long a sample can be left between collection and analysis (and how quickly precision may be lost), the designs of AirCore and sub-sampler, the temperature of the AirCore in flight, and the effect of using a Gas Concentration Analyzer from Picarro. This AirCore technique is a versatile one and this chapter aims to confirm and expand the utility of this method to investigate and monitor trace gases, in addition to investigating and refining best practices for doing so.

#### **2.1.4 Satellites**

Satellites can avoid some of the problems experienced by in-situ sampling; unlike balloon or aircraft-borne measurements, satellites can be utilised over a wide geographical range. Limitations to coverage still exist and there is usually a trade-off between the resolution of satellite images and the special coverage they can provide, with greater coverage usually resulting in lower spatial resolution (Kim *et al.*, 2020; Dubovik *et al.*, 2021).

Satellite measurements have been used to great success in monitoring many abundant trace gases such as CO<sub>2</sub> and NO<sub>2</sub> (Richter *et al.*, 2004; Reuter *et al.*, 2014; Chevallier *et al.*, 2017, 2019). However, satellites are not yet able to resolve many less abundant trace gases such as some CFCs though Stiller *et al.* (2024) has made considerable progress in resolving two of the most abundant CFCs: CFC-11 and CFC-12. However the CFCs studied in Chapter 3 and Chapter 4 are currently not resolvable using satellite

measurements. In addition satellites require ‘ground truthing’ via the collection of whole air samples in order to be and remain reliable (Long *et al.*, 2020). The process of designing, constructing, launching, and monitoring satellites is also prohibitively expensive, usually running to hundreds of millions of dollars. Failures at or following launch are a hazard, and damage taken once a satellite is in position is extremely difficult (and expensive!) to repair. The strength and reception of a satellite’s signal can also vary due to errors made by the satellite (or those working on it), interference from adverse weather conditions, or sunspot activity.

This thesis did not directly use satellite data. However, it does reference research performed using it, and discusses how satellite measurements and in-situ measurements may be used to support each other.

## 2.2 Atmospheric Chemistry Transport Models

Models provide certain advantages over in-situ observations. It is possible to simulate conditions that are difficult or impossible to sample under real world conditions and can conduct experiments it would be impractical and severely unethical to perform in the real world (for example testing the results of adding varyingly large quantities of ozone-depleting substances into the atmosphere). They can provide estimates over wide geographical areas that balloon- or aircraft-based measurements are generally impractical over.

However, models also need to be validated via reliable input from both lab-based experiments and in situ measurements. They also rely on parameterisations which by necessity simplify particular processes and can therefore miss certain relevant processes and feedback mechanisms. An example of this is the polar Ozone Hole, as the chemical models missed the relevant mechanisms of ozone depletion (Bhartia *et al.*, 2018). So as with other research methods (such as balloon or aircraft sampling), modelling has both advantages and disadvantages, so can only provide the most reliable data in conjunction with other techniques.

There are a number of different ‘types’ of models that deal with atmosphere, climate and weather. Alongside research aircraft data Chapter 3 uses data from two models: the Chemical Lagrangian Model of the Stratosphere (CLaMS), which is a modular 3-D Chemistry

Transport Model (CTM) system developed at the Forschungszentrum Jülich, Germany (McKenna *et al.*, 2002a, 2002b; Konopka *et al.*, 2004), and the Goddard Space Flight Centre (GSFC) 2-D coupled chemistry-radiation-dynamics (Fleming *et al.*, 1999, 2001, 2002, 2011) based at Washington, D.C., the United States, which is an Idealised and Simplified Model (see section 3.2.3 for details). CTMs are driven by real world meteorological data and dynamics (such as wind fields) to calculate the chemistry and transport of chemical tracers. This allows them (among other things) to simulate the processes affecting air parcels in 3 dimensions. However, the more complex a model, the more time consuming (potentially taking years) and expensive it can be to run. Idealised and Simplified models as the name suggests are models which simplify the processes involved, in order to minimise computational power. Both types of model have strengths and weaknesses, and as these are relevant to the results in Chapter 3, these will be discussed in more detail there (section 3.2.3).

## 2.3 Gas Chromatography/Mass Spectroscopy

Once the air samples had been collected, from either research aircraft flights, large balloon flights, or AirCore flights, they needed to be analysed. Samples analysed in Chapter 3 typically have a volume between 200-300 ml, while samples analysed in Chapter 4 have volumes between 20 and 50 ml. Samples are introduced to the GC-MS system via a valve in the inlet system (see Figure 2.2).

The samples discussed in Chapter 3 and Chapter 4, were analysed primarily by Dr Laube, Dr Leedham-Elvidge, and Dr Adcock. Samples for Chapter 3 were analysed at the University of East Anglia (UEA), while only samples used in Chapter 4 collected before 2019 were analysed at UEA, with those collected from 2019 onwards analysed at the Forschungszentrum Jülich (FZJ). Samples used in the archived air section (3.2.6) were analysed at FZJ. I was fortunate enough to have the opportunity to assist in some of the Gas Chromatography/Mass Spectroscopy done for Chapter 3 and Chapter 4. Each chapter of this thesis will include details of any analysis techniques and equipment that varied between the different campaigns (3.2.2 and 4.2.4 for Chapter 3 and Chapter 4 respectively), but here I will detail the general procedure used.

The samples were first dried by passing through a magnesium perchlorate ( $\text{Mg}(\text{ClO}_4)_2$ ) drying tube, then cryogenically trapped by passing through a stainless steel sample loop packed with Hayesep D absorbent; this loop was immersed in a cold bath (made up of a dry-ice and ethanol mixture) at  $\sim -78^\circ\text{C}$ , in order to give quantitative retention and release (a procedure which has been used to great success on numerous papers (Adcock *et al.*, 2020, 2021; Laube *et al.*, 2020, 2025)). The sample loop was then submerged in boiling water, heating it to near  $100^\circ\text{C}$ , thus providing immediate and complete desorption of the analytes (see Figure 2.2). The sample is then separated using Agilent 6890 Gas Chromatograph, which is connected to a high-sensitivity Waters AutoSpec tri-sector mass spectrometer. Samples were also measured at FZJ, Jülich (using the same model GC-MS system), and the results were the same within measurement uncertainties for these compounds. Each day a ‘blank’ sample of pure, research-grade helium was measured to ensure to check for leaks or possible contamination.

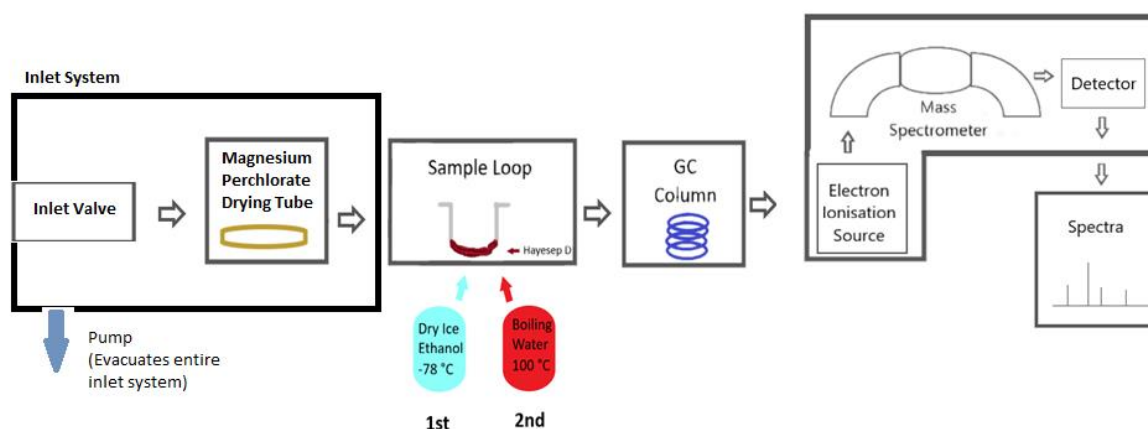


Figure 2.2. The stages of sample preparation. The sample is introduced via the inlet (which is attached to a pump that can evacuate the entire inlet system), is passed through the magnesium perchlorate drying tube to remove moisture, then into the sample loop. Here it is first cooled to  $-78^\circ\text{C}$  by a dry-ice and ethanol mixture to trap the required sample, then heated by boiling water to  $\sim 100^\circ\text{C}$  to release the sample to the GC Column.

The Inlet System connected to the GC-MS in Figure 2.2 has undergone a series of improvements throughout the course of this PhD project. The most notable improvement was a partial automation of the system. Initially all valves needed to be opened or closed manually. This required precise timing and was thus labour intensive. It also left an increased risk of operator error, particularly since the operator would need to be present for long stretches of the day and may become fatigued. The improved system utilises Valco pneumatic valves that can be controlled electronically. In addition to relieving the burden on the operator and allowing for consistently precise timing, this automation meant that the

entire inlet system could be enclosed and heated to a consistent temperature (~60 C) in order to avoid issues of condensation and to aid in the drying process.

The initial plan to automate the heating and cooling of the sample loop using heated/cooled air in a contained environment around the sample loop, did not prove successful as it was not possible to cool sufficient air, fast enough, to cool the sample loop in a time effective manner. However, all other automation elements were successfully implemented. My contributions to this project included assisting in the physical assembly of the system, extensive leak testing, extensive testing of the system itself, troubleshooting both hardware and software issues, writing the program to control the automation, and writing a user guide for the system.

Within the gas chromatograph system separation of the compounds within a sample is achieved through the use of a 'column' which is long, narrow tube. The sample is carried along by a continuous flow of inert gas. In this case the carrier gas is research grade helium. Separation occurs because different components within the sample will pass through at different rates, which are dependent on chemical or physical properties, and the interactions with the column lining (stationary phase).

The samples analysed for Chapter 3 used two different columns (separately) depending on which compounds were the focus. As the sample size for Chapter 3 was reasonably large (200-300 ml, compared to the 20-50 ml samples in Chapter 4) it was possible to run some samples on multiple columns. The type of columns used were gas chromatograph capillary PLOT (porous layer open tubular) columns: the 'GasPro', which was an Agilent GS GasPro column with a silica (silicon dioxide) stationary phase (length ~50 m, ID 0.32 mm) and the 'AIPLOT' an Agilent KCl-passivated Al<sub>2</sub>O<sub>3</sub>-PLOT column with an aluminium oxide (Al<sub>2</sub>O<sub>3</sub>) deactivated by potassium chloride stationary phase (length: 50 m, ID 0.32 mm). For Chapter 3 the AIPLOT column was essential as it uses polarities and boiling points to separate compounds which enables the separation of isomers (notably CFC-114 and CFC-114a) which would not be possible with the GasPro column (Laube *et al.*, 2016). However, it was necessary to also use the GasPro column as the AIPLOT column produces carbon dioxide and has a stronger affinity for carbon dioxide than the GasPro column. An Ascarite® (NaOH coated silica) trap is used to remove carbon dioxide when using the AIPLOT column, but this Ascarite® trap can reduce or distort the signal of some compounds, most strongly those containing both hydrogen and chlorine. In addition, the column coating is responsible

for a reaction which removes HCl. For Chapter 4 the samples were analysed on only the GasPro column, as the comparatively small sample size possible from AirCores (see sections 4.2.1 and 4.2.2 for details) meant that multiple analyses of a single sample was rarely possible.

The GC-column is within a temperature-controlled oven; prior to sample injection the GC oven is cooled to -10 °C using the process of expansion of liquid CO<sub>2</sub>. The column is held at that temperature for 2 minutes before being heated by increments of 10 °C min<sup>-1</sup>, till the oven reaches 180 °C for the ALPlot column, and 200 °C for the GasPro. This allows consistent retention times for the compounds of interest, and as compounds are separated by (among other things) boiling point, this incremental temperature increase allows analysis of compounds with a wide array of boiling points (Laube *et al.*, 2016).

Having been separated out in the GC column, they then pass to the mass spectrometer portion of the device. Here the sample is subjected to electron ionisation from a heated metal filament (tungsten) which emits a stream of electrons at the compounds; this breaks them down into electrically charged fragments. Each fragment has a particular mass, which divided by its charge gives the mass-to-charge ratio ( $m/z$ ). The fragments are then accelerated and deflected while exposed to multiple electro-magnetic fields, which separates the fragments by their  $m/z$ . Selected fragments then reach a photomultiplier detector which amplifies and records a voltage. The detector then sends this data to a linked computer which provides the results.

Repeats of samples would be done each day in order to account for instrument precision and to ensure that samples were being measured consistently. Approximately 12 samples (including samples of standard and a helium blank) are run in a day, so samples from a single flight may need to be analysed on separate days. During analysis every two to three samples a 'working standard' ('SX-3591' for KAL17, and 'AAL-071170' for all other campaigns, ratios between the two standards derived from multiple intercomparisons were used to ensure consistency) was used to bracket the samples. Standards were supplied by the National Oceanic and Atmospheric Administration's Global Monitoring Laboratory Monitoring Division, which maintains calibration scales for a number of trace gases. Mixing ratios (as dry air mole fraction) in the standard are reported based on compressed gas standards prepared in-house by gravimetric methods. Scales are named according to the year they are adopted. While the two standards here are assigned codes, and these are

mentioned here to distinguish between the two standards. Intercomparisons between samples were performed to ensure that they could be compared, and regular (usually once every 6 months) analysis of the standard is done to identify any drift that may occur.

As the standard has known quantities of each species, the measurement of the standard can be compared to the measurement for the sample, resulting in a response relative to the standard. From this the mixing ratio of the species in the sample can be calculated (as the mixing ratio in the standard is already known). As the instrument precision may 'drift' throughout the day, bracketing samples with standard throughout the day gives a measure of the drift on that day, and means this can be accounted for. This method is the same as that used in multiple works (Laube *et al.*, 2016, 2020; Adcock *et al.*, 2021). Drift in an instrument's sensitivity has a number of causes. These include small fluctuations in many internal currents, the burning of the filament in the ion source, increasing or decreasing amounts of more abundant species (e.g. H<sub>2</sub>O, O<sub>2</sub>) coming into the source and removing different amounts of electrons.

We used the single ion monitoring (SIM) mode of the device, so magnetic and electric fields were set to dwell on one mass at a time. The results are then analysed using 'integration'. The time that a peak elutes depends on various factors (notably boiling point), which allows identification of the compound. The size of the peak, either height or area, corresponds to the compound's abundance. Integration is the process of calculating the height and area of the peak. We use a program coded in IDL to automatically integrate peak height and area, though manual integration is necessary when peaks are difficult for the software to resolve. Automatic integrations are displayed visually and are checked to ensure that they are not missing sections of a peak or including sections of later peaks. I did some of the integrations for Chapter 3 and Chapter 4; the rest were done primarily by Dr Laube, Dr Leedham-Elvidge, and Dr Adcock.

From the peak area/height, a response factor is calculated based on the peak area/height and the concentration of the injected compound. The response factor for a compound in a sample where that compound's abundance is known (i.e. in the 'working standard'), can be compared to the response factor for the sample with unknown concentrations, giving a 'relative response' (RR). For most compounds the peak area is used (as it is usually the more reliable) but in some cases the peak area is harder to accurately measure. This is primarily due to interference from a nearby peak that overlaps the peak of

interest and therefore complicates peak area determination. If this is the case, then the height of the peak may be used instead. This relative response can then be multiplied by the known mixing ratio of the compound in the standard to give the mixing ratio of the compound in the sample (in the case of all compounds analysed here, the mixing ratio is in the 'parts per trillion' ppt range). The sample is also 'blank corrected'; research grade helium was analysed as a 'blank' as it should give either no peaks or peaks that were an order of magnitude (or more) smaller than the peaks expected in the sample. This provides a 'baseline' for what the spectra would look like if the compound were absent, and this makes it possible to account for the background 'noise'; a 'blank corrected' relative response for the sample is obtained using the relative response for the blank and the relative response for the sample (Equation 2-1).

$$\text{'Blank Corrected Relative Responce'} = (\text{'Sample RR'} - \text{'Blank RR'}) / (1 - \text{'Blank RR'})$$

*Equation 2-1. Equation for obtaining a blank corrected relative response.*

## 2.4 Bivariate Data

When using Excel (and most calculation software) to plot a trendline or regression, the program assumes that all the uncertainty is on the y axis, and none is on the x axis. This is appropriate for datasets where x is fixed (for example dates), but not where the x axis also contains considerable uncertainty.

This is potentially a problem as the datasets used to predict FRFs in sections 3.2.4 and 4.3.9, and lifetimes in section 3.2.5, include uncertainty on both x and y axes, and it is necessary to account for this. Cantrell, (2008) provides a useful spreadsheet that uses the Williamson-York Iterative Bivariate Fit Shell to plot a regression that takes both x and y uncertainty into account. This is very effective for linear regression but cannot be applied to polynomial regression. A viable method/software of bivariate polynomial regression was not available during my thesis. Instead this research uses a bootstrapping method (more details in Section 2.5, and a worked example in Appendix section D.ii), described by Barreto & Howland, (2010), in an attempt to account for uncertainty in both x and y axis.

Given that both methods and the original data agree within uncertainties (see Appendix section D.i for worked example that demonstrates this), the question remains why add the extra step and use either method? Firstly, the uncertainty range for the original data is only a rough estimate, using instrument precision. But real variation is more complex than that, with a distribution of values which might be a mix of higher or lower values. The original data is able to create a mean; however, if for example dozens of measurements were taken under the same conditions, their means would vary. Actually doing those extra measurements might not be possible, but bootstrapping the data is able to treat the single sample (the original dataset) as only one of many random samples that could theoretically have been collected, and the resampling (with replacement in this case) allows analysis of sample distribution and uses this as the foundation for confidence intervals. Bootstrapping does not make assumptions about the distribution of the data; it simply resampled the data and gives you the sampling distribution.

When compared in detail (section Appendix D for this worked example), both methods had some small differences but agreed within the uncertainties. The Cantrell, (2008) method seems to give less uncertainty and is able to perform a true bivariate fit. The Barreto & Howland (2010) method has greater uncertainty but is able to give an approximation of a bivariate fit (which is otherwise extremely difficult to achieve for a polynomial regression). The Cantrell method is more precise and should ideally be used where greater precision is required and a linear regression is possible, but the Barreto & Howland (2010) method does provide a suitable alternative where this is not possible, notably for other types of regression (such as polynomial regression).

## **2.5 Bootstrapping and statistical analysis**

To investigate the uncertainty in the data I used the bootstrapping method described in Barreto & Howland, (2010) to bootstrap the data. Bootstrapping the data was necessary to explore and account for uncertainty in the data; it was vital to understand what effect outliers might have on the outcome of the analysis, and to quantitatively demonstrate the degree of variation both within the dataset, and within the predictions drawn from it.

When explaining the bootstrapping method, it is helpful to think of each number from the dataset is painted on a marble, all of these marbles are placed in a bag and shaken. They

are then removed, one at a time, and the number on the marble is recorded. This is ‘resampling’, for ‘resampling with replacement’; the marble is returned to the bag and the bag shaken again. This means certain marbles (or data points in this case) may either not be drawn, be drawn once, or be drawn multiple times.

For ‘dummy’ data this does not matter, and it is impossible to say what degree of variation is statistically relevant. However, when using real data such variation needs to be accounted for and quantified. For example: the trendlines of datasets are used to predict FRFs in sections 3.2.4 and 4.3.9, and lifetimes in section 3.2.5, and thus variation in the trendline will result in variation in the results from those predictions. If only the original dataset is used, it would be impossible to know how strongly an abnormally high or low value has affected the trendline (and in turn, the predictions drawn from it).

In this technique resampling with replacement takes place 2000 times, and the predictions for each of the resulting 2000 trendlines is recoded. This provides not just what the result was, but how often it occurred. For example, result A may have occurred 456 times, while result B may have occurred 23 times. In order to exclude extreme outliers, the top and bottom 2.5 % of results are excluded. The remaining distribution of results gives a mean, minimum and maximum value, thus providing an uncertainty range that takes into account variation in the dataset.

A worked example of this entire method can be found in Appendix D.

## **2.6 Fractional Release Factors: Background, Context, and Calculation**

As discussed in section 1.4, FRFs are the fraction of a species that has been disassociated into its reactive (and thus ozone-depleting) form (Solomon *et al.*, 1992b) over a set number of years (here 3 and 5 years, in order to be as consistent as possible with previous studies such as Leedham-Elvidge *et al.* (2018)) after being injected into the stratosphere. FRFs, aside from being used to calculate other metrics such as lifetimes and ozone depletion potentials, are a useful metric in their own right. A compound with a high FRF will be contributing more to ozone depletion in the immediate future but will not be present for as long as a compound with a low FRF. This in turn will contribute less ozone depletion short term but will continue to be present in the stratosphere and thus deplete ozone for significantly

longer. This is a useful concept that has undergone substantial development and improvement over the years.

As FRFs are needed to calculate Ozone Depletion Potentials (ODPs), their use (and definition) developed alongside ODPs (Solomon *et al.*, 1992b, 1992a). It was necessary to calculate relative stratospheric chlorine release as the ratio between the fraction of chlorine released by the target molecule, compared to that of CFC-11, multiplied by the chlorine loading potential. The chlorine loading potential is a metric which indicates the fraction of surface emission input to the stratosphere and the timescale in which the compound is present in the atmosphere (Solomon *et al.*, 1992a). Solomon *et al.* (1992a) also suggested that in some latitudes and seasons, the ozone depletion potential could be affected by nonlocal processes or slow chemistry, resulting in time-dependent effects.

Newman *et al.*, (2007) developed a formulation of Equivalent Effective Stratospheric Chlorine (EESC) that included the effects of age-of-air dependent fractional release values and age of air spectrum. Due to this dependence on mean age of air, Newman *et al.* argued it could be more appropriately applied to various parts of the stratosphere. This was a significant development in the calculation of FRFs but relied on the assumption that mean age of air and fractional release values were time independent. FRFs are calculated by comparing the mixing ratio of the tracer when it entered the stratosphere ('entry mixing ratio') and the mixing ratio observed at a point in the stratosphere. The difference between these two mixing ratios is the quantity of the species that has disassociated since entering the stratosphere (Equation 2-2). So, when an ODS enters the stratosphere, it has a FRF of 0, after this the air parcels containing the compound are distributed into different transport pathways in the stratospheric circulation and will then pass through their photochemical loss regions where the ODS is dissociated. As the compound is disassociated the FRF increases, until the ODS is totally depleted and the FRF is 1.

$$f(r) = \frac{\int_0^{\infty} \chi_{trop}(t - t')G(r, t')dt' - \chi_{strat}(r, t)}{\int_0^{\infty} \chi_{trop}(t - t')G(r, t')dt'}$$

*Equation 2-2. The formulation used to derive FRFs in Newman et al., (2007) and Laube et al., (2013) , reproduced in (Ostermüller et al., 2017), where it is referred to as the 'current formulation of FRF'.*

In Equation 2-2,  $f(r)$  denotes a single fractional release factor,  $\chi_{\text{strat}}(r,t)$  is the observed mixing ratio in the stratosphere at location  $r$  and time  $t$ .  $\chi_{\text{trop}}$  is the observed mixing ratio in the troposphere at location  $r$  and time  $t$ . A parcel of air in the stratosphere will have a mixture of fluid elements with varying transit times  $t'$ , depending on the pathways they travelled.  $G$  denotes the age spectrum. Thus Equation 2-3 compares the observed stratospheric mixing ratio at a specific point and time, and compares it to the mixing ratio of that compound when it entered the stratosphere from the tropopause (Equation 2-3).

$$FRF = (\text{Entry Mixing Ratio} - \text{Observed Mixing Ratio}) / \text{Entry Mixing Ratio}$$

*Equation 2-3. The summary of Equation 2-3, in simplified terms.*

To calculate FRFs for a compound, the entry mixing ratio of that compound is needed, and to find this the mean age of the air parcel is required. The mean age of the air parcel is an average of the time that air parcel has spent in the stratosphere. However, the relationship between stratospheric inorganic chlorine and mean age differs between models, depending on the representation of transport and chemistry used by the model (Vaughn *et al.*, 2007). There are numerous other assumptions and dependencies in how EESC and FRFs are calculated. EESC can only be seen as a valid proxy for anthropogenic ozone depletion, provided other parameters such as atmospheric transport remain unchanged, and FRFs were calculated assuming that chemically active gas propagates in the same manner as a chemically inert one (Engel *et al.*, 2018). The age spectrum, which is used in calculating the propagation of a chemically inert trace gas into the stratosphere, and to calculate mean age (necessary for the calculation of FRFs), does not take chemical loss into account (as the calculation assumes that the gas is inert and thus not subject to chemical loss). Due to the factors such as actinic flux of short wavelengths, circulation and stratospheric mixing, chemical loss does not happen uniformly throughout the stratosphere (Engel *et al.*, 2018).

Mean age of air is by its nature an average of the ages of the fluid elements within an air parcel. For example, a mean age of 3 years could include fluid elements that entered the stratosphere 2.5 years and fluid elements that enter the stratosphere 3.5 years ago. If the tropospheric mixing ratio of the compound has remained constant, then the entry mixing ratio will be the same regardless of how old the different fluid elements in the air

parcel are. However, if the tropospheric mixing ratios of the compound are changing, then this needs to be corrected for (Ostermüller *et al.*, 2017). Inconsistencies between FRF values derived at different times and from different observations have been observed (Laube *et al.*, 2013; L J Carpenter *et al.*, 2014). It was unclear whether this represented real changes to FRFs or was due to variability in tropospheric mixing ratios not being corrected for, as the older formulation for calculating FRFs (Newman *et al.*, 2007) treated the transport and mixing of chemically active species in similar fashion to chemically inert species.

Ostermüller *et al.*, (2017) discussed possible reasons for these discrepancies, which included: real changes to FRF, changing atmospheric conditions, or deficiencies in the way tropospheric trends are accounted for in calculating FRFs. Their paper goes on to argue that the latter is very likely, noting that when data from different time periods are compared, and when trends differ (in both magnitude and potentially direction), there is potentially a large impact on the way tropospheric trends are considered when calculating FRFs.

Ostermüller *et al.*, (2017) presents an improved method of calculating FRFs which takes into account chemical loss in the calculation of stratospheric mixing ratio, which they argue reduces and ‘almost’ compensates for time dependence in FRF calculation. The ‘almost’ is important here (and is the word used in the paper), as the paper admits that while their method is a substantial improvement, it does not completely compensate for time dependence in FRF calculations.

Ostermüller *et al.*, (2017) showed that tropospheric trends had a significant impact on the resulting FRFs, and presented a new method for calculating FRFs which largely corrects for the impact of tropospheric trends. This is the method used here to derive FRFs. Ostermüller *et al.*, (2017) defines a new loss weighted distribution function in which the arrival time distribution is normalised ( $G^*_N$ ) Equation 2-4.

$$\chi_{entry}(r, t) = \int_0^{\infty} \chi_{trop}(t - t') G^*_N(r, t') dt$$

*Equation 2-4. The time-independent equation for entry mixing ratios, from Ostermüller *et al.*, (2017) (equation 20).*

One drawback of this approach is that  $G^*$  is the combination of  $G$  with the chemical loss term ( $1-f(r, t')$ ) (see Equation 2-5). This means that calculating entry mixing ratios by this method requires that the chemical loss of a species already be well understood. So, calculating FRFs using entry mixing ratios derived using Equation 2-4, is somewhat circular.

However, the method laid out in Ostermüller et al., (2017) did demonstrate significant improvement in accounting for age spectrum when compared to the previous formulation, and without it the formulation for FRFs would not be time independent.

$$G^*(r, t') \equiv (1 - f(r, t')) G(r, t')$$

*Equation 2-5. Formula for the new loss weighted distribution function  $G^*$ . (Appears as equation 9 in (Ostermüller et al., 2017).)*

The common method used here to calculate mean age of air is based on Hall and Plumb, (1994) and assumes that air enters the stratosphere at the tropics and that this process is irreversible. This definition is used as we do not know precisely where emissions have come from, and this definition allows an approximation to compensate for this. However, in reality not all air enters the stratosphere at the tropics and the process is not always irreversible. In the extra-tropics and at the tropopause region there can be rapid exchanges of air, while conversely not all air at the tropical tropopause region will cross into the stratosphere. Air parcels at the tropopause are assumed to have a mean age of air that is zero. This means that our calculations will often produce negative values for mean age when evaluating tropospherically influenced samples. As this thesis is solely focused on the stratosphere this effect is only seen in samples at or close to the tropopause. As these negative mean age values are not actually representative of a sample's 'true' mean age, samples with negative mean ages beyond the uncertainty range expected of the age tracer ( $\sim\pm 0.5$  years), are excluded from calculations and discussions.

## Chapter 3 Long Lived CFCs.

### 3.1 Introduction

#### 3.1.1 Why the focus on long lived CFCs?

As discussed in section 1.4, in the case of CFCs it is more useful to look at the 'stratospheric steady-state lifetime'. When in 'steady-state' (i.e. source strength = sink strength), the atmospheric burden of a gas equals the product of its lifetime and emissions. Therefore, the longer the stratospheric lifetime of an ODS, the longer it will contribute towards ozone depletion, and the longer it will take for ozone levels to return to pre-1970s levels. While the most common CFCs (CFC-11, CFC-12, and CFC-113), have stratospheric lifetimes of 55, 103, and 94.5 years respectively, the 'long-lived' CFCs examined here (CFC-113, CFC-114, and CFC-115), are believed to have lifetimes of 640, 189, and 540 years respectively (CFC-114's isomer, CFC-114a has a shorter lifetime of 82-133 years) (Table 1-1).

When discussing the abundance of chlorine in the troposphere, the metric 'total tropospheric chlorine' can be useful. This metric is a way to quantify the contribution of the major chlorine-containing ODSs to the combined global average abundance of chlorine in the troposphere. Each ODS's contribution to total tropospheric chlorine is the product of the number of chlorine atoms it contains, and its mean mole fraction. So, compounds with a higher number of chlorine atoms would contribute higher total tropospheric chlorine than a compound with less chlorine atoms present in the same abundance.

The total tropospheric chlorine in 2016 was 3287 ppt., By 2020 it had decreased to 3220 (approximately 1.8% lower) and was ~12 % lower than its peak value in 1993. CFCs account for 60% of this. The remaining 40% is made up from both anthropogenic sources such as methyl chloroform ( $\text{CH}_3\text{CCl}_3$ ), carbon tetrachloride ( $\text{CCl}_4$ ), hydrochlorofluorocarbons (HCFCs), and halon-1211, and natural sources such as methyl chloride ( $\text{CH}_3\text{Cl}$ ). The most common CFCs (CFC-11, CFC-12, and CFC-113) had mole fractions listed in the comprehensive ODS assessment in 2020, of 224 ppt, 497.2 ppt, and 68.9 ppt respectively (Table 1-1) (Burkholder *et al.*, 2022).

While full destruction of CFCs in the atmosphere will still take many years, we are already seeing a significant decline for most of them. We are able to see such decline because, in addition to their much-decreased emissions, the lifetimes of these compounds

(CFC-11, CFC-12, and CFC-113) are comparatively short compared to the very long-lived CFCs (see Table 1-1). However, CFC-13, CFC-114, and CFC-115 have significantly longer lifetimes than the more common CFCs, so while their total abundance may be lower, they will continue to pose a threat to the ozone layer for significantly longer. It should also be noted that the uncertainty for these lifetimes is high, ranging from  $\pm 12\%$  to  $\pm 22\%$ , with one compound (CFC-13) missing lifetime uncertainty (lifetime uncertainties taken from (Ko *et al.*, 2013) with the exception of CFC-114a which took its lifetime uncertainty from (Laube *et al.*, 2016)). I am not aware of any lifetime uncertainties for CFC-13 at this time. CFC-113 and CFC-115 have the same relative lifetime uncertainties:  $\pm 17\%$ . For CFC-113 with a lifetime of 93 years, this represents  $\pm 15.81$  years, but for CFC-115's 540-year lifetime, the uncertainty represents a substantially larger  $\pm 91.8$  years. Improvements to our knowledge of these compounds' lifetimes (and their uncertainties), are vital to accurate estimates of ozone recovery and CFC-emissions.

Even the 'shorter' lived CFCs still persist for a considerable amount of time and are both ODSs and greenhouse gases. The extremely long atmospheric lifetimes and strong infrared absorptions of CFC-13, CFC-114 and CFC-115 result in large GWPs. For example, while CFC-11 (lifetime of 52 years) has a GWP of 5160 over 100 years, CFC-13 with a lifetime of 640 years has a GWP of 13,900 over 100 years. This is more than double the GWP of CFC-11, so while CFC-13 has a lower abundance its potential for global warming is substantial.

This demonstrates the importance of three things: compliance with the Protocol, swift identification of new emissions or ozone-depleting compounds, and closing of 'loopholes' in the Protocol that allow for unreasonably high emissions.

### **3.1.2 Long lived CFCs: Sinks, Sources, Abundance and Emission trends**

For these CFCs, the only sinks are in the stratosphere. The two main pathways for removal of these compounds from the stratosphere are believed to be reaction with excited atomic oxygen ( $O(^1D)$ ) and short-wavelength UV photolysis. Photolysis is a dominant loss process for most of the CFCs; however,  $O(^1D)$  reaction loss is significant for CFC-13 (80%) and CFC-115 (63%). The 2013 SPARC report (Ko *et al.*, 2013) placed the contribution of  $O(^1D)$  reactions for CFC-114 at 25%. However, this was based on studies which did not account for

the potential presence of CFC-114a, which would have biased the CFC-114 UV absorption spectra because CFC-114a's UV absorption is significantly stronger than that of CFC-114. The O(<sup>1</sup>D) kinetics for these two isomers is however similar (Vollmer *et al.*, 2018), though the reaction of CFC-114 with O(<sup>1</sup>D) is believed to be slower than CFC-114a.

CFC-13's main sources are low temperature refrigeration, some aluminium plants, and it is potentially present as impurity in CFC-12 due to over-fluorination during production. According to Vollmer *et al.*, (2018), the compounds first appeared in the atmosphere in the late 1950s through to the early 1960s. The compound's growth rates were highest in the 1970s and 1980s, before then declining in the late 1980s. CFC-13's emissions were at their maximum in the mid-1980s at  $\sim 2.6 \pm 0.25$  kt yr<sup>-1</sup>. By the 2007-2016 period emissions had decreased to  $\sim 0.48 \pm 0.15$  kt yr<sup>-1</sup>. This may have been the consequence of reduced emissions in response to the restrictions imposed by the Montréal Protocol in non-article 5 countries. In 2016 CFC-13's global tropospheric abundance was 3 ppt, and its growth rate was 0.03 ppt yr<sup>-1</sup> (Vollmer *et al.*, 2018). By 2020 atmospheric abundance had increased to 3.32 ppt, and its growth rate was 0.04 ppt yr<sup>-1</sup>, (Table 1-1). So, it is one of the few CFCs for which sources continue to outweigh sink processes.

CFC-114 and CFC-114a have frequently been referred to in combination due to the difficulty in separating the two. This is mainly because the two have virtually identical boiling points, so separation for analysis is difficult. They also have similar mass spectra, further complicating their analysis and detection using mass spectrometric techniques. Because of this, the two isomers are usually reported as their sum, with the assumption that CFC-114a makes up approximately 10% of the total (Carpenter *et al.*, 2014). However, Laube *et al.*, (2016) found that there was a steadily increasing contribution from CFC-114a, which started at 4.2% of the total in 1978, and had increased to 6.9% by 2014. This means that the  $\sim 10$  % value Carpenter *et al.* (2014) used previously constituted an overestimate, and the assumption that the ratio between the two isomers remained constant was incorrect. So, CFC-114 and CFC-114a have different trends, and this would suggest at least in part different origins since if their origins were identical, the ratio between them should remain largely constant (Laube *et al.*, 2016).

Vollmer *et al.*, (2018) reported a growth rate in 2016 of -0.1 ppt yr<sup>-1</sup> (CFC-114) and -0.02 ppt yr<sup>-1</sup> (CFC-114a), the global abundance 15 ppt (CFC-114) and 1 ppt (CFC-114a); however, this paper does not separate the isomers, so cannot give reliable trends or

abundances. CFC-114's growth rate remained  $-0.01 \text{ ppt yr}^{-1}$  in 2020 with an atmospheric abundance of 16.3 ppt. CFC-114a had a growth rate in 2020 of  $0.02 \text{ ppt yr}^{-1}$ , with an abundance of 1.11 ppt (Table 1-1). It should be noted that Table 1-1 uses data from UEA/FZJ flask measurements for CFC-114 and CFC-114a, rather than from AGAGE ([agage.eas.gatech.edu](http://agage.eas.gatech.edu)) in situ measurements, as UEA/FZJ were able to quantify the isomers separately (Laube *et al.*, 2022). Western *et al.*, (2023) saw the mole fractions of CFC-114a increase from 2013.

However, with estimated lifetimes of 189 years (CFC-114) and 82–133 years (CFC-114a), these compounds will take a long time to decrease in abundance to pre-1970s levels. Laube *et al.*, (2016)'s estimate of 82-133 years for CFC-114a were not based on observational data, but a rough estimate to facilitate estimation of emissions. Currently there are no good measurement-based lifetime estimates aside from the lab-based kinetics by Burkholder's group (Ko *et al.*, 2013).

Both CFC-114 and CFC-114a were used primarily as blowing agents and aerosol propellants. CFC-114 was also used heavily as a refrigerant and had uses in heat-pumps, while CFC-114a was used in polyolefin foams. If CFC-114a has a stratospheric lifetime shorter than that of CFC-114, then an increasing CFC-114/CFC-114a ratio in the atmosphere can only stem from different (higher CFC-114a) emissions.

Emissions are believed to have started in the 1930s with significant release quantities by the late 1940s; the growth rate was highest in the 1970s and 1980s with peak emissions in 1986/1987. While global emissions have declined from their two maxima of  $21 \pm 0.28 \text{ kt yr}^{-1}$  (mid-1970s) and  $22 \pm 0.19 \text{ kt yr}^{-1}$  (1988), to  $1.9 \pm 0.84 \text{ kt yr}^{-1}$  (2007-2016) they remain surprisingly stable and high (Vollmer *et al.*, 2018). However, as mentioned previously, most analytical equipment is unable to differentiate between CFC – 114 and its asymmetric isomer form CFC–114a, and as such most of the peer-reviewed literature has not addressed these molecules as separate.

CFC–115 was used as a refrigerant, as part of air-conditioning, as an aerosol propellant and to a lesser extent as a dielectric fluid (to prevent electric discharges) (Fisher and Midgley, 1993). First appearing in the atmosphere around the 1960s, (a decade later than CFC–13 and CFC–114), emissions increased to maximum of  $12.5 \pm 1.3 \text{ kt yr}^{-1}$  in the late 1980s. Emissions strongly declined to a minimum of  $0.59 \pm 0.51 \text{ kt yr}^{-1}$  (mean 2007-2010), but has steadily increased since 2010 to  $1.14 \pm 0.50 \text{ kt yr}^{-1}$  (mean 2015-2016), which gives

mean yearly emissions for 2007-2016 as  $0.80 \pm 0.50 \text{ kt yr}^{-1}$ . This increase has been led by Northern Hemisphere sites and has been clearly seen in recent in-situ measurements.

By 2016 CFC-115 had a growth rate of  $0.03 \text{ ppt yr}^{-1}$  and a global abundance of 8.5 ppt (Vollmer *et al.*, 2018). By 2020 the growth rate remained  $0.03 \text{ ppt yr}^{-1}$ , and abundance had risen to 8.7 ppt (Table 1-1). A transport analysis of CFC-115 pollution peaks observed at Gosan (Cheju Island, Republic of Korea) indicate that the potential emission sources are mainly located in mainland China. CFC-115 emissions may stem from HFC-125 production and use. (Vollmer *et al.*, (2018) hypothesises that the increase in CFC-115 emissions is potentially due to production of hydrofluorocarbons, as these are produced in large quantities; CFC-115 is a known by-product of HFC – 125 production. Excess CFC-115 was found in laboratories in the Advanced Global Atmospheric Gases Experiment (Prinn *et al.*, 2020) sites during air-conditioning leakages. The primary constituents of those air conditioners were 50-55% by mass HFC-125, the rest HFC-32; as CFC-115 is used in the production of HFC-125 it could be present as impurities in HFC-125, leading to the excess CFC-115 found during air-conditioner leaks (Vollmer *et al.*, 2018). Western *et al.*, (2023) reported an increase in mole fraction of CFC-115 from 2011.

### 3.1.3 Archived Air Introduction

The majority of this chapter will focus on samples taken relatively recently, with the earliest flight from 2009. Over the years the sophistication and versatility of sample collection has improved, and new methods have been developed for doing so in a cost-effective manner (such as the AirCore technique discussed in Chapter 4. However, emissions of ODSs (including the compounds of interest to this chapter), date back a lot further. In order to put the compounds discussed in this chapter into their historical context, and to further investigate potential changes to FRFs over time, archived air from 1 further recent (2015) and 5 historical flights (of both large balloons and research aircraft) was reanalysed (Table 3-1). These samples were reanalysed using more sophisticated techniques, notably it was previously not possible to differentiate the isomers CFC-114 and CFC-114a from each other, but this was possible on reanalysis.

Table 3-1. The Location (including latitude and longitude) of each flight, the date, and the Code used to identify them in this text.

Code	Location	Lat	Long	Date
TEX15	Texas, USA	38.79926	93.9576	28/10/2015
Gap 99	Gap, France	44.5596	6.0798	23/06/1999
AIRE93	Aire-sur-l'Adour, France	43.7001	0.2623	30/09/1993
PAL82	Palestine, Texas	31.7621	95.6308	15/05/1982
PAL81	Palestine, Texas	31.7621	95.6308	20/09/1981
PAL76	Palestine, Texas	31.7621	95.6308	27/01/1976

While samples and data from these flights have been analysed before, their focus was on compounds such as CO<sub>2</sub>, SF<sub>6</sub>, C<sub>2</sub>F<sub>6</sub>, and CF<sub>4</sub>, with the goal being investigating Age of Air and total chlorine. None of these papers focused on the compounds examined in this chapter. As there is a dearth of older data for these compounds, this presents an opportunity to investigate previously neglected compounds in their historical context. These flights are discussed in: (Schmidt *et al.*, 1991; Nakazawa *et al.*, 1995; Harnisch *et al.*, 1996; Andrews *et al.*, 2001; Engel *et al.*, 2002, 2006, 2009, 2017; Moore *et al.*, 2003)

### 3.2 Methodology

Having as accurate an estimate of lifetime as possible for a compound is essential. If for example a compound has a shorter lifetime than previously estimated, this means that emissions must be higher in order to account for it. In order to more accurately estimate lifetimes for these long-lived CFCs, FRFs at 3 and 5 years mean ages for a number of well-studied compounds, are plotted against their mean ages. We can use this correlation and compare it to the correlation between the long-lived CFCs' (CFC-13, CFC-114, CFC-114a and CFC-114a) FRFs and lifetimes, to establish how well (or not) they fit. Next, comparisons of model data to observational data are used in order to investigate the effect of varying chemistry and circulation conditions on the CFCs' lifetimes, and to support and explain the new lifetime estimates generated using the FRF-mean age correlation method.

### 3.2.1 Flight dates and other details.

Data have been collected from multiple flights of the M55 Geophysica high altitude research aircraft (Section 2.1.1) during three different campaigns (see Table 3-2). The flights in Oberpfaffenhofen, Bavaria, Germany in 2009 and Kiruna, Sweden in 2010, were part of the RECONCILE campaign (von Hobe *et al.*, 2013). The 2011 flight in Kiruna, Sweden, was part of the ESSenCe campaign, which itself was a part of the ESA project PremierEx (ESSenCe - Earth Online, accessed 13/07/2023; Kaufmann *et al.*, 2013). The Kalamata, Greece campaign in 2016 and the Kathmandu, Nepal 2017 campaigns (Johansson *et al.*, 2020; Adcock *et al.*, 2021; Lee *et al.*, 2021) were part of the StratoClim EU project ([www.stratoclim.org](http://www.stratoclim.org)).

This chapter largely uses results from measurements on samples from Geophysica flights but does include data from archived air samples (see section 3.1.3). Most of the archived air samples were collected cryogenically via high-altitude research balloons. CFC-115 is explored further using additional AirCore flights in Chapter 4, which also investigates the complexities of FRFs in more detail.

Air samples were collected in the manner described in Adcock *et al.*, (2020)'s supplementary material. In short, the samples were collected in 3 litre Silco-treated, stainless steel canisters (Restek) (some of which were Silco-treated). These canisters were repeatedly evacuated and repressurized prior to sampling.

Table 3-2 The campaigns, their dates, which columns they were analysed with, which standard was used (see section 2.3 for detailed explanation of the columns and standards used) and the abbreviations used for them.

Abbreviation	Campaign	Campaign location, Lat/long (average)	Campaign Dates	Altitude ranges	Columns used	Standard used
OB09	RECONCILE, 2009	Oberpfaffenhofen, Bavaria, Germany. 47.8N 9.8E	01/11/2009	10-20 km	GasPro only	AAL-071170
KIR10	RECONCILE, 2010	Kiruna2010, Lapland, Sweden. 70.3N 19.8E	30/01/2010	9-19 km	Al-Plot & GasPro	AAL-071170
KIR11	ESSenCe, 2011	Kiruna2011, Lapland, Sweden. 67.9N 15.4E	01/12/2011	9-19 km	Al-Plot & GasPro	AAL-071170
KAL16	StratoClim, 2016	Kalamata, Peloponnese peninsula, Greece. 36.0N 26.7E	03/09/2016	10-21 km	Al-Plot & GasPro	AAL-071170
KAT17	StratoClim, 2017	Kathmandu, Nepal. 26.6N 84.3E	27/07/2017-06/08/2017	9-21 km	Al-Plot & GasPro	SX-3591

### 3.2.2 Details specific to the processing of these samples.

There were numerous challenges in using these datasets. For example, different columns (see section 2.3) were used to analyse the samples. The two columns used were the ‘Gaspro’ column, and the ‘AL-Plot’. In order to use this data, it was necessary to compare the results and evaluate whether or not they were comparable, before merging them.

After comparing residuals, and percentage differences between column data, I found there was generally good agreement between measurements on different columns for KIR10 and KAL16. This fits with previous research showing good agreement between different columns in general (Sturges *et al.*, 2012) and these two columns specifically (Newland *et al.*, 2013; Adcock *et al.*, 2018). For KAT17 this was the case for all compounds except CFC-13 where the precision was poor for the ‘Gaspro’ column, possibly due to CFC-13’s proximity to CO<sub>2</sub> (see section 2.3 for discussion on this effect). For this reason, I used only ‘AL-Plot’ data for CFC-13 for KAT17. For KIR11 the ‘AL-PLOT’ column data had a high bias which we believe to be due to CO<sub>2</sub> accumulation from the AL-PLOT column as at the time these samples were analysed, the CO<sub>2</sub> was not filtered out, and if there was not a

sufficient waiting period for the CO<sub>2</sub> to clear, the accumulation of CO<sub>2</sub> could significantly lower the precisions of compounds (such as C<sub>3</sub>F<sub>8</sub> and CFC-115) with retention times close to that of CO<sub>2</sub>. Knowing this, I have excluded the KIR11\_AL data.

### 3.2.3 A sensitivity study of the Model

Metrics such as FRFs, ODPs, and lifetimes, are vital in understanding the atmospheric processes involved in ozone depletion and recovery, as well as monitoring and enforcing the Montréal Protocol. Different techniques have their own advantages and disadvantages, so using a variety of techniques allows for a more thorough investigation. The use of models allows for investigations on a much larger scale than is feasible for in-situ measurements and can explore hypothetical scenarios such as changes to circulation or chemistry, that could not be practically or ethically studied under real world conditions.

As discussed in section 2.2, models require ground truthing from in-situ measurements. For this reason, this chapter will investigate how well models can predict FRFs and lifetimes, compared to in-situ measurements, and explore what challenges are faced when using this method.

To do this we collaborated with Dr Eric Fleming and Dr Qing Liang of the Goddard Space Flight Centre (GSFC) to use the 2-D coupled chemistry-radiation-dynamics model developed there (henceforth referred to as the GSFC model). The model's domain extends from the ground to ~92 km, so covers the area being considered (the stratosphere, ~8-15km to ~55 km), as well as the areas either side of it. The grid resolution used for chemistry calculations is 4° latitude by 1 km altitude, while the grid used for the radiation and dynamics calculations was ~4.9 latitude by 2 km altitude. This 'coarser' grid is used because finer resolution was found to not improve model dynamical simulations while still adding to computational burden (Fleming *et al.*, 2011). The model has undergone extensive developments, improvements and evaluation (Considine *et al.*, 1994; Bacmeister *et al.*, 1995; Jackman *et al.*, 1996, 2016; Rosenfield *et al.*, 1997, 2002; Fleming *et al.*, 2007, 2011, 2015).

This model was chosen as it is able to examine the compounds of interest in the specific area of the atmosphere required, and was able to produce multiple simulations to explore the potential effect of variation to stratospheric chemistry and circulation. Given

the time and expense needed to run a detailed 3D model, using a 2D model was more viable given their much smaller computational requirements.

As it is necessary to be consistent when comparing modelled and in-situ observed stratospheric tracer compounds distributions and lifetimes, we provided our measured tropospheric trends for both the long-lived CFCs under examination (CFC-13, CFC-114, CFC-114a, and CFC-115) and the three most common CFCs (CFC-11, CFC-12, and CFC-113). This data was then inputted to the 2D model in order to generate predicted mixing ratios and lifetime estimates for these compounds.

For a 3D perspective, Dr Felix Ploeger of Forschungszentrum Jülich (FZJ) provided data from the Chemical Lagrangian Model of the Stratosphere (CLaMS). This is a modular chemistry transport model (CTM) system developed at Forschungszentrum Jülich (FZJ), Germany (Grooß et al., 2002; McKenna, Grooß, et al., 2002; McKenna, Konopka, et al., 2002, 2002a; Konopka et al., 2004). CLaMS simulates dynamics and chemistry of multiple air parcels along their trajectories, and the mixing (interaction between air parcels) is introduced by combining air parcels and the addition of new air parcels. The chemistry scheme incorporates over a hundred chemical reactions, and 30+ chemical species, including CFC-11 and CFC-12 (Grooß *et al.*, 2002). While CLaMS does not have the chemical schemes for the long lived CFCs (CFC-13, CFC-114, and CFC-115) implemented at this time, it was possible to compare CLaMS' model data for CFC-11 to GSFC predictions to assess how well the two models fit the observational data.

Data from the GSFC 2D model was available for each year from 1977 to 2017 (broken down by month and latitude). As one of the key goals in this section is to test the sensitivity of the model, it was necessary to restrict analysis to data that corresponded to the campaigns listed in section 3.2.1. However, not all campaigns were particularly suited to this analysis; notably KAL16 and KAT17. There are a number of reasons for this. Firstly, both campaigns had significantly younger mean ages of air (with a max mean age of around 3 years for KAL16, and 2.5 years for KAT17). The model features (including chemistry and circulation effects) under examination here predominantly occur at or after 3 years mean age. Therefore, there would be little benefit in including these campaigns. The second reason is that KAT17 was timed to coincide with and catch the (highly polluted) air from the Asian monsoon (Adcock *et al.*, 2021). The KAL16 campaign caught the Asian monsoon's outflow, so data from this campaign would be affected by the highly polluted air (Hottmann

*et al.*, 2020). For these representativity limitations, these two campaigns are excluded from the model analysis in section 3.3.4

The chemical loss uncertainty in the GSFC chemistry scenarios is calculated based on a range of laboratory measurements of the relevant reaction or process (in the case of the compounds studied here, this refers to photolysis and O(<sup>1</sup>D) reactions). This data was taken from the 2013 SPARC Lifetime report (Ko *et al.*, 2013). However, the model does not provide separate uncertainty ranges, so figures illustrating model data will not have traditional error bars attached to that data. The GSFC produced not only a baseline simulation, but simulations of changes to the chemistry or circulation, and plotted alongside the baseline scenario these provide some visualization of the potential uncertainty range that might result from such changes.

### **3.2.4 FRFs and how they were derived for this Chapter**

As discussed in section 2.6 deriving FRFs is a vital step in calculating important policy relevant metrics, notably stratospheric lifetime, and ODP. This chapter makes use of the Cape Grim tropospheric time series, which uses air taken at ground level at the Cape Grim (CG) observation station in Tasmania. This observation station was established in 1976 and has been collecting air samples since (all compounds studied in this chapter have a time series beginning in 1978, or 1977 if shifted backwards in time by half a year to create a ‘pseudo-global’ time series). As the area is so remote, the air should be as ‘clean’ (free from industrial pollution, traffic pollution etc...) as possible. Samples have been taken regularly for decades, creating an archive of air samples, which are used in this chapter for the tropospheric ‘baseline’ and for the calculation of entry mixing ratios. The Cape Grim tropospheric trend series was used to generate an updated version of the data used in (Laube *et al.*, 2016). This provided time series for all four compounds. The archived Cape Grim air is believed to contain a trace gas record representative of unpolluted southern hemisphere air, and thus is a useful means of determining a trend, largely free of big pollution events which might obscure it.

The CG trend for CFC-13 and CFC-115 are unpublished but the UEA Cape Grim time series has been proven to be of high quality for multiple species (Laube *et al.*, 2013, 2016; Leedham-Elvidge *et al.*, 2018). For further quality assurance purposes, I compare the CG

trend to that published in Vollmer et al., (2018) taken from the same location. The two datasets do not initially match; this is a calibration issue as the datasets used different scales (AGAGE for Vollmer, UEA for Laube). By comparing the fit of each dataset, it was possible to generate a conversion factor for each compound. For CFC-13 (conversion factor 0.8) and CFC-115 (conversion factor 0.953), the two datasets line up closely (within the uncertainties) (Figure C.1 a and b). Vollmer et al. did not distinguish between CFC-114 and CFC-114a, and so the data is summed together to give 'ΣCFC-114' (the 'Σ' here used to represent that the isomers have been summed together). Having summed CFC-114 and CFC-114a from the Laube et al. data, the two are compared. Looking at Figure C.1c it is clear that while using a conversion factor (of 1.0234) does bring the datasets closer together, they still do not line up. This further confirms (Laube et al., . (2016)'s conclusion that CFC-114 and CFC-114a have varying ratios over time and should be examined separately (Figure C.1).

In order to see how the campaign samples compare to the tropospheric trend, the data from campaigns sampling (mostly stratospheric, but includes some tropospheric) air was added to the previously plotted tropospheric trend (Figure 3.1).

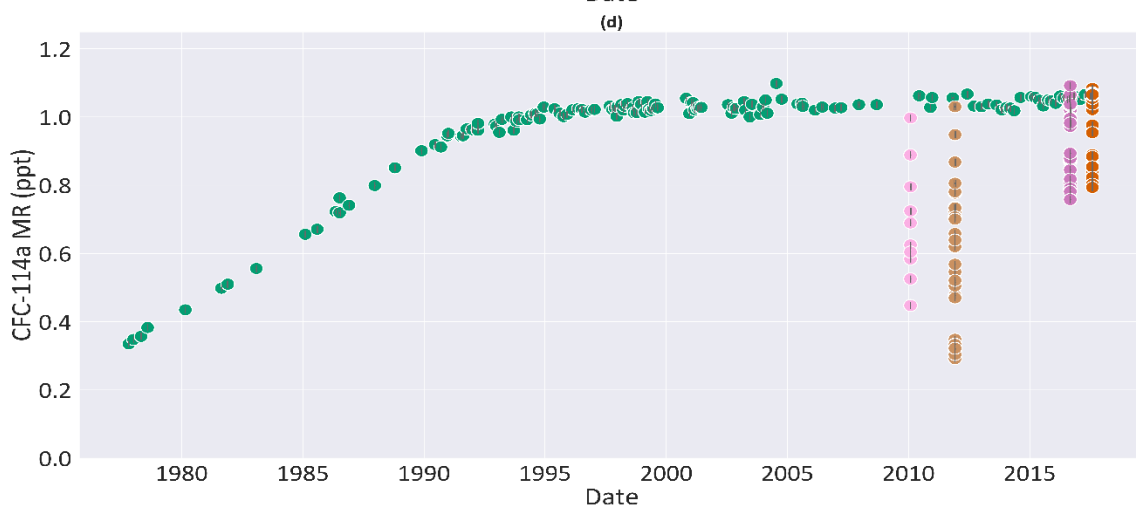
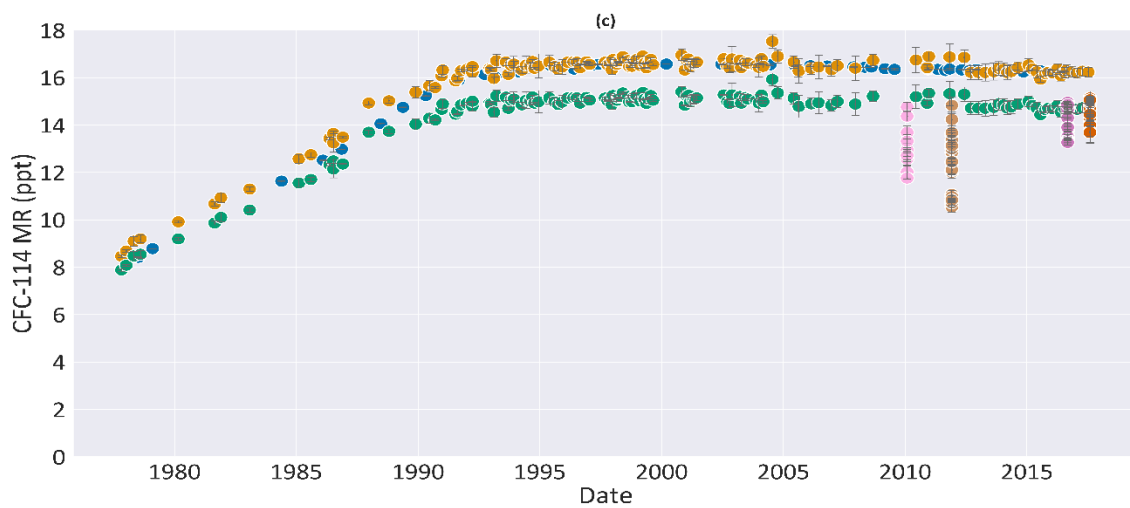
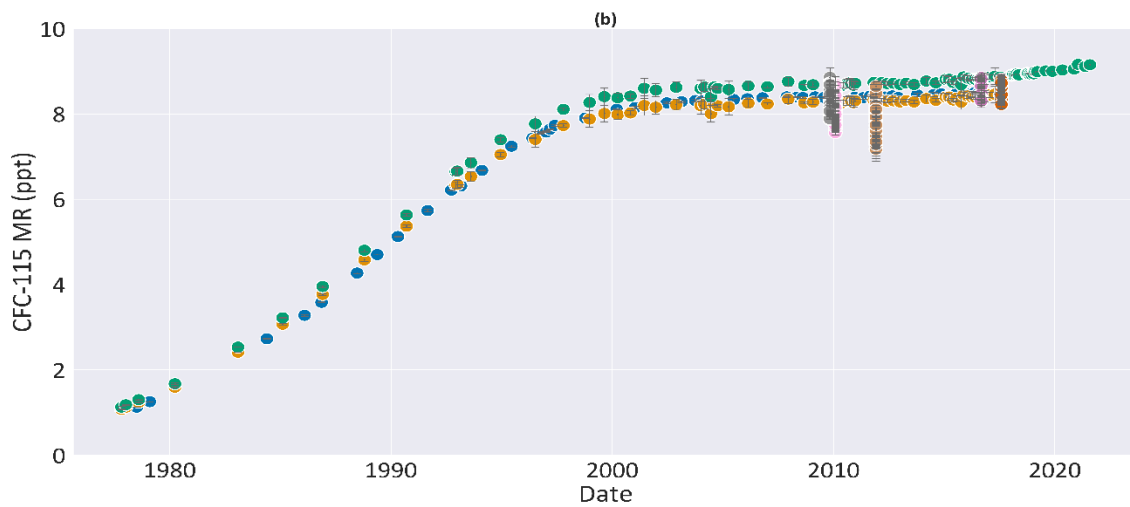
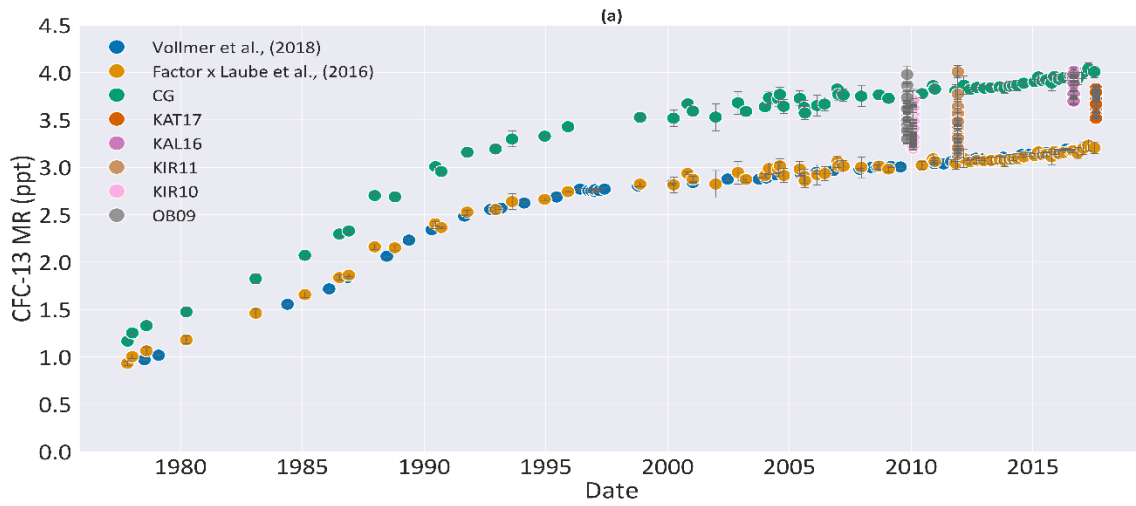


Figure 3.1. Mixing ratio (ppt) of (a) CFC-13, (b) CFC-115, (c) CFC-114, and (d) CFC-114a, from five campaigns using the M55 Geophysica, plotted against date. 'CG' refers to measurements taken at the Cape Grim research station, which is updated from Laube et al., (2016). This is compared to Vollmer et al., (2018). The 'Factor x Laube et al., (2016)' trend is the CG trend multiplied by a conversion factor in order to test that it is consistent with the Vollmer et al., (2018) trend. This is absent for CFC-114a as Vollmer et al., (2018) used the sum of both CFC-114 and CFC-114a, so cannot easily be compared to the much less abundant CFC-114a. There is no data from OB09 for (c) CFC-114 and (d) CFC-114a as the samples from this campaign were not analysed using the AIPlot column due to time constraints, and thus could not differentiate between the isomers.

Measurements from OB09 are missing from Figure 3.1c and d. This is because the samples were all run on the 'gaspro' column, which is unable to distinguish between CFC-114 and CFC-114a (see section 2.3). As Cape Grim is in the Southern Hemisphere, a six-month time-shift was applied in order to approximate the global tropospheric trend. It should be noted that all campaigns were in the Northern Hemisphere and may have been exposed to more pollution events. A figure with an inverted axis would be difficult to parse, but it should be noted that for each campaign, the mixing ratio of the compound decreases with increasing altitude (though due to circulation and mixing of air parcels, the mean age of the air may not line up neatly with altitude). So the lower the mixing ratio in the sample, the higher up in the stratosphere it was collected (and the greater mean age it will have).

Figure 3.1 shows how each campaign's samples provide a 'snapshot' of stratospheric composition at the time of flight. Each campaign has samples gathered at or below the tropopause and extending into the stratosphere (though as discussed in section 2.1.1, research aircraft cannot sample the full range of the stratosphere). In Figure 3.1a-d, at least one campaign shows data points above the tropospheric trend, for example in Figure 3.1a, the Cape Grim tropospheric trend for CFC-13, if we look at the data points for OB09, we can see they cross the Cape Grim trend. This could mean that the samples were taken at or below the tropopause, or that a pollution event occurred, and the measured concentrations of CFC-13 were higher than average.

FRFs are a measure of what fraction of a compound has disassociated since injection into the stratosphere. Figure 3.1 is a visual representation of this process: the Cape Grim tropospheric trend is around what we would expect the mixing ratio of a compound to be as it enters the stratosphere, and the campaign samples have progressively smaller mixing ratios the further from the tropopause they get (and this also reflects increased mean age). The mixing ratio of the compound decreases with increasing mean age as it dissociates. For example, in Figure 3.1d the mixing ratio for CFC-114a from the KIR11 campaign, decreases

from around 1 ppt at the troposphere (the highest point in Figure 3.1d), to around 0.3 ppt at the highest point where a sample was taken (which was around 21 km altitude).

Dr Laube calculated the entry mixing ratios for CFC-13, CFC-114, CFC-114a, and CFC-115, for the five campaigns (OB09, KIR10, KIR11, KAL16, and KAT17), using the method described in Ostermüller et al. (2017), which takes into account transit times and chemical loss in the calculation of stratospheric mixing ratios and reduces the time dependence in FRFs. Stratospheric mixing ratios cannot be accurately calculated for these compounds of interest solely by propagating the tropospheric trend into the stratosphere, as there are non-linearities in the tropospheric trend for these compounds (as they are not inert in the stratosphere, and simple propagation into the stratosphere assumes they are), and thus the width of the age spectrum can impact the propagation of these trends (Engel *et al.*, 2002).

Using these entry mixing ratios and the ratios observed in the Geophysica campaign samples, I calculated FRFs for each individual sample using Equation 2-3 (as described in detail in section 2.6). In order to calculate FRFs at 3 and 5 years mean age, I combined the FRFs and mean ages from each campaign (sample 1n), and quintupled it by including FRFs and mean ages calculated to 2 sigma (sample 5n), in similar fashion to (Laube *et al.*, 2020). This was because each campaign had a limited number of samples; some campaigns did not measure certain compounds, and since the greatest mean ages for KAL16 and KAT17 were 3.02 and 2.53 respectively, extrapolation from either campaign alone to 3 or 5 years produces unreliable results. Using the combined 5n dataset for each compound, FRF was plotted against mean age and a 2<sup>nd</sup> order polynomial trendline was plotted through the data (see Figure 3.2).

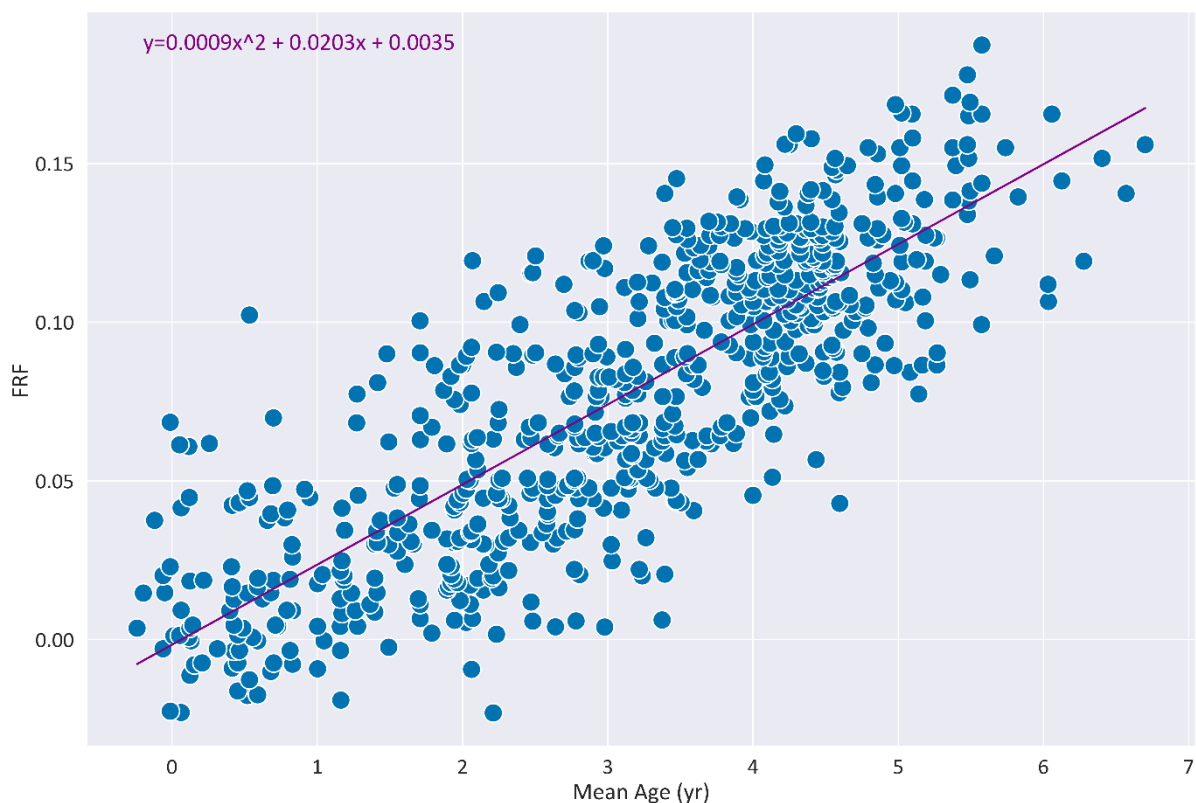


Figure 3.2. Fractional Release Factors (FRF) plotted against Mean Age (yr) for all flights (expanded to 5n), for CFC-13. A 2<sup>nd</sup> order polynomial trendline is plotted through the dataset, and the equation of the line is shown.

The trendline was used to calculate the FRF at 3 and 5 years for each compound. To test the robustness of the polynomial's prediction, I used the bootstrapping procedure designed in (Barreto & Howland, 2010) and described in more detail in section 2.5. From this was derived the highest and lowest prediction (to give an error range), and the mean (these results will be covered in section 3.3.1). This was done for all four compounds of interest. In addition, since SF<sub>6</sub> does not have estimates of FRF available, the same process was used for this compound. This was necessary as the method used in this thesis to calculate the stratospheric lifetime of compounds relies on the correlation between FRF and lifetime for well-studied compounds, without an estimate for FRF, SF<sub>6</sub> could not be used in this correlation.

### 3.2.5 FRF and lifetime correlation: lifetime estimation

There are a number of ways that stratospheric lifetimes can be calculated. Lifetimes have been estimated using model simulations and ground-based kinetics experiments;

however, both have their limitations. The chemical loss rate of a compound in the stratosphere is affected by atmospheric conditions that are difficult (or impossible) to properly replicate in the lab. Modeling can simulate a range of dynamical and chemical processes, but still require 'ground truthing'. Potential biases in the modelled transport of air through a loss region compared to real atmospheric conditions, are a source of uncertainty in estimates of trace gas lifetimes from model simulations (Ray *et al.*, 2017). Douglass *et al.*, (2008) demonstrated that model simulations that incorporated realistic mean age and FRF distributions, in turn predicted longer atmospheric lifetimes for CFCs.

Daniel *et al.* (1995) used stratospheric air samples and model calculations to derive FRFs relative to CFC-11 and used the assumption that most halocarbons show a linear correlation with CFC-11 throughout the stratosphere. The technique was later improved by deriving FRFs as a function of mean age of air collected via research aircraft (Schauffler, 2003; Newman *et al.*, 2006). While mixing does occur, air masses in similar stratospheric regions have experienced similar transport pathways, and thus there is a correlation between long-lived halocarbons which is characteristic for a given region. This correlation is not perfect; for example HCFC-22 ( $\text{CHF}_2\text{Cl}$ ) decomposes very slowly in comparison to CFC-11, and as the primary sink for HCFC-22 is reaction with OH it has a less variable vertical distribution of loss when compared to compounds with loss primarily from absorption of radiation (Laube *et al.*, 2010).

The stratospheric lifetime and FRF of a compound are related; the stratospheric lifetime refers to how long after injection into the stratosphere the compound will take to fully disassociate, while the FRF is the fraction of the compound that has disassociated since injection. A compound with a larger FRF at 3 years mean age will in turn have a shorter lifetime, while a compound with a smaller FRF at 3 years mean age will have a comparatively longer lifetime. As the halocarbons within an air mass experienced similar transport pathways, there will be a correlation between their concentrations (Plumb, 2007). Knowing this it is possible to estimate the lifetime of a compound from its FRF at 3 years mean age if one compares that to the FRFs at 3 years mean age of compounds with well documented lifetimes. This was done to good effect in Kloss *et al.*, (2014) for three compounds: CFC-216ba, CFC-216ca and HCFC-225ca. This thesis uses the correlation between FRF and stratospheric lifetime to derive new estimates for the stratospheric lifetimes of CFC-13, CFC-114, CFC-114a, and CFC-115.

Leedham-Elvidge et al., (2018) calculated mean ages and FRFs for 10 compounds, using the same air samples and the same instrument as my own measurements (reproduced in Table 3-3 for ease of comparison). To calculate mean ages Leedham-Elvidge used the method described in Engel et al., (2002). Leedham-Elvidge used the same data as Laube et al. (2013), but utilised improved mean age and FRF calculations.

Table 3-3. Mean ages, FRF at 3 and 5 years mean ages, for ten compounds from Leedham-Elvidge et al., (2018) for both high and mid latitudes, compared to Burkholder et al. (2022). Lifetime here refers to stratospheric lifetime.

Compound	Formula	FRF	Lifetimes	High latitude		Mid-latitude		WMO,2022
				3- year	5-year	3- year	5-year	Lifetimes
CFC-11	CFCl <sub>3</sub>	0.47	60 (54–67)	0.48	0.93	0.47	0.92	55
CFC-113	CF <sub>2</sub> ClCFCl <sub>2</sub>	0.3	83 (75–94)	0.32	0.70	0.30	0.64	94.5
CFC-12	CF <sub>2</sub> Cl <sub>2</sub>	0.26	(102)	0.28	0.61	0.26	0.55	103
HCFC-141b	CH <sub>3</sub> CFCl <sub>2</sub>	0.31	101 (64–221)	0.33	0.75	0.31	0.69	49.4
HCFC-142b	CH <sub>3</sub> CF <sub>2</sub> Cl	0.13	178 (103–459)	-	-	0.13	0.27	148
HCFC-22	CHF <sub>2</sub> Cl	0.13	129 (94–204)	0.14	0.29	0.13	0.26	120
Halon-1301	CF <sub>3</sub> Br	0.39	78 (72–85)	0.41	0.84	0.39	0.80	73.5
Halon-1211	CF <sub>2</sub> ClBr	0.66	37 (32–42)	0.64	1.03	0.66	1.05	41
Carbon Tetrachloride	CCl <sub>4</sub>	0.76	53 (46–63)	0.51	0.94	0.55	1.00	44
Methyl chloroform	CH <sub>3</sub> CCl <sub>3</sub>	0.69	37 (26–52)	0.56	0.95	0.59	0.96	38

This thesis is able to use updated FRFs and stratospheric lifetimes than were available for Kloss et al., (2014), primarily relying on values found in Leedham-Elvidge et al., (2018); however, these are not always the same as those listed in Burkholder et al. (2022). For example in the case of HCFC-141b, Leedham-Elvidge et al., (2018) estimated 101 (64–221) years stratospheric lifetime while Burkholder et al. (2022) 49.4 years stratospheric lifetime. The FRFs listed in Burkholder et al. (2022) are taken from Engel et al., (2018), and Leedham-Elvidge et al., (2018) uses the same time-independent method as Engel. Engel et al., (2018) lists FRFs at 5.5 years rather than the 5 years used with the Leedham-Elvidge et al., (2018) data. For lifetimes for the compounds in question, Burkholder et al. (2022) primarily uses lifetime estimate from the 2013 SPARC lifetime report (Ko *et al.*, 2013), which relied upon kinetics and modeling data. There are two exceptions: HCFC-142b which used the lifetime estimate from Papanastasiou et al., (2018) and CCl<sub>4</sub> which used the 2016 SPARC

report (Liang *et al.*, 2016). It is worth noting that the stratospheric lifetimes of many compounds are subject to substantial uncertainty.

For this reason the calculations were performed (separately) both using the FRFs and lifetimes from Leedham-Elvidge *et al.*, (2018), and those using those listed in Burkholder *et al.* (2022), and the resulting correlations (using FRFs at 3 years mean age) can be seen in Figure 3.3 and Figure 3.4.

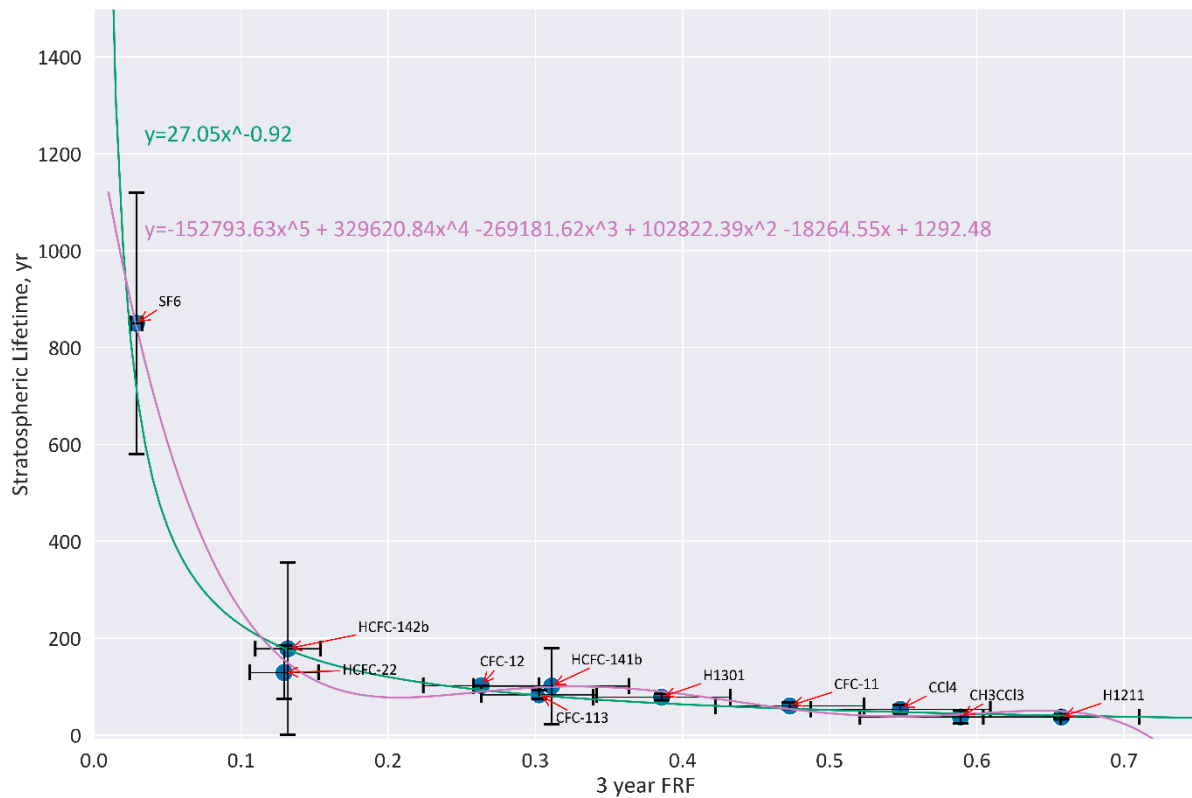


Figure 3.3. Plotting FRF at 3 years mean ages against Lifetime (yr) for mid latitude, FRFs and lifetimes from Leedham-Elvidge *et al.*, (2018), with the exception of SF6, where the lifetime from Ray *et al.*, (2017) is used. FRF uncertainties were derived from instrument precision and the uncertainty range generated by the bootstrapping procedure. For SF6 the FRF uncertainty was small enough that the x- error bar cannot be easily distinguished. Some compounds have small enough uncertainty ranges that they are hard to distinguish.

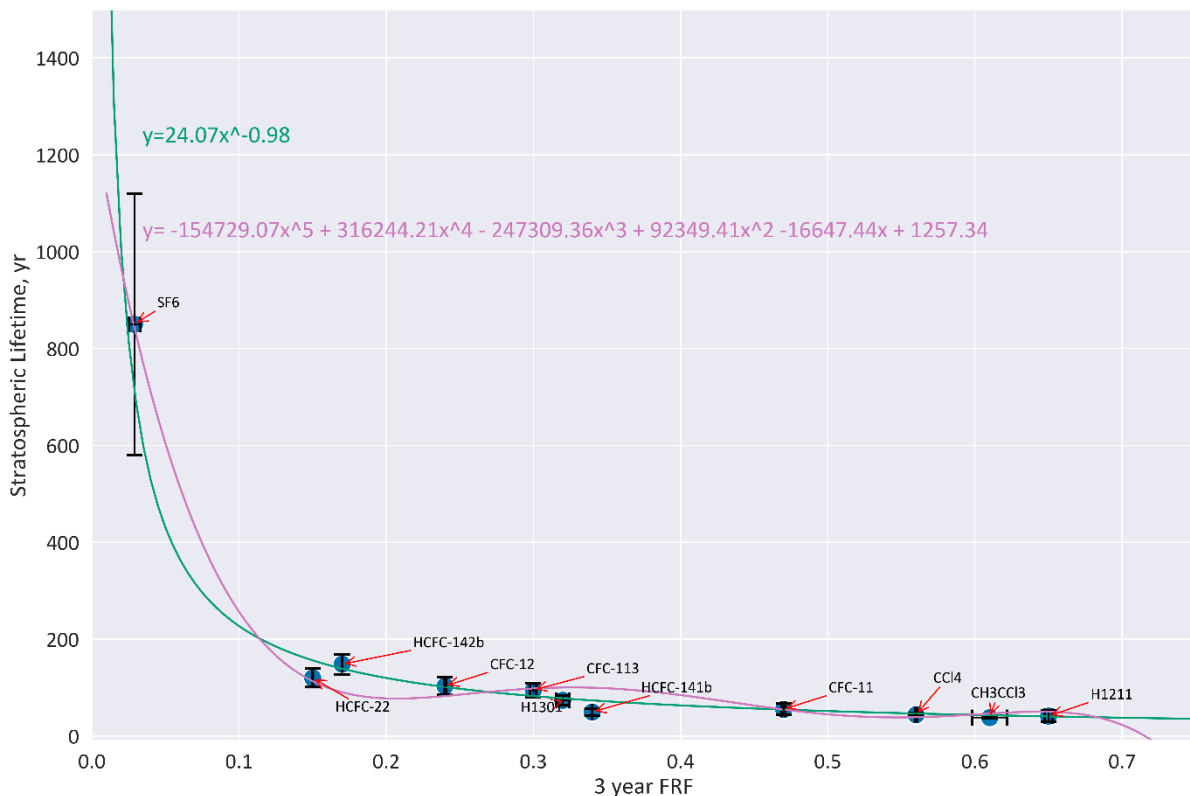


Figure 3.4. Plotting FRF at 3 years mean ages against Lifetime (yr) for mid latitude, FRFs and lifetimes from Burkholder *et al.* (2022) with the exception of SF<sub>6</sub>, where the lifetime from (Ray *et al.*, 2017). FRF uncertainties were listed in Engel *et al.*, (2018) and are often so small that they are not visible in the plot. For SF<sub>6</sub> the FRF uncertainty was small enough that the x-error bar cannot be easily distinguished. No uncertainty values were provided for CCl<sub>4</sub>'s lifetime estimate, so it is missing the y-error bar. Included in plot are the 'power' and 6th order polynomial trendlines with their respective equations.

Figure 3.3 and Figure 3.4 both show the correlation between FRF and lifetime of a compound. As several of the compounds examined in this chapter are believed to have lifetimes in excess of 200 years, for this correlation to be applicable to them, a long-lived compound with known FRF and lifetime was needed; SF<sub>6</sub> is used for that purpose. As discussed in section 3.2.4 FRFs for all 4 compounds, as well as SF<sub>6</sub>, were derived. When calculating FRFs for SF<sub>6</sub> two campaigns were excluded: Kiruna 2010 as it could have captured SF<sub>6</sub> depleted mesospheric air due to the polar vortex (when the vortex breaks down each spring, compounds with mesospheric loss such as SF<sub>6</sub> will be transported into the stratosphere (Ray *et al.*, 2017), and Kalamata 2017 as this campaign took place during the Asian Monsoon and as such contained elevated trace gas levels from the highly polluted air masses that are transported in the upper troposphere and lower stratosphere (UTLS) by the Asian Monsoon (Adcock *et al.*, 2021).

However, the lifetime of SF<sub>6</sub> is subject to some dispute. Engel & Rigby *et al.*, (2018) notes that the widely used value of 3200 years (Ravishankara *et al.*, 1993) may be a

substantial overestimate. Kovács, et al., (2017) estimated an average lifetime of 1,278 (1120-1475) years using model data, while (Ray *et al.*, 2017) estimated a lifetime of 850 (580-1400) years using observations of SF<sub>6</sub> in the Arctic polar vortex. Ravishankara et al., (1993) lists a lower limit for the lifetime of SF<sub>6</sub> as 580 years, so the range of 580-3200 years encompasses the estimates of both Ray et al., (2017) and Kovács et al., (2017). Kouznetsov et al., (2020) used a model study which gave a range for SF<sub>6</sub>'s lifetime between 600 and 2900 years, while Loeffel et al., (2022) proposed a value of 2100 years (1900-2600 years range). As there is growing evidence that the 3200 year figure is an over-estimate, this thesis will focus primarily Kovacs's 1278 year stratospheric lifetime estimate, and Ray's estimate of 850 years stratospheric lifetime for SF<sub>6</sub>. The estimate for Kouznetsov et al., (2020) gave too wide a spread of possible lifetime for SF<sub>6</sub>, for this method to be practical. Loeffel et al., (2022) was a modelling paper and does not focus on defining the lifetime of SF<sub>6</sub> and the lifetimes listed are time-dependent lifetimes and varied over the spread of the simulation. For the calculations in this thesis, equilibrium lifetimes are required, so lifetimes listed in Loeffel et al., (2022) are not used.

Calculations using both the Ray et al., (2017) and Kovács et al., (2017) lifetime estimates were performed, for FRFs at both 3 and 5 years mean age, and the resulting lifetime estimates for our compounds of interest are included in section 3.3.2.

With these lifetimes and FRFs I needed to plot a trendline and use the correlation to generate predicted lifetimes for my compound. To do this it was necessary to choose the appropriate trendline. As is clear in Figure 3.3 and Figure 3.4, while it is possible to get a better 'goodness of fit' by increasing the order of the polynomial fit function, this results in an increasing number of inflexion points and a 'bumpy' trendline. The fit function with the lowest degree of freedom that produces robust results is the power function as it has only 2 rather than the 6 degrees of freedom given by the 5<sup>th</sup> order polynomial. As the power trendline function gives a much smoother line while still retaining a robust goodness of fit, this fit was selected.

Using the power trendline from the correlation between FRF (at 3 and 5 years mean age) with lifetime shown in Figure 3.3 and Figure 3.4, the lifetimes for the compounds used for the correlation were estimated. The results are displayed in Figure 3.5, and with the exception of CCl<sub>4</sub> (which does not have a lifetime uncertainty range listed), all estimated lifetimes agreed within the uncertainties with the previous estimate, demonstrating the

robustness of fit for the trendline used in the calculation. This trendline equation was then used to estimate lifetimes for CFC-13, CFC-114, CFC-114a, and CFC-115, and the results are detailed in section 3.3.2.

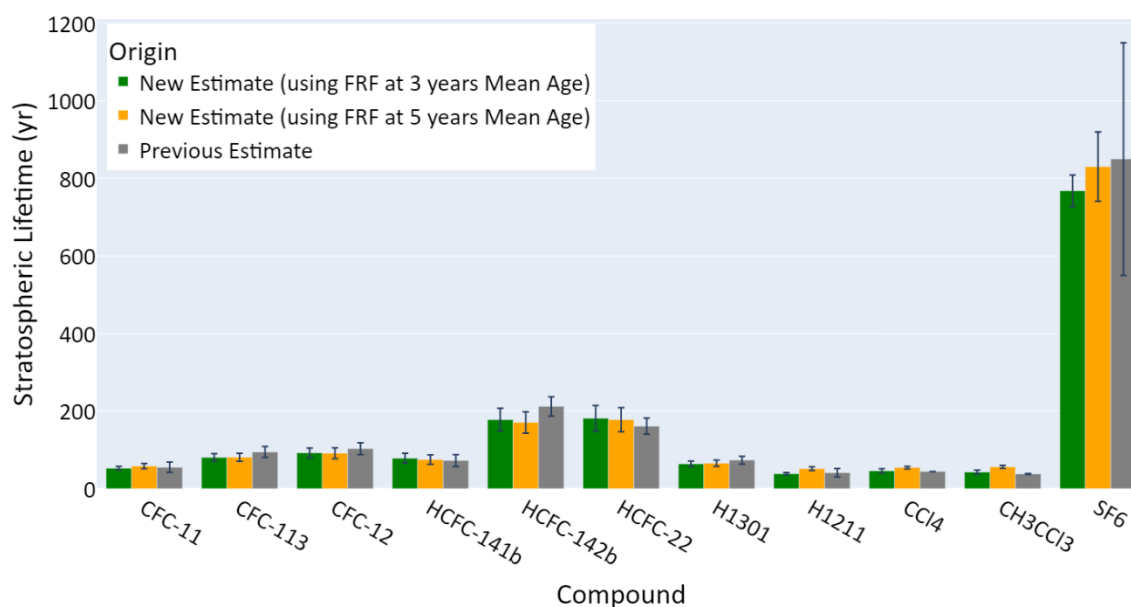


Figure 3.5. A comparison estimated stratospheric lifetimes (generated using the ‘power’ trendline), using either FRFs at 3 or 5 years mean age. Compared to the previous estimates listed in WMO 2022(Burkholder et al., 2022) . Error bar for CCl4’s ‘previous estimate’ is missing because there are no error estimates for that compound. Error is to 2 sigma.

### 3.2.6 Archived Air Methods

All flights except TEX15 (which used the WB57 high altitude aircraft) utilised high altitude balloons for sample collection. The balloon-borne observations were taken using large whole air samples collected using cryogenic samplers. Flights reached altitudes of up to ~35 km in the northern hemisphere mid-latitudes between 32° N and 51° N (Schmidt *et al.*, 1991; Engel *et al.*, 2009, 2017). The archived air samples were reanalysed in 2019 and 2021 at UEA and FZJ primarily by Dr Laube. This used the same methodology as described in sections 2.3 and 3.2.2.

The resulting entry mixing ratios, mean ages and FRFs were calculated using the same methods as described in sections 2.5, 2.6, and 3.2.4, and thus are comparable to the other results for this chapter. As will be discussed in more detail in section 4.3.9 the time-independent method (Ostermöller *et al.*, 2017; Engel *et al.*, 2018a) that is used here for

calculating entry-mixing ratios, mean ages and from them, FRFs, largely but not completely compensates for changes in the tropospheric background trend of a compound over time. However, there are limitations to the method; for example, the background trend prior to the sample’s collection date needs to stretch back at least 10 years, but ideally 15-20 years or more. The latest flights discussed in section 3.1.3 (TEX15 from Texas in 2015, GAP99 from Gap, France 1999, and AIRE93 from Aire-sur-l'Adour, France in 1993) are late enough that there are established background trends for all compounds examined here that stretch back at least 10 years. However, the older three flights (all from Palestine, Texas) were from 1982, 1981 and 1976, and while the background trends for some compounds may stretch this far back, they do not extend sufficiently far back in time for the Ostermüller et al., (2017) method to produce reliable entry mixing ratios. For this reason, while all 6 flights will be represented in background trend plots in section 3.3.5, only the later 3 flights have FRFs calculated for them. Unless otherwise specified, the mean ages used in this section were derived using PFC-116 as an age tracer in order to avoid the high bias associated with SF<sub>6</sub> (Leedham-Elvidge *et al.*, 2018; Garny *et al.*, 2024b).

### 3.3 Results

#### 3.3.1 FRF results

Having generated FRFs at 3 and 5 years mean age in the manner described in section 3.2.4 we can now examine them (Table 3-4).

*Table 3-4. Fractional Release factors for this chapter’s compounds of interest. Includes both FRFs 3 and 5 years mean ages, and their uncertainty range. Compared to previous Time independent FRF estimates from Engel et al., (2018) , as cited in Burkholder et al. (2022).*

Compound	FRF at 3 years Mean Age	FRF at 5 years Mean Age	Previous Estimates (FRF at 3 years mean Age)
CFC-13	0.071 (±0.003)	0.126 (± 0.003)	N/A
CFC-114	0.121 (±0.007)	0.227 (± 0.012)	0.13 (± 0.00014)
CFC-114a	0.313 (±0.015)	0.571 (± 0.026)	N/A
CFC-115	0.060 (± 0.002)	0.118 (±0.005)	0.07 (±0.00032)
SF <sub>6</sub>	0.029 (±0.002)	0.046 (±0.005)	N/A

Previous estimates for the FRF at 3 or 5 years mean age are not available for all compounds. However, they do exist for CFC-114, and CFC-115. CFC-114 estimated FRF at 3 years mean age in Table 3-4 is 0.121 (±0.007), and if the full uncertainty range is taken into

account and the value rounded up to 2 significant figures, it would overlap within the uncertainties with the value previously estimated in Engel et al., (2018) of  $0.13 (\pm 0.00014)$ . For CFC-115 the new estimated FRF at 3 years mean age was  $0.06 (\pm 0.002)$ , which does not overlap within the uncertainties with the previous estimate of  $0.07 (\pm 0.00032)$ . However FRFs display a significant variability; this will be explored in more detail in section 4.4.2, but the 0.07 value is well within the range seen across all campaigns (Figure 4.27).

If we compare the FRFs calculated for Leedham-Elvidge et al., (2018) (Table 3-3) to those calculated for the long-lived CFCs for each campaign (Table 3-4), we begin to see some useful patterns (Figure 3.6).

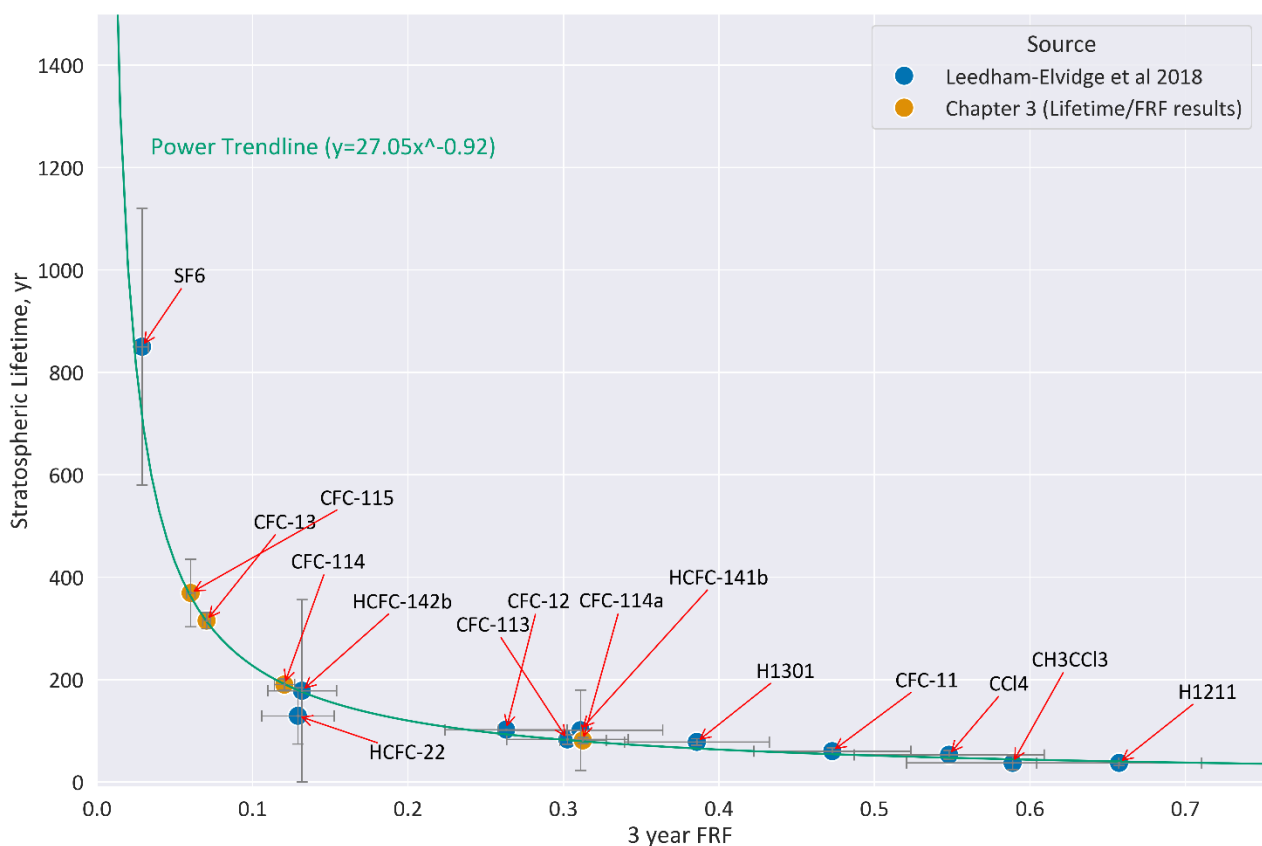


Figure 3.6. FRF at 3 years mean age, plotted against Stratospheric lifetime (yr). Includes the FRFs and lifetimes calculated by Leedham-Elvidge et al 2018, and those calculated in this chapter (sections 3.3.1 and 3.3.2)

Since CFC-114a is believed to have a similar lifetime to CFC-12, we can compare the FRF at 3 years mean ages of the two compounds (Figure 3.6). Leedham-Elvidge et al., (2018) gave a FRF at 3 years mean age for CFC-12 of 0.26 (0.23–0.30). Compare this to the FRF at 3 years mean ages calculated for CFC-114a in Table 3-4: 0.313 (0.298-0.328) which is higher than Leedham-Elvidge et al., but still within the uncertainty range.

The FRF at 3 years mean age for CFC-114a is on the higher end (even within uncertainties) of CFC-12's range, and a higher FRF than CFC-12 would give CFC-114a a shorter lifetime. This is feasible: CFC-12's lifetime is 102 years, while CFC-114a's lifetime has previously been estimated at 82-133 years (Table 1-1). We can see something similar with HCFC-22, which has an estimated FRF at 3 years mean age of 0.13, and lifetime of 129 (94-204) in Leedham-Elvidge et al., (2018) and 161 in (Carpenter *et al.*, 2018). CFC-114 has a similar FRF at 3 years mean age (0.121), and an estimated lifetime of 189, which falls within the uncertainty range for HCFC-22's lifetime estimate in Leedham-Elvidge et al., (2018).

### **3.3.2 Stratospheric Lifetime Results**

With solid fractional release factors established for these compounds, lifetimes were predicted using the method discussed in Section 3.2.5. Lifetime estimates were generated for FRFs at both 3 and 5 years mean ages, and for each of the potential lifetimes for SF<sub>6</sub> (see Section 3.2.5 for discussion on the different lifetimes and how they were estimated).

In Figure 3.7 we can see that the greater the lifetime of SF<sub>6</sub>, the higher the new estimated lifetime, which is to be expected as this is the only compound used in the correlation that has a stratospheric lifetime greater than 300 years. So a variation in the lifetime of the longest lived of the compounds results in larger changes in estimates derived from the correlation. The effect is most pronounced in the longer-lived CFCs (CFC-13, CFC-115 and to a lesser extent, CFC-114). CFC-114a, having a shorter lifetime, is affected much less, for some correlations CFC-114a's lifetime actually decreases with increasing SF<sub>6</sub> lifetime (though to a very small extent, and still within the uncertainties).

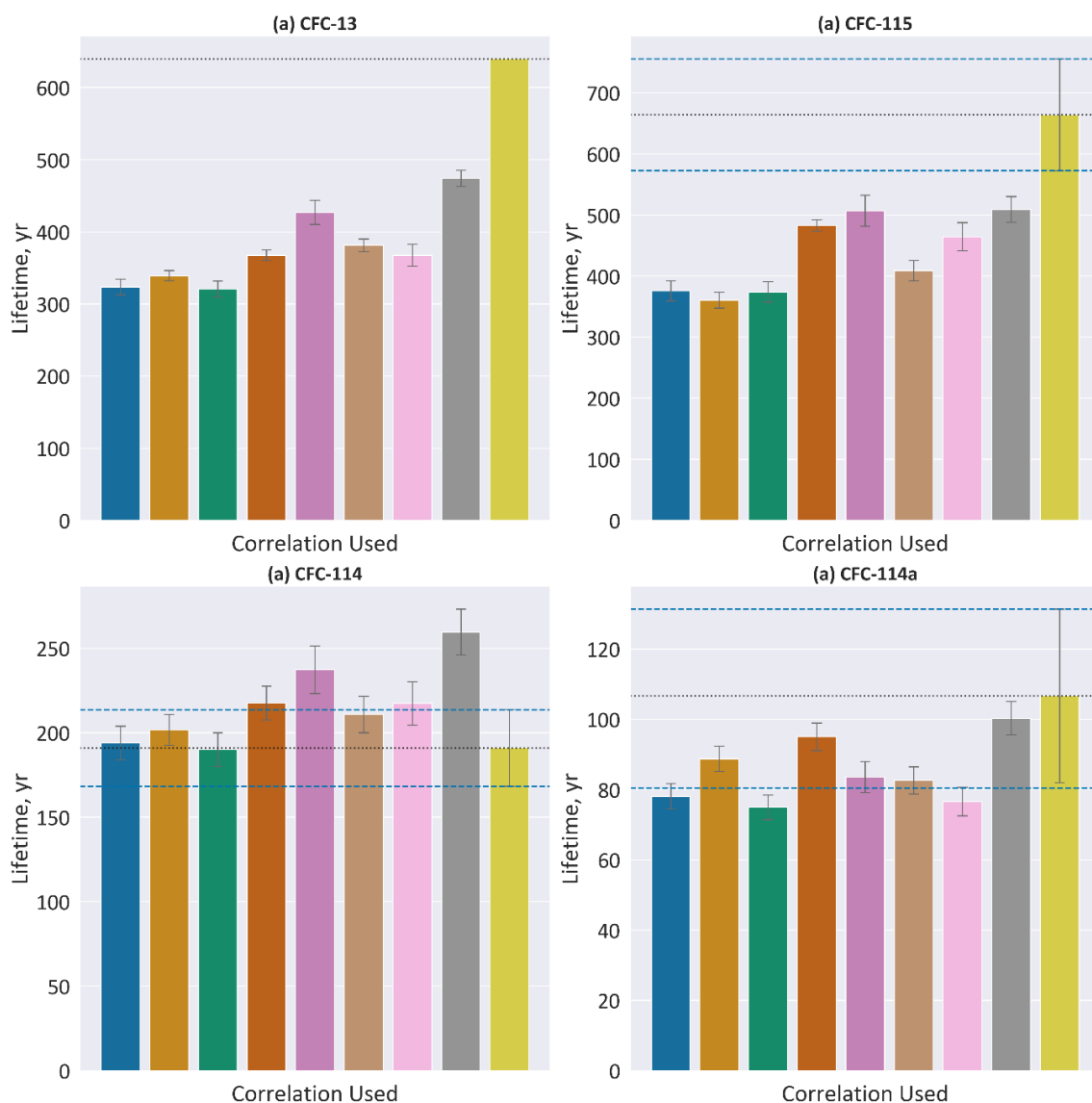
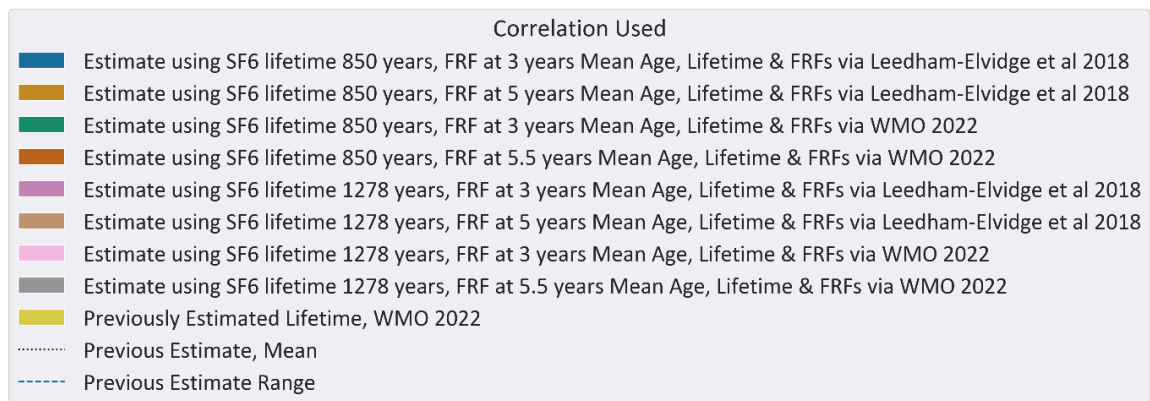


Figure 3.7. Newly estimated stratospheric lifetimes for each compound, using the correlation between FRF at 3 or 5 years mean ages and lifetimes of well-studied compounds, taken either from Leedham-Elvidge et al., (2018) or Burkholder et al. (2022). These are compared to previous estimates in Burkholder et al. (2022). As the lifetime of SF6 is disputed, two different correlations were used, one containing the lifetime estimates of 850 years from Ray et al., (2017), and one using the lifetime estimate of 1278 years from Kovács et al., (2017). Error bars are to 2 sigma uncertainty. Uncertainty range unavailable for CFC-13.

Table 3-5. The previous estimates (P) for stratospheric lifetime Burkholder et al. (2022) and the newly estimated lifetimes depending on which correlation was used. Correlations used FRF and lifetime data from either (L) Leedham-Elvidge et al., (2018) or (B) Burkholder et al. (2022). FRFs at either 3 or 5 years mean age (5.5 for Burkholder et al. (2022)). As the lifetime of SF<sub>6</sub> is disputed, two different correlations were used, one containing the lifetime estimates of 850 years from Ray et al., (2017), and one using the lifetime estimate of 1278 years from Kovács et al., (2017) Kovács et al., (2017).

CFC-13 Lifetime, yr	CFC-114 Lifetime, yr	CFC-114a Lifetime, yr	CFC-115 Lifetime, yr	FRF at mean age (yr):	Lifetime of SF <sub>6</sub> (yr)	Source
6401	191 (± 12%)	106.7 (82–133)	664 (± 17%)	-	-	P
324 (313-335)	194 (184-204)	78 (75-82)	376 (360-393)	3	850	L
303 (297-309)	181 (173-204)	80 (77-83)	397 (404-389)	5	850	
427 (411-444)	237 (224-252)	84 (79-88)	507 (483-534)	3	1278	
381 (373-390)	211 (200-222)	83 (79-87)	409 (393-426)	5	1278	
321 (310-332)	190 (181-201)	95 (72-79)	374 (358-391)	3	850	
368 (360-375)	218 (208-228)	95 (91-99)	483 (474-492)	5.5	850	B
368 (376-407)	217 (205-231)	77 (73-81)	464 (442-489)	3	1278	
474 (463-486)	260 (247-274)	100 (96-105)	509 (489-531)	5.5	1278	
315 (287-331)	190 (176-201)	81 (76-87)	369 (328-435)	Average L		
387 (310-486)	222 (181-274)	89 (72-105)	458 (358-531)	Average B		

1. Tropospheric lifetime. Stratospheric lifetime not listed. Lifetime uncertainty unknown.

Comparing each compound's original estimated lifetime to the new one, there are a few notable differences. CFC-114a has the shortest lifetime, and regardless of whether the FRF at 3 or 5 years mean age was used, or which SF<sub>6</sub> lifetime was used, the newly derived stratospheric lifetime estimates for CFC-114a are lower than but overlap within the uncertainties of the previous estimate. As CFC-114a has a lifetime which is comparable to the bulk of compounds used for the correlation, it will be less affected by changes to the lifetime of the longest-lived compound SF<sub>6</sub>.

All newly derived estimates for CFC-114's stratospheric lifetime overlapped within the uncertainties with the previously estimated stratospheric lifetime. CFC-114 is believed to have a similar lifetime to HCFC-142b (212 years) and HCFC-22 (161 years), and both compounds were included in the correlation. This should result in a comparatively accurate estimate, depending on how accurate the stratospheric lifetime estimates for HCFC-142b and HCFC-22 are.

The newly estimated stratospheric lifetimes for both CFC-13 and CFC-115 are substantially lower than the previous estimates, which is outside the uncertainty range for CFC-115. We do not have an uncertainty for CFC-13's previous lifetime estimate, so we cannot definitively state whether this is outside the uncertainty range. However, this strongly suggests that previous stratospheric lifetime estimates for these compounds are a significant overestimate. The longer-lived CFC-13 and CFC-115 both showed greater variation in their estimated lifetime at different mean ages and depending on which SF<sub>6</sub> lifetime was used, when compared the shorter-lived CFC-114 and CFC-114a.

### 3.3.3 Ozone Depletion Potentials.

Now that lifetimes and FRFs at 3 years mean age have been derived for all four compounds, these can be used to calculate their respective Ozone Depletion Potentials (ODPs) (Table 3-6), using Equation 1-12, as discussed in section 1.4.

*Table 3-6. Ozone Depletion Potentials (ODPs) predicted using FRFs at 3 and 5 years mean age, compared to those listed in WMO 2022 (Burkholder et al., 2022). (There is no ODP uncertainty range listed for CFC-13 or CFC-114a in WMO 2022).*

Compound	WMO 2022	Newly estimated; using FRFs at 3 years mean age	Newly estimated; using FRFs at 5 years mean age
CFC-13	0.3	0.38 (0.36-0.39)	0.34 (0.34-0.35)
CFC-114	0.53 (±0.02)	0.48 (0.45-0.5)	0.46 (0.43-0.48)
CFC-114a	0.72	0.53 (0.5-0.55)	0.49 (0.47-0.51)
CFC-115	0.45 (±0.01)	0.25 (0.25-0.27)	0.26 (0.24-0.27)

Both ODPs derived using FRFs at 3 years and those using FRFs at 5 years are in fairly good agreement within the uncertainties. Despite being isomers CFC-114 and CFC-114a have noticeably different ODPs. Even a comparatively small difference in FRF and lifetime produce different ODPs, and thus CFC-114a has a higher ODP than its isomer. None of the newly derived ODPs overlap (within the uncertainty range) with those listed in Burkholder et al. (2022), though CFC-114 is fairly close.

It is worth noting that these are the first in-situ observation-based ODPs to be derived for these compounds. The estimate for CFC-13 is higher than previous estimates, while those for CFC-114a and CFC-115 are lower. This evidence changes the policy relevant danger of these compounds with respect to the ozone layer, increasing it for CFC-13 and decreasing it for CFC-114a and CFC-115.

### 3.3.4 Model results.

#### 3.3.4.a Mean Age-Tracer correlation

In sections 3.3.1 and 3.3.2 the in-situ measurements were used to investigate fractional release factors and stratospheric lifetimes respectively. But as discussed in section 3.2.3, it is worth investigating how accurately these metrics can be modelled, and what challenges are faced when doing so. To that end, this section will compare two models, both to each other, and to the in-situ data. As the samples taken by the Geophysica high-altitude research aircraft had mean ages largely ranging from 0 to 5 years (KIR11 has 5 samples with mean ages older than 5 years mean age, the oldest of which was 5.2 years mean age), comparison of model data to Geophysica data was only possible up to around 5 years mean age.

The bulk of the model data examined in this section came from the National Aeronautics and Space Administration (NASA)/ Goddard Space Flight Center two-dimensional model (GSFC2D), which has full stratospheric chemistry, and due to computational efficiency, it is ideal for running numerous scenarios. For example Fleming et al. (2020) did this with scenarios for global emission scenarios for CFC-11.

The GSFC model provided data first on the baseline conditions, assuming no changes to the chemistry or circulation patterns currently recognised. This was the 'original' or 'baseline' scenario. There were then four circulation scenarios in which the transport parameterisation (consisting of diffusion and advection) was tuned: two in which the circulation was speeded up by 10% (P10) and 20% (P20), and two in which the circulation was slowed by 10% (M10) and 20% (M20). Additionally there were 6 more scenarios exploring changes in chemistry (reaction rates), which consisted of: three scenarios where the chemistry (photolysis and O(<sup>1</sup>D) reactions) were speeded up, both together and separately (fast chemistry scenarios: O1D\_fast, Photolysis\_fast, and O1D + Photolysis\_fast). The remaining three scenarios consisted of those same chemical processes but slowed down (slow chemistry scenarios: O1D\_slow, Photolysis\_slow, and O1D + Photolysis\_slow).

Each scenario included data on mixing ratios for the compounds of interest, altitude, pressure, mean age, and temperature. Using this data I also calculated potential temperature. Also included were lifetime estimates for the compounds, for global atmosphere, troposphere, stratosphere, and mesosphere. As this study is focused on

stratospheric lifetimes, these are what were explored here. The model generates the predicted lifetimes by computing the global burden (total number of molecules) and dividing it by the globally integrated loss (molecules per year), and both are taken over the entire vertical extent of the atmosphere. This means that model transport and loss rate of a compound are what control how its lifetime is computed.

Using these predicted stratospheric lifetimes, it is possible to compare the lifetimes generated for each scenario and show how strongly (or not) different factors such as increases or decreases in circulation or chemistry, may impact a compound's stratospheric lifetime. First the observational data from the three campaigns was compared to the GSFC baseline scenario (GSFC\_O). The mixing ratio (in ppt) for CFC-11 was plotted against (a) Mean Age (yr), (b) Potential Temperature (K), and (c) Altitude (km). The results can be seen in Figure 3.8, Figure 3.9 and Figure 3.10, where some of the strengths and weaknesses of this model become apparent.

When mixing ratio is plotted against potential temperature or altitude, for CFC-11 (Figure 3.8, Figure 3.9 and Figure 3.10 b & c), the model simulates conditions well until around an altitude of 15-20 km or potential temperature of 400-450 K, (samples from about 2.5-3 years mean age and older). After that the Geophysica data plateaus while the GSFC\_O data points increase steadily in altitude or potential temperature. This pattern is broadly the same for all compounds, though an offset was observed for CFC-114 when plotting mixing ratio against mean age, altitude or potential temperature (Figure C.5b & c). The reasons for this will be explored presently.

The GSFC 2D model simulates the mean age-tracer correlation robustly. However, the model uses a 2D zonal mean to create a potential temperature profile, and this is naturally different to the observed singular potential temperature profiles. To investigate further the GSFC's model data and data generated by the Chemical Lagrangian Model of the Stratosphere (CLaMS), were compared to in-situ observational data. As discussed in section 2.2, CLaMS is a modular chemistry transport model (CTM) system (Groß *et al.*, 2002; McKenna *et al.*, 2002a, 2002b). As a 3D CTM, CLaMS is able to represent real world meteorological conditions; this allows 'point-to-point' comparisons between the observational data from the campaigns (listed in section 3.2.1) and the model data.

A comparison between a 2D model, a 3D model, and in-situ measurements is not straightforward. For the GSFC, the x-Dimension (longitude) is missing, but provides data for

latitudes between -88 and 88 degrees, in 4-degree increments. Both models were compared to three in-situ campaigns (OB09, KIR10 and KIR11), and thus used the same latitude, month and year as the corresponding campaign. For CLaMS it was possible to match the exact date and time each sample was taken, so the CLaMS dataset is being compared 'point-to-point' with the in-situ data, while the GSFC dataset is only an average for the latitude, month and year.

As the chemical schemes for the compounds being examined here (CFC-13, CFC-114, CFC-114a, and CFC-115) are not yet implemented in CLaMS, but are for CFC-11, this is the compound used for comparison to the GSFC data. As can be seen in Figure 3.8- Figure 3.10, both models simulate the tracer-mean age correlation well, but CLaMS data better fits the in-situ data when the tracer is plotted against altitude or potential temperature. This is because as mentioned CLaMS can compare data 'point-to-point', and this works well for mean age-tracer correlations as these are driven by transport processes (advection and eddy diffusion), which do not depend strictly on spatial position.

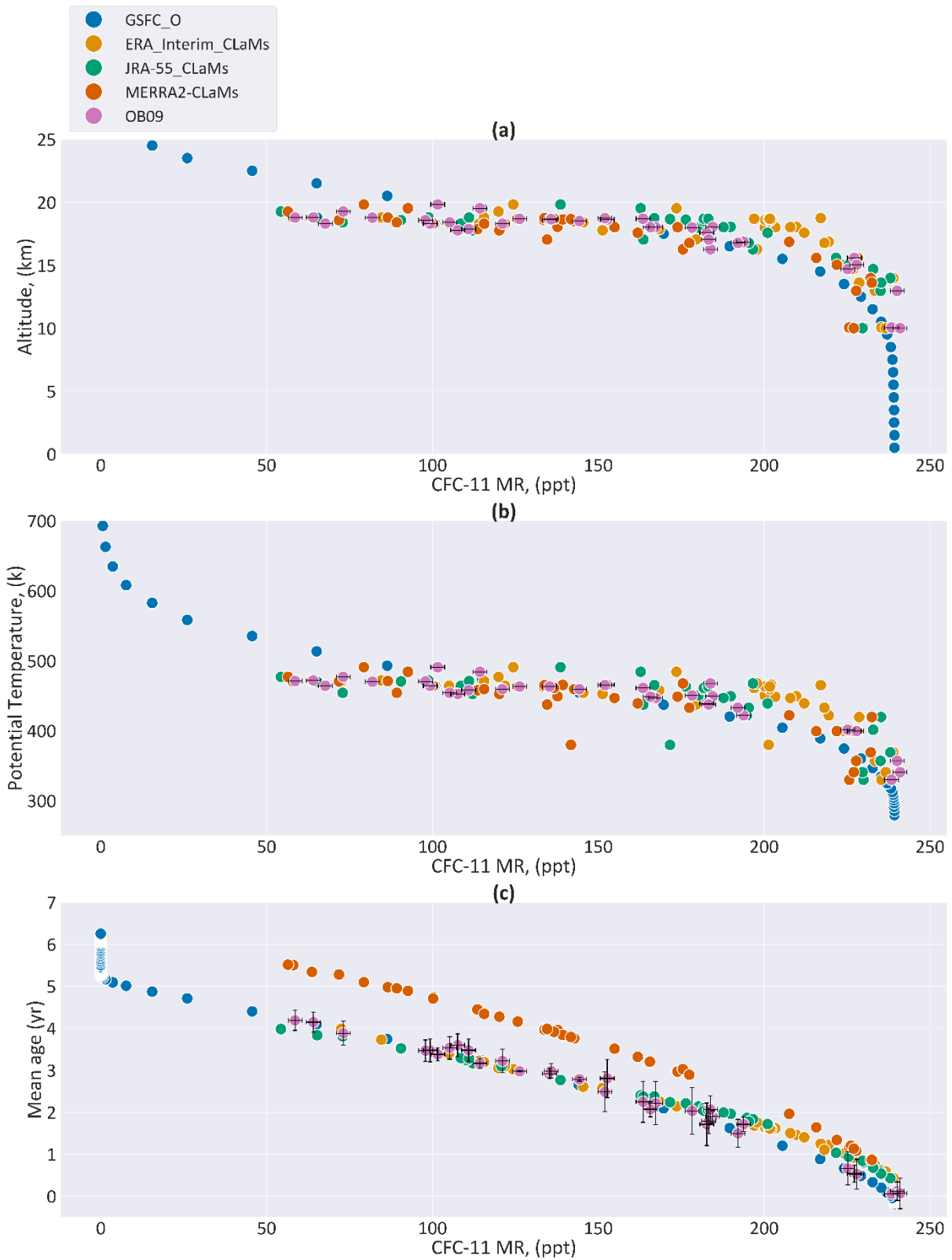


Figure 3.8. OB09. Comparison between GSFC baseline scenario (GSFC\_O), CLaMS (driven by three reanalyses: ERA Interim, FRA-55, and MERRA-2), and the observational data from the OB09 flight. (a) Mixing ratio (ppt) v Altitude for CFC-11. (b) CFC-mixing ratio b Mean Age (yr) (k). (c) CFC-11 mixing ratio versus mean age (yr). Neither model provided uncertainty data, the observational data includes error bars derived from instrument precision for Mean Age and mixing ratio.

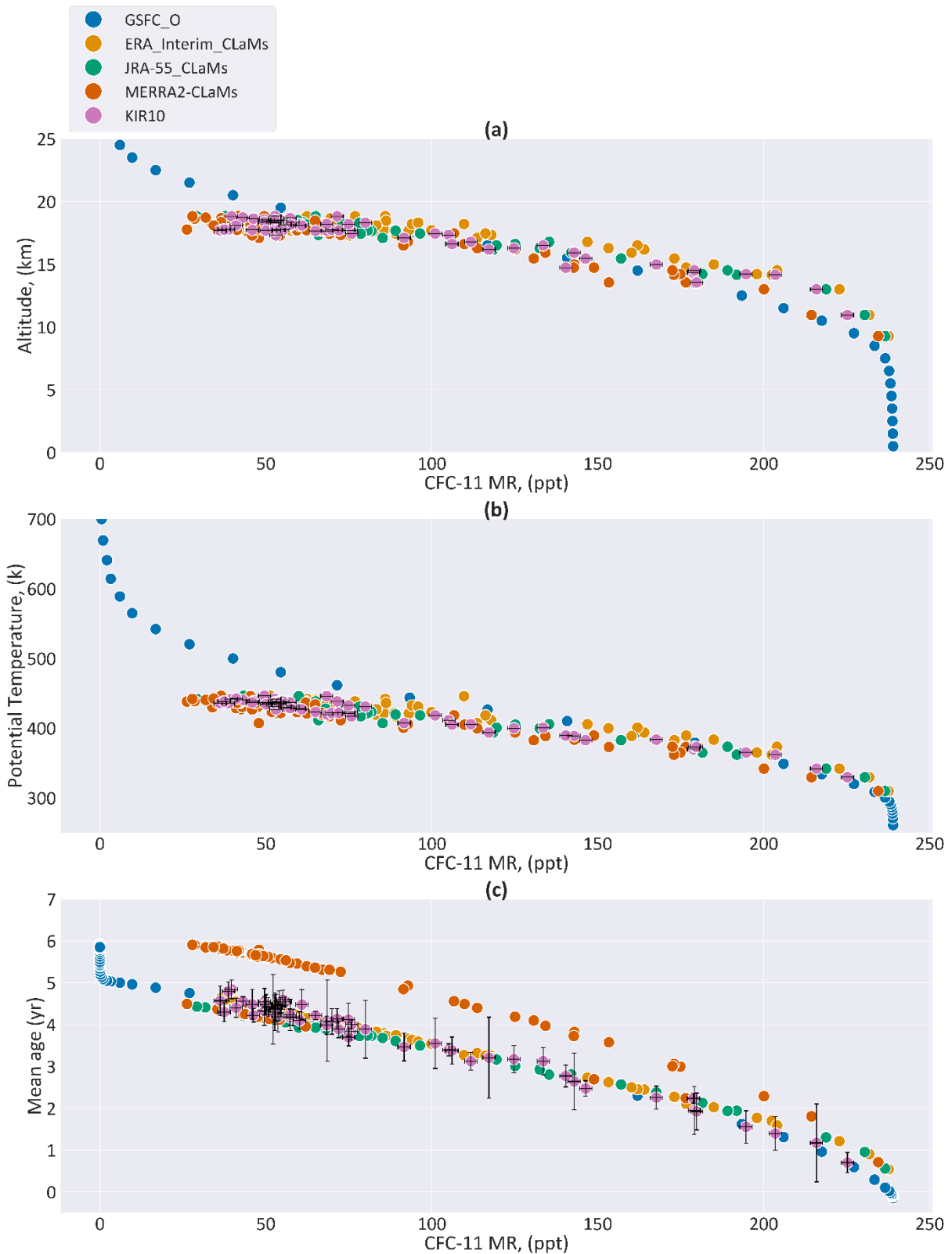


Figure 3.9. KIR10. Comparison between GSFC baseline scenario (GSFC\_O), CLaMS (driven by three reanalyses: ERA Interim, FRA-55, and MERRA-2), and the observational data from the KIR10 flight. (a) Mixing ratio (ppt) v Altitude for CFC-11. (b) CFC-11 mixing ratio v Mean Age (yr) (k). (c) CFC-11 mixing ratio versus mean age (yr). Neither model provided uncertainty data; the observational data includes error bars derived from instrument precision for Mean Age and mixing ratio.

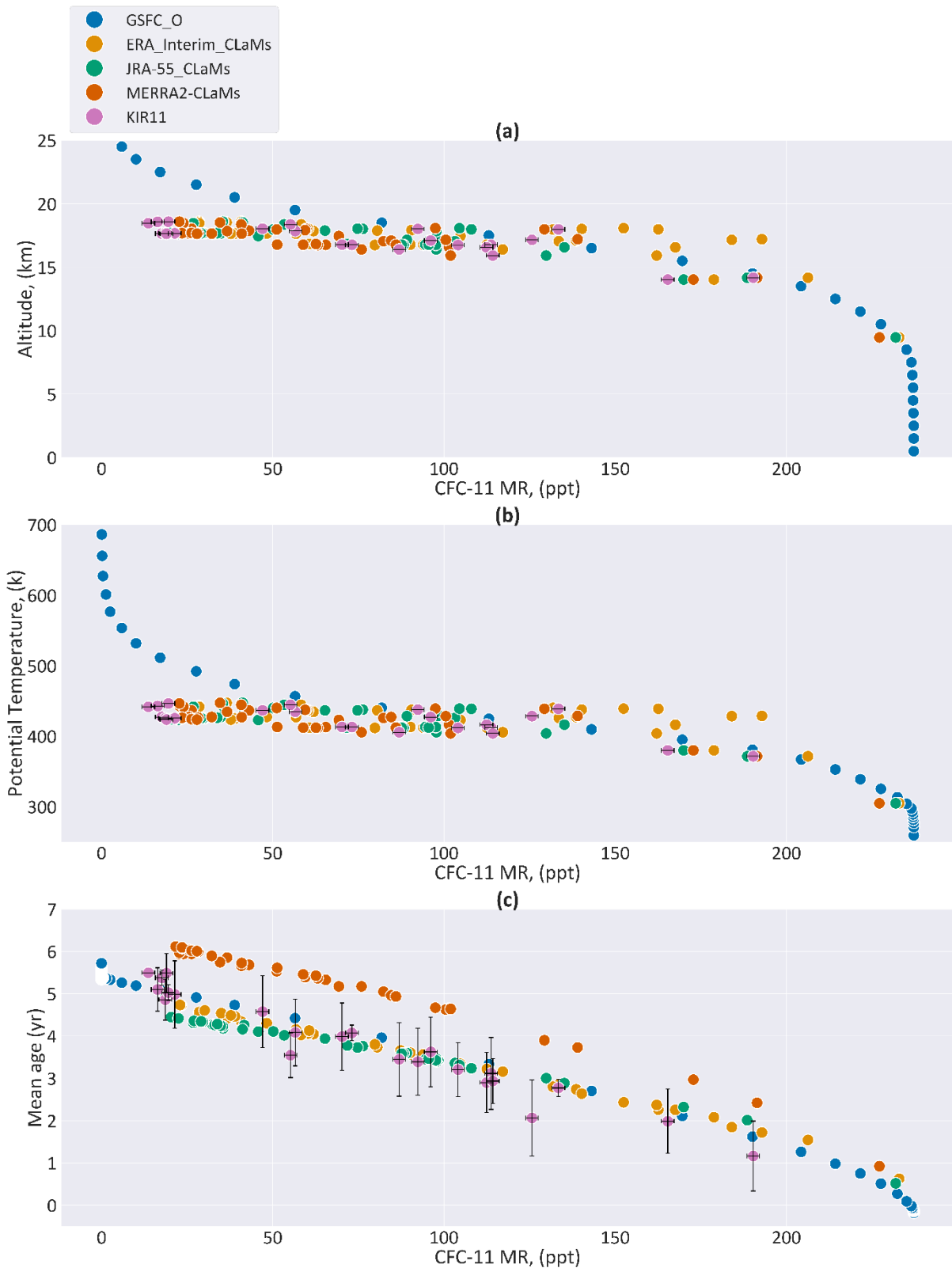


Figure 3.10. KIR11. Comparison between GSFC baseline scenario (GSFC\_O), CLaMS (driven by three reanalyses: ERA Interim, FRA-55, and MERRA-2), and the observational data from the KIR11 flight. (a) Mixing ratio (ppt) v Altitude for CFC-11. (b) CFC-11 mixing ratio v Mean Age (yr) (k). (c) CFC-11 mixing ratio versus mean age (yr). Neither model provided uncertainty data; the observational data includes error bars derived from instrument precision for Mean Age and mixing ratio.

Examining Figure 3.8, Figure 3.9, and Figure 3.10 some of the strengths and weaknesses of different modelling techniques become clear. It is possible to compare CLaMS and GSFC when looking at mean age-tracer correlation as this involves a coordinate system that does not depend on spatial position and local meteorological conditions. When modelling mean age (Figure 3.8c, Figure 3.9c, and Figure 3.10c), both models agree with the observational data, though CLaMS seems to have slightly higher mean ages between 1.5 years mean age and 0 years mean age (appears in all three figures, but is most clear in Figure 3.8c) than either the GSFC data or the in-situ data; this is within the uncertainties for the observational data. As can be expected for a 3D model, when looking at vertical coordinates such as altitude (and to a lesser extent Mean Age (yr), which does not increase linearly with altitude).

The reason that the GSFC simulates the mean age-tracer correlation accurately but is less accurate for tracer-potential temperature or tracer-altitude correlations is because the GSFC 2D model is highly parameterised. The model accurately simulates the mixing ratio versus mean age correlation because mean age is a general characteristic of each air parcel as it is the mean transit time from the tropopause to the specific location of the specific air parcel in the stratosphere. The correlation between long-lived tracers (in this case CFCs) and mean age is strongly influenced by seasonality, and both the modelled and the observed tracer distributions in theory share the same seasonal varying transport patterns. This correlation in the stratosphere generally holds, providing the tracer's local lifetime (not necessarily the same as global stratospheric lifetime) is longer compared to the local transport timescale.

The mean age-tracer correlation is mainly shaped by the strength of the Brewer-Dobson circulation, and this is included in the GSFC model, because transport parameters are calculated from observed climatological values of temperature, H<sub>2</sub>O, zonal wind, and ozone, see e.g. Weisenstein et al., (2004). However, the in-situ measurements were taken at very specific times and places, while the GSFC 2D model data only provide average for that month and latitude (plus or minus 4 degrees of latitude), so may not accurately reflect the precise local conditions experienced by the M55 Geophysica. This means that the mean age and compound concentration at any given altitude, is a mean for the season and latitude. As a 2D simplified model it does not use the real-world meteorological conditions and cannot easily take into account more localised transport processes.

Potential temperature however, in contrast to altitude, is sensitive to the strength of the Brewer-Dobson circulation. It is important to remember that it is not possible to compare ‘point to point’ between in-situ observational data, and the data generated by this 2D simplified model. In Figure 3.11 it is clear that while the relationship between mean age and potential temperature (and by extension altitude) behaves similarly between campaigns it still shows a non-trivial non-linear correlation. The OB09 campaign, which took place during an earlier season and at a lower latitude than the KIR10 and KIR11 campaigns, shows lower mean ages at higher potential temperatures/altitudes.

It should also be noted that since modelled trace gas profiles are so dependent on the strength of mixing between the tropics and extra-tropics, this can lead to an overcompensation of higher up- and downwelling velocity in the BDC overturning circulation, particularly closer to the tropics.

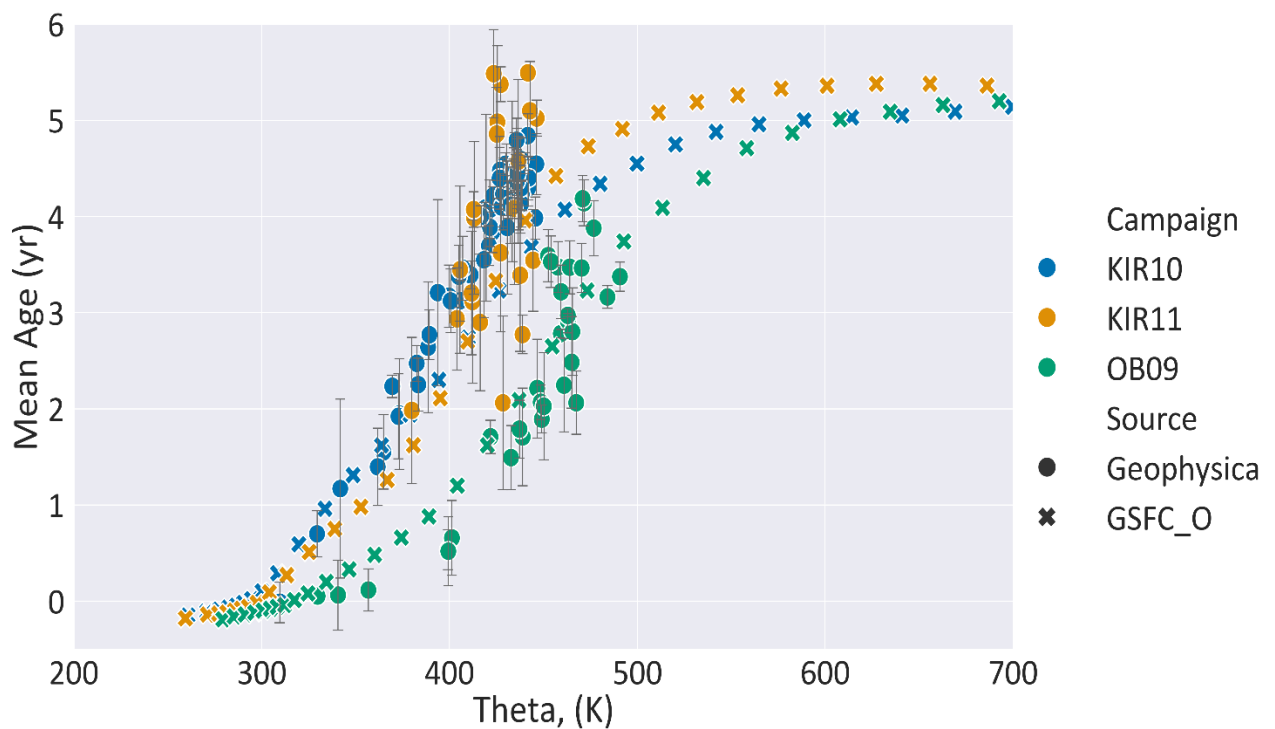


Figure 3.11. Potential temperature (K) plotted against Mean Age (yr) for all three campaigns, and both data from M55 Geophysica research flights, and the GSFC baseline scenario (GSFC\_O).

The rest of section 3.3.4 will focus primarily on the tracer-mean age correlation as the GSFC is able to simulate this much more precisely than the correlation between tracer and altitude or potential temperature.

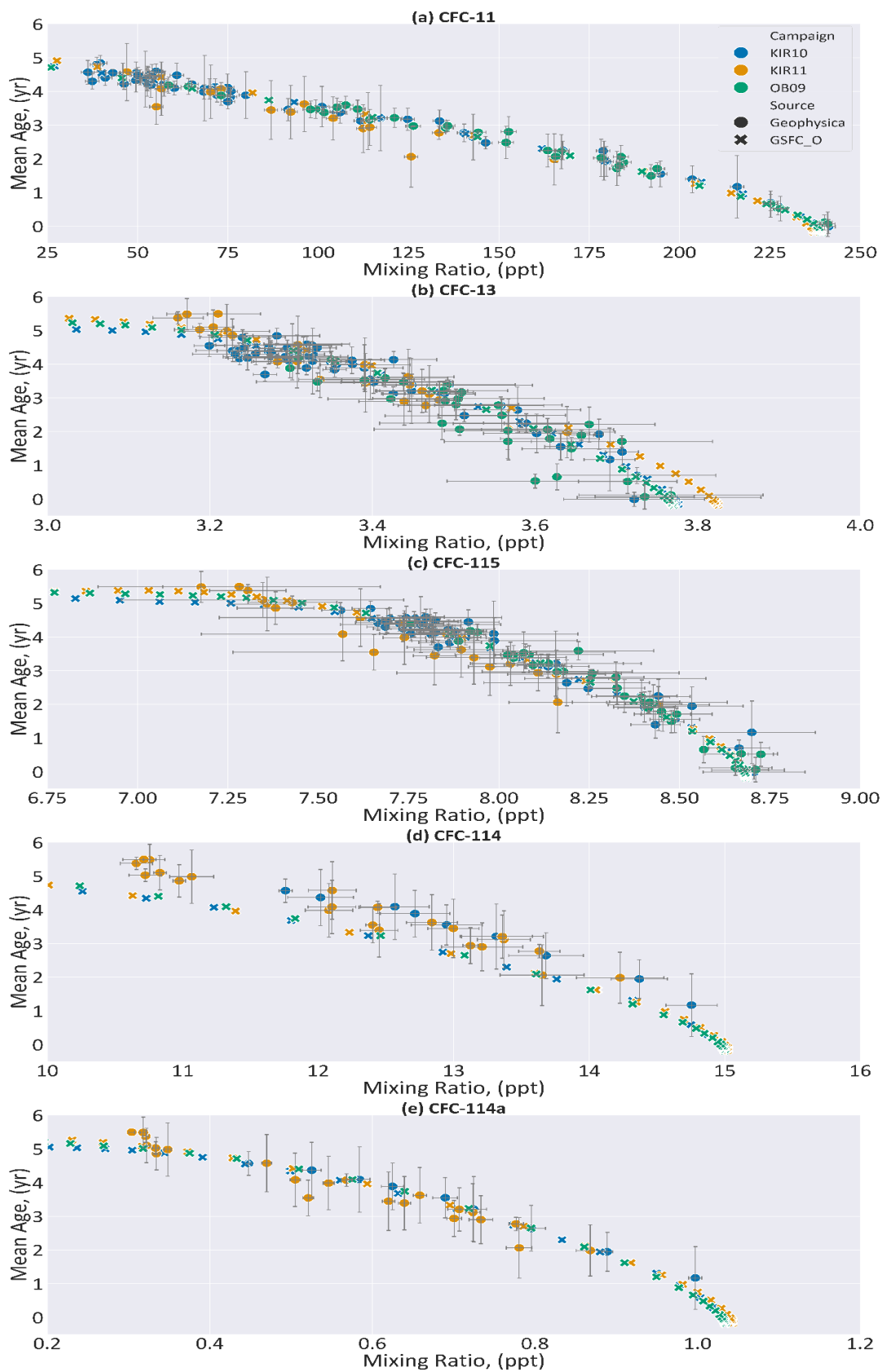


Figure 3.12. Mixing ratios (ppt) for all compounds, plotted against mean age (yr). Shows data derived using both Geophysica high-altitude research flights, and GSFC model data. Includes the OB09, KIR10, and KIR11 campaigns (with the exceptions of CFC-114 and CFC-114a where the samples for OB09 were analysed on a column that could not differentiate these isomers, see section 2.3 for details).

If we look first at CFC-11 mixing ratio plotted against mean age, the model fits closely with the in-situ observations (Figure 3.12a). For the other compounds we can see that there is a compact visual correlation between mean age and mixing ratio. This compact correlation would suggest that the model is accurately simulating the transport history of these compounds. However, there is one notable outlier: CFC-114. As can be seen in Figure 3.12d the data points from the Geophysica flights are notably offset from the GSFC baseline scenario, resulting in anomalously high mean ages.

Precisely why CFC-114 is an anomaly is difficult to ascertain. If the problem was that the model does not simulate circulation correctly, one would expect to see the same effect across compounds. Both compounds with shorter lifetimes than CFC-114, CFC-11 (Figure 3.12a) and CFC-114a (Figure 3.12e) showed a compact correlation between mean age and mixing ratio, as did the two compounds with longer lifetimes CFC-13 (Figure 3.12b) and CFC-115 (Figure 3.12c). CFC-114 and CFC-114a are isomers and have often been studied as their sum rather than separately (Vollmer *et al.*, 2018). If the chemistry the GSFC used for these compounds had done this, we might expect erroneous results for both compounds. Figure 3.12 shows that CFC-114a is simulated as well as CFC-11, CFC-13 and CFC-115.

The chemical loss (photolysis and  $O(^1D)$ ) of CFC-114, and the  $O(^1D)$  loss of CFC-114a were taken from the JPL-15 recommendations (Sander *et al.*, 2006), and the chemistry has not been updated as of JPL-19 (Burkholder *et al.*, 2020). The photolysis of CFC-114a was from Davis *et al.*, (2016). Vollmer *et al.*, (2018) notes that the laboratory studies which derived the UV absorption spectra and  $O(^1D)$  reaction rates used in the JPL – 17 report (Sander *et al.*, 2011), did not give consideration to the potential presence of impurities of CFC-114a in CFC-114. As these impurities were likely to be present (Laube *et al.*, 2016), and the UV absorption of CFC-114 is significantly weaker than that of CFC-114a (Davis *et al.*, 2016; Vollmer *et al.*, 2018), this could lead to CFC-114's lifetime being underestimated. The  $O(^1D)$  kinetics of the isomers are however sufficiently similar that lifetime estimates would not be affected significantly (as a result of incorrect  $O(^1D)$  kinetics) if impurities were present. The kinetics data listed for CFC-114 has remained the same for all three JPL reports mentioned here (15, 17, 19). In Figure 3.12 the model gives lower mean ages than are seen in the Geophysica samples; if the model uses kinetics parameters that assume CFC-114's UV absorption is stronger than it is, this would result in the compound disassociating faster in the model than in the actual stratosphere.

To further investigate how well the GSFC models the mean age-tracer correlation, and which factors had the greatest effect on lifetime, I compare the mean age generated by the model, and the mean age found in my in-situ samples. As mean age of air is a diagnostic for the stratospheric circulation (e.g. Hall et al. (1994)), the comparison between the baseline scenario and the in-situ data could be an indication that the circulation is being modelled accurately.

In order to use data from the GSFC that was comparable to the in-situ data, I used the correlation from a chemical tracer (first CFC-11 for quality assurance purposes, then for each of the compounds of interest; CFC-13, CFC-114, CFC-114a and CFC-115) and mean age to generate a conversion function from tracer mixing ratio to mean age using a second order polynomial (see Figure 3.13). If for example the in-situ dataset had a sample with CFC-11 at mixing ratio of 55 ppt, the conversion function from Figure 3.13 would be used with 55 ppt as 'X', and from this derive 'Y' which would be the mean age of the air sample when the mixing ratio of CFC-11 was 55 ppt. To check how well the conversion function worked, I also used the original mixing ratio as 'X' and used the conversion function to derive 'Y', which was then compared to the original mean age for that sample, and from this I derived residuals.

As a bivariate fit is difficult to achieve for a polynomial (see section 2.4), I used a similar method as that described in section 2.4: I derived 'Y' using the original mixing ratio (MRO), the mixing ratio plus the uncertainty (MR+), and the mixing ratio minus the uncertainty (MR-). From this I calculated the average range between MR+ and MR-, which was multiplied by the standard deviation of the residuals (derived from the comparison between the original mean age, and the mean age derived using the original mixing ratio and the conversion function). This provided an average uncertainty that took into account the variability of the original data.

Using this technique, I could compare the mean age in the in-situ sample when the mixing ratio of CFC-11 was 55 ppt, to the mean age in the GSFC dataset at the point where the mixing ratio of CFC-11 was 55 ppt. From this I derived comparable mean ages from each dataset, for all 5 compounds, for all 3 campaigns, and for all GSFC scenarios (Figure 3.13 as example using CFC-11).

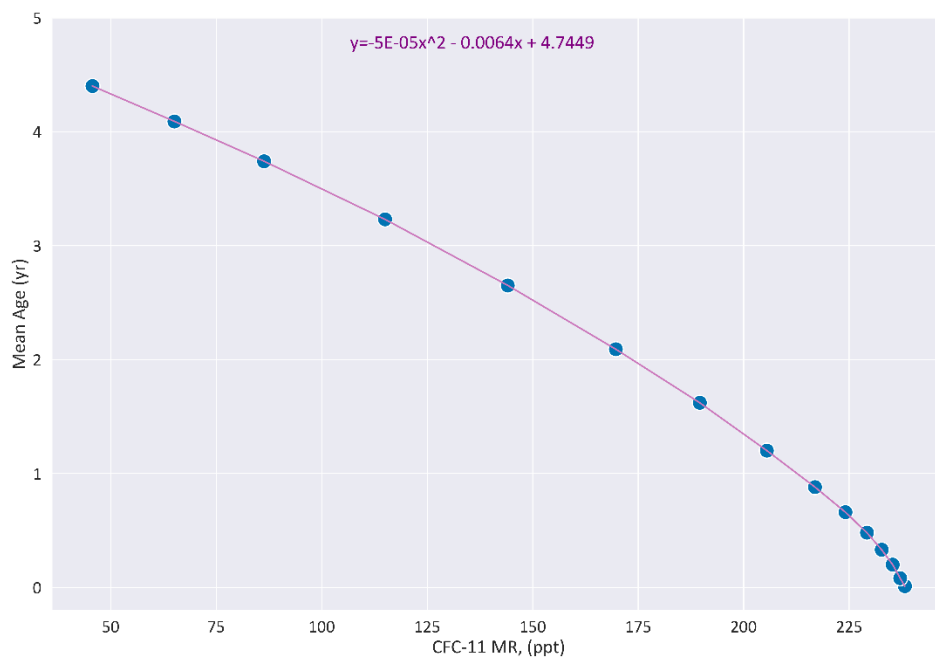


Figure 3.13. The correlation between CFC-11 mixing ratio (ppt) and mean age (yr) from GSFC\_0 for OB09 campaign. Trendline is a second order polynomial.

### 3.3.4.b Chemistry and Circulation scenarios

If the model perfectly fitted the in-situ data, when plotting mean ages derived using in-situ data against mean ages derived via the model, we would expect to see a 1,1 trendline (so when the real world mean age is 1, then the mean age from the GSFC 2D model would also be 1). However, this was not the case and thus it was necessary to determine to what extent the baseline and different scenarios differed from a 1,1 line, and whether this difference is statistically relevant.

To determine the average uncertainty I first plotted mixing ratio against mean age for the original Geophysica collected data (including the mixing ratios plus or minus the instrument precision to give an uncertainty range, expanding the dataset to 5n, as described in section 3.2.4), then calculated the residuals between it and the 1,1 line. By combining the range of mean age variation and the standard deviation of the residuals, I derived an average uncertainty range that reflected the natural variation in the original dataset.

Having done this I then compared the mean age-mean age correlation from each of the 11 GSFC model scenarios, to the 1,1 line, and calculated the average residuals (in years mean age), see Figure 3.14 and Figure 3.15.

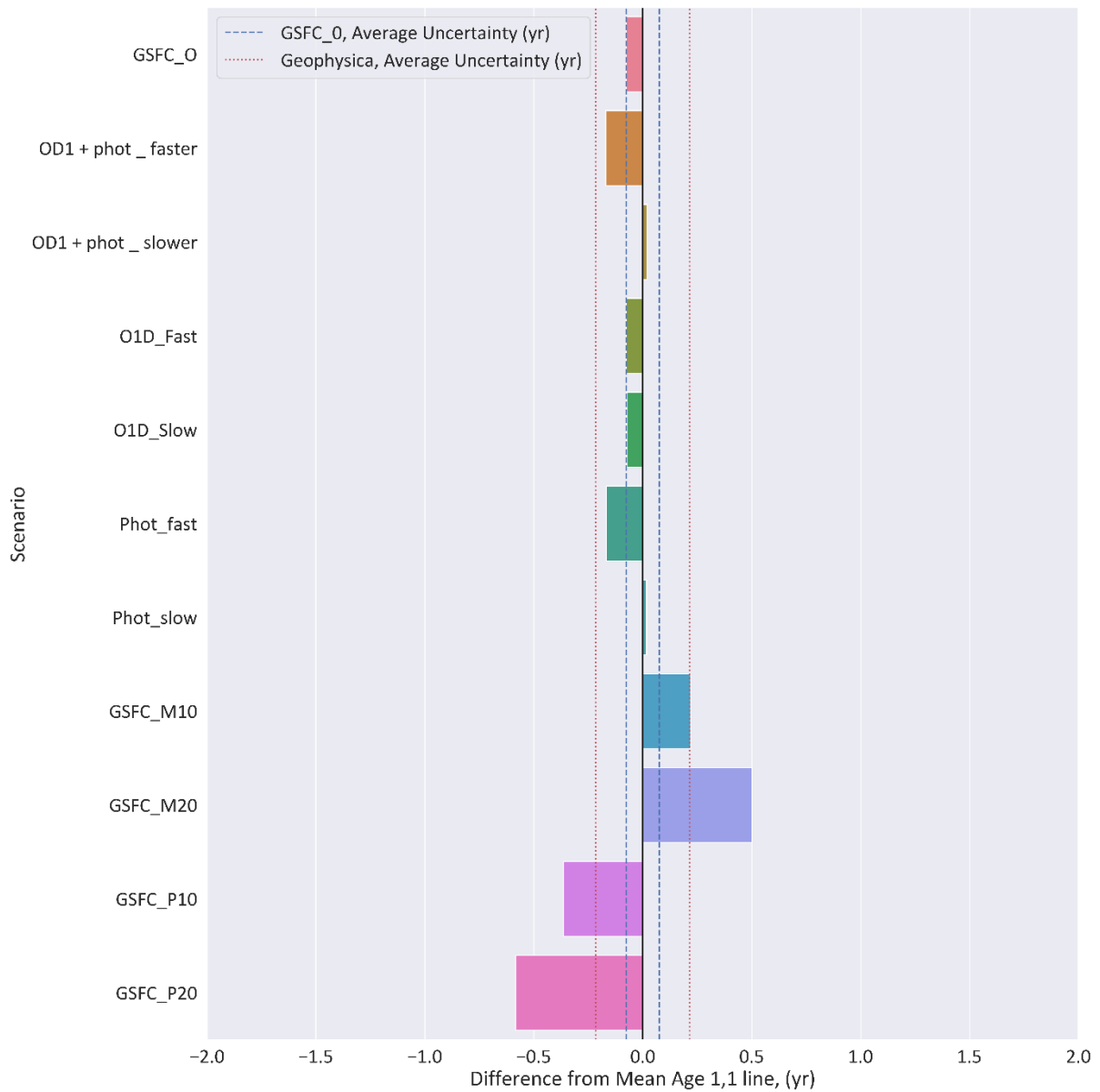


Figure 3.14. The difference (in yr) (average residuals) between the mean age-mean age correlations and a 1,1 line CFC-11. Results are the average of all three campaigns (OB09, KIR10, and KIR11). Blue dashed lines represent how far GSFC\_0 (the baseline scenario) differs from a 1,1 line (both plus and minus), in order to compare to the other scenarios. The orange dotted line is the 'average uncertainty', e.g. how much variation from the baseline can be explained by variation in the original data.

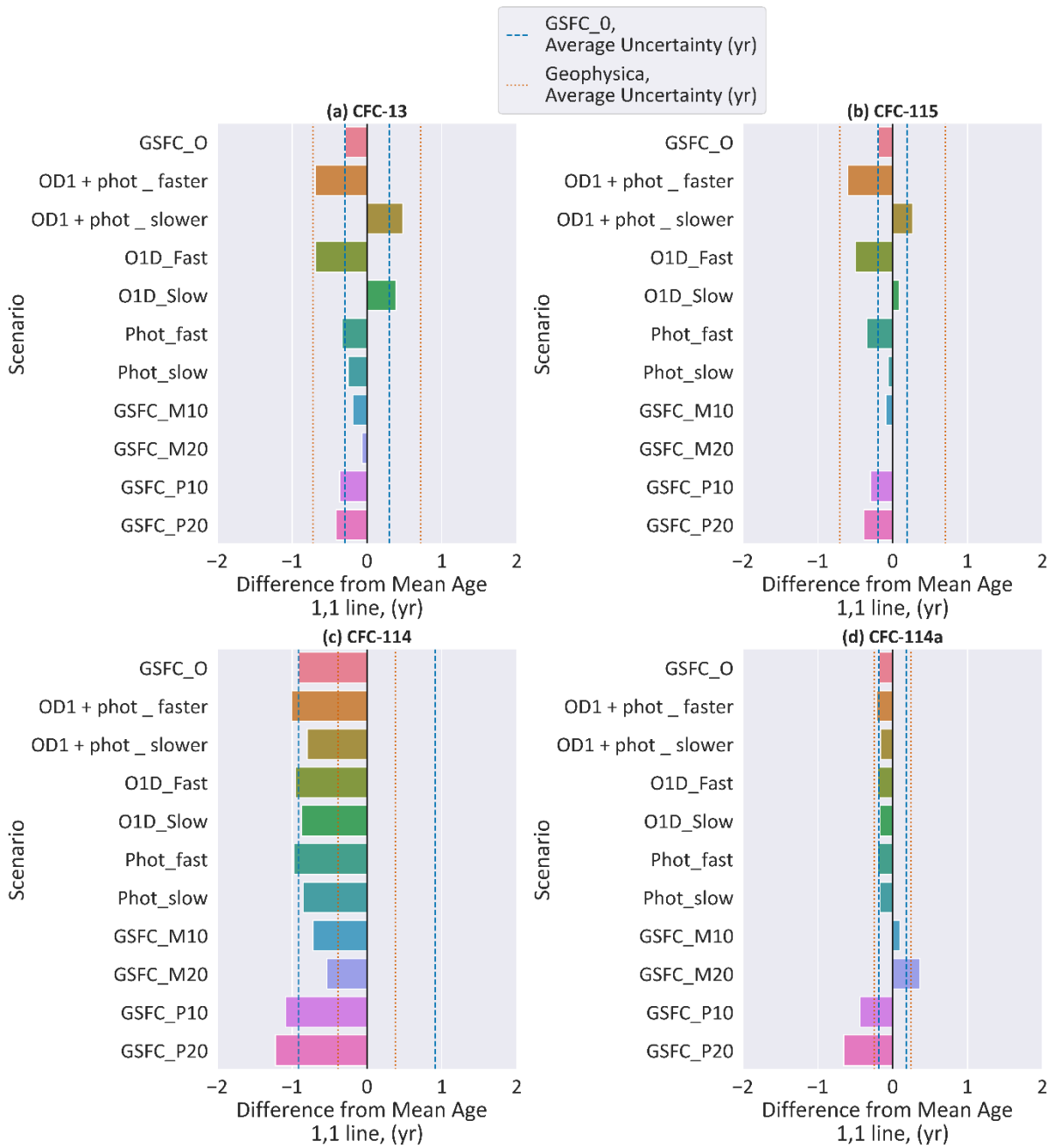


Figure 3.15. The difference (in yr) (average residuals) between the mean age-mean age correlations and a 1,1 line for (a) CFC-13, (b) CFC-115, (c) CFC-114, and (d) CFC-114a. Results are the average of all three campaigns (OB09, KIR10, and KIR11). Blue dashed lines represent how far GSFC\_0 (the baseline scenario) differs from a 1,1 line (both plus and minus), in order to compare to the other scenarios. The orange dotted line is the 'average uncertainty', e.g. how much variation from the baseline can be explained by variation in the original data.

When interpreting Figure 3.14 and Figure 3.15., it should be noted that as the reference (to which the model is compared) are the in-situ observations, deviation against a reference is given by:

$$\textit{Deviation against reference} = \textit{Value} - \textit{Value\_Reference}$$

*Equation 3-1. Deviation against reference*

So if the average residual is positive, then the mean age from the model was greater than the 1,1 line, while if the residual was negative, the mean age was less than the 1,1 line. The closer to zero a scenario's average residual is, the closer it is to the observational data. However, if the scenario's average residual is less than the average error, then the difference is not statistically relevant. If the scenario's average residual is greater than the average error, then that difference cannot be explained by the error range of the original Geophysica data.

In Figure 3.14 and Figure 3.15 all five compounds have negative average residuals (and thus their baseline scenario predicted smaller mean ages than the real world samples showed). As discussed previously the tracer-mean age correlation for all five compounds is robust. Figure 3.14 and Figure 3.15 would suggest that the GSFC\_baseline scenario's estimates agree within the uncertainty range with the in-situ measurements for all compounds except CFC-114, for which all scenarios, including the baseline scenario, fell outside the average error.

It can be informative to compare the scenarios to the baseline (GSFC\_0) rather than just to the 1,1 line; with scenarios which speed up the chemistry or circulation having more negative residuals (meaning smaller mean ages) when compared to the 1,1 line than the baseline scenario does, this is expected as scenarios which speed up chemistry or circulation would result in smaller mean ages. This is why Figure 3.14 and Figure 3.15 feature lines to indicate the extent of the baseline scenario's difference from a 1,1 line. This allows comparison against the other scenarios.

In Figure 3.14 in terms of chemistry CFC-11 was not affected by changes to the O(<sup>1</sup>D) rate of reaction, as these scenarios gave the same result as the baseline scenario. Increasing the photolysis rate (in the 'Phot\_fast' and 'O1D+Phot\_faster' scenarios) gave a difference from 0 of more than double that of the baseline scenario. The 'Phot\_slow' and 'O1D+Phot\_Faster' scenarios give residuals closest to zero of any of the scenarios when looking at CFC-11; however, the baseline and chemistry scenarios had residuals less than the average uncertainty. Only the circulation scenarios produced residuals greater than the average uncertainty, and thus had a statistically relevant impact on the mean age.

As photolysis is the dominant loss process for CFC-11 increasing the reaction rate would be expected to have a significant effect. However if CFC-11 were already at saturation point, increasing the reaction rate would not have a noticeable impact on the predicted mean age. The  $O(^1D)$  scenarios show no discernible change compared to the baseline scenario, so either these reaction pathways are at saturation point, or account for such a small percentage of the loss rate for CFC-11 that any change to them has little noticeable impact in Figure 3.14. The photolysis scenarios have a noticeable impact relative to the baseline scenario, though this is small compared to the circulation scenarios and still less than the average uncertainty. This suggests that photolysis pathways are not at saturation point, but there are still other limiting factors, and that how quickly the compound can be transported into loss regions has a greater bearing on dissociation than the speed of the photolysis reaction rate.

In terms of circulation, all scenarios which change the speed of circulation result in change of mean age, more than double that of the baseline scenario, with the M10 and M20 scenarios (in which circulation was slowed by 10 and 20% respectively) had a greater impact than the P10 and P20 scenarios. So in comparison to the baseline scenario, for CFC-11 circulation had a significantly bigger impact than the chemistry, and only the circulation scenarios had residuals that were greater than the average uncertainty.

Having assessed model performance with a well-constrained CFC (CFC-11), we can now turn to the four CFCs this chapter is primarily focused on. CFC-13 (Figure 3.15a) demonstrates that when changing photolysis reaction rates, the photolysis scenarios give average residuals very close to the baseline scenario. However, changing the  $O(^1D)$  reaction rate has a much greater effect, with speeded up  $O(^1D)$  scenarios giving residuals more than double those from the baseline scenario, and those with slower  $O(^1D)$  reactions giving residuals that were 25%/50% greater than those of the baseline scenario. Of the chemistry scenarios, 'Phot\_slow' was the scenario closest to zero (and thus the observational data) and was the only chemistry scenario with smaller average residuals than the baseline scenario.

Reactions with  $O(^1D)$  are the dominant loss process (80%) for CFC-13, so changes to the photolysis rate are unlikely to have a big impact here (as they only account for 20% of CFC-13's loss rate). So Figure 3.15a would suggest that reactions with  $O(^1D)$  are not yet at saturation rate, as increasing the reaction rate significantly lowers the resulting mean age,

which is to be expected for a long-lived compound. In terms of circulation the P10 and P20 scenarios gave average residuals somewhat larger than the baseline scenario, while the M10 and M20 scenarios gave significantly smaller average residuals, notably M20. Both the chemistry and circulation scenarios had notable effects on the mean ages, compared to the baseline scenario, with the P20 scenario having the largest impact, followed closely by the O1D+Phot\_Faster scenario. When compared to the observational data, the scenarios that match most closely are the 'Phot\_slow', M10 and M20 scenarios. However, none of the scenarios produced average residuals greater than the average uncertainty. The O(<sup>1</sup>D) scenarios are the closest to the average uncertainty, but still just under it, and thus all scenarios fell within the uncertainty range expected of the original data.

In the case of CFC-115 (Figure 3.15b), with the exception of 'O1D + Phot slower' all scenarios (both chemistry and circulation) gave smaller mean ages than the in-situ observations. In terms of chemistry, both the 'O1D+Phot\_faster' and 'O1d\_fast' scenarios produced average residuals double those of the baseline scenario, with 'Phot\_fast' around 50% greater than the baseline. The 'O1D\_Phot\_slower' scenario has average residuals somewhat greater than those of the baseline scenario, while 'Phot\_slow' and 'O1D\_slow' both gave residuals significantly smaller than those of the baseline scenario, and thus closest to the in-situ measurements. In terms of circulation, both 'fast' scenarios (P10 and P20) gave larger residuals than the baseline, with P20 being close to double. The slower scenarios (M10 and M20) however had average residuals much smaller than those of the baseline, with M20's value being so low as to be invisible in Figure 3.15b. The compound's known chemistry is displayed here, as both the O(<sup>1</sup>D) and Photolysis scenarios have an effect on the mean ages relative to the baseline scenario, with the O(<sup>1</sup>D) scenarios having a slightly stronger effect. As with CFC-13, both chemistry and circulation scenarios had a sizable effect on mean age relative to the baseline scenario. The M20, M10, Phot\_slow, and O1D\_slow scenarios matched most closely the 1,1 line (and thus were closest to the observational data); however, all scenarios fell within the average uncertainty range.

For CFC-114 (Figure 3.15c) all scenarios had negative residuals, so all scenarios simulated smaller mean ages for this compound, relative to in-situ samples. This supports section 3.3.4.a, where there was an offset between in-situ measurements and the model data, with the model predicting smaller mean ages for a given mixing ratio than were seen in the in-situ measurements. In Figure 3.15c the scenarios showed very little variation from

each other, with both circulation and chemistry having similar levels of impact. In terms of chemistry the faster scenarios ('O1D+Phot\_faster', 'Phot\_fast' and 'O1D\_fast') gave slightly higher average residuals when compared to the baseline. The slow scenarios 'O1D\_slow', 'Phot\_slow' and 'O1D+Phot\_slower' give progressively lower residuals. With the combined slow scenario giving the closest to zero (and therefore closest match to the observational data). In terms of circulation, the scenarios had slightly more noticeable effects. The P10 and P20 scenarios gave somewhat larger residuals than the baseline, while the M10 and M20 scenarios gave smaller residuals, with M20 being the closest of all scenarios to zero. However, CFC-114 differs from the other compounds examined here in that all scenarios for this compound had greater residuals than the average uncertainty. This means all scenarios, including the baseline scenario, were statistically different from the in-situ data. This is consistent with the possibility that the model used incorrect kinetics data for this compound, which is discussed in section 3.3.4.a.

The lack of substantial impact from any scenario is unlikely to be down to CFC-114's shorter (relative to CFC-13 and CFC-115) lifetime alone as CFC-11 (Figure 3.14) and CFC-114a (Figure 3.15d) (which both have shorter lifetimes than CFC-114) show some impact from changes in chemistry, and substantial impacts from changes in circulation. When compared to the baseline scenario, the other scenarios have relatively little impact; however, when compared to the observational data, the slow chemistry and circulation scenarios are (as with other compounds) the ones that most closely match the observational data, but all scenarios fall outside the uncertainty range.

As with CFC-13 and CFC-115, all scenarios for CFC-114a (Figure 3.15d) except two had negative residuals and thus the model predicted mean ages which were too small for a given mixing ratio, compared to the in-situ measurements. However, unlike CFC-115 and CFC-13 which only saw positive results for chemistry scenarios, the only positive residuals for CFC-114a were for the circulation (M10 and M20) scenarios. When looking at the chemistry scenarios, they all gave average residuals that were extremely close to those of the baseline scenario. The 'Phot\_slow' and 'O1D+Phot\_slower' scenarios gave marginally smaller average residuals, so were the closest of the chemistry scenarios to the 1,1 line (and the observational data). The circulation scenarios however had a much greater impact. The P10 and P20 scenarios had average residuals more than double that of the baseline scenario, while M20 had average residuals just short of double. M10 on the other hand had

average residuals less than half the magnitude of the baseline scenario. So the 'Phot\_slow', 'O1D+Phot\_slower' and M10 scenarios were the ones that most closely matched the 1,1 line (with M10 being the closest) and were therefore closest to the observational data. However, only the M20, P10, and P20 scenarios had greater average residuals than the average uncertainty, and thus only these circulation scenarios showed a statistically relevant difference from the 1,1 line (and the observational data).

In shorter-lived compounds such as CFC-114a and CFC-11, reaction rates may not be the limiting factor in disassociation, whereas Brewer-Dobson circulation would transport the compound from the source region (the tropical tropopause) to sink regions in the stratosphere faster or slower, and thus impact how quickly the compound can be disassociated.

To sum up, the scenarios which most closely fit the observational data would be those with average residuals closest to zero; residuals that fall below the average error can be accounted for by the uncertainty range of the original data. For CFC-11, the scenarios which were closest to the 1,1 line were the Phot\_Slow, and O1D+Phot\_Slow scenarios, but all scenarios fell within the uncertainty range. For CFC-115 the scenario closest to zero is M20, followed by Phot\_slow, then O1D\_slow, and all scenarios fell within the uncertainty range. For both CFC-13 and CFC-114 the closest scenarios to zero were M20, M10, and Phot\_slow; however, all scenarios for CFC-13 were within the uncertainty range, while all scenarios for CFC-114 were outside the uncertainty range. And for CFC-114a the M20, P10 and P20 scenarios fell outside the average uncertainty range, with the closest scenario to zero being M10, with all other scenarios giving values extremely close to that of the baseline scenario. In order of smallest difference to largest difference between the 1,1 line and the baseline scenarios: CFC-11 (-0.07 yr), CFC-114a (-0.19 yr), CFC-115 (-0.20 yr), CFC-13 (-0.29 yr), and CFC-114 (-0.91 yr).

Figure 3.14 and Figure 3.15 allow us to compare how strongly the mean age-tracer correlation was affected by different scenarios and compare this between compounds. Notably the compounds with the shortest lifetimes (CFC-11 with 55 years, CFC-114a with around 80 years) show a much bigger impact from circulation than from chemistry. The longer-lived compounds are affected by both to a similar (though not uniform) degree. A compound's lifetime reflects how quickly the compound is broken down, so shorter-lived compounds are already being broken down comparatively quickly, thus changes to their

reaction rate would have minimal effect. The limiting factor would be how quickly the compound arrives in a loss region (high up in the deep branch of the BDC), which is heavily parameterised by the model, not how quickly it is broken down when it arrives. The relationship between tracer and mean age changes differently for the chemistry scenarios than it does in the circulation scenarios.

Comparing CFC-13 (Figure 3.15a) to CFC-115 (Figure 3.15b) the difference between their respective loss processes is clear. For CFC-13 photolysis barely has any effect on the mean age shift, while for CFC-115 both photolysis and  $O(^1D)$  have an impact, with  $O(^1D)$  having a somewhat stronger impact. CFC-114 (Figure 3.15c) is barely affected by changes to the chemistry, and CFC-114a (Figure 3.15d) is virtually unchanged. In the case of CFC-114, it is that the modelled mean age-mixing ratio correlation for CFC-114 systematically underestimates mean ages for CFC-114 (see Figure C.5). For CFC-115, processes that speed up either chemistry or circulation seem to have the greatest impact compared to the baseline scenario, while those that slowed the chemistry or circulation most closely matched the observational data. As with CFC-11 and CFC-114, the mean age-mixing ratio correlation for CFC-115 systematically underestimates mean age.

CFC-13 and CFC-115 share the same characteristic of very long-lived species: both circulation and chemistry matter to similar degrees in their dissociation. However, the pattern is different, with  $O(^1D)$  kinetics having a much stronger impact on CFC-13 than on CFC-115, and circulation having a somewhat stronger impact on CFC-13 than CFC-115. These are the two compounds that have their lifetimes revised down significantly in section 3.3.2. This might suggest these compounds are behaving (or being subject to conditions) in ways that were not previously taken into consideration, either by previous studies of the compounds, or by the way the GSFC simulates them. This theme will be continued in the following sections, where the relationship between tracer and mean age, the GSFC 2D model, and the resulting FRFs (section 3.3.4.d) and stratospheric lifetimes (section 3.3.4.c), are explored in depth.

#### *3.3.4.c Model Lifetimes*

The GSFC 2D model did generate predicted stratospheric lifetimes for each compound in each scenario. This allows an exploration of how strongly each compound's

lifetime is affected by different conditions, and speculation as to why some of the stratospheric lifetimes produced in section 3.3.2 differ so greatly from previous estimates. Figure 3.16 shows the steady-state stratospheric lifetimes the GSFC baseline scenario predicted for each year. There are significant fluctuations in the lifetimes for the early decades, and after that the lifetimes stabilise, which is a general feature of model simulations. When the model initialises, the tracer distribution within it is unknown (and may not be the same as found in observations). Time is needed to run ('spin up') the simulation with the same meteorological and boundary conditions; during this time the model stabilises as it runs, which can take 15-25 years for a long-lived tracer. This is seen in Figure 3.16; by the time the model reaches 2009 the lifetime estimates do not fluctuate so heavily: from 2009 to 2011 the lifetime changes by 13 years for CFC-13, 18 years for CFC-115, 14 years for CFC-114 and 6 years for CFC-114a.

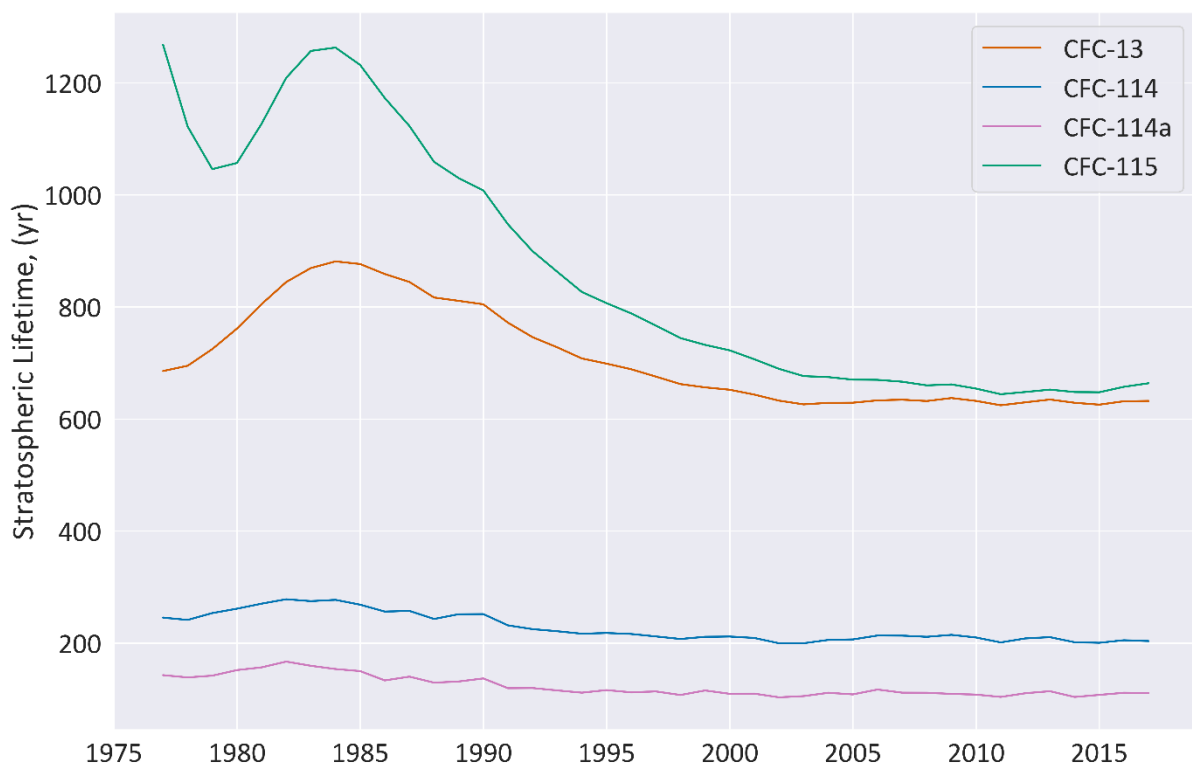


Figure 3.16. Steady-state stratospheric lifetime (yr) from the GSFC baseline scenario, for CFC-13, CFC-114, CFC-114a, and CFC-115, plotted against date.

The stratospheric lifetime for each scenario was compared to the 'baseline' scenario, and the percentage difference was calculated in Figure 3.17.

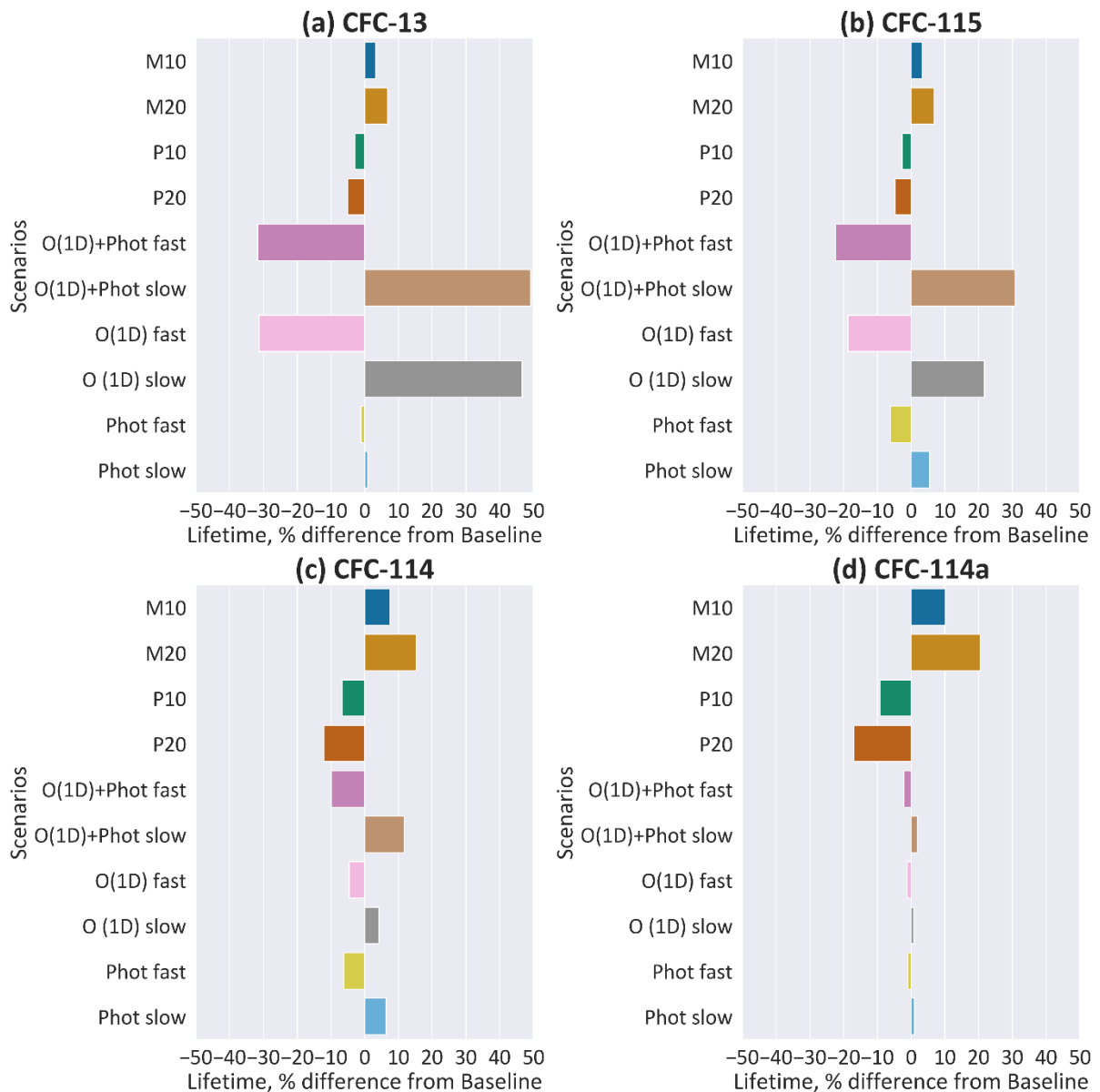


Figure 3.17. Shows the % difference in stratospheric lifetime for each scenario, compared to the unaltered 'baseline' scenario. Positive numbers reflect an increased lifetime compared to baseline, while negative numbers refer to a decrease in lifetime compared to baseline. Stratospheric lifetimes for (a) CFC-13, (b) CFC-115, (c) CFC-114, and (d) CFC-114a. Lifetimes are the average from those generated for the different GSFC simulation scenarios for 2009 to 2011.

Looking at Figure 3.17a, changes in circulation have only a limited effect on CFC-13's stratospheric lifetime (less than  $\pm 10\%$ ), while changes to the  $O(^1D)$  reaction rates have a significant impact on the lifetime with  $O(^1D)$ \_fast producing a lifetime -31% smaller than the baseline, and  $O(^1D)$ \_slow producing a lifetime 47% larger than the baseline. Photolysis rates have a much lower impact on lifetime with the 'Phot fast' and 'Phot slow' scenarios producing results (-1.15% smaller and 1% larger respectively), the  $O(^1D)$ +Photolysis fast

scenario gave a lifetime that was -31.3% smaller than baseline, while the O(<sup>1</sup>D)+Photolysis slow scenario gave a lifetime that was 49.2% larger than baseline. This is barely changed from the O(<sup>1</sup>D) only scenarios. In the 'O(<sup>1</sup>D)+Photolysis' scenarios both O(<sup>1</sup>D) and Photolysis rates were altered, and these scenarios are not the sum of the two separate O(<sup>1</sup>D) and Photolysis scenarios. While it is not always clear in the Figure 3.17, the 'O(<sup>1</sup>D)+Photolysis' fast/slow scenarios do have a greater effect on tracer lifetime than the separate scenarios do when combined. This demonstrates the interdependence between the loss reaction pathways. Figure 3.17a reflects the known reaction pathways for CFC-13, as O(<sup>1</sup>D) is the dominant loss reaction.

For CFC-115 (Figure 3.17b), as with CFC-13 the circulation has a much lower impact on stratospheric lifetime than the chemistry. The O(<sup>1</sup>D) scenarios seem to have the greatest impact on the stratospheric lifetime of CFC-115, though not to the same extent as with CFC-13. This also reflects the known chemistry of CFC-115.

CFC-114 is impacted to a similar degree by both circulation and chemistry changes (Figure 3.17c). Both O(<sup>1</sup>D) reaction rates and photolysis reaction rates have an effect on the lifetime of the compound, but photolysis has a slightly greater effect. In section 3.3.4.a it was noted that the photolysis kinetics for CFC-114 in the model may have been based on studies which did not account for contamination with CFC-114a, which has much stronger UV absorption. If this is the case, then Figure 3.17c may not accurately reflect CFC-114's chemistry.

CFC-114a on the other hand (Figure 3.17d) is noticeably more affected by circulation than it is by chemistry, which barely affects the lifetime. While changes to circulation resulted in much larger (~±20%) changes in stratospheric lifetime, increases or decreases in reaction rates results in only small (~±1-2%) changes in stratospheric lifetime.

Noticeably the compounds with the shorter lifetimes are the ones most affected by circulation; CFC-114a is the shortest-lived compound, and the one most affected by circulation changes. With shorter lifetimes, the reaction pathways may already be saturated, this is seen most clearly with CFC-114a in Figure 3.17d, where changes to the rate of reaction have very little effect on lifetime. Neither CFC-114 nor CFC-114a saw their lifetimes dramatically affected by changes in chemistry or circulation, with only the most extreme scenarios changing the lifetimes by more than 10%, while the longer-lived CFC-13 and CFC-115 saw increases/decreases of 30-50% on their most extreme scenarios.

In contrast, the longer-lived compounds see much smaller impact from circulation changes, and larger impact from chemistry changes. This is a consequence of the fact that (as discussed in section 3.3.4.b) longer-lived compounds such as CFC-13 and CFC-115 have such low loss rates in their main sink region (upper stratosphere), that even a much faster circulation resulting in shorter transport times into the main sink region would not result in a significant increase in the total stratospheric loss rate of the compound or decrease of the stratospheric lifetime, respectively.

In Figure 3.17, the effects of different scenarios are compared to the baseline scenario, but how do these lifetimes compare to estimates in 3.3.2 and to previous estimates in WMO 2022 (Burkholder *et al.*, 2022)? This is shown in Figure 3.18.

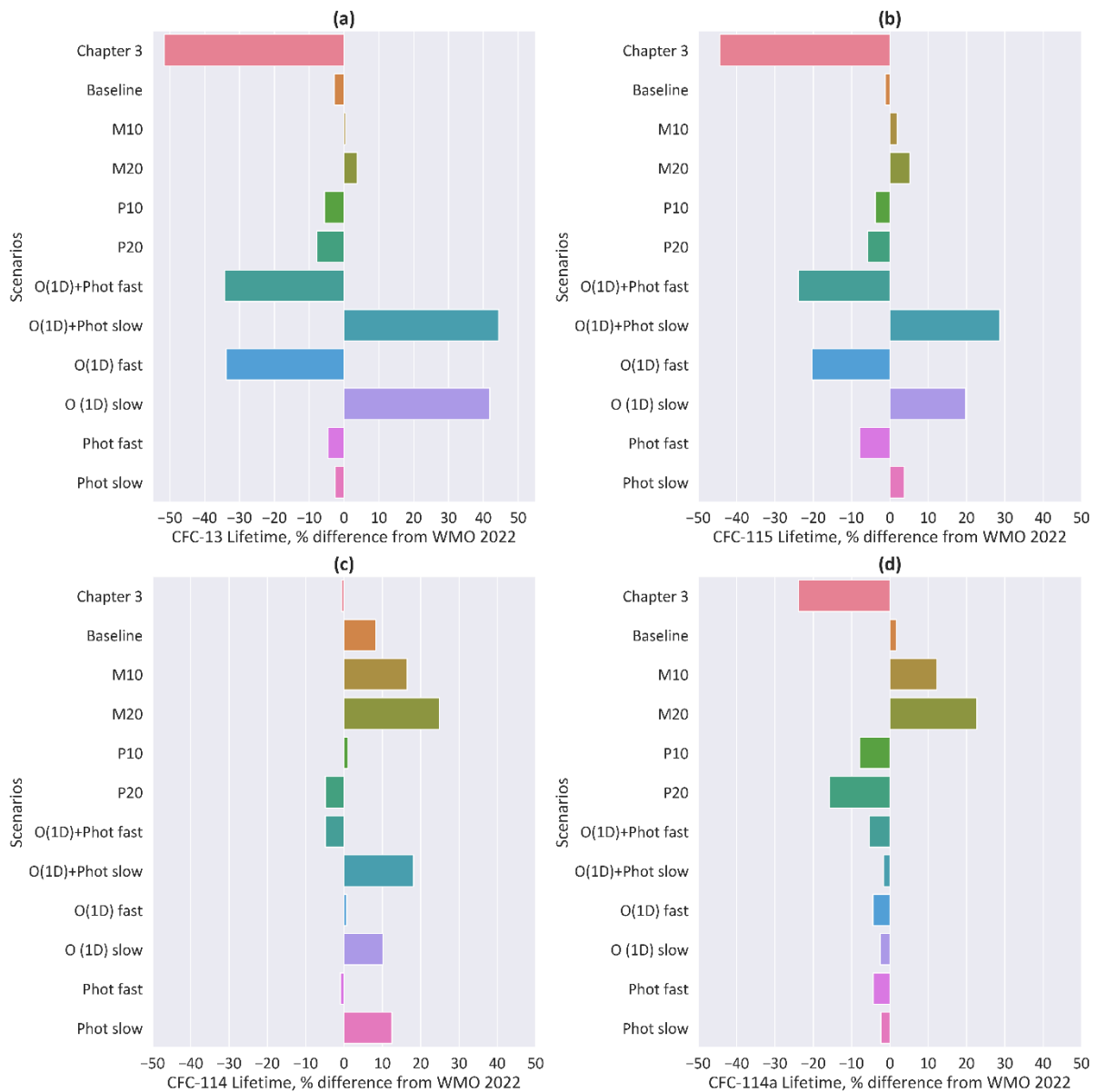


Figure 3.18. Percentage difference in lifetime for the scenario (or Chapter 3), compared to the previous estimate in WMO 2022 (Burkholder et al., 2022), for (a) CFC-13, (b) CFC-115, (c) CFC-114, and (d) CFC-114a. Average for all campaigns.

Looking at Figure 3.18 the baseline scenario produces lifetime estimates that match the WMO 2022 values for CFC-13, -115 and -114a nearly perfectly and that agree with CFC-114 within less than 10%. The lifetimes predicted for CFC-13 and CFC-115 in section 3.3.2 were substantially shorter than those in WMO 2022. As can be seen in Figure 3.18 a-b, even the scenarios with the most extreme increases in circulation or chemistry do not produce lifetimes as short as those derived in section 3.3.2. For CFC-114 the lifetime derived from observations in section 3.3.2 is closer (though within the uncertainties) to the WMO 2022 estimate than the GSFC baseline scenario (Figure 3.18c). CFC-114a also has a shorter

lifetime estimate in section 3.3.2 than the GSFC baseline scenario or the estimate in WMO 2022, but the difference is just within the uncertainties of the WMO estimate (Burkholder *et al.*, 2022).

One feature of Figure 3.17 and Figure 3.18 that stands out is the lack of symmetry. For example, in Figure 3.17a the O(<sup>1</sup>D)+Photolysis fast scenario lifetime is 31.2% smaller than the baseline while the O(<sup>1</sup>D)+Photolysis slow scenario lifetime is 49.2% larger than baseline. This asymmetry is most evident in the chemistry scenarios but is still present in the circulation scenarios as well. I have corresponded with Dr Fleming (of the Goddard Space Flight Centre, who provided the model data from this model) and this asymmetry is a known feature of the model; he speculates it could be related to asymmetry in the ozone response from the associated chlorine changes, which then feeds back on the lifetimes, but its exact cause is currently unknown.

The second reason for the asymmetry between scenarios, and bias with regard to the observational data, is that there are always additional factors which influence how quickly a compound is broken down. If the only limiting factor for how quickly a compound is disassociated is the reaction rate, then speeding or slowing that reaction rate in the model will be reflected in the decrease or increase in mean age shown in Figure 3.14 and Figure 3.15. This should generally be true for circulation scenarios (where there is a clear relationship between mean age and circulation speed/strength). It should also be true for the chemical scenarios, provided only the reaction rates change with the circulation remaining constant with no significant feedback mechanism via radiation. The GSFC does not appear to have implemented such radiation feedbacks (Fleming *et al.*, 2002).

However, if the factor being changed is not the limiting factor (or is not the only limiting factor), for example because the reaction has already reached saturation point, then there will be less (or even no) change in the tracer's mixing ratio, and this is reflected in Figure 3.14 and Figure 3.15.

#### *3.3.4.d Fractional Release Factors from the GSFC*

As noted in section 3.3.4.a the correlation between mean age and mixing ratio was compact; however, the model predicts much longer stratospheric lifetimes (section 3.3.4.c) than were found in section 3.3.2. If the model is accurately simulating the mean age -tracer

correlation, but not the lifetime, this poses the question of whether FRFs derived using the GSFC data would be comparable to those from in-situ measurements (section 3.3.1). So I calculated FRFs for each compound both individually for each campaign, and combined for all campaigns. I did this for both the Geophysica data, and the GSFC data.

Figure 3.19 shows the FRFs (from both Geophysica and GSFC) for each campaign and compound, plotted against mean age. I used the same method as described in section 3.2.4. I did this for the baseline scenario, for the most extreme (M20 and P20) circulation scenarios, and the combined O(<sup>1</sup>D) and Photolysis plus/minus scenarios. I left off the other scenarios primarily because the plots would become increasingly visually confusing, and the most extreme scenarios would show most clearly what effect (if any) changing those factors had on the FRFs. For the aircraft based FRFs, as in section 3.2.4, a 5n dataset was created using both the original mean age and FRF pairs, and the uncertainty range. This 5n dataset is represented in Figure 3.19, so the figure does not include error bars, but the spread of data points does give an indication of what that range is. This is for several reasons; firstly, each campaign has few samples compared to the GSFC data, so representing the data in this way cuts down on the signal-to-noise ratio present. Secondly, with such a large dataset and such a complex multiplot figure it was difficult to use traditional error bars in a way that was visually distinct without obscuring the data. In short this design choice was in aid of visual clarity, and should still represent the uncertainty from both FRFs and mean ages (in both cases this ultimately is derived from instrument precision).

As was explored in sections 3.3.4.a, b and c, long lived compounds show an effect from changes to circulation and chemistry, while the shortest lived compound was only effected by changes in circulation, and this is seen in Figure 3.19.

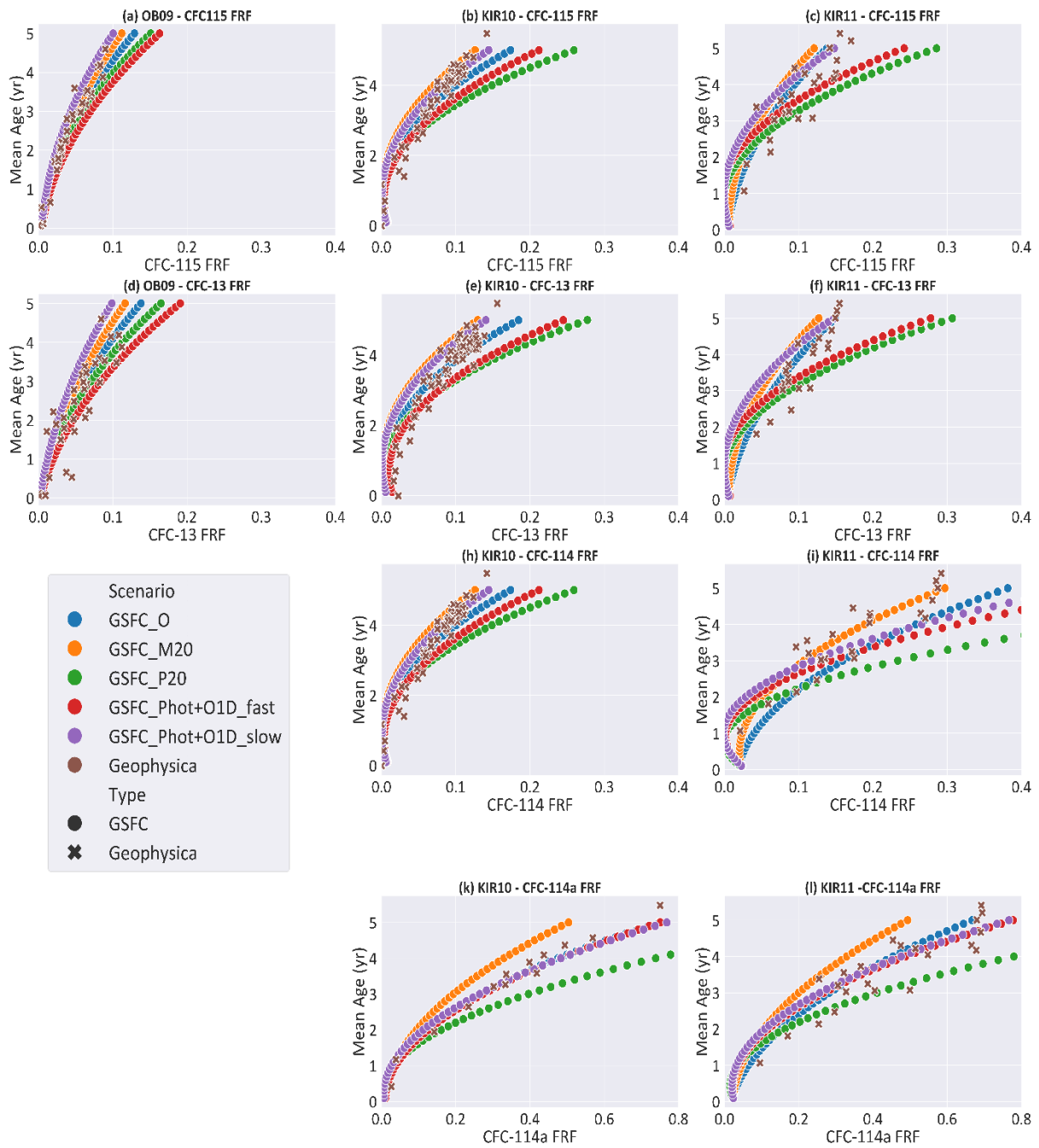


Figure 3.19. The FRF for each compound, for each campaign, plotted against Mean Age (yr). Includes both Geophysica data, and data from the GSFC. GSFC scenarios included were: GSFC\_O (Baseline), GSFC\_M20, GSFC\_P20, GSFC\_Phot + O1D fast, and GSFC\_Phot + O1D slow. OB09 data is absent for CFC-114 and CFC-114a. Please note x axis is the same for all compounds except CFC-114a. This is because CFC-114a has FRFs larger than 0.4, but if all x axes were expanded to 0.8 it would be increasingly difficult to see details for other compounds.

One conclusion that can be drawn from Figure 3.19 is that the mean age-FRF correlation is not unique, so seasonality and spatial variations cannot be neglected. This raises the question of how many observations are needed to quantitatively describe the

mean age-FRF relation. Looking at CFC-115 (Figure 3.19a-c), and CFC-13 (Figure 3.19d-e), in the OB09 campaign, the chemistry scenarios have the greater impact on the magnitude of the FRFs, but for the two Kiruna campaigns, the circulation scenarios seem to have the greater impact. As OB09 does not have data for CFC-114 and CFC-114a, we can't compare these, but for their respective Kiruna campaigns, circulation had the strongest impact for both, and chemistry had little noticeable effect for CFC-114a (the shortest-lived compound of the four).

Each campaign shows a different pattern. In the OB09 campaign all scenarios have profiles which are relatively straight and vertical. The KIR10 campaign shows a curve that is most pronounced below 2 years mean age (and is clearest for CFC-114a Figure 3.19k). KIR11 has a significantly more dramatic curve, and more rapid flattening out. This can be seen most clearly in Figure 3.19i, where the P20, and both chemistry scenarios bend sharply away from the baseline scenario (with the M20 scenario having a less pronounced but still notable curve). The shortest-lived compound, CFC-114a flattens out most.

There are a few possible explanations for these different profiles. In the OB09 and KIR10 campaigns, the observational data points are more tightly clustered, than in the KIR11 campaign where they appear more scattered. Perhaps the KIR11 campaign was naturally more varied for some reason, and the model struggled to accurately reproduce it. Oberpfaffenhofen and Kiruna differ in latitude by roughly 20 degrees, which could explain some of the differences in their respective profiles. This is due not due to the 20 degrees specifically but transport barriers in the stratosphere, particularly for the Kiruna 2010 campaign which took place in a region close to the polar vortex.

As discussed in section 3.3.4.a the campaigns occurred at similar times of year (with Oberpfaffenhofen in early November, Kiruna 2010 in late January, and Kiruna 2011 in early December), so the effect of season on FRF was not expected to be large. However, transport patterns during November in the midlatitudes are rather different from patterns in the high latitudes in December and January, and this could potentially account for some of the differences seen here. Section 3.3.4.c saw that the steady-state stratospheric lifetimes estimated for each compound varied year to year (Figure 3.27), so the model is showing some variation in conditions between years. The exact reason for the pattern observed in Figure 3.19 is difficult to discern given the large number of potential variables, such as the

effects of season, latitude, and the difficulties of comparing a 2D model's dataset 'point-to-point' with in-situ measurements.

So there is variation between years and scenarios, so next I investigated how strongly does this variation affect the FRF at 3 or 5 years mean ages derived from the data. Figure 3.20-Figure 3.23, show the FRF at 3 or 5 years mean ages derived for each compound, using either GSFC data or Geophysica data. As the chemistry scenarios used the JPL-15 recommendations (Sander *et al.*, 2006) we could be confident that the underlying chemistry (though not necessarily how it is handled in the model) was largely reliable (kinetics for CFC-114 aside), while the circulation scenarios carried more unknowns. Therefore FRFs 3 and 5 years mean ages were generated for the baseline FRFs, in which I included only data from the baseline scenario. For the '+ chemistry' FRFs I included the baseline scenario, the increased O(<sup>1</sup>D) and Photolysis scenario, and the decreased O(<sup>1</sup>D) and Photolysis scenario. The '+chemistry+circ' included all of these as well as the P20 and M20 data.

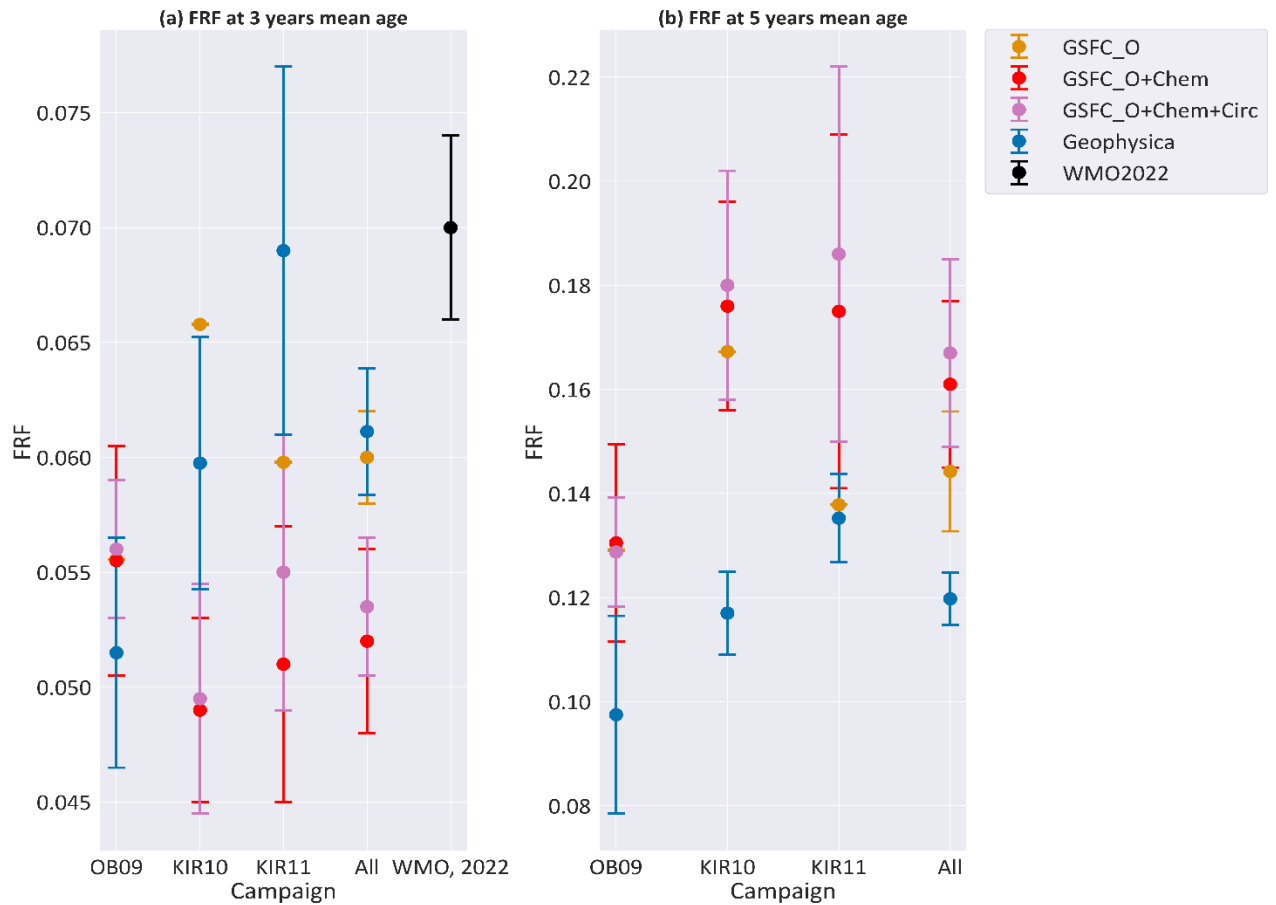


Figure 3.20. FRFs at (a) 3 years and (b) 5 years mean age, for CFC-115 derived using either data from the corresponding Geophysica flight, compared to FRFs derived using GSFC data, with the FRF listed in the WMO 2022 (Burkholder et al., 2022) for comparison (only present for FRF at 3 years mean ages). Error bars represent the span of possible FRFs at 3 or 5 years mean age, as generated by the bootstrapping procedure (see section 2.5). This is either done using only FRFs-mean ages from a single campaign, or all FRFs and mean ages from all campaigns (the 'All' value).

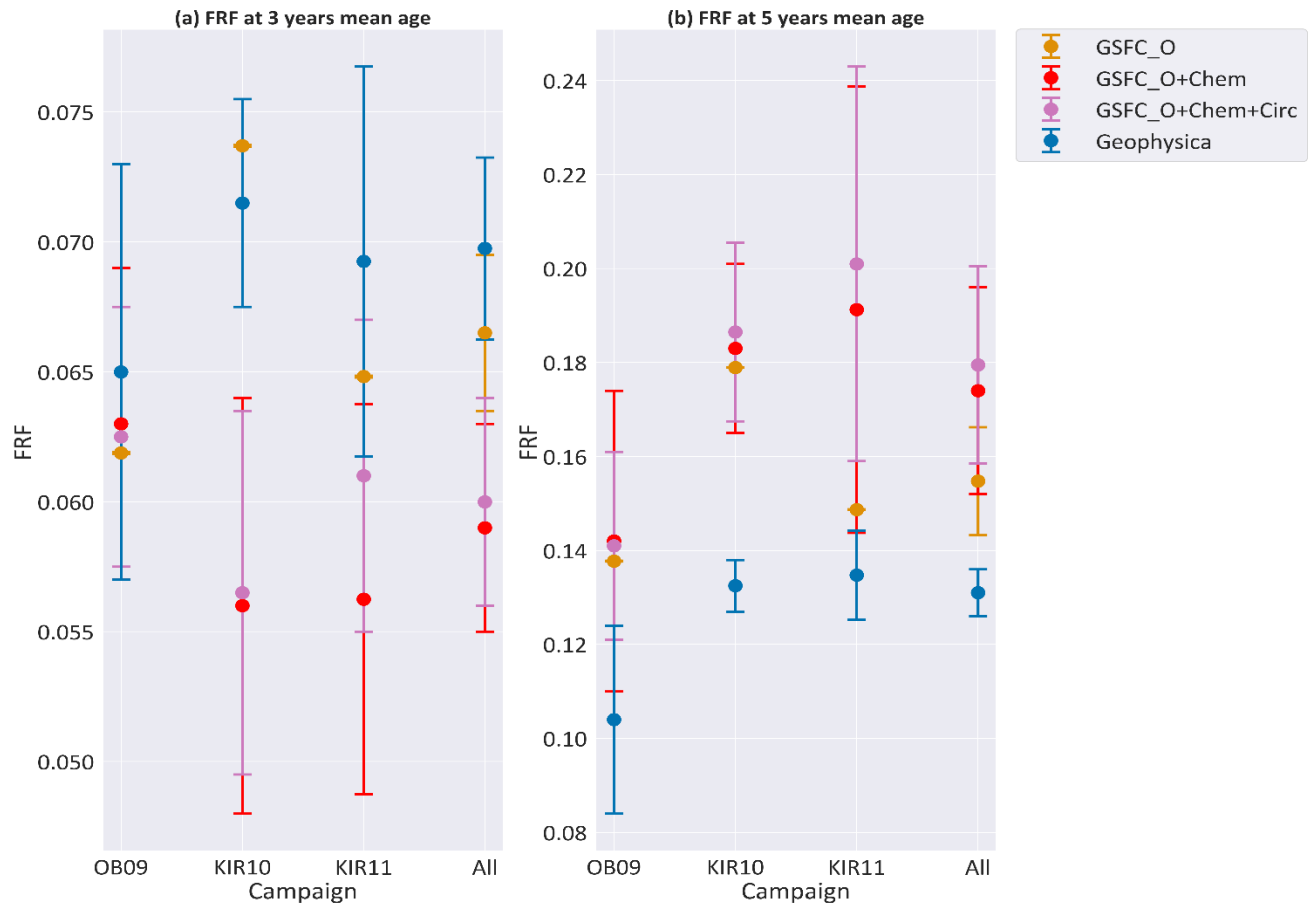


Figure 3.21. FRFs at (a) 3 years and (b) 5 years mean age for CFC-13 derived using either 'real' data from the corresponding Geophysica flight, compared to FRFs derived using GSFC data. Error bars represent the span of possible FRFs at 3 or 5 years mean age, as generated by the bootstrapping procedure (see section 2.5). This is either done using only FRFs-mean ages from a single campaign, or all FRFs and mean ages from all campaigns (the 'All' value).

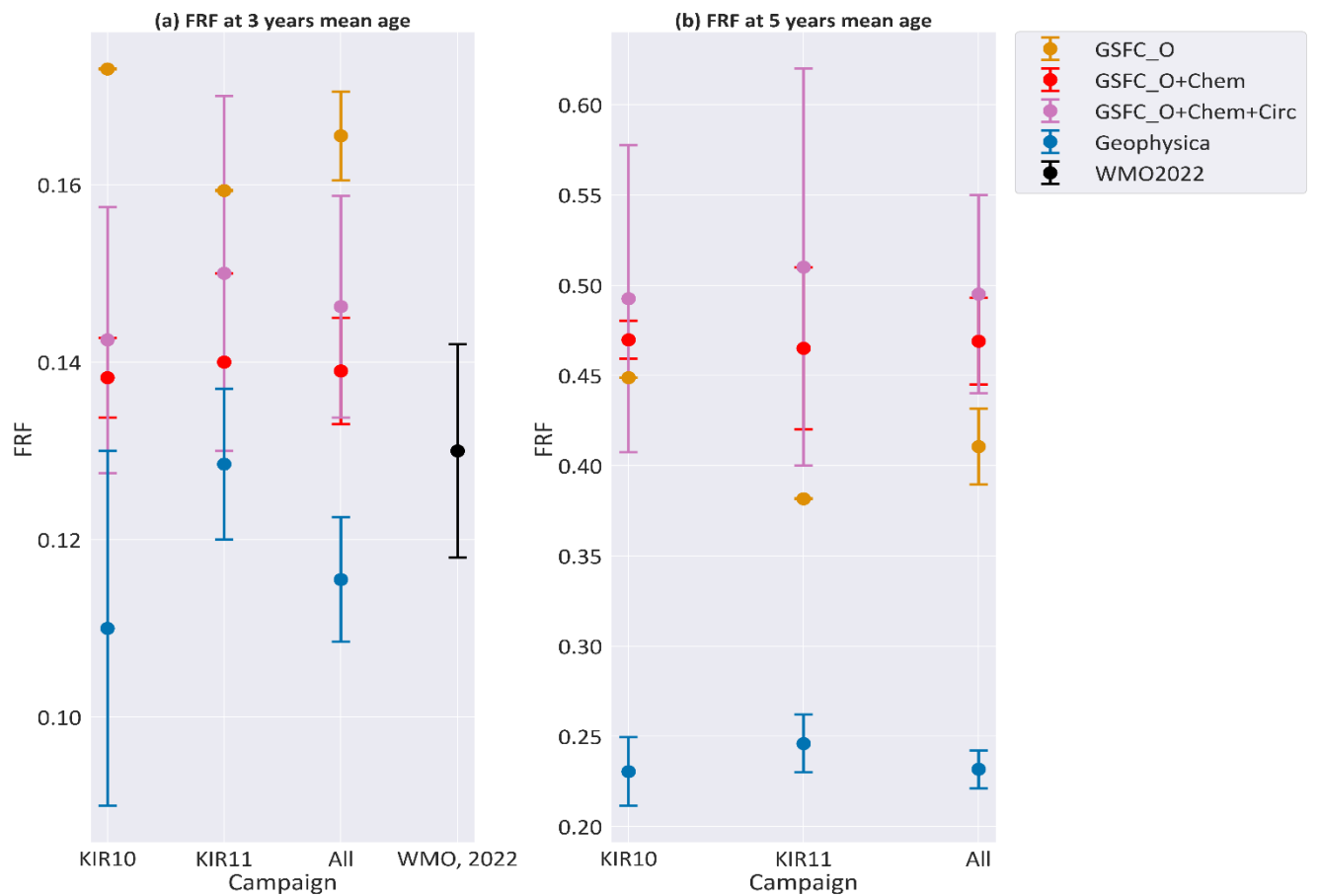


Figure 3.22 FRFs at (a) 3 years and (b) 5 years mean age for CFC-114 derived using either ‘real’ data from the corresponding Geophysica flight, compared to FRFs derived using GSFC data. Includes the estimate for FRF at 3 years mean age from WMO 2022 (Burkholder et al., 2022). Error bars represent the span of possible FRFs at 3 or 5 years mean age, as generated by the bootstrapping procedure (see section 2.5). This is either done using only FRFs-mean ages from a single campaign, or all FRFs and mean ages from all campaigns (the ‘All’ value).

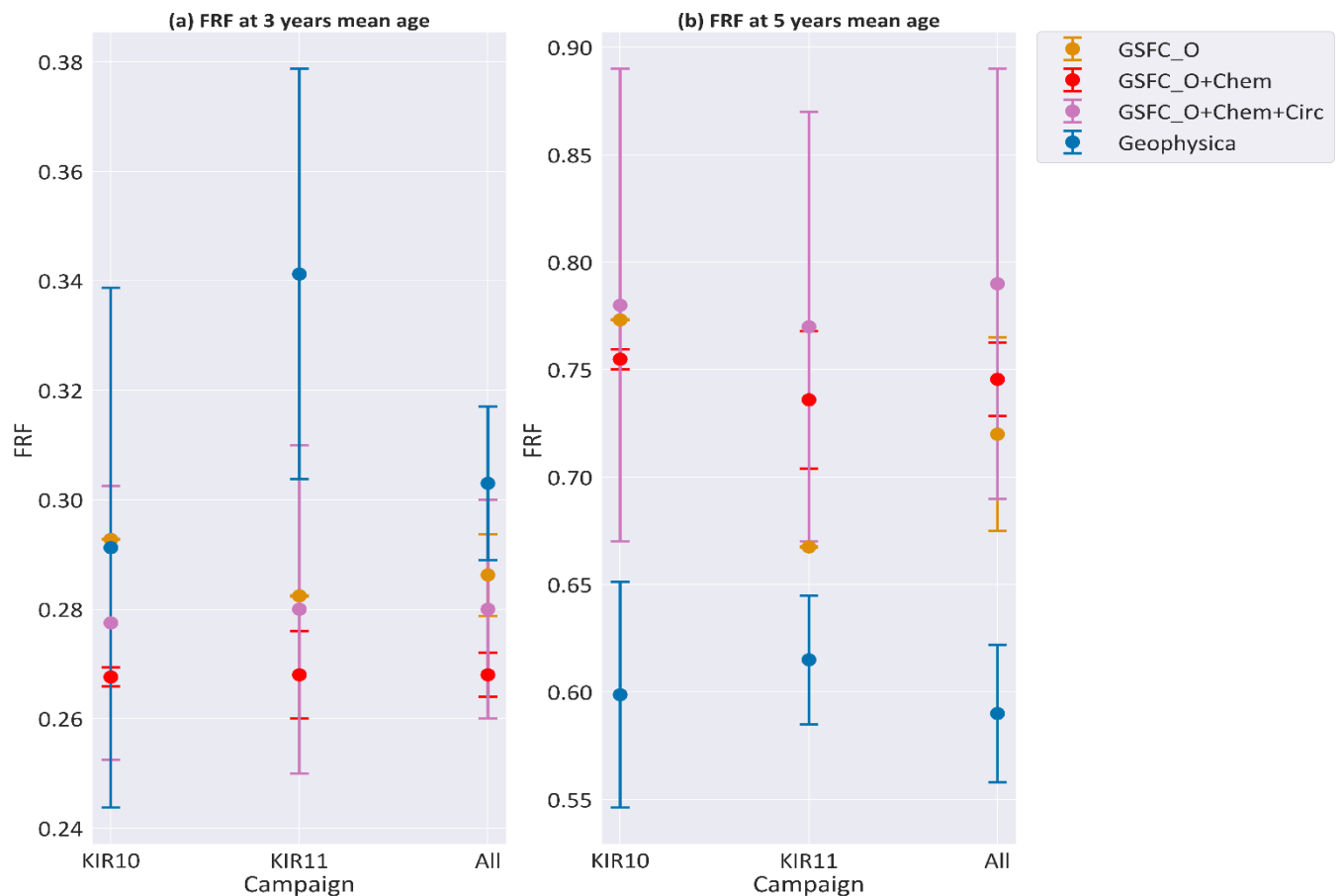


Figure 3.23 FRFs at (a) 3 years and (b) 5 years mean age for CFC-114a derived using either ‘real’ data from the corresponding Geophysica flight, compared to FRFs derived using GSFC data. Error bars represent the span of possible FRFs at 3 or 5 years mean age, as generated by the bootstrapping procedure (see section 2.5). This is either done using only FRFs-mean ages from a single campaign, or all FRFs and mean ages from all campaigns (the ‘All’ value). There is no FRF value for this compound listed in WMO 2022 (Burkholder *et al.*, 2022).

Looking at the FRF at 3 years mean ages for CFC-115 (Figure 3.20) only the KIR11 Geophysica derived FRF overlapped with the WMO 2022 (Burkholder *et al.*, 2022) estimate. The uncertainty range for the GSFC chemistry and circulation FRFs is not noticeably larger than the uncertainty range from just the chemistry and baseline scenarios. The uncertainty range of the GSFC derived FRFs often, though not always, overlaps the FRFs derived from the Geophysica data. Due to the asymmetrical nature of the scenario data, it is not surprising that incorporating these scenarios when calculating FRFs gives FRFs that are skewed somewhat, giving higher or lower FRFs than the baseline scenario. For the FRF at 3 years mean ages, the Geophysica FRFs are usually higher than those derived from the GSFC data. However, in the FRF at 5 years mean ages, the reverse is true. If we refer to Figure

3.19a-c, at 3 years mean age the profiles are relatively close together, but by 5 years they have diverged considerably. At higher mean ages the differences in the scenarios are significantly more pronounced, and this is reflected in the FRF at 5 years mean ages. This may also explain why the OB09 FRFs at 3 and 5 years mean ages show relatively good agreement between the GSFC FRFs and the Geophysica FRFs. As can be seen in Figure 3.19a the OB09 profiles are the most compact and least curved. This is a consequence of where and when the OB09 campaign sampled (November, midlatitude, in an area of the stratosphere which is well mixed), compared to the later Kiruna campaigns (winter, close to the polar vortex, a strong, localised transport barrier in December and January).

This is also seen in Figure 3.21 where the FRFs at 3 and 5 years mean ages for CFC-13 for the OB09 campaign generally agree within the uncertainty ranges, while there is greater spread for the Kiruna campaigns. And as with CFC-115, there is relatively little increase in the uncertainty range between the GSFC baseline and chemistry FRFs, and the GSFC baseline, chemistry and circulation FRFs.

For CFC-114 the Geophysica FRF at 3 years mean ages all overlapped with the WMO 2022 estimate (Figure 3.22). The FRFs from the GSFC baseline scenario do not overlap with the WMO 2022 estimate and was notably higher; however, both the chemistry only and chemistry + circulation scenarios did. The chemistry only scenarios give a notably smaller range of uncertainty than the chemistry and circulation scenarios.

In Figure 3.23 the Geophysica FRF at 3 years mean ages for CFC-114a overlap within the uncertainty ranges of at least the chemistry and circulation scenarios. However, this ceases to be the case for the FRF at 5 years mean ages. In Figure 3.19k-j the profile for both KIR10 and KIR11 is very curved and flattens out more quickly than for other compounds. As CFC-114a is the shortest lived of these compounds, this makes sense. It should also be noted that in Figure 3.23 the uncertainty range for the GSFC FRFs that included both circulation and chemistry are significantly larger than those that just included chemistry.

Lifetimes for these compounds were generated using these FRF-mean age correlations in section 3.3.4.c, and this was done for the baseline scenario, the 'Baseline+Chemistry' scenario, and the 'Baseline+Chemistry+Circulation' scenario. These will be compared to the lifetimes the GSFC directly predicted which will be labelled 'GSFC\_Prediction'. The result is Figure 3.24.

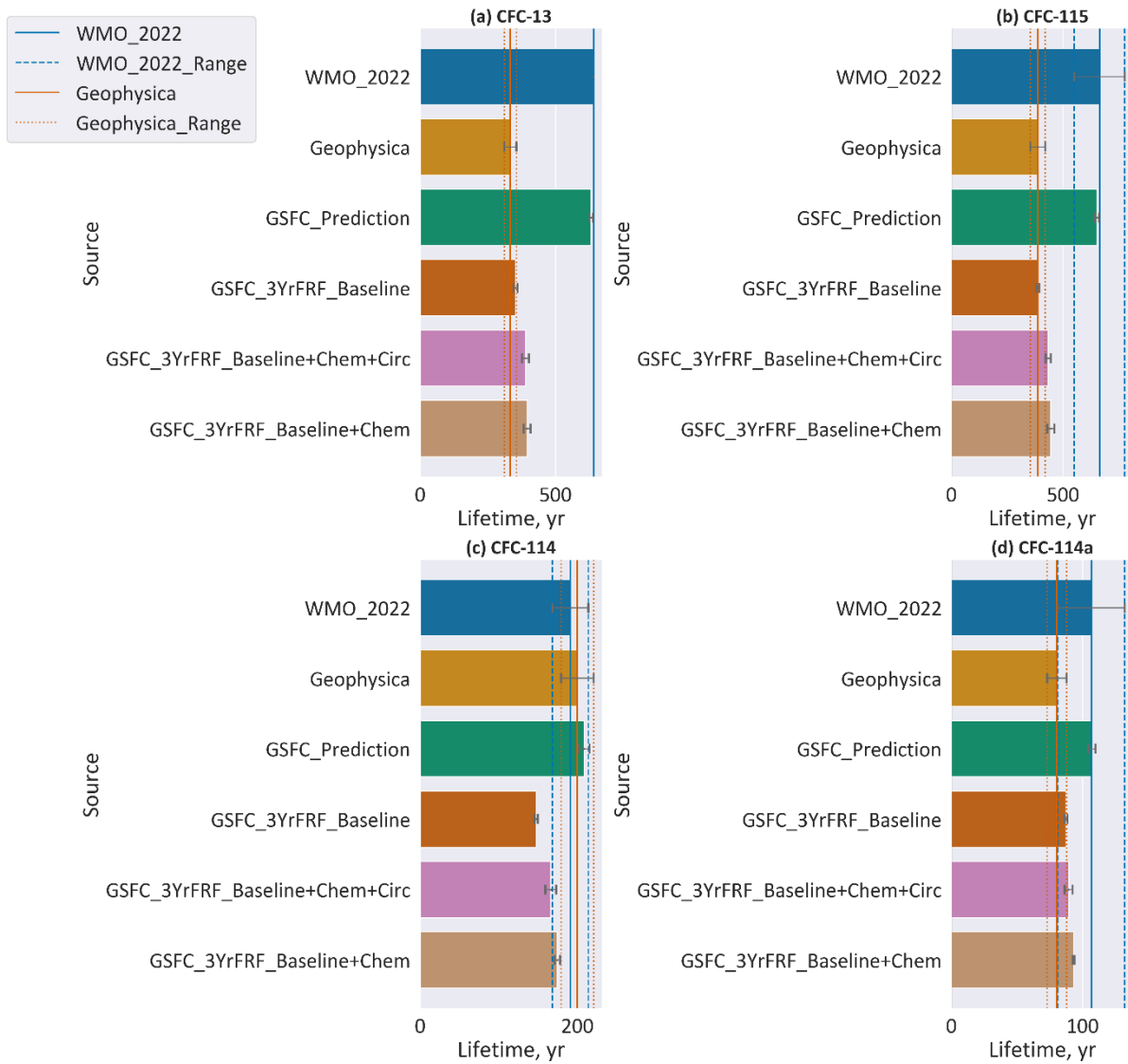


Figure 3.24. The steady-state stratospheric lifetimes (yr) of (a) CFC-13, (b) CFC-115, (c) CFC-114, and (d) CFC-114a, generated using different methods, and compared to the estimate in the WMO 2022 (Burkholder *et al.*, 2022) ‘Geophysica’ refers to lifetimes generated using FRFs using the Geophysica research flight; these lifetimes are listed in section 3.3.2. ‘GSFC\_Prediction’ refers to the steady-state stratospheric lifetimes generated by the GSFC baseline scenario (section 3.3.3.d). The remaining sources are the lifetimes derived using the FRF at 3 years mean ages derived from the GSFC tracer-mean age correlation, using baseline scenario only, baseline +chemistry+ circulation scenarios, and baseline + chemistry scenarios respectively.

As can be seen from Figure 3.24 the lifetimes predicted by the GSFC are in agreement with those used in WMO 2022 (Burkholder *et al.*, 2022). However for CFC-13 and CFC-115 (Figure 3.24a-b), none of the lifetimes derived using FRFs, either from Geophysica research flights, or from the GSFC’s data, line up with the WMO 2022 lifetime estimate or the GSFC’s predicted lifetime. For CFC-114 (Figure 3.24c) the uncertainty range for WMO 2022 just overlaps with the ‘baseline +chemistry+ circulation scenarios’ and ‘baseline +

chemistry scenarios', but not the baseline-only lifetime. And for CFC-114a (Figure 3.24d), all lifetimes agree within the uncertainties.

As mentioned in section 3.2.5, Douglass et al., (2008) discusses model simulations which had used realistic mean ages and FRF distribution and resulted in predictions of longer atmospheric lifetimes for CFCs, than those predicted from observations. Why the GSFC 2D model data gives tracer-mean age correlations (and from this, FRFs and lifetimes) that match the in-situ measurements, but the direct predictions provided by the model do not, is unclear, and outside the scope of this thesis as it would necessitate a thorough investigation of the model source code. However, it is worth highlighting as an example of why in-situ measurements are so vital for providing ground-truthing to models.

One possible explanation is the effect of seasonality on FRFs at the 3 year mean age level; Figure 3.11 shows potential temperature plotted against mean age for all three campaigns), and there is a notable difference between the OB09 campaign which took place in autumn and the KIR10 and KIR11 campaigns which took place in winter. There may also be effects from different latitudes (tropical, extra tropical, polar etc...) and potential influence from the polar vortex. It is possible for two parcels of air to have the same 'mean' age, but different tracer mixing ratios (and thus different FRFs). As the chemical sinks or sources have non-uniform distributions in both the stratosphere and the mesosphere, the combination means that there are different pathway distributions for the same mean age (as well as for the same age spectra/transit time distribution). Lower tracer mixing ratios (and thus higher FRFs) can be found in the 3 year mean age level in the extra tropics during winter, the phase in which there is the strongest downwelling in the northern hemisphere's stratosphere (Young *et al.*, 2011). This feature can be seen in Figure 3.19 where the baseline GSFC scenario shows a systematic shift between mid-latitude OB09 campaign in autumn and the winter campaigns in Kiruna 2010 and 2011. While this is visible in the observational data, it is less visible due to the comparatively sparse data and the large internal variability. KIR11 may also have contained samples affected by intrusion by the polar vortex, and in Figure 3.19 for KIR11 the mean age-FRF correlation is the one that sees the strongest increase of FRFs with mean age.

As the air samples stemmed from regions and seasons with the highest FRFs at the 3 years mean age level (taking place in autumn or winter), the estimated lifetime is lower than that computed by the model as this is an annual global mean, calculated using the relation

between burden, loss and/or sinks. The difficulty of accounting for seasonality and latitude with regards to FRFs will be explored further in Chapter 4 section 4.4.2.

#### *3.3.4.e Stratospheric tracer transport in CLaMS and GSFC.*

To model atmospheric processes accurately, models need extensive observations of the systems they seek to reproduce, for as great a span of time as possible. These observations include meteorological parameters, wind, pressure, temperature, etc... as well as potentially some chemical species such as water and ozone. However, observations are not always evenly distributed or may contain gaps due to the practical considerations of collecting observations. They will also come with their own set of uncertainties from, for example, instrument precision. Models use 'reanalyses' to fill those gaps in the observational record. These reanalyses are able to combine atmospheric observations with a global weather forecast model, and using a data assimilation system to sequentially compare new observations to previous model forecasts, and this allows consistent reprocessing of the meteorological observations, and this can span large periods of historical data. Reanalysis should do this in a way that should be consistent in time, allowing a consistent reprocessing of the in-situ observations; this enables the creation of gridded datasets for a broader range of variables than might otherwise be (Dee *et al.*, 2011; Gelaro *et al.*, 2017; Ploeger *et al.*, 2019).

The two models have some differences in terms of tracer transport. CLaMS' transport is driven by meteorological 'reanalysis' datasets (e.g. ERA-Interim, ERA5, JRA55, MERRA-2) (Ploeger *et al.*, 2019), while the GSFC calculates transport parameters from climatological values of temperature, H<sub>2</sub>O, zonal wind, and ozone. These were derived from a meteorological reanalysis dataset (MERRA-2).

CLaMS used the all three reanalysis for the model run shown in Figure 3.8, Figure 3.9, and Figure 3.10. And this demonstrates that the reanalysis used can substantially influence the results. Notably Ploeger *et al.*, (2019) ran CLaMS using three different reanalyses including MERRA-2 and found that the age spectrum tail was much more pronounced for MERRA-2, and age spectrum values were more than twice as large as the JRA-55 and ERA-Interim values at transit times larger than ~ 8 years. This results in MERRA-2

giving a substantially larger fraction of very old air. The MERRA-2 showed slower transport, and thus larger transit times (and older ages), and consistently gave substantially older mean ages compared to the other reanalyses.

Given that the MERRA-2 reanalysis consistently provides older AoA, the question remains why in Figure 3.8c, Figure 3.9c, and Figure 3.10c, as well as Figure 3.12, does the GSFC (which uses the MERRA-2) simulate mean ages that are comparable with the observational data? To explore this I analysed CLaMS data for each campaign using three different reanalyses: ERA-Interim, MERRA-2, and JRA-55, and compared it to the corresponding GSFC data (Figure 3.25, Figure 3.26, and Figure 3.27).

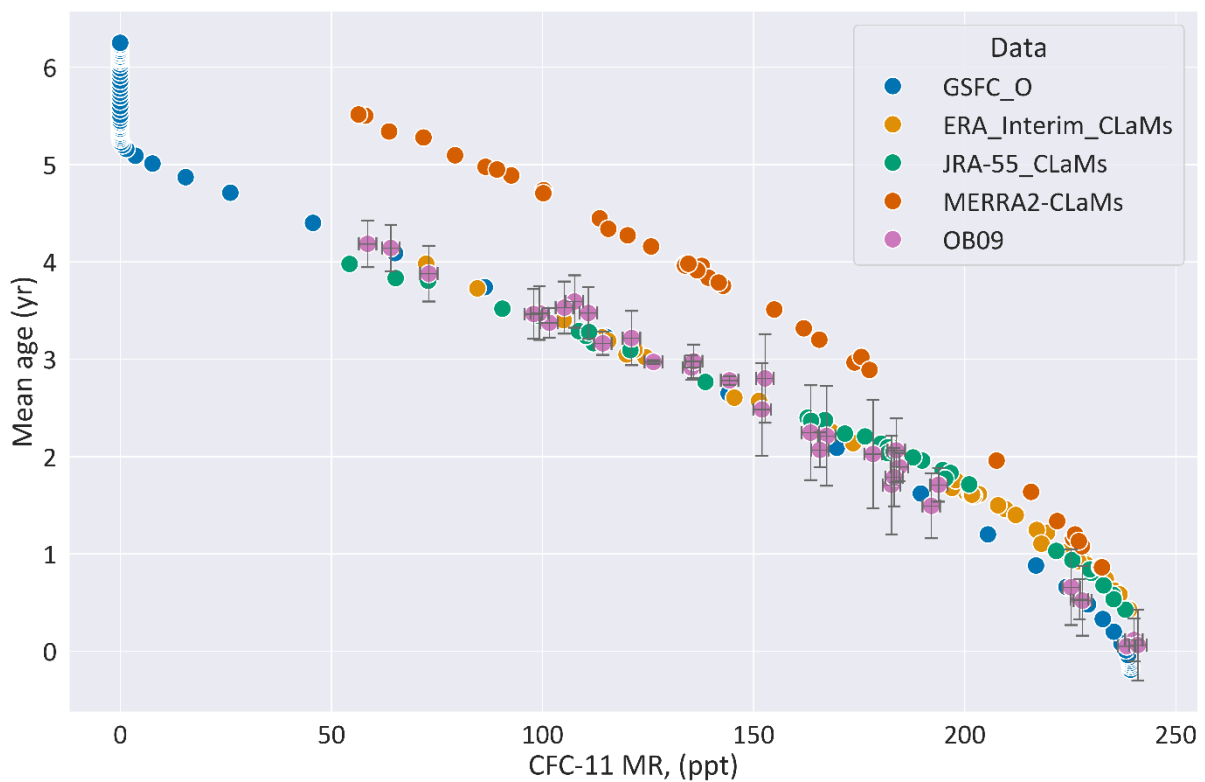


Figure 3.25. CFC-11 MR (ppt) plotted against mean age for the OB09 campaign. Included are the observational data, the baseline GSFC scenario, and the output from CLaMS using the ERA\_Interim, JRA-55, and MERRA-2 reanalysis. Neither model provided uncertainty ranges. Error bars for the observational data are derived from instrument precision uncertainty.

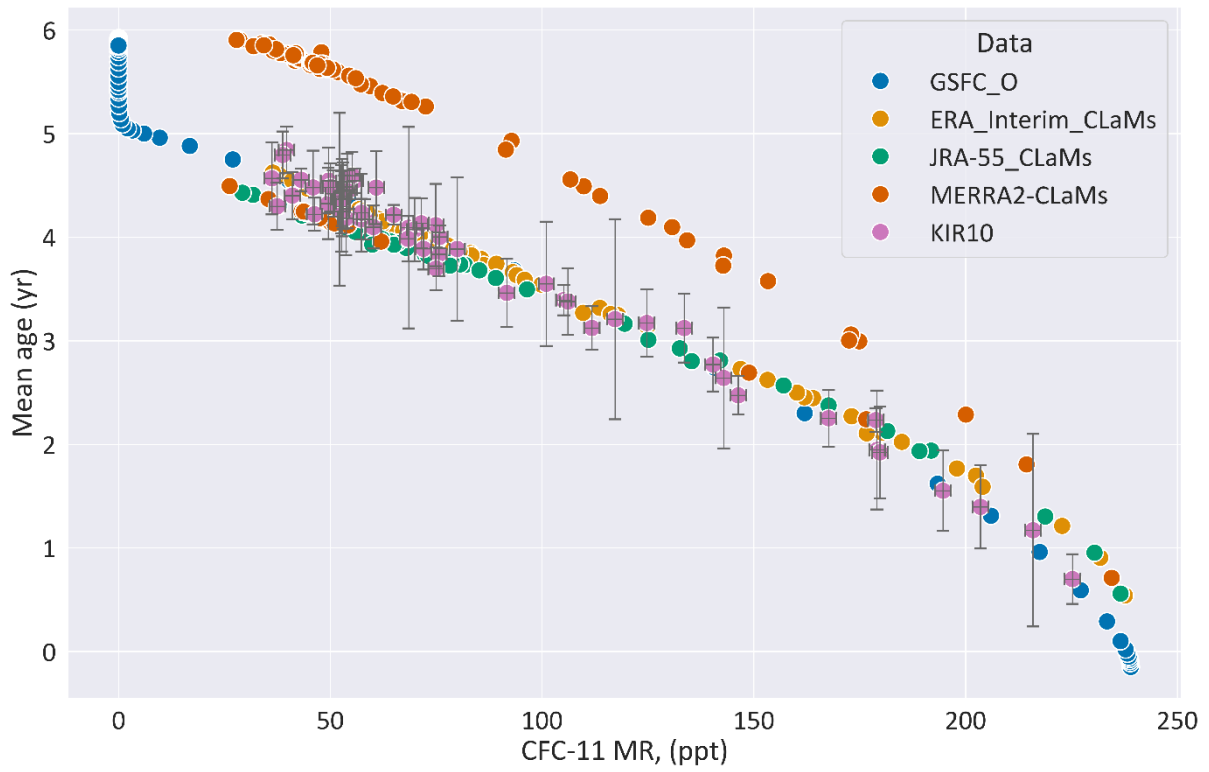


Figure 3.26. CFC-11 MR (ppt) plotted against mean age for the KIR10 campaign. Included are the observational data, the baseline GSFC scenario, and the output from CLaMS using the ERA\_Interim, JRA-55, and MERRA-2 reanalysis. Neither model provided uncertainty ranges. Error bars for the observational data are derived from instrument precision uncertainty.

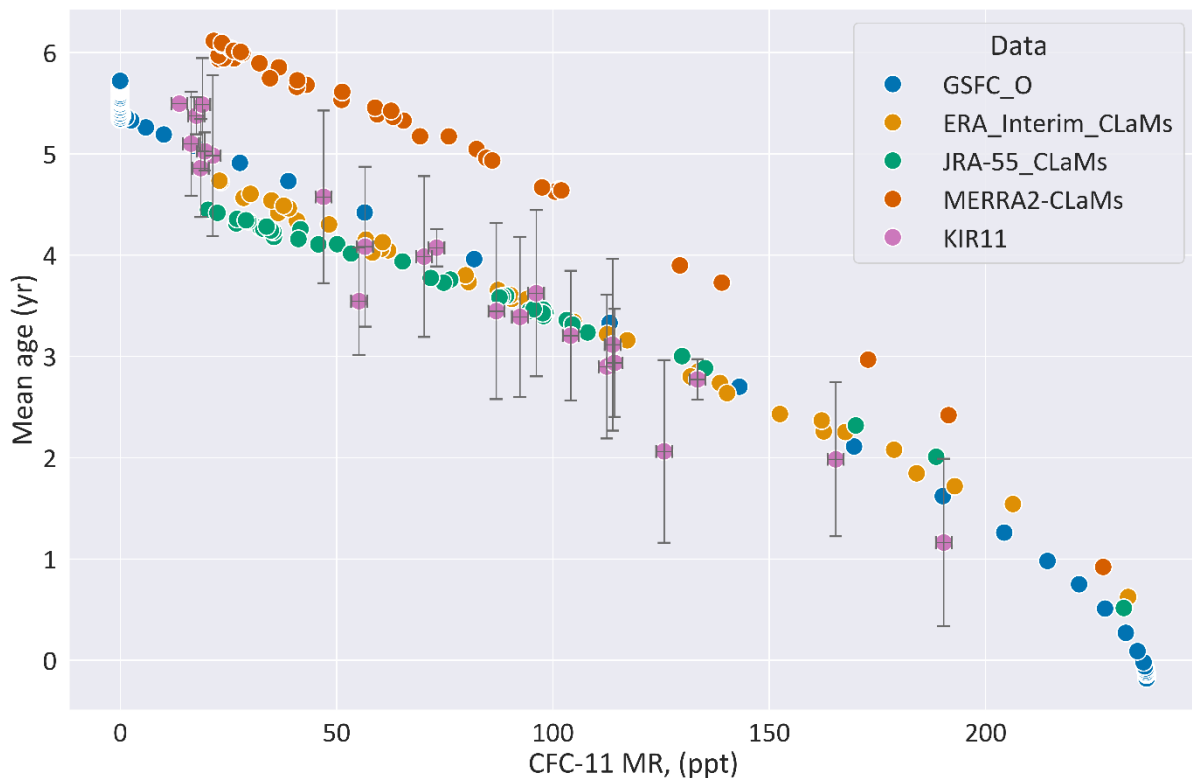


Figure 3.27. CFC-11 MR (ppt) plotted against mean age for the KIR10 campaign. Included are the observational data, the baseline GSFC scenario, and the output from CLaMS using the ERA\_Interim, JRA-55, and MERRA-2 reanalysis. Neither model provided uncertainty ranges. Error bars for the observational data are derived from instrument precision uncertainty.

As can be seen clearly in Figure 3.25, Figure 3.26, and Figure 3.27 the model data for CLaMS' Merra-2 run has a significant bias towards higher mean ages. This is not seen in GSFC data, which is unexpected as it uses the same reanalysis. However, the GSFC model uses a 'nudged' MERRA-2 reanalysis. Normally 'nudging' refers to the process within a model in which the calculated temperature and wind fields are constrained to observed fields, and those fields can be relaxed or strengthened across a given model time step. However, in the GSFC 2D model, the model transport fields (residual meridional circulation, eddy mixing etc...) are computed offline from the MERRA-2 temperatures, winds and heating rates. The resulting residual circulation and eddy transport fields are then input into the model and used to transport chemical constituents. This could explain why the GSFC data in Figure 3.25, Figure 3.26, and Figure 3.27 is largely comparable to the observational data, and to CLaMS\_JRA-55 and CLaMS\_ERA-Interim.

#### *3.3.4.f Summary of Model Results*

Section 3.3.4 set out to investigate a number of questions relating to the model data provided by the GSFC 2D model, and how well it compared to in-situ measurements. The mean age to tracer correlation is the basis for the calculation of lifetime using observational data in section 3.3.2. Section 3.3.4.a investigated how well the model was able to simulate this correlation. It found that the mean-age tracer correlation for in-situ measurements in comparisons to the GSFC data, were inside the uncertainties, with the exception of CFC-114. CFC-114 is an outlier throughout this section, and the most plausible mechanism for this is that the GSFC used kinetics data which did not take into account impurities of CFC-114a, and thus overestimated photolysis rates for CFC-114.

In section 3.3.4.b the intention was to look at the impact of changing circulation or chemistry on the distribution of tracers, and what effect this might have on their lifetimes. For circulation, the baseline scenario and observational data agree within the uncertainties, with the exception of CFC-114. CFC-114 seemed to fit better to the M20 (slowest circulation simulation), which fits with the hypothesis that the photolysis rates for CFC-114 are overestimated within the model. As with the circulation simulations, chemistry results also saw the baseline scenario and the observational data agreeing within the uncertainties, with the exception of CFC-114.

In section 3.3.4.c the intention was to compare the model-derived lifetimes to the lifetimes derived using observational data, and to understand the differences. Longer-lived compounds (CFC-13 and CFC-115) were more affected by chemistry than circulation, and conversely the shortest-lived compound explored here (CFC-114a) was most strongly affected by changes to circulation. CFC-114 has a lifetime longer than CFC-114a and shorter than either CFC-13 or CFC-115, and was impacted by circulation and chemistry to a roughly equal extent. When compared to the lifetimes listed in WMO 2022, for all compounds except CFC-114 the baseline scenario fits best. As CFC-114 had several scenarios (notably those with faster circulation or photolysis) which provided lifetimes that were more consistent with the WMO 2022 listed lifetimes than the baseline scenario provided. It should be noted that as discussed in section 1.3 the GSFC changes the speed of the BDC uniformly, but in reality the different branches may speed or slow at different rates. As the sink regions for the CFCs examined here are high in the stratosphere, they would reach

them via the deep branch. So the GSFC may be predicting changes to stratospheric lifetimes for these compounds assuming that the deep branch circulation changes are the same as the shallow branch.

To continue the investigation of how well the model simulates mean-age tracer correlation and lifetime, section 3.3.4.d calculated lifetimes from the GSFC data using the same mean age-FRF correlation method used in section 3.3.2, and compared the results to the GSFC's own lifetime estimates. The resulting GSFC derived lifetimes had good agreement with the observation derived lifetimes; however, they were significantly different from the lifetimes predicted by the GSFC. Section 3.3.4.d speculates that this is potentially because lifetimes derived from local observations do not cover the whole season and only a select part of the stratosphere. In contrast, lifetimes derived from the GSFC model are steady-state lifetimes calculated by the balance of stratospheric burden/loading and loss/sink. While the values of the model are internally consistent, the model uses parameterisation simplifying atmospheric processes. As seen in section 3.3.4.e the MERRA-2 reanalysis used by the GSFC results in elevated mean ages, and needed to be de-coupled from the model at a key stage to avoid bias. We also saw that the kinetics data used for CFC-114 is most likely incorrect, also resulting in a bias. So models can provide many data points, but these are not as well constrained as those gathered from (the less numerous) in-situ measurements. It is also more difficult to calibrate models for compounds with atmospheric lifetimes of 200 years or more so that will be an area of large uncertainty in model output.

Section 3.3.4.e used CLaMS to investigate the impact of the MERRA-2 reanalysis on the GSFC simulations. It found that while driven by MERRA-2 the GSFC produces a good mean age-tracer correlation, but CLaMS showed a significant difference between the profile using MERRA-2 and those using different reanalysis or the observational data. The GSFC is not affected by this due to the transport parameters being 'de-coupled' and calculated separate from the MERRA-2 reanalysis.

### **3.3.5 Archived Air Results**

In addition to calculating FRFs for each compound, the sample mixing ratios were also plotted against the tropospheric background trend for each compound, alongside available data from other campaigns. For CFC-13, CFC-114, and CFC-114a this only included

the Geophysica research aircraft flights detailed in section 3.2.1. For CFC-115, in addition to the Geophysica flights, the AirCore flights that will be covered in depth in Chapter 4 were also included. This is to put the archived air data into its proper historical context, and to allow comparison between methods. Due to both the KAT17 and the TEX15 flights producing very low mean ages (rarely exceeding 2.5 years mean age, with no samples even approaching 3 years mean age), it was not appropriate to extrapolate to FRF at 3 or 5 years mean age for these flights.

It should be noted that while this section does derive FRFs and compares them to those derived using Geophysica flights only, the FRFs derived from archived air samples are not included in section 3.3.1, or this chapter's overall conclusions. This was for a number of reasons, primarily consistency. The Geophysica flights took place between 2009 and 2017, while the archived air samples which provided data from which FRFs could be derived occurred in 1993 and 1999, so there is a ten-year gap between sampling periods. In addition, as will be seen in each compound's results section, both flights (AIRE 93 and GAP 99) have elevated FRFs and unusually large uncertainty ranges (for reasons that will be explored). Therefore, these are not included in the FRFs presented in this chapter's conclusions.

### 3.3.5.a Archived Air Samples of CFC-13 – Results

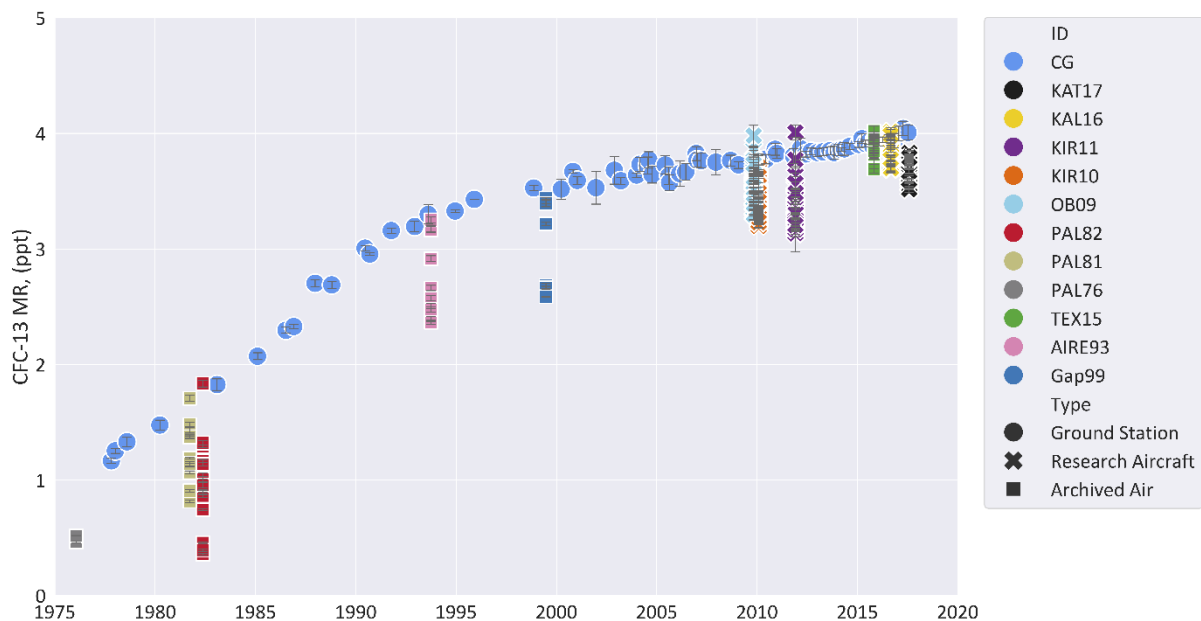


Figure 3.28. Mixing ratios (ppt) for CFC-13, plotted against date. Includes the Geophysica research aircraft flights detailed in section 3.2.1, the archived air samples detailed in section 3.1.3, along with the Cape Grim (CG) tropospheric background trend.

As can be seen in Figure 3.28 the archived air data seems to be as consistent with the tropospheric background trend, as the Geophysica flights. As the trend stretches back in time there are fewer samples for the background trend, and it is harder to assess whether the archived air overlaps or exceeds the background trend for those samples that have been collected near or below the tropopause. However, the fact that most archived air datasets are consistent with the background trend, gives confidence that the archived samples have not been contaminated, were well-preserved and leak-free. For the earliest flight (PAL76) the background trend does not extend far enough back in time to compare the flight to it. This helps illustrate why the oldest 3 flights are not suitable for calculating FRFs; the available background trend simply does not extend far enough back in time for a reliable comparison to be made.

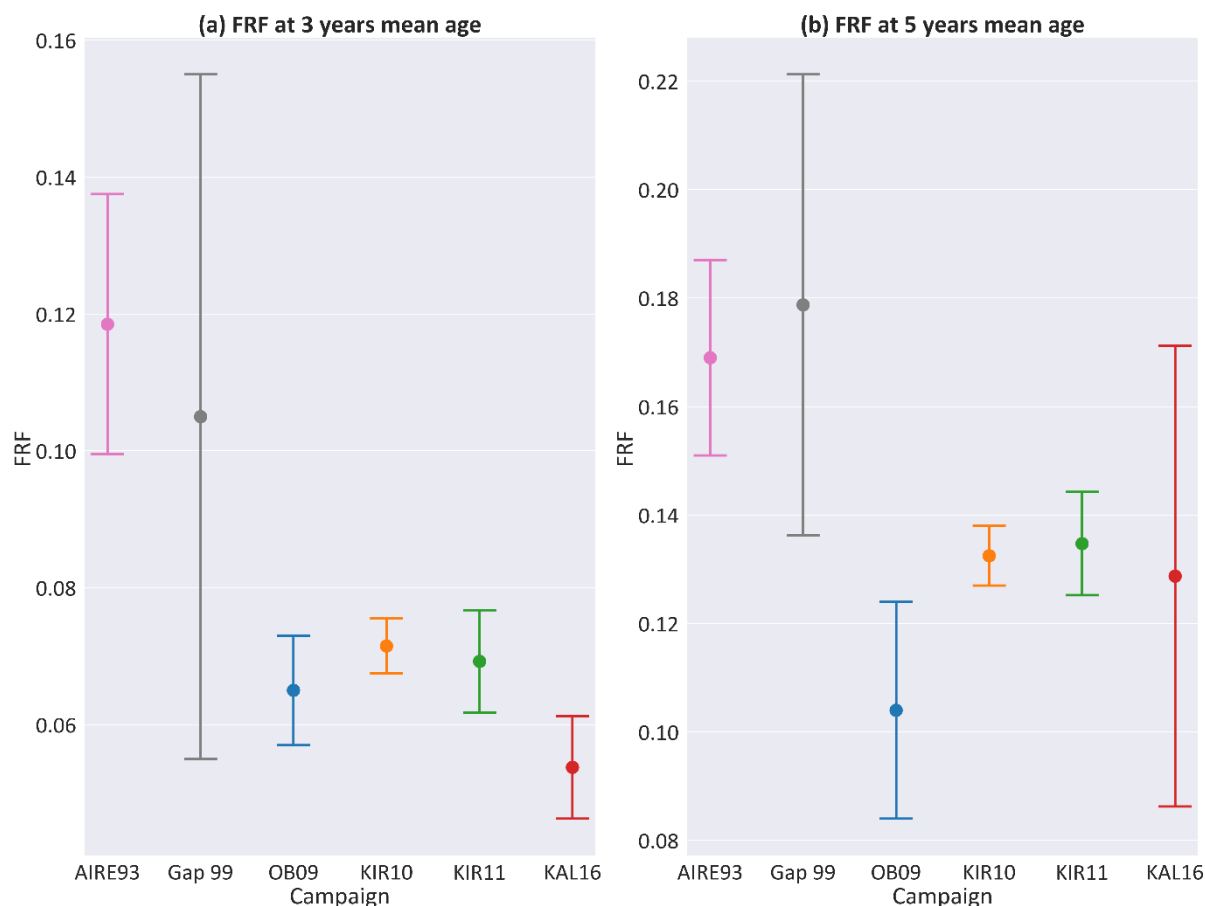


Figure 3.29. For CFC-13, the FRF at (a) 3 and (b) 5 years mean age for each campaign for which data was available for this compound. Uncertainty is to  $1\sigma$  uncertainty and reflects the range for each FRF seen during the bootstrapping procedure detailed in section 2.5.

As can be seen in Figure 3.29 there is variation between the different flights both for FRFs at 3 and 5 years mean age. The archived air samples had the largest uncertainty ranges. This may be due to poor instrument precision when analysing samples, as the device used is known to have had some precision and sensitivity problems at the time. The large uncertainty seems to stem from the larger than average uncertainty spread for mean age seen in these samples, which affected both possible age-tracers PFC-116 and SF<sub>6</sub>. There does not appear to be any clear pattern to the FRFs at 5 years mean age. However, for the FRFs at 3 years mean age the earlier archived air samples (AIRE93 and GAP99) appear to have higher FRFs than all later flights. Despite the variation of FRFs between flights, when uncertainty ranges are taken into account there is substantial overlap. The AIRE93 flight produces a notably higher FRF at both 3 and 5 years mean age. This could be due to latitude (both AIRE93 and GAP99 took place in France, while other flights take place at higher

latitudes, and both flights have higher than average FRFs at 3 and 5 years mean age). It may also be due to season, as the AIRE93 flight takes place in late September (early autumn), while all other flights took place in different seasons (winter, spring, and summer). Ray et al., (2024) found that FRFs collected in the summer were higher than those collected in winter. Sections 4.3.9 and 4.4.2, look more closely at the effects of latitude and season on FRF, so for the sake of brevity this section will not examine them in detail. However, it is worth noting that the effect may be present in the long-lived CFCs examined here.

#### *3.3.5.b Archived Air Samples of CFC-115 -Results*

CFC-115 is the compound for which there is the most included data, with sampling done by high altitude research aircraft, the traditional large high-altitude balloon-borne measurements, and the newer small balloon-borne AirCore technique. This makes Figure 3.30 and Figure 3.31 somewhat harder to parse than the figures for other compounds, but also allows a much broader examination of the compound, the different sampling techniques used, and any effects this may have on the resulting FRFs.

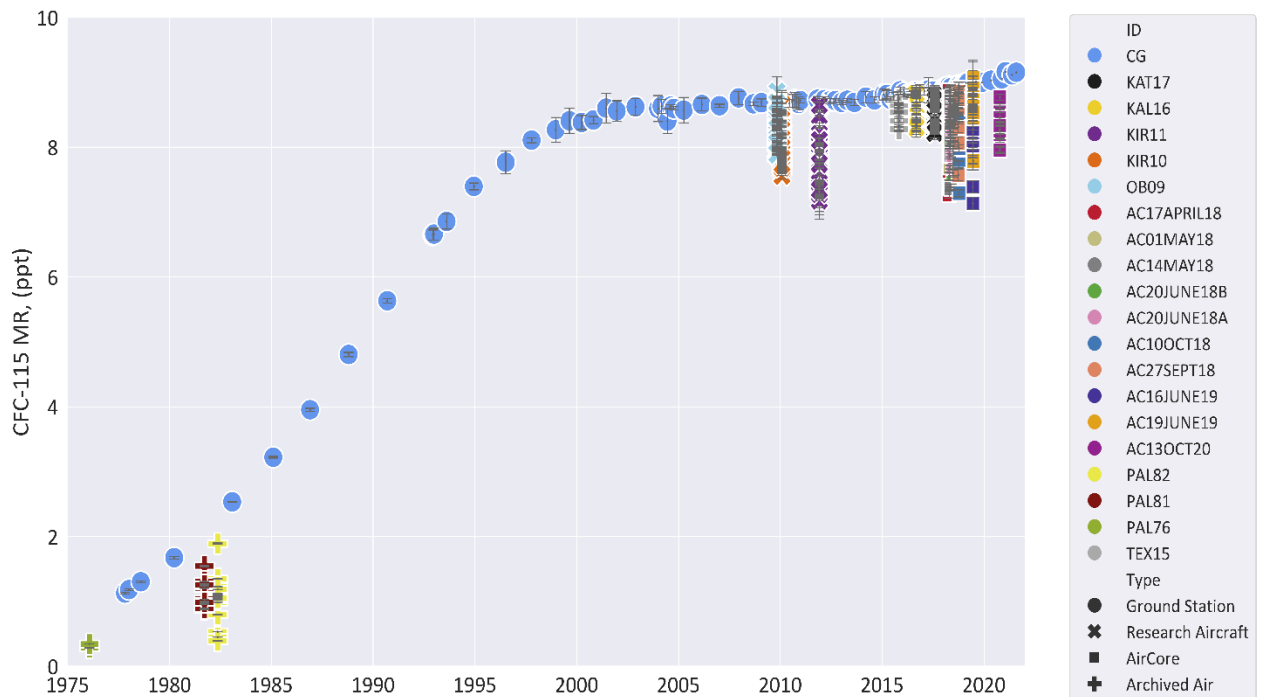


Figure 3.30. Mixing ratios (ppt) for CFC-115, plotted against date. Includes the Geophysica research aircraft flights detailed in section 3.2.1, the archived air samples detailed in section 3.1.3, along with the Cape Grim (CG) tropospheric background trend.

The background trend (CG) in Figure 3.30 again does not quite reach back far enough to overlap with the PAL76 flight, but extrapolating it backwards in time would potentially overlap with the PAL76 flight assuming that the slope of the trend had remained constant. The PAL81 and PAL82 flights do seem to be consistent with the background trend, but there are fewer data points during these years so it is hard to be certain precisely what point these samples came up to on the background trend. All other flights (including the TEX15 archived air, the Geophysica flights, and the AirCore flights) appear to be consistent with the background trend.

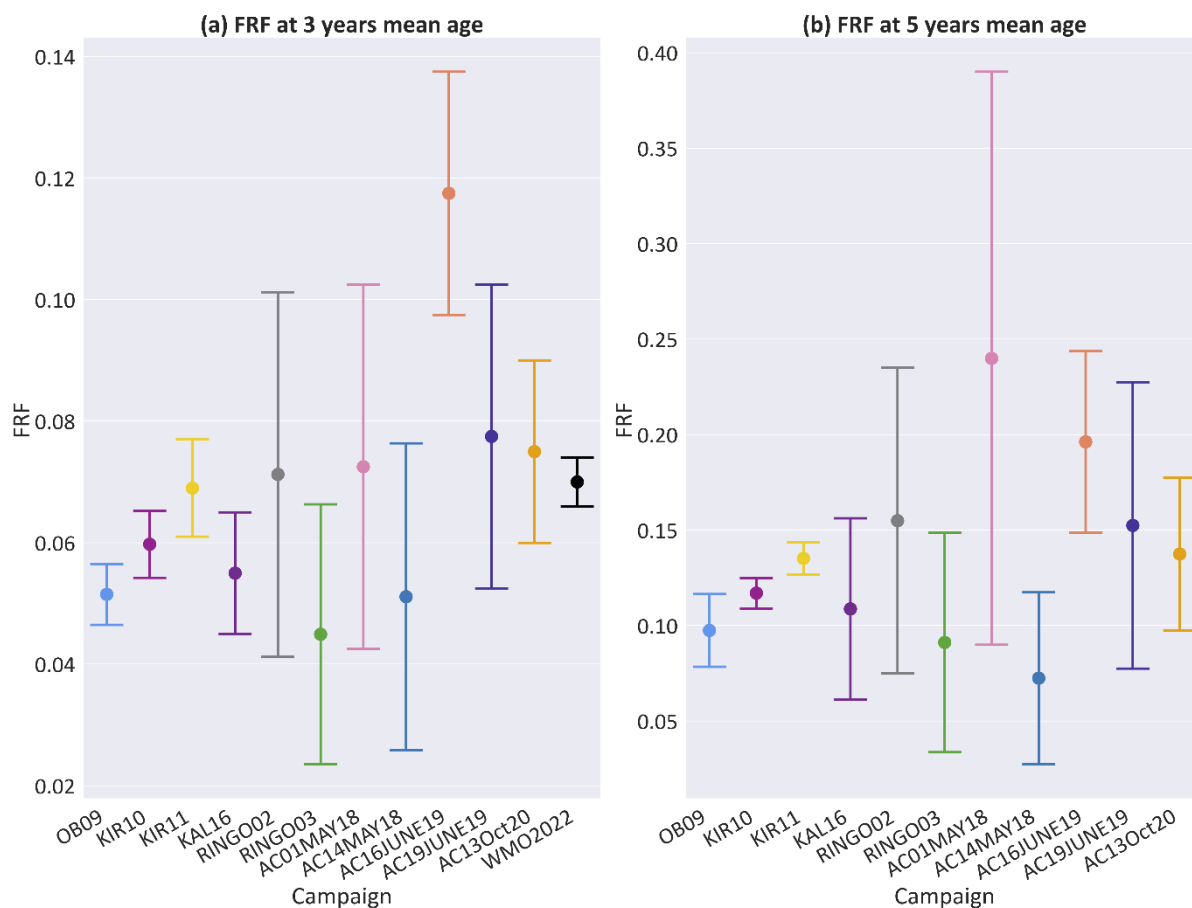


Figure 3.31. For CFC-115, the FRF at (a) 3 and (b) 5 years mean age for each campaign for which data was available for this compound. Uncertainty is to  $1\delta$  uncertainty, and reflects the range for each FRF seen during the bootstrapping procedure detailed in section 2.5.

Unfortunately, data for CFC-115 is available for neither AIRE93 or Gap 99, so FRFs from these campaigns could not be derived for this compound. However, this section does allow for a more detailed examination of FRF variation for a compound where many data points are available. In Figure 3.31 we can see the natural variation in FRFs for the compound. The uncertainty ranges for the FRFs derived using the data from Geophysica flights is the smallest, with AireCore derived FRFs having the largest uncertainty range. The AirCore flight on 01<sup>st</sup> of May 2018 has the largest uncertainty range for this compound, section 4.3.4 explores some of the possibilities and it is unclear as to why the uncertainty range for this flight was unusually large. There were no clear factors that could have impacted the uncertainty range to this extent, but this flight did have a large uncertainty range for most compounds. The AirCore flight on the 16<sup>th</sup> of June 2019 gives an unusually high FRF at 3 years mean age (though the effect is not seen for FRFs at 5 years mean age).

Section 4.3.4 looks into this in more depth, but the effect may be due to the type of AirCore used.

Despite the variation between FRFs, they largely overlap within the uncertainties for both FRFs at 3 and 5 years mean age. While most FRFs at 3 years mean age are broadly consistent with those stated in WMO 2022 (Daniel *et al.*, 2022), the general spread trends towards a lower value, which is consistent with the results seen in section 3.3.1. The variation in FRFs will be explored in more detail in section 4.3.9, but FRFs are by their nature an ‘average’ and may be impacted by a number of factors such as season, latitude, and the polar vortex, so it is to be expected that there will be variation between flights.

### *3.3.5.c Archived Air Samples of CFC-114 - Results*

As CFC-114 and CFC-114a require specific equipment and techniques to be differentiated from one another (see section 2.3 and section 3.2.2 for details), data for these compounds is available from fewer flights. However there are two flights from the archived air samples that do include these compounds; AIRE93 and GAP99.

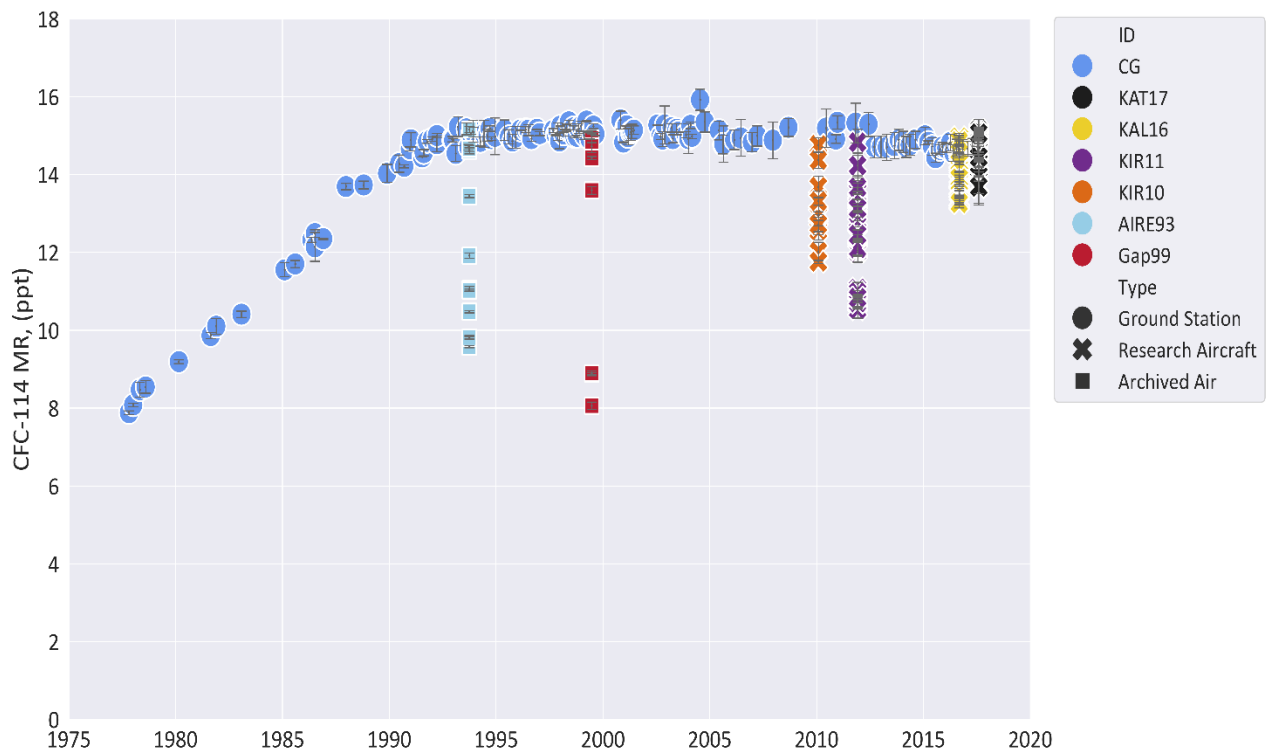


Figure 3.32. Mixing ratios (ppt) for CFC-114, plotted against date. Includes the Geophysica research aircraft flights detailed in section 3.2.1, the archived air samples detailed in section 3.1.3, along with the Cape Grim (CG) tropospheric background trend.

While the number of data points in the Cape Grim (CG) background trend make it hard to discern, in Figure 3.32 the data from both AIRE93 and GAP99 overlap with that background trend. The GAP99 data and to a much lesser extent the KIR11 data show a pronounced gap between samples collected near the troposphere and those collected higher (those with the lowest concentration of the compound). This can happen when either samples aren't taken in the intervening range of the stratosphere, and it can happen regardless of the method used (GAP99 utilised balloon-borne measurements, while KIR11 used the Geophysica high altitude research aircraft). This aside, all flights did capture a reasonable range of stratospheric air.

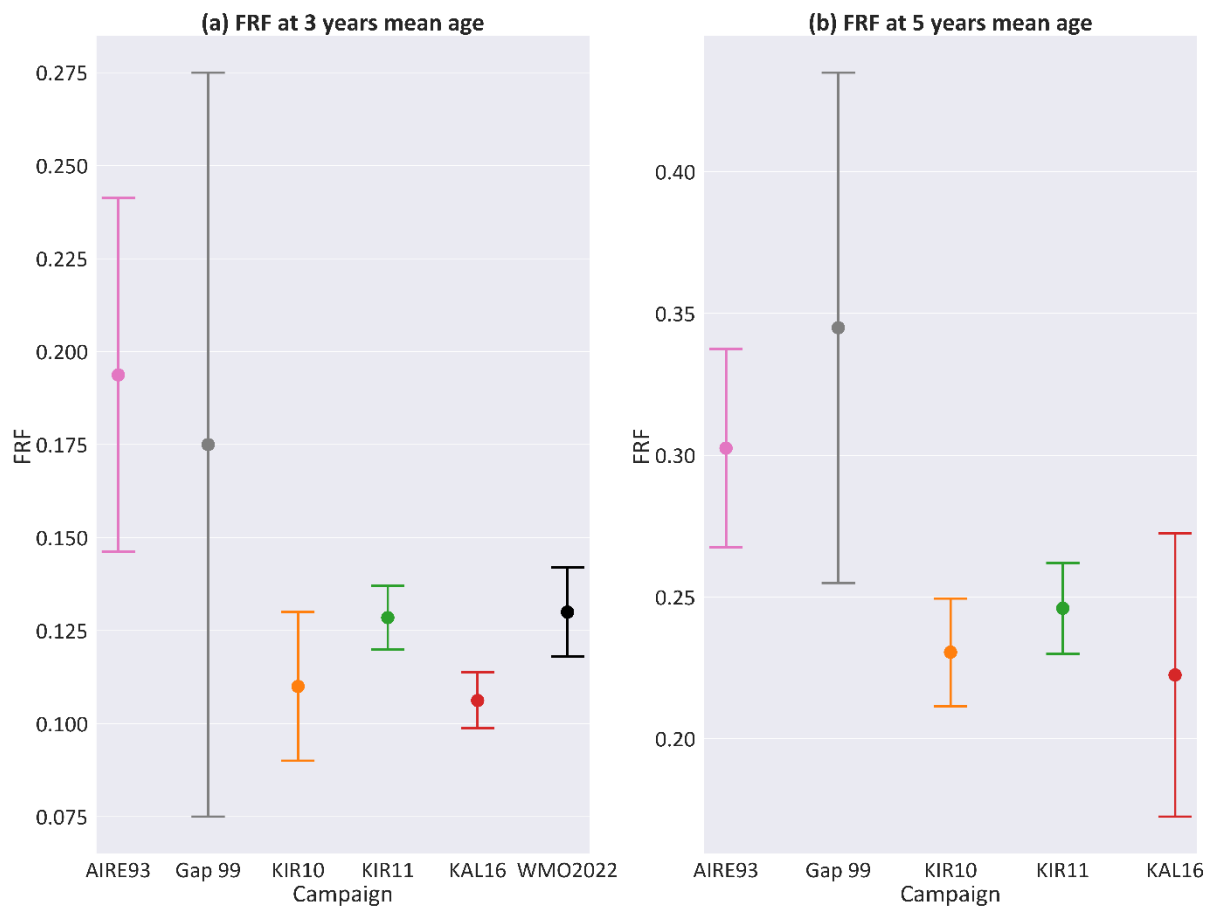


Figure 3.33. For CFC-114, the FRF at (a) 3 and (b) 5 years mean age for each campaign for which data was available for this compound. Uncertainty is to  $1\delta$  uncertainty, and reflects the range for each FRF seen during the bootstrapping procedure detailed in section 2.5.

In Figure 3.33 the AIRE93 and GAP99 flights have the largest uncertainty range and have higher FRFs at both 3 and 5 years mean age. Due to this large uncertainty range the GAP99 flight's range overlaps all other flights at 3 years mean age, and all but KIR10 at 5 years mean age. As discussed in section 3.3.5.a this large uncertainty range seems to derive from a lower precision for the age tracer used (PFC-116) which had limited precision on the AIPlot column (see section 2.3 for details on columns), resulting in a much larger uncertainty for mean age. Most FRFs at 3 years mean age overlap within the uncertainties with the value stated in WMO 2022 (Daniel *et al.*, 2022), with the exception of KAL16 which is just too low, and AIRE93 which is too high. This again illustrates the range of values for FRF that can be derived and highlights the importance of using a composite dataset rather than relying on individual flights alone.

### 3.3.5.d Archived Air Samples of CFC-114a – Results

As with CFC-114, data for CFC-114a is available from fewer flights, but the AIRE93 and GAP99 flights do include data for CFC-114a.

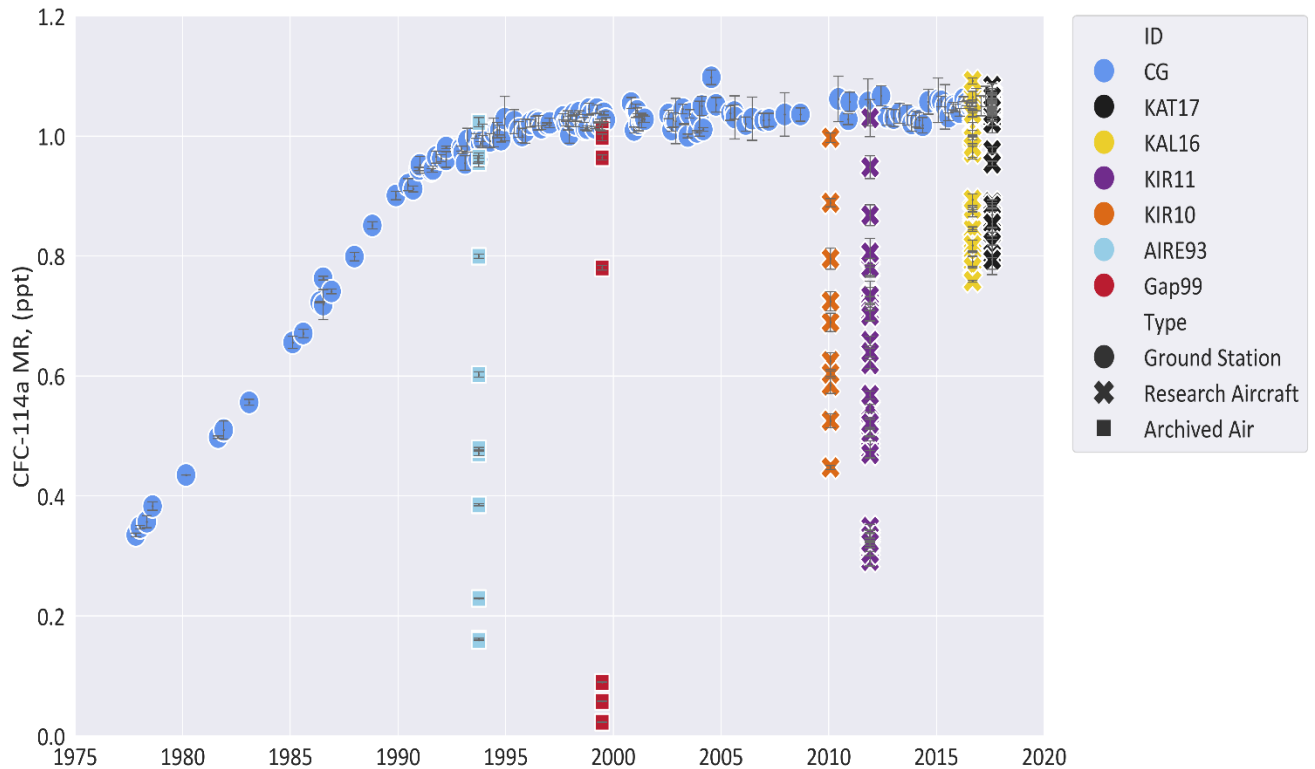


Figure 3.34. Mixing ratios (ppt) for CFC-114a, plotted against date. Includes the Geophysica research aircraft flights detailed in section 3.2.1, the archived air samples detailed in section 3.1.3, along with the Cape Grim (CG) tropospheric background trend.

In Figure 3.34 we can see that all flights, both from Geophysica and the balloon-borne archived air data overlap the background trend to a similar degree. As the AIRE93 flight takes place shortly after the rise in abundance for CFC-114a has begun to plateau, it is interesting to see that one data point is just above the background trend, though this does overlap within the uncertainties.

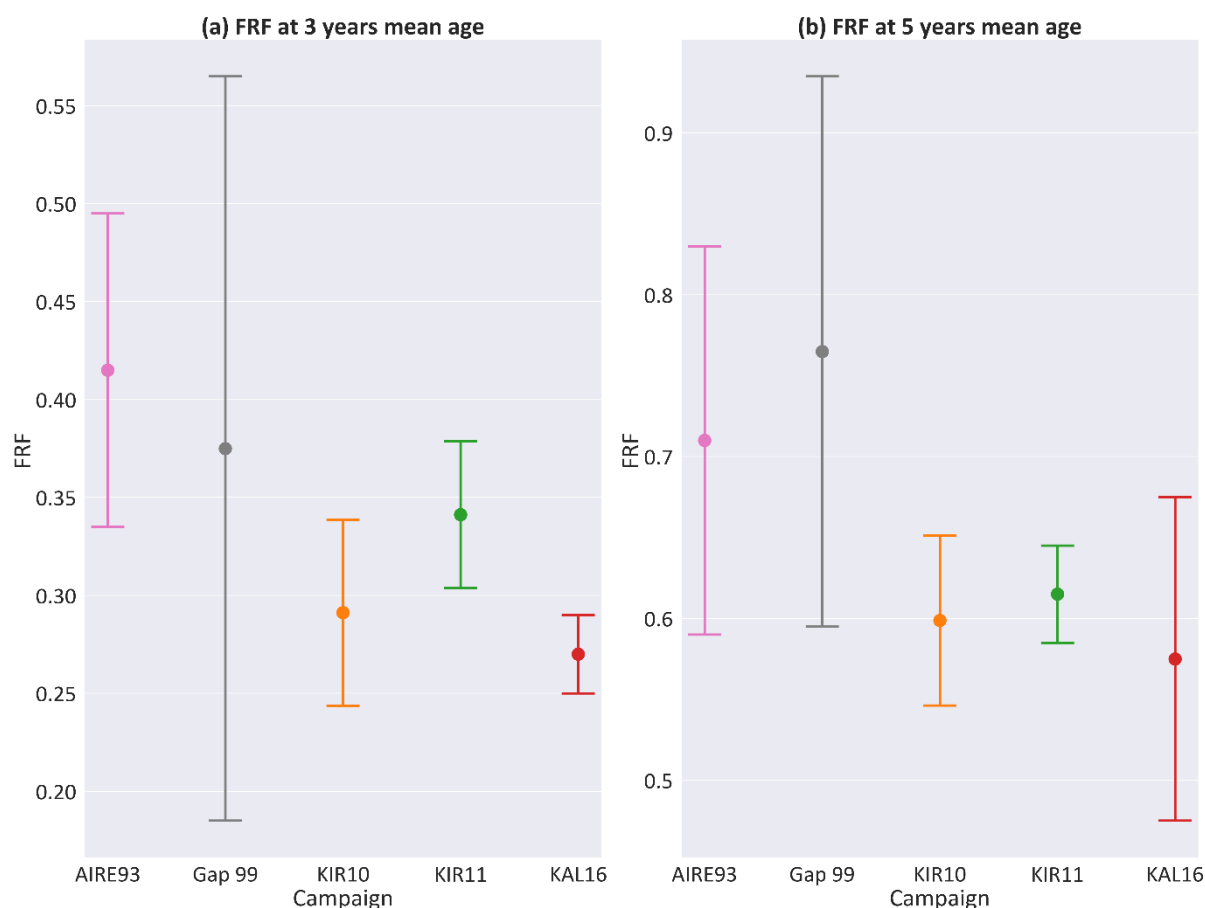


Figure 3.35. For CFC-114a, the FRF at (a) 3 and (b) 5 years mean age for each campaign for which data was available for this compound. Uncertainty is to  $1 \delta$  uncertainty, and reflects the range for each FRF seen during the bootstrapping procedure detailed in section 2.5.

In Figure 3.35, as seen for CFC-114 in section 3.3.5.c the FRFs at 3 years mean age for AIRE93 and GAP99 are notably higher than for other flights and have notably large uncertainty ranges. As previously noted, instrument sensitivity and precision on the days these flights were analysed was poor, leading to larger uncertainty ranges. The background trend for these two compounds was largely consistent from AIRE 93 onwards, and the FRFs were derived using the time-independent method, so this should not have caused the earlier FRFs to be higher. For the FRFs at 3 years mean age, 4 out of 5 overlap within the (sometimes ample) uncertainty ranges, and for the FRFs at 5 years mean age, all 5 values overlap within the uncertainties.

### 3.4 Discussion

Section 3.3.4 used model data to explore how changes in circulation might impact stratospheric lifetimes for these compounds. Due to the way the GSFC 2D model works, it is not possible to use it to predict new lifetimes for those compounds. However, it does give some insight into how strongly chemistry and circulation affects those lifetimes.

Models have predicted a strengthening of the Brewer-Dobson Circulation in response to climate change (Butchart *et al.*, 2006; Garcia *et al.*, 2008; McLandress *et al.*, 2009; Okamoto *et al.*, 2011; Bunzel *et al.*, 2013; Lin *et al.*, 2013; Oberländer *et al.*, 2013). A stronger Brewer-Dobson Circulation could result in shorter lifetimes and would be particularly noticeable for longer-lived compounds such as CFC-13 and CFC-115. Previous stratospheric lifetime estimates for these compounds relied on lab-based kinetics experiments only (Ko *et al.*, 2013) Section 3.3.3 showed that changes to the best estimates of the reaction rates for CFC-13 and CFC-115 would have a significant impact on their stratospheric lifetimes. It is possible that the chemistry in the stratosphere does not match that done in the lab, and thus the lifetimes predicted from field-work observational data and lifetimes predicted from lab-based kinetics experiments, might not match. On the other hand, it is worth considering that the observation-based estimates also have associated uncertainties, for example that arising from instrument precision.

Section 3.3.1 presents newly derived FRFs for compounds which previously either did not have values or had no values derived using in-situ measurements. Section 3.3.2 proposed a revision of stratospheric lifetime estimates for CFC-13 and CFC-115, as these newly derived observation-based lifetimes are significantly different from previous estimates. Section 3.3.3 presented revised, in-situ derived ODPs for these compounds. Combined, these results sections present some additional questions.

If the stratospheric lifetimes of these compounds are significantly shorter than previously believed, then this would suggest that emissions are higher than previously estimated in order to account for the compounds' abundance. While precise emissions estimates were initially outside the scope of this thesis, it is possible to generate some rough estimates for the emissions of CFC-13, CFC-114, CFC-114a and CFC-115, both using the lifetime listed in Burkholder *et al.* (2022), and the new lifetime estimates for these compounds using the average stratospheric lifetime derived using FRFs and lifetimes from

Leedham-Elvidge, et al., (2018) (section 3.3.2, Table 3-5) in order to illustrate how great a difference in emissions would potentially be. To do this requires an understanding of how the atmospheric lifetime of a compound relates to its atmospheric burden, sources and sinks, using Equation 3-2, Equation 3-3 and Equation 3-4 (Ko *et al.*, 2013).

$$\frac{\delta B(t)}{\delta t} = S(t) - R(t)$$

*Equation 3-2. Equation relating the time evolution of the atmospheric burden (B(t) of in this case a compound in the atmosphere, to its sources S(t) and removal processes R(t). ( Equation 1.1 in Ko et al., 2013)*

$$\tau(t) = \frac{B(t)}{R(t)}$$

*Equation 3-3. Equation relating Global Atmospheric lifetimes  $\tau(t)$ , to Atmospheric burden B(t) and Removal processes (sinks) R(t). (Equation 1.2 in Ko et al., 2013)*

$$T_{ss} = \frac{B}{R} = \frac{B}{S}$$

*Equation 3-4. Equation relating the steady state lifetime (Tss) to globally integrated loss/removal processes (R) (molecules/yr), Globally integrated sources (S) (molecules/yr), and global burden (B) (e.g. total number of molecules). (Originally Equation 2.7 from (Ko et al., 2013), in which loss is represented with 'L', changed here to avoid confusion with equations Equation 3-2 and Equation 3-3).*

The atmospheric lifetime used is either the one derived in section 3.3.2, or those listed in Burkholder et al. (2022), and as the atmospheric lifetimes for these compounds is assumed to be in steady-state, burden/emissions should balance burden/loss (Equation 3-4). This means that when Equation 3-3 is re-arranged so that Removal Processes are equal to burden divided by lifetime, this also gives the emissions (sources) as loss and emission should be equal.

This requires a value for the global burden, which is approximately the product of the mixing ratio near the ground and the atmospheric mass (Ko *et al.*, 2013). So, for each compound, first the abundance (ppt) and the molecular mass were multiplied to give the number of grams of the compound in 1 trillion moles, and this value was then multiplied by the approximate number of Trillion moles in atmosphere to give the total grams of the compound in the atmosphere. This was converted to kilotons, was then divided by the

global lifetime to give an estimate of the emissions for that compound. These initial estimates are shown in Figure 3.36.

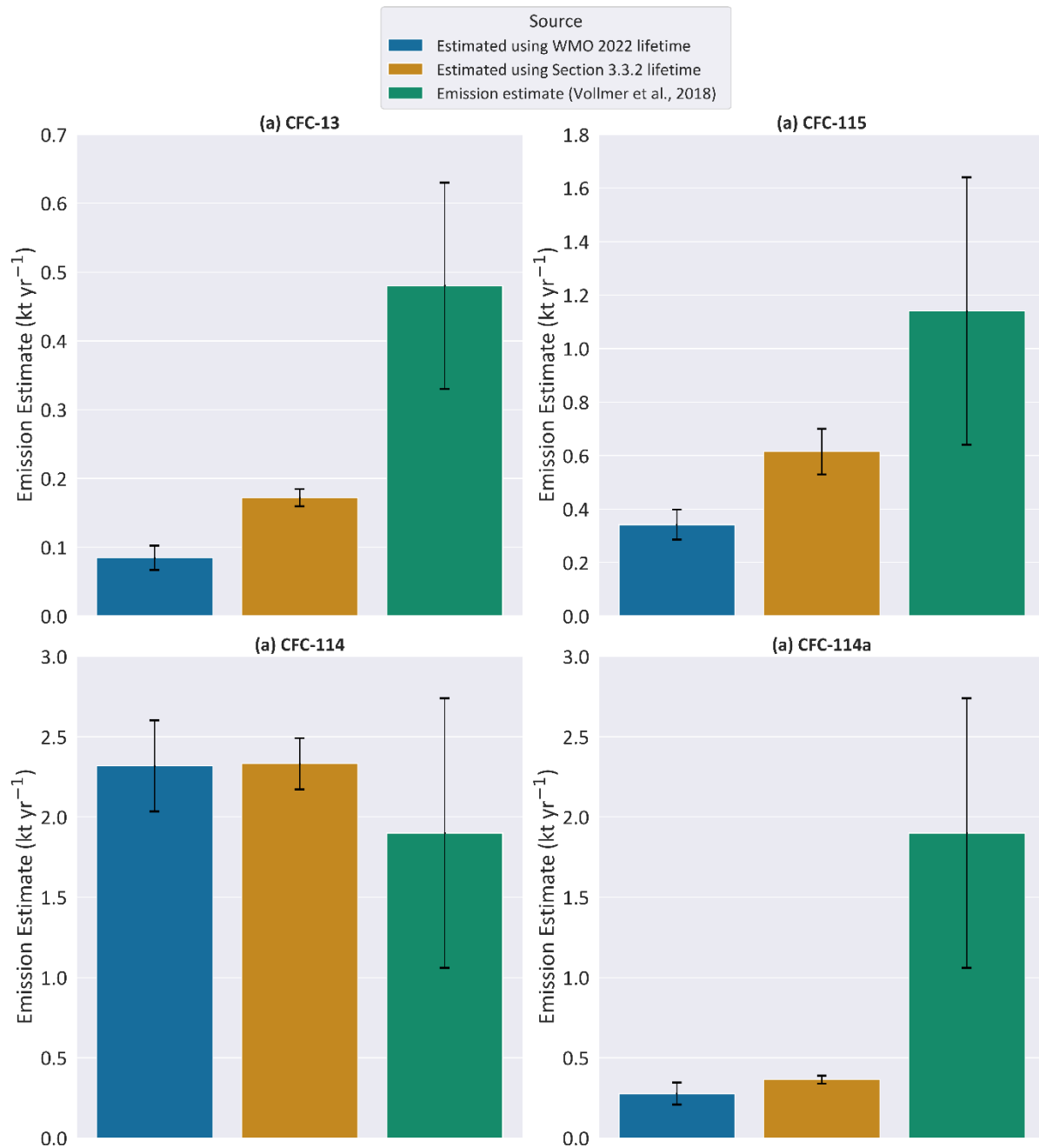


Figure 3.36. Showing emissions calculated for all four compounds, first using the new lifetime estimates from section 3.3.2, then using the lifetime estimates listed in Burkholder et al. (2022). This is then compared to the emissions estimates listed in (Vollmer et al., 2018). Emission estimates from Vollmer et al. (2018) are global mean yearly emissions (2007–2016). The estimates using either WMO 2022 lifetimes or lifetime estimates from section 3.3.2, are global mean yearly emissions for the period between 2009–2017.

It should be noted that the emissions estimates in Figure 3.36 do not match those calculated by Vollmer et al., (2018). Firstly Vollmer looked at the sum of CFC-114 and CFC-114a; if the emissions for both from Figure 3.36, are combined we get 2.69 (2.54–2.91) (kt

yr<sup>-1</sup>), which is within the range of 1.9 (1.06-2.74) (kt yr<sup>-1</sup>) in Vollmer et al., (2018). Both CFC-13 and CFC-115 are increasing in abundance, and the rough calculations used here by necessity assume a source-sink equilibrium, which means that the resulting numbers will be somewhat smaller than those listed in Vollmer et al., (2018). The calculations in this section will naturally have some high bias, as they rely on the assumption that the mole fraction near to the ground is the same as in the entire atmosphere; however, we know in practice that the mole fractions are lower in the stratosphere, particularly for the shorter-lived CFC-114a. However, the other gases are comparatively long-lived so this should have only a small impact on the resulting emission estimates.

As can be seen in Figure 3.36 the effect of a change in lifetime is most dramatic for longer-lived compounds. For CFC-13, compared to the longer lifetime estimate in Burkholder et al. (2022) (640 years) the shorter lifetime estimated in section 3.3.2 of 315 (287-331) years would require roughly double (103.3%) the emissions to account for the compound's abundance, even when taking the uncertainty range into account. CFC-115 also requires significantly greater emissions (79.9%) to account for its abundance if the shorter lifetime estimated in section 3.3.2 of 369 (328-435) years, which is not accounted for by the uncertainties.

However, the emissions for CFC-114 and CFC-114a do not change significantly when the different lifetimes are used. This is because, as discussed in section 3.3.2, the 'new' lifetime estimates for these compounds were within the uncertainty range for the original lifetimes. A dominant factor in emissions estimate uncertainty is the lifetime uncertainty of the compounds, so it is to be expected that the emissions estimates in Figure 3.36 for CFC-114 and CFC-114a overlap within the uncertainties.

As these estimates are somewhat simplistic, I reached out to Luke Western (NOAA Global Monitoring Laboratory, Boulder, CO, USA, correspondence 08/2024) to ask if he could provide updated (from the Western et al., (2023) paper) using section 3.3.2's revised lifetimes. He was kind enough to do so, and the results can be seen in Figure 3.37.

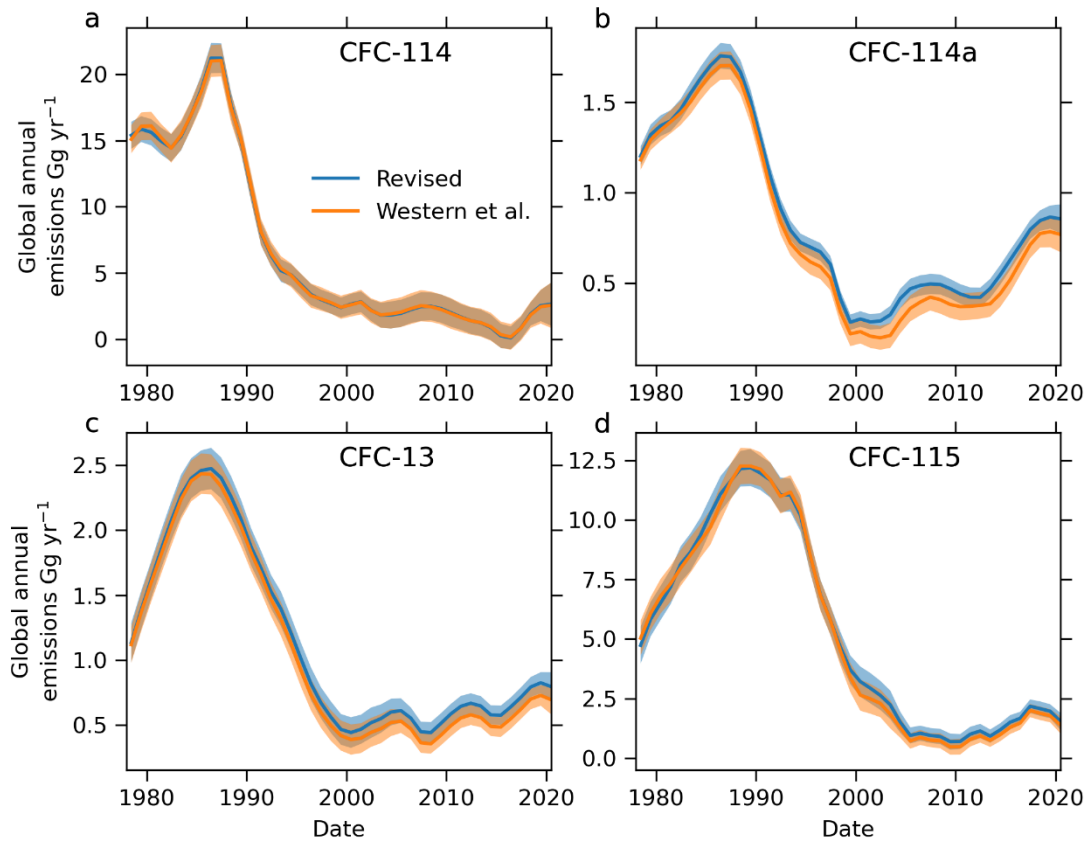


Figure 3.37. The emissions estimates for all four compounds, showing the original emissions estimates from Western et al., (2023), and revised estimates that use the revised lifetime estimates from section 3.3.2. Courtesy of Luke Western (NOAA Global Monitoring Laboratory; Boulder, CO, US).

Figure 3.37 shows a less dramatic increase in emissions compared to Figure 3.36, but there are still notable differences between the two sets of emissions estimates. Using the global mean annual emissions estimate (from 2009 to 2017), and the newly derived ODP estimates listed in 3.3.3, I derived OPD weighted emissions estimates for each compound. This was done using both the original Western et al., (2023) emissions estimates and the revised estimates (which used the same process, the only change was that the lifetimes for the compounds were those derived in section 3.3.2).

Table 3-7. Table showing emission estimates and ODP-weighted emissions estimates calculated for all four compounds. All emissions estimates are the global mean for the period of 2009-2017. 'Original' refers to data from Western et al., (2023), while 'revised' estimates are emissions estimates supplied by Luke Western, using the same technique, with the only difference being the lifetimes used (which the revised estimates using the lifetime estimates from section 3.3.2, while the 'original' estimates used the lifetimes listed in WMO 2022 in Burkholder et al. (2022)). The ODPs used for the ODP-weighted emissions estimates are those from section 3.3.3. Uncertainty range is to 1  $\delta$ .

Compound	CFC-13	CFC-114	CFC-114a	CFC-115
Original Emissions estimate, kt yr <sup>-1</sup>	0.53 ±0.08	1.22 ±1.04	0.46 ±0.07	1.02 ±0.29
Revised Emissions estimate, kt yr <sup>-1</sup>	0.62 ±0.08	1.21 ±0.96	0.54 ±0.05	1.22 ±0.30
ODP weighted emission estimate (Western et al., 2023), kt yr <sup>-1</sup>	0.20 ±0.03	0.59 ±0.50	0.25 ±0.04	0.25 ±0.07
ODP weighted emission estimate (Revised), kt yr <sup>-1</sup>	0.23 ±0.03	0.58 ±0.46	0.29 ±0.03	0.31 ±0.07

As can be seen in Table 3-7, we can see that with the exception of CFC-114 (which had a slightly higher lifetime estimate in section 3.3.2 than the previous estimate), all compounds have average emissions estimates that are higher when the revised lifetimes are used. The uncertainty range is broad and overlaps for all compounds, however it is clear that longer stratospheric lifetimes would result in higher emissions. When weighted by ODP, CFC-114a and CFC-115 have identical values despite very different base emissions and lifetimes. CFC-13 has the lowest value for ODP-weighted emissions, while CFC-114 has more than double the value of any of the other compounds. So while their overall emissions are much smaller than those of the most abundant CFCs (such as CFC-11, CFC-12 and CFC-113, Table 1-1), their contribution to ozone depletion is still a concern.

The question remains whether these increased estimated emissions for CFC-13 and CFC-115 are due to release from long-term banks, or from new emissions. If they are from new emissions this would have important implications to enforcement of the Montréal Protocol. Whether from long-term banks or new emissions, higher emissions need to be taken into account when assessing the ozone recovery timeline.

Different applications of ODSs result in banks that would release their contents at different rates. For example, propellants and aerosols generally make up short term banks, while refrigerants, heat pumps and air-conditioning constitute long term banks. As CFCs spray applications were banned early on, emissions stemming from short-term banks largely peaked around 1990, while emissions from medium and long-term banks became the dominant emission sources. The long-term banks for the compounds of interest in this paper were largely low-temperature refrigerant (CFC-13, CFC-114, CFC-115), heat-pumps

(CFC-114), and air-conditioning (CFC-115). Long-term banks are estimated to lose roughly 2% of their material per year and combined with the relatively long atmospheric lifetimes of these compounds, releases from these banks could continue to harm the ozone layer for a substantial amount of time before finally depleting (Ashford *et al.*, 2004a, 2004b; Lickley *et al.*, 2021, 2022, 2024; Bourguet *et al.*, 2024).

Estimates of bank emissions vary widely; they are estimated using different techniques which utilise incomplete or imprecise information (WMO, 2003; TEAP, 2009). Lickley *et al.*, (2022) argues that production assumptions for several CFCs (including CFC-115 but not CFC-13) have a low bias stemming from underreporting, leading to published bank estimates that also have a low bias, and thus banks are likely to be larger than previously assumed.

Lickley *et al.*, (2022) found a discrepancy for CFC-115 in which the modelled mole fraction increased through the simulation period, which is in contrast to observed real world mole fractions which were comparatively constant. Lickley *et al.*, notes that a shorter lifetime would result in modelled mole fractions declining more rapidly after 1990 and would better match observations. Thus, the discrepancy could be explained by the substantial uncertainties in the atmospheric lifetimes of CFC-115, suggesting that the compound has a significantly shorter lifetime than previously estimated. This fits the results shown in Figure 3.36, where emissions estimates using the new, shorter lifetime, are significantly greater than those derived using the original lifetime.

Vollmer *et al.*, (2018) found that growth rates for both CFC-13 and CFC-115 were significantly larger than would have been predicted based on zero emissions, though the paper uses the assumption of unaltered lifetimes and atmospheric transport patterns. Emissions from aluminium smelters (CFC-13) and impurities of CFC-115 in the refrigerant HFC-125 did not fully account for the lingering global emissions found in atmospheric observations. Significant emissions observed from the Gosan, Korea AGAGE site suggest that a large percentage of global emissions of CFC-115 and CFC-13 occur in north-eastern Asia in general, and the Chinese mainland specifically. Emissions seem to originate from pollution events rather than a steady emission, and Vollmer *et al.*, (2018) speculate that it is unlikely that CFC-13 is being used as a process agent as it would need to be recorded and controlled under the Montréal Protocol and suggest that it could be emitted as by-product of

fluorochemical manufacture, being released either during the process or as an impurity in the end product.

Western et al., (2023) found that CFC-115 emissions are probably the result of the production of hydrofluorocarbons, and that CFC-13 emissions can be the result of deliberate plasma arc destruction of CFC-12. As discussed in section 1.2 illegal production and trade of CFCs has occurred, notably in the case of CFC-11 (UNEP, 2018; Lin *et al.*, 2019; Zeng *et al.*, 2020; Benish *et al.*, 2021; Huang *et al.*, 2021; Park *et al.*, 2021; Yang *et al.*, 2021), so it is plausible that the same could happen for other CFCs such as CFC-115 and CFC-13. Bourguet and Lickley, (2024) argues that unreported feedstock production for HFCs may be responsible for higher than expected emissions of CFC-114 and CFC-115.

Both Lickley et al., (2022) and Vollmer et al., (2018) assume unaltered lifetimes for these compounds, which section 3.3.2 has shown are not the case. Shorter lifetimes for these two compounds would require greater emissions in order to account for their atmospheric abundance. While it is not possible to conclude decisively whether the increased emissions reflected in Figure 3.36 are due more to long-term banks or new emissions. Both appear to be a factor.

### **3.4.1 Archived Air Discussion**

It should be noted that the background trend may not match up perfectly with any given flight as the background trend is taken from the southern hemisphere. This creates a time lag which may not be completely accounted for by applying an adjustment (of half a year) to the background trend. The background trend is taken from a remote area where pollution levels should be as low as possible. For these reasons the background trend may not be perfectly comparable to samples taken in the northern hemisphere, particularly in more polluted regions. When comparing the archived air data to background trend data, Geophysica data and where available AirCore data, it was found that the archived air data was consistent with the background trend (where the background trend extended far enough into the past), to the same extent as data derived from other sources.

Archived air data from only 2 of the 6 flights was suitable for calculating FRFs, though only AIRE93 and GAP99 were available for all compounds except CFC-115. TEX15 had such

young mean age of air it was not appropriate to derive FRFs at 3 or 5 years mean age. However, despite these limitations, the data has yielded some relevant results.

The FRFs at 3 years mean age from AIRE93 and GAP99 were on average higher than those for later flights. This was still the case at 5 years mean age but the difference was less noticeable. The FRFs from AIRE93 and GAP99 displayed larger uncertainty ranges, with the FRFs from GAP99 displaying a particularly large uncertainty range. The high uncertainty is believed to have been due to low instrument precision at the time these samples were analysed, as all samples analysed at this time demonstrated poor precision. The AIRE93 and GAP99 flights took place in summer/autumn, where concentrations of these tracers might have been higher. It may also reflect the fact that entry mixing ratios (which are necessary to calculate FRFs) require a background trend with data stretching back a substantial number of years. As the earlier flights had around 15 years of background trend prior, this should be sufficient. Notably for CFC-13 and CFC-114a the AIRE93 and GAP99 flights were at or just after the point in time where the abundance of the compound in the atmosphere began to plateau. However, this is not the case for CFC-114, which also sees a large uncertainty range in FRFs derived for these flights. Therefore, the most probable explanation for the large uncertainty is poor instrument precision during analysis and the effects of seasonality.

Possible effects from seasonality on FRFs (as will be explored in more detail in section 4.4.2) for these compounds were investigated. Figure C.2 shows the FRF at 3 years mean age for the compounds of interest in Chapter 3 (CFC-115, CFC-13, CFC-114 and CFC-114a), plotted against fraction of year. The only compound with sufficient data points that any pattern from seasonality could be apparent is CFC-115, though Figure C.2a does not show any significant pattern. However, all compounds have comparatively long lifetimes, and thus relatively low FRFs. This would be expected to dampen any seasonal signal if there is one.

### **3.5 Conclusion.**

This is the first study using in-situ based stratospheric data for these four gases and used this data to investigate these compounds in detail, deriving policy-relevant metrics such as FRF, stratospheric lifetime, and ODP, in addition to new ODP-weighted emissions

estimates. This in-situ data was largely derived from samples taken by high-altitude research aircraft, but also uses model data to further explore how these compounds behave in the stratosphere. In addition, data from archived air samples was examined to help contextualise the existing samples and to further explore their FRFs.

Comparison of the archived air sample data to the tropospheric background trend, alongside data from high-altitude research aircraft flights and where available AirCore flights, showed that all three methods produced profiles that were consistent with the background trend. At 3 and 5 years mean age the FRFs from each flight showed substantial variation; FRFs from different flights largely overlapping within the uncertainties, but the range was significant (section 3.3.1).

In section 3.3.2, by using the correlation between lifetime and FRF for well-studied compounds, I was able to derive updated estimates for their stratospheric lifetimes of CFC-13, CFC-114, CFC-114a, and CFC-115. CFC-13's lifetime substantially decreased from previous estimate (640 years) to 315 (287-331) years. There was also a large change in CFC-115's estimated lifetime, from 664 years to 369 (328-435) years. My stratospheric lifetime estimate for CFC-114a of 81 (76-87) years agrees within the uncertainties with the previous estimate 106.7 (82–133) years. CFC-114's previous stratospheric lifetime estimate was 191 ( $\pm 12\%$ ) years the uncertainties of which comfortably overlaps my own findings of 190 (176-201) years.

Exploration of the GSFC model did provide some insight into the underlying dynamics and chemistry of stratospheric circulation within the model. Notably the model produced robust visual correlation between mean age and tracer mixing ratio; however, the lifetimes estimated by the model itself were significantly different from those that can be derived via the mean age-tracer correlation of its own data. With the exception of CFC-114 (whose kinetics data was impacted by impurities of CFC-114a), the model accurately simulates the known chemistry of the four compounds examined here. The comparison between GSFC and CLaMS showed that the nudging of the MERRA-2 reanalysis accelerates the transport, and thus brings the mean age-mixing ratio correlation in the GSFC in line with observations.

In section 3.3.5 archived air from largely historic large balloon flights was analysed, with FRFs at 3 and 5 years mean age derived (where appropriate). This section helped to

expand on the challenges of deriving representative FRFs from a limited number of flights, but where data is available it supports the conclusions of other sections.

This chapter also derived ODPs for all four compounds (section 3.3.3), and none of these overlapped within the uncertainties with Burkholder et al. (2022), though CFC-114 is fairly close.

Using these newly derived stratospheric lifetimes and ODPs, section 3.4 derived new ODP-weighted emission estimates for these compounds and compared them to existing estimates. The estimates show that the revised lifetimes (with the exception of CFC-114) resulted in larger average emissions, though the uncertainty range was broad enough to overlap, the trend is still clear: greater stratospheric lifetimes required greater emissions in order to account for them.

## Chapter 4 Exploring the Stratosphere with AirCores

### 4.1 Introduction

#### 4.1.1 Exploring the stratosphere with AirCores

As discussed in 2.1.3 the AirCore technique has previously been used to investigate more abundant trace gases ( $\text{CO}_2$  and  $\text{CH}_4$ ), and Laube et al. (2020) expanded the range of compounds analysed via AirCore by six species with abundances in the ppt range. Li et al. (2023) also used the AirCore method to examine a number of trace gases ( $\text{N}_2\text{O}$ ,  $\text{SF}_6$ , CFC-11, CFC-12, H-1211, and CFC-113), and expanded the capabilities of the technique to investigate trace compounds.

This chapter sets out to expand that number by seven additional compounds: PFC-116/hexafluoroethane ( $\text{C}_2\text{F}_6$ ), methyl chloride ( $\text{CH}_3\text{Cl}$ ), CFC-113 ( $\text{C}_2\text{Cl}_3\text{F}_3$ ), CFC-115 ( $\text{C}_2\text{ClF}_5$ ), HFC-125 ( $\text{C}_2\text{HF}_5$ ), HCFC-141b ( $\text{C}_2\text{H}_3\text{Cl}_2\text{F}$ ), and HCFC-142b ( $\text{C}_2\text{H}_3\text{ClF}_2$ ). These were initially identified as the most promising candidates for further trace species quantifiable in the stratosphere with the AirCore technique.

As discussed in Section 2.6, there are a lot of assumptions involved in the calculation of FRFs, so a key aim in this chapter is to first establish that AirCore sampling can reliably generate FRFs for its target compounds, and second, to explore those assumptions (see Section 4.3.9). Section 2.1 gave an overview of the various sampling techniques available, and their individual strengths and weaknesses.

My goal is to answer a series of questions about each compound:

1. Can AirCore sampling provide viable mixing ratios at acceptable precision for the compound?
2. What factors affect the precision and usability of data?
3. How can we improve the sampling process to improve the usability of the data?
4. What can be learned from this AirCore data regarding this compound?

If the AirCore technique can reliably be used to gather data on these compounds, this will substantially improve our ability to study and monitor them efficiently and affordably.

### 4.1.2 Introducing the Compounds

For some of these compounds (i.e., the chlorine-containing ones), this chapter's primary interest is in monitoring changes in abundance, as this determines their impact on stratospheric ozone.

Two compounds examined in this chapter (HFC-125 and C<sub>2</sub>F<sub>6</sub>) have applications as age-tracers, so investigating their viability in AirCore sampling allows a more nuanced exploration of Age of Air (AoA). As discussed in Section 1.4 the AoA is not homogenous, nor does it increase linearly with altitude. Most relevant to this chapter is the use of AoA in calculations regarding stratospheric lifetime and ozone depletion potentials, which are vital to assessing the state of ozone recovery in the ozone layer (Volk *et al.*, 1997; Brown *et al.*, 2013; Laube *et al.*, 2013).

The mean AoA can be derived by using the observed abundance of a suitable stratospheric tracer compound, and comparing it to that compound's tropospheric time series. Doing this requires that the trace gas is (largely) chemically inert in the stratosphere, and it should have a monotonically (ideally linearly) changing tropospheric concentration (Hall *et al.*, 1994). Commonly used tracers such as sulfur hexafluoride (SF<sub>6</sub>) and carbon dioxide (CO<sub>2</sub>) both have limitations. CO<sub>2</sub> has a complicated tropospheric trend, partially due to the seasonal cycle's influence (Bönisch *et al.*, 2009), it also has a stratospheric source (the oxidation of hydrocarbons). As discussed in section 3.2.5 there is strong evidence that SF<sub>6</sub>'s mean age has been overestimated (and thus may give high-biased mean ages).

Because of these complications, additional options for age-tracer compounds are required. Leedham-Elvidge *et al.*, (2018) expanded the list of potential age-tracers by six (CF<sub>4</sub>, C<sub>2</sub>F<sub>6</sub>, C<sub>3</sub>F<sub>8</sub>, CHF<sub>3</sub>, HFC-125, HFC-227ea) and, with the exception of HFC-227ea, demonstrated their viability as age-tracers. However, most of these compounds have very low abundance so, when combined with the low volume of air collected in an AirCore sample (20-50 ml rather than the 200-300 ml collected using traditional sampling techniques), this may mean that they cannot be reliably detected in the sample. This chapter will examine how well C<sub>2</sub>F<sub>6</sub> and HFC-125 can be resolved from AirCore samples, and thus whether they can be reliably used in age of air calculations using samples collected via AirCore.

Laube et al., (2020) showed that AirCore samples are a viable way to examine six gases which are important for understanding stratospheric ozone depletion and circulation (CFC-11, CFC-12, HCFC-22, H-1211, H-1301, and SF<sub>6</sub>). This thesis aims to expand the number of compounds for which AirCore sampling can reliably be used to study by a further seven.

#### 4.1.2.a A short introduction to PFC-116

PFC-116 (C<sub>2</sub>F<sub>6</sub>) is a perfluorocarbon (PFC), a fully fluorinated hydrocarbon and, like many PFCs (though not all), PFC-116 is both a potent and long-lived greenhouse gas. It is released predominantly during semiconductor and aluminium production and makes a small contribution to the R-508 refrigerant blend. With no identified natural sources (Trudinger *et al.*, 2016), PFC-116 has a 100-yr global warming potential of 11,100, and a lifetime of 10,000 years (Burkholder et al., 2018), which means it is the most potent (in terms of global warming potential) PFC, and fourth most potent greenhouse gas listed under the Kyoto protocol (Say *et al.*, 2021).

Possible sink processes for PFC-116 have been investigated, including reactions with oxygen and hydrogen atoms, reactions with vibrationally excited OH, and with ions in the stratosphere and above; however, PFC-116's sink processes have been found to be dominated by unintentional thermal destruction during high temperature combustion on the ground, with few sinks in the troposphere or stratosphere, leading to a very long atmospheric lifetime (10,000 years) (Cicerone, 1979; Ravishankara *et al.*, 1993; Morris *et al.*, 1995; Mühle *et al.*, 2010; Trudinger *et al.*, 2016).

High demand for aluminium during the second world war may be behind a peak of emissions of PFC-116 in the 1940s. Emissions of PFC-116 peaked in the early to mid-2000s, due to improvements to the smelting process and other mitigation efforts. However, these decreases in emissions appeared to have halted (Trudinger *et al.*, 2016), and there is a weak growth in emissions since 2009 (Say *et al.*, 2021). Though emissions have declined, the abundance of PFC-116 is still increasing by 0.1 ppt per year from 4.6 ppt in 2016, to 4.7 ppt in 2017, and 4.8 ppt in 2018 (AGAGE global network (Prinn *et al.*, 2020)).

Due to its long lifetime and apparent stability, Leedham-Elvidge et al., (2018) evaluated PFC-116 as a potential age tracer. Their study used Cape Grim archived air for the tropospheric trend, and aircraft and balloon data for stratospheric data. It found PFC-116 to

be a suitable age tracer using these samples. The viability of using this compound as an age tracer, when utilising the AirCore technique, has yet to be investigated thoroughly.

#### 4.1.2.b A short introduction to HFC-125

With the phasing out of ODSs such as the CFCs, replacement compounds were needed for processes that had previously been dependent on them; for example, major refrigeration blends, and air conditioning. HFC-125 also has a minor application in fire protection. Hydrofluorocarbons (HFCs) were used as ODS substitutes for many applications, as they do not contain ozone-depleting chlorine or bromine. Many HFCs also have smaller climate impacts per molecule than the ODSs they replaced, but not all. Long-lived HFCs are potent greenhouse gases; HFC-125 has a global warming potential (GWP) of 3450 or 4800 (depending on whether the calculation is based on models or kinetic studies) (Ko *et al.*, 2013; Burkholder *et al.*, 2022), and because of this HFC-125 is one of the HFCs controlled by the Kigali Amendment: an Amendment to the Montréal Protocol that aims to gradually reduce the consumption and production of HFCs (Stanley *et al.*, 2020).

As would be expected from the replacement of many ODSs with HFCs, most of the currently measured HFCs show increasing atmospheric mole fractions at accelerating rates. HFC-125 is one of the most abundant HFCs and has seen a significant increase in abundance; for the 2012-2016 period, mole fractions for HFC-125 increased by an average of 2.1 ppt yr<sup>-1</sup> (Burkholder *et al.*, 2022) and from 21.1 ppt in 2016, to 25.2 ppt in 2018 (NOAA (*National Oceanic and Atmospheric Administration*), NOAA/ESRL Global Monitoring Division., 2020).

The radiative forcing from HFCs also continues to increase. In 2018 it amounted to approximately 1% of the total forcing from all long-lived greenhouse gases, the radiative forcing for HFC-125 contributing around 15% of that with 4.70 (4.62–4.79) mW m<sup>-2</sup>. This means that the GWP of HFC-125 is substantial at 3820 (100-yr<sup>1</sup>) (Table 1-1).

While HFC-125 has a tropospheric lifetime of 32 years, it has a significantly longer stratospheric lifetime of 595 years (Burkholder *et al.*, 2022). Like the majority of hydrogen-containing compounds, the dominant loss process for HFC-125 is reactions with OH, both in the troposphere and the stratosphere. HFCs are also removed in the stratosphere by reactions with O(<sup>1</sup>D). The altitudinal distribution of OH and O(<sup>1</sup>D) is different, with concentrations of O(<sup>1</sup>D) increasing more rapidly with altitude in the lower stratosphere, compared to OH.

Reactions with O(<sup>1</sup>D) in the upper stratosphere can be a significant loss process for HFCs. With concentrations of O(<sup>1</sup>D) small in the troposphere and lower stratosphere, O(<sup>1</sup>D) reactions are only a significant contribution to the lifetimes of compounds that actually reach the upper stratosphere. Orkin et al., (2020) estimated the partial lifetime for HFC-125 subject only to O(<sup>1</sup>D) reactions to be 5500 years (and the GSFC-2D model, also used in that paper, estimated the partial lifetime as 5860 years), which demonstrates OH reactions are the dominant atmospheric loss process even for slower reacting HFCs.

Leedham-Elvidge et al., (2018) evaluated HFC-125 as a potential age-tracer, and found that CF<sub>4</sub>, C<sub>2</sub>F<sub>6</sub>, C<sub>3</sub>F<sub>8</sub>, CHF<sub>3</sub> and HFC-125, produce very similar mean ages of air, allowing them to produce a new best-estimate mean age which they compared to SF<sub>6</sub> derived mean ages. Their paper proved that these compounds could be used, with a time-shift, as a proxy for stratospheric input into the tropical stratosphere. So, provided the precision and accuracy of the sampling technique is sufficient, stratospheric measurements of HFC-125 (and PFC-116) mixing ratios can be used to determine mean age of air. This chapter will investigate whether AirCore sampling provides sufficient precision to use HFC-125 as an age tracer for these samples.

#### *4.1.2.c A short introduction to CFC-113*

As most CFCs, CFC-113 (CCl<sub>2</sub>FCClF<sub>2</sub>) was used as a refrigerant, but it was also used as an aerosol propellant, and as a cleaning agent for electrical components. CFC-113 has no sinks in the troposphere, and its sink reactions in the stratosphere are with O(<sup>1</sup>D) and photolysis which is the dominant loss process. Concentrations have slowly decreased since their peak of 84.2 ppt in around 1995. By 2016 concentrations were 71.4 ppt, declining to 70.8 ppt in 2017, and to 70.3 in 2018 (NOAA background trend, reported in Burkholder et al. (2022)). It has a stratospheric lifetime of 94.5 years, and with a high ODP of 0.81 is a substantial threat to the ozone layer. It is also a potent greenhouse gas, with a direct GWP (100 yr) of 6080 (Table 1-1).

Continued monitoring is necessary to ensure that concentrations continue to decrease, and to spot rogue emissions or emissions from sources not previously covered by the Montréal Protocol. CFC-113 (and CFC-113a) emissions modelling was done in (Adcock et al., (2018), and (Lickley et al., (2020) found ongoing emissions of CFC-113 which were

considerably larger than would be expected from known banks and other sources, which suggests that there is a greater contribution to climate change and ozone depletion from this compound than previously thought. As such it is worth investigating the viability of AirCore sampling to monitor this compound.

#### 4.1.2.d A short introduction to CFC-115

CFC-115 ( $\text{CClF}_2\text{CF}_3$ ) is a particularly long-lived chlorofluorocarbon, compared to CFC-11's lifetime of 52 years. CFC-115's lifetime was estimated to be 540 years ( $\pm 17\%$ ) via a 2-D model for 2000 steady-state conditions, in which the model input kinetic and photochemical parameters to derive the steady state lifetime estimate (Ko *et al.*, 2013). Chapter 3 of this thesis produced an observation-based steady state lifetimes of 369 (328-435) years utilising measurements of air samples collected in the stratosphere.

CFC-115's only sinks are in the stratosphere, and the main pathways for its removal are reactions with excited atomic oxygen  $\text{O}(^1\text{D})$  which accounts for roughly 63% of its loss, and short-wavelength UV photolysis (37%) (Ko *et al.*, 2013). CFC-115 has an ozone depletion potential (ODP) of 0.27 ( $\pm 0.02$ ) (Table 1-1). While this is smaller than the ODP of 1 for CFC-11, its significantly longer lifetime means that CFC-115 can do damage to the ozone layer for much longer.

As discussed in section 3.1.2 CFC-115's growth rate of  $0.03\text{ppt yr}^{-1}$  has remained the same from 2016 to 2020 and abundance had risen from 8.5 ppt to 8.7 ppt (Table 1-1). While the overall abundance is low, CFC-115 has a global warming potential (GWP) of 7,310, so even small concentrations of it (particularly considering the compound's long lifetime), are a concern. Like many CFCs, CFC-115 has been used in refrigerants; in addition, CFC-115 is a known by-product of HFC-125 production and has been found in laboratories during air-conditioning leakages (Vollmer *et al.*, 2018).

CFC-115 has been studied via archived air, firn air samples and in situ measurements (Vollmer *et al.*, 2018), modelling (Totterdill *et al.*, 2016), research aircraft (Daniel *et al.*, 1996), and kinetic experiments (Baasandorj *et al.*, 2013; Ko *et al.*, 2013). Totterdill *et al.*, (2016) used model data to present updated values for CFC-115's atmospheric lifetime, infrared absorption spectra, radiative forcing and global warming potential. The study also found that omitting stratospheric adjustment could result in underestimates of radiative forcings (by between 5-

35%) and omitting clouds can result in a significant overestimate (60%). Stratospheric adjustment involved adjusting stratospheric temperatures using an iterative process in which changes in heating rate over 100 days resulted in the stratospheric temperatures returning to radiative equilibrium. As clouds absorb across the same spectral region as CFC-115, they can result in a reduction of radiative forcing.

Daniel et al., (1996), did not study CFC-115 directly, but used it, along with CO<sub>2</sub> as an age tracer. Baasandorj et al., (2013) presented total and reactive rate coefficients for the O(<sup>1</sup>D) reaction for a number of compounds, including CFC-115. While the SPARC report (Ko et al., 2013) consolidated the known kinetics of CFC-115 along with a large number of compounds.

In order to expand and enhance the available methods for studying CFC-115, this chapter will examine the use of the AirCore technique. This would be particularly useful in circumstances where a larger, more expensive campaign, is not possible.

#### *4.1.2.e A short introduction to Methyl Chloride*

Methyl chloride (CH<sub>3</sub>Cl) is an ozone-depleting substance, and is the shortest lived compound examined in this thesis, with a tropospheric lifetime of 1.57 years, and a stratospheric lifetime of 30.4 years (Burkholder et al., 2022). Its sources are largely natural in origin, and it is not controlled by the Montréal Protocol. Major sources include tropical and subtropical plants, biomass burning, the ocean, salt marshes, and fungi (Rhew, Miller and Weiss, et al., 2000; Yokouchi et al., 2000; Mead et al., 2008; Archibald et al., 2015). The major anthropogenic source is believed to be coal combustion, with a smaller component from the chemical industry (McCulloch et al., 1999). Major sinks are oxidation by hydroxyl radical, uptake by soils, degradation in oceans, and photolysis in the stratosphere. Global source strength is about 20% lower than the magnitude of known sinks (World Meteorological Organization, 2010) and as the background trend remains largely stable (if seasonal variation is taken into account) this implies there must be other sinks not currently identified in order to account for the stable abundance of the compound.

While it is not as potent a greenhouse gas as some of the other compounds investigated here, it is still 6 times more potent than CO<sub>2</sub> (though miniscule in abundance compared to CO<sub>2</sub>) (Table 1-1).

Non-controlled substances contribute approximately 20% of total tropospheric chlorine, of which 17% is due to CH<sub>3</sub>Cl. Concentrations of CH<sub>3</sub>Cl fluctuate, with seasonal and regional differences. For example, the 2018 WMO report noted that the 2016 global mean mole fraction from NOAA global networks was 559 ppt, approximately 2-3% higher than the 2012 values, but this is consistent with historic variability (Engel et al., 2018). Li et al., (2017) found that measurements of atmospheric CH<sub>3</sub>Cl concentrations at a remote background site in East Asia, revealed significant pollution events, on top of seasonal variation. The paper highlighted the importance of accounting for emissions from the chemical industry, so that global anthropogenic emissions are not underestimated.

Significant uncertainty remains regarding anthropogenic emissions of CH<sub>3</sub>Cl; AirCore measurements could be used to supplement monitoring for pollution events, and to better constrain transport estimates. In addition, AirCore measurements could also be used to determine variability in the amount of CH<sub>3</sub>Cl reaching the stratosphere, as while this may be substantial it is not very well understood (Umezawa *et al.*, 2014; Adcock *et al.*, 2021). So this chapter will investigate whether AirCore measurements are a viable method for investigating CH<sub>3</sub>Cl.

#### 4.1.2.f A short introduction to HCFC-141b

HCFC-141b (CH<sub>3</sub>CCl<sub>2</sub>F) is the second most abundant HCFC after HCFC-22 (Laube *et al.*, 2020). As a hydrochlorofluorocarbon (HCFC), it was used primarily as a foam-blowing agent, as well as a solvent in electronics and precision cleaning. Global mean growth rates reached their first maximum in 1998 at 1.9 pmol mol<sup>-1</sup> yr<sup>-1</sup>, then a second in 2011 at 1.0 mol<sup>-1</sup> yr<sup>-1</sup>. Between 2011 and 2015 the compound showed a 70% decline with a growth rate of ~0.3 pmol mol<sup>-1</sup> yr<sup>-1</sup> (Burkholder *et al.*, 2022). As discussed in section 1.2 HCFCs were used as a replacement for CFCs because as they pass through the troposphere, they react with hydroxyl radicals (OH) rapidly, and this reduces the chlorine that reaches the stratosphere (and in turn depletes ozone). While HCFCs have ocean sinks, the primary sink mechanism in the atmosphere is via OH radicals (Western *et al.*, 2022).

The 2007 adjustment to the Montréal Protocol required the accelerated phase-out of emissions of HCFCs, and this seems to have been effective as the annual average growth rate of chlorine from HCFCs has decreased from 9.2 ± 0.3 ppt yr<sup>-1</sup> for 2008-2012, to 5.9 ± 1.3 ppt

yr<sup>-1</sup> for 2012-2016. Emissions of HCFC-141b have decreased by 10%, between 2012 and 2016. However, as the total chlorine from HCFCs has continued to increase, it is important to continue monitoring the compound (Simmonds *et al.*, 2017). HCFC-141b's global emissions in 2020 were  $58.1 \pm 8.8$  Gg yr<sup>-1</sup> and  $56.4 \pm 8.2$  Gg yr<sup>-1</sup> from AGAGE and NOAA respectively. This is smaller than in 2016; however, after this initial drop emissions rose each year since 2017, amounting to a total rise in emissions of ~4.5 Gg (Burkholder *et al.*, 2022).

HCFC-141b has a stratospheric lifetime of 72.3 years which contrasts with its much shorter tropospheric lifetime of 10.7 years (the shorter lifetime was an important factor in choosing HCFCs as first-stage replacements for CFCs), and an FRF of 0.34. With an ODP of 0.102 and a direct GWP (100 yr) of 800, this compound is both a threat to stratospheric ozone and to global warming (values in Table 1-1).

#### 4.1.2.g A short introduction to HCFC-142b

HCFC-142b (CH<sub>3</sub>CClF<sub>2</sub>) is the second HCFC examined here. It was used primarily as a foam-blowing agent, and additionally as an aerosol propellant and as a refrigerant. HCFC-142b's global mean growth rate saw its first maximum in 2008 at 1.1 pmol mol<sup>-1</sup> yr<sup>-1</sup>. This was followed by a strong decline of 90% in 2015, dropping to 0.11 pmol mol<sup>-1</sup> yr<sup>-1</sup> (Simmonds *et al.*, 2017).

Concentrations of HCFC-142b has decreased from 22.54 ppt (AGAGE)/ 22.02 ppt (NOAA) in 2016, 22.23 ppt (AGAGE)/ 21.69 ppt (NOAA) in 2020 Burkholder *et al.* (2022). HCFC-142b has a stratospheric lifetime of 212 years, and an FRF of 0.17. It has a lower ODP (0.057) than HCFC-141b (0.102), but a higher global warming potential (2070 versus HCFC-141b's 800) (Table 1-1). So both compounds are investigated here.

## 4.2 Methodology.

For this initial analysis I looked at eleven flights from April 2018 to October 2020. Each AirCore and subsampler was given a name in order to more easily differentiate between them (Table 4-1).

Table 4-1. The locations of each launch, the dates of launches, the dates those flights were analysed with the number of days delay between launch and analysis, whether a Picarro was used (and its type), which AirCore and Sub-sampler were used. Details on the exact configuration of each AirCore (4.2.1) and Sub-Sampler (4.2.2) is found in their respective sections.

Location of Launch	Flight date	Delay (days)	Picarro	AirCore	Subsampler
Sodankylä, Finland. (67.42 N, 26.59 E)	17/04/2018	36-42	Yes	AIRCORE#1	Luna (simple)
Elsworth, England. (52.26 N, 0.07 W)	01/05/2018	0-9	No	Hester	Ed (complex)
Elsworth, England. (52.26 N, 0.07 W)	14/05/2018	0-8	No	Hester	Ed (complex)
Sodankylä, Finland. (67.42 N, 26.59 E) (RINGO 02)	20/06/2018A	34-35	Yes	AIRCORE#1	Ed (complex)
Sodankylä, Finland. (67.42 N, 26.59 E) (RINGO 03)	20/06/2018B	36	Yes	Hester	Shaun (complex)
Elsworth, England. (52.26 N, 0.07 W)	27/09/2018	125-126	No	Hester	Ed (complex)
Elsworth, England. (52.26 N, 0.07 W)	10/10/2018	113-121	No	Synflex-Serafina	Shaun (complex)
Trainou, France (47.97 N, 2.09 E)	16/06/2019	436-438	No	Lyra_v2	Shaun (complex)
Trainou, France (47.97 N, 2.09 E)	19/06/2019	449-450	Yes	Lyra_v2	Luna (simple)
Jülich, Germany (50.91 N, 6.41 E)	25/04/2020	117-122	Yes	Lyra_v2	Ed (complex)
Jülich, Germany (50.91 N, 6.41 E)	13/10/2020	1-2	No	Lyra_v2	Shaun (complex)

#### 4.2.1 AirCores

An AirCore consists of a long (around 150 m), thin, coiled tube of stainless steel. This is usually divided into two sections; a shorter (~10-30 m) section with a wider diameter of ½ inch, and a much longer (~120+ m) section with a narrower diameter of 1/8 inch. These sections of tubing are connected together. At the other end of the 1/8 inch tubing is a 3-way valve which is closed, while the ‘open’ end of the ½ inch tubing connects to first a drier, then an inlet valve, which is opened prior to launch. As this can be complex to visualise Figure 4.1 shows an annotated photograph of one AirCore being prepared for launch. Attached to the AirCore will be 3-5 sensors for temperature and pressure, at different points of the coil, and these will be attached to an Arduino feather which logs the data. (Not shown in Figure 4.1, as these have yet to be added to the AirCore at this stage of the launch).

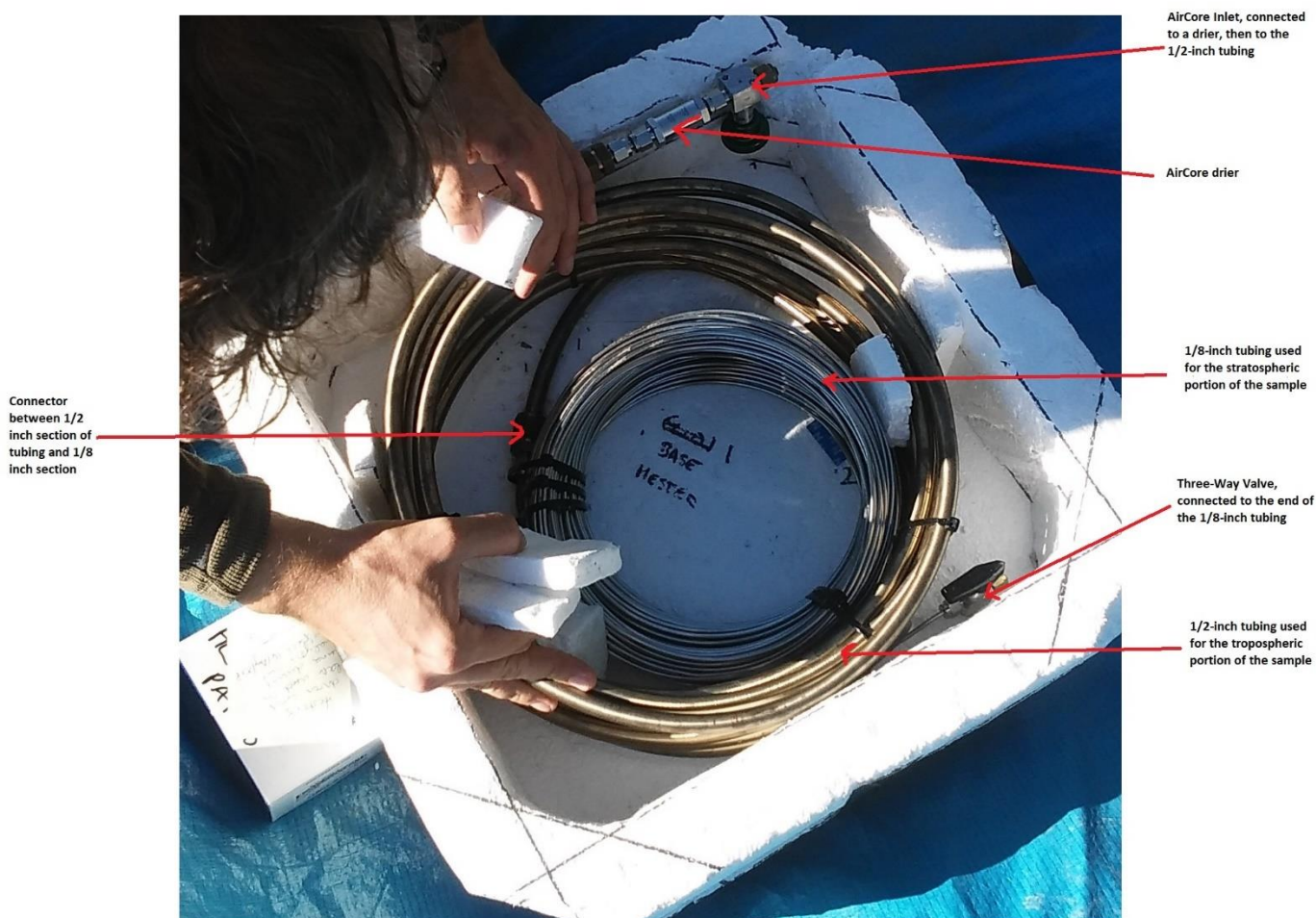


Figure 4.1. The AirCore 'Hester'. Note smaller 1/8 inch tubing on the inside, and the larger 1/2 inch tubing on the exterior with the inlet valve positioned at a hole in the polystyrene packing, which the AirCore will be deployed in in order to protect the sensitive equipment, particularly on landing.

As discussed in 4.1.1, the AirCore technique was developed at NOAA (Karion *et al.*, 2010). Prior to further development at UEA the technique had only been used to analyse CO<sub>2</sub>, CO, and CH<sub>4</sub> and some of their isotopes (Mrozek *et al.*, 2016), and continues to be further refined (Li *et al.*, 2023). This design was used as the basis of the UEA AirCore design, with some modifications to allow measurement of a range of halocarbons. The AirCore is primarily made up of stainless steel (with the exception of the thin plastic (polyethylene) layer in the Synflex<sup>®</sup> tubing), and the AirCore uses tubing specially designed to maximise the quantities of air sampled in the stratosphere. While previous versions of the AirCore (such as described in Karion *et al.*, (2010)), the section of the AirCore that samples tropospheric

air consisted of ¼-inch tubing. Here that section is replaced with 1/2-inch tubing, which increases the internal volume collected into the 1/8-inch tubing used for the stratospheric sample.

However, as this is a technique which has undergone (and continues to undergo) substantial development, data for this chapter was derived from a variety of AirCore iterations. The 4 AirCores and 11 flights discussed in this chapter showcase a variety of differences in AirCore design and sample collection. These are outlined in (Table 4-1).

All AirCores used in this chapter were comprised of two sections, the larger ½ inch tubing for the tropospheric portion of the sample, and the smaller 1/8-inch tubing for the stratospheric sample (see Figure 4.1). In order to prevent reactions and interactions between the sample and the walls of the AirCore, most AirCores underwent the SilcoNert® process which is an inert non-reactive silicon coating process that makes flow paths inert for consistent sampling and analytical results. This is applied via chemical vapor deposition (CVD), to allow an even distribution and a strong cohesion with the material it is applied to (which is important for AirCores, so that the coating is not damaged when the tube is flexed). The three AirCores used during the 2018 flights were named ‘AirCore#1’, ‘Synflex-Serafina’, and ‘Hester’. ‘AirCore#1’ is fully Silco-treated, ‘Hester’ was the first UEA-made AirCore, originally the 1/8-inch section was not Silco-treated, but this was added by May 2018, so was present for all flights discussed here. ‘Synflex-Serafina’ is fully Silco-treated on the 1/8-inch section, but the ½ inch section is Synflex® tubing, which has a thin inner layer of aluminium, covered by a thin layer of plastic. This material was chosen because it is light (an important consideration when a balloon’s payload must be kept under 4 kg total), the downside is that it cannot be coated/Silco-treated, and thus it may allow reactions with certain compounds and the wall of the tube. This is one possibility this chapter will investigate. The last AirCore featured here is ‘Lyra’, which is of similar design to the others. Both the ½ and the 1/8<sup>th</sup> inch tubing (the latter being the portion of the AirCore used for stratospheric sampling) is made of Silco-1000 coated stainless steel. These AirCores each feature a Swagelok 3-way valve, which is greased with a perfluorocarbon-containing compound (this grease is also used in the 2-way valves for the Picarro G2401 and the 3-way valves used in the ‘Luna’ simple sub-sampler). This grease could contaminate the sample (resulting in a high concentration of PFC-116) but should be buffered by the presence of fill-gas (see section 4.2.2).

In order to prevent contamination, prior to launch the AirCore is initially filled with a nearly trace gas-free fill gas. In order to identify contamination from fill gas into atmospheric samples, the fill gas needed to be spiked with something that could be measured on the GC-MS system but is not normally present in air (or in only very low quantities). For this we use Perfluorotriethylamine (PFTEA), of which there is very little in the atmosphere (i.e., at its current atmospheric abundance it is undetectable with our high-sensitivity mass spectrometer which has detection limits in the lower to sub-ppq range). The rest of the fill gas is primarily nitrogen; however, the lab that creates the PFTEA is not totally free of contaminants, so small quantities of SF<sub>6</sub> and some of the compounds we examine here are present in the remaining fill gas.



*Figure 4.2. Preparing for launch: The balloon is being filled with helium. Attached to it is (aside from the tube filling it with helium) a strong cord, which has been securely fastened to the AirCore (large white box in the foreground). Between the AirCore and the balloon a plastic object is affixed to the cord, this contains a Radiosonde which monitors temperature, pressure and relative humidity. At the very end of the cord (beyond the AirCore) is a small black object, which is one of the 3 GPS trackers used to ensure location and retrieval of the instruments. Behind the balloon, at the far edge of the blue tarpaulin is the red and blue parachute which has been attached to the cord. (The large white bottles under the balloon are simply additional weight to assist in tethering the balloon while it is filled).*

In order to launch a careful evaluation of upcoming weather conditions is performed, to assess whether it will be a. safe to launch (high winds for example could prove hazardous), and b. that the balloon will land safely in an area that is isolated (to avoid property damage or injury to people), and safe to retrieve from (we cannot retrieve our equipment from water). Once a suitable launch 'window' appears, relevant notices are given (in the UK this consists of a 'Notice to Airmen' (NOTAMs) but different countries have their own requirements/forms of notice).

To launch an AirCore, all equipment to be launched is laid out on the ground (usually on a water-proof sheet, as can be seen in Figure 4.2), along the cord that will attach all components. Some monitoring equipment is inside the box containing the AirCore, but some need to be outside to be effective (and because there are legal limits on the weight of individual sections of a balloon's payload). Equipment is then attached to the cord, and the balloon is steadily filled with helium. The equipment included can vary (depending on which conditions one is monitoring) but typically includes a radio-sonde (to monitor pressure, relative humidity and temperature, multiple (in case of failure) GPS trackers so that the equipment can be located after landing, and a parachute to ensure safe landing of equipment. (On one occasion the parachute failed. The packing for the AirCore proved excellent and while it sustained slight damage, this was quickly repaired, though the sample from that flight was lost). Once launched the balloon will be tracked using the GPS trackers, and upon landing will be retrieved as quickly as possible. It is then returned to the lab, where the sample from the AirCore can be transferred into a sub-sampler.

#### **4.2.2 Sub-sampling**

Once an AirCore has been recovered after a flight, the stratospheric portion of its contents are swiftly transferred into a sub-sampler, in order to better preserve the vertical profile by preventing mixing along the entire length of an AirCore.



*Figure 4.3. The simple sub-sampler 'Luna'. Note the extensive copper-coloured coils, each loop is a sample loop, attached to a 3-way valve at the exterior of the sub-sampler.*

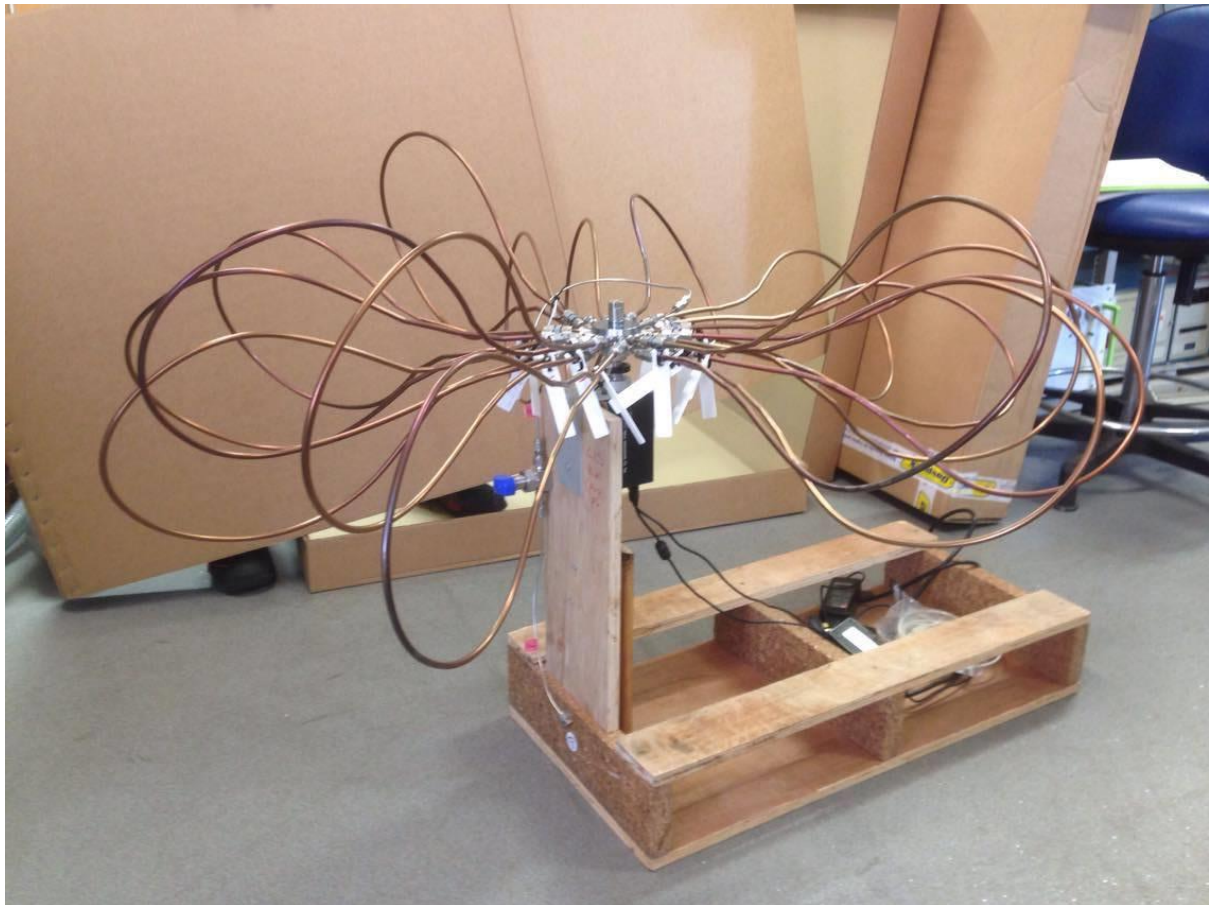


*Figure 4.4. Complex sub-sampler 'Ed'. Note each copper-coloured loop connected to the stainless-steel rotary valve in the centre. Ed is here supported by a wooden scaffold, and there is a flow-meter attached to the valve.*

The three subsamplers used to store samples from the flights listed in Table 4-1 can be divided into two categories: simple and complex. The simple subsampler, named 'Luna' (Figure 4.3), is a continuous series of Sulfinert® coated tubing intersected with three-way valves (Swagelok catalogue numberSS-43GXS4). This was constructed following the blueprint given in Mrozek et al., (2016), and consists of 10 loops each with a volume of 20 ml and 5 loops with a volume of 50 ml each.

The simple sub-sampler is conditioned with 'fill gas', then filled from the AirCore, and the three-way valves are closed after a pre-determined time when the stratospheric air should have reached the end of the last loop. The valves in-between each loop are then closed. This is the same technique described in Mrozek et al., (2016). As the uppermost sample loops (usually only 1-2 of them) still contain a significant portion of the fill gas, and correcting for this is complex and introduces uncertainties, these samples are excluded for analysis here, in the same manner as Laube et al., (2020).

The total stratospheric portion of the AirCore sample (total volume of 1.2-1.4 litres) is only around 200-300 ml (at ambient temperature and pressure), and this is split into multiple segments of the sub-sampler. The sample size accommodated by each loop is approximately 20 or 50 ml, which is 2 orders of magnitude smaller than typically measured amounts from samples collected using aircraft-based sampling techniques (200-300 ml). The loops are each approximately 2m long with 1/4-inch diameter (Laube *et al.*, 2020).

The remaining two subsamplers are complex subsamplers, named 'Ed' and 'Shaun' (Figure 4.4). These are a series of separate Sulfinert® coated loops, connected to a multiport Valco SC valve (<https://www.vici.com/vval/sc.php>), an 1/8-inch 16 position selector. In this valve the 'common-in' port is open, while the 'common-out' port is plugged, the 'default position' used for transport purposes is also plugged. The remaining 30 ports are connected in pairs to 15 sample loops, each with a volume of ~20 ml. In contrast to the simple sub-samplers, these are evacuated before filling. Each loop is filled for a set amount of time determined by tests we carried out to determine how long it takes to get a stable pressure inside those loops, which is a maximum of 15 seconds, then the valve is switched, and the next loop is filled. A retrieval algorithm is used to assign average altitudes to each sample and was developed by Alex Lojko as part of his MSc at UEA. This uses the minimum pressure measured by the radiosonde (a device which measures various atmospheric parameters such as altitude, pressure, and temperature, then transmits them by radio to a receiver at ground level), which is launched alongside each AirCore, to determine the top of the profile (see supplement to (Laube *et al.*, 2020) for details).

The complex sub-samplers have a single valve, and ports are closed by moving the internal rotor to a position where there is no loop, but instead a plug. There is a slight progression between 'Ed' and 'Shaun'; 'Shaun' used shorter loops with a larger internal diameter. . Shorter loops were hoped to be 'sturdier' and thus minimise vibrations during shipping of the samplers, which could cause leakages. This did however change the surface-to-volume ratio slightly, but not the internal volume of each loop.

The complex-subsampler technique is much more convenient to analyse as one need only connect the sub-sampler once before analysis. This theoretically leaves less room for mistakes or accidents and so might provide more viable data than the simple-subsampler. In addition, the evacuation procedure of the complex sub-samplers prior to filling, should be better at preventing contamination of the samples with fill gas. However, the three-way

valves (used in the simple sub-samplers) are typically much less prone to internal leakage between loops as compared to the multi-position Valco valve. Some compounds may be more susceptible to such problems, while others may show no effect. Which compounds were affected and to what extent, is a question explored further in section 4.3.

While the AirCores discussed here were retrieved quickly and their samples transferred into a sub-sampler within hours of landing, there were varying delays between their transfer to a sub-sampler and their analysis via GS-MS. There are a few reasons this happened; if a sample was collected on campaign (such as those that took place in France during the RINGO campaign), then it would take time for the sub-samplers to be safely shipped back for analysis. Another possible cause of delay might be that the GS-MS system was non-functional at the time as it is a delicate device, and repairs can take considerable time to arrange.

For the purposes of this chapter, delay was divided into three broad categories: ‘small’ refers to 2 weeks or less, ‘medium’ refers to up to a month, and ‘long’ refers to delays of greater than 3 months (there were no flights where the delay was between 1 and 3 months). Some compounds may remain stable during storage, others may decay, become contaminated or react with the walls of the sub-sampler. So, it was important to learn which compounds were affected by delays, and to what extent they were.

### **4.2.3 Stability Tests**

A number of stability tests were performed by Dr Laube and his team in order to identify more precisely the effects of storage procedures, delay between sampling and analysis, Picarro G2401 use (this device measures CO<sub>2</sub>, CH<sub>4</sub>, and CO), and AirCore temperature. It should be noted that two different Picarro G2401 devices were used: the one situated at the Forschungszentrum, Jülich (which is used for all stability tests discussed here, and most AirCore flights where a Picarro G2401 is used), and a device from the Finnish Meteorological Institute (FMI) which is denoted in this thesis as ‘Picarro FMI-G2401’.

To test the effect of storage over time, the complex sub-sampler ‘Shaun’ was filled using the same procedure as would be used for a ‘real’ stratospheric sample. Shaun was filled with either the SX3600 standard (unpolluted tropospheric air collected in June 2019), research grade Helium, synthetic air, or lab air. In addition, both a dilution series (prepared

via mixing the standard with ultra-pure N<sub>2</sub> in various Silco canisters) and the lab air were not filled into the sampler, but simply measured via the AirCore inlet of the inlet system. The samples of the SX3600 standard were left for 1, 3, 9, 15, 20, or 23 days, then tested (using the procedure detailed in section 4.2.4).

To simulate the effect of leaving a collected sample in the AirCore for an extended period of time (as would happen if the AirCore cannot be located quickly after it lands), our most advanced AirCore (named 'Lyra') was filled with standard (SX360), then tested the next day.

After several of the flights examined in this chapter, the AirCores' sample was passed through the G2401 Gas Concentration Analyzer from Picarro before sub-sampling. To transfer the sample from the AirCore to the Picarro then onto a sub-sampler, the working standard (SX3600) is used as a 'push gas' and a pressure controller is used to maintain a stable flow that is regularly checked by a flowmeter. To test what effect this procedure might have on a sample, standard was sampled through a G2401 Gas Concentration Analyzer which measures CO, CO<sub>2</sub>, CH<sub>4</sub>, and H<sub>2</sub>O. The sample was then passed from the analyser into the 'Shaun' sub-sampler and was then analysed immediately afterwards. The Picarro used in the stability tests, and that used during the RINGO campaign are the same model, however the Picarro used during the RINGO campaign (Picarro FMI-G2401) had a different pump in which most connectors and tubes were replaced with stainless steel Swagelok versions.

Another factor to be investigated is the effect of temperature on AirCores. One mechanism is that as the temperature alternatively increases and decreases it can inhibit or accelerate the mixing of the air samples. This would potentially 'smear' the altitude resolution. Another mechanism is that if the AirCore cools down too much, higher boiling gases (in this chapter this refers to CFC-113 and HCFC-141b) can condense on available surfaces such as the stainless-steel tubing or the drier. The drier is filled with magnesium perchlorate powder, and has a large surface area, which is located close to the inlet (the coldest part of the AirCore).

To investigate the effect of temperature on AirCore samples, the 'Lyra' AirCore was placed in a climate simulation chamber, cooled to -10 degrees C, then filled with SX3600 standard over 10 minutes in 20 torr increments. It was allowed to equilibrate before the next 20 torr was added. This was an attempt to better simulate in-situ conditions, as an

AirCore would not be filled immediately in the stratosphere, but over the time during which it falls. The AirCore was left to equilibrate to 20 degrees (to simulate the time between landing and sub-sampling after retrieval), the sample was then transferred to the 'Shaun' sub-sampler and measured the same day.

#### **4.2.4 Analysis of Samples**

The data in this section was processed and analysed in much the same way as described in section 2.3, but due to the nature of sample collection via AirCore, there are a few differences. At approximately 15-20 ml, the sample volume for AirCore samples is substantially lower than the canister sampling used in Chapter 3, which were around 200-300 ml. The detection limit for the GS-MC is dependent on several factors, notably the trapping amount, the species measured, and the ion used for quantification. For the trapping amounts seen from AirCore samples, the detection limits would typically be between 0.01 and 0.2 ppt. The detection limit is defined as a signal-to-noise ratio of 3, the noise being determined as root mean square (RMS).

Smaller sample volumes can make it more difficult to detect some low abundance compounds and make repeating samples (as described in section 2.3) difficult or impossible. This is why one of the aims of this chapter is to demonstrate the robustness of the data collected from AirCore sampling, particularly with regard to age tracer species.

#### **4.2.5 Mean Ages derived from AirCores Measurements**

The concept of Age of Air, and that of mean age of air was discussed in section 1.4 and features prominently in Chapter 3, notably in Section 3.2.4. However, Chapter 3 used data collected via traditional sampling techniques on a research aircraft; sampling age tracers in this way is confirmed to be reliable (Leedham-Elvidge *et al.*, 2018). SF<sub>6</sub> collected via AirCore sampling has been shown to be reliable (Laube *et al.*, 2020), and this chapter will demonstrate the reliability and comparability to samples collected via research aircraft, of two additional age tracers: PFC-116 and HFC-125.

The first step was to exclude AirCore flights where the data was clearly affected by the factors discussed earlier (e.g. delay between flight and analysis, using simple sub-sampler, contamination from the use of a Picarro G2401, etc.). In their respective results sections

(section 4.3.1 for PFC-116, and section 4.3.2 for HFC-125), the factors affecting each flight are examined and discussed at length, so will not be repeated here. In short, of the flights that took place in 2018, only the May flights had sufficient precision and robust profiles to be used reliably as age tracers. (Due to time constraints mean ages derived using HFC-125 and PFC-116 were not derived for the 2019 and 2020 flights). Therefore, only the May flights utilise the (merged) mean ages derived using these tracers. For all other flights mean ages were derived using SF<sub>6</sub>, with the correction proposed in Leedham-Elvidge et al., (2018) applied.

In order to investigate the use of C<sub>2</sub>F<sub>6</sub> and HFC-125 as age tracers for AirCore samples, mean ages were derived for each compound, using the process described in section 2.6 (Ostermüller *et al.*, 2017; Engel *et al.*, 2018a; Fritsch *et al.*, 2020). From Leedham-Elvidge et al., (2018) we know that the ratio between the mean ages derived from SF<sub>6</sub> and the other compounds (CF<sub>4</sub>, C<sub>2</sub>F<sub>6</sub>, C<sub>3</sub>F<sub>8</sub>, CHF<sub>3</sub>, HFC-125) is in the region of 1:0.8, so when examining the slope of these mean age correlations, I wanted to see how close they were to 0.8, and whether that was within the uncertainties. The process to generate entry mixing ratios and mean ages requires specific (licensed) software which I did not have access to while analysing the 2019 and 2020 flights. Dr Laube was able to generate entry mixing ratios and mean ages using SF<sub>6</sub> data, but due to time constraints was unable to do this for PFC-116 and HFC-125. So for the 2019 and 2020 flights mean ages derived using SF<sub>6</sub> data, and the 0.8 conversion factor described in Leedham-Elvidge et al., (2018) was used so that the mean ages and entry mixing ratios used were comparable. Section 4.3.8 explores how comparable methods for deriving mean age were, and while differences were observed, they did prove sufficiently comparable.

To test this I used both the bootstrapping method of Barreto & Howland, (2010) and the Williamson-York Iterative Bivariate Fit Shell method from Cantrell, (2008) (both described in detail in section 2.4 Bivariate Data). The correlation between the SF<sub>6</sub> derived mean ages and the PFC-116 or HFC-125 derived mean ages, was subjected to these two processes separately. From each method I derived the slope and intercept for each correlation.

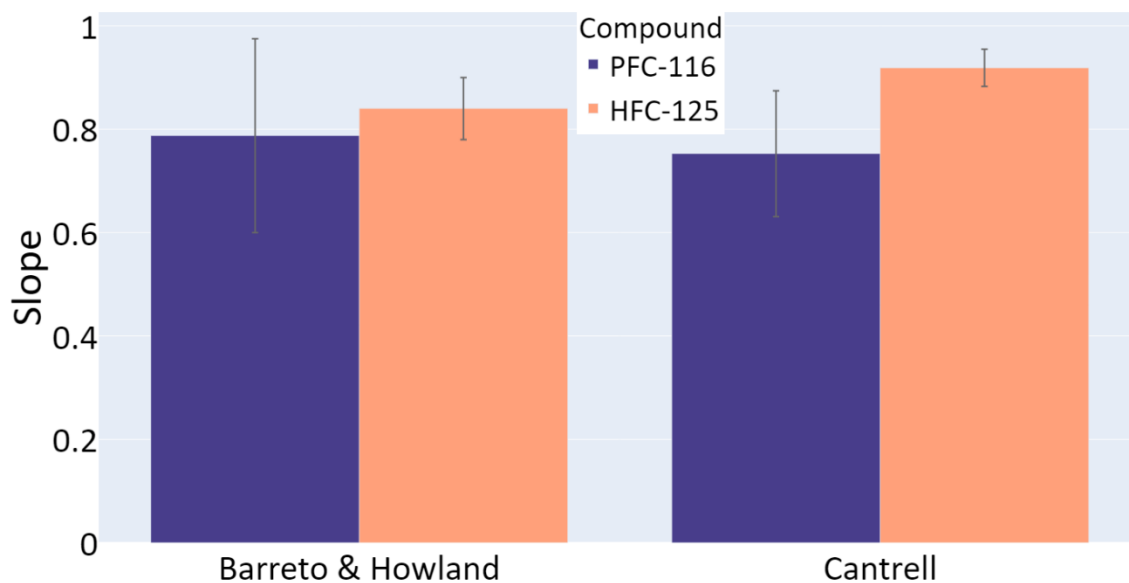


Figure 4.5. The mean slope for the correlation between the SF<sub>6</sub> derived mean ages and the PFC-116 or HFC-125 derived mean ages, using either the Barreto & Howland, (2010) or the Cantrell, (2008) methods. Error bars are to 1 sigma uncertainty, and represent the range of values for the slope derived using each method.

While there is some variation, in Figure 4.5 the error range for the slope encompassed 0.8 for all but the HFC-125 v SF<sub>6</sub> slope as analysed by the Cantrell method. As seen in Figure 4.8 even when obvious outliers are removed, HFC-125 saw some considerable scatter (for reasons discussed in section 4.3.2), and by excluding those outliers there were fewer flights to analyse here. If the error range in Figure 4.5 were extended to two sigma, it would encompass the 0.8 figure.

The intercept was harder to interpret, as there is a limited dataset. If the dataset either does not include or includes only a small number of samples at or around zero years mean age, then an extrapolation from the trendline would be required. If the AirCore sampled tropospheric air, it could erroneously generate negative values for mean age. However, for both compounds the intercept was within  $\pm 0.5$  of 0 years mean age, which is within the expected uncertainty range.

In order to calculate an entry mixing ratio for a sample, a tropospheric trend of each compound was required. The background trends were acquired from either the AGAGE Data Base (Prinn *et al.*, 2020) the NOAA data base (NOAA (National Oceanic and Atmospheric Administration), NOAA/ESRL Global Monitoring Division., 2020), or Cape Grim archived air, analysed at UEA. UEA data is updated (to 2020) from those previously published in Laube et

al., (2013) for HCFC-141b, HCFC-142b, and CFC-113, Laube et al., (2016) for CFC-114 and CFC-114a, and Leedham-Elvidge et al., (2018) for PFC-116 and HFC-125.

AGAGE uses different calibration scales to UEA and NOAA for PFC-116, so in order to account for an offset between AGAGE data and UEA/NOAA, a conversion calculation was used (Equation 4-1) based on Trudinger et al., (2016). The linear equation of the line for each dataset (both AGAGE and UEA data) was plotted, the difference between these equations was calculated, then applied to the AGAGE dataset to account for the offset.

$$N = \left( S_N * \frac{A + I_A}{S_A} \right) - I_N$$

*Equation 4-1. Equation for the conversion between the AGAGE dataset and the NOAA dataset. In which NOAA dataset is "N", AGAGE dataset (date and mixing ratio, ppt) is "A", NOAA slope =  $S_N$ , NOAA intercept =  $I_N$ , AGAGE slope =  $S_A$ , AGAGE intercept =  $I_A$ . This equation takes a concentration value for an AGAGE measurement and gives an equivalent for NOAA.*

The method of comparing the trendline equation in order to derive a conversion factor was employed for other compounds where two different scales had been used. For CFC-115, the background trend from 1977 to 2017 used Cape Grim archival air, analysed at UEA (the same data as in Chapter 3, Figure 3.1) and shifted in time by 6 months as Cape Grim is in the Southern Hemisphere. A 6-month shift is required to accurately reflect the time when the air was in the tropics (see section 1.1 for a more detailed explanation). However, as this trend has yet to be updated, and it was not reasonable to extrapolate a trend that ends in mid-2017 into late 2018, I needed to use AGAGE's Cape Grim data for 2018 and 2019, with the same 6 month shift applied. As AGAGE and UEA use different calibration scales it was then necessary to apply a conversion factor to the AGAGE CFC-115 data (dividing the AGAGE data by a factor of 0.96847).

When using NOAA background data for CFC-113 and HCFC-142b the conversion factor found in (Laube *et al.*, 2013) was applied to the AirCore data so that it would be comparable to the NOAA background trend. For quality assurance purposes I also analysed CFC-11 as this has already been well studied (Laube *et al.*, 2020), and it is known that the compound can be analysed reliably.

In order to quantify the uncertainty in mean age estimates, I applied the sample analysis uncertainties to each age tracer for each flight to generate the maximum and minimum mixing ratio of each compound. I used these to generate maximum and minimum

means for all compounds, to 2-sigma uncertainty (uncertainty derived from instrument precision).

### 4.3 Results

Firstly, a brief look at the precision achieved for each compound using AirCore samples, compared to the precision achieved for these compounds using high-altitude research aircraft (taken from the Supplementary information of Adcock et al., (2021)). The results can be seen in Table 4-2. ‘Precision’ here refers to the precision of the measurements (instrument precision).

*Table 4-2. The precision for the compounds examined in Chapter 4, from Adcock et al., (2021), and from AirCore measurements. Shows both the percentage precision uncertainty (from instrument precision), and what that represents in terms of mixing ratio (ppt). AirCore precision includes only flights where the data for that compound was robust, the reasons why this might not be the case for certain flights and certain compounds, are explored in each compound’s respective result section.*

Compound	F113	F115	F141b	F142b	HFC-125	C <sub>2</sub> F <sub>6</sub>	CH <sub>3</sub> Cl
Adcock et al., (2021), % precision	0.9%	0.7%	1.0%	0.8%	0.8%	0.8%	0.6%
Adcock et al., (2021), precision mixing ratio (ppt)	0.64	0.06	0.28	0.19	0.24	0.03	3.33
AirCore precision, %	0.9%	1.0%	1.2%	1.4%	1.4%	1.5%	1.2%
AirCore precision, mixing ratio, (ppt)	0.64	0.09	0.33	0.34	0.43	0.06	6.72

For CFC-113 the precision is the same between Adcock et al., (2021), and the AirCore flights. For the rest of the compounds, AirCore precision was on average 0.4% worse than the precision seen in Adcock et al., (2021). This is to be expected as the sample volume for AirCores is an order of magnitude smaller than those of the canisters used in Adcock et al., (2021). The impact of this worsening precision (if there is a statistically significant impact), will be explored in each compounds’ respective results chapter.

#### 4.3.1 PFC-116

As the tropospheric abundance of PFC-116 around this time was 4.94 ppt (Table 1-1), with a growth rate of around 0.1 ppt (2%) annually (Laube *et al.*, 2022) the average precision is lower than the trend (Table 4-2). This is promising as it shows PFC-116 can be sampled using AirCores and still have good enough precision to potentially be used as an age tracer,

though other factors may still impact its usability, and care must be taken during analysis to optimise precision. Some analysis days or samples may need to be discarded if instrument precision is too poor.

To investigate the quality of data for this compound each flight resulted in, I first plotted (Figure 4.6) PFC-116 mixing ratio (ppt) against CFC-11 mixing ratio (ppt), which has been well-studied in AirCores (Laube *et al.*, 2020).

The majority of the flights form a comparatively visually compact profile; however, there were extremely high mixing ratios seen in the 19.06.2019 and 17.04.2018 flights, and to a lesser but still noticeable extent the 25.04.2020 flight. The 25.04.2020 flight had anomalous data for all compounds (to varying degrees), and this was found to be due to fill-gas contamination (see section 4.2.2 for details on fill-gas). The common denominator for the 19.06.2019 and 17.04.2018 flights is that both used the simple sub-sampler 'Luna', which is known to contain a source of PFCs, which would explain the massive elevation of PFC-116 for these flights. Excluding these three flights gives a clearer picture. This can be seen in Figure 4.6 where the data is colour coded to differentiate a. which AirCore was used, b. which sub-sampler was used, c. how long a delay was experienced between flight and analysis, and d. whether or not a Picarro G2401 was used.

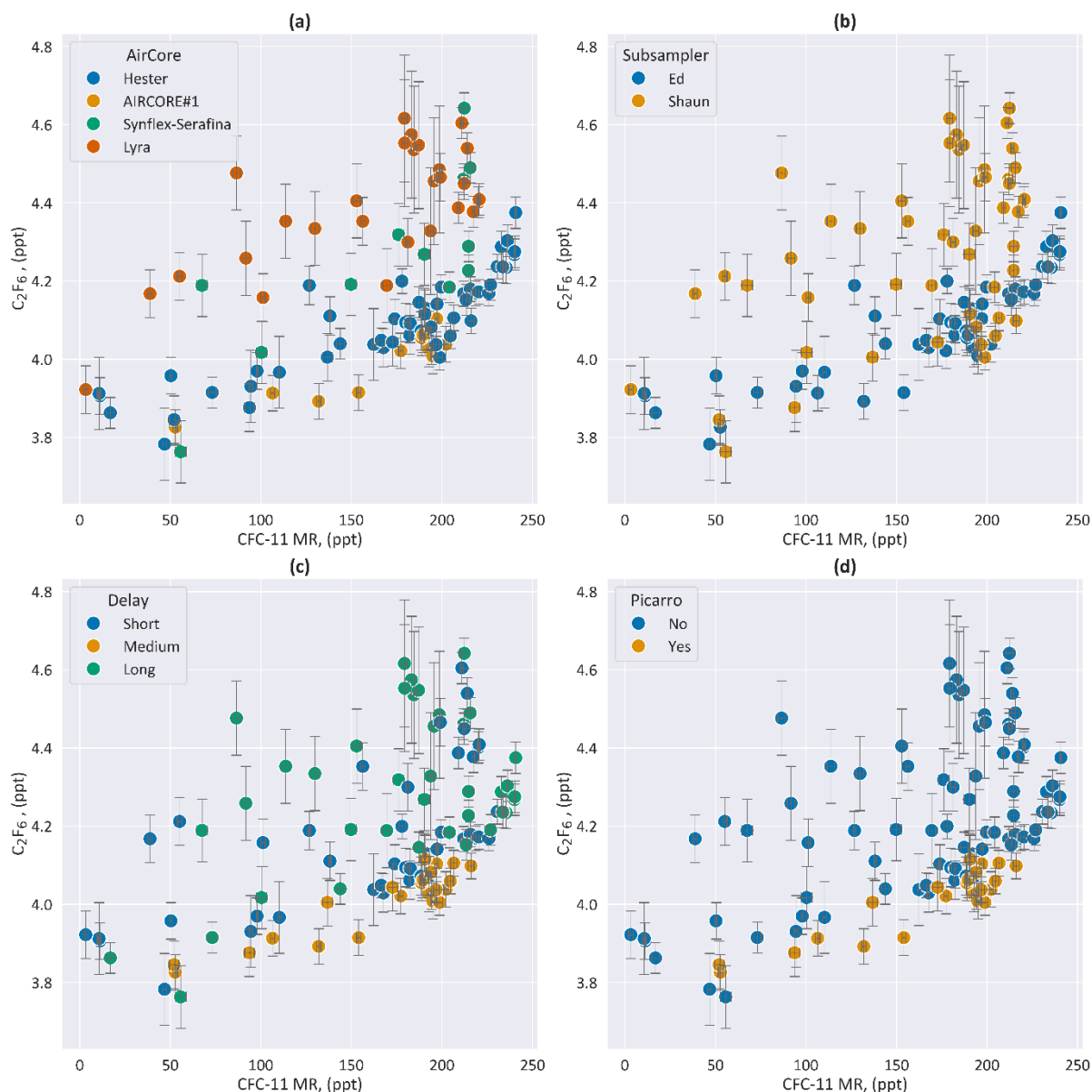


Figure 4.6. Showing factors potentially affecting PFC-116 ( $C_2F_6$ ) mixing ratio (ppt) plotted against CFC-11 mixing ratio (ppt), for all AirCore flights listed in section 4.1.1, (excluding 25.04.2020 and the two flights which used the ‘Luna’ sub-sampler). Hue identifies (a) which AirCore was used, (b) which subsampler, (c) How long the delay between flight and analysis was, and (d) whether or not a Picarro was used. Errors derived using instrument precision, to 1 sigma uncertainty.

Having excluded the clear outlier flights, examining Figure 4.6 still provides some interesting insight into the data. In Figure 4.6 the flights that used the ‘Lyra’ AirCore seem to be those with the highest scatter, followed by the ‘Synflex-Serafina’ AirCore, in Figure 4.6b the most scattered data used the ‘Shaun’ sub-sampler; however, many flights using the ‘Shaun’ sub-sampler did not show this scatter. The same can be said for Figure 4.6d, in which the most scattered data did not use the Picarro G2401, but not all flights that did not

use the Picarro G2401 are scattered. Figure 4.6c shows several flights with either short or long delays had scatter, while the flights with 'medium' delay did not have this scatter. In the stability tests the 'Lyra' AirCore seemed to show some elevation in PFC-116 concentration (Figure B.4) and saw heavy elevation when passed through a Picarro G2401 (Figure B.5). It is possible that the perfluorocarbon grease used in the 3-way valve for these AirCores resulted in some contamination of the samples for these flights.

Another question is how the data from AirCore flights intersects with the tropospheric background trend, as the bulk of the air sampled is in the stratosphere. The AirCore will sample a continuous profile from its highest point to the ground. However, the sub-samplers used only have so much capacity, and as the focus of the research being conducted is stratospheric air, this is what was prioritised. Therefore, when the sample is transferred to the sub-sampler, it may be completely filled with the stratospheric sample before reaching the tropospheric part of the AirCore sample. As discussed in section 1.1 the precise height of the tropopause varies by latitude and season, and as such identifying whether an AirCore sample contains tropospheric air is not as simple as checking the altitude at which it was collected. As PFC-116 is an age tracer, it is particularly important to be able to relate the AirCore data for this compound, to the tropospheric trend.

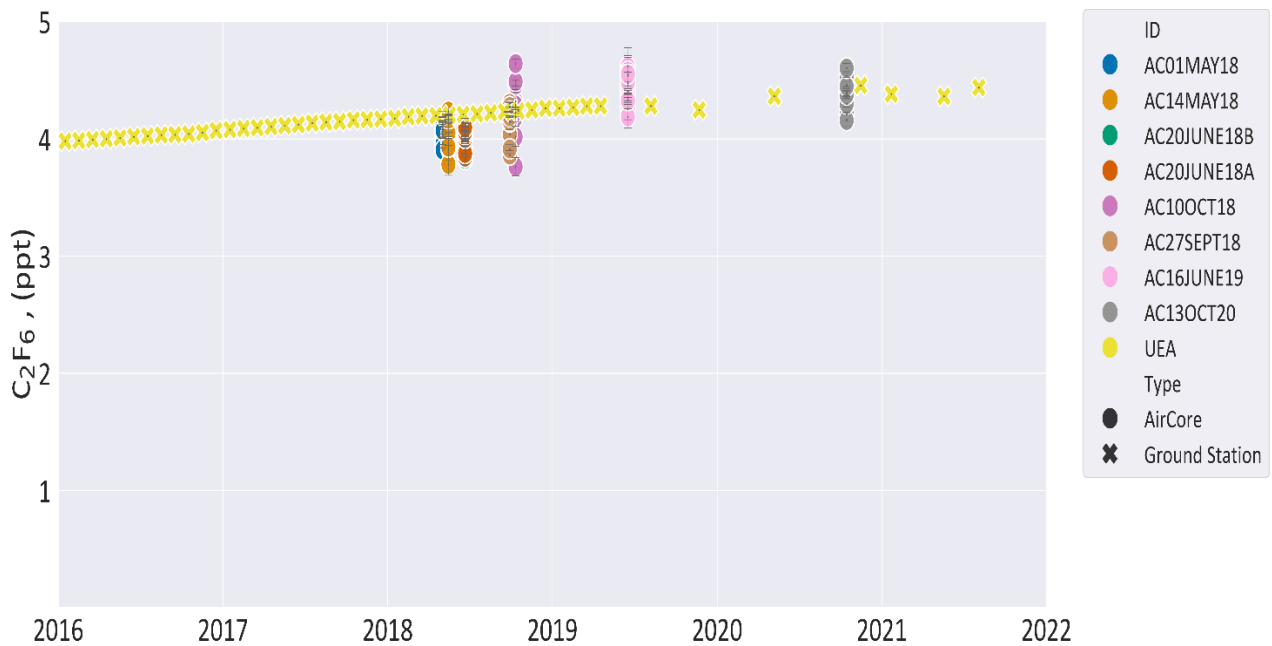


Figure 4.7. 'Selected' Flights only. The mixing ratio of PFC-116 (ppt) in the tropospheric background trend (measured at UEA, updated from Leedham-Elvidge et al., (2018)) and the AirCore flights examined here excluding those with extremely poor data for this compound, plotted against date (yr). Background trend prior to 2016 is excluded here for ease of viewing, but is available for much further back (see Figure A.13)

Examining Figure 4.7 it seems that the flights that intersect but do not exceed the tropospheric background trend are the AC01MAY18, AC14MAY18, AC20JUNE18A&B, and AC27SEPT18 flights. In contrast, the 10.10.2018, 16.06.2019 and 13.10.2020 flights exceed the background trend. It is unclear why these flights had somewhat elevated data for this compound; all three used the 'Shaun' sub-sampler, but this sub-sampler was used on the 20.06.2018A flight and this was not affected. Two of the flights were in mid-October, but the other was in June, so seasonality does not appear to be the cause. They each took place in different countries (Sodankylä Finland, Cambridgeshire England, and Jülich, Germany) so a localised effect is unlikely. These flights take part months or years apart, so while it is possible that all three flights captured air from a pollution event, it does not seem highly probable. As discussed in section 4.2.1 these AirCores do contain a 3-way valve which is coated with perfluorocarbon grease, and the stability tests did show a small effect from the Lyra AirCore (Figure B.4), in Figure 4.7 the flights that exceed the background trend used either Lyra or Synflex-Serafina AirCores (very similar in construction), so this may be the cause.

### 4.3.2 HFC-125

The growth rate for HFC-125 is 3-3.3 ppt yr<sup>-1</sup> or 10-11 % yr<sup>-1</sup> (Liang *et al.*, 2022), so uncertainty from instrument precision for HFC-125 using the AirCore technique is within that range (Table 4-2).

When the mixing ratio of HFC-125 (ppt) is plotted against that of CFC-11 (ppt) there is significant scatter. The one major factor affecting this is the delay between flight and analysis. When those flights are removed, we can examine the data more closely. As can be seen in Figure 4.8 the visual correlation between CFC-11 and HFC-125 is much more compact, though the AirCore flights have more scatter than the Geophysica flight.

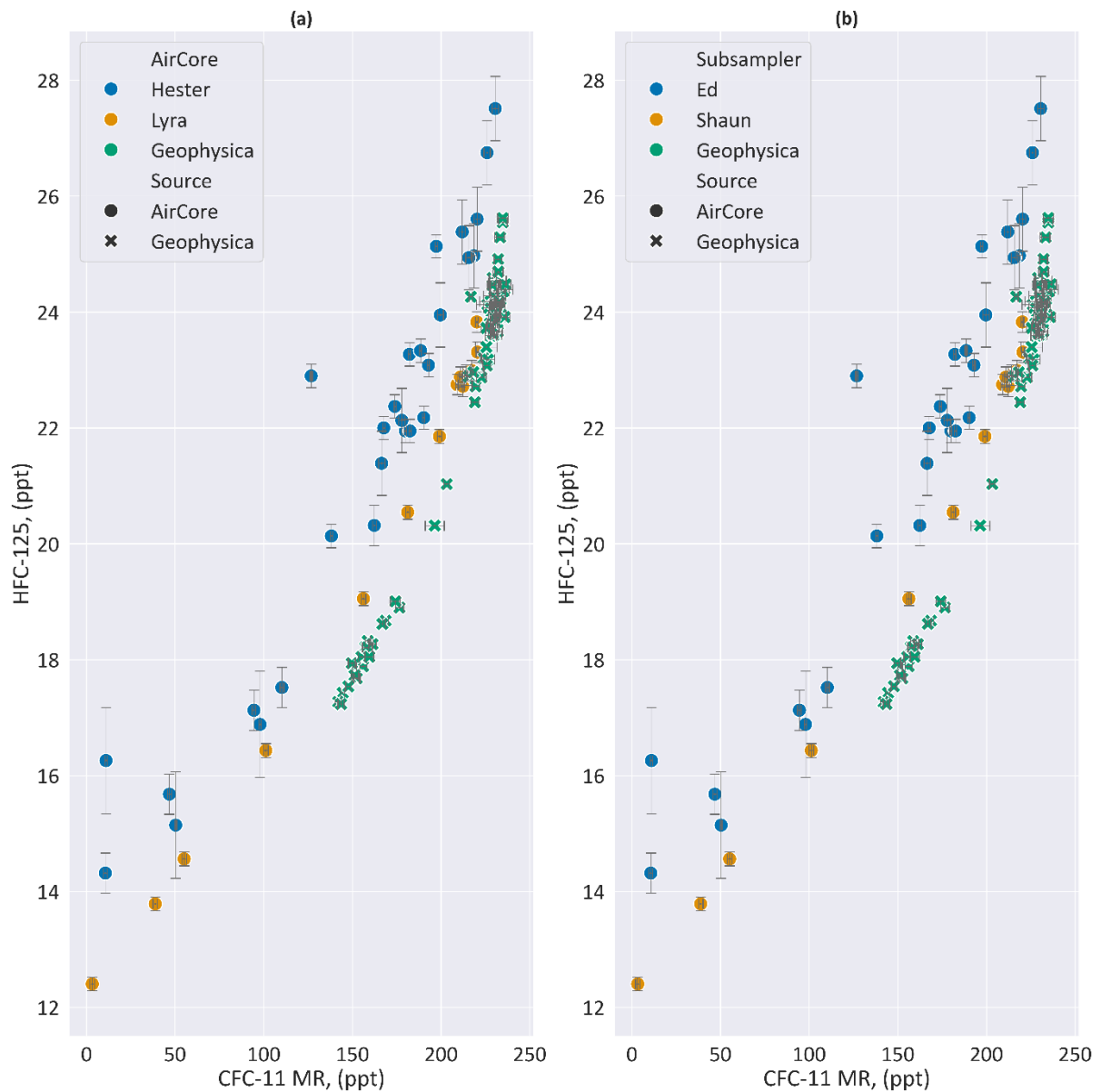


Figure 4.8. Showing Factors affecting HFC-125 mixing ratio (ppt) plotted against CFC-11 mixing ratio (ppt), for all AirCore flights listed in section 4.2, and Geophysica flight KAT17. Hue identifies (a) which AirCore was used, (b) which subsampler. Errors derived using instrument precision, to 1 sigma uncertainty.

Examining Figure 4.8, having accounted for the scatter caused by delay, there are three remaining flights including one from the Geophysica flights, so it is hard to draw conclusions from this. The most scattered flights use Hester and Ed (AirCore and subsampler respectively); however, these flights were the May 2018 flights, while the flight which used Lyra and Shaun occurred in October 2020. It is possible that improvements to sampling or analysis techniques could account for the decreased scatter. It could also be a coincidence. None of these flights used the Picarro G2401.

As with PFC-116 (section 4.3.1), HFC-125 is an age tracer and therefore it is important to be able to relate the AirCore data for this compound to the tropospheric background trend (Figure 4.9).

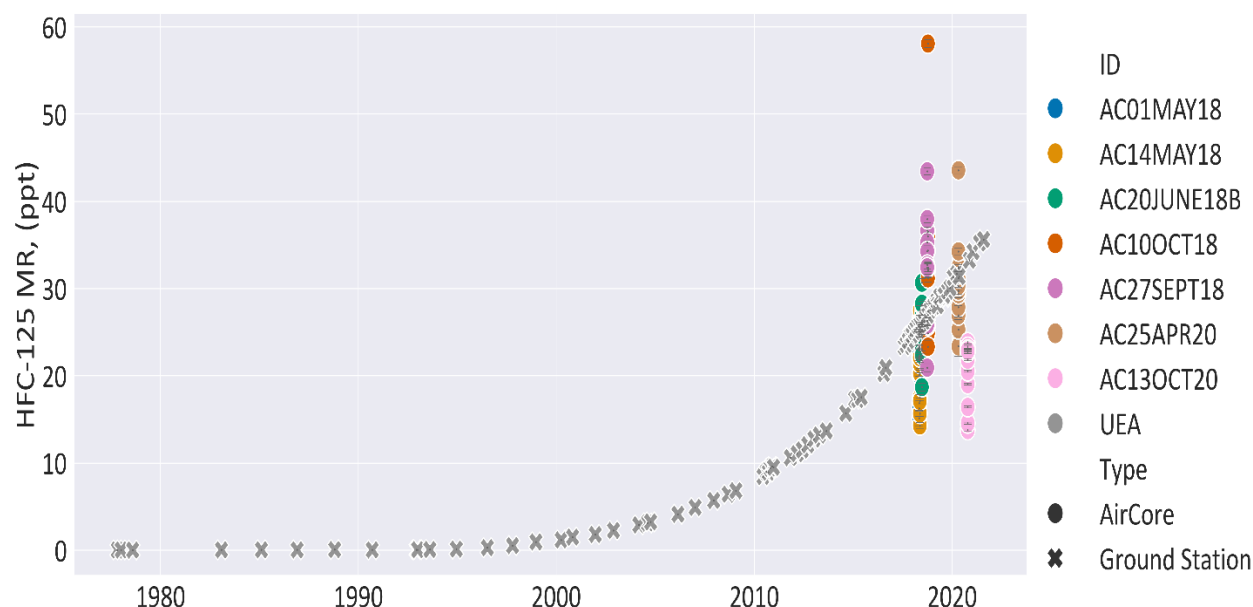


Figure 4.9. Mixing ratio for HFC-125 (ppt), plotted against date, for the tropospheric background trend (measured at UEA, updated from Leedham-Elvidge *et al.*, (2018)) and the AirCore flights examined here.

As demonstrated in Figure 4.8 c HFC-125 was heavily affected by delays between flight and analysis, and this is reflected again in Figure 4.9. Flights that had the least delay were more consistent with the background trend, than those that had longer delays (which produced many above trend measurements). This re-affirms that for HFC-125 to be viable from AirCore samples, those samples must be analysed as soon as possible after the flight, and ideally less than 2 weeks after.

### 4.3.3 CFC-113

CFC-113’s average instrument precision from AirCore samples was the same as that of the Geophysica flights (see supplementary material for Adcock *et al.* (2020)) (Table 4-2). The annual growth rate for CFC-113 (between 2019-2020) was  $-0.5/-0.7 \text{ ppt yr}^{-1}$  ( $-1\%/-0.7\% \text{ yr}^{-1}$ ) (Laube *et al.*, 2022), and the precision for both AirCore and Geophysica flights was within that range.

Looking at Figure 4.10 the visual correlation between CFC-113 and CFC-11 is fairly compact; however, there are several notable outliers. There is a single outlier for the 20.06.2018 'RINGO02' flight; the remaining outliers are all from the 27.09.2018 flight, which has a noticeably different gradient.

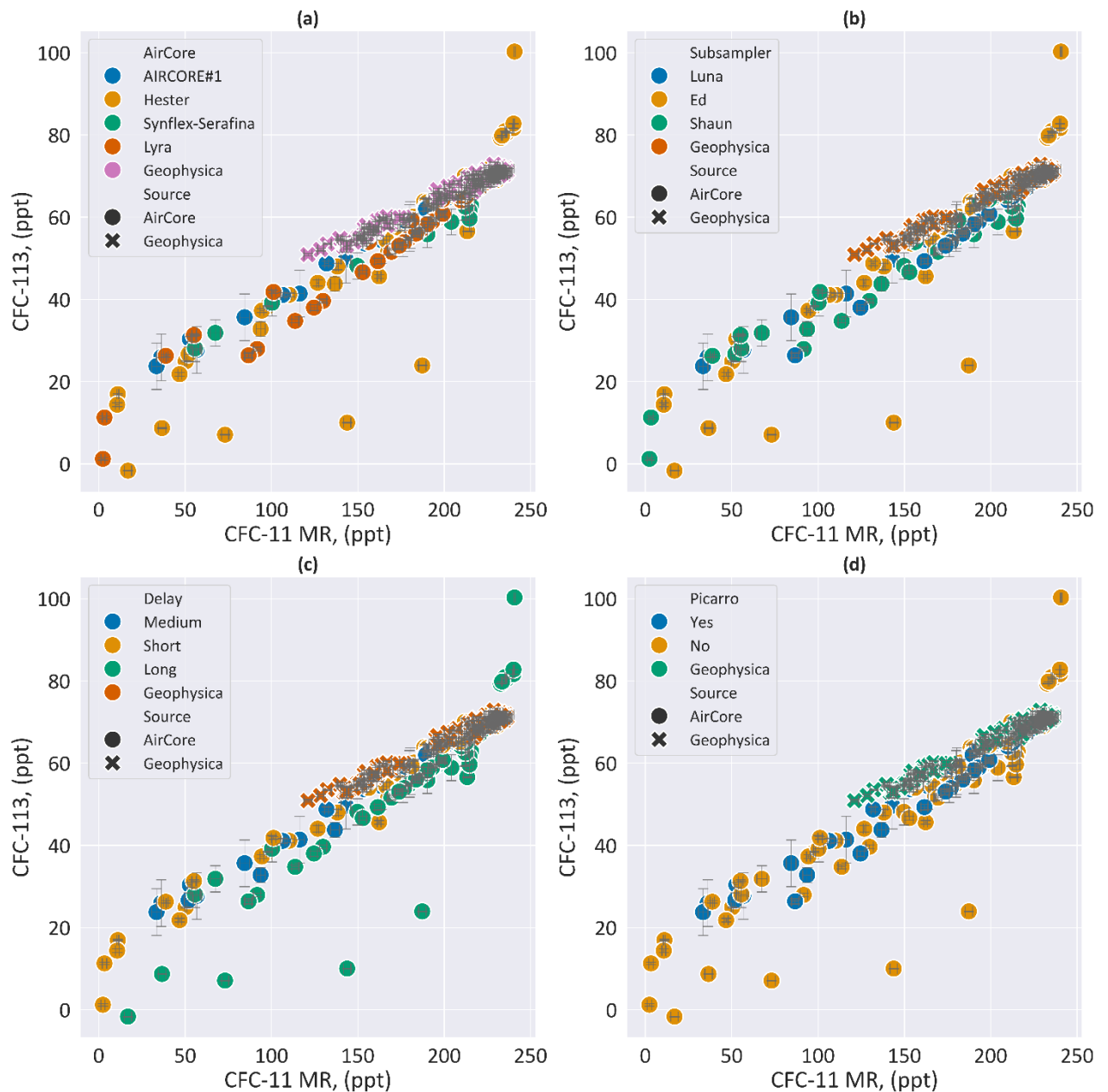


Figure 4.10. Factors affecting CFC-113 mixing ratio (ppt) plotted against CFC-11 mixing ratio (ppt), for all AirCore flights listed in section 4.2, and two Geophysica flights (KAL16, and KAT17). Hue identifies (a) which AirCore was used, (b) which subsampler, (c) How long the delay between flight and analysis was, and (d) whether or not a Picarro was used. Errors derived using instrument precision, to 1 sigma uncertainty.

Figure 4.10 does not provide clear answers as none of the variables explored can adequately explain all the outliers. A single outlier (from 20.06.2018 ‘RINGO02’ flight) could be explained as a leak or mistake during analysis of the sample.

The abnormal data for the 27.09.2018 flight might be explained by the effect of temperature on the AirCore. In section 4.2.3 one of the factors potentially affecting AirCore

sample viability was the temperature of the AirCore. Only two of the studied compounds are sufficiently high-boiling to be within the range that could be affected by AirCore temperature; CFC-113, and HCFC-141b.

As this effect has been suspected for some time, precautions to avoid it were put into effect from 2019. For example, none of the AirCore flights were launched at night (when heating from the sun is missing) and the AirCore parcel was well insulated; the inlet and drier were wrapped in halocarbon-free felt. Looking at Figure 4.10, none of the flights from 2019 onwards (after insulation was implemented) show the ‘smear’ (a large cluster of data points near the tropopause, then a rapid drop in concentration of the compound as it moves into the stratosphere) predicted in section 4.2.3, so the insulation appears to be working. Therefore, examination of the effect of temperature on AirCores will focus on pre-2019 flights.

*Table 4-3. The minimum temperatures experienced by the AirCores, and the length of time they were below zero degrees C. Exact flight times varied between flights, but averaged 5 hours.*

Flight	Min temp (°C)	Time below 0°C (min)
01.05.2018 (Hester, Ed, No Picarro)	7.5	0
14.05.2018 (Hester, Ed, No Picarro)	3	0
20/June/2018 (RINGO03)	2	0
20/June/2018 (RINGO02)	2	0
27.09.2018 (Hester, Ed, no Picarro)	-2.1	25.7
10.10.2018 (Synflex-Serafina, Shaun, no Picarro)	-8.2	18.6

Looking at Figure 4.10 (CFC-113 mixing ratio v CFC-11 mixing ratio) and Figure 4.19 (HCFC-141b mixing ratio v CFC-11 mixing ratio), for both compounds, the September flight showed abnormally high concentrations at the top of the profile, which is the highest altitude and corresponds to the lowest mixing ratios. These concentrations abruptly drop, giving an extremely steep profile (compared to other flights).

Since the October flight had the lowest AirCore temperature, it could be expected to have the steepest gradient, but this is not the case. For both compounds though we see a cluster of higher concentrations at the top of the profile, which is similar to what we saw in the September flight, though the feature in the September flight is more pronounced.

The mixing ratio for CFC-113 nearest the tropopause was 100.3 ppt for the September flight, and 62.8 ppt for the October flight. The tropospheric trend (National Oceanic and Atmospheric Administration (NOAA), 2020) for that time period gives a mixing ratio for CFC-113 as 70 ppt, so only the value for the September AirCore flight is abnormally high. For HCFC-141b the mixing ratio nearest the tropopause was 37.9 ppt for the September flight, and 23.9 ppt for the October flight. The tropospheric trend (using NOAA's Moana Loa station) gave mixing ratios at these times of 24.7 ppt and 25.51 ppt respectively. So only the September flight saw mixing ratios of HCFC-141b that were elevated above the background trend.

The October flight does not show samples as close to the tropopause as the September flight, so the effect might not be as pronounced when looking only at a comparison between these samples and the tropospheric mixing ratio. Another reason the October flights may not have shown as strong an effect as the September flights was how long temperatures remained sufficiently cold. As can be seen in Table 4-3 the AirCore in the September flight was exposed to sub-zero temperatures for significantly longer than the October flights. As is seen in the stability tests for temperature (Figure B.6) holding the AirCore at -10 degrees C for 10 minutes had little effect on either CFC-113 or HCFC-141b. So the evidence indicates that not only the temperature of the AirCore matters, but also how long the AirCore was at that temperature.

In Figure 4.8 a cluster of data points from the 27.09.2018 flight show elevated concentrations of CFC-113, and this is reflected in Figure 4.11. Aside from this flight, all others reach or slightly exceed the tropospheric background trend, but this is largely within the uncertainties. This includes both Geophysica flights and AirCore flights, so is not a feature exclusive to AirCore flights.

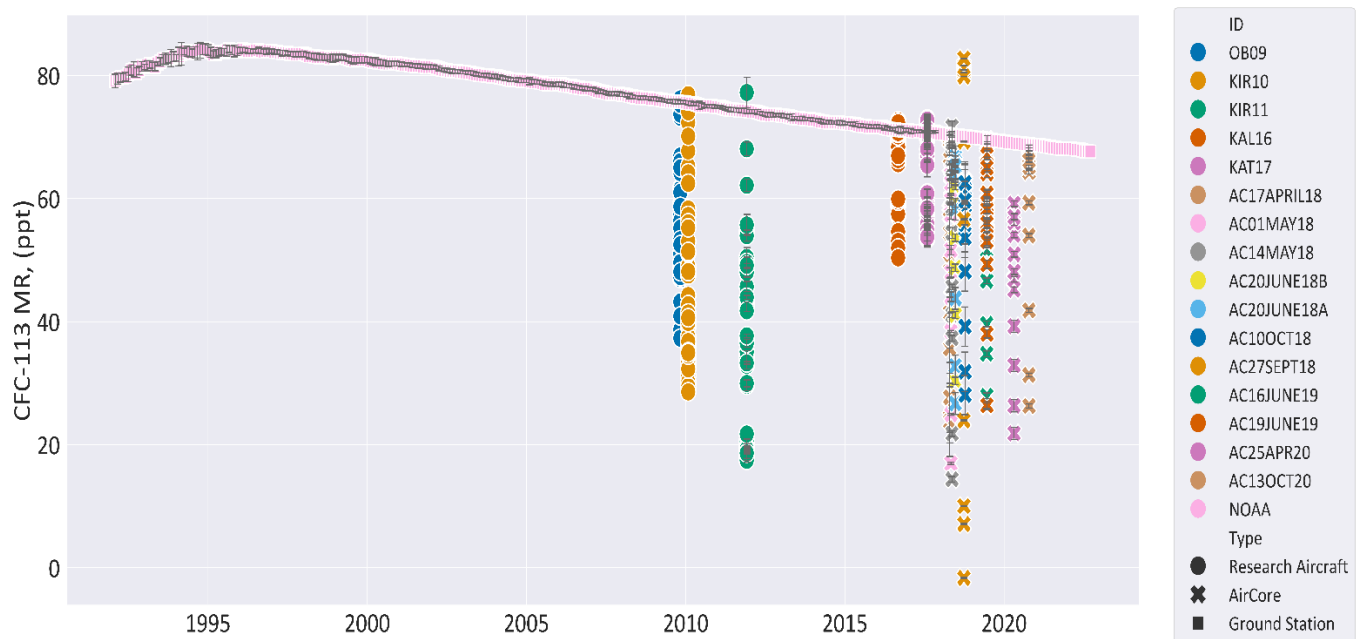


Figure 4.11. Mixing ratio of CFC-113 (ppt) plotted against date (yr), for the NOAA global background trend, the 5 Geophysica flights explored in section 3.2.1, and the AirCore flights explored here.

As discussed in section 1.4 a vital component in calculating FRFs is the background trend of the compound. So it is necessary to know how precisely AirCore data relates to the background trend of the compound, and one way to explore that is to plot FRFs against mean age (yr) and this is shown in Figure 4.12. Samples include the original dataset (sample 1n), then expand the dataset to 5n by including in the analysis the maximum and minimum mean age (to two sigma) from each compound, and the maximum and minimum FRF, thus giving a 5n or quintupled dataset (the same procedure as seen in section 3.2.4).

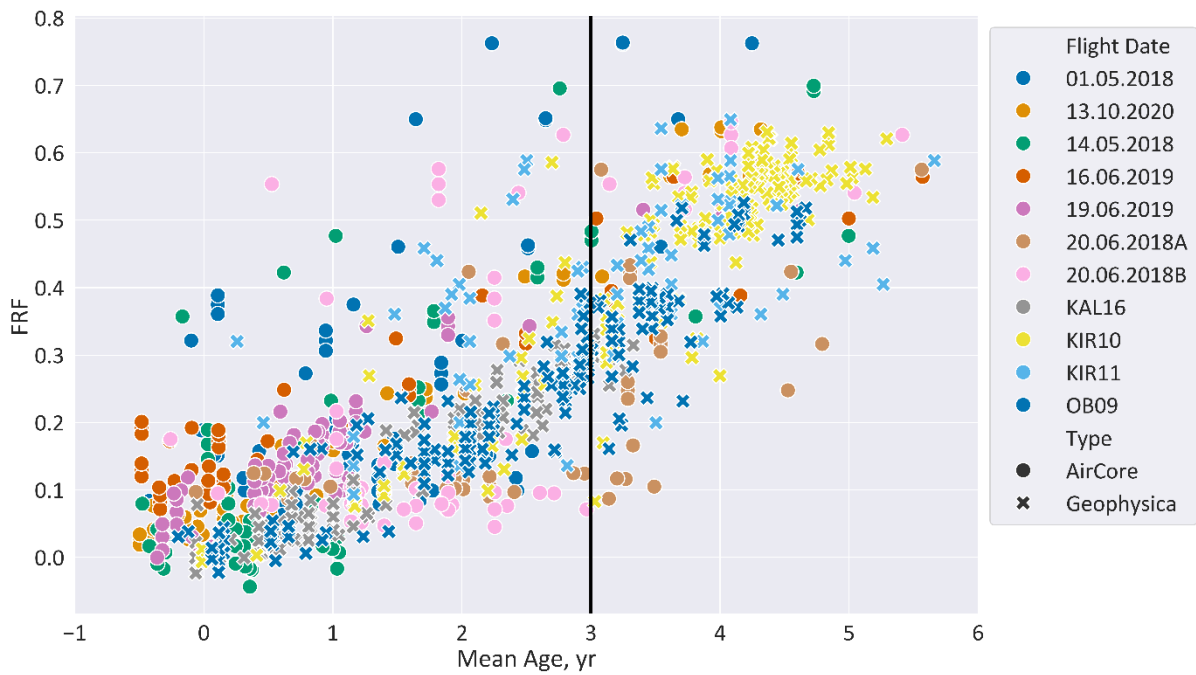


Figure 4.12. FRFs for CFC-113 plotted against mean age (yr) for 4 Geophysica flights, and all AirCore flights where there was sufficient age tracer and CFC-113 data to calculate FRFs. Samples are 5n, including original FRF-Mean Age data pairs, FRF+, FRF-, Mean Age+ and Mean Age-. Vertical line indicates 3 years mean age.

As can be seen from Figure 4.12 FRFs are not a neat, linear line, but a broad cluster of data points that generally have higher values for FRF as mean age is increased. The Geophysica data points are more closely clustered and while most AirCore do cluster around this, there are notable outliers (though the 5n sampling means that instead of a single outlier, there will be 5 in a rough cross pattern). When looking at the vertical line at 3 years mean age, that line encompasses a significant range of FRF values, and this is explored more thoroughly in section 4.3.9. This means that the AirCore values largely overlap the Geophysica values, and this is promising for the AirCore’s utility for studying this compound. Note that negative mean age values reflect the technique used, rather than reality (see section 2.6 for more details), and values beyond -0.5 were excluded from calculations in section 4.3.9, as were flights where the data for that compound was poor (as discussed in each compound’s relevant results section).

#### 4.3.4 CFC-115

For CFC-115 the change in abundance between 2019-2020 for this compound was 0.03 ppt yr<sup>-1</sup> or 0.4 % yr<sup>-1</sup> (Laube *et al.*, 2022), the precision for AirCore samples is lower than that of Geophysica samples (Table 4-2), and both exceed this change in abundance.

As with CFC-113 (section 4.3.2) most flights resulted in a compact correlation for CFC-115 and CFC-11. The lowest outlier is from the 13.10.2020 flight, and the sample is the second loop of the 'Shaun' sub-sampler. Early loops are more likely to still contain 'fill gas'. It was also the earliest sample analysed on that day (after several samples of standard, and a helium blank), and the GC-MS system might have still been equilibrating for the day. The single point from 27.09.2018 (which was ~74% lower than the other samples), which was also the first sample analysed on that analysis day, and two points from 10.10.2018 (which were 29% and 49% lower abundance than the other samples), can also be accounted for as they were all early loops and analysed early on their respective analysis days (excluded data points can be seen in Figure C.12, but are excluded from Figure 4.13 as they make it difficult to parse). As discussed in section 4.3.1 flight 25.04.2020 gave poor data for most compounds. Removing these outliers gives a much clearer profile (Figure 4.13).

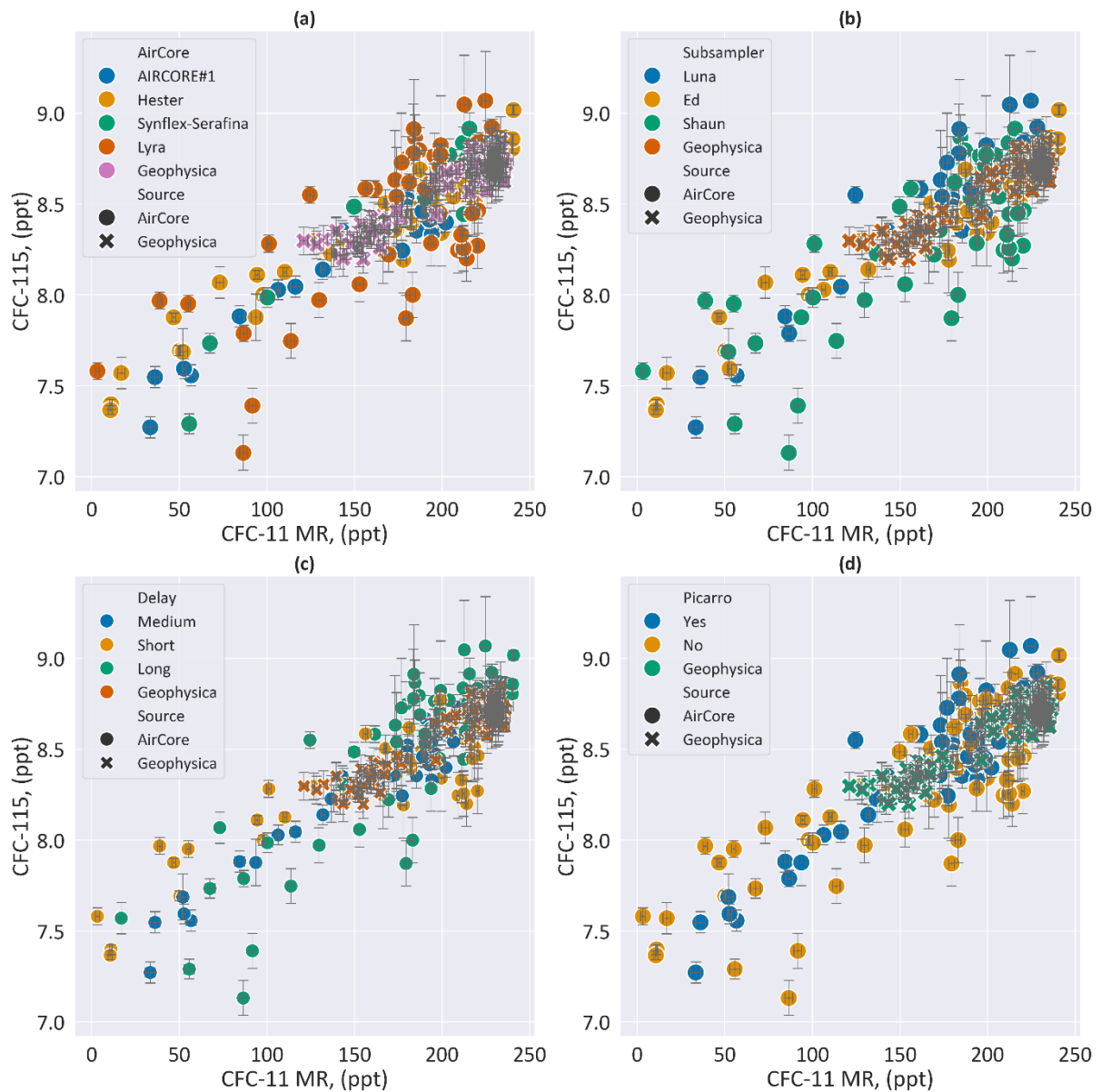


Figure 4.13. Factors affecting CFC-115 mixing ratio (ppt) plotted against CFC-11 mixing ratio (ppt), for all AirCore flights listed in section 4.2, and two Geophysica flights (KAL16, and KAT17). Hue identifies (a) which AirCore was used, (b) which subsampler, (c) How long the delay between flight and analysis was, and (d) whether or not a Picarro was used. Errors derived using instrument precision, to 1 sigma uncertainty.

Figure 4.13 demonstrates none of the explored variables (AirCore, Sub-Sampler, delay, and Picarro) had any noticeable effect on the mixing ratios for CFC-115. This is encouraging, as it shows that when outliers are accounted for, the data for CFC-115 from AirCore samples is of comparable quality to data gathered via Geophysica flights and the Cape Grim Background trend (Figure 4.14).

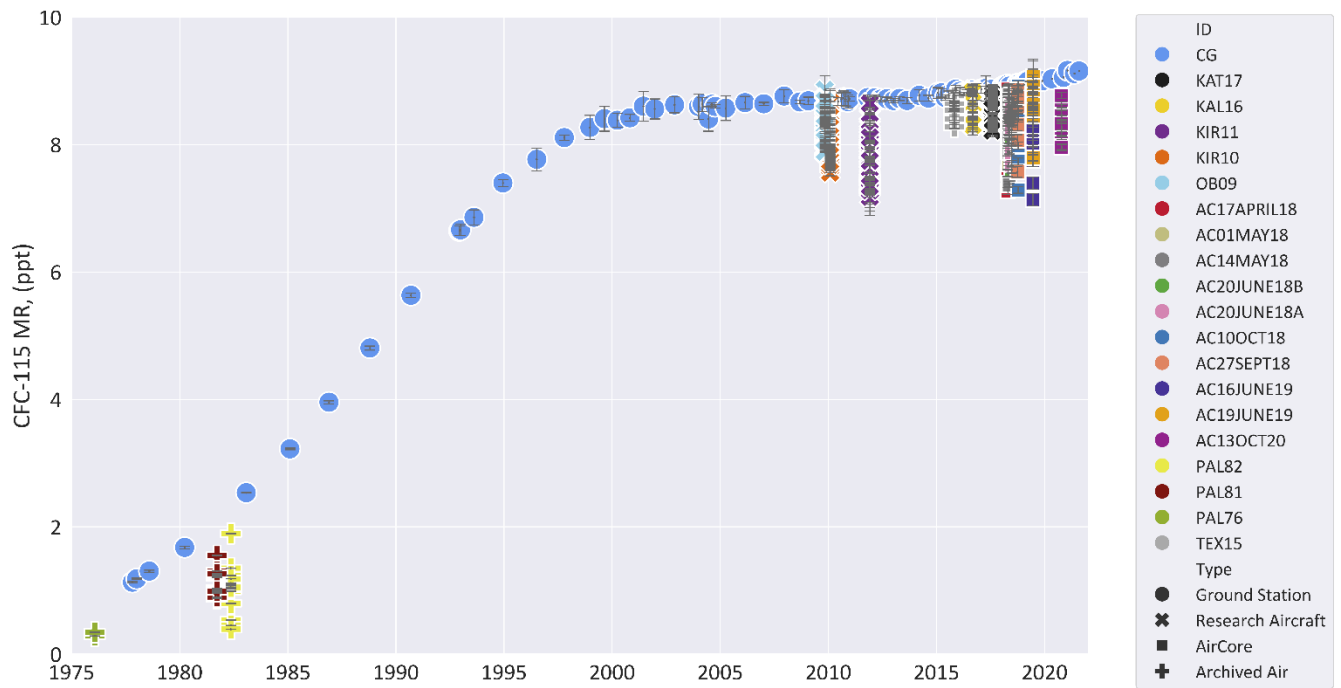


Figure 4.14. Mixing Ratio for CFC-115 (ppt) plotted against date (yr). For the five Geophysica flights examined in section 3.2.1, the AirCore flights examined here, the archived air data discussed in section 3.1.3, and the Cape Grim (CG) tropospheric background trend. This is a repeat of Figure 3.30, for ease of reading.

In terms of FRFs, examining Figure 4.15, most (with the exception of KIR11) Geophysica flights form a fairly tight profile, the AirCore flights have a greater range of scatter, and on average give higher FRFs than the Geophysica samples at the same mean age. The vertical line at 3 years mean age encompasses a range of values, but the generation of FRFs in section 4.3.9 uses the bootstrapping technique detailed in section 2.5, and can take into account uncertainty ranges and the presence of outliers.

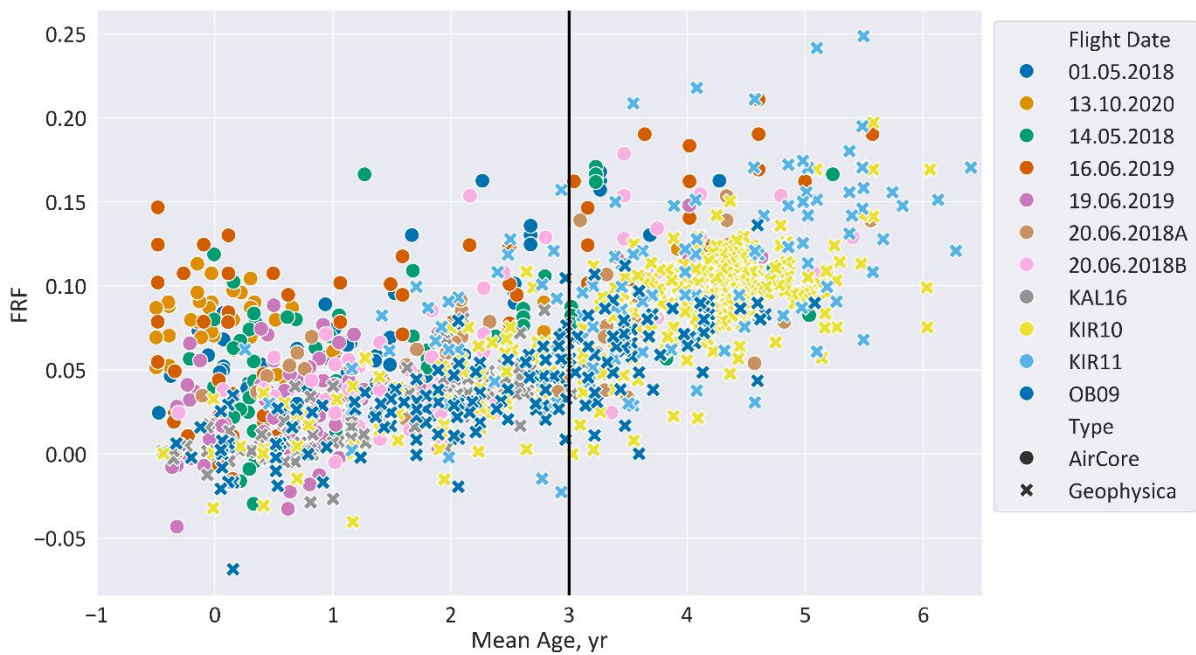


Figure 4.15. FRFs v Mean Age for CFC-115. This includes most AirCore flights examined here (the 25.04.2020 flight is excluded due to excessive outliers which obscured the data), and four of the Geophysica flights.

#### 4.3.5 Methyl Chloride

The annual growth rate between 2019 and 2020 was 3.3 ppt yr<sup>-1</sup> or 0.6 % ppt yr<sup>-1</sup> (Laube *et al.*, 2022). As it is the compound with the greatest abundance of those studied here, even small changes, mistakes or improvements to technique might be more visible. The precision for AirCore samples, was significantly worse than those of Geophysica samples (Table 4-2); the precision from Geophysica flights was the same as the growth rate for this compound, while the precision uncertainty from AirCore flights was higher.

The correlation between the mixing ratios of methyl chloride (ppt) and CFC-11 (ppt) show significant scatter and the factor all affected flights had in common was delay. Excluding these flights gives a clearer picture (Figure 4.16).

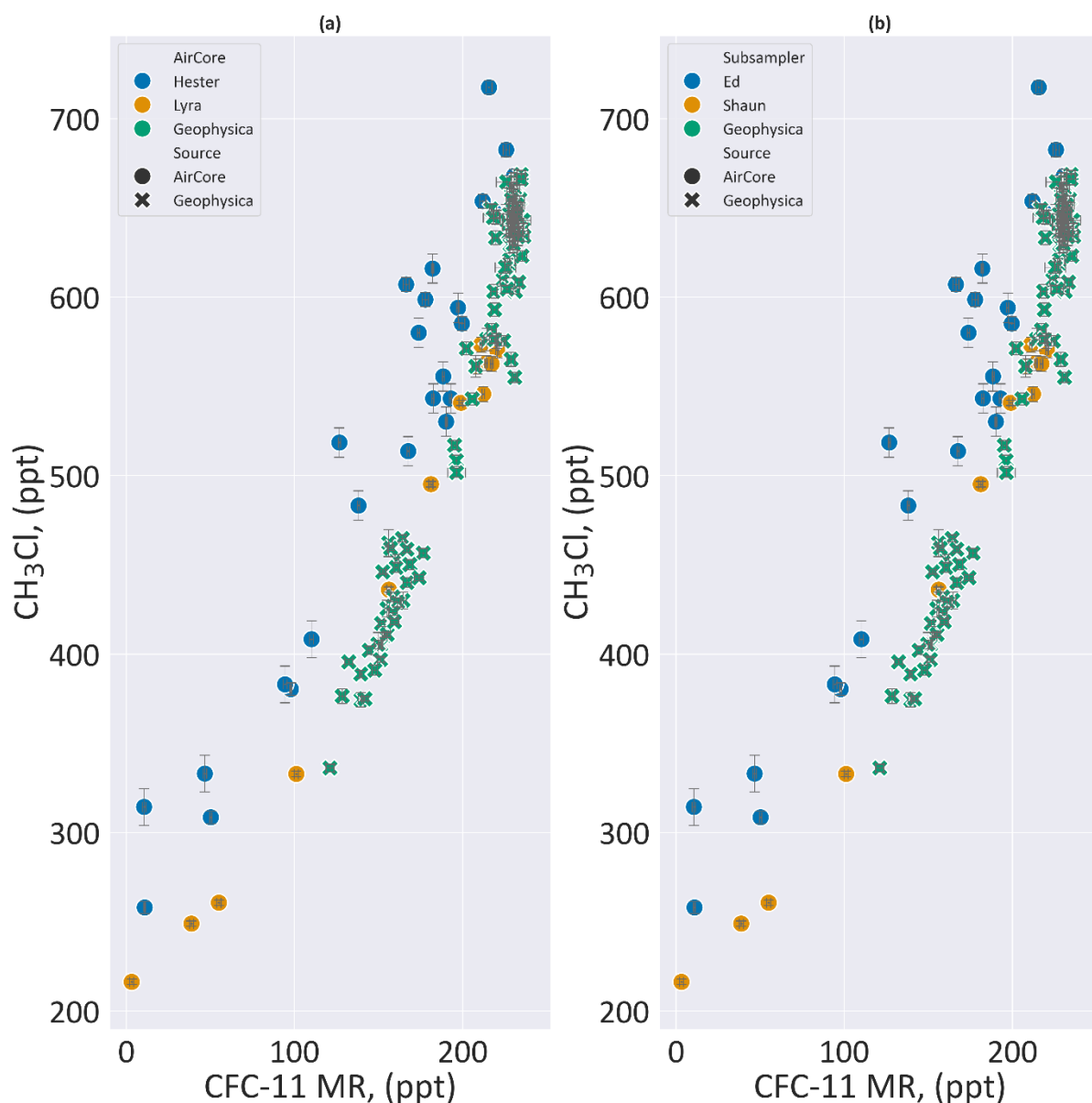


Figure 4.16. Factors affecting Methyl Chloride mixing ratio (ppt) plotted against CFC-11 mixing ratio (ppt), for all AirCore flights listed in section 4.2 (excluding flights where the delay was 'long' or 'medium'), and two Geophysica flights (KAL16, and KAT17). Hue identifies (a) which AirCore was used, (b) which subsampler, (c) How long the delay between flight and analysis was, and (d) whether or not a Picarro was used. Errors derived using instrument precision, to 1 sigma uncertainty.

In Figure 4.16, having removed the flights delays between sample and analysis of more than 2 weeks, no other factor seems to heavily influence the quality of the data. And as discussed for HFC-125 (section 4.3.2) the later 2020 flight seems to have better precision, but as there are so few flights, one cannot draw concrete conclusions from this.

The effect from delay was so pronounced that it meant many AirCore flights did not have usable data for this compound. In stability tests (Figure B.1) the effect is noticeable by

15 days, and by 20 days is responsible for over a 20% increase in Methyl Chloride mixing ratio. In Laube et al., (2008) an increase of 0.73% (22.4 ppt) per month for Methyl Chloride was observed, and attributed to wall reactions. In wall reactions compounds can 'bump' into the wall of their container and fall apart in a 0 order kinetic reaction. If the wall has reactive spots, such as impurities (e.g. carbon, sulphur, trace metals etc...) in the stainless steel of the AirCore or sub-sampler, compounds that are being stored there may react at those spots. Cold surfaces also allow compounds to condense; this is particularly the case with water vapour, though in our experiments a dryer is used to remove water vapour from the sample, and the Picarro G2401 is used to test how well that water vapour has been removed. As discussed, the stratospheric portion of the AirCore sample contains ozone, which can oxidise substances (e.g. steel).

In Laube et al., (2008) the increase observed was small, while that observed in the stability tests (conducted for this thesis, see section 4.2.3 for details and Appendix B for results) was over 20% in less than a month. The difference between these two results are the conditions in which the samples were stored. In Laube et al., (2008) the samples were stored in stainless steel canisters, while in Section 4.3.5 and in Appendix B – Stability Test Results, Figure B.4, the samples were stored in sub-samplers, with vastly smaller volumes. If wall reactions are responsible for these changes, the significantly greater surface area to volume ratio in the sub-samplers would explain the stronger drift as compared to Laube et al., (2008).

One possible explanation for this drift is hinted at in Laube et al., (2008). While Methyl Chloride concentrations increased, carbon tetrachloride decreased by 1.57% (4.06 ppt) per month. It is possible that the chlorine released during this decay then reacts with methane to form Methyl Chloride. In the absence of darkness (UV light would catalyse the reaction) the reaction would be slow, and is therefore most likely to be caused by a slow, first order wall reaction. Testing this hypothesis further is outside the scope of this thesis, but it does offer a possible explanation for Methyl Chloride's increase with delay.

The poor precision from delay made any comparison between flights and background trend extremely difficult, so these flights are excluded for Figure 4.17.

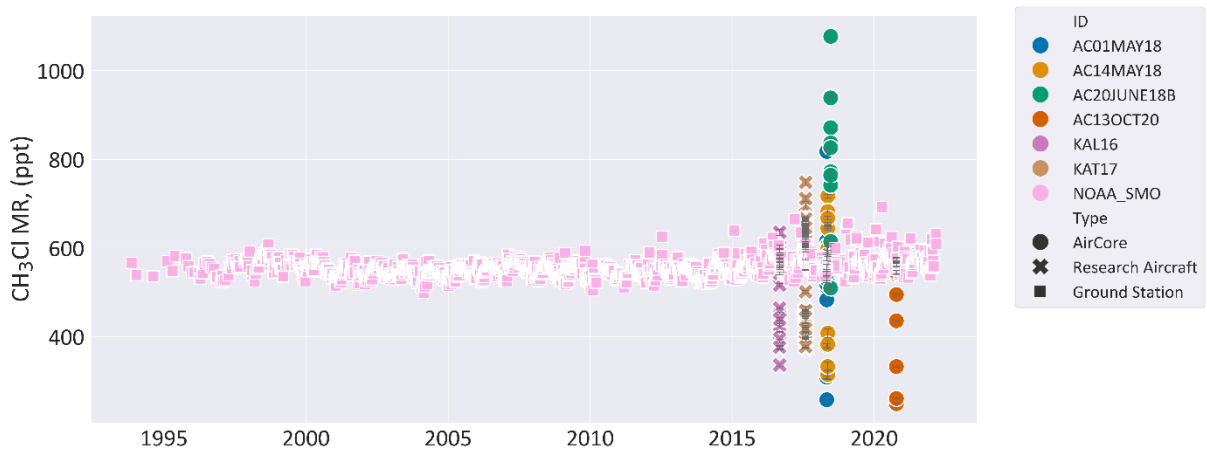


Figure 4.17. Selected flights only. Methyl chloride ( $\text{CH}_3\text{Cl}$ ) Mixing Ratio (ppt) plotted against date, for the AirCore flights examined here excluding those for which the data was excessively bad for this compound, the KAL16 and KAT17 Geophysical flights, and the NOAA tropospheric trend from the American Samoa Observatory (SMO). As methyl chloride has a seasonal cycle a global trend was unsuitable. There are a limited number of observation stations, so SMO was chosen as it was the closest in latitude.

In Figure 4.17 only the flights measured in under 2 weeks (01.05.2018, 14.05.2018, and 13.10.2020) were comparable to the tropospheric trend. This means that only these flights could meaningfully be used in the FRF calculation in section 4.3.9, and as can be seen in Figure 4.18 there are very few suitable flights, and these have on average lower mean ages, though the vertical line at 3 years mean age still encompasses a range of values.

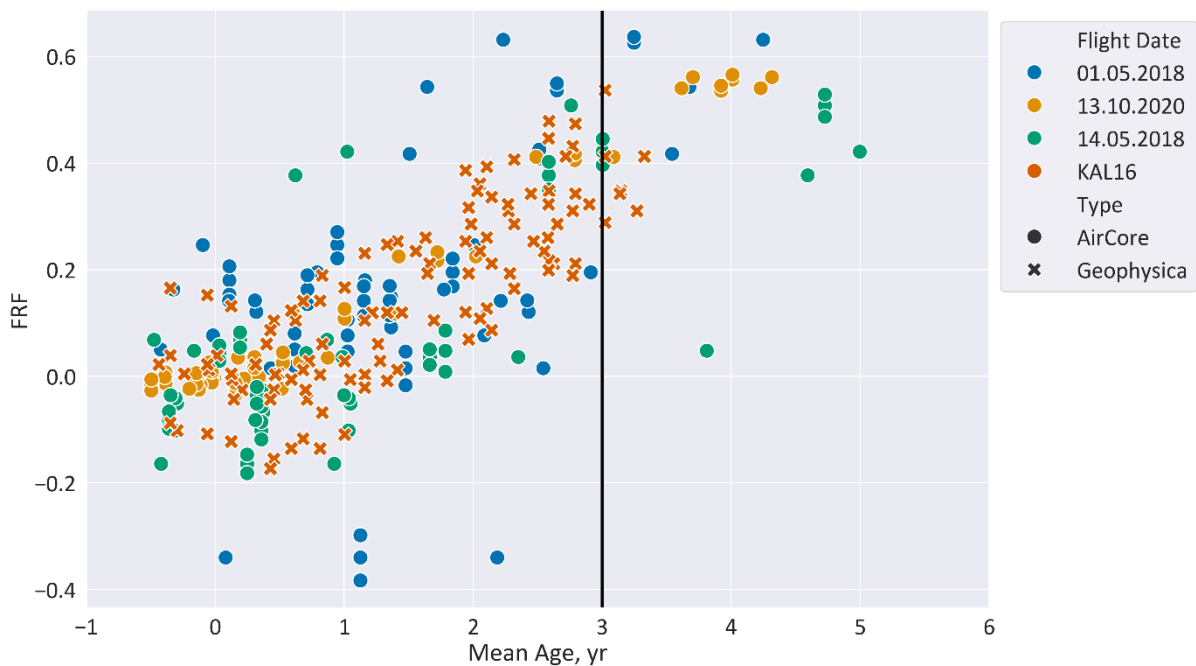


Figure 4.18. FRFs plotted against Mean Age (yr) for Methyl Chloride. Including the KAL16 Geophysica flight for reference, and the 13.10.2020, 14.05.2018 and 01.05.2018 AirCore flights.

#### 4.3.6 HCFC-141b

Growth of abundance between 2019 and 2020 was  $0.12\text{-}0.14 \text{ ppt yr}^{-1}$  or  $0.58\text{-}0.5 \%$   $\text{yr}^{-1}$  (Laube *et al.*, 2022). The precision seen for both Geophysica and AirCore derived samples (Table 4-2), exceeded this.

The profile of mixing ratios between HCFC-141b (ppt) and CFC-11 (ppt) has some similarities with those of CFC-113 (section 4.3.2) and CFC-115 (section 4.3.4). There is an outlier for 20.06.2018 from 'RINGO02' which is the same sample that is an outlier for CFC-113 in section 4.3.2. As seen for CFC-115 there is one notable outlier for HCFC-141b from the 13.10.2020 flight, and two from the 10.10.2018 flight. These are the same samples as discussed in section 4.3.4 and are outliers due to issues arising during the analysis process, rather than from AirCore sampling techniques. When these outliers are excluded, we can examine the compound more clearly (Figure 4.19).

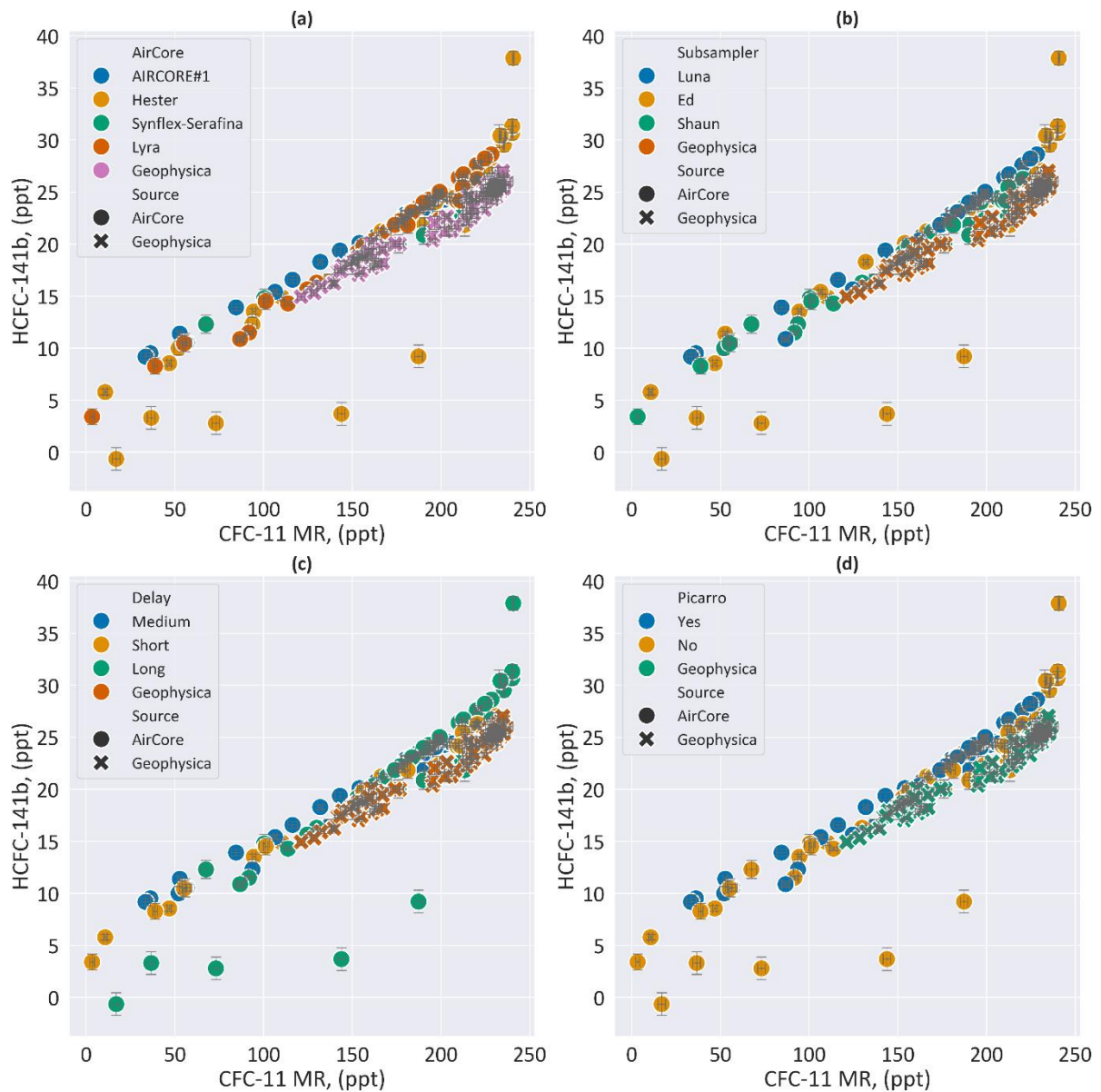


Figure 4.19. Factors affecting HCFC-141b mixing ratio (ppt) plotted against CFC-11 mixing ratio (ppt), for all AirCore flights listed in section 4.2., and two Geophysica flights (KAL16, and KAT17). Hue identifies (a) which AirCore was used, (b) which subsampler, (c) How long the delay between flight and analysis was, and (d) whether or not a Picarro was used. Errors derived using instrument precision, to 1 sigma uncertainty.

In Figure 4.19 there is no clear correlation between any of the explored factors (AirCore, Sub-Sampler, Delay and Picarro use), that would explain the remaining scatter from flight 27.09.2018. This is a similar pattern of scatter (and substantially different gradient for one flight) as seen for CFC-113, and this is most likely due to the effect of temperature on the sample (see discussion in section 4.3.2).



Figure 4.20. Mixing Ratio for HCFC-141b plotted against date (yr), for the AirCore flights examined here, and the NOAA tropospheric trend from Mauna Loa Observatory (MLO). As HCFC-141b has a seasonal cycle a global trend was unsuitable. There are a limited number of observation stations, so MLO was chosen as it was the closest in latitude.

In Figure 4.20 there are some clear outliers. The effect of temperature on the AC27SEPT18 flight is very noticeable. While temperature is not shown, we can see a large cluster of data points above the background trend, some close to the trend, then a large gap before the remaining data points which show abnormally low mixing ratios (if compared to other flights). The AC14MAY18 and AC19JUNE19 flights also seem to have somewhat elevated concentrations of HCFC-141b, though this was not noticeable in Figure 4.19. They used different AirCores (Hester and Lyra respectively) and different sub-samplers (Shaun and Luna respectively), so it is unclear why this effect exists. That stability tests (Appendix B) did see some effect from the use of the Lyra AirCore on concentrations of HCFC-141b (Figure B.4), and as the Lyra and Hester AirCores are very similar, this could be a possible cause. As discussed in section 4.2.1 both AirCores are Silco-treated, but wall reactions are still possible, and the presence of perfluorocarbon grease in the 3-way valves used could have resulted in contamination (at present there are no viable alternatives).

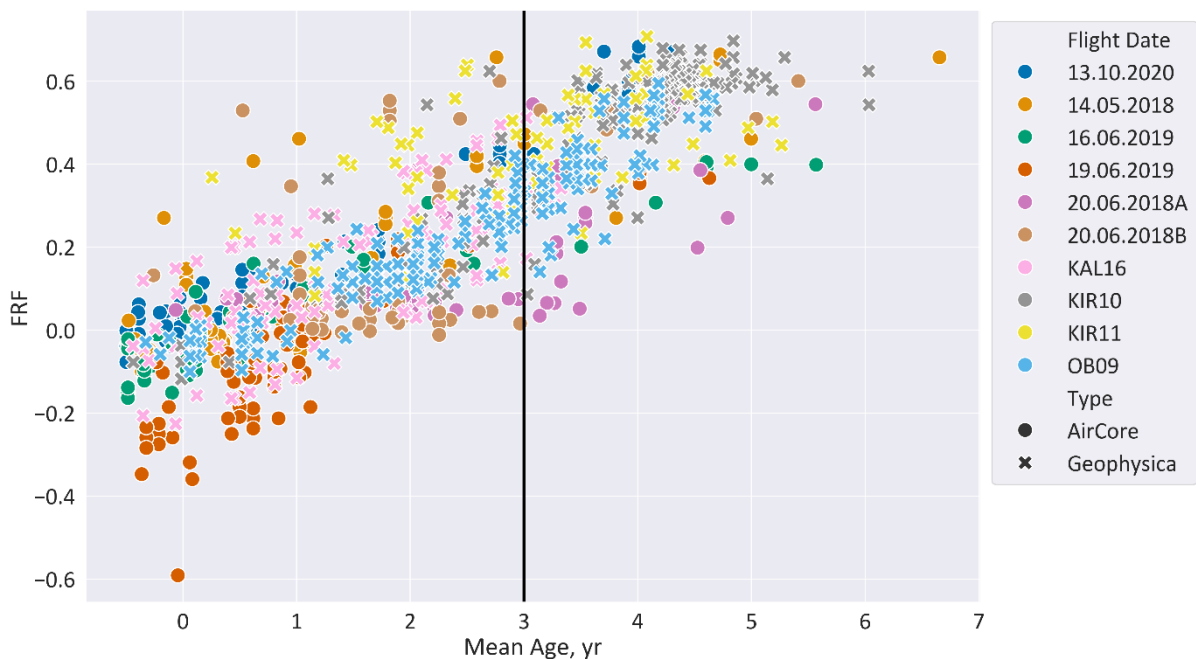


Figure 4.21. FRFs plotted against Mean Age for HCFC-141b, for the AirCore flights examined here that had reasonable data for this compound, and from the Geophysica flights OB09, KIR10, KIR11, and KAL16. The vertical line marks 3 years mean age.

In Figure 4.21 we can see what impact the quality of different flights had on the resulting FRFs, and how this compares to FRFs generated using Geophysica data. With the exception of the 25.04.2020 (which is excluded from the figure and from calculations used for the FRF results in section 4.3.9, due to known contamination problems), the visual correlation here is fairly compact, and the AirCore FRFs are largely consistent with the Geophysica FRFs.

### 4.3.7 HCFC-142b

Growth between 2019-2020 for this compound was  $-0.23/-0.26$  ppt  $\text{yr}^{-1}$  or  $-1/01.2\%$   $\text{yr}^{-1}$  (Laube *et al.*, 2022). The instrument precision achieved for the Geophysica flights was within this range, while the precision achieved for AirCore flights just exceeded it (Table 4-2).

When plotting the correlation between the mixing ratios of HCFC-142b and CFC-11 (ppt) several flights are clear outliers. Two flights with abnormally high concentrations of HCFC-142b: the 25.04.2020 flight, which as discussed had poor quality data for most compounds examined here, and 20.06.2018 (RINGO02) flight, which aside from a single

outlier for CFC-113 and HCFC-141b, otherwise provided good data for other compounds studied here. As the 20.06.2018 (RINGO02) flight did not use any procedure that was not used elsewhere, and this flight has good data for the other compounds studied here, it is unclear as to why the data is so poor for HCFC-141b.

Removing these flights gives a clearer picture of the data in Figure 4.22 we can see some scatter, and the AirCore data has greater scatter than the Geophysica data, but aside from a few outliers, which have already been discussed for other compounds, the profile appears reasonably compact.

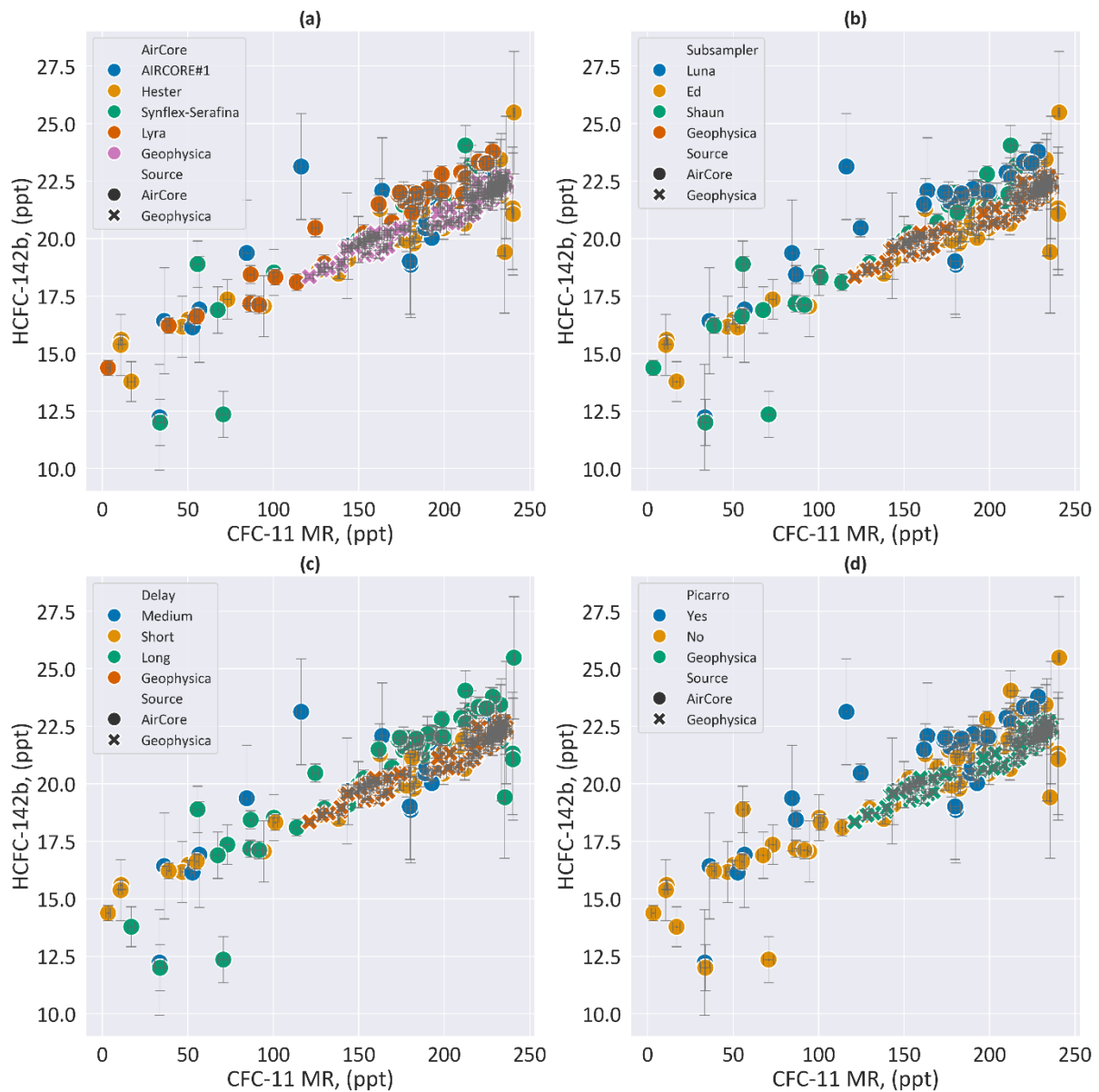


Figure 4.22. Factors affecting HCFC-142b mixing ratio (ppt) plotted against CFC-11 mixing ratio (ppt), for all AirCore flights listed in section 4.2 (excluding 25.04.2020 and 20.06.2018 (RINGO02), and two Geophysica flights (KAL16, and KAT17). Hue identifies (a) which AirCore was used, (b) which subsampler, (c) How long the delay between flight and analysis was, and (d) whether or not a Picarro was used. Errors derived using instrument precision, to 1 sigma uncertainty.

In Figure 4.22 there is no clear influence from AirCore type, Sub-Sampler type, delay, or Picarro use. Though the worst scatter is from flights with a longer delay time, there are still flights with long and medium delay that are part of the compact profile.

Two flights were identified as having poor quality data for this compound: 20.06.2018 and 25.04.2020, and these two flights are excluded from Figure 4.23. Here we

see that most AirCore flights had reasonably good agreement (within the uncertainties) with the tropospheric background trend.

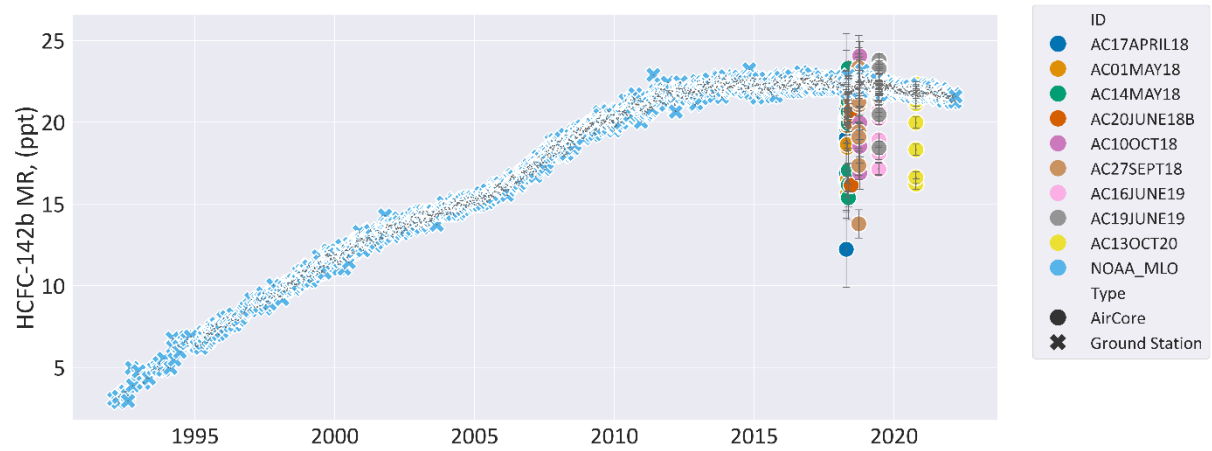


Figure 4.23. 'Good' flights only. Mixing Ratio for HCFC-141b plotted against date, for the AirCore flights examined here (excluding 20.06.2018A and 25.04.2020 flights), and the NOAA tropospheric trend from Mauna Loa Observatory (MLO). As HCFC-142b has a seasonal cycle a global trend was unsuitable. There are a limited number of observation stations, so MLO was chosen as it was the closest in latitude.

Taking this into account, the next step was to see how well FRFs generated from this data correlated with mean age, and how comparable they were to those generated using Geophysica data (Figure 4.24).

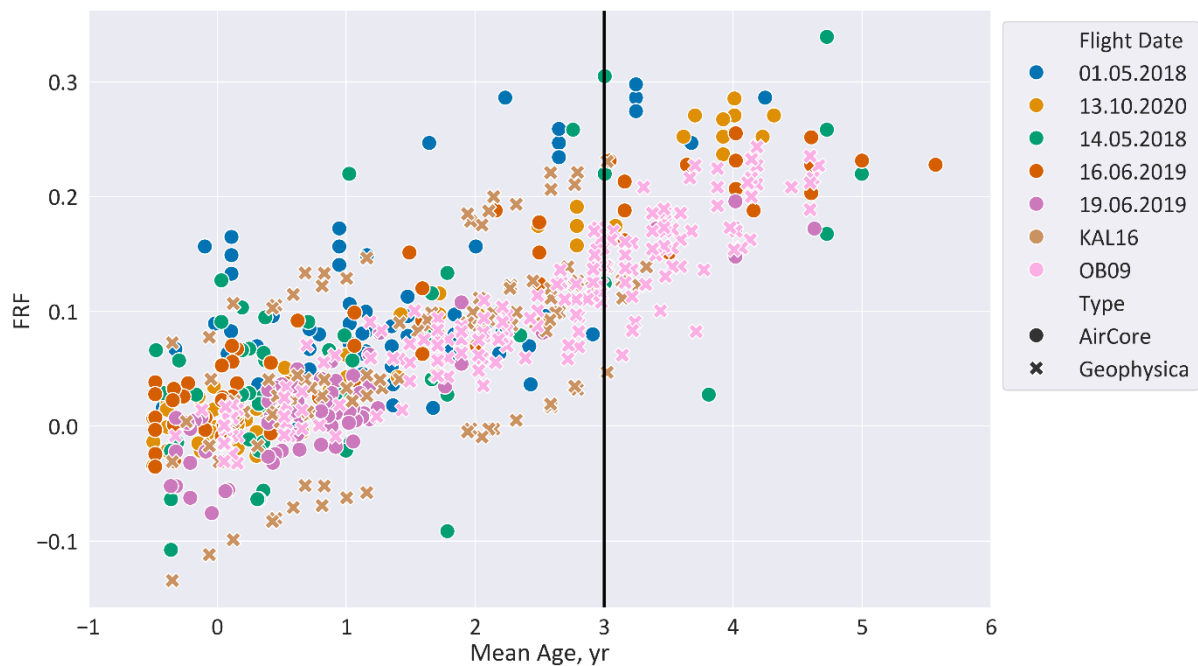


Figure 4.24. FRFs plotted against Mean Age for HCFC-142b, for the AirCore flights examined here that had reasonable data for this compound, and from the Geophysica flights OB09 and KAL16. The vertical line marks the 3 years mean age.

In Figure 4.24 the data from the 25.04.2020 flight is excluded, as this flight's samples were contaminated with fill gas. Excluding that, we see that the Geophysica data has the most compact correlation, but most AirCore data points cluster around this. The vertical line at 3 years mean age still encompasses a range of values, but this is to be expected as FRFs are affected by a number of factors (such as season, latitude, the transport pathways experienced etc... see section 4.3.9).

#### 4.3.8 Mean Ages

Ultimately, improvements in AirCore technique need to provide improvements in scientific advancement. One way for them to do this is to contribute to updated policy relevant metrics such as FRFs and ODPs. In order to derive these metrics, it is first necessary to derive mean ages for the samples (see section 4.2.5, for details).

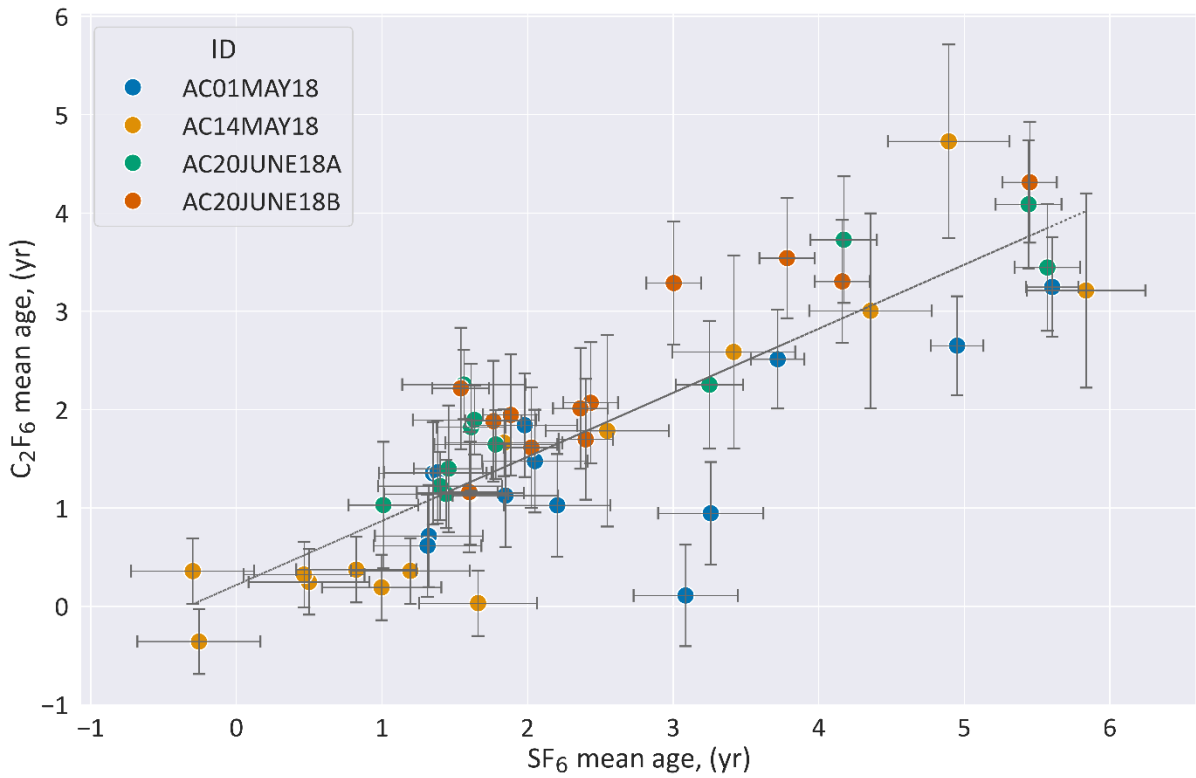


Figure 4.25. SF<sub>6</sub> derived mean ages (yr) plotted against C<sub>2</sub>F<sub>6</sub> derived mean ages (yr), for the 2018 flights where data was available for this compound. Error range is derived from instrument precision uncertainty.

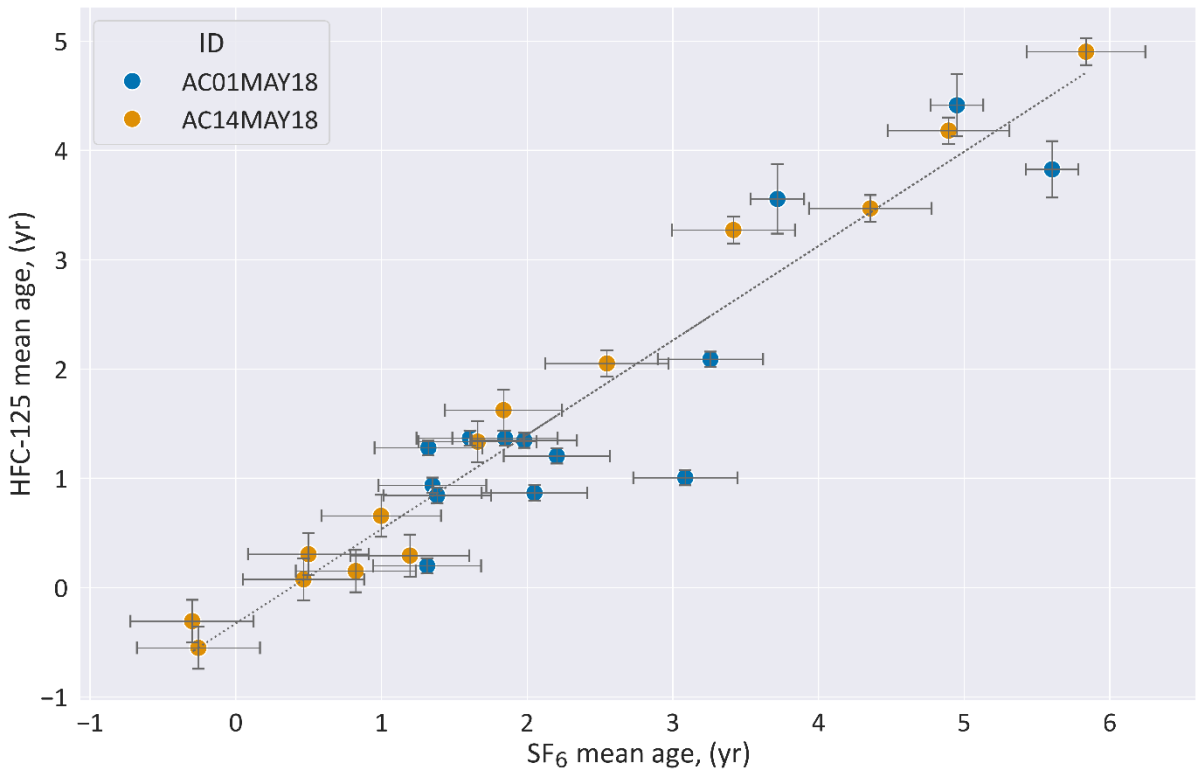


Figure 4.26. SF<sub>6</sub> derived mean ages (yr) plotted against HFC-125 derived mean ages (yr), for the 2018 flights where data was available for this compound. Error range is derived from instrument precision uncertainty.

As can be seen from Figure 4.25 and Figure 4.26, there was some variation between AirCore flights and their respective uncertainty; however, using the bootstrapping technique detailed in section 2.5 with the expanded dataset (expanded to 2 sigma uncertainty, thus giving a sample of 5n, as described in section 3.2.4 and Appendix D) actually decreased the overall uncertainty of slope and intercept considerably (Table 4-4). C<sub>2</sub>F<sub>6</sub> derived mean ages had slightly higher average uncertainty, but usable data was only available from two flights for HFC-125 while C<sub>2</sub>F<sub>6</sub> used four flights, so this may not reflect a true comparison of the uncertainties of the two compounds.

*Table 4-4. The slope and intercept values for the correlation between SF<sub>6</sub> derived mean ages and C<sub>2</sub>F<sub>6</sub> or HFC-125 derived mean age averages with their respective uncertainties. Includes both the original sample range (1n) and the expanded 5n dataset (as described in sections 3.2.4 and 4.2.2).*

Sample	Average slope	Average Intercept, yr
C <sub>2</sub> F <sub>6</sub> 1n Sample	0.75 ± 0.17	-0.07 ± 0.4
C <sub>2</sub> F <sub>6</sub> 5n Sample	0.61 ± 0.23	0.18 ± 0.69
HFC-125 1n Sample	0.77 ± 0.16	-0.18 ± 0.33
HFC-125 5n Sample	0.84 ± 0.16	-0.36 ± 0.4

From Table 4-4 the average slope for C<sub>2</sub>F<sub>6</sub> (using the 5n dataset) was 0.61 (±0.23), and the average slope for HFC-125 (using the 5n dataset) was 0.84 (±0.16). In Leedham-Elvidge et al., (2018) the mean ages derived from SF<sub>6</sub> were compared to the average mean age from the new age tracers. The slope of the correlation varied from 0.74 to 0.96 (a difference of 22%), depending on whether all (non-tropical) data, polar data, mid-latitude data, or tropical data was used to determine the mean ages. The average uncertainty of the mean ages was in the region of 6 months to a year. Leedham-Elvidge et al., (2018) therefore observed a similar level of variation and uncertainty to what is seen in Table 4-4.

In addition, archived air data discussed in section 3.1.3 included mean ages derived both from C<sub>2</sub>F<sub>6</sub> and SF<sub>6</sub> (HFC-125 was present in too small abundance for its use as an age-tracer to be feasible). The mean ages derived from C<sub>2</sub>F<sub>6</sub> and SF<sub>6</sub> were plotted against each other, with the slope and the intercept listed in Table 4-5.

Table 4-5. The slope and intercept of  $C_2F_6$  and  $SF_6$  derived mean ages from archived air data. Includes the mean from all campaigns plotted simultaneously, and the slope/intercept for campaigns plotted individually.

Sample	Slope	Intercept
Mean	0.91	0.06
TEX15	0.79	0.14
AIRE93	0.89	0.01
GAP99	0.95	0.14

In Table 4-5 we can see that there is variation between the flights, similar to that observed in Table 4-4. TEX15 had the slope with the smallest value (0.79) which is close to the 0.80 observed in Leedham-Elvidge et al., (2018). The slopes for  $C_2F_6$  v  $SF_6$  mean ages from AirCore flights varied between 0.58 to 0.90, with an average uncertainty of 0.20. Leedham-Elvidge et al., (2018) saw the slope of the correlation (when mean ages derived from  $SF_6$  were compared to the average mean age from the new age tracers, a comparison to just  $C_2F_6$  is not included) varied from 0.74 to 0.96, depending on which dataset was used (e.g. all data, polar, mid-latitude or tropical data), and had an average uncertainty within the region of 6-12 months.

From the data in Table 4-4 and Table 4-5, along with the spread observed in Leedham-Elvidge et al., (2018), we can conclude that the mean age estimates derived from both  $C_2F_6$  and HFC-125 can be both reliable and comparable, assuming other factors (such as those discussed earlier in this section) do not reduce their viability. Calculations in section 4.3.9 use a mean age that is the average of both the  $C_2F_6$  and HFC-125 derived mean ages, or where these are not available, either due to factors discussed in sections 4.3.1 or 4.3.2 or for later flights where time constraints meant that mean age data for these compounds could not be compiled (the 2019 and 2020 flights), the 0.8 conversion factor (as proposed in Leedham-Elvidge et al., (2018)) applied to the  $SF_6$  derived mean ages, in order to make them comparable.

#### 4.3.9 FRFs

As discussed in Section 2.6, there are a number of assumptions implicit in the calculations of FRFs, and several factors that can affect them. The method used in FRF calculations in both Chapter 3 and Chapter 4, is that described in Ostermüller et al., (2017).

Ostermüller et al., (2017) argues that the FRF for a trace gas should not be dependent on the tropospheric trend of that trace gas. But Adcock et al., (2021) who used the same method as Ostermüller et al., found an offset between the background trend for certain compounds, and the actual entry mixing ratio. This was particularly noticeable for short-lived compounds such as CH<sub>3</sub>Cl, and a large reason for this offset is that the Adcock paper was investigating the Asian Monsoon. The Asian Monsoon, due to deep convection and anticyclonic flow in the upper troposphere and lower stratosphere (UTLS), provides an efficient transport pathway for air containing elevated levels of tropospheric trace gases (and in particular ozone-depleting substances), from the surface into the lower stratosphere in a few days to a few weeks.

In contrast the background trends (in this thesis) for CH<sub>3</sub>Cl were taken from surface stations in remote and largely unpolluted regions (Mauna Loa and American Samoa). However, even in less polluted sampling regions (Northern Europe), the AirCore samples also featured a noticeable offset where both May 2018 AirCore flights, and the KAT17 Geophysica flight have samples with mixing ratios far higher than the American Samoa or Mauna Loa background trends. CH<sub>3</sub>Cl is subject to seasonal variations, and as it has many natural sources the local background trend may vary significantly to that measured at remote sensing stations. It should also be noted that, as discussed earlier in this chapter, of the compounds covered here CH<sub>3</sub>Cl is the one most sensitive to delay and often gives abnormally high mixing ratios if not analysed swiftly enough.

There is a mismatch for some of the gases, between what we measured in the stratosphere and what would be expected from the tropospheric trend. This is particularly the case for a very long-lived gas such as CFC-115, where the observed positive FRF offset at or near the tropopause cannot be caused by chemical decay. This means that less CFC-115 is entering the stratosphere in this region than would be expected from the shifted Cape Grim trend. There are strong sources in East Asia, which is far distant (and south) from the AirCore flights, so air that arrives at Cape Grim may have higher mixing ratios for this compound as the East Asian emissions will only mix in later on their way to the southern hemisphere.

In addition there could also be a seasonal effect as the Asian Monsoon mixes polluted air masses into the stratosphere, particularly in late summer and early autumn. This leads to (during these months), higher than expected mixing ratios in the northern

hemisphere stratosphere. This can lead (particularly for shorter-lived species such as methyl chloride), to negative FRFs near the tropopause.

As accurate FRFs are needed for the calculation of various policy-relevant metrics such as stratospheric lifetime and ozone depletion potential, a better understanding of potential variability, its causes and mitigation, is vital. To investigate variability in FRFs, FRF at 3 years mean ages were generated for each compound, for each flight of each campaign (i.e. every individual Geophysica and AirCore flight). This was done using the same method as detailed in section 3.2.4.

This allowed an investigation into some of the factors that might influence FRF at 3 years mean ages, such as potential changes in background trend (Figure 4.27 shows all flights in chronological order, so any influence from changes to background trend, might be visible), latitude (Figure 4.28), and the fraction of year (Figure 4.29) as a proxy for seasonality. In addition to a FRF at 3 years mean age for each flight, I also calculated a weighted average FRF at 3 years mean age for all Geophysica flights, a weighted average FRF at 3 years mean age for all AirCore flights, and a weighted average FRF at 3 years mean age for all flights combined. The averages were weighted inversely to the magnitude of each flight's uncertainty, so that a flight with good precision would be weighted more heavily compared to a flight with poor precision. This was to minimise the impact of any outliers on the resulting FRF at 3 years mean age.

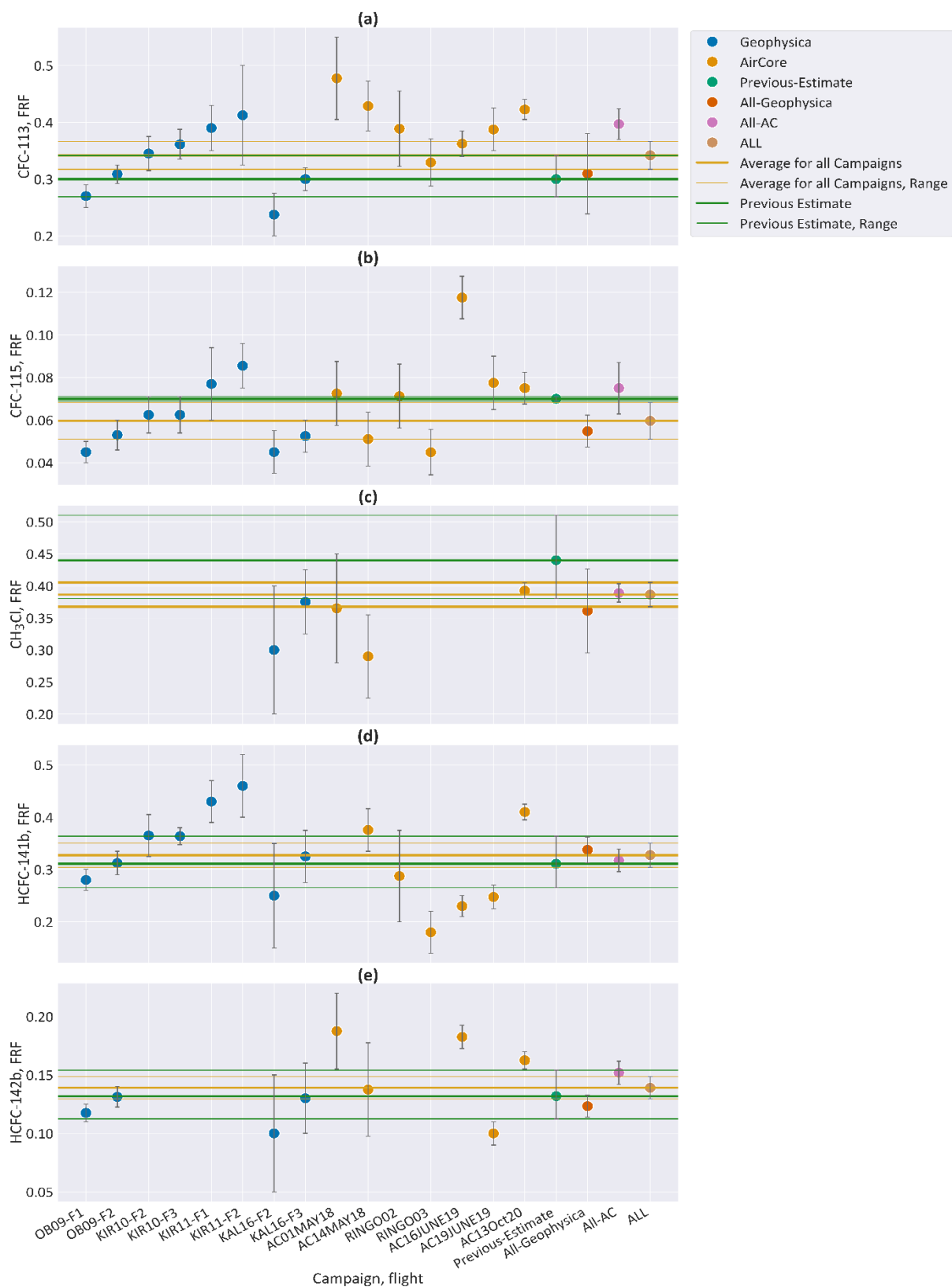


Figure 4.27. The FRF at 3 years mean age of different compounds, calculated for each flight. 'All Geophysica' refers to the average of all Geophysica derived FRFs. 'All-AC' refers to the average of all AirCore FRFs. A thick line is plotted through the mean for 'All' (yellow) and 'previous estimate' (green), with thin lines of the same colour indicating the extent of their range (a). CFC-113, 'previous estimate' = Leedham-Elvidge et al 2018. (b). CFC-115, 'previous estimate' refers to estimate in Chapter 3. (c) CH<sub>3</sub>Cl, 'previous estimate' refers to Adcock et al 2020. (d) HCFC-141b, 'previous estimate' = Leedham-Elvidge et al 2018. (e) HCFC-142b, 'previous estimate' = Leedham-Elvidge et al 2018.

In Figure 4.27 we can see that for all compounds' FRF at 3 years mean ages, there is considerable variation and range between individual flights. For CFC-113 the 'previous estimate' range overlaps the 'All' range within the uncertainties; however, there is still substantial variation between FRFs from different flights. Several Geophysica points occur outside the previous estimates range. Most AirCore data points are outside the previous estimate range. Many AirCore and Geophysica data points occur outside the range marked by the 'all' line, which is the average for all flights. While the 'all Geophysica' and 'all AC' data points do overlap within the uncertainties, AirCore flights on average produced higher FRFs than Geophysica flights. All AirCore Flights took place after the Geophysica flights, and CFC-113's abundance has been in slow decline (see Table 1-1 and Figure 4.11). This should not affect the compound's FRF as the time-independent formulation described in Ostermüller et al., (2017) was used to derive FRFs.

For CFC-115 the 'previous estimate' range does not overlap with the 'all' range, which is consistent with results in section 3.3.1 where the FRF at 3 years mean age for CFC-115 was significantly higher than previous estimates. In Figure 4.27 there is no clear trend, though AirCore FRFs seem to be on average higher than Geophysica derived FRFs. There is one unusually high FRF at 3 years mean age for the flight on the 16<sup>th</sup> June 2019, but as this does not appear to be anomalous on any other compound, and no error was found with the sampling or analysis procedures for this flight, the data point has been included here. It helps illustrate the variability for FRFs, even between flights with very similar conditions (the flight on the 19<sup>th</sup> of June 2020 gives a FRF at 3 years mean age that is in line with others for this compound).

As there are fewer data points for CH<sub>3</sub>Cl, forming any concrete conclusions is difficult. However, most data points fall within the uncertainty range of the previous estimate. All but one data point fell within both the 'all' range and the 'previous estimate' range, though it should be noted that as CH<sub>3</sub>Cl was the compound most heavily affected if not analysed swiftly after capture, only the best samples could be used to generate FRFs, as poorer quality samples had such extreme outliers as to be unusable.

For HCFC-141b, the 'all' range and the 'previous estimate' range, have substantial overlap. Around two thirds of the data points fall within these ranges, with more AirCore samples falling outside the range than Geophysica samples. Again there is substantial variation of the three year FRFs from both Geophysica and AirCore samples observed.

For HCFC-142b all the Geophysica samples overlapped the 'all' and the 'previous estimate' range, while only one of the AirCore flights fits within these ranges. There is a notable variation and range between AirCore samples, while the Geophysica ones are fairly consistent.

All compounds showed noticeable variation, with outliers far outside the average. For all compounds the 'all' range and 'previous estimate' ranges are overlapped. With the exception of HCFC-141b, for all compounds the 'All-AC' range was higher than that of the 'All-Geophysica' ranges. In the case of HCFC-141b, both ranges still heavily overlapped each other. This would suggest that using data from multiple flights using different techniques, does result in notable variation between flights, but that when taken as a whole can result in representative FRF at 3 years mean ages.

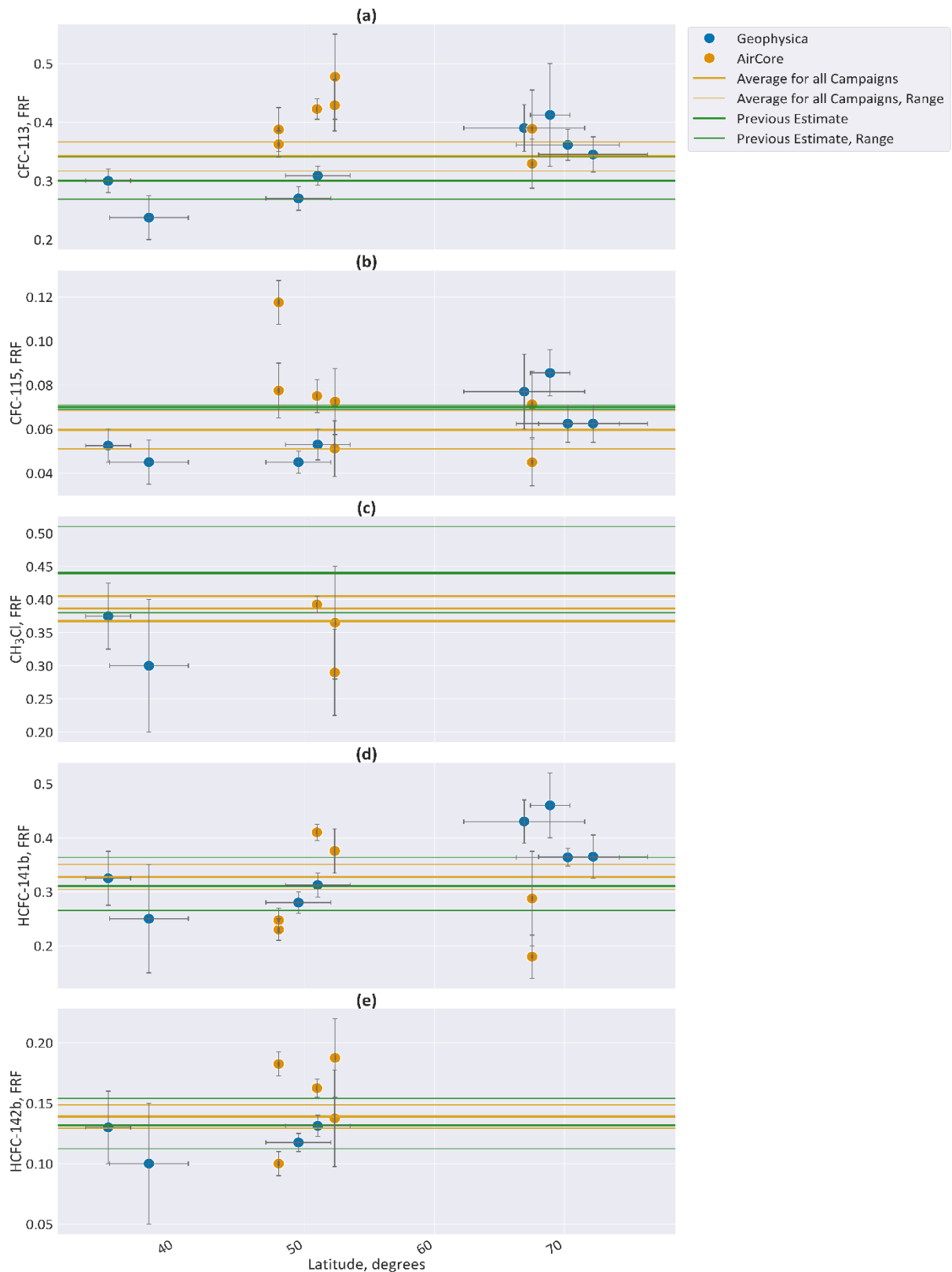


Figure 4.28. The FRF at 3 years mean age of different compounds, calculated for each flight, plotted against latitude. 'All Geophysica' refers to the average of all Geophysica derived FRFs. 'All-AC' refers to the average of all AirCore FRFs. A thick line is plotted through the mean for 'All' (yellow) and 'previous estimate' (green), with thin lines of the same colour indicating the extent of their range (a). CFC-113, 'previous estimate' = Leedham-Elvidge et al 2018. (b). CFC-115, 'previous estimate' refers to estimate in Chapter 3. (c) CH<sub>3</sub>Cl, 'previous estimate' refers to Adcock et al 2020. (d) HCFC-141b, 'previous estimate' = Leedham-Elvidge et al 2018. (e) HCFC-142b, 'previous estimate' = Leedham-Elvidge et al 2018.

In Figure 4.28 there is no clear variation correlated with latitude for CFC-113, CFC-115, or CH<sub>3</sub>Cl (though with so few data points, any pattern would need to be extremely clear to be noticeable). CFC-115 may have slightly higher FRFs on average at higher latitudes, but the uncertainty ranges still heavily overlap. For HCFC-141b there is possible variation with latitude; Geophysica flights in higher latitudes have higher FRFs; however, most fall within the average range so no firm conclusion can be reached from this. As samples for higher latitude are absent for HCFC-142b, there are insufficient data points to reliably suggest a correlation with latitude.

So, from Figure 4.28 it is not possible to rule out variation as a result of different latitudes; the data points presented here are insufficient to support this. More samples and a greater range of latitudes might shed more light on this. However, at present Figure 4.28 can only hint at an effect from latitude.

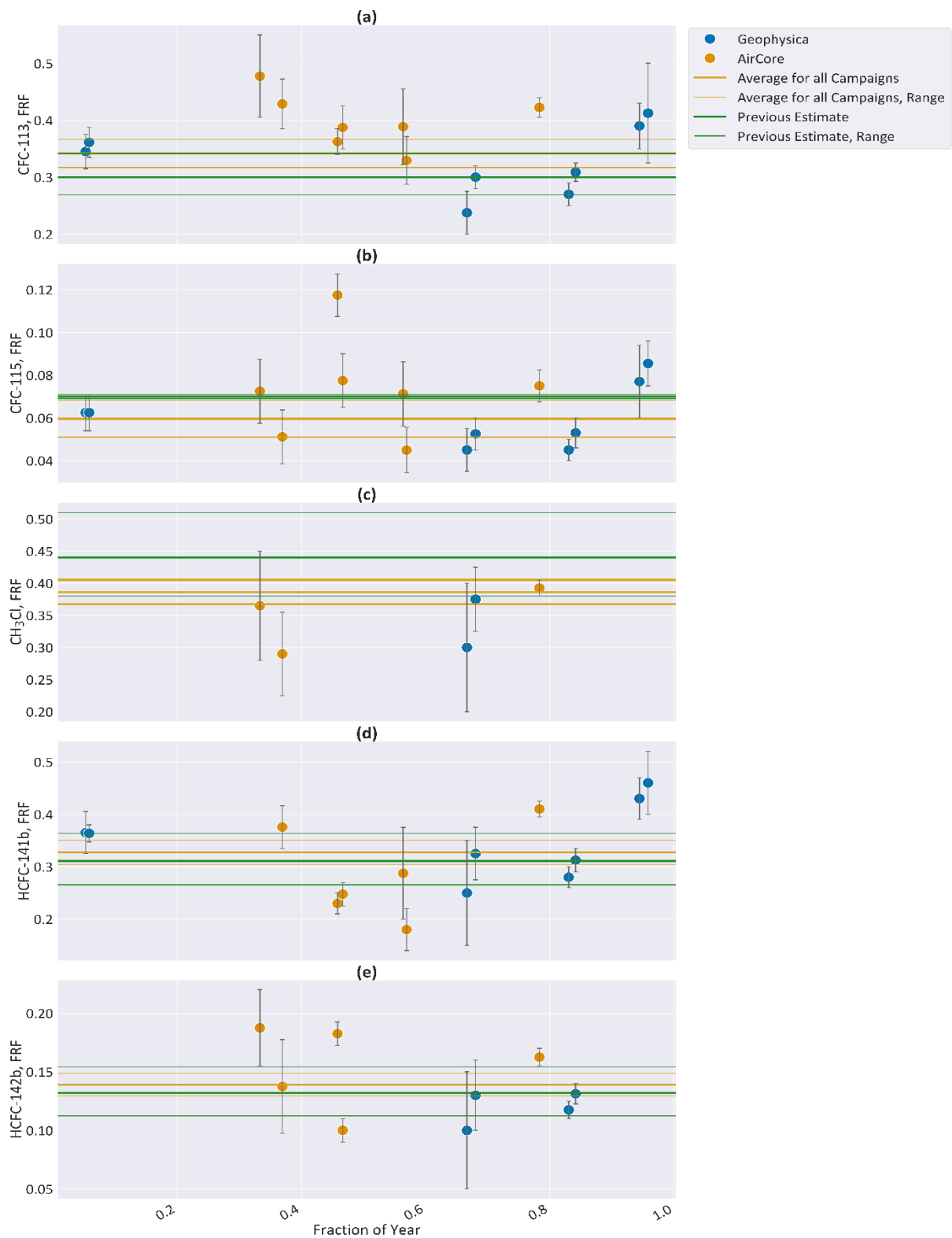


Figure 4.29. The FRF at 3 years mean age of different compounds, calculated for each flight, plotted against fraction of year. 'All Geophysica' refers to the average of all Geophysica derived FRFs. 'AC-Merged' refers to AirCore data that used mean ages derived from different compounds (SF6\*0.8, HFC-125, and/or C2F6), then merged. 'All-AC' refers to the average of all AirCore FRFs. A thick line is plotted through the mean for 'All' (yellow) and 'previous estimate' (green), with thin lines of the same colour indicating the extent of their range (a). CFC-113, 'previous estimate' = Leedham-Elvidge et al 2018. (b) CFC-115, 'previous estimate' refers to estimate in Chapter 3. (c) CH<sub>3</sub>Cl, 'previous estimate' refers to Adcock et al 2020. (d) HCFC-141b, 'previous estimate' = Leedham-Elvidge et al 2018. (e) HCFC-142b, 'previous estimate' = Leedham-Elvidge et al 2018.

In Figure 4.29 some compounds have what might be a seasonal pattern, notably CFC-113 and HCFC-141b, which both appear to vary with the fraction of year (this is discussed more in section 4.4.2). It should be noted that the uncertainties shown are the result of the methods used.

Variability from the atmosphere should be expected; for example, transport times will vary, flights over different altitudes will vary, the exact transport conditions of air parcels vary. So variation around the average reflects this. FRFs are by their nature an average, and will differ over flights and different parts of the stratosphere due to their slight dependence on the exact path the sampled air has previously taken inside the stratosphere. It is also encouraging that the uncertainty ranges from both Geophysica and AirCore flights are both small and comparable. Very low latitude FRFs tend to be lower; however, they are still broadly within the uncertainties. During the polar vortex we can expect to see higher FRFs, because the air inside the polar vortex has descended from the upper stratosphere and mesosphere, regions where destruction of chlorine-bearing compounds is heightened. Within the polar vortex, conditions for the destruction of ozone are optimal, so air from the polar vortex will necessarily be depleted of ODSs. However, this effect should only be seen during specific seasons and within certain latitudinal zones.

The figures show only a small effect (higher altitude FRFs seem on average slightly higher than lower latitude FRFs), and this is consistent with those flights only capturing small quantities of mesospheric air. So, while the average of large numbers of samples gives a result that is usually in good agreement with previous estimates, variation between flights will be a factor if a smaller dataset is used (Table 4-6).

*Table 4-6. FRF results for each compound, compared to the previously estimated FRFs. For CFC-115 the previous estimate FRF is from Chapter 3, Section 3.3.1. For CH<sub>3</sub>Cl the previous estimate figure is from Adcock et al., (2021). All other compounds' previous estimates FRFs are derived from updated data for Leedham-Elvidge et al., (2018). All-Geophysica refers to FRF at 3 years mean ages calculated using all available data from Geophysica flights, but does not include AirCore flights. All-AirCore refers to FRFs calculated using all appropriate AirCore flights. 'All' Refers to FRFs derived using both AirCore and Geophysica data.*

	Previous-Estimate	All-Geophysica	All-AirCore	ALL
CFC-113	0.3 (0.27-0.34)	0.31 (0.29-0.43)	0.4 (0.37-0.42)	0.34 (0.32-0.37)
CFC-115	0.07 (0.6-0.8)	0.05 (0.05-0.14)	0.08 (0.06-0.09)	0.06 (0.05-0.07)
CH <sub>3</sub> Cl	0.44 (0.38-0.51)	0.36 (0.3-0.43)	0.39 (0.37-0.4)	0.39 (0.37-0.41)
HCFC-141b	0.31 (0.27-0.36)	0.34 (0.31-0.6)	0.32 (0.3-0.6)	0.33 (0.3-0.35)
HCFC-142b	0.13 (0.11-0.15)	0.12 (0.11-0.19)	0.15 (0.14-0.16)	0.14 (0.13-0.15)

### 4.3.10 ODPs

Using the method described in section 3.3.3, and the new FRFs derived from AirCore and Geophysica samples (Section 4.3.9), ODPs for each compound were generated. This was done three times: using AirCore only FRFs, using Geophysica only derived FRFs, and combined Geophysica and AirCore FRFs. In Table 4-7 these are compared to the previous estimates from the most recent WMO 2022 report (Daniel *et al.*, 2022).

*Table 4-7. ODPs derived from Table 4-6 FRF results, using either FRFs from AirCore flights only, or a combination of AirCore and Geophysica derived FRFs. These are compared to those listed in WMO 2022 (Daniel et al., 2022). For CFC-115 two sets of ODPs were generated, one using the new FRF and lifetime estimate from Chapter 3, and the other using the ODP listed in WMO 2022. As an uncertainty range for ODPs was not listed in WMO 2022, I have used the uncertainty range given in Velders et al. (2014).*

Compound	Geophysica + AirCore	AirCore Only	Geophysica Only	WMO2022
CFC-113	0.92 (0.85-0.98)	1.06 (0.99-1.14)	0.83 (0.77-1.15)	0.82 (0.74-0.93)
CFC-115 (Lifetime and FRF from WMO 2022)	0.45 (0.39-0.52)	0.57 (0.48-0.66)	0.417 (0.36-1.049)	0.45 (0.44-0.47)
CFC-115 (Lifetime and FRF from Chapter 3, section 3.3.2)	0.26 (0.23-0.3)	0.33 (0.28-0.39)	0.243 (0.21-0.61)	0.27 (0.26-0.28)
Methyl Chloride	0.012 (0.012-0.013)	0.012 (0.012-0.013)	0.011 (0.009-0.013)	0.015 (0.009-0.021)
HCFC-141b	0.087 (0.081-0.094)	0.085 (0.079-0.159)	0.09 (0.084-0.16)	0.102 (0.096-0.108)
HCFC-142b	0.044 (0.041-0.047)	0.048 (0.045-0.051)	0.039 (0.036-0.06)	0.057 (0.051-0.063)

Examining Table 4-7 and Figure 4.30 the variation between ODPs derived from different sources and using different techniques is clear. There are also some anomalies that need to be discussed. Firstly, that the ODP given for CFC-113 using FRFs derived only from AirCore data, is 1.06. As ODPs are relative to CFC-11 which by definition has an ODP of 1, an ODP of 1.06 for a compound with 2 fewer chlorine atoms than CFC-11 should not be possible. CFC-113 has the same number of chlorine atoms as CFC-11, but a longer lifetime, so a higher ODP for CFC-113 is probably an anomaly. To understand why this anomalously high ODP was reached, we can look back to section 4.3.9 and in particular Figure 4.27a, in which we see that FRFs for each flight varied notably from each other, though largely overlapped the ‘average’ and the ‘previous estimate’ ranges. The AirCore flights in particular seem to have on average higher FRFs than the Geophysica flights, and these higher FRFs seem to have biased the resulting ODP unreasonably high. The FRFs were weighted inversely to the size of the uncertainty, but that uncertainty was derived from instrument

precision, if another factor (such as atmospheric conditions) was the cause of unusually high FRFs, then this would not have been accounted for.

However as can be seen more clearly in Figure 4.30, when combining FRFs from both AirCore and Geophysica flights, the resulting FRF, while high, does overlap within the uncertainties with the previous estimate in (Daniel *et al.*, 2022). The Geophysica-only derived FRF also has a range that exceeds 1, so the issue is not confined solely to AirCore flights. This illustrates one of the challenges of this method to derive FRFs from individual flights: that it results in a wide range that can be biased by a few individual flights. Even the Geophysica flights, which are of well documented quality, saw variation between flights. This also demonstrates the necessity of combining FRFs from multiple flights and campaigns, as doing so can help account for variations from atmospheric conditions, seasonality, location and any variations in technique.

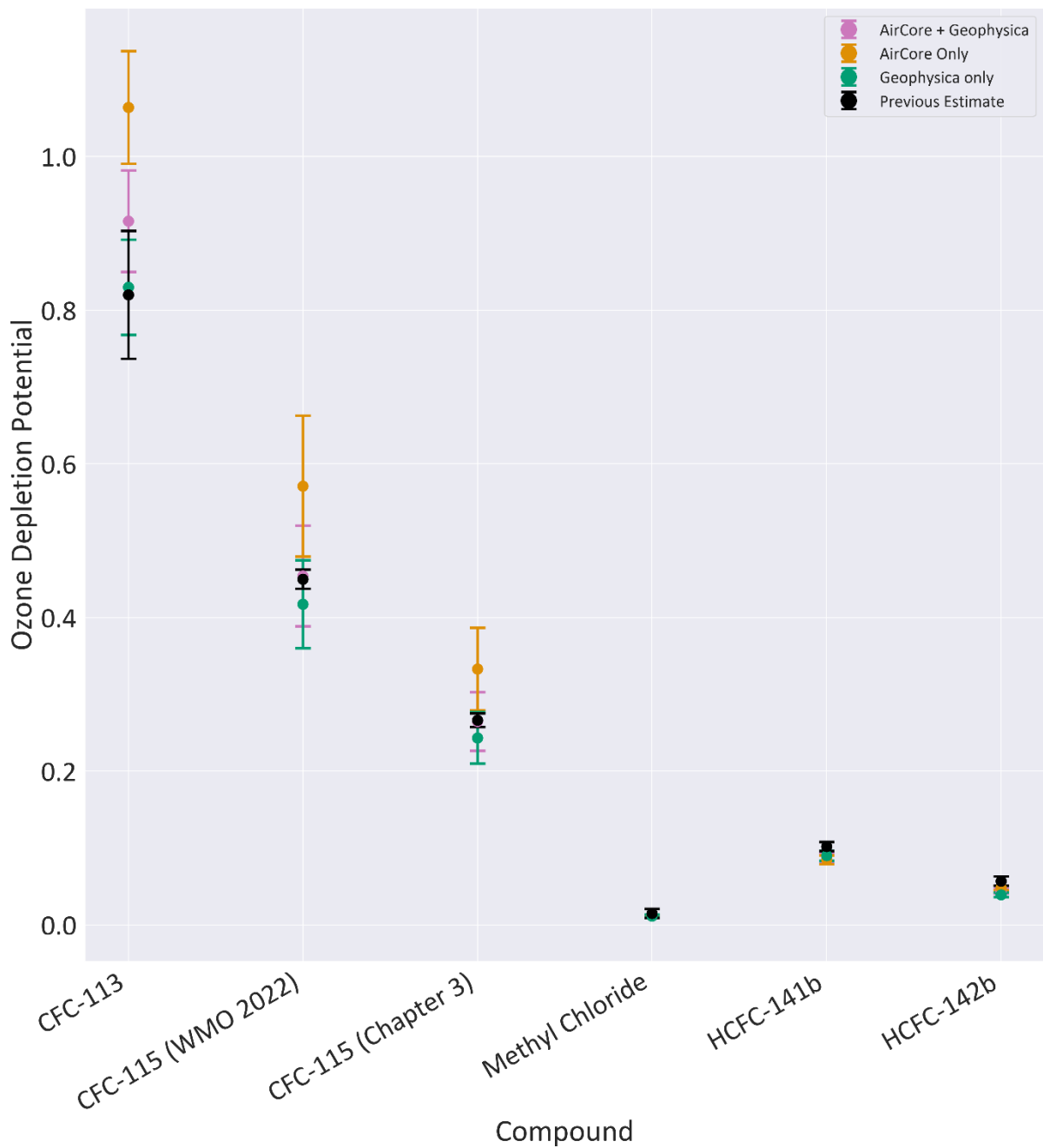


Figure 4.30. A plot of Table 4-8, showing ODPs derived from Chapter 4, FRF results, using either FRFs from AirCore flights only, Geophysica flights only, or a combination of AirCore and Geophysica flight derived FRFs. These are compared to the 'Previous Estimate' listed in WMO 2022 (Daniel *et al.*, 2022). For CFC-115 two sets of ODPs were generated, one using the new FRF and stratospheric lifetime estimate from Chapter 3 and the other using the FRF and stratospheric lifetime value estimate listed in WMO 2022. As an uncertainty range for ODPs was not listed in WMO 2022, I have used the uncertainty range given in Velders *et al.* (2014).

CFC-115 is more complex to analyse as two different estimation methods were used to derive lifetime: once to compare ODPs derived using the previously estimated lifetime for CFC-115, and again using the lifetime estimated in section 3.3.2. Please note that the ODP value for 'CFC-115 (WMO 2022)' uses the FRF and lifetime values listed in (Daniel *et al.*,

2022), while the ODP 'CFC-115 (Chapter 3)' was derived using the FRF and lifetime estimates derived in Chapter 3. Looking at Figure 4.30 CFC-115, both 'WMO 2022' points overlap closely with the combined AirCore and Geophysica derived ODP values, and in both cases the AirCore-only derived ODPs were notably higher (though still overlapped within the uncertainties) than the previous estimate. The Geophysica only derived ODPs are lower than the previous estimate for both 'CFC-115 (WMO 2022)' and 'CFC-115 (Chapter 3)', but in both cases they overlap with the previous estimate within the uncertainty range.

One detail of note is that the ODP value for CFC-115 derived using the newly derived lifetime estimate and FRF estimate in section 3.3.3 is  $0.27 (\pm 0.02)$ , the value calculated here in this section using the combined AirCore and Geophysica data is 0.26 (0.23-0.3), which would be consistent with the ODP value listed in the previous WMO (2018) report which was 0.26 (Carpenter *et al.*, 2018), but not the value of 0.45 listed in WMO 2022 (Daniel *et al.*, 2022). This was derived using the atmospheric lifetimes and FRFs for mid-latitude conditions from Engel *et al.*, (2018).

It is difficult to see from Figure 4.30 but the values for CH<sub>3</sub>Cl from both the AirCore-only data and the AirCore plus Geophysica data are virtually identical, are slightly lower than the previous estimate, and the Geophysica-only ODP is the lowest value, but all values overlap within the uncertainties.

In the case of HCFC-141b the ODP using the combined AirCore and Geophysica data is slightly higher than the AirCore-only value, and the Geophysica only ODP is highest of the three. All three values are lower than the value listed in WMO 2022 (Daniel *et al.*, 2022), and only the combined Geophysica and AirCore derived ODPs does not overlap with the previous estimate within the uncertainties. Similarly, HCFC-142b also has lower ODPs from Geophysica plus AirCore and the AirCore, than the previous estimate. Unlike HCFC-141b however, HCFC-142b's AirCore-only value is higher than the AirCore plus Geophysica values, with the Geophysica-only ODP being the lowest. Only the AirCore-only data overlaps with the previous estimate within the uncertainties. This may be due to firstly to the ODPs for these compounds being such small numbers that even tiny changes to them are noticeable, as such the fact that the AirCore-derived ODPs tended to have slightly larger error ranges may have led them to overlap the previous estimate, when the AirCore plus Geophysica derived ODPs did not.

For all compounds except the HCFCs, the combined AirCore and Geophysica derived ODPs overlapped with the previous estimates, within the uncertainties. For most compounds the AirCore-only ODPs were notably higher than those derived using both AirCore and Geophysica data, for CH<sub>3</sub>Cl the values were virtually identical (with such small numbers, one would need to go down to 5 decimal places to see a difference), and HCFC-141b where the combined AirCore and Geophysica derived ODP was fractionally larger than that of the AirCore-only ODP. With the exception of HCFC-141b, the Geophysica-only derived FRFs were lower than the AirCore-only derived FRFs.

#### 4.4 Discussion

Looking at both the AirCore flights (section 4.3) and stability tests (Appendix B ) for most compounds, collection via AirCore provided robust data. However, there were a few factors which did influence the quality of the data for some compounds (Table 4-8).

*Table 4-8. The compounds explored in this chapter, the potential factors that might have affected them, and whether or not this was found to be the case in section 4.3 or the stability tests (Appendix B).*

Compound	AirCore	Subsampler	Delay	Picarro (G2401)	Temp
CFC-113	No	No	No	No	Maybe
CFC-115	No	No	No	No	No
HCFC-141b	Maybe	No	No	No	Maybe
HCFC-142b	No	No	No	No	No
HFC-125	No	No	Yes	Yes	No
C <sub>2</sub> F <sub>6</sub>	Maybe	Yes (Luna)	No	Yes	No
CH <sub>3</sub> Cl	No	No	Yes	No	No

As can be seen in Table 4-8 only CFC-115 and HCFC-142b saw no effect from any of the proposed factors. All other compounds saw some effect, and this should be taken into account when using AirCores to sample them.

##### 4.4.1 Idiosyncrasies of technique.

There are a few features which are particular to the technique used to derive FRFs, described in section 3.2.4, which constrain the range of uncertainty. When using a polynomial to derive FRF at 3 years mean ages, the closer the correlation between mean

age and FRF for that flight/compound/dataset, the more reliable the results. Very few flights will have a 'perfect' profile with an even distribution of data, in which samples start precisely at the troposphere and extend through the stratosphere to a mean age of 4-5 years. Some flights will have large numbers of samples at a low mean age, but few at a higher mean age, and vice versa. This is somewhat compensated for by quintupling the dataset (5n), using the same technique described in section 2.5. While this does help compensate for high or low mean age skews, it also produces a more 'scattered' plot (e.g. Figure 4.15) which is harder to draw a representative polynomial trendline through. However, as the polynomial is bootstrapped, we do get a better representation of the possible range

Ultimately most of these issues can be easily compensated for by consolidating data for a particular compound from all flights. This however is only possible if all flights are genuinely comparable. As can be seen from Figure 4.27, the overall mean overlaps most flights within the uncertainties, but there is substantial variation between flights.

#### **4.4.2 Seasonality and Latitude**

As mentioned in earlier sections (2.6 and 4.3.9), nonlocal processes such as different transport pathways can impact the chemistry in time-dependent ways (Solomon *et al.*, 1992a, 1992b). Ostermüller *et al.*, (2017) noticed a seasonality in FRF, which they attributed to seasonal variations in transport, chemistry and mixing. They argued that the changes were consistent with an acceleration of the Brewer-Dobson circulation due to climate change. A stronger circulation would on average lead to faster transport of air parcels into their loss regions, and therefore give an increased FRF on a given mean age level.

As photolysis is a major sink for the compounds of interest in both Chapter 3 and Chapter 4, they should decompose fastest in the tropical stratosphere where the highest actinic fluxes occur, as opposed to higher latitude (Schauffler *et al.*, 1999; Laube *et al.*, 2013). Vertical transport above 20km is slower in the northern hemisphere's summer than in its winter (Boering *et al.*, 1994). This would be particularly pronounced in areas that are subject to the polar vortex, which is characterised by rapid descent, with regular mesosphere intrusion. This means the stratospheric polar vortex contains, at least in its upper levels, a substantial amount of mesospheric air. Any trace gas that experiences

mesospheric loss, will be depleted in air that is transported through (or into) the polar vortex (Ray *et al.*, 2017).

Therefore, both seasonality and latitude could plausibly influence the abundance of the trace gases under examination here, and thus their fractional release factors. Figure 4.28 showed FRFs for all compounds, plotted against latitude, and no compound shows any clear impact from latitude. It is possible that more campaigns in different latitudes might demonstrate an effect, but Figure 4.28 does not.

In regard to seasonality, it is also challenging to determine a correlation. In Figure 4.29 FRF at 3 years mean age for each flight is plotted against fraction of year. Most compounds show no pattern; however, CFC-113 does appear to follow an oscillating cycle throughout the year. Any relationship would be non-linear (alternately increasing and decreasing throughout a year). Any pattern could be coincidental, though there are indications it may not be. The cycle potentially shown in Figure 4.29 suggests that CFC-113's FRFs at 3 years mean age are at their maximum in spring, and their minimum in autumn. This would suggest we are seeing CFC-113 depleted air in spring following the polar vortex, with an increase in concentrations in the run up to the next polar vortex. Ray *et al.*, (2024) observed that FRFs were noticeably higher in summer than in winter.

While there are too few data points to be certain, and one clear outlier, in Figure 4.31 the FRFs at 3 years mean age do appear to display some seasonal variation, with undulation similar to a sine wave. However without further data points – especially ones that capture seasonality over several consecutive years, it is difficult to draw firm conclusions. Please note the obvious outlier at fraction of year 0.79 was the 19<sup>th</sup> of October 2020 flight, which for CFC-113 and HCFC-141b was affected by the very low temperatures experienced by the AirCore (see section 4.3.3), so the high FRF could be explained by temperature.

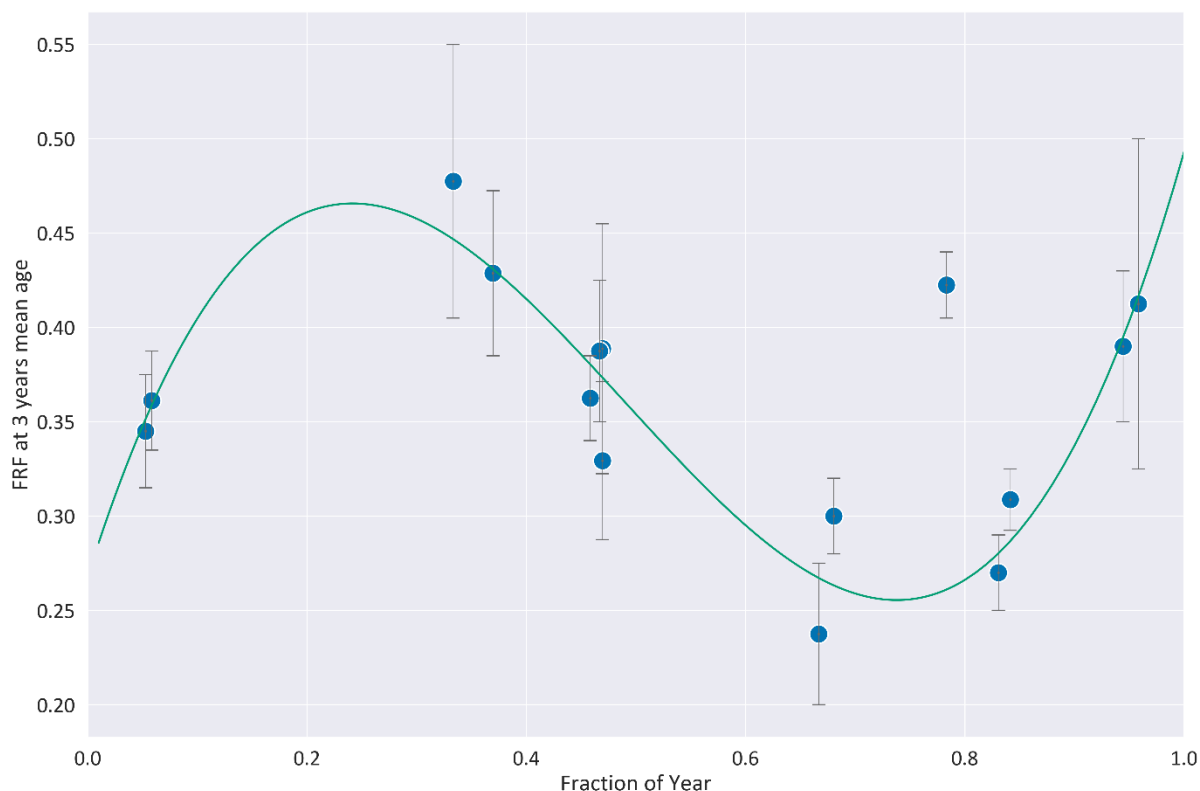


Figure 4.31. The FRF at 3 years mean age for CFC-113, plotted against Fraction of year. A 3<sup>rd</sup> order polynomial is plotted through the data points to illustrate the potential seasonal cycle.

It is possible to plot a 3<sup>rd</sup> order polynomial regression line through the data (see Figure 4.31), but how representative of any correlation between FRF and seasonality is the polynomial? To test the variability within the polynomial's fit, I used the same bootstrapping technique as I used with the FRF v Mean age correlation, but instead plotted fraction of year against FRF. Fraction of year here describes what fraction of the year had elapsed at the time the sample was collected, so a fraction of year value of 0.5 would correspond with the month of June, while a value of 1 would correspond with December. Using this polynomial, I calculated the FRF at 0.5 (fraction of year), and 1 (fraction of year). For June the predicted FRF at 3 years mean age was 0.36 (0.34-0.38), and December predicted an FRF at 3 years mean age of 0.48 (0.4-0.55). This shows substantial variation and no overlap.

The reason why CFC-113 would be affected by seasonality but not all the other compounds may be due to its comparatively short stratospheric lifetime. Of the compounds examined here only CH<sub>3</sub>Cl has a shorter lifetime, and HCFC-141b has a similar lifetime to CFC-113. CH<sub>3</sub>Cl has too few data points to identify a pattern; however, in the case of HCFC-141b, in Figure 4.32 a 2<sup>nd</sup> order polynomial is plotted through the data points (FRF at 3 years

mean age, and Fraction of year). This suggests that the FRF at 3 years mean age is lower (in the northern hemisphere) mid-year than it is in winter. As with CFC-113 I applied the bootstrapping technique to analyse variation in HCFC-141b's FRFs at 3 years mean age. For June the predicted FRF at 3 years mean age was 0.24 (0.14-0.38) and in December this became 0.45 (0.41-0.5).

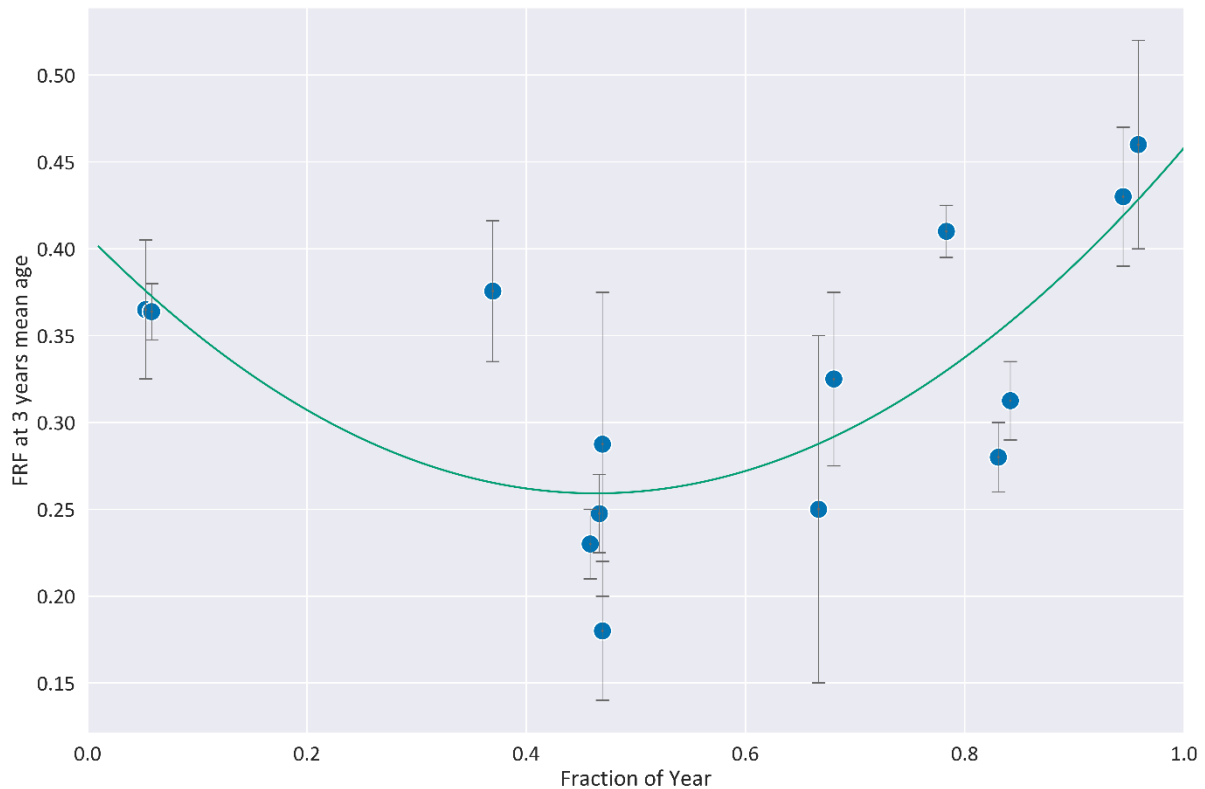


Figure 4.32. FRF at 3 years mean age for HCFC-141b plotted against fraction of year. 2<sup>nd</sup> order polynomial is plotted through to illustrate potential seasonal variation.

Given how different the FRF at 3 years mean age for either CFC-113 or HCFC-141b is during June compared to December, if seasonality does indeed affect the FRF of CFC-113 and HCFC-141b, it does so quite substantially, but differently for each compound. A reason for this is the differences between the sink reactions of the two compounds. In autumn the lower stratosphere receives an influx of tropospheric air through isentropic transport in the extra-tropics, in addition to the Asian Monsoon, and this brings extra water vapour, resulting in enhanced stratospheric OH (Klonecki *et al.*, 2003; Zheng *et al.*, 2024). As discussed in section 4.1.2.f the primary loss pathway for HCFCs is via the OH radical, so an influx of air containing enhanced quantities of OH should see a decrease in HCFC-141b's concentrations during autumn (and by extension result in greater values for FRFs). In Figure

4.32 the values for FRF at 3 years mean age does indeed increase during autumn for HCFC-141b.

In contrast the dominant loss pathway for CFC-113 is photolysis (with O(<sup>1</sup>D) reactions being largely responsible for the rest). This means the autumn influx of air with increased concentrations of OH would not lower the concentrations of CFC-113. On the contrary, an influx of tropospheric air would increase the concentrations of CFC-113, resulting in lower FRFs during that time of year, which is reflected in Figure 4.31.

#### 4.4.3 ODPs

From Figure 4.30 it is clear that the AirCore derived ODPs and the ODPs derived in the published literature, largely agree within the uncertainty range. AirCore-only derived ODPs were usually higher than those derived from combined Geophysica and AirCore data, and Table 4-7 shows the range resulting from variation between flights. For reasons explored in more detail in Section 4.3.9 and Section 4.4.2, there is variation in FRF at 3 years mean ages between flights, possibly due to season and latitude. When data from many flights is combined to derive FRFs, this variation is largely averaged, but it is helpful to be aware of this variation.

Another factor to be aware of is that changing the lifetime used for ODP calculation (described in Section 3.3.3) naturally changes the resulting ODP. This can be seen clearly seen in Section 4.3.10, where the ODP of CFC-115 is calculated twice, once using the FRF and lifetime listed in Burkholder et al. (2022) and once using the FRF and lifetime generated in Section 3.3.1 and Section 3.3.2 respectively. The resulting ODPs were significantly different. The ODP calculation requires the total global atmospheric lifetime of a compound. For the CFCs this should be roughly equivalent to stratospheric lifetime as there are no significant sinks outside of the stratosphere. However, in Burkholder et al. (2022) CFC-115 is listed as having a global lifetime of 540 years, but a stratospheric lifetime of 664 years. There are a number of factors for this discrepancy. Firstly the 'total lifetime' estimate for CFC-115 included loss from Lyman- $\alpha$  photolysis in the mesosphere, though it is unclear how strong an impact this is expected to have. Only a small percentage of air reaches the mesosphere each year (Ray *et al.*, 2017), so the effect should be minimal.

Another factor is that the lifetime estimates are taken from the SPARC 2013 lifetime report (Ko *et al.*, 2013). A footnote (L5) in Burkholder *et al.* (2022) mentions that there are differences between the recommended total atmospheric lifetime listed and the results of combining partial lifetimes. This is attributed to the fact these lifetimes were derived from multi-model results and field observations. So the multi-model results and field observations may not have all derived the same specific lifetime (they may have only derived partial lifetimes and will have used different methods). The discrepancy between total and stratospheric lifetime for CFC-115 may be due to skewing from different model results, rather than reflecting real differences in lifetime.

The ODP value for CFC-115 listed in WMO 2022 used FRFs from Engel *et al.*, (2018) while the lifetime uncertainties were based on the SPARC (2013) lifetime report, as evaluated by Velders *et al.* (2014). As this predates the time-independent method for calculating entry mixing ratios and FRFs (Ostermüller *et al.*, 2017), the FRFs used would not have been time independent, though as CFC-115 had a relatively small trend that had largely plateaued by 2000, any effect should be minimal.

CFC-113 also shows some differences between total lifetime and stratospheric lifetime, with a total lifetime of 93 years and a stratospheric lifetime of 94 years in Burkholder *et al.* (2022), which agrees within the uncertainties with the estimate of 83 (75–94) years in Leedham-Elvidge *et al.*, (2018). The total lifetime analysis for CFC-113 included tropospheric photolysis partial lifetimes, but as CFCs are largely inert in the troposphere this is unlikely to change the resulting lifetime greatly. As with CFC-115, atmospheric lifetimes for CFC-113 in Burkholder *et al.* (2022) were taken from the SPARC (2013) lifetime report and discrepancies may arise from the use of lifetimes derived from multi-model results and field observations. ODPs were derived using FRFs from Engel *et al.*, (2018), though a greater ODP value was derived in Davis *et al.*, (2016).

The atmospheric lifetimes and ODPs of HCFC-141b, HCFC-142b, and CH<sub>3</sub>Cl, listed in Burkholder *et al.* (2022) were derived from the same sources as CFC-113 and CFC-115, and this explains some of the discrepancies between the values given in Leedham Elvidge *et al.*, (2018) and Burkholder *et al.* (2022). However, unlike the CFCs, these compounds have loss processes which occur before they enter the stratosphere. All three compounds have tropospheric and ocean loss processes, and in addition CH<sub>3</sub>Cl has soil loss processes.

As ODP calculations are extremely sensitive to even small changes in the FRF and lifetimes used, the resulting ODP values may have greater uncertainty than is initially apparent. However, for the compounds examined here, provided care is taken during collection, and where AirCore data and data derived from research flights can be shown to be sufficiently comparable, then AirCore data can be used to generate policy relevant metrics such as ODPs. However, there are a number of factors to consider; firstly, that careful quality control measures are needed, secondly that the small quantities of air retrieved via AirCore have an increased chance of sampling a non-representative air mass, and thirdly that the AirCore precisions are not quite as good due to the smaller signals.

These added uncertainties can be compensated for somewhat when data from a larger number of flights (which due to their flexibility and cheapness AirCores are eminently suitable to provide) are included. Given the relative cost-effectiveness and flexibility of the AirCore technique compared to large balloon flights or high-altitude research aircraft campaigns, some additional precautions and the occasional poor-quality flight could be seen as fairly minor inconveniences.

## **4.5 Conclusion**

### **4.5.1 AirCore and sampling techniques**

All seven of these compounds showed acceptable-to-robust precision, particularly when necessary precautions are taken. Such precautions include analysing samples as soon after collection as possible, using a complex sub-sampler, using suitable thermal insulation for the AirCore during deployment, and ensuring that the AirCore is coated to prevent wall reactions. Though not all precautions were required for all compounds, CFC-115, for example, did not appear affected by any of these factors, while CH<sub>3</sub>Cl was extremely sensitive to delay between collection and analysis.

Both HCFC-125 and PFC-116 were investigated in Leedham-Elvidge et al., (2018) as potential age-tracers, and this chapter investigates whether the AirCore sampling technique gives strong enough precision for these compounds to be used as age-tracers. Provided the samples are analysed quickly after collection (to preserve HCFC-125) and both using a complex sub-sampler and a Silco-treated AirCore is used (for PFC-116), both compounds do appear to give robust enough precisions and vertical profiles to be useful.

The AirCore sampling technique has proven to be extremely versatile, being able to sample both long-lived compounds (such as PFC-116) to much shorter-lived compounds (methyl chloride), and a wide range of different families of compounds (CFCs, HFCs, PFCs, HCFCs, etc.). It is also apparent that these different compounds do not seem to have conflicting requirements for sampling but are necessary if a suite of compounds is being studied. So theoretically improvements to sampling technique aimed at improving the reliability of data for one compound, should not decrease the reliability of others, and may in fact improve it.

#### 4.5.2 Mean Ages

As discussed in Section 4.3.8 the average ratio between mean ages derived via SF<sub>6</sub> and C<sub>2</sub>F<sub>6</sub> or HFC-125, were consistent, within the uncertainties, with the 1:0.8 ratio found in Leedham-Elvidge et al., (2018).

HFC-125 is clearly very sensitive to the effect of delay, and only three flights contained usable data for this compound. During stability tests concentrations of HFC-125 had begun to increase very slightly by 20+ days (Figure B.1), but the tests did not run long enough to pinpoint precisely what timeframe is crucial for HFC-125. If there is contamination from lab-air, HFC-125 concentrations increase while PFC-116 concentrations decrease (Figure B.2). Both compounds were found to be affected by the use of a Picarro G2401 spectrometer, with PFC-116 being affected most dramatically (Figure B.5)

From the available data, it seems that C<sub>2</sub>F<sub>6</sub> is more reliable (there were more usable flights as C<sub>2</sub>F<sub>6</sub> was less sensitive to adverse conditions) than HFC-125 as an age tracer in AirCore samples. C<sub>2</sub>F<sub>6</sub> is affected by the type of sub-sampler used and potentially whether the AirCore is coated. HFC-125 is heavily impacted by a delay between flight and analysis.

Both can potentially be used as age tracers for AirCore samples, but each are sensitive to different conditions. Having two potential age tracers means that one can be used when the other is missing, and when both are present, they could be averaged to better account for uncertainty. SF<sub>6</sub> derived mean ages have their own set of uncertainties; Leedham-Elvidge et al., (2018) shows the uncertainty range, and this tracer is particularly sensitive to the effect of the Polar Vortex producing a high-biased mean age for SF<sub>6</sub>. This

means that HFC-125 and C<sub>2</sub>F<sub>6</sub> make a useful addition to the options for AoA analysis for AirCore samples, particularly those taken during or in the vicinity of the Polar Vortex.

### **4.5.3 FRFs**

Having evaluated (in section 4.3.9) the FRF at 3 or 5 years mean age for each individual flight, notable variability between flights can be observed. After taking into account idiosyncrasies in calculation, and excluding heavily polluted regions, this variability remains. Some of this is due to an offset between ground-based background trends, and actual mixing ratios. Some variation may also be attributed to the latitude and season of the flight, though the uncertainty here is high.

At present the best solution to this variability is to combine FRFs and mean ages from a large number of flights (preferably over a wide latitude range and across different seasons), to achieve an 'average' FRF at 3 or 5 years mean age. This may necessitate the exclusion of flights performed during high pollution events (such as the Asian Monsoon), or other events that might impact the composition of stratospheric air such as during the polar vortex.

It is also clear that, provided appropriate precautions are taken (see Table 4-8), useful, policy relevant metrics (such as FRFs) can be derived using samples collected via AirCore technique. Due to the comparative cost-effectiveness and flexibility of the technique, this opens many possibilities for monitoring of compounds of interest.

### **4.5.4 ODPs**

Ozone Depletion Potentials are particularly useful as policy relevant metrics as they provide a simple scale differentiating compounds by their potential to deplete ozone. AirCore data allows sampling on a smaller, more localised scale than is possible via research flights or large balloon flights. Sections 4.3.10 and 4.4.3 demonstrate that ODPs for these compounds can be reliably derived from AirCore data, and while the uncertainty range is broader than for the published literature, it is still in agreement. Section 4.4.3 also illustrates that the ODP calculations are sensitive to uncertainty in total atmospheric lifetime estimates and FRF estimates. This highlights the importance of robust data collection for these

estimates, which AirCores can provide in a cost-effective manner. It also suggests that some uncertainty around ODP estimates is to be expected.

## Chapter 5 Summary, conclusions, future work.

### 5.1 Overview of major research findings.

Throughout this thesis, the focus has been on ozone-depleting and related substances and has explored a number of ways that they can be studied. Chapter 3 focused on 4 long-lived ODSs, and data gathered via high altitude research aircraft flights. In addition two models were used to investigate how changes to circulation or chemistry would affect these compounds. Archived air samples were also used to investigate these compounds where possible. Chapter 4 on the other hand explored CFC-115 along with 6 additional compounds using a (comparatively novel) technique for sampling the stratosphere: the AirCore technique.

#### 5.1.1 Overview from 'Chapter 3: Long Lived CFCs'

The four CFCs examined in Chapter 3 had previously been understudied, particularly CFC-13 and CFC-115. The updated stratospheric lifetimes, FRFs, and ODPs for these compounds (Table 5-1) are therefore able to fill gaps in existing knowledge. While some values for these metrics exist for some of these compounds, this is the first time in-situ measurements have been used to derive them for these compounds. A better understanding of these compounds is vital for monitoring and legislating threats to the ozone layer.

Section 3.3.1 saw updated FRF values for all four compounds under examination. In the most recent WMO (2022) report (Burkholder *et al.*, 2022; Daniel *et al.*, 2022), estimates for the FRF at 3 years mean age were available for CFC-114 and CFC-115. These had been sourced from Engel *et al.*, (2018). For CFC-114 the previous estimate of 0.13 ( $\pm 0.00014$ ) is very similar to the FRF at 3 years mean age from this work (section 3.3.1) which is 0.121 ( $\pm 0.007$ ), and if the uncertainty range is extended to 2-sigma, agrees within the uncertainties. The previously estimated value for CFC-115 was 0.07 ( $\pm 0.00032$ ), while my new estimate from section 3.3.1 was 0.06 ( $\pm 0.002$ ). In the case of CFC-13 and CFC-114a, there is a dearth of information on these compounds, and no FRFs were listed in WMO 2022. So the FRFs derived here for these compounds (0.071  $\pm 0.003$  and 0.313  $\pm 0.015$  respectively at 3 years mean age), fill a gap in the existing literature. As the concept of FRFs

is essential for assessing and quantifying the potential for ozone depletion of a compound, this is useful both in terms of its scientific merit alone, and as a policy-relevant metric that can aid in policy decisions.

While the stratospheric lifetimes derived in this work for CFC-114 and CFC-114a of 190 (range of 176-201) and 81 (range of 76-87) years respectively are within the uncertainty range of the original estimates of 191 (168-214) and 107 (82–133) years respectively, CFC-13's newly estimated stratospheric lifetime of 315 (287-331) years is around 50% smaller than the previous estimate (640 years, tropospheric lifetime only available with an unknown uncertainty range), while CFC-115's newly estimated stratospheric lifetime of 369 (328-435) years is around 44% smaller than the previous estimate of 664 (551-777) years.

While these newly estimated lifetimes for CFC-13 and CFC-115 from my work are shorter than previously estimated, they still represent a very long time during which these compounds can contribute to ozone depletion. Additionally, in order to account for both the current abundance of CFC-13 and CFC-115, and their newly estimated stratospheric lifetimes, emissions would need to be higher than previously believed. Precisely how much greater emissions would need to be is currently unclear, section 3.4 estimates that for CFC-13 the shorter lifetime might necessitate roughly double the current emissions estimates, and for CFC-115 80% increased emissions might be required. The model estimates updated from Western et al., (2023) however suggest a more modest increase.

Either way this could have implications, both in terms of ozone recovery, and in the enforcement of the Montréal Protocol. The question remains as to where these additional emissions are coming from. Unidentified banks (e.g. storage or in landfill), illegal manufacture, trade or use of the compounds, or inappropriate disposal methods (e.g. methods that destroy the compound and do not release it, such methods are discussed in Yazici et al. (2014)), are all possibilities. Western et al., (2023) concluded that emissions for CFC-115 and CFC-114a probably arise from the production of hydrofluorocarbons, while the drivers for CFC-13 are more uncertain, though emissions are known to result from the deliberate plasma arc destruction of CFC-12.

With newly derived FRFs and stratospheric lifetimes, it is necessary to quantify how great an impact on the ozone layer each compound can have, when compared to CFC-11. For this I derived ODPs for these compounds. The previous estimate for CFC-13's ODP, listed in WMO 2022 (Burkholder *et al.*, 2022), which was taken from the Montréal Protocol, was

0.3. The newly derived ODPs in section 3.3.3 were 0.38 (0.36-0.39) when using FRFs at 3 years mean age, and 0.34 (0.34-0.35) when using FRFs at 5 years mean age (the uncertainty for the latter was so small that rounding up the lowest estimate to 2 significant figures, produces the same number as the 'mean' figure). These ODP estimates are somewhat higher than the previous estimate, as the previous estimate would have used a larger lifetime for CFC-13, so would have produced a lower ODP.

CFC-114's previous estimate of 0.53 as listed in WMO 2022 (Burkholder *et al.*, 2022), and was derived using the FRF and lifetime figures (0.13 and 189 years respectively) listed alongside it in Table 7-2 Chapter 7 of WMO 2022 (confirmed via personal correspondence with chapter lead author John Daniel, 03/2024) (Daniel *et al.*, 2022). This is close to the uncertainty range found in section 3.3.3 of 0.48 (0.45-0.5) using FRFs at 3 years mean age, and 0.46 (0.43-0.48) using FRFs at 5 years mean age. This is lower than but largely consistent with the 0.50 semi-empirical ODP listed in Davis *et al.*, (2016).

CFC-115 had an ODP value of 0.45 listed in WMO 2022 (Burkholder *et al.*, 2022), and as with CFC-114 this was derived using the FRF and Lifetime values (FRF of 0.07 and lifetime of 540 year) in Table 7-2 Chapter 7 of WMO 2022 (Daniel *et al.*, 2022). This is substantially higher than those derived in section 3.3.3, which were 0.25 (0.25-0.27) using FRFs at 3 years mean age and 0.26 (0.24-0.27) using FRFs at 5 years mean age. Given that the newly estimated stratospheric lifetime of CFC-115 was significantly lower than the previous estimate, and that the FRF at 3 years was similar to (but smaller than) the previous estimate, it is to be expected that the newly derived ODP value will be smaller than the previous estimate.

For CFC-114a the previous estimate listed in WMO 2022 (Burkholder *et al.*, 2022) was 0.72. This was taken from the 2-D model ODP values in Davis *et al.*, (2016), which does not list a semi-empirical value for this compound. However, Burkholder *et al.* (2022) notes that it is consistent with the semi-empirical ODP reported in Laube *et al.*, (2014), though these have a larger uncertainty range. The newly estimated ODP value for CFC-114a from section 3.3.3 was 0.53 (0.5-0.55) for FRFs at 3 years mean age, and 0.49 (0.47-0.51) for FRFs at 5 years mean age. This is substantially lower than the previous estimate. However in Davis *et al.*, (2016), there is a noticeable difference between the semi-empirical ODP and the 2-D model derived ODP for CFC-114 (being 0.50 and 0.78 respectively), and this difference (where the 2-D model ODP is higher than the semi-empirical ODP) is seen for all but one of

the other compounds listed (when both types of ODPs were listed). The 2-D model utilised was the Goddard Space Flight Center (GSFC) 2-D atmospheric model, which was also used in section 3.2.3 this thesis, as discussed in that section; if aspects of the chemistry are incorrect then the resulting data may produce erroneous conclusions.

Table 5-1. Shows the newly derived metrics as well as their previous estimates. Revised FRFs are from section 3.3.1, Table 3-4. Revised lifetimes are stratospheric steady state lifetimes from section 3.3.2, Table 3-5. ODPs are from section 3.3.3, Table 3-6. Previous estimates for all metrics taken from Burkholder *et al.* (2022).

Metric	CFC-13	CFC-114	CFC-114a	CFC-115
Revised FRF	0.07	0.12	0.31	0.06
Previously Estimated FRF	-	0.13	-	0.07
Revised Lifetime	315	190	81	369
Previously Estimated Lifetime	-	191	106.7	664
Revised ODP	0.40	0.50	0.52	0.27
Previously Estimated ODP	0.30	0.53	0.72	0.45

Sections 3.3.1, 3.3.2, and 3.3.3 focused on deriving stratospheric lifetimes and other policy relevant metrics and did so using in-situ measurements. The final section (3.3.4) of the chapter explored how well the Goddard Space Flight Centre 2D model could simulate these observed conditions, some of the challenges faced when using a 2D model to do this, and to explore the effect changing the speed of circulation or chemical reactions, would have on our target compounds.

When the model data was compared to the in-situ data, several features became apparent. For CFC-11, CFC-13, CFC-115 and CFC-114a, when mixing ratio (ppt) was plotted against mean age (yr) the model data was in good agreement with the in-situ data (within the uncertainties). Such a compact correlation indicates that the model is able to accurately simulate the transport history of these compounds. However, for CFC-114 the mean ages were higher for the in-situ measurements than for the model data. As explored in section 3.3.4.a the kinetics data used for CFC-114 in the GSFC 2D model was taken from the Jet Propulsion Laboratory (JPL) report (JPL-15) recommendations (Sander *et al.*, 2006), which Vollmer *et al.*, (2018) notes did not take into account the potential presence of CFC-114a impurities in CFC-114. As the UV absorption of CFC-114 is weaker than that of CFC-114a, the GSFC would assume a faster disassociation rate for CFC-114 than would actually be the case.

When examining the effect of changes to circulation on the resulting mixing ratio-mean age correlation, the natural variation in the mean ages for air parcels in-situ was substantial. For all compounds, excluding CFC-114, the mean ages of the in-situ samples

largely fell within the range encompassed by the most extreme increased (P20) and decreased (M20) circulation simulations; with the in-situ data uncertainty range sometimes extending a short distance beyond these extreme scenarios. This is because the GSFC can only provide average values while the in-situ measurements will reflect the transport conditions experienced by the individual air parcels sampled. For reasons already discussed, CFC-114's in-situ data showed higher mean ages than the GSFC scenarios and was most consistent with the slower circulation scenario M20.

The speed of circulation affected the mixing ratio-mean age correlation at earlier mean ages for longer-lived compounds (CFC-13 and CFC-115), than it did shorter-lived compounds (CFC-114 and CFC-114a). Shortest mean ages were the result of the fastest circulation scenario (P20), and this was particularly striking for the longer-lived compounds.

In terms of chemistry the data produced by the GSFC largely reflected the known chemistry of the compounds, and the longer-lived compounds saw a greater divergence from the baseline scenario by the chemistry scenarios than the shorter-lived compounds. Once again CFC-114 was an outlier, with the model data generating lower mean ages than the in-situ data. The in-situ data has most in common with the slow chemistry (particularly photolysis) scenarios, and this is consistent with the interpretation that the kinetics data used in the model did not take into account impurities of CFC-114 and thus assumed a faster UV photolysis rate than was actually present.

The 2D GSFC model data was compared to the data from the 3D CLaMS model, the 3D model (CLaMS) was better able to simulate coordinates that had a spacial component (such as altitude and potential temperature), and the main focus of this section was on the mean age-tracer correlation which both models should handle well. The GSFC model utilizes the MERRA\_2 'reanalyses', while CLaMS can use different 'reanalyses'. However, when comparing the in-situ data to GSFC data and CLaMS using 3 different reanalyses, only the CLaMS-MERRA\_2 produced anomalously high mean ages. The reason for this is that the GSFC 2D model decouples the transport fields from the MERRA-2 temperatures, winds and heating rates, before inputting the resulting residual circulation and eddy transport fields back into the model.

Chapter 3 also investigated the impact of these changes in circulation or chemistry on a compound's stratospheric lifetime as predicted by the GSFC. It found that for long-lived compounds (CFC-13 and CFC-115) the impact from changes to circulation was minimal,

while the effect from changes to reaction rates was significant. For shorter lived compounds (CFC-114 and CFC-114a) both circulation and chemistry had a similar impact on the stratospheric lifetimes of these compounds. That said, CFC-114 and CFC-114a did not see a substantial ( $\pm 10\%$ ) change in stratospheric lifetime regardless of which scenario was enacted. CFC-13 and CFC-115 however saw increase/decrease to their stratospheric lifetimes of 30-50% from their most extreme scenarios. When compared to the stratospheric lifetimes listed in WMO 2022 and those calculated earlier in Chapter 3 (using in-situ measurements), the baseline GSFC scenario produces lifetime estimates that match closely with the lifetime listed in WMO 2022 (Burkholder *et al.*, 2022) for all compounds. However, the stratospheric lifetimes estimated in section 3.3.2 for CFC-13 and CFC-115 were substantially shorter than even the most extreme of the GSFC scenarios could produce. For CFC-114 and CFC-114a the stratospheric lifetimes derived in section 3.3.2 agree within the uncertainty range with both the estimates in WMO 2022 and the estimate derived by the GSFC.

The mean age-tracer correlation for all compounds examined here is robust, though CFC-114 sees an offset for reasons discussed in section 3.3.4.a. However, it was also necessary to investigate how well the mean ages derived by the GSFC compared to the mean ages observed via in-situ measurements. For CFC-11 only the P10, P20, and M20 scenarios produced mean ages that were outside the uncertainty/natural variability range established for the in-situ measurements. For CFC-13 and CFC-115 none of the GSFC's scenarios produced mean ages outside the expected range of natural variability. For CFC-114a the M20, P10 and P20 scenarios produced mean ages which exceeded the natural variability range. The mean ages for CFC-114 from all GSFC scenarios exceeded the natural variability range, which is further evidence that there is an error in how the GSFC handles the compound. For all compounds the GSFC baseline scenario predicted smaller mean ages than were observed in the in-situ samples, but with the exception of CFC-114, these still fell within the natural variability range. Again, it was seen that the longer-lived compounds were less affected by circulation and more affected by reaction rates, which appeared to be a limiting factor for those compounds' dissociation. Shorter-lived compounds seemed to be affected equally by changes to both circulation and chemistry.

As the mean age to tracer correlation in the GSFC data seemed robust, it was used to calculate FRFs for the compounds studied, and those FRFs were compared to those derived

using in-situ measurements. When examining FRFs derived using GSFC data, their uncertainty range often (though not always) overlaps the range of FRFs derived using in-situ data. For CFC-114 and CFC-114a circulation had the greatest impact on FRFs, while for CFC-13 and CFC-115 which factor dominated (circulation or chemistry) varied between campaigns. Variation was seen between all campaigns, for all compounds, suggesting that a variety of factors impacted the FRFs, from latitude to season. Section 4.4.2 explored the effects of season and latitude on FRFs in more detail, and while it was impossible from the available data to completely unpick the effects from multiple factors, there were indications that both season and region impact FRFs.

As the FRFs at 3 years mean age generated using the GSFC data (using the mean age-tracer correlation) were usually close to the FRFs at 3 years mean age generated using data from the Geophysica research flights, they were used to estimate stratospheric lifetimes for their respective compounds. These were compared to the stratospheric lifetimes the GSFC had predicted. For all compounds except CFC-114, the 'predicted' stratospheric lifetimes that were derived using FRFs and mean ages from the GSFC data were consistent with those derived using aircraft-based in-situ measurements. For CFC-13 and CFC-115 this meant that the lifetimes derived using FRFs and mean ages from the GSFC were substantially lower than both those listed in WMO 2022 and those predicted by the GSFC itself. For CFC-114 all lifetime estimates were consistent with each other. For CFC-114a the lifetime estimate using FRFs and mean ages from the GSFC baseline scenario were shorter than the lifetime estimates for WMO 2022, those that the GSFC predicted, and those derived using in-situ data.

It should be noted that there are always additional factors which can influence how quickly a compound can be broken down, such as the speed of the reaction rate, the time taken for compounds in different air parcels to reach a loss region, and how long they remain in the loss region. This means that the model can only approximate an average value, and the in-situ conditions may vary somewhat from the data predicted by the model. The FRF-mean age correlation using the GSFC 2D model data produced estimated lifetimes that match those predicted using in-situ measurements, but the direct GSFC lifetime predictions did not. While an extremely useful tool, these factors, along with the necessity to decouple key parts of the process and the reliance on accurate inputs (such as the

kinetics data used) demonstrates the importance of reliable in-situ data for ‘truthing’ of models.

### 5.1.2 Overview from ‘Chapter 4: AirCores’

One of the unfortunate realities in the research field is that funding is limited, and access to it extremely competitive. Awarding of funding may be prioritised by a number of different factors such as environmental urgency, corporate interest, or recent discoveries sparking renewed interest in a topic. In such a competitive and mercurial market, an adaptable, comparatively low-cost technique that allows sampling of a wide variety of atmospheric gases, including little-studied trace gases, has a lot of advantages. This is where the AirCore technique comes into its own. Aside from small balloon launches of a single AirCore, AirCores can be packed as part of the payload for much larger flights. The technique allows sampling using multiple (non-destructive) instruments; for example, in Chapter 4 for some flights the sample was first passed through a non-destructive cavity ring-down spectrometer (Picarro G2401), before being admitted into the GC-MS instrument (where the sample is used up). While this is not practical if one is examining PFCs (see discussion in section 4.3.1), the ability to analyse a sample more than once demonstrates the versatility of the technique. In this case samples were passed through the Picarro G2401 in order to analyse the presence of CO<sub>2</sub>, CO, methane and water vapour for other projects (unrelated to this research).

In order to make the most of the AirCore technique it is necessary to establish a set of ‘best practice’ guidelines, particularly when sampling low abundance trace gases, and in particular compounds that might be vulnerable to contamination or decay. Chapter 4 explored a number of factors which could theoretically impact the viability of compounds within a sample: the type of AirCore used, the type of sub-sampler used, the delay between collection and analysis, the use of a Picarro G2401, and the effect of temperature on the AirCore (summary Table 5-2). The type of AirCore used appeared to have little effect on the viability of most compounds, though some small contamination from use of fluorocarbon grease in certain parts of the AirCore may have impacted PFC-116 and HCFC-141b. For the same reasons, the simple sub-sampler Luna had a profoundly negative effect on the viability of PFC-116, and the Picarro G2401 had this effect on PFC-116 and to a lesser extent HFC-

125. So while technically passing a sample through the Picarro G2401 is non-destructive, for certain compounds which are sensitive to the grease contained within, using this device essentially destroys the usability of these compounds in a sample.

The delay between collection and analysis was shown to affect both HFC-125 and methyl chloride. While a precise timeline could not be established with the available data (and would require substantially more stability tests), it is clear that from approximately 2 weeks onward, the viability of samples deteriorates. If these compounds are of interest to a study, the samples should be analysed as quickly as is feasible. However, it is encouraging that all other compounds seemed to weather delays without significant changes.

The effect of temperature on AirCore samples was difficult to study as the precise conditions that would result in reduced viability of a sample were poorly constrained. From the available data, it seems that for temperature to have an effect on the sample it must be below 0 degrees Celsius for an extended period of time (20+ minutes). However, the practice of insulating the inlet of the AirCore should minimise the risk of this effect coming into play, and the effect (if present) only encompasses those compounds with freezing points within a narrow range. In Chapter 4 this included CFC-113 and HCFC-141b.

CFC-115 and HCFC-142b showed no discernible effect from any of these factors, while no compound saw a significant effect from more than two of the examined variables. This suggests that with the appropriate practices a wide range of compounds may be sampled in this way, allowing a cost-effective and flexible approach to stratospheric data collection.

This is particularly notable with regards to the two age tracers examined here: PFC-116 and HFC-125. While PFC-116 is sensitive to contamination when using a simple sub-sampler or the Picarro G2401, HFC-125 was sensitive to delay between collection and analysis. That these two age tracers are affected by different conditions means that if one is not available, for example because use of a Picarro G2401 was necessary for other research objectives, then the other age tracer could still be used. Under the 'best practice' guidelines discussed, both compounds can be sampled at an acceptable precision using the AirCore technique, and the ratio between SF<sub>6</sub> derived mean ages and those derived using either PFC-116 or HFC-125 was consistent with the 1:0.8 ratio reported in Leedham-Elvidge et al., (2018). This further increases the versatility of the AirCore technique as it is not reliant

solely on SF<sub>6</sub> derived mean ages which can be biased by mesospheric intrusion from the polar vortex.

*Table 5-2. (A repeat of Table 4-8, as it serves as a useful summary of which factors affected which compounds). The compounds explored in this chapter, the potential factors that might have affected them, and whether or not this was found to be the case in section 4.3 or the stability tests (Appendix B).*

Compound	AirCore	Subsampler	Delay	Picarro (G2401)	Temp
CFC-113	No	No	No	No	Maybe
CFC-115	No	No	No	No	No
HCFC-141b	Maybe	No	No	No	Maybe
HCFC-142b	No	No	No	No	No
HFC-125	No	No	Yes	Yes	No
C <sub>2</sub> F <sub>6</sub>	Maybe	Yes (Luna)	No	Yes	No
CH <sub>3</sub> Cl	No	No	Yes	No	No

A possible offset in FRF was investigated for methyl chloride and CFC-115. When plotting FRF against mean age, the FRF at mean age 0 years should be 0. However, for methyl chloride there was an average offset of -0.05, while for CFC-115 the offset was 0.02. Having tested varying offset it was found that while the offset did have an effect on the resulting FRF at 3 years mean age from around 0.01 onwards, the effect was small, and overlap was within the uncertainties. It was noted that compounds that had larger FRFs at 3 years mean age (and thus shorter stratospheric lifetimes) were less impacted by these offsets than compounds with smaller FRFs at 3 years mean age (and therefore longer stratospheric lifetimes). For compounds where an overset of or beyond  $\pm 0.01$  was present, an appropriate correction was applied. This meant that potential offsets between mixing ratio and background trend could be accounted for.

An important question was whether the AirCore technique could produce data of sufficient precision and reliability for these compounds, that FRFs (and ODPs) could be derived. With the exception of CFC-113 the range for the average FRF at 3 years mean age derived using AirCore flights, overlapped the range for the previously estimated FRF. For all compounds the 'all' range (which averaged the FRFs at 3 years mean age for both Geophysica flights and AirCore flights) overlapped the range for the previous estimated FRFs. CFC-113 was influenced by two AirCore flights which produced unusually high FRFs at 3 years mean age. For all compounds discussed here there was substantial variation in the FRFs at 3 years mean age, derived for individual flights, both for Geophysica and AirCore

flights. This highlights the importance of using as wide a dataset as possible in order to account for outliers.

With the exception of HCFC-141b the average range for AirCore flights was higher than for the Geophysica flights, though both ranges still overlap. It is unclear whether this reflects a difference stemming from the sampling technique used, or whether this may reflect a shift in the FRF at 3 years mean age. If the latter there are several possible explanations. The time-independent method for calculating entry mixing ratios (and thence FRFs) used is that of Ostermüller et al., (2017), which largely but not entirely accounts for changes in background trends for the compound in question. So, it is possible that long-term changes in background trends were not entirely accounted for in the calculations. Another possibility, in light of the fact AirCore derived FRFs were on average higher than the earlier sampled Geophysica derived FRFs, is that changes to stratospheric circulation (such as the suspected speed-up of the Brewer-Dobson circulation) could have shortened the compounds' stratospheric lifetime somewhat, resulting in slightly higher FRFs at 3 years mean age.

The reasons for variation between the FRFs for different flights was explored. Little supportive evidence for an effect from latitude was seen; there were some hints that HCFC-141b may experience some influence from latitude, but this was not conclusive. The latitude span examined spanned from 67.42 N to 47.97 N, but there were many variables affecting every flight, and it was difficult, verging on impossible, to identify effects from latitude alone using these flights. Seasonality was also a challenge to confirm as a factor in varying FRFs. CFC-113, one of the shorter-lived compounds studied in this chapter, did seem to have some seasonal cycle. Methyl chloride had the shortest lifetime of any compounds studied in this chapter; however, due to its sensitivity to delay, viable samples for this compound were sparse, so no conclusion could be reached on whether or not seasonality affected the compound's FRFs.

The ODPs derived for these compounds using the FRFs from either just AirCore flights, or both AirCore and Geophysica flights, largely overlapped or were close to overlapping within the uncertainties, the values listed in Burkholder et al. (2022). For CFC-113, the AirCore value is too high, but the combined value overlaps the previous estimate. For CFC-115, when using the lifetime and FRF cited in Burkholder et al. (2022), the ODP from both AirCore only derived FRFs and Geophysica + AirCore derived FRFs, overlap within the

uncertainties. When using the lifetime and FRF at 3 years mean age derived in sections 3.3.2 and 3.3.1, the ODPs arrived at in section 4.3.10 do not overlap with that cited in Burkholder et al. (2022), but do with the ODP for CFC-115 derived in Chapter 3. Methyl chloride's ODPs (both from 'All' and 'AirCore Only') overlap within the uncertainties with Burkholder et al. (2022). For both HCFC-141b and HCFC-142b the 'all' ODP does not overlap with Burkholder et al. (2022), while the 'AirCore Only' ODP does. In both cases the ODP derived in Chapter 4 was notably lower than that cited in Burkholder et al. (2022). For most compounds the AirCore only derived ODPs were somewhat higher than those that used the expanded dataset, and the uncertainty range was greater.

## **5.2 Suggestions for future work/policy implications.**

Chapter 3 (section 3.3.2) demonstrated that CFC-13 and CFC-115 had significantly lower stratospheric lifetimes than previously estimated, and to account for this the emissions of these gases must be greater than previously estimated. Further research could focus on the potential sources of these additional emissions. Western et al., (2023) notes that the sources for CFC-13 in particular are difficult to identify. This could indicate illegal production, trade or use, inappropriate disposal of waste, or as-yet unidentified banks of the compound. It is clear from Chapter 3 that there is much more we need to learn about these neglected compounds. Regardless of the source, greater emissions and shorter stratospheric lifetimes for these compounds would need to be taken into account during ozone recovery time estimates, as well as for monitoring and enforcement of the Montréal Protocol. While Chapter 3 cannot prove the existence of a speed-up in the Brewer-Dobson circulation, the shorter lifetimes for these longer-lived compounds are not incompatible with this possibility.

One way to further explore both the emissions origins of these long-lived compounds and changes to the speed of the Brewer-Dobson circulation (using trace gases as proxies for circulation), would be the use of AirCores. Due to the comparative affordability of AirCores and their versatility, they could cover a much greater spacial range than is an option for other sampling techniques.

An 'ideal' project to do this would include as many locations as possible, probably featuring collaboration across multiple research institutes. It should include locations within both the southern and northern hemispheres, tropical, sub-tropical, mid, high and polar latitudes. For best resolution multiple AirCore launches a month would be necessary (4 a month would allow a decent snapshot of conditions as the month progresses), and this could include double launches (meaning two different balloons, each with their own AirCore) to account for failures in individual flights. In areas where larger payloads are safe and legal, 'Mega' AirCores as described in Laube et al. (2025), could be deployed. This would significantly increase the volume of air collected, allowing for samples to be analysed multiple times.

Chapter 4 found tantalising indications of variability for FRFs from seasonality and latitude. The above proposed project would allow for further exploration of this topic. One of the issues experienced in section 4.4.2 was that there were simply too few data points to reliably reach a conclusion. With more flights, in a greater variety of locations and seasons, much of the ambiguity here would evaporate.

The flexibility of the AirCore technique, coupled with the improved practices and reliability proposed in Chapter 4 would allow for a great range of atmospheric questions to be explored. As the AirCore technique is non-destructive, depending on how the sample is analysed (e.g. whether or not that technique is destructive) it can be analysed multiple times. For example, some of the samples explored in Chapter 4 were analysed first using the Picarro analyser, before being used up in the GC-MS system. Thus, adding CO, CO<sub>2</sub>, CH<sub>4</sub> and water vapour to the list of compounds captured for analysis by the AirCore. This means that one does not need to choose only the compounds that are in most urgent need of study, but can cast a 'wide net', and produce data on a large number of compounds. The AirCore can be adapted to sample tropospheric air, stratospheric air, or both. It can be launched in areas where flight restrictions limit or prohibit larger balloon-borne measurements. It can be used to monitor for pollution events, or novel compounds arriving in the atmosphere, significantly aiding in the monitoring and enforcement of the Montréal Protocol as well as other measures to curb pollution and improve air quality.

The efficiency of the technique, coupled with its affordability makes the AirCore an invaluable tool for atmospheric exploration. Doing so would allow for examining a significant array of compounds, could investigate important atmospheric processes such as

the polar vortex and Brewer-Dobson circulation, and aid in the enforcement of the Montréal Protocol.

## Glossary

- Actinic flux – The light or radiation flux from the sun at a point in the earth's atmosphere. This is particularly used to describe the light/radiation available for the photochemical processes.
- BDC – Brewer-Dobson Circulation.
- CG – Cape Grim tropospheric background trend.
- CLaMs - Chemical Lagrangian Model of the Stratosphere
- CTM - Chemistry Transport Model. A type of model which primarily simulates atmospheric chemistry and circulation/transport.
- Chemical Vapor Deposition (CVD) – a technique to deposit thin films of a substance on a heated substrate via a chemical reaction of gas-phase precursors.
- DU – Dobson Unit. Unit that measures ozone column thickness. 1 DU refers to the number of molecules of ozone needed to form a layer 0.01 mm thick at temperature 0° degrees C and 1 atmosphere of pressure.
- Equivalent Effective Stratospheric Chlorine (EESC) is a parameter use to estimate the total effective quantity of halogens in the stratosphere. It is the sum of chlorine and bromine which is derived from the tropospheric abundances of ozone-depleting substances (ODSs), and weighted in order to reflect their predicted depletion of stratospheric ozone
- Fractional Release Factor (FRF) – The fraction of a compound that has disassociated since entering the stratosphere.
- FZJ – Forschungszentrum (Research Center), Jülich, Germany.
- Global Warming Potential (GWPs)- a metric which measures the radiative forcing for a given greenhouse gas, compared to the same mass of CO<sub>2</sub>, summed over a given period of time (typically 20 or 100 years).
- GSFC – Goddard Space Flight Centre, refers to the 2D model developed at the Goddard Space Flight Centre, NASA, Washington DC.
- Heterogeneous reactions – Chemical reaction where reactants are in two or more phases (e.g. solid, liquid, gas etc...) or in which a reaction takes place at an interface such as on the surface of a solid catalyst.

- Isentropic transport – transport in which there is no change in entropy.
- JPL – Jet Propulsion Laboratory.
- Ozone Depletion Potential (ODP) – The potential for a compound to deplete ozone, relative to CFC-11.
- Ozone-Depleting Substance (ODS) – A substance which has the potential to deplete ozone.
- Polar Stratospheric ‘Clouds’ (PSCs) – These are ‘wave clouds’ that form in polar stratosphere during the winter. They form at very high altitudes (15 and 25 km) and at very low temperatures -78°C or lower.
- UEA – University of East Anglia
- Upper Troposphere and Lower Stratosphere (UTLS) – The boundary region comprised of the upper portion of the troposphere and the lower portion of the stratosphere.
- Wave Clouds – A type of cloud formed when stable air moves over a raised feature, which forces it upwards. Gravity causes the air to fall back, the air begins to oscillate, and this creates a rippled effect.

## Appendix A – Background trends and Flights

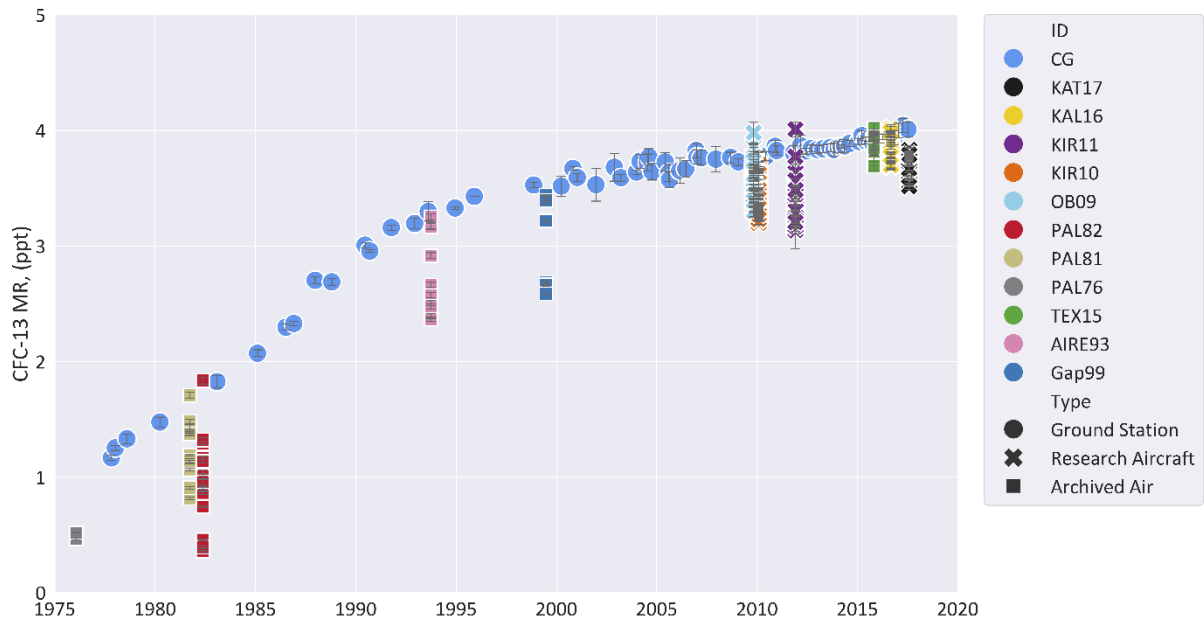


Figure A.1 Mixing ratio (ppt) for CFC-13, plotted against date. Includes Archived Air data and Geophysica flights, with the Cape Grim background trend ('Ground Station'/'CG'), for reference.

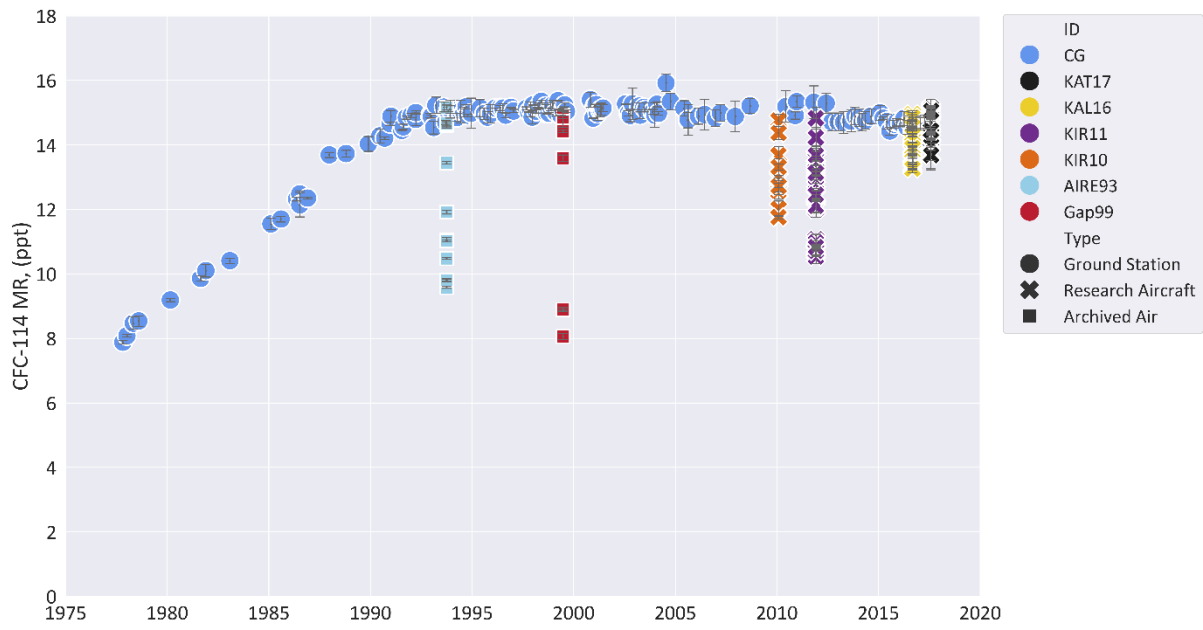


Figure A.2 Mixing ratio (ppt) for CFC-114, plotted against date. Includes Archived Air data and Geophysica flights, with the Cape Grim background trend for reference.

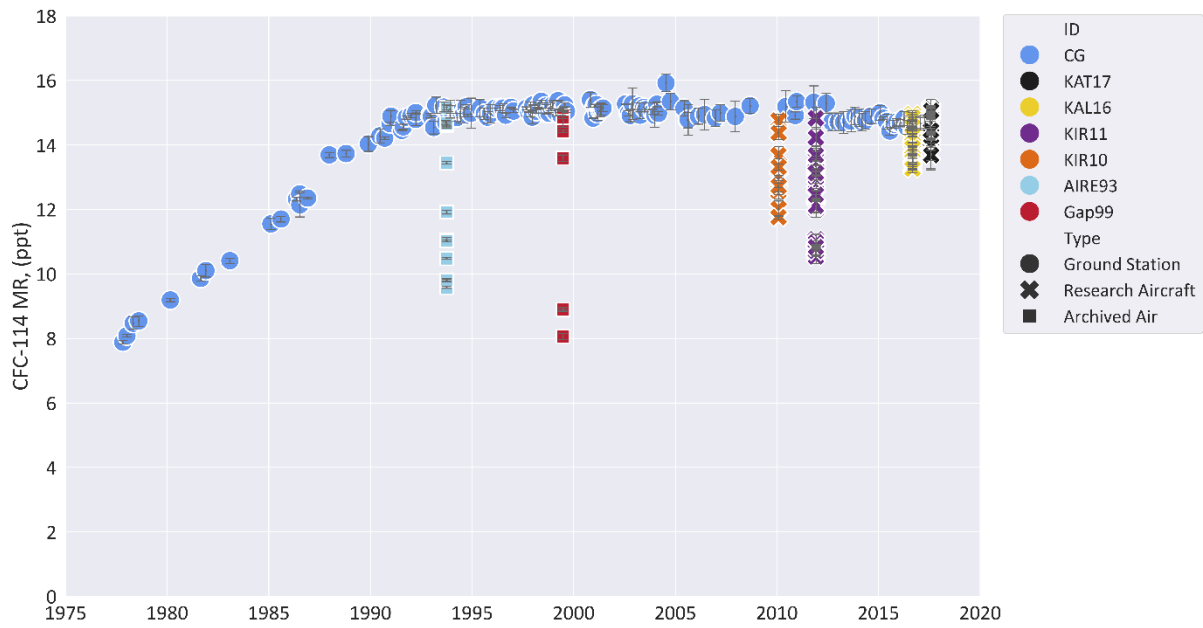


Figure A.3. Mixing ratio (ppt) for CFC-114a, plotted against date. Includes Archived Air data and Geophysica flights, with the Cape Grim background trend for reference.

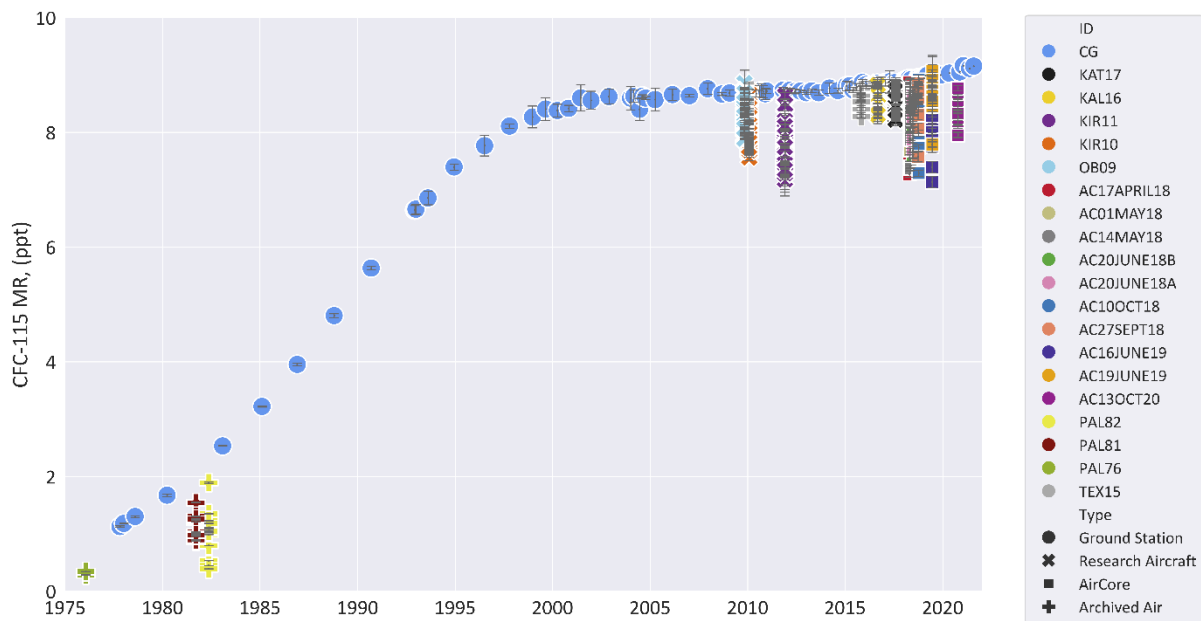


Figure A.4. CFC-115 mixing ratio (ppt) plotted against date. Includes the Cape Grim background trend ('Ground Station'/'CG'), Archived Air data, Geophysica flights, and AirCore Flights.

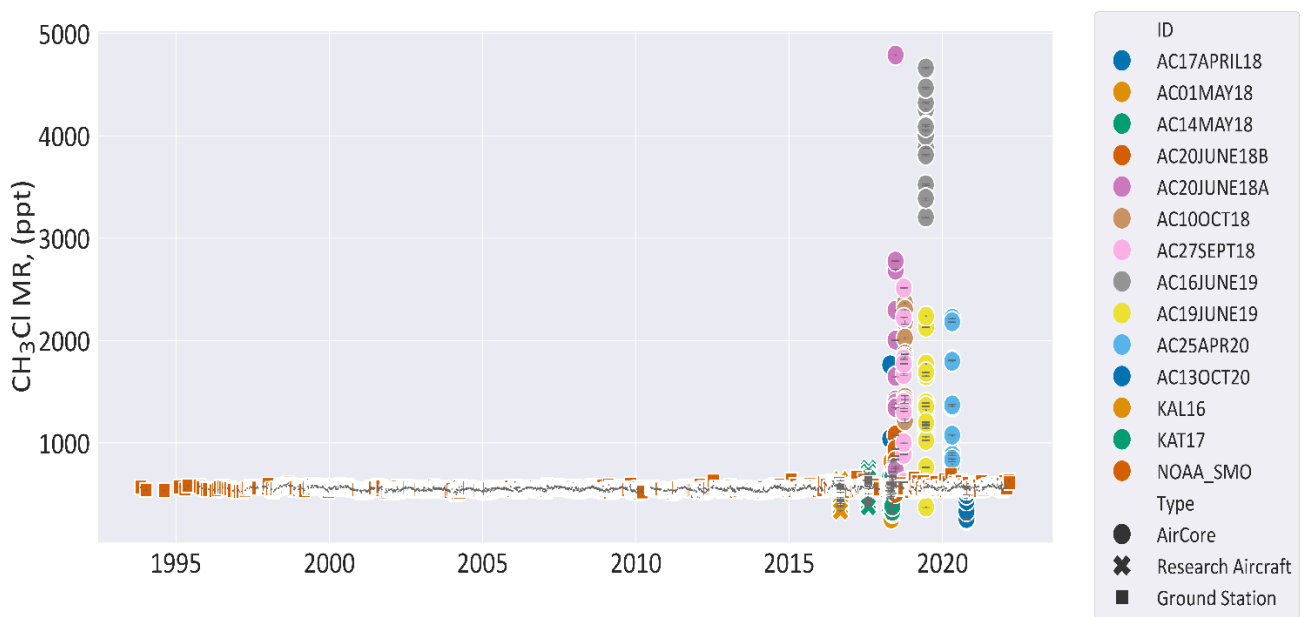


Figure A.5. CH<sub>3</sub>Cl mixing ratio (ppt) plotted against date (All Flights). Includes the ground station readings from SMO, three large balloon flights, two Geophysica flights, and 10 AirCore flights. Note that as most of the AirCore flights were analysed a month or more after the flight itself, the CH<sub>3</sub>Cl mixing ratio is significantly affected by delay. (See section 4.3.5 for details).



Figure A.6.  $CH_3Cl$  mixing ratio (ppt) plotted against date (yr) (selected flights). Includes the ground station readings from SMO, two Geophysica flights, and 3 AirCore flights.



Figure A.7. CFC-113 mixing ratio (ppt) plotted against date. Includes the background trend ('Ground Station'/'NOAA'), Geophysica flights, and AirCore flights.

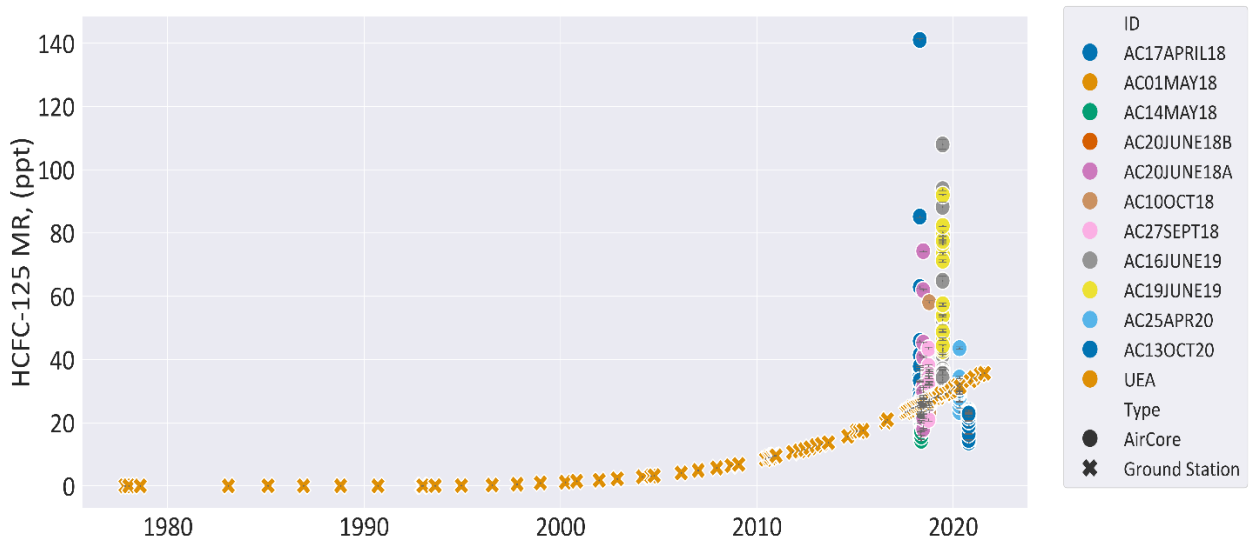


Figure A.8. HFC-125 mixing ratio (ppt) plotted against date (All available flights). Includes the background trend ('Ground Station'/'UEA'), Geophysica flights, and AirCore Flights.

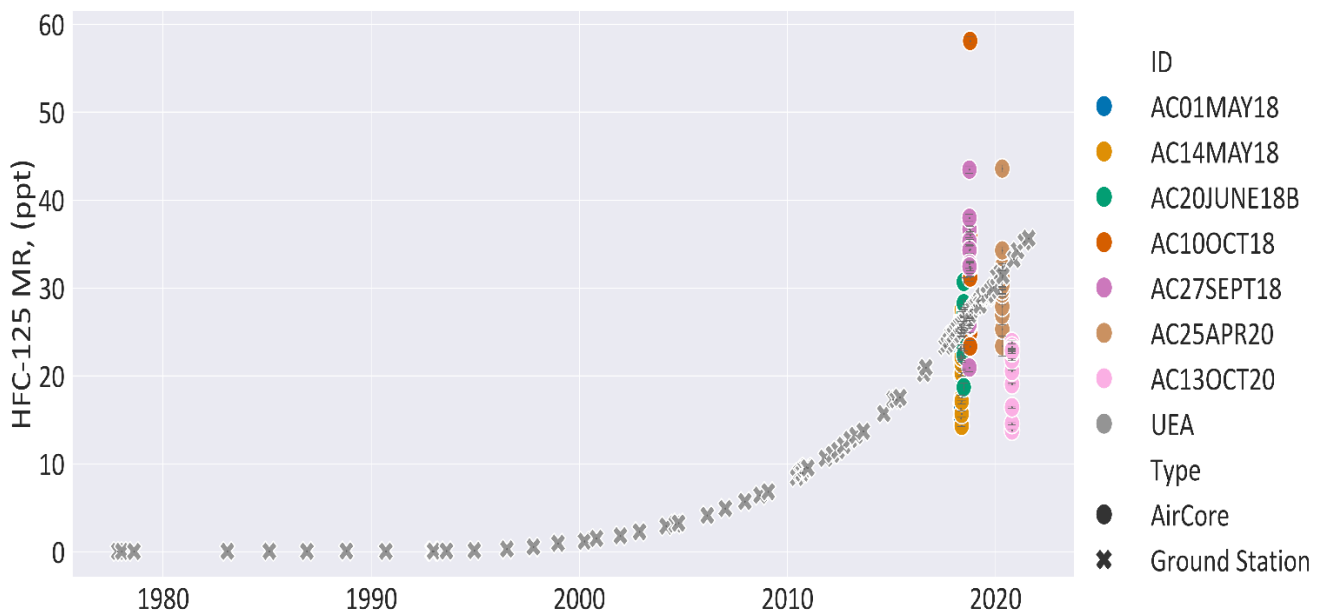


Figure A.9. HFC-125 mixing ratio (ppt) plotted against date (selected flights). Includes the background trend ('Ground Station'/'UEA'), Geophysica flights, and AirCore Flights. [Flights with poor data removed.]

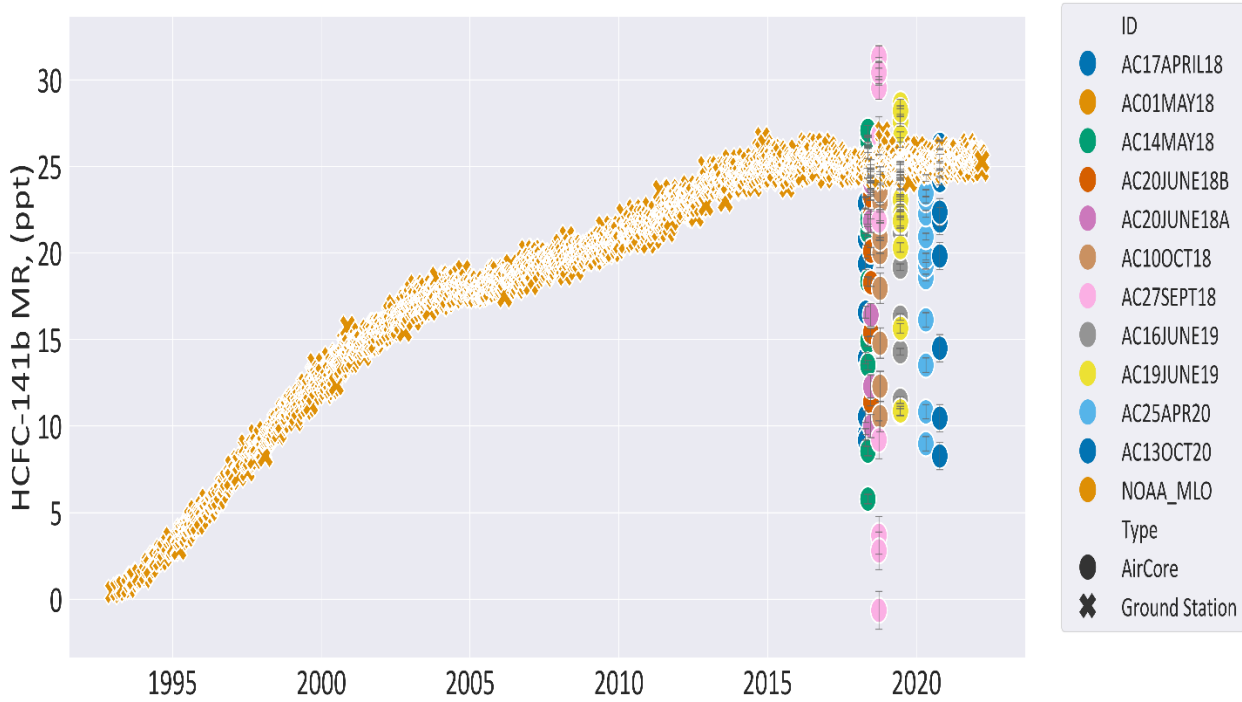


Figure A.10. HCFC-141b mixing ratio (ppt) plotted against date. Includes the NOAA\_MLO background trend ('Ground Station'/'NOAA\_MLO'), and AirCore flights.

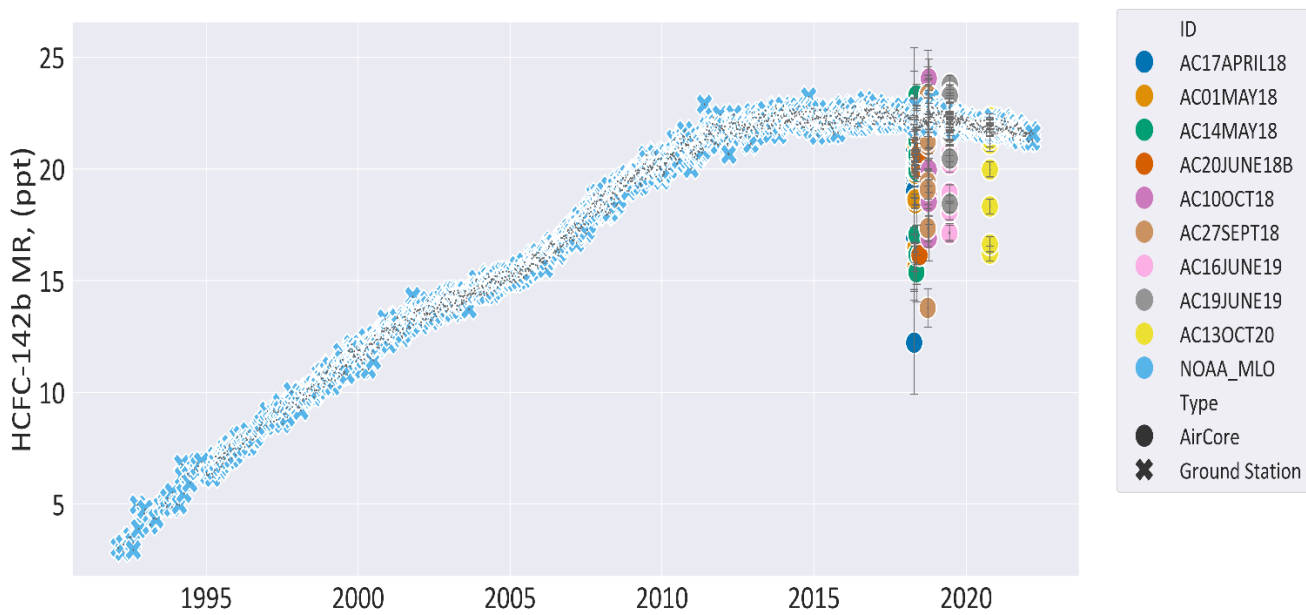


Figure A.11. HCFC-142b mixing ratio (ppt) plotted against date (selected flights). Includes the NOAA\_MLO background trend ('Ground Station'/'NOAA\_MLO'), and AirCore flights.

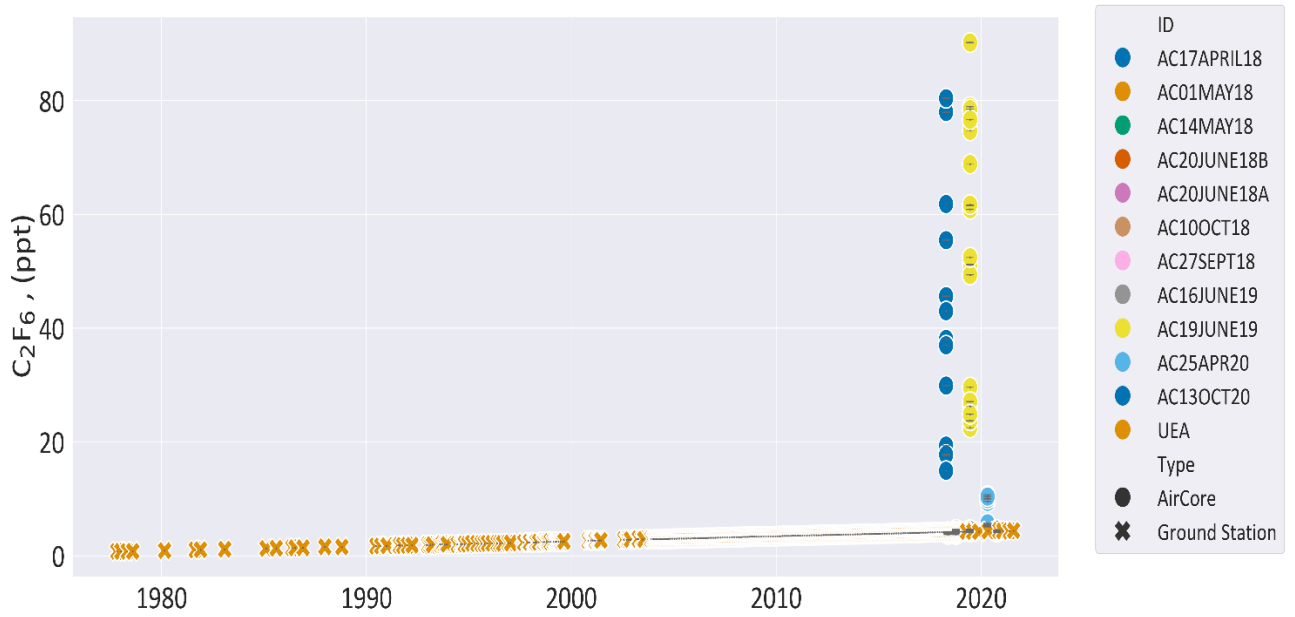


Figure A.12.  $C_2F_6$  mixing ratio (ppt) plotted against date (All Flights). Includes the background trend ('Ground Station'/'NOAA'), and AirCore flights.

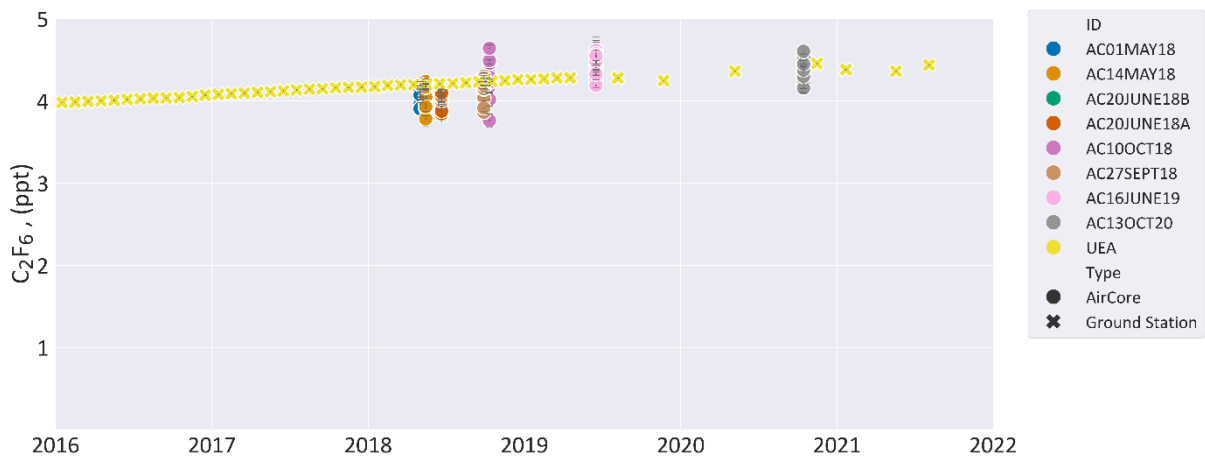


Figure A.13.  $C_2F_6$  mixing ratio (ppt) plotted against date (Selected Flights). Includes the background trend ('Ground Station'/'NOAA'), and AirCore flights.

## Appendix B – Stability Test Results

First test is of delay between fill and analysis. This includes standard (SX3600) stored in the Shaun complex sub-sampler for 1, 20, or 23 days ('Delay'), when only standard (SX3600) was stored in the loops. It also includes the tests where half of Shaun's loops were filled with standard (SX3600), and the other half with Helium, then left for 3 or 9 days ('ShaunHelium3' and 'ShaunHelium9'). And the test where half of Shaun's loops were filled with standard (SX3600) and the other half with synthetic air, for 15 days ('ShaunSynthetic14'). So Figure B.1 shows both the effect of delay and should highlight any effect from cross contamination between sample loops.

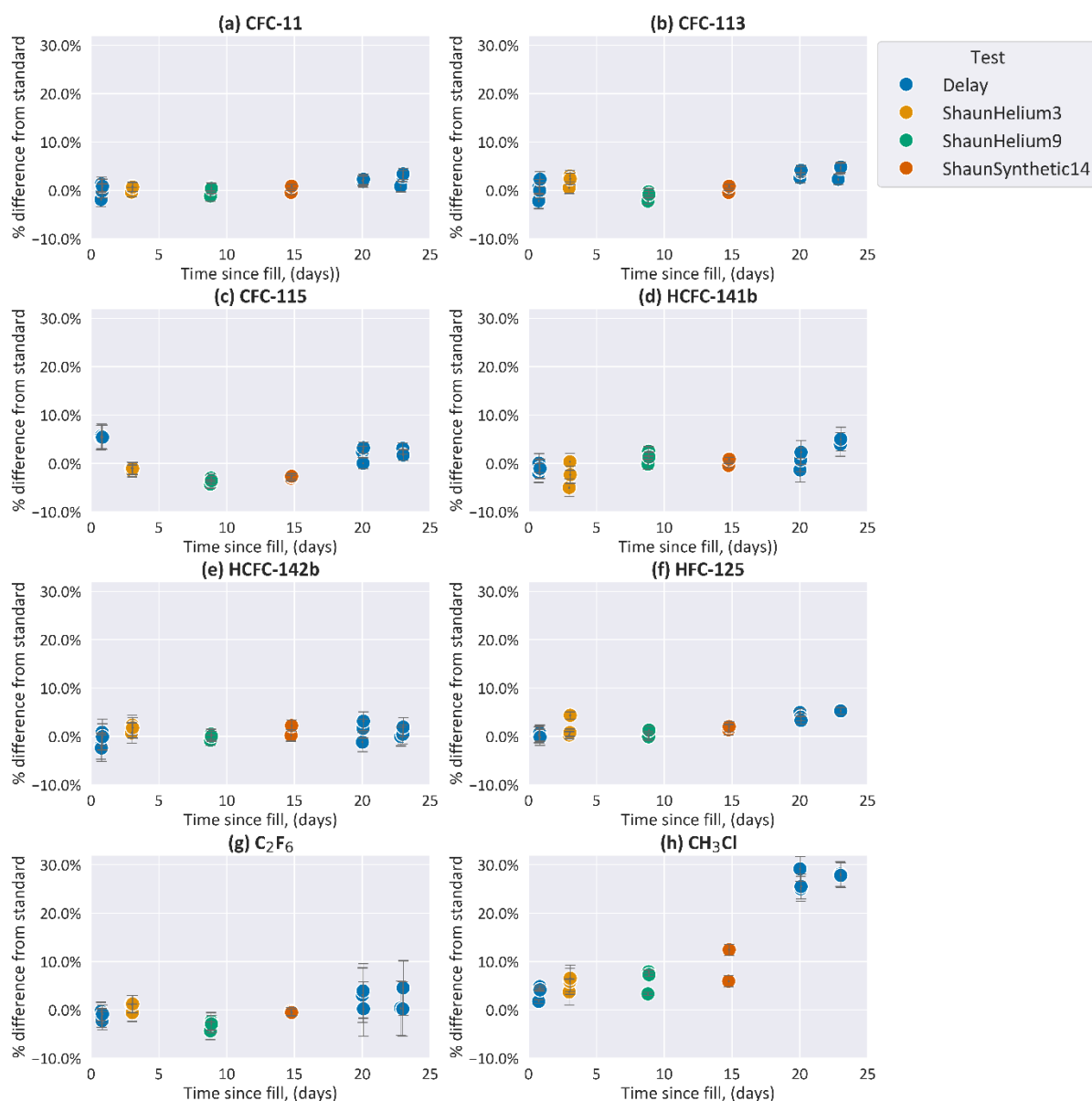


Figure B.1. Time since fill (days), plotted against percentage difference from the standard. (a). CFC-11. (b). CFC-113. (c) CFC-115. (d) HCFC-141b. (e) HCFC-142b. (f) HFC-125. (g)  $C_2F_6$ . (h)  $CH_3Cl$ . Error range is instrument precision.

In Figure B.1 most compounds see only small changes from the standard (usually less than 5% with 2.5% error range). In section 4.3.2 we saw a pronounced effect from delay on HFC-125, but that is not seen in Figure B.1f. This may be because the delay used in the stability tests was not long enough to noticeably impact the levels of HFC-125. In section 4.3.5 delay is shown to have a significant effect on  $CH_3Cl$  concentrations, and this is reflected in Figure B.1h, where from 20 days onwards the effect from delay sees  $CH_3Cl$  concentrations increase by an average of 27%. In Laube et al., (2008) an increase of 0.73% (22.4 ppt) per month was observed for  $CH_3Cl$ , however the  $CH_3Cl$  in this study was stored in stainless steel canisters,

which had a significantly larger surface area to volume ratio than an AirCore or sub-sampler. If wall reactions are responsible for the increase in CH<sub>3</sub>Cl, then there would be much greater scope for those reactions in a sub-sampler than in a stainless-steel canister.

For the tests where half of the sub-sampler's loops were filled with standard, and half with either Helium or synthetic air, some data points showed anomalously low concentrations. This may be due to the difference in concentrations of the compound between the fill gases, causing some small leak between sample loops. However, this is an extreme test, and during a normal AirCore filling, no large concentration gradient should be present. That the effect is small even during such an extreme test is encouraging.

Another test was to analyse lab air, introduced at valve 3 of the inlet system. The mixing ratio of the compounds in the lab air is compared to the mixing ratio found in the standard. In Figure B.2 most compounds (CFC-11, CFC-113, CFC-115, HCFC-141b, and PFC-116) had noticeably lower mixing ratios than the standard. HCFC-142b had a virtually identical mixing ratio to that of the standard, while HFC-125 and CH<sub>3</sub>Cl had noticeably higher mixing ratios than the standard.

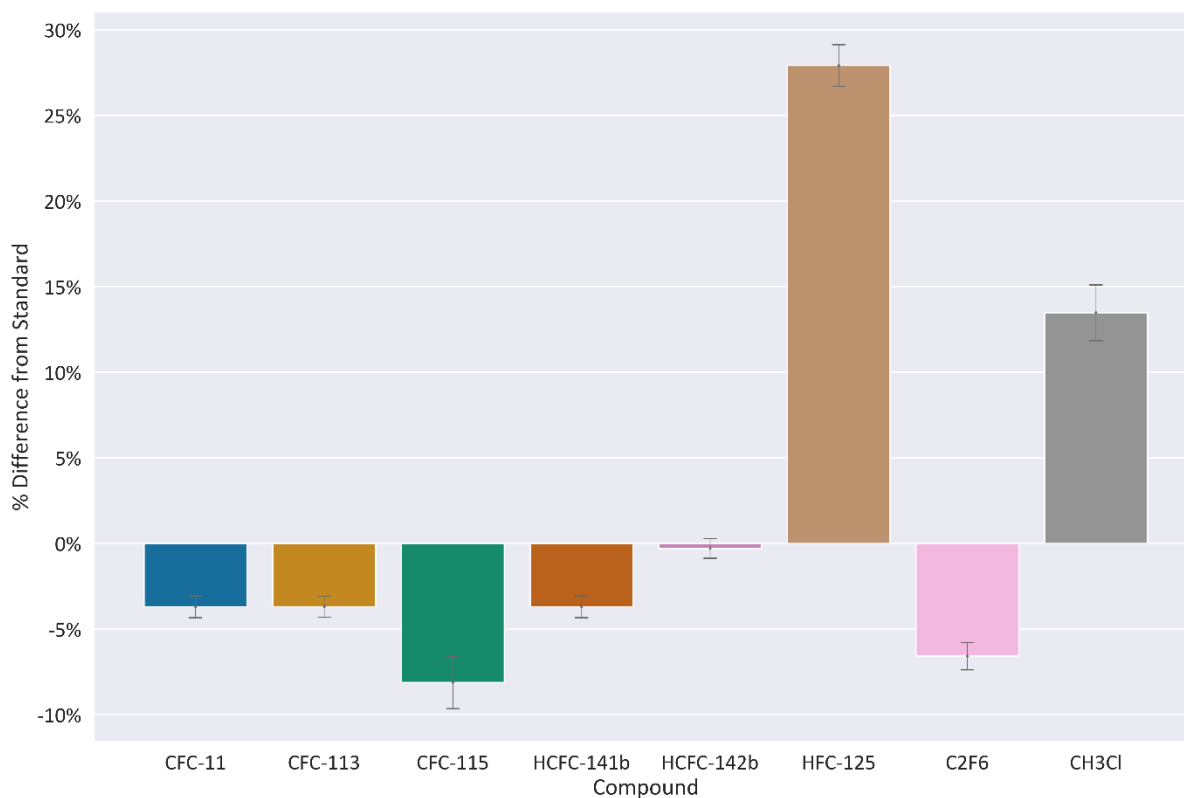


Figure B.2. Percentage difference from standard for all compounds, when sampling lab-air introduced via valve 9.

There are a number of possible explanations for this variation from the standard seen in Figure B.2. The standard was collected in June 2019 in the remote Rocky Mountains in North America. One of the purposes of choosing air from such a remote location is to capture air that is as ‘clean’ (as free from pollution and pollution events) as possible. The lab air in contrast was collected in a laboratory in Jülich, North Rhine-Westphalia, Germany. So, the composition of these compounds in the lab air is likely to be somewhat different than for the standard. This is particularly relevant for CH<sub>3</sub>Cl, which has biogenic sources (section 4.1.2.e) which would have been far more common in lush landscape around Jülich, than in the remote Rockies. This is reflected in Figure B.2 where CH<sub>3</sub>Cl is around 27% more abundant in the lab air than in the standard.

The elevated levels of HFC-125 relative to the standard may be due to a leak in the lab air conditioning (the tests were conducted in late autumn and winter, so the use of air conditioning would be minimal), HFC-125 also has a rapidly increasing global trend so would be expected to be somewhat higher in late 2020 than it was mid 2019.

Figure B.2 gives a rough overview of what the mixing ratios for each compound would look like if either due to contamination or a leak in the system, lab air were introduced. For most compounds the effects would be fairly minor (less than 5%), however the effect would be much more noticeable for HFC-125 and CH<sub>3</sub>Cl.

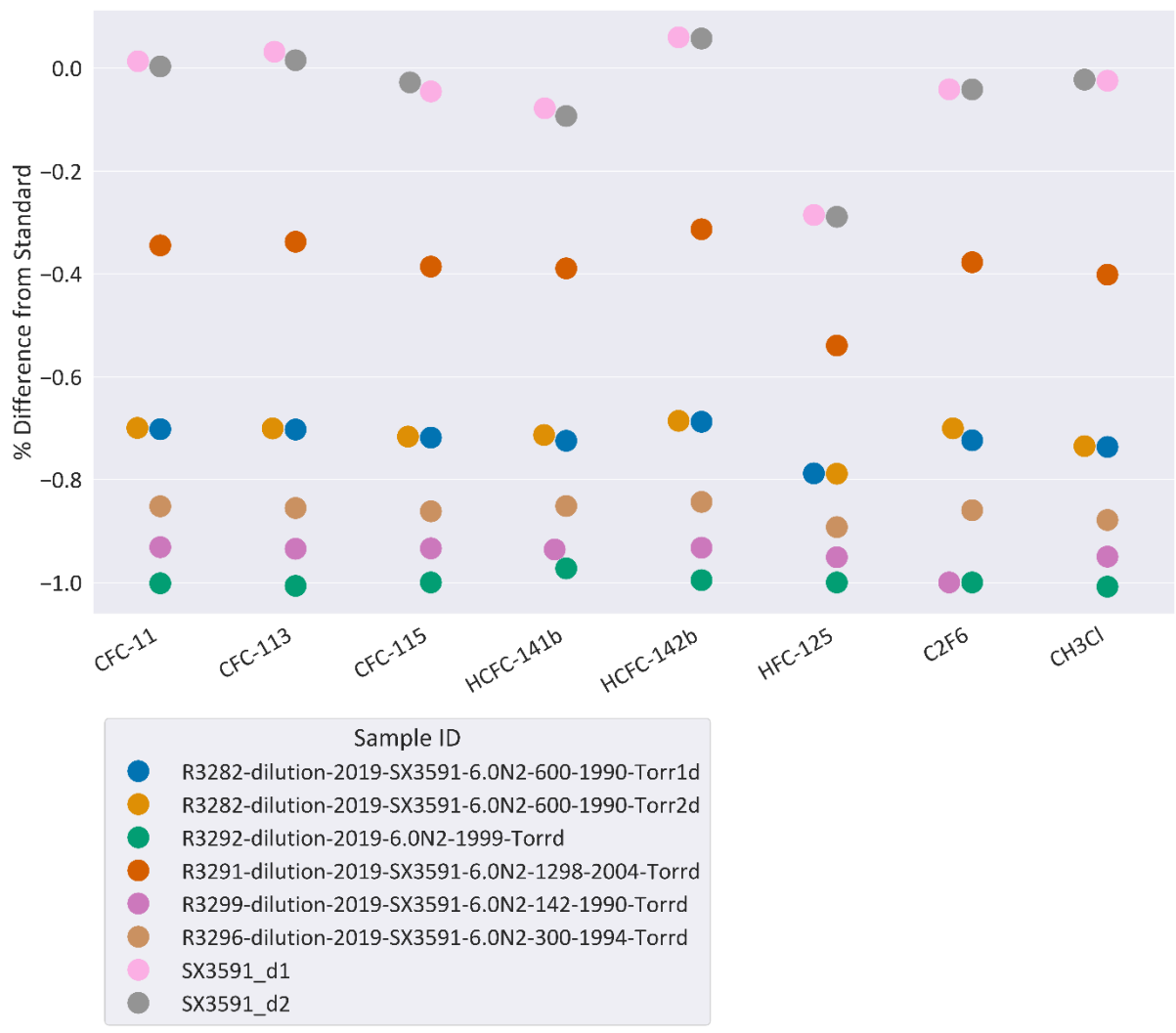


Figure B.3. Dilution series for the standard SX3591, for each compound, compared to (in percentage difference) the SX3600 standard.

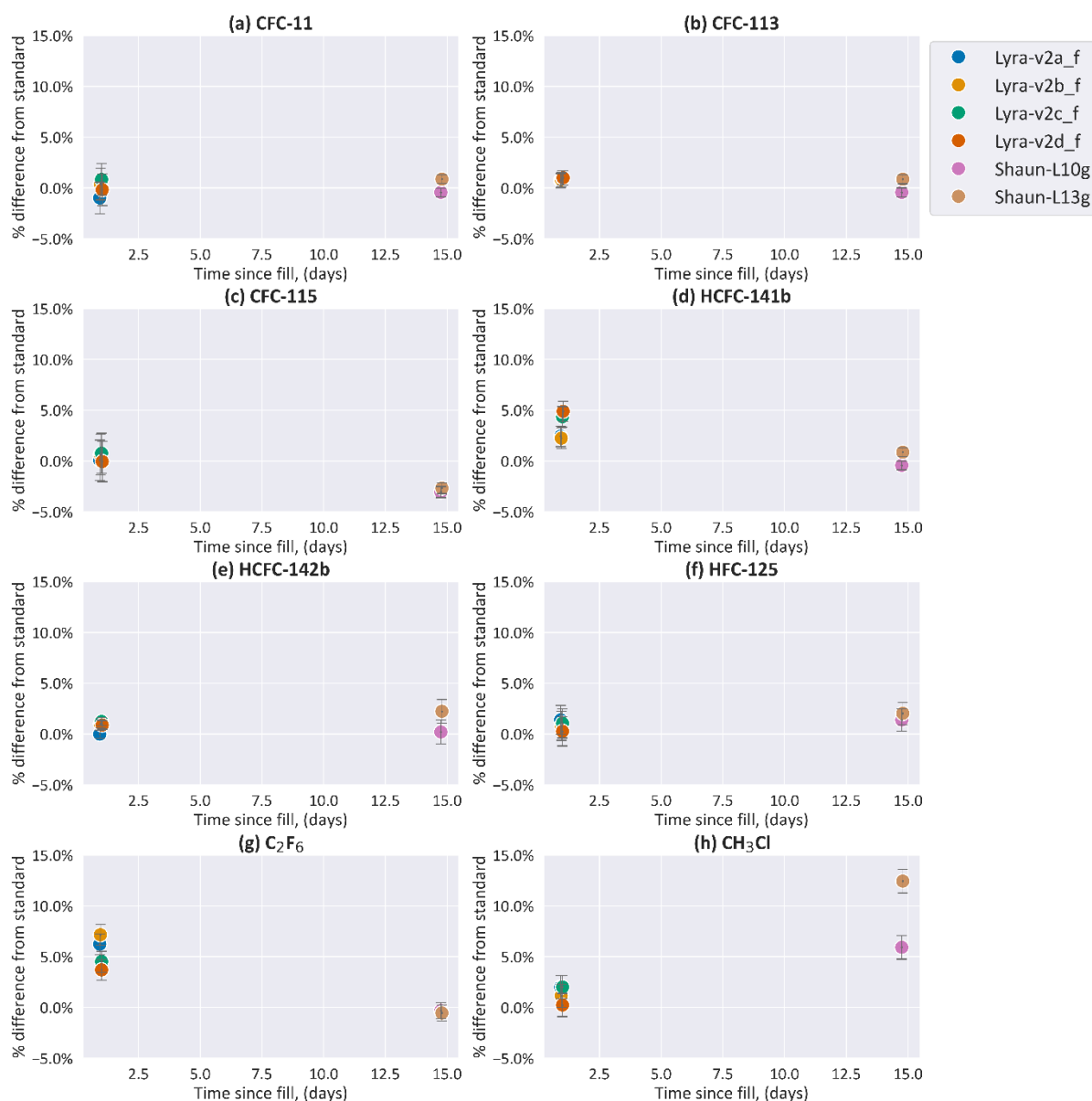


Figure B.4. Percentage difference from standard when stored in either the Lyra AirCore, or the Shaun sub-sampler.

In Figure B.4 we see the effect of storing standard in either the AirCore Lyra or in the Shaun sub-sampler. For most compounds, variations in concentration are within the uncertainty/error range. CH<sub>3</sub>Cl (Figure B.4h) shows an increase in concentration in the Shaun sub-sampler, but this is consistent with the already discussed effect of delay on this compound.

HCFC-141b and C<sub>2</sub>F<sub>6</sub> (Figure B.4 d & g) have somewhat elevated levels compared to the standard when stored in Lyra. One possible explanation for this is that the stratospheric end of the AirCore has a 3-way valve which is greased with a perfluorocarbon grease. This same grease is used in 2-way valves for the Picarro, as well as the simple sub-sampler Luna.

But is not present for the Shaun or Ed sub-samplers. In theory, since some fill gas remains in the AirCore, only the fill gas should be exposed to the 3-way valve, thus minimising the risk of contamination of the sample. It is necessary to use this 3-way valve as it was the lightest valve available that was suitable for the task. The noticeable increase in mixing ratio of  $C_2F_6$  (Figure B.4g) could be caused by the presence of this grease.

Time constraints meant it was not possible to test every AirCore and sub-sampler like this. But Lyra and Ed are reasonably representative, and from this we can take that both performed well in this test, though some compounds may be affected by the AirCore they are stored in, since AirCores are retrieved quickly and samples are transferred into sub-samplers, the effect of the AirCore on samples should be minimal.

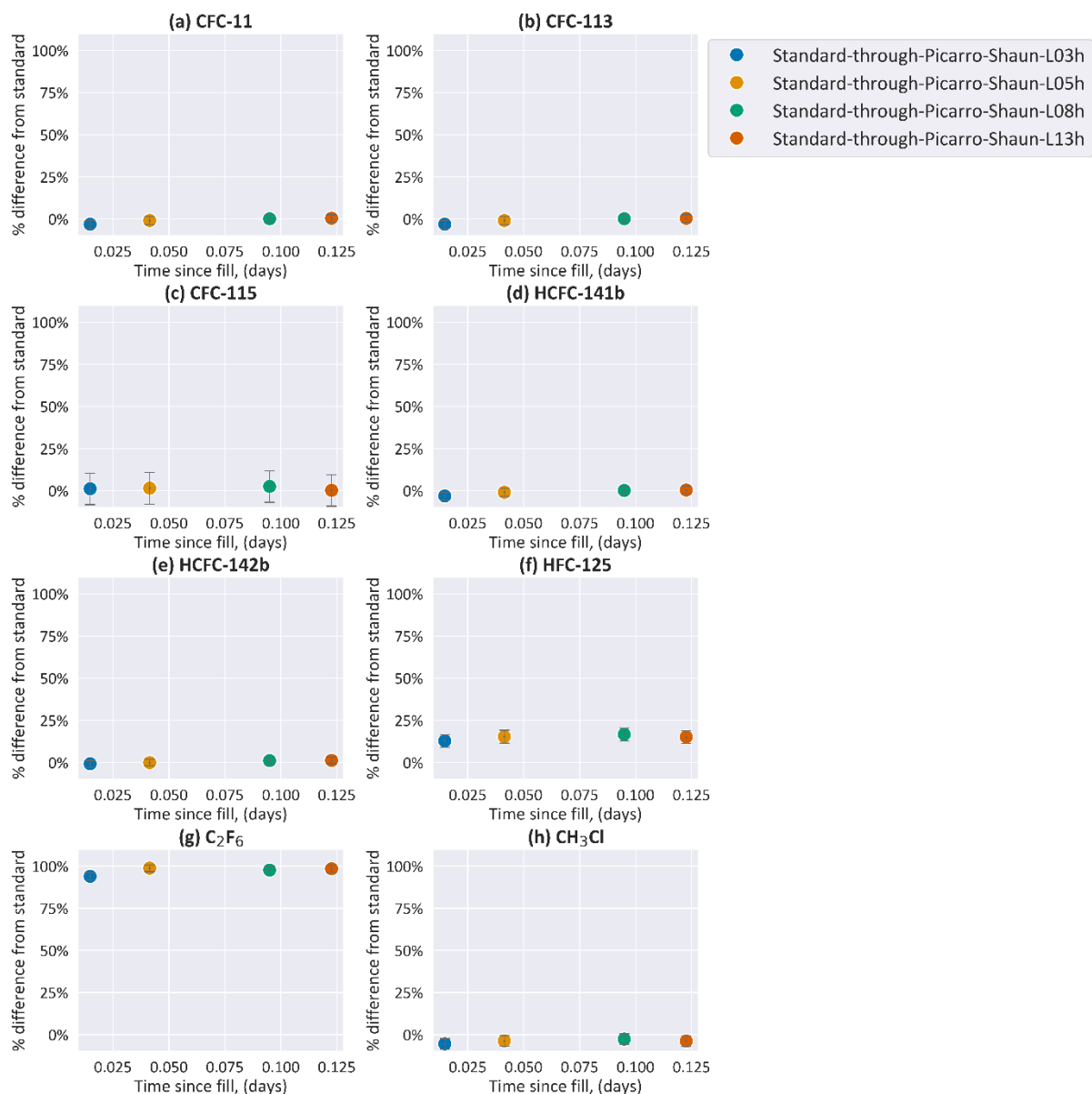


Figure B.5. The effect on each compound from being passed through a Picarro G2401.

In Figure B.5 most compounds are not noticeably affected by exposure to the Picarro G2401; however, HFC-125 and to a much greater extent C<sub>2</sub>F<sub>6</sub>, see elevated mixing ratios as compared to the standard. There is a Polytetrafluoroethylene (PTFE) filter on the exhaust and membrane pump of the Picarro G2401, and perfluorocarbon grease is present on 2-way valves found on the Picarro G2401.

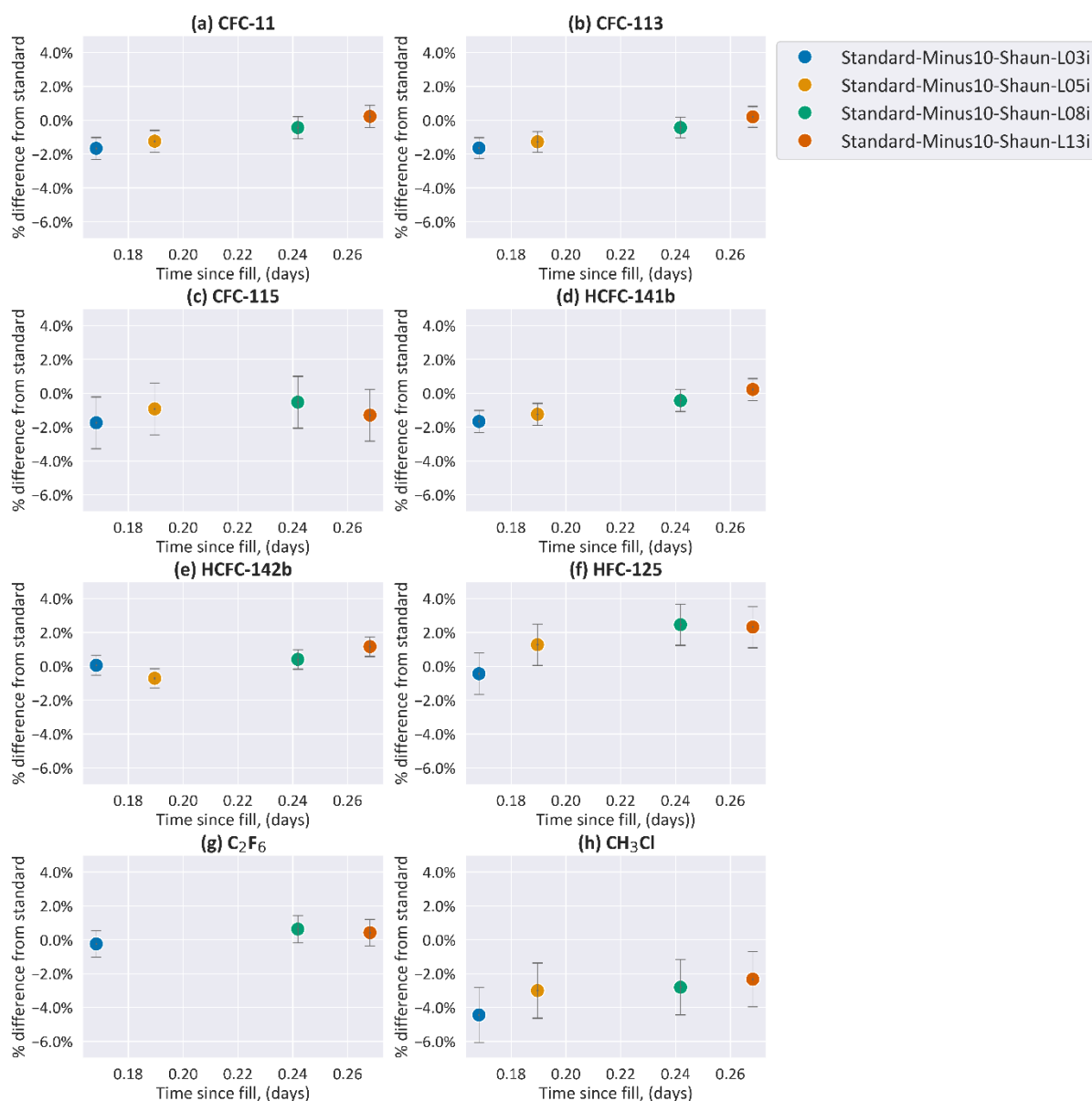


Figure B.6. Effect of temperature on each compound. All samples were kept at -10 degrees C for 10 minutes before being allowed to warm to room temperature and then analysed normally. One data point for C<sub>2</sub>F<sub>6</sub> is excluded due to suspected contamination.

As discussed in section 4.2.3, it is suspected that exposing the AirCore's inlet to sub-zero temperatures may cause certain compounds to precipitate out there, leading to anomalous results. This is potentially seen for CFC-113 (4.3.2) and HCFC-141b (4.3.6), where two autumn flights (September and October 2018) had some samples which contained anomalously high mixing ratios for these compounds, while other samples had anomalously low mixing ratios of those compounds. Figure B.6 shows the results of the temperature stability test discussed in section 4.2.3, and no compound shows dramatic changes from the

effect of temperature. CH<sub>3</sub>Cl seems to have somewhat lower mixing ratios than the standard (approximately -5%), CFC-113, HCFC-141b and HFC-125 seemed to show a tiny increase in concentration with 'time since fill' but this is so small and their error ranges overlap, so this does not seem to be statistically relevant.

The discrepancy between the AirCore flights and the stability tests suggests that the full picture is yet to be revealed. Neither CFC-113 nor HCFC-141b were strongly affected by delay in analysis, which is the primary distinguishing feature for the Autumn 2018 flights. It is possible that while the stability tests were designed to be as close to atmospheric conditions as possible, they could not perfectly replicate them, and were thus unable to reproduce the specific conditions that lead to anomalous results for CFC-113 and HCFC-141b during those two autumn 2018 flights.

Of note is that during the stability tests the AirCore was only kept at sub-zero temperatures for 10 minutes. The September and October flights remained at sub-zero temperatures for 25.7 and 18.6 respectively. It is possible that the effect becomes more pronounced the longer the AirCore is held at freezing temperatures. After these two flights the AirCore inlet was insulated, which could explain why this effect is seen in no further flights.

## Appendix C – Additional Figures

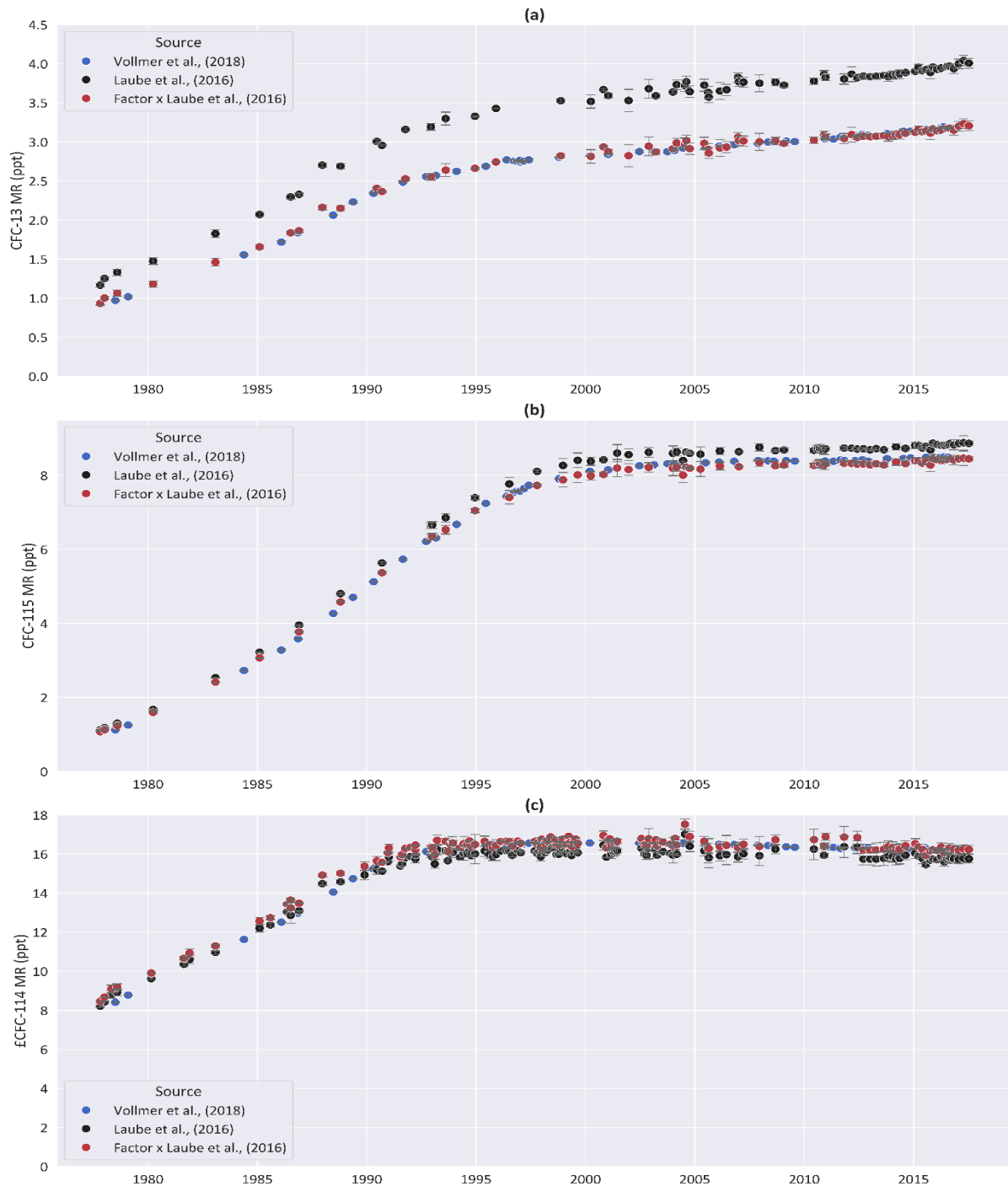


Figure C.1. Comparison between Laube et al (2016) and Vollmer et al (2018). Tropospheric trend mixing ratio (ppt) for CFC-13 (a), CFC-115 (b), and ECFC-114 (c), plotted against date. ECFC-114 refers to the sum of both CFC-114 and CFC-114a. Using data from (Laube et al., 2016; Vollmer et al., 2018), and the Laube et al., data with a conversion factor applied. (Conversion factor was 0.8 for CFC-13, 0.953 for CFC-115 and 1.0234 for ECFC-114). Error bars use instrument precision to 1 sigma. For a and b, the Laube et al (2016) data has the same shape as the Vollmer et al (2018) data, but has higher mixing ratios for each sample. This is due to a difference in calibration scale between each dataset. 'Factor x Laube et al., (2016)' refers to the Laube et al., (2016) dataset which has the conversion factor applied to it. Both datasets used the same archival time series but did not analyse the exact same set of samples, so for example between 1995 and 2000 the Vollmer et al., (2018) dataset includes several data points that do not have corresponding data points in the Laube et al., (2016) dataset.

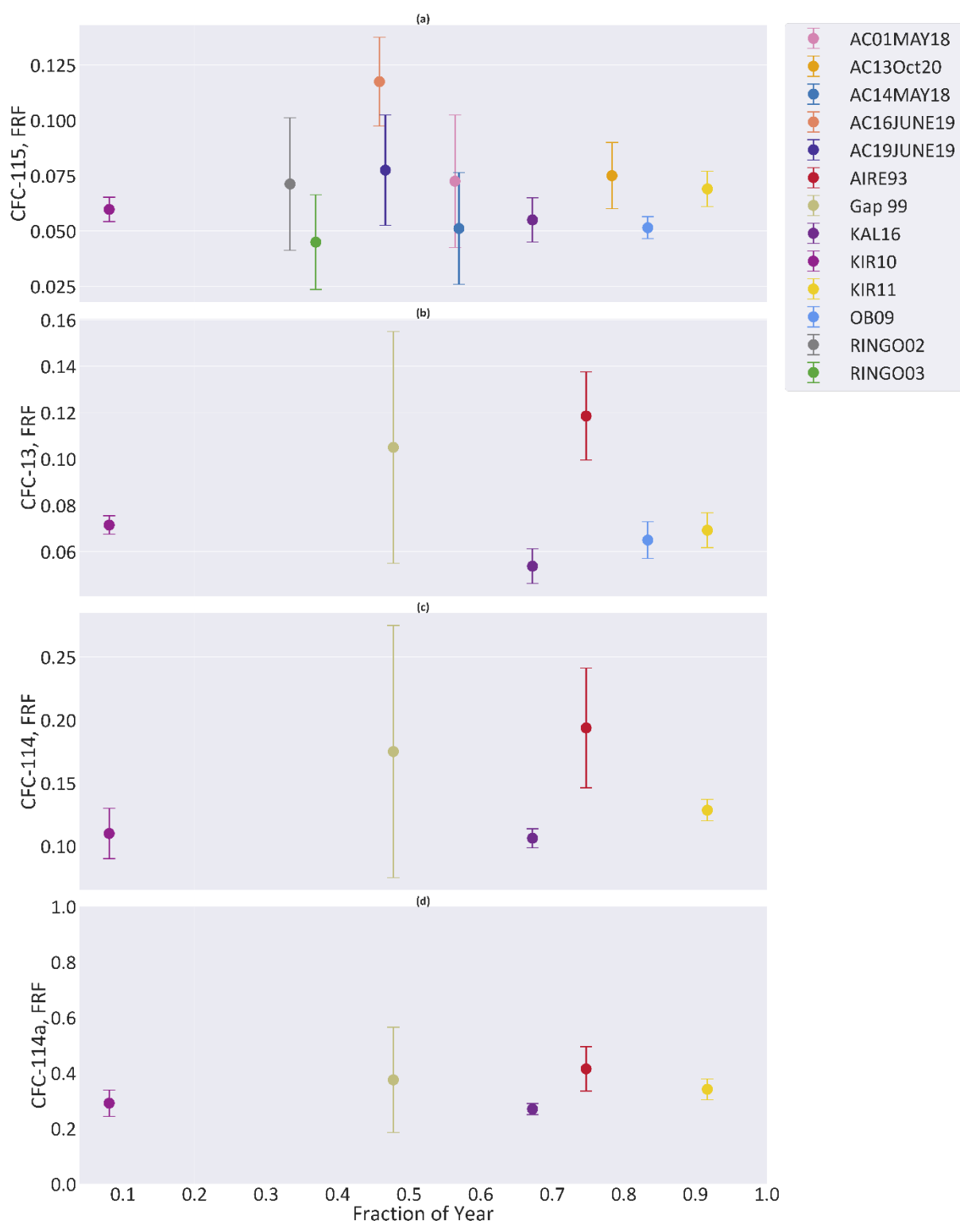


Figure C.2. FRFs at 3 years mean age from Archived Air Data (section 3.3.5), plotted against Fraction of Year, for (a) CFC-115, (b) CFC-13, (c) CFC-114, and (d) CFC-114a. Includes all flights where data was available for the compound, error range is to 1  $\delta$  uncertainty, and was derived from instrument precision.

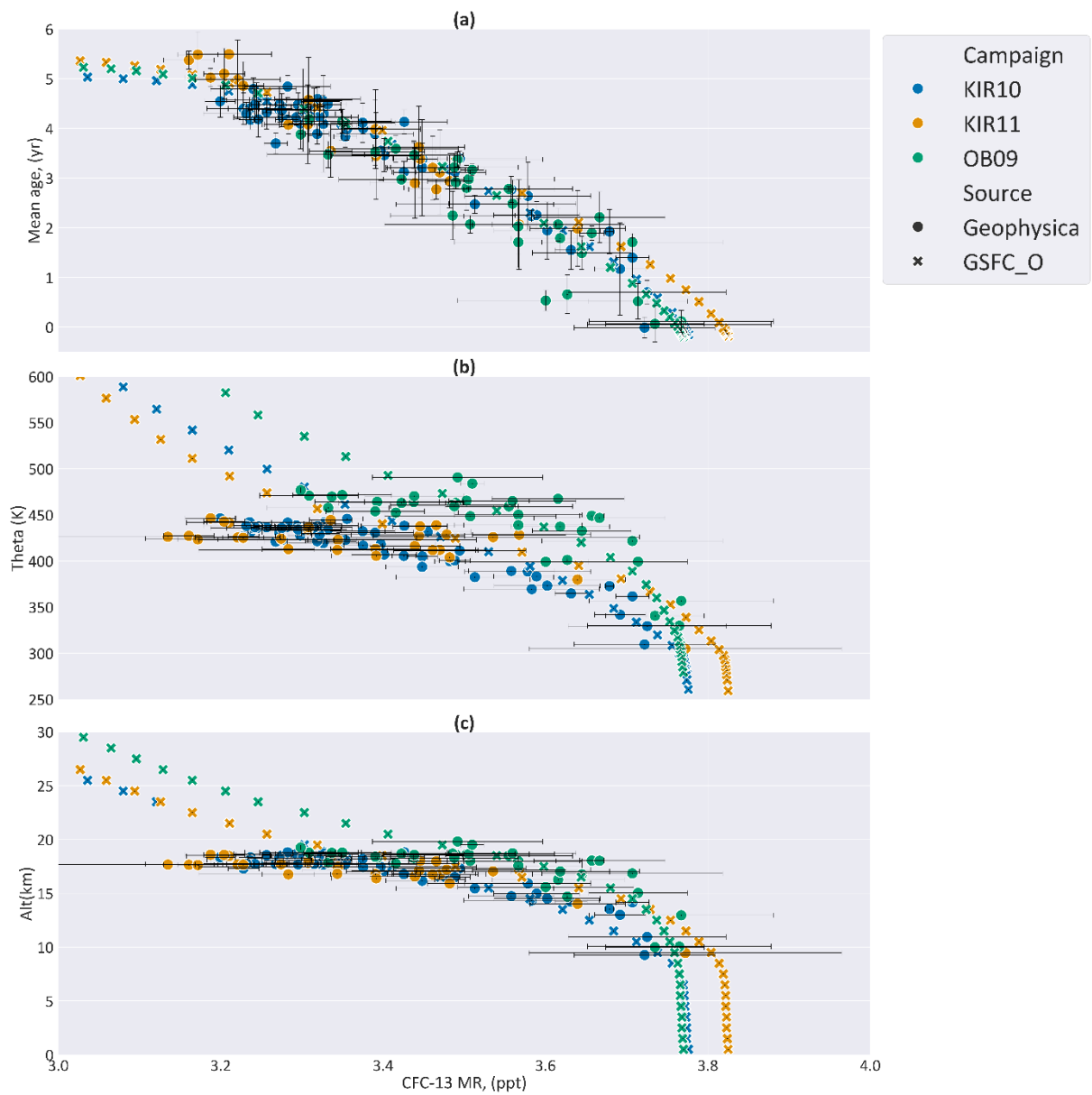


Figure C.3 CFC-13 mixing ratio (ppt) for OB09, KIR10, and KIR11 campaigns, using both GSFC baseline scenario (GSFC\_O) data and M55 Geophysica data, plotted against (a) mean age (yr), (b) Potential Temperature (K), and (c) Altitude (km). Error range for Geophysica data is from instrument precision, and is to 1 sigma uncertainty.

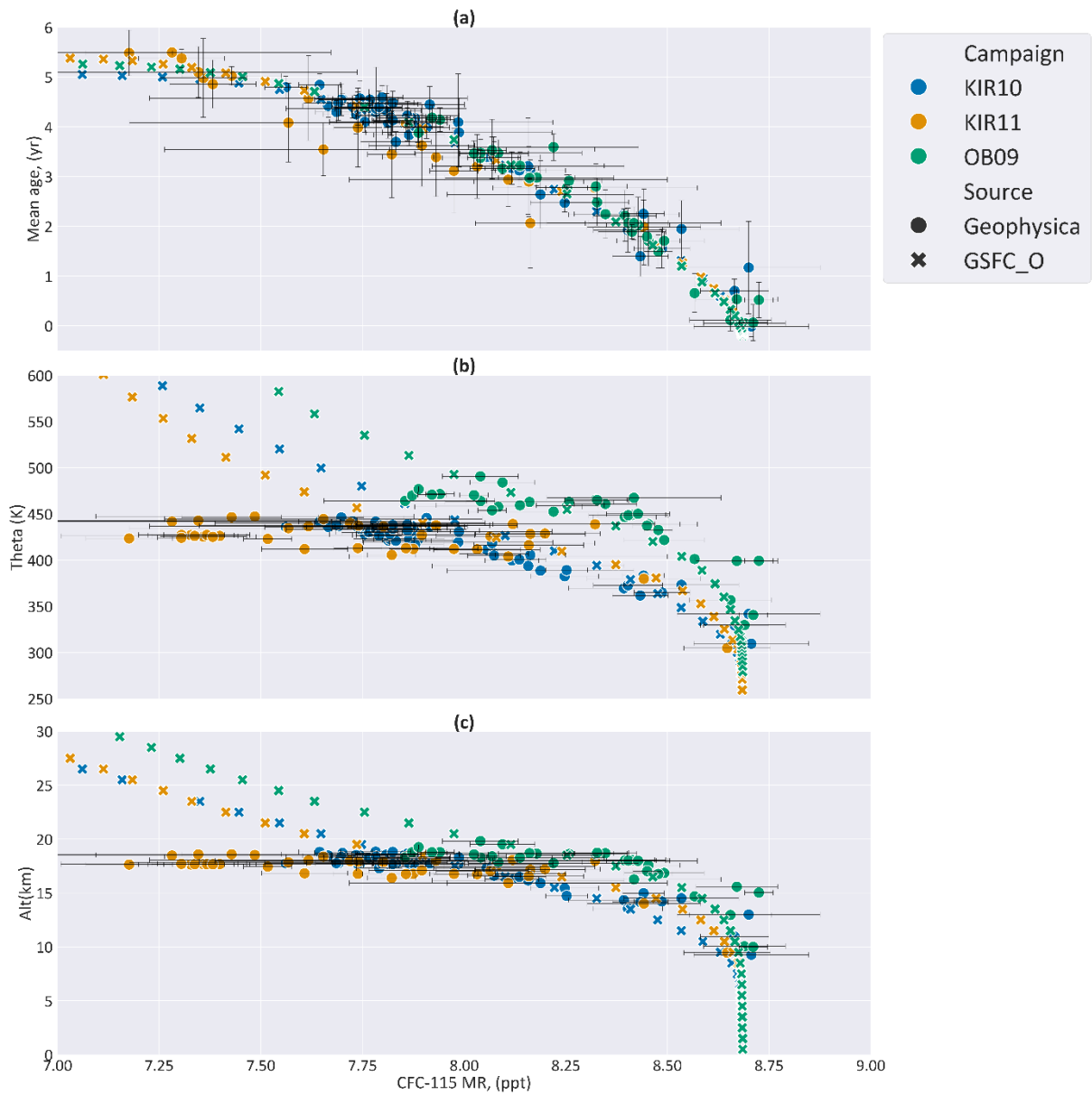


Figure C.4. CFC-115 mixing ratio (ppt) for OB09, KIR10, and KIR11 campaigns, using both GSFC baseline scenario (GSFC\_O) data and M55 Geophysica data, plotted against (a) mean age (yr), (b) Potential Temperature (K), and (c) Altitude (km). Error range for Geophysica data is from instrument precision, and is to 1 sigma uncertainty.

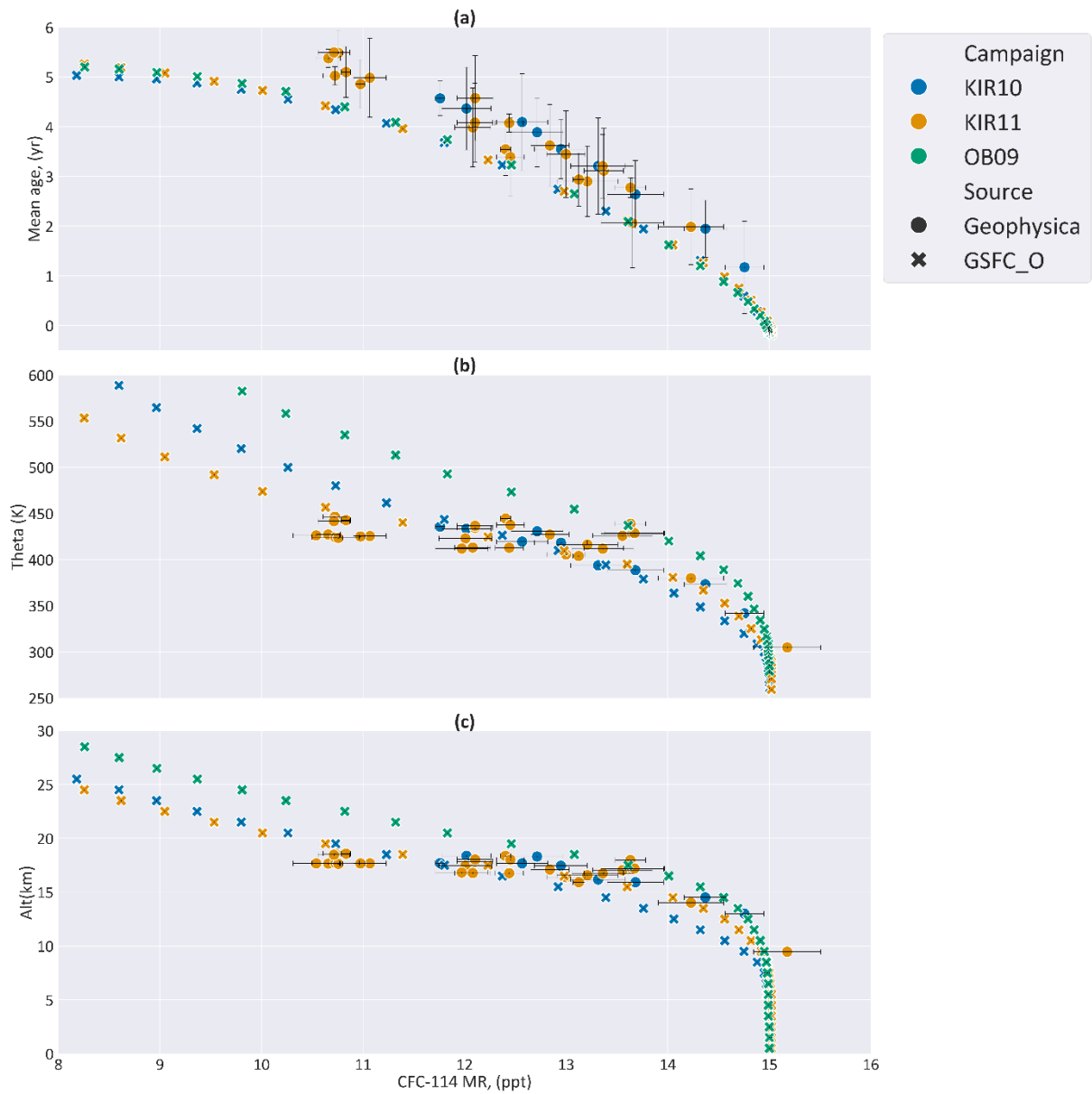


Figure C.5. CFC-114 mixing ratio (ppt) for OB09, KIR10, and KIR11 campaigns, using both GSFC baseline scenario (GSFC\_O) data and M55 Geophysica data, plotted against (a) mean age (yr), (b) Potential Temperature (K), and (c) Altitude (km). Geophysica data is absent for OB09 as these samples were not run on the AI-Plot column, so we do not have results for this compound. Error range for Geophysica data is from instrument precision, and is to 1 sigma uncertainty.

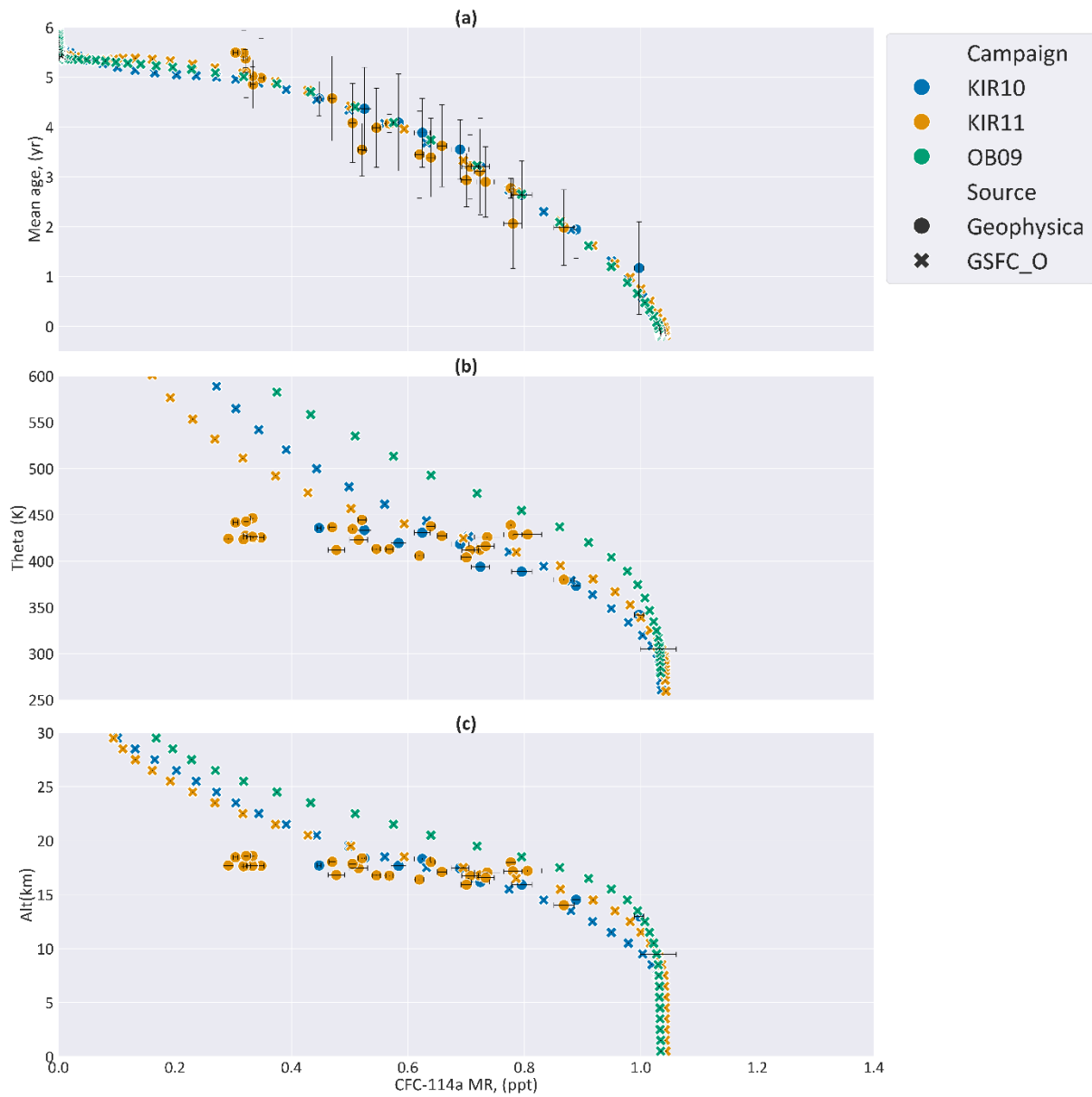


Figure C.6. CFC-114a mixing ratio (ppt) for OB09, KIR10, and KIR11 campaigns, using both GSFC baseline scenario (GSFC\_O) data and M55 Geophysica data, plotted against (a) mean age (yr), (b) Potential Temperature (K), and (c) Altitude (km). Geophysica data is absent for OB09 as these samples were not run on the AI-Plot column, so we do not have results for this compound. Error range for Geophysica data is from instrument precision, and is to 2 sigma uncertainty.

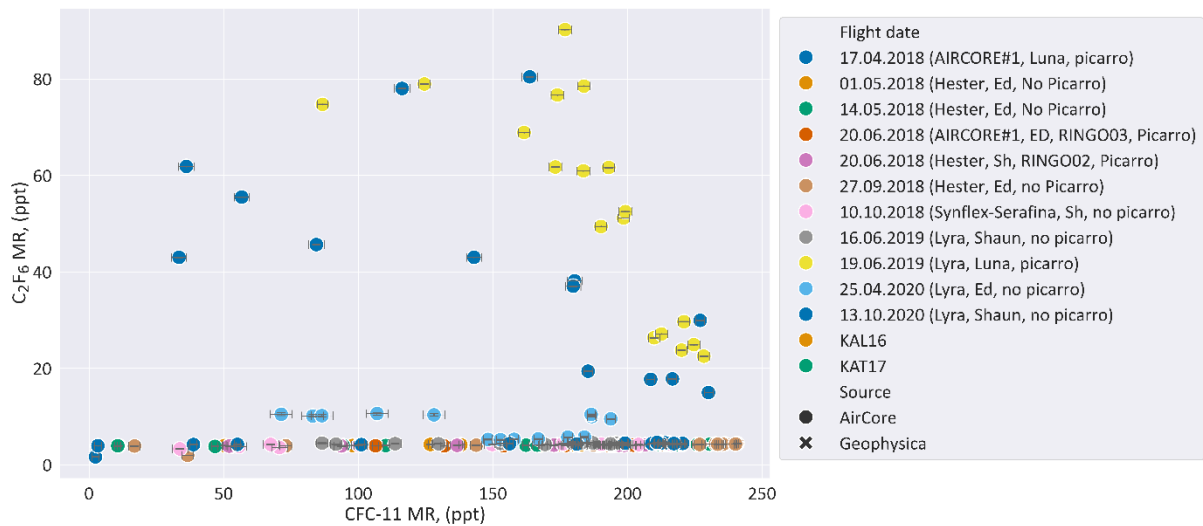


Figure C.7. PFC-116 ( $C_2F_6$ ) mixing ratio (MR, ppt) plotted against CFC-11 mixing ratio (MR, ppt), for all AirCore flights listed in section 4.2, and two Geophysica flights (KAL16, and KAT17). Errors derived using instrument precision, to 1 sigma uncertainty.

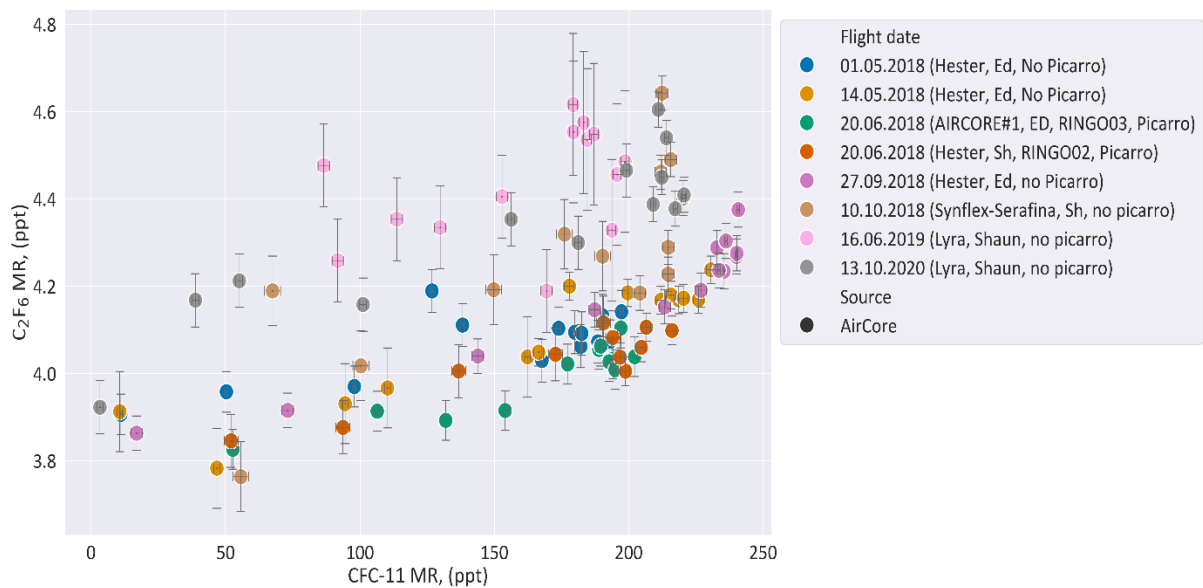


Figure C.8. 'Selected' Flights only. PFC-116 ( $C_2F_6$ ) mixing ratio (ppt) plotted against CFC-11 mixing ratio (ppt), for all AirCore flights listed in section 4.2, (excluding 25.04.2020 and the two flights which used the 'Luna' sub-sampler) and two Geophysica flights (KAL16, and KAT17). Errors derived using instrument precision, to 1 sigma uncertainty.

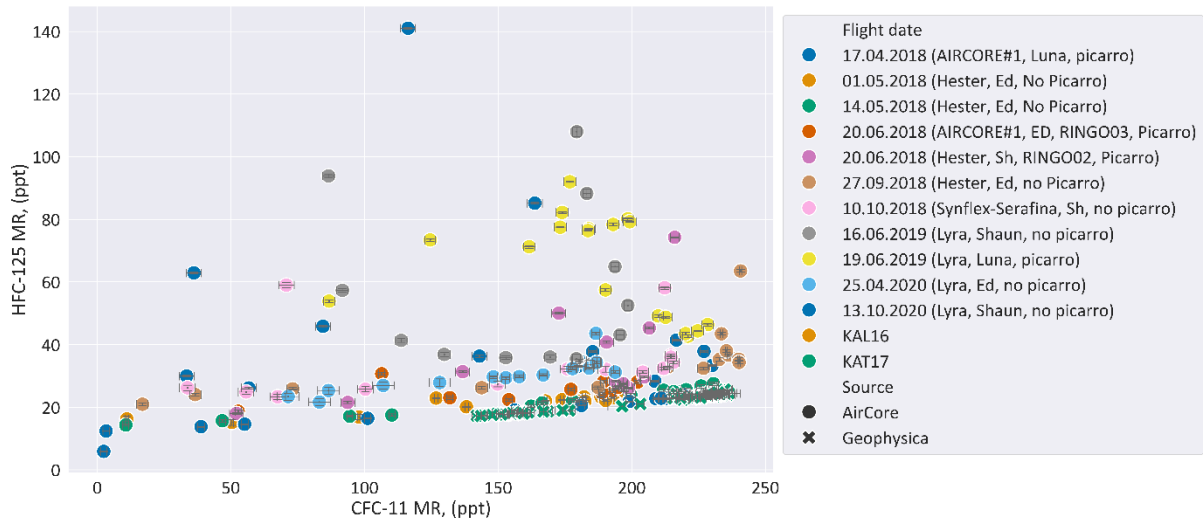


Figure C.9. HFC-125 mixing ratio (ppt) plotted against CFC-11 mixing ratio (ppt), for all AirCore flights listed in section 4.2, and two Geophysica flights (KAL16, and KAT17). Errors derived using instrument precision, to 1 sigma uncertainty.

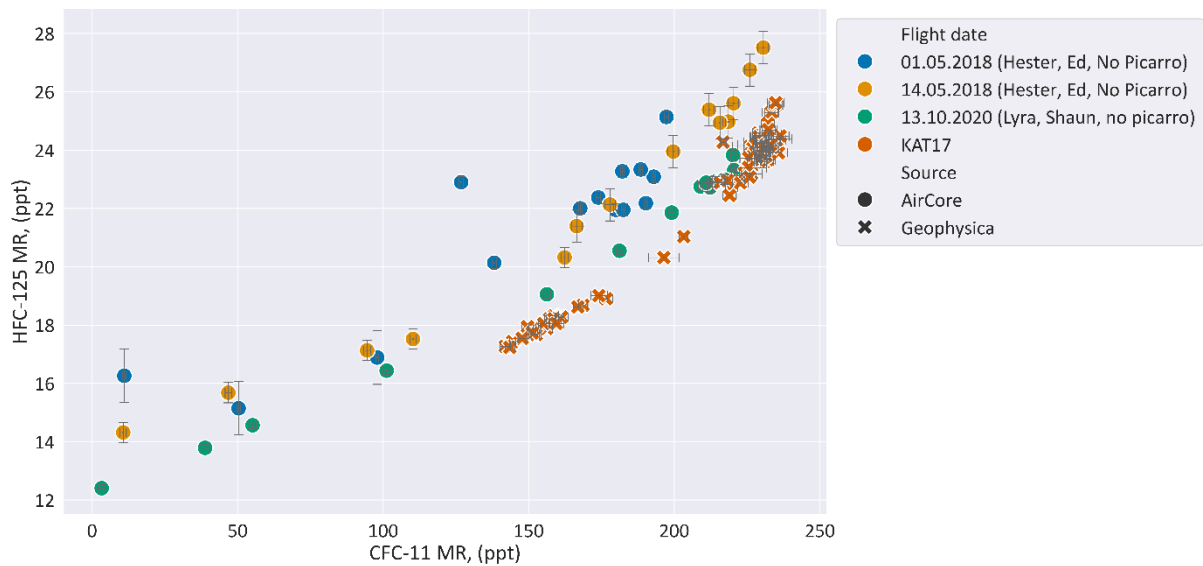


Figure C.10. 'Selected' Flights only. HFC-125 mixing ratio (ppt) plotted against CFC-11 mixing ratio (ppt), for all AirCore flights with only a 'short' delay between flight and analysis, and Geophysica flight KAT17). Errors derived using instrument precision, to 1 sigma uncertainty.

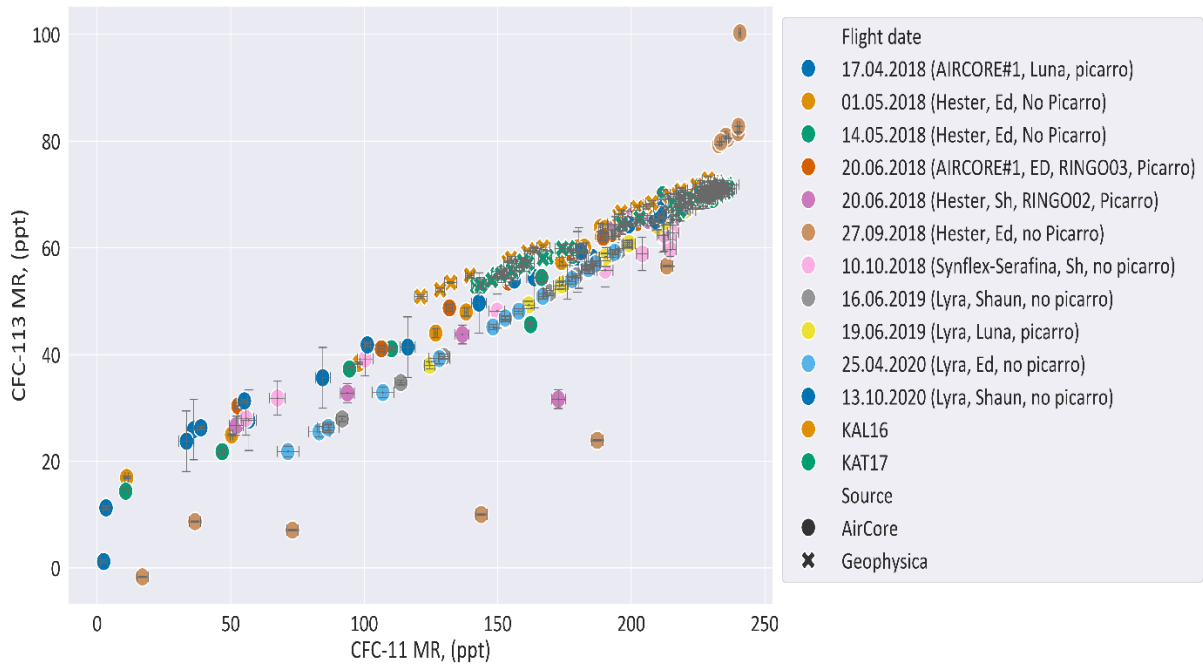


Figure C.11. CFC-113 mixing ratio (ppt) plotted against CFC-11 mixing ratio (ppt), for all AirCore flights listed in section 4.2, and two Geophysica flights (KAL16, and KAT17). Errors derived using instrument precision, to 1 sigma uncertainty.

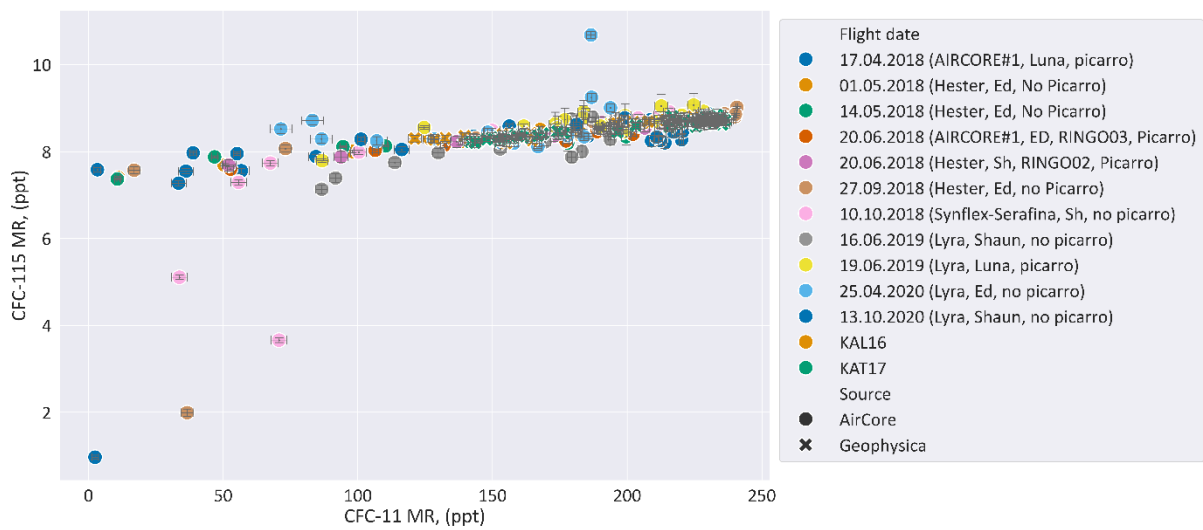


Figure C.12. CFC-115 mixing ratio (ppt) plotted against CFC-11 mixing ratio (ppt), for all AirCore flights listed in section 4.2, and two Geophysica flights (KAL16, and KAT17). Errors derived using instrument precision, to 1 sigma uncertainty.

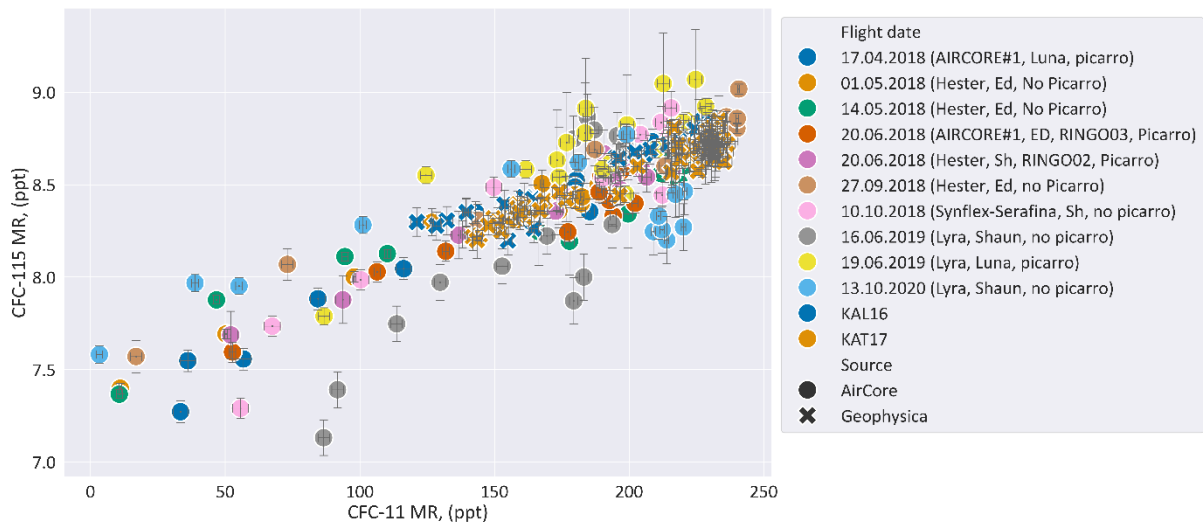


Figure C.13. ‘Selected’ flights only. CFC-115 mixing ratio (ppt) plotted against CFC-11 mixing ratio (ppt), for all AirCore flights listed in section 4.2 (excluding the 25.04.2020 flight and the outliers discussed), and two Geophysica flights (KAL16, and KAT17). Errors derived using instrument precision, to 1 sigma uncertainty.

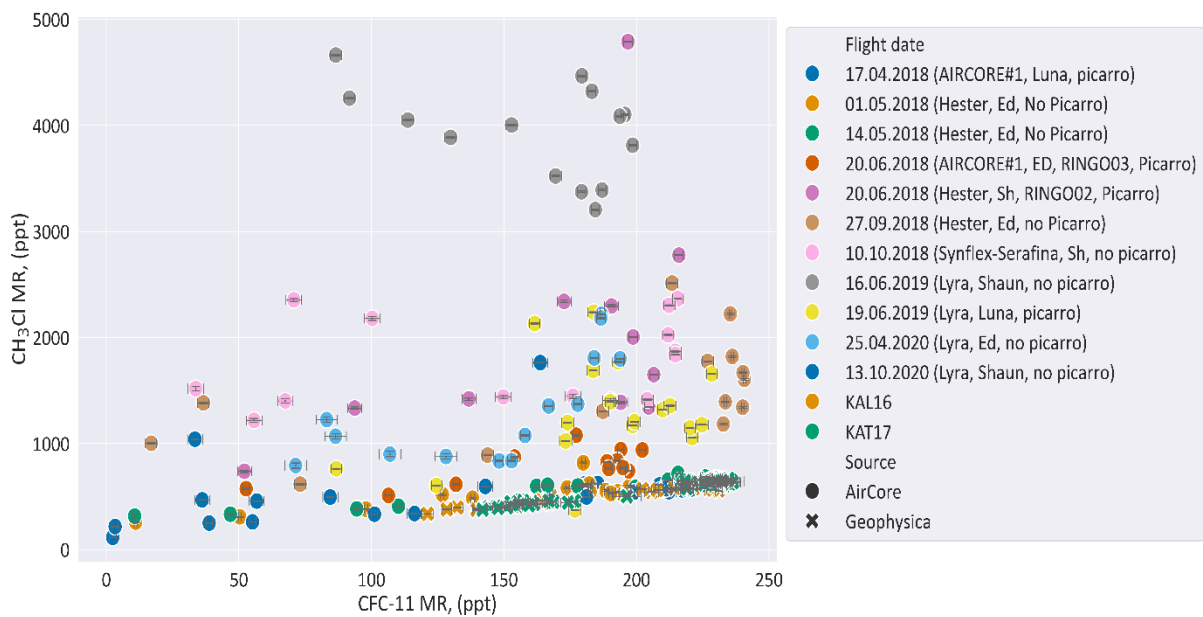


Figure C.14. Methyl Chloride mixing ratio (ppt) plotted against CFC-11 mixing ratio (ppt), for all AirCore flights listed in section 4.2, and two Geophysica flights (KAL16, and KAT17). Errors derived using instrument precision, to 1 sigma uncertainty.

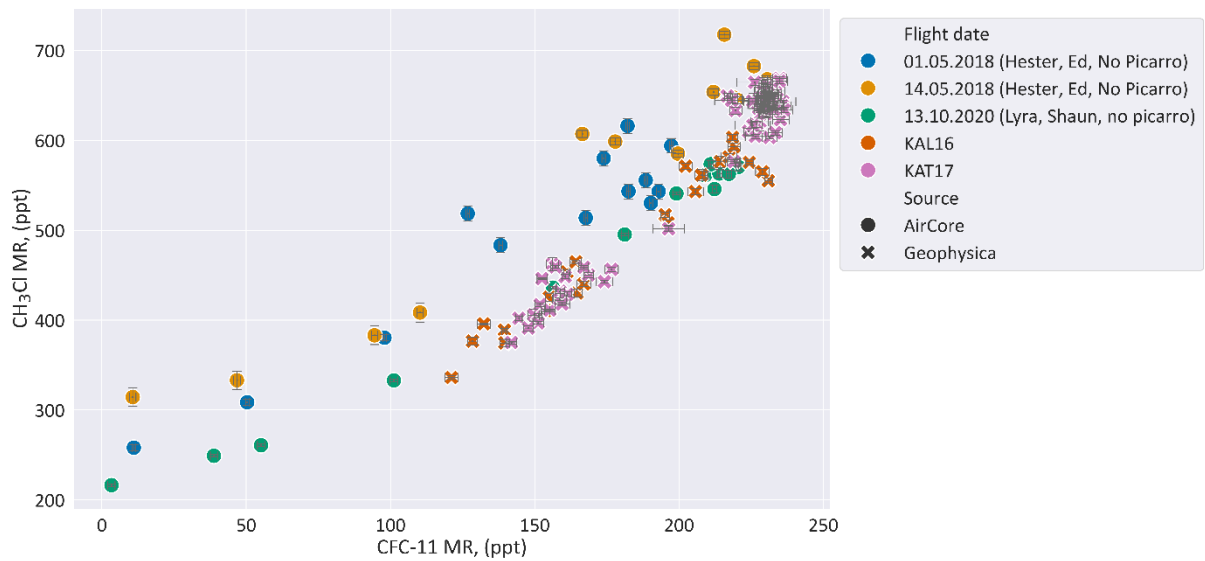


Figure C.15. 'Selected' flights only. Methyl Chloride mixing ratio (ppt) plotted against CFC-11 mixing ratio (ppt), for all AirCore flights listed in section 4.2 (excluding flights where the delay was 'long' or 'medium'), and two Geophysica flights (KAL16, and KAT17). Errors derived using instrument precision, to 1 sigma uncertainty.

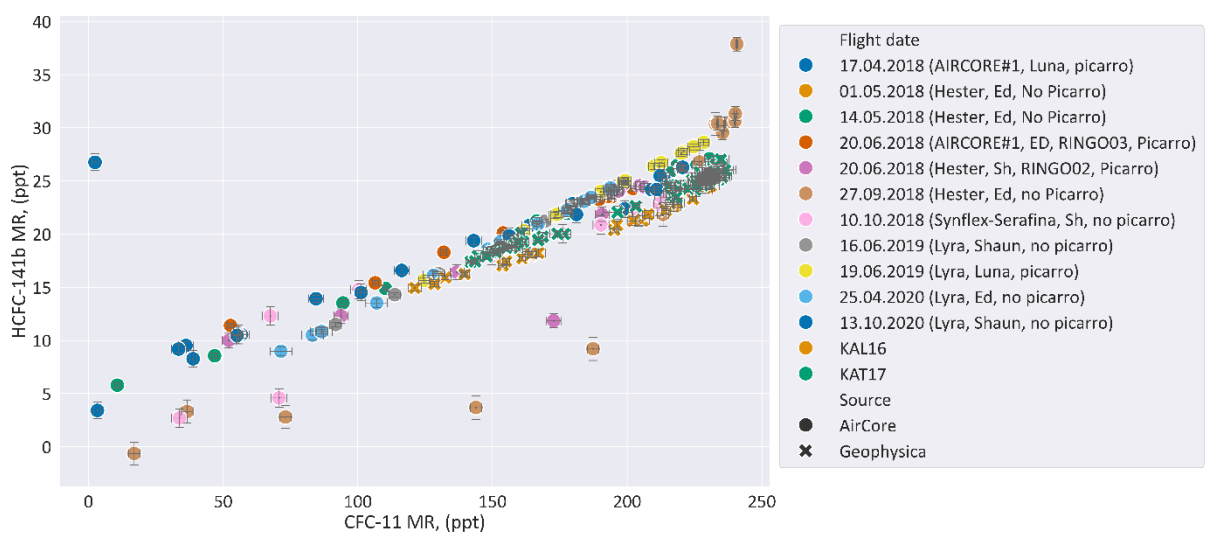


Figure C.16. HCFC-141b mixing ratio (ppt) plotted against CFC-11 mixing ratio (ppt), for all AirCore flights listed in section 4.2, and two Geophysica flights (KAL16, and KAT17). Errors derived using instrument precision, to 1 sigma uncertainty.

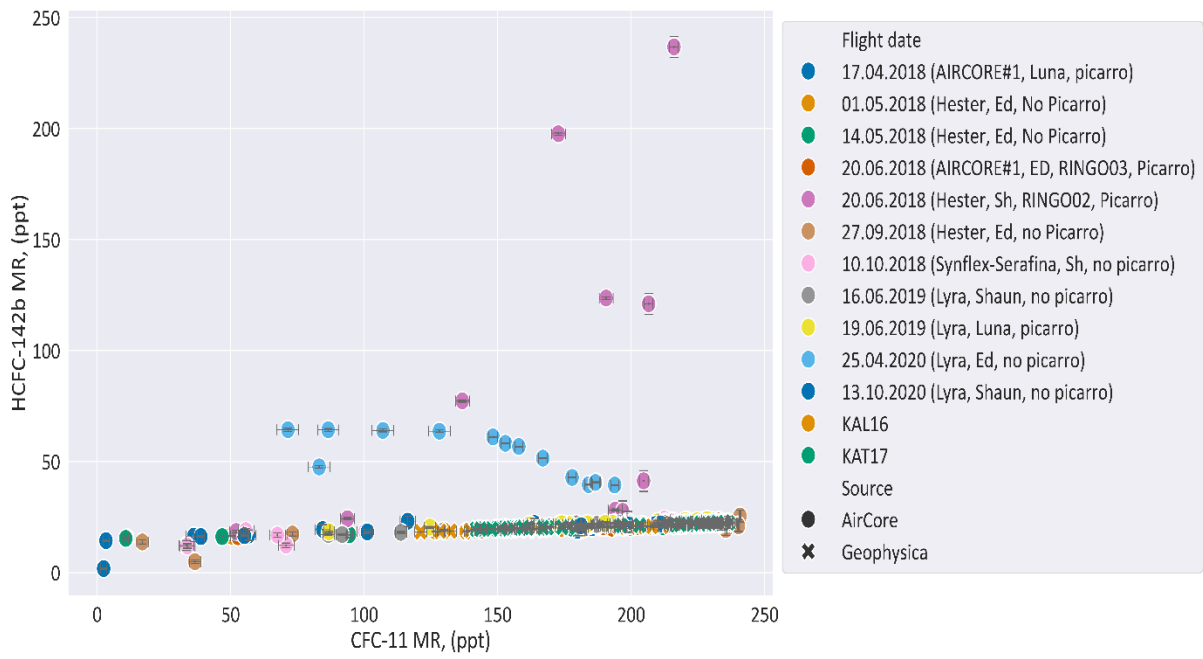


Figure C.17. All Flights. HCFC-142b mixing ratio (ppt) plotted against CFC-11 mixing ratio (ppt), for all AirCore flights listed in section 4.2, and two Geophysica flights (KAL16, and KAT17). Errors derived using instrument precision, to 1 sigma uncertainty.

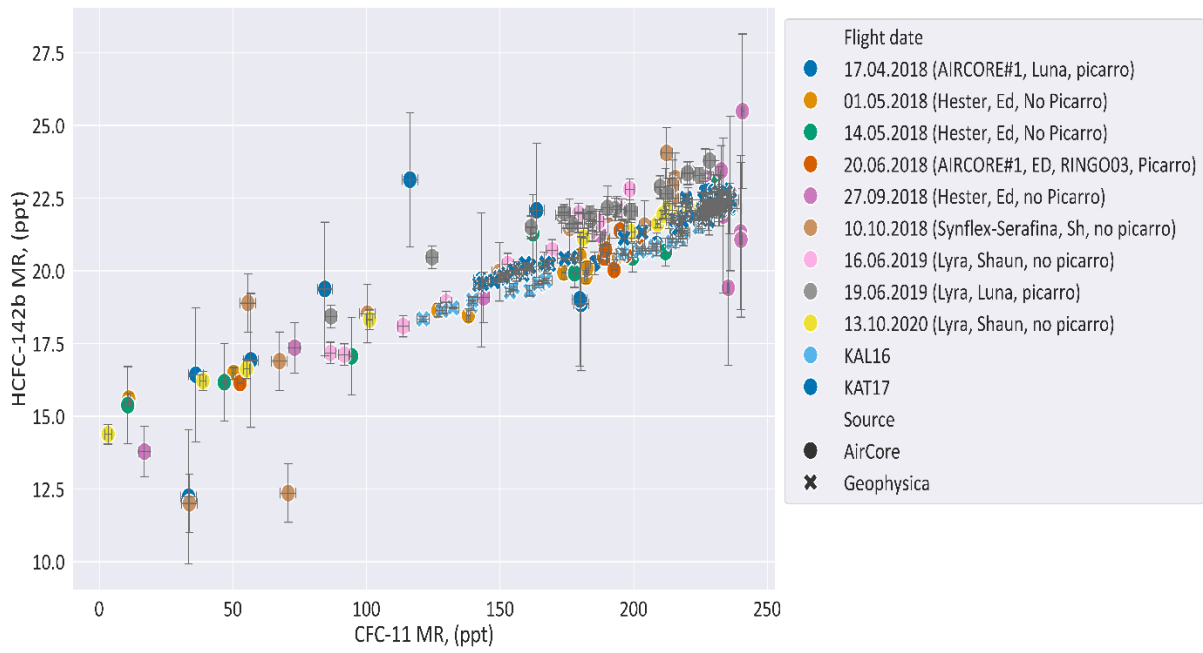


Figure C.18. 'Selected' flights only. HCFC-142b mixing ratio (ppt) plotted against CFC-11 mixing ratio (ppt), for all AirCore flights listed in section 4.2 (excluding 25.04.2020 and 20.06.2018 (RINGO02)), and two Geophysica flights (KAL16, and KAT17). Errors derived using instrument precision, to 1 sigma uncertainty.

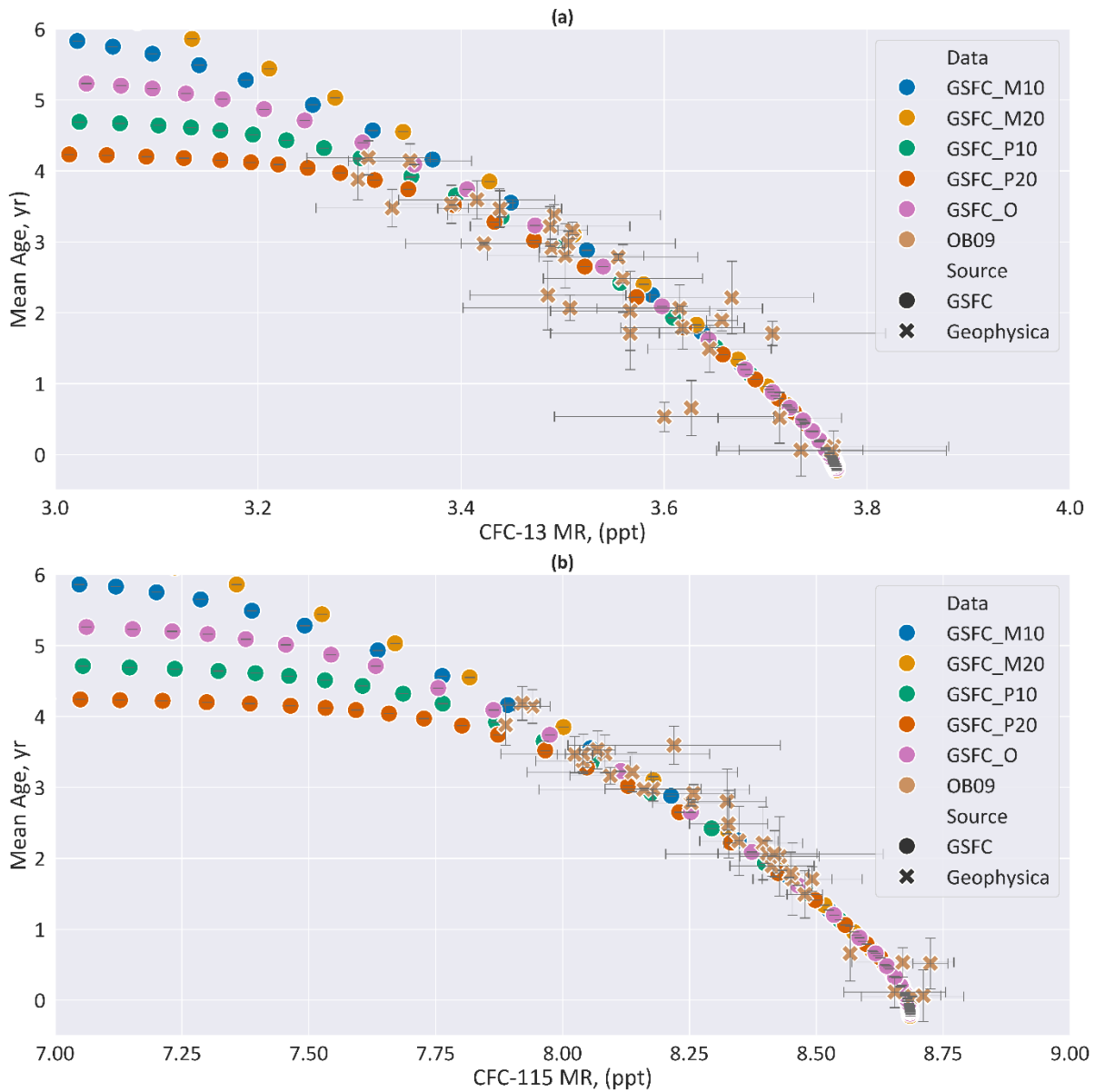


Figure C.19 Mixing ratio (ppt) of (a) CFC-13 and (b) CFC-115, plotted against mean age (yr). Data for the OB09 campaign from both the M55 Geophysica flights, and the GSFC 2D model. Includes the GSFC baseline scenario (GSFC\_O), scenarios where the speed of the circulation is slowed by 10% (GSFC\_M10) and 20% (GSFC\_M20), and scenarios where the speed of the circulation was increased by 10% (GSFC\_P10) and 20% (GSFC\_P20). CFC-114 and CFC-114a were not measured for this campaign. Error bars use instrument uncertainty measurements for the observational data, there were no error ranges for the GSFC data, but the varied scenarios act as a proxy error range.

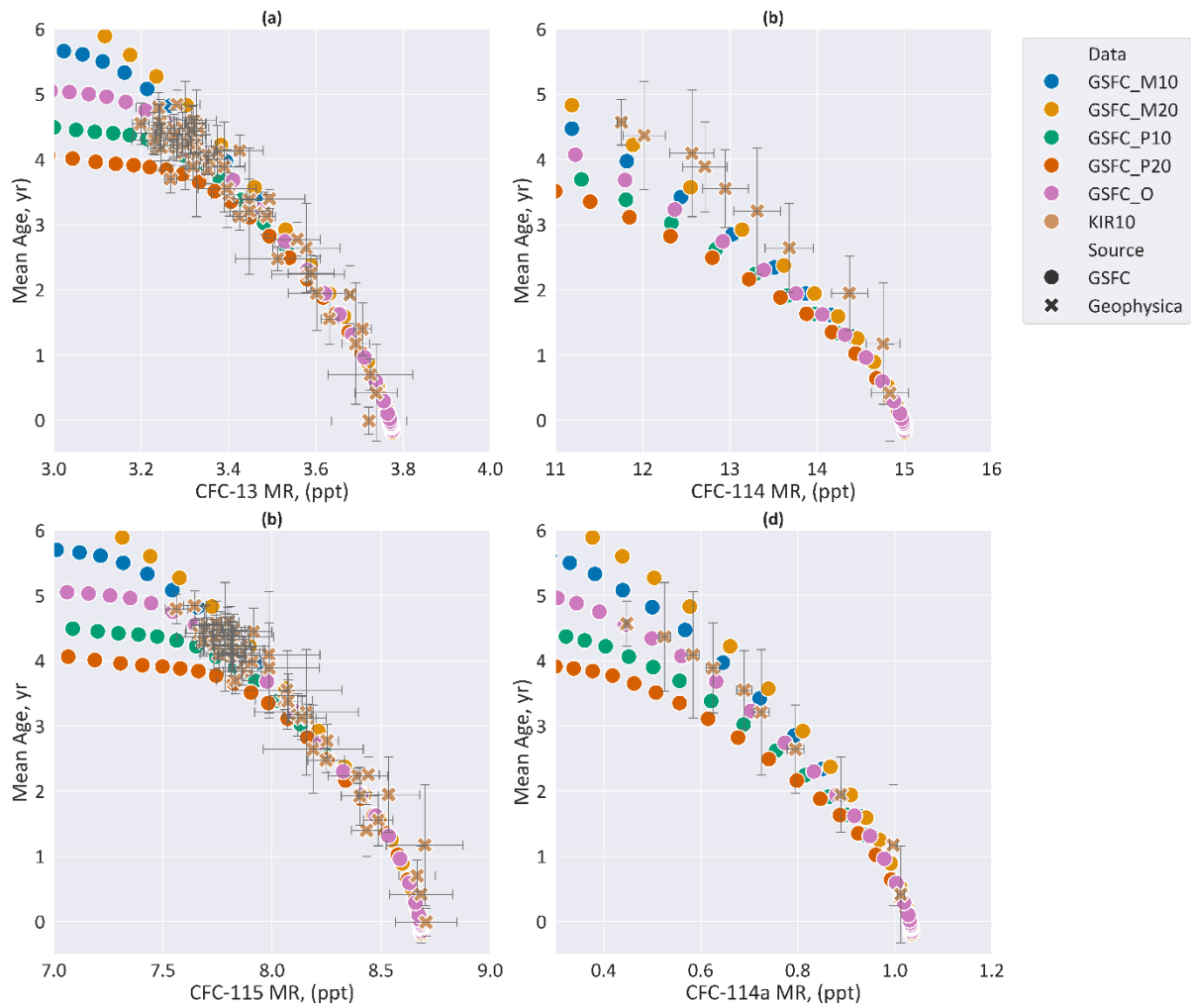


Figure C.20. Mixing ratio (ppt) of (a) CFC-13, (b) CFC-115, (c) CFC-114, and CFC-114a, plotted against mean age (yr). Data for the KIR10 campaign from both the M55 Geophysica flights, and the GSFC 2D model. Includes the GSFC baseline scenario (GSFC\_O), scenarios where the speed of the circulation is slowed by 10% (GSFC\_M10) and 20% (GSFC\_M20), and scenarios where the speed of the circulation was increased by 10% (GSFC\_P10) and 20% (GSFC\_P20). Error bars use instrument uncertainty measurements for the observational data, there were no error ranges for the GSFC data, but the varied scenarios act as a proxy error range.

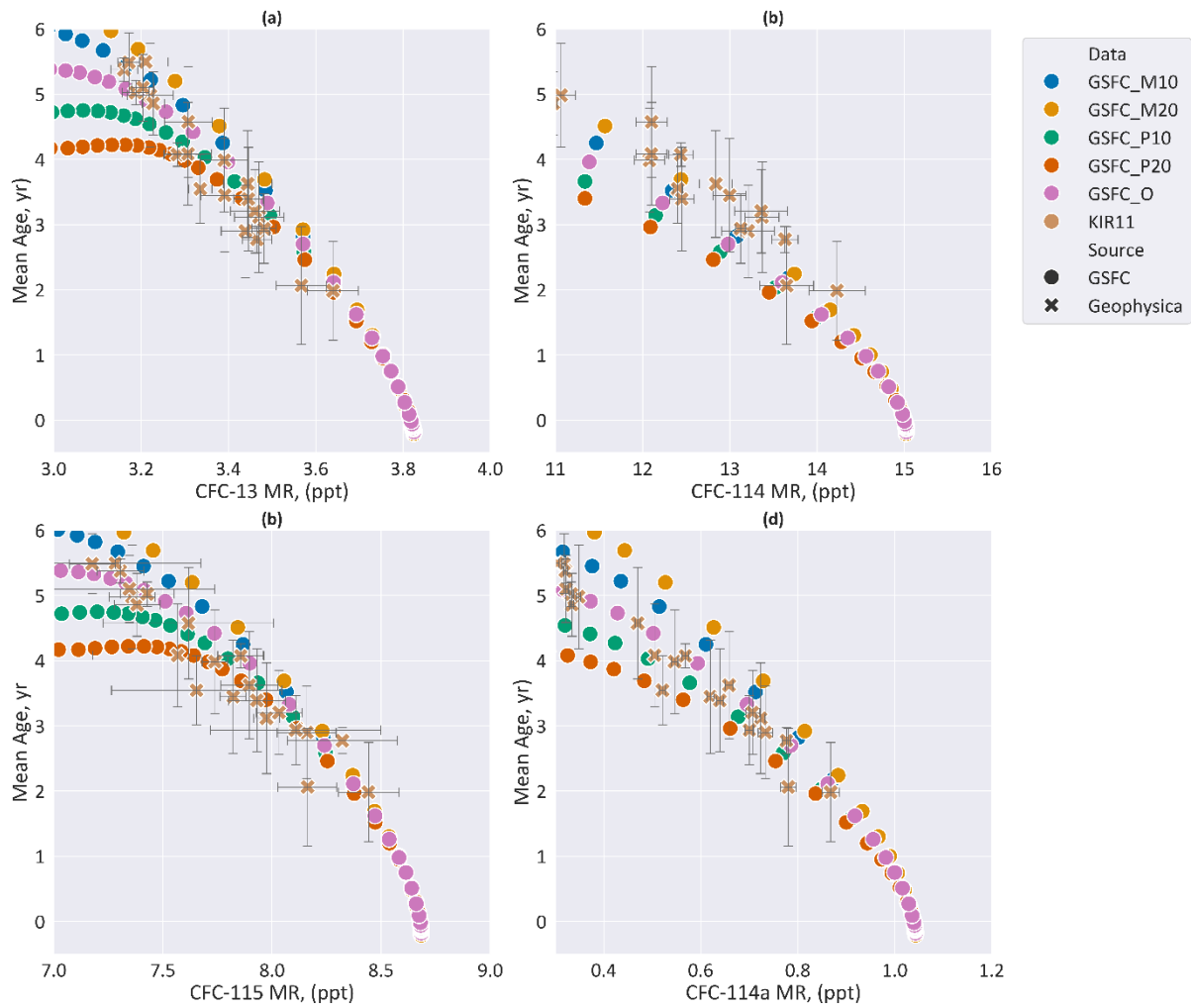


Figure C.21. Mixing ratio (ppt) of (a) CFC-13, (b) CFC-115, (c) CFC-114, and CFC-114a, plotted against mean age (yr). Data for the KIR11 campaign from both the M55 Geophysica flights, and the GSFC 2D model. Includes the GSFC baseline scenario (GSFC\_O), scenarios where the speed of the circulation is slowed by 10% (GSFC\_M10) and 20% (GSFC\_M20), and scenarios where the speed of the circulation was increased by 10% (GSFC\_P10) and 20% (GSFC\_P20). Error bars use instrument uncertainty measurements for the observational data, there were no error ranges for the GSFC data, but the varied scenarios act as a proxy error range.

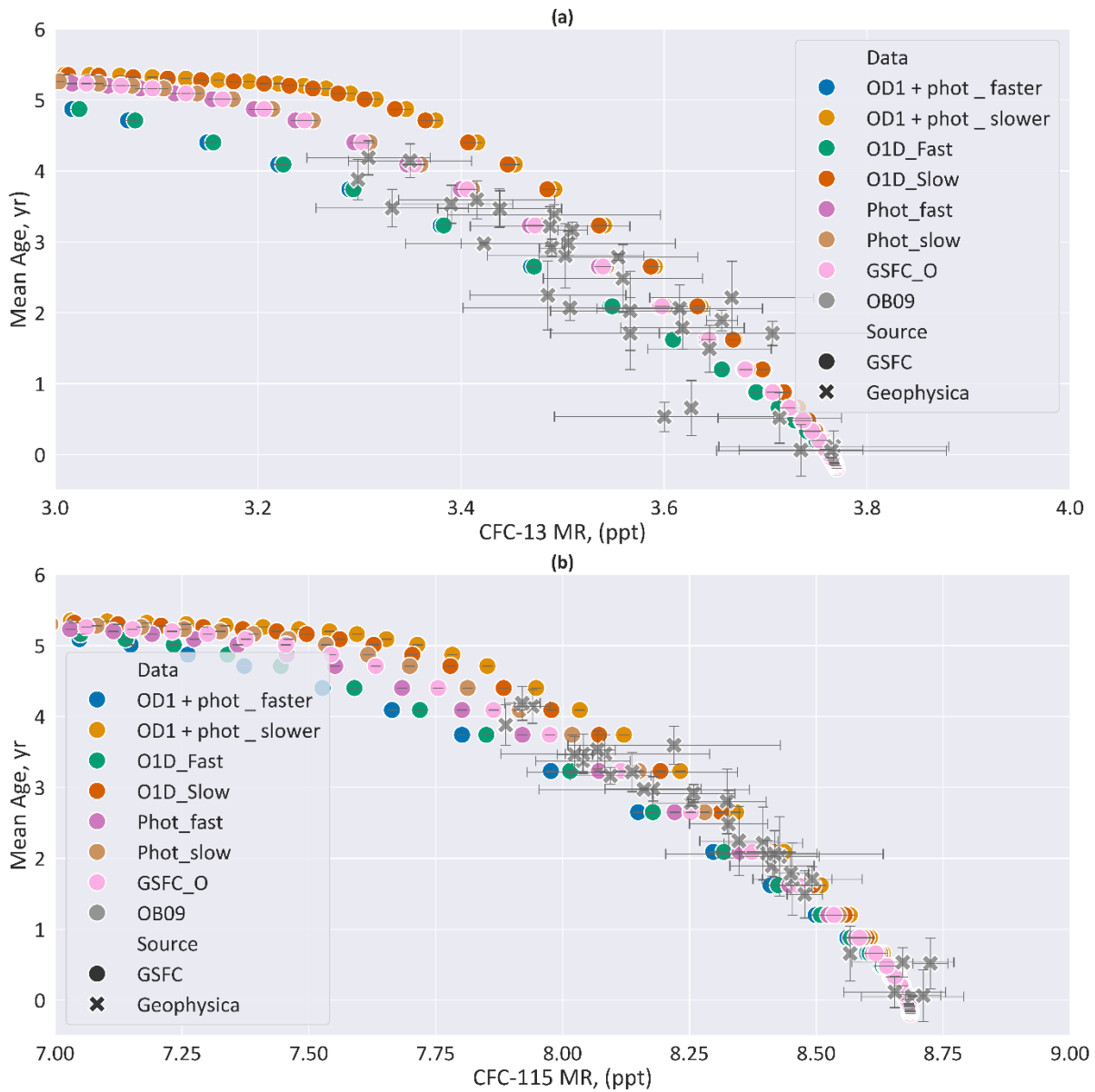


Figure C.22. Displays the 6 chemistry scenarios from the GSFC-2D model for the OB09 campaign, the 'baseline' scenario in which circulation and chemistry are normal (GSFC\_O), and observational data (OB09). Mixing ratio (ppt) is plotted against Mean Age (yr). Mixing ratio is for (a) CFC-13, (b) CFC-115. As only the gaspro column was used for the samples from this campaign, it could not distinguish between CFC-114 and CFC-114a. Error bars use instrument uncertainty measurements for the observational data, there were no error ranges for the GSFC data, but the varied scenarios act as a proxy error range.

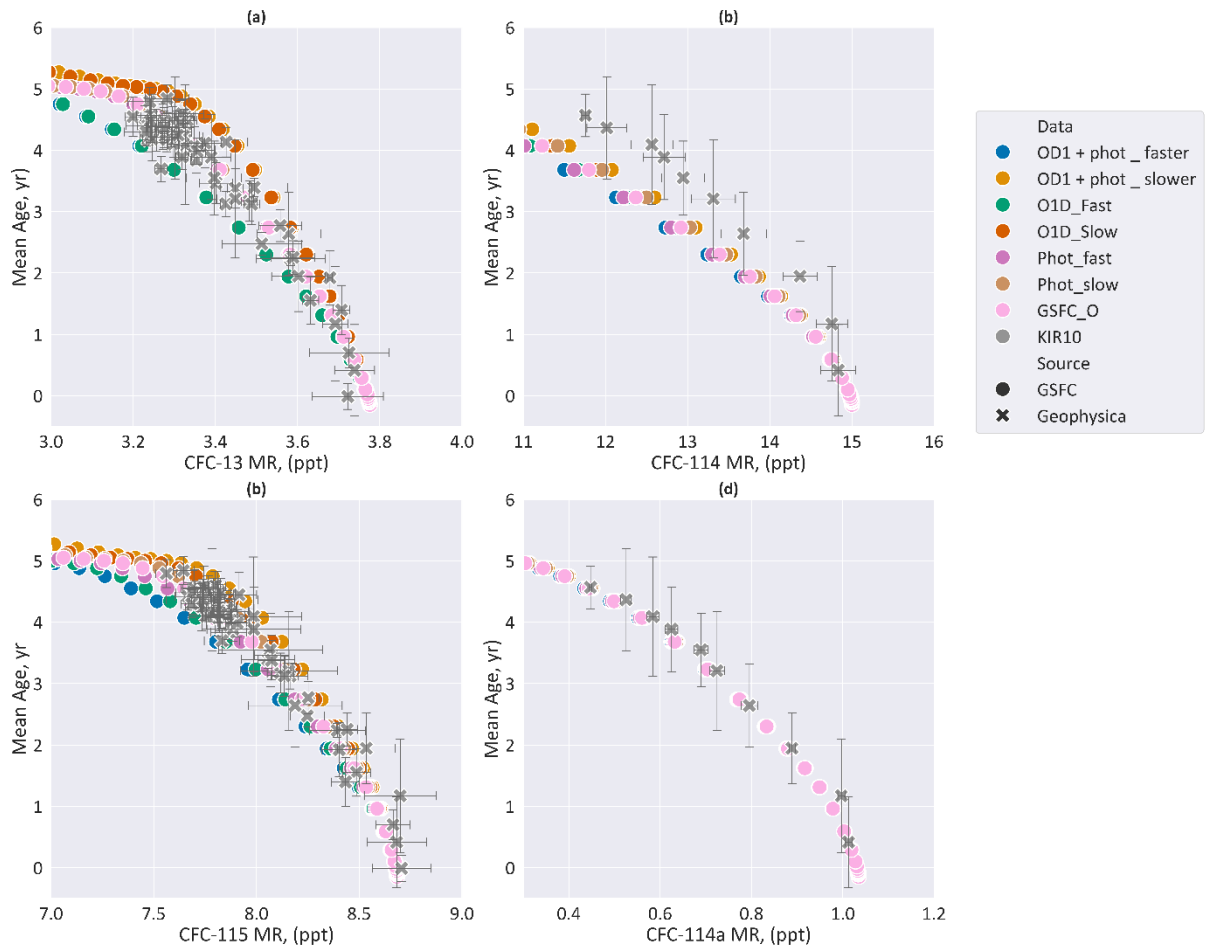


Figure C.23. Displays the 6 chemistry scenarios from the GSFC-2D model for the KIR10 campaign, the 'baseline' scenario in which circulation and chemistry are normal (GSFC\_O), and observational data (KIR10). Mixing ratio (ppt) is plotted against Mean Age (yr). Mixing ratio is for: (a) CFC-13, (b) CFC-114, (c) CFC-115, (d) CFC-114a. Error bars use instrument uncertainty measurements for the observational data, there were no error ranges for the GSFC data, but the varied scenarios act as a proxy error range.

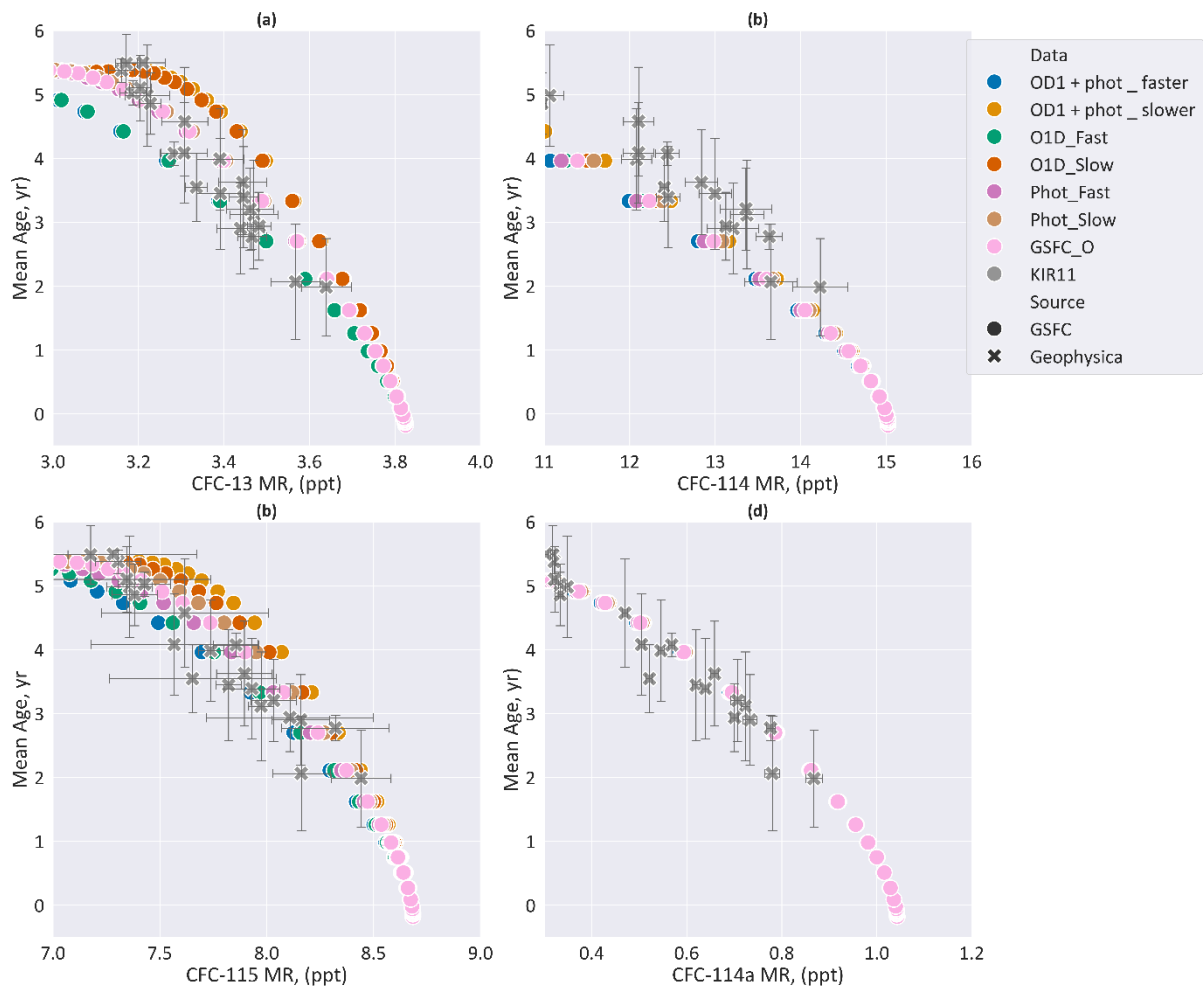


Figure C.24 Displays the 6 chemistry scenarios from the GSFC-2D model for the KIR11 Campaign, this also includes the 'baseline' scenario in which circulation and chemistry are normal (GSFC\_O), and observational data (KIR11). Mixing ratio (ppt) is plotted against Mean Age (yr). Mixing ratio is for: (a) CFC-13, (b) CFC-114, (c) CFC-115, (d) CFC-114a. Error bars use instrument uncertainty measurements for the observational data, there were no error ranges for the GSFC data, but the varied scenarios act as a proxy error range.

## Appendix D Statistical techniques – technical details

### D.i Bivariate data – worked example

The same base data from the 14<sup>th</sup> of May flight (explored in detail in Chapter 4) was used for each method: the mean ages derived for SF<sub>6</sub>, plotted against mean ages derived for PFC-116 or HFC-125. As discussed in section 4.3.8, the slope of this data is used to determine how different the derived mean ages from PFC-116 and HFC-125 are from SF<sub>6</sub>, and to calculate a conversion factor for SF<sub>6</sub> derived mean ages. Both the x axis (SF<sub>6</sub>) and the y axis (PFC-116 or HFC-125) contain uncertainty, and this needs to be taken into account when using the trendline of this slope in any predictions or calculations.

In this worked example the Barreto & Howland., (2010) bootstrapping method is compared to the method described in Cantrell, (2008). This was a linear regression as there was no way to compare a polynomial regression done with Barreto & Howland., (2010) to Cantrell's method. The two methods use different techniques to account for variation. For Cantrell, the variance is included in the calculation (to two sigma). For Barreto & Howland., (2010) however, an extra step is necessary. We start with the original dataset (sample 1n), then expand the sample to 5n by including in the analysis the maximum and minimum mean age (to two sigma) from each compound, e.g. SF<sub>6</sub> original mean age plotted against C<sub>2</sub>F<sub>6</sub> minimum mean age, SF<sub>6</sub> plotted against C<sub>2</sub>F<sub>6</sub> maximum mean age, SF<sub>6</sub> minimum mean age against C<sub>2</sub>F<sub>6</sub> original mean age, SF<sub>6</sub> maximum mean age against C<sub>2</sub>F<sub>6</sub> original mean age. Thus, giving a 5n or quintupled dataset.

This 5n dataset was then analysed using the spreadsheet created by Barreto & Howland., (2010), using the procedure detailed in Section 2.4. The results, along with the results from using Cantrell's method, are in Table D-1.

*Table D-1. Results of analysis by the methods in Barreto & Howland, and Cantrell. Showing the predicted slope, intercept, and relative uncertainties, for SF<sub>6</sub> plotted against C<sub>2</sub>F<sub>6</sub> and HFC-125.*

Method	C <sub>2</sub> F <sub>6</sub>		HCF-125	
	Slope	Intercept	Slope	Intercept
Barreto & Howland (2010)	0.79 (0.6-0.98)	-0.3 (-0.58--0.03)	0.84 (0.78-0.9)	-0.18 (-0.34--0.02)
Cantrell, (2008)	0.75 (0.63-0.87)	-0.22 (-0.42--0.02)	0.92 (0.88-0.95)	-0.31 (-0.41--0.2)

These resulting slopes and intercepts are then compared to each other and to that of the original data. For the original data depicted in Figure D.1 and Figure D.2, the error range is a rough estimate; using the known uncertainty from instrument precision (to 2 sigma) to generate high and low versions of the data, from which slope and intercept could be calculated.

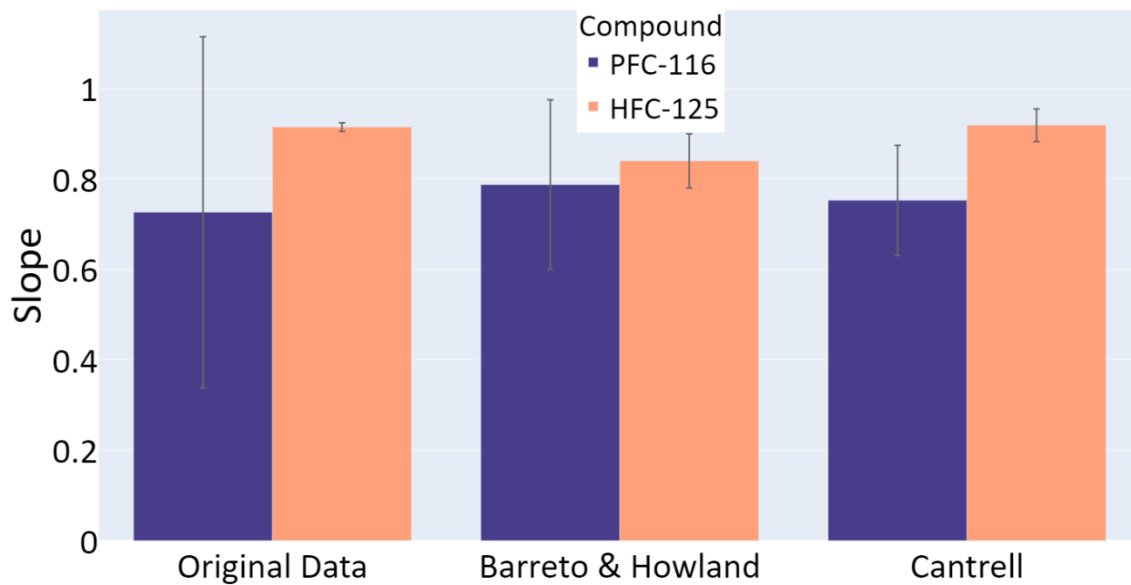


Figure D.1. Slopes predicted by Barreto & Howland (2010) and Cantrell (2008), compared to the original data.

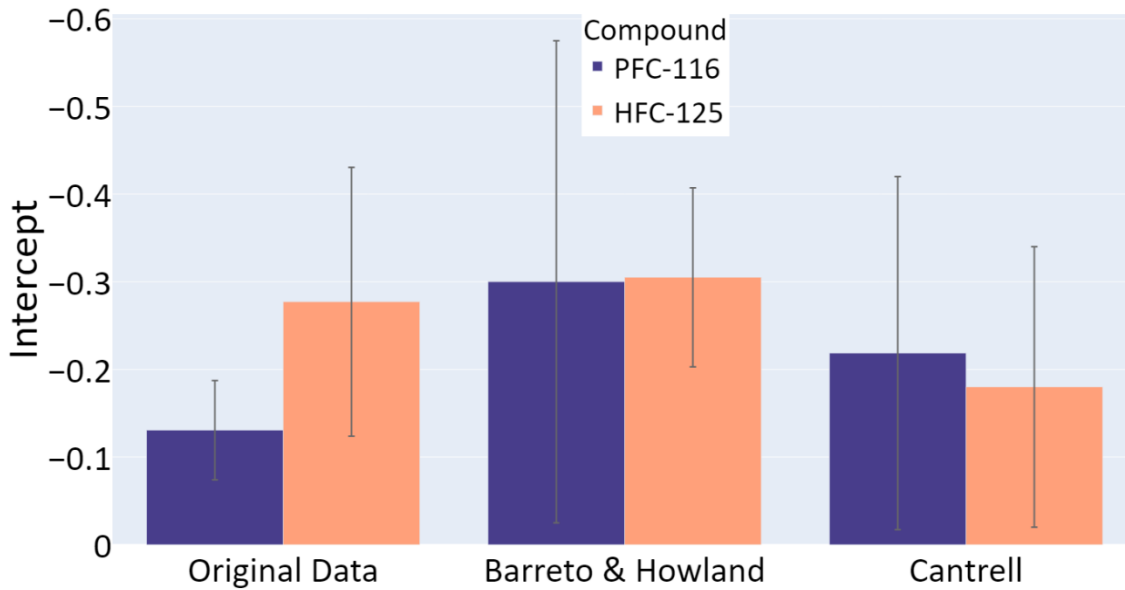


Figure D.2. Intercepts predicted by Barreto & Howland (2010) and Cantrell (2008), compared to original data.

As can be seen from Figure D.1 and Figure D.2, while the methods produce different results, they still agree within the uncertainties. In Figure D.1, while Cantrell’s uncertainties are smaller than Barreto & Howland’s, they nevertheless overlap considerably. In Figure D.2 the uncertainties seem so large because the intercept is such a small number, and the intercept seems to have been more sensitive to changes in the dataset than the slope was. In both cases the slope and intercept derived by each method agree with each other and with the original dataset within the uncertainties.

## D.ii Bootstrapping - worked example

In Table D-2 as an example, the numbers in columns A and B are pairs, so sticking to the marble example (section 2.5), instead of each number being painted on a different marble, imagine both numbers are painted on the same marble, so from the first row, the number ‘10’ from column A and the number ‘5’ from column B are both painted on the marble. From here the bootstrapping process then randomly selects data pairs from the original dataset. For example, the fifth ‘pair’ in the original data is 5 and 2, and if ‘picked’ for resampling ‘5’ will appear in the column for resampled A, and ‘2’ will appear in the column for resampled B. As this is resampling ‘with replacement’ a pair is not removed from the potential pool of data pairs that the resampling draws from, therefore the same data pair may

appear multiple times (or not at all) in the resampled dataset. For example, in the dataset in Table D-2 the first row of data in the original dataset is absent in the resampled data, but the fourth row is represented twice. The last two columns in Table D-2 show how this variation from random resampling with replacement affects the slope and intercept of the data, and this can be seen clearly in Figure D.3 and Figure D.4.

*Table D-2. A simplified example of resampling with replacement using dummy data for ease of comprehension. The first two (green) columns show the original dataset, the second two show the resampled (with replacement) dataset. The final two columns show the slope and intercept for both the original and resampled datasets, calculated using the Slope and Intercept functions respectively.*

A	B	Resample Dataset A	Resample Dataset B
10	5	14	10
6	12	23	23
14	10	5	2
23	23	23	23
5	2	10	5
	Original Dataset	Resample Dataset	
Slope	0.76	0.8	
Intercept	3.72	4.97	

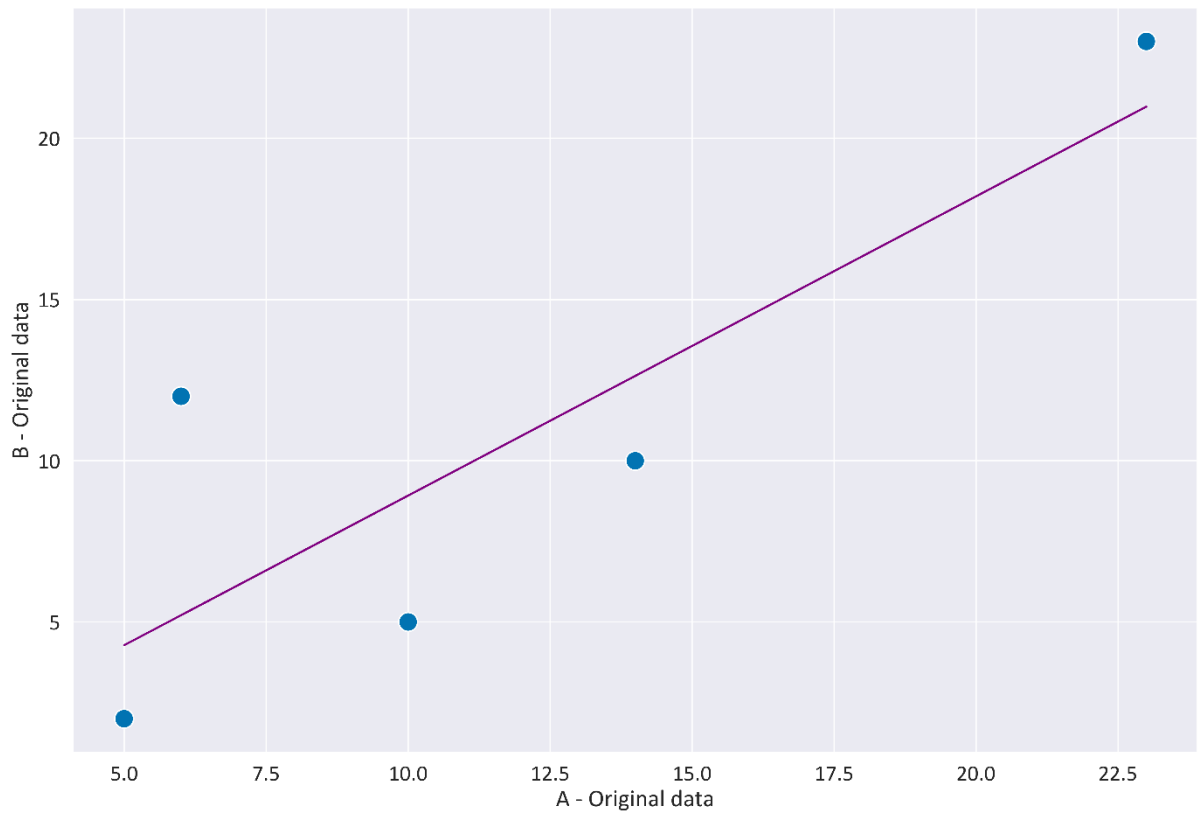


Figure D.3. The 'original' data plotted with a linear trendline.

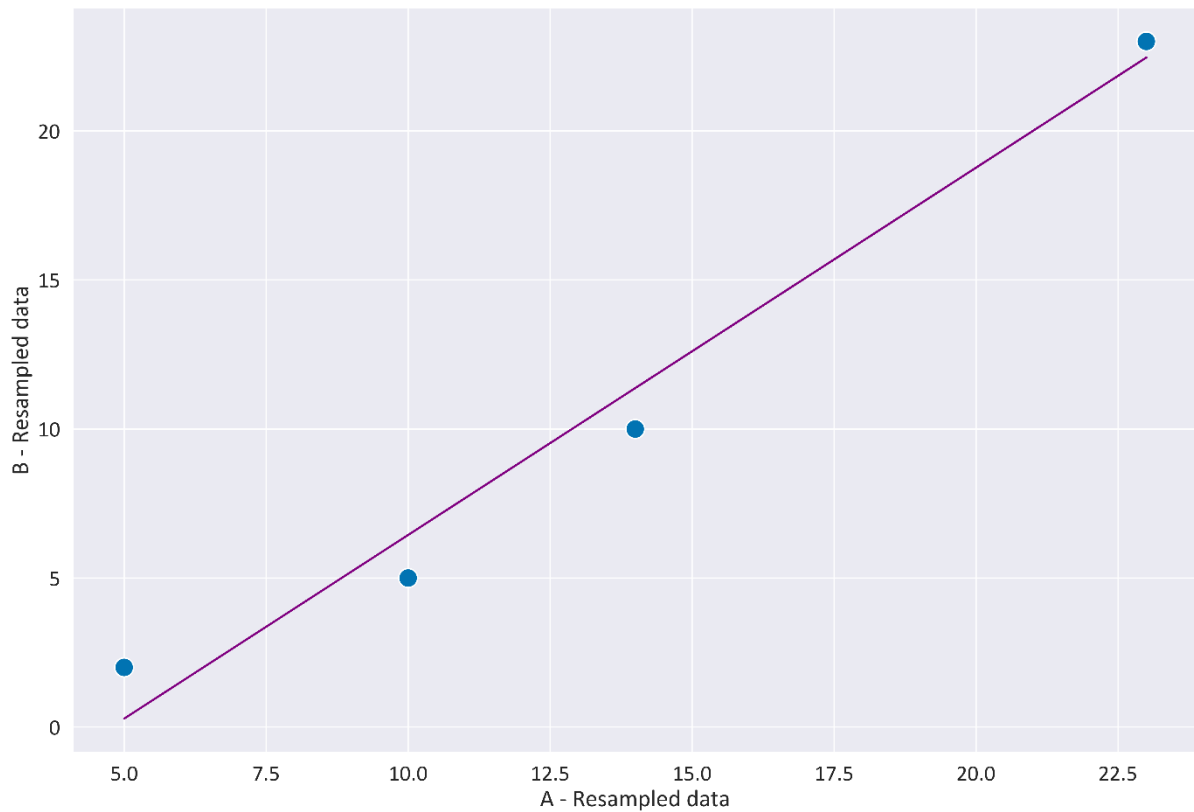


Figure D.4. The resampled data, with a linear trendline through the data points.

As can be seen from Figure D.3 and Figure D.4 the slope derived from the data changes; becoming steeper with the presence of 'outlier' points (the 'marble' with 23,23 on, was drawn twice, and thus this higher point changes the shape of the slope).

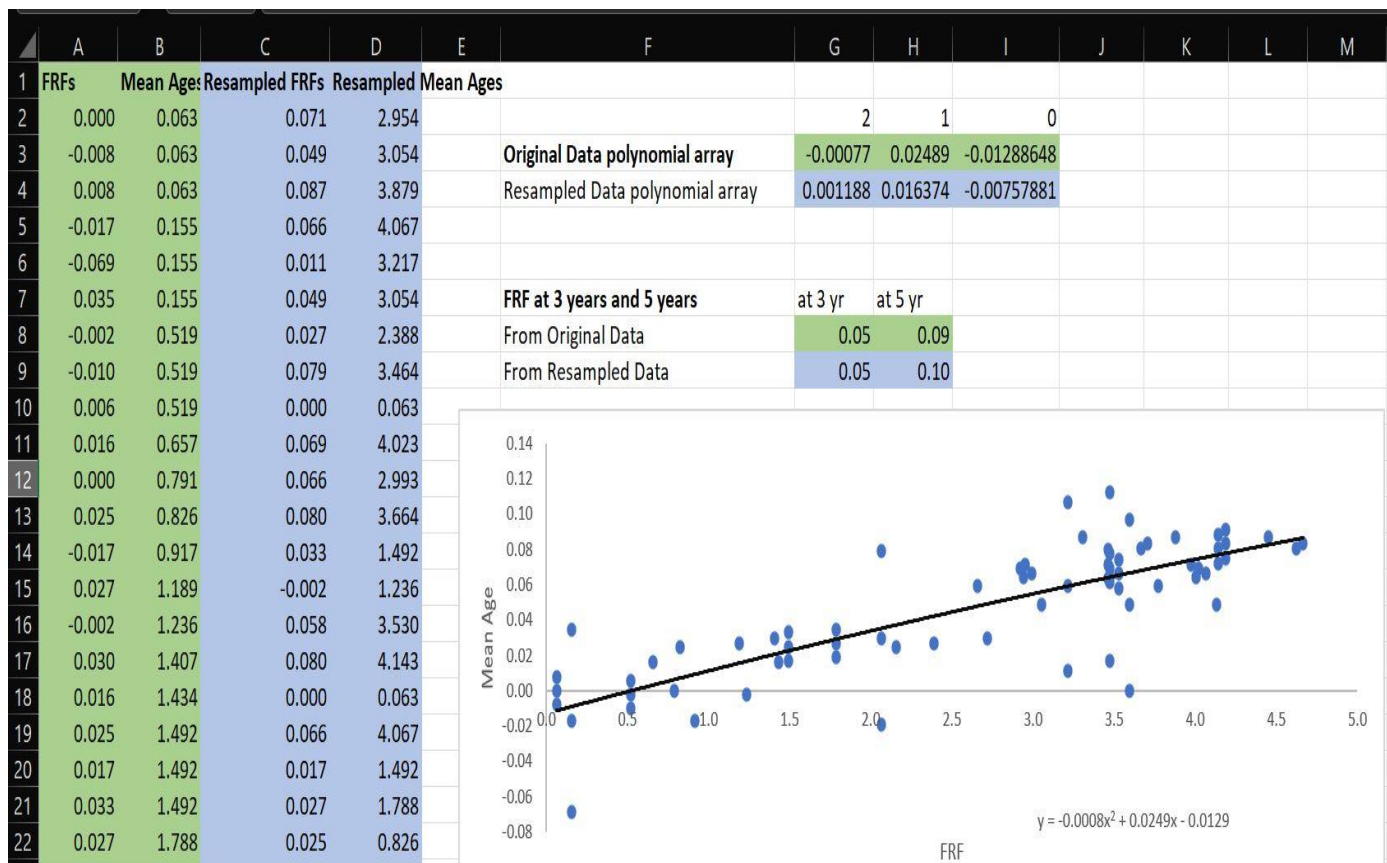


Figure D.5. The initial layout of the bootstrap excel sheet, using CFC-115 FRF and Mean Age data from the 2009 Oberpfaffenhofen campaign. 'Original data' highlighted in green, while the 'resampled data' highlighted in blue. Shows the top portion of both the original dataset and the resampled dataset. Also shows the 2<sup>nd</sup> order polynomial array derived for each dataset, and the 3<sup>rd</sup> and 5<sup>th</sup> year FRFs predicted from these arrays. The original data can also be seen plotted with the 2<sup>nd</sup> order polynomial trendline.

The data in Figure D.5 is a dataset from Chapter 3 and features an abbreviated segment of CFC-115 FRF and Mean Age data from the 2009 Oberpfaffenhofen campaign. The method can however be applied to many other datasets. The original data is placed in columns A and B (highlighted green), and the LINEST function used to calculate the equation of a 2<sup>nd</sup> order polynomial trendline of FRFs (x) plotted against Mean Ages (y), with results shown in cells G3-I3 (highlighted in green). The bootstrapping program performed a 'resampling with replacement' of the original dataset, randomly selecting a pair of FRF and Mean Age (so for example an FRF of 0.08 paired with a Mean Age of 4.6) for 'resampling', and that each pair is equally likely to be selected. As this is resampling with replacement, some pairs from the original sample may not appear, and others may appear more than once. This 'resample' is placed in columns C and D (highlighted blue), which effectively samples from an infinite population with the same distribution (pattern) as the original sample. The 2<sup>nd</sup> order

polynomial trendline for the 'resample' data appears in cells G4-I4 (highlighted blue), and this will change with each 'resampling'. This resampling was done 2000 times, meaning the polynomial array was derived 2000 times.

Using the polynomial trendline for the original and resampled datasets, I then derive the FRF at 3 and 5 years mean ages, these are shown in cells G8-H8 for the original dataset, and G9-H9 for the resampled dataset. As the resampling is repeated 2000 times, the values in G9 and H9 change to reflect the new trendline for the resampled data. The bootstrapping program 'watched' the cells G9 and H9, and recorded those results, along with how often each result occurred. For example a FRF at 3 years mean age of 0.056 might occur 209 times while a FRF at 3 years mean age of 0.04 might occur 2 times.

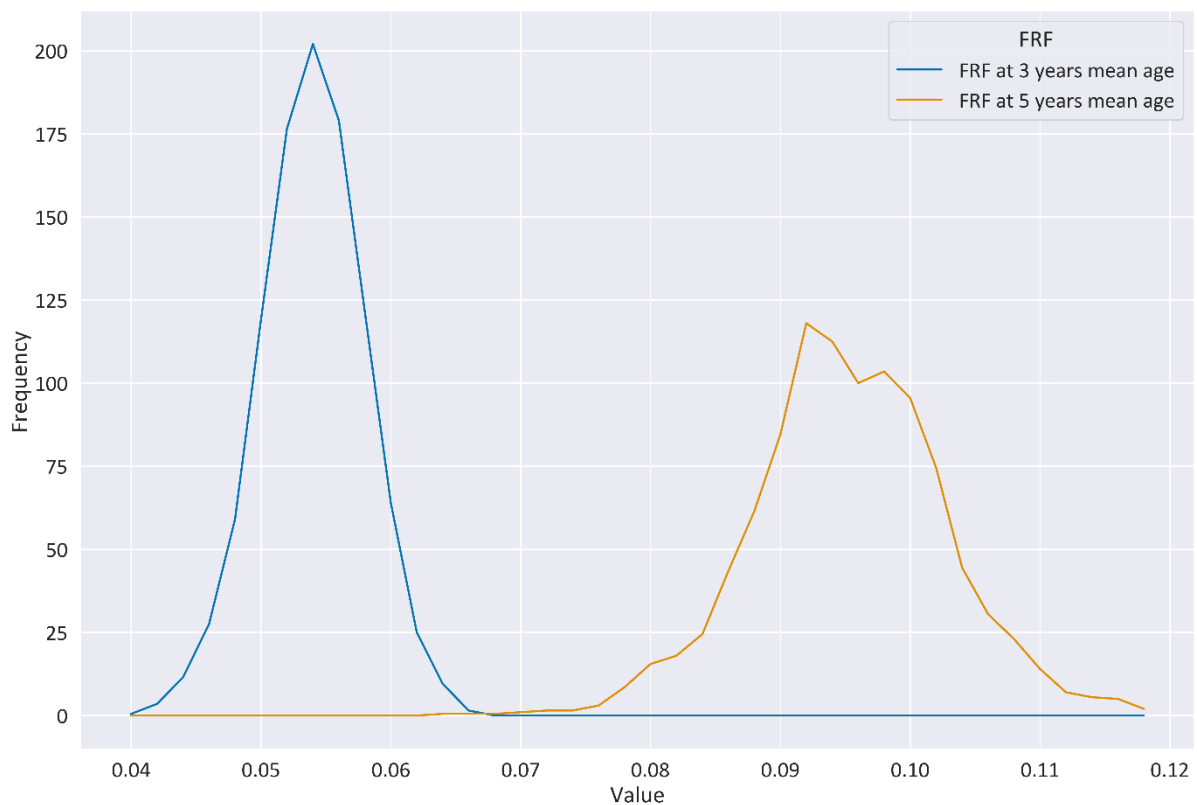


Figure D.6. A plot of the relative distribution of FRFs at 3 and 5 years mean age, these are the results from resampling of the original data.

As can be seen from Figure D.6 the results for 3 years mean age show that the bulk of the predicted FRFs fall around 0.056, and results that are higher or lower, occur with decreasing frequency. Resampling with replacement occurred 2000 times however, so a small number of results will be abnormally high or low. It was therefore necessary to exclude

extreme outliers and after some experimentation I found that excluding the highest and lowest 2.5% would most reliably removed extreme outliers while retaining an accurate distribution. From this I derived mean values, using the spread of values (see the distribution in Figure D.6) to give a measure of uncertainty.

## Bibliography

Abalos, M. *et al.* (2021) 'The Brewer-Dobson circulation in CMIP6', *Atmospheric Chemistry and Physics*, 21(17), pp. 13571–13591. Available at: <https://doi.org/10.5194/acp-21-13571-2021>.

Abalos, M. and de la Cámara, A. (2020) 'Twenty-First Century Trends in Mixing Barriers and Eddy Transport in the Lower Stratosphere', *Geophysical Research Letters*, 47(21). Available at: <https://doi.org/10.1029/2020GL089548>.

Abbatt, J.P.D. and Molina, M.J. (1992a) 'Heterogeneous interactions of nitryl hypochlorite and hydrogen chloride on nitric acid trihydrate at 202 K', *The Journal of Physical Chemistry*, 96(19), pp. 7674–7679. Available at: <https://doi.org/10.1021/j100198a036>.

Abbatt, J.P.D. and Molina, M.J. (1992b) 'The heterogeneous reaction of HOCl + HCl → Cl<sub>2</sub> + H<sub>2</sub>O on ice and nitric acid trihydrate: Reaction probabilities and stratospheric implications', *Geophysical Research Letters*, 19(5), pp. 461–464. Available at: <https://doi.org/10.1029/92GL00373>.

Adcock, K.E. *et al.* (2018) 'Continued increase of CFC-113a (CCl<sub>3</sub>CF<sub>3</sub>) mixing ratios in the global atmosphere: Emissions, occurrence and potential sources', *Atmospheric Chemistry and Physics*, 18(7), pp. 4737–4751. Available at: <https://doi.org/10.5194/acp-18-4737-2018>.

Adcock, K.E. *et al.* (2020) 'Investigation of East Asian Emissions of CFC-11 Using Atmospheric Observations in Taiwan', *Environmental Science & Technology*, 54(7), pp. 3814–3822. Available at: <https://doi.org/10.1021/acs.est.9b06433>.

Adcock, K.E. *et al.* (2021) 'Aircraft-Based Observations of Ozone-Depleting Substances in the Upper Troposphere and Lower Stratosphere in and Above the Asian Summer Monsoon', *Journal of Geophysical Research: Atmospheres*, 126(1). Available at: <https://doi.org/10.1029/2020JD033137>.

Andersen, T. *et al.* (2018) 'A UAV-based active AirCore system for measurements of greenhouse gases', *Atmospheric Measurement Techniques*, 11(5), pp. 2683–2699. Available at: <https://doi.org/10.5194/amt-11-2683-2018>.

Andrews, A.E. *et al.* (2001) 'Mean ages of stratospheric air derived from in situ observations of CO<sub>2</sub>, CH<sub>4</sub>, and N<sub>2</sub>O', *Journal of Geophysical Research Atmospheres*, 106(D23), pp. 32295–32314. Available at: <https://doi.org/10.1029/2001JD000465>.

Archibald, A.T. *et al.* (2015) 'Long-term high frequency measurements of ethane, benzene and methyl chloride at Ragged Point, Barbados: Identification of long-range transport events', *Elementa*, 3. Available at: <https://doi.org/10.12952/journal.elementa.000068>.

Ashford, P. *et al.* (2004a) 'Emission profiles from the foam and refrigeration sectors comparison with atmospheric concentrations. Part 1: Methodology and data', in *International Journal of Refrigeration*. Elsevier Ltd, pp. 687–700. Available at: <https://doi.org/10.1016/j.ijrefrig.2004.07.025>.

Ashford, P. *et al.* (2004b) 'Emission profiles from the foam and refrigeration sectors comparison with atmospheric concentrations. Part 2: Results and discussion', in *International Journal of Refrigeration*. Elsevier Ltd, pp. 701–716. Available at: <https://doi.org/10.1016/j.ijrefrig.2004.08.003>.

Baasandorj, M. *et al.* (2013) 'O(1D) kinetic study of key ozone depleting substances and greenhouse gases', *Journal of Physical Chemistry A*, 117(12), pp. 2434–2445. Available at: <https://doi.org/10.1021/jp312781c>.

Bacmeister, J.T. *et al.* (1995) 'Descent of long-lived trace gases in the winter polar vortex', *Journal of Geophysical Research*, 100(D6), p. 11669. Available at: <http://doi.wiley.com/10.1029/94JD02958>.

Barreto & Howland (2010) '*Introductory Econometrics: Using Monte Carlo Simulation with Microsoft Excel Add-In*', Cambridge University Press; Har/Cdr edition. Available online at: <http://www3.wabash.edu/econometrics>. Cambridge University Press. Available at: <http://www3.wabash.edu/econometrics>.

Battle, M. *et al.* (1996) 'Atmospheric gas concentrations over the past century measured in air from firn at the South Pole', *Nature*, 383(6597), pp. 231–235. Available at: <https://doi.org/10.1038/383231a0>.

Benish, S.E. *et al.* (2021) 'Airborne Observations of CFCs Over Hebei Province, China in Spring 2016', *Journal of Geophysical Research: Atmospheres*, 126(18). Available at: <https://doi.org/10.1029/2021JD035152>.

Bergamaschi, P. *et al.* (2009) 'Inverse modeling of global and regional CH<sub>4</sub> emissions using SCIAMACHY satellite retrievals', *Journal of Geophysical Research Atmospheres*, 114(22). Available at: <https://doi.org/10.1029/2009JD012287>.

Bernhard, G.H. *et al.* (2020) 'Record-Breaking Increases in Arctic Solar Ultraviolet Radiation Caused by Exceptionally Large Ozone Depletion in 2020', *Geophysical Research Letters*, 47(24). Available at: <https://doi.org/10.1029/2020GL090844>.

Bhartia, P.K. and McPeters, R.D. (2018) 'The discovery of the Antarctic Ozone Hole', *Comptes Rendus - Geoscience*, 350(7), pp. 335–340. Available at: <https://doi.org/10.1016/j.crte.2018.04.006>.

Birner, T. and Bönisch, H. (2011) 'Residual circulation trajectories and transit times into the extratropical lowermost stratosphere', *Atmospheric Chemistry and Physics*, 11(2), pp. 817–827. Available at: <https://doi.org/10.5194/acp-11-817-2011>.

Boering, K.A. *et al.* (1994) 'Tracer-tracer relationships and lower stratospheric dynamics: CO<sub>2</sub> and N<sub>2</sub>O correlations during SPADE', *Geophysical Research Letters*, 21(23), pp. 2567–2570. Available at: <https://doi.org/10.1029/94GL01985>.

Bönisch, H. *et al.* (2009) 'Quantifying transport into the lowermost stratosphere using simultaneous in-situ measurements of SF<sub>6</sub> and CO<sub>2</sub>', *Atmospheric Chemistry and Physics*, 9(16), pp. 5905–5919. Available at: <https://doi.org/10.5194/acp-9-5905-2009>.

Bönisch, H. *et al.* (2011) 'On the structural changes in the Brewer-Dobson circulation after 2000', *Atmospheric Chemistry and Physics*, 11(8), pp. 3937–3948. Available at: <https://doi.org/10.5194/acp-11-3937-2011>.

Bourguet, S. and Lickley, M. (2024) 'Bayesian modeling of HFC production pipeline suggests growth in unreported CFC by-product and feedstock production Bayesian modeling of HFC production pipeline suggests growth 1 in unreported CFC by-product and feedstock production 2'. Available at: <https://doi.org/10.21203/rs.3.rs-4718479/v1>.

Brewer, A.W. (1949) 'Evidence for a world circulation provided by the measurements of helium and water vapour distribution in the stratosphere', *Quarterly Journal of the Royal Meteorological Society*, 75(326), pp. 351–363.

Brown, A.T. *et al.* (2013) 'Stratospheric lifetimes of CFC-12, CCl<sub>4</sub>, CH<sub>4</sub>, CH<sub>3</sub>Cl and N<sub>2</sub>O from measurements made by the Atmospheric Chemistry Experiment-Fourier Transform Spectrometer (ACE-FTS)', *Atmospheric Chemistry and Physics*, 13(14), pp. 6921–6950. Available at: <https://doi.org/10.5194/acp-13-6921-2013>.

Bunzel, F. and Schmidt, H. (2013) 'The brewer-dobson circulation in a changing climate: Impact of the model configuration', *Journal of the Atmospheric Sciences*, 70(5), pp. 1437–1455. Available at: <https://doi.org/10.1175/JAS-D-12-0215.1>.

Burkholder, J.B. *et al.* (2020) 'Chemical Kinetics and Photochemical Data for Use in Atmospheric Studies, Evaluation No. 19', *JPL Publications 19-5*, (19), pp. 1–153. Available at: <http://jpldataeval.jpl.nasa.gov/>.

Burkholder, J.B. and Hodnebrog, Ø. (2022) 'ANNEX - Summary of Abundances, Lifetimes, ODPs, REs, GWPs, and GTPs', *World Meteorological Organization (WMO). Scientific Assessment of Ozone Depletion: 2022, GAW Report No. 278*,. Geneva. Available at: <https://ozone.unep.org/science/assessment/sap> (Accessed: 11 June 2024).

Butchart, N. *et al.* (2006) 'Simulations of anthropogenic change in the strength of the Brewer-Dobson circulation', *Climate Dynamics*, 27(7–8), pp. 727–741. Available at: <https://doi.org/10.1007/s00382-006-0162-4>.

Butchart, N. *et al.* (2010) 'Chemistry-climate model simulations of twenty-first century stratospheric climate and circulation changes', *Journal of Climate*, 23(20), pp. 5349–5374. Available at: <https://doi.org/10.1175/2010JCLI3404.1>.

Butchart, N. (2014) 'The Brewer-Dobson circulation', *Reviews of Geophysics*, 52(2), pp. 157–184. Available at: <https://doi.org/10.1002/2013RG000448>.

Byrne, B. *et al.* (2020) 'Improved Constraints on Northern Extratropical CO<sub>2</sub> Fluxes Obtained by Combining Surface-Based and Space-Based Atmospheric CO<sub>2</sub> Measurements', *Journal of Geophysical Research: Atmospheres*, 125(15). Available at: <https://doi.org/10.1029/2019JD032029>.

Cantrell, C.A. (2008) 'Technical Note: Review of methods for linear least-squares fitting of data and application to atmospheric chemistry problems', *Atmospheric Chemistry and Physics*, 8(17), pp. 5477–5487. Available at: <https://doi.org/10.5194/acp-8-5477-2008>.

Carpenter, L. and Daniel, J.S. (2018) 'Chapter 6, Scenarios and Information for Policymakers', *Scientific Assessment of Ozone Depletion: 2018, Global Ozone Research and Monitoring Project, World Meteorological Organization, Geneva, Switzerland*, Report no. Available at: <http://ozone.unep.org/science/assessment/sap>.

Carpenter, L.J. *et al.* (2014) 'World Meteorological Organization (WMO)-Update on Ozone-Depleting Substances ( ODSs ) and Other Gases of Interest to the Montreal Protocol,

Chapter 1 in Scientific Assessment of Ozone Depletion: 2014, Global Ozone Research and Monitoring Project-Report No', *World Meteorological Organization*, p. 416.

Chen, X., Huang, X. and Strow, L.L. (2020) 'Near-Global CFC-11 Trends as Observed by Atmospheric Infrared Sounder From 2003 to 2018', *Journal of Geophysical Research: Atmospheres*, 125(22). Available at: <https://doi.org/10.1029/2020JD033051>.

Chevallier, F. *et al.* (2017) 'Probabilistic global maps of the CO<sub>2</sub> column at daily and monthly scales from sparse satellite measurements', *Journal of Geophysical Research*, 122(14), pp. 7614–7629. Available at: <https://doi.org/10.1002/2017JD026453>.

Chevallier, F. *et al.* (2019) 'Objective evaluation of surface- and satellite-driven carbon dioxide atmospheric inversions', *Atmospheric Chemistry and Physics*, 19(22), pp. 14233–14251. Available at: <https://doi.org/10.5194/acp-19-14233-2019>.

Chipperfield, M.P. *et al.* (2014) 'Multimodel estimates of atmospheric lifetimes of long-lived ozone-depleting substances: Present and future', *Journal of Geophysical Research*, 119(5), pp. 2555–2573. Available at: <https://doi.org/10.1002/2013JD021097>.

Chipperfield, M.P. *et al.* (2017) 'Detecting recovery of the stratospheric ozone layer', *Nature*, 549(7671), pp. 211–218. Available at: <https://doi.org/10.1038/nature23681>.

Cicerone, R.J. (1979) 'Atmospheric carbon tetrafluoride: A nearly inert gas', *Science*, 206(4414), pp. 59–61. Available at: <https://doi.org/10.1126/science.206.4414.59>.

Considine, D.B., Douglass, A.R. and Jackman, C.H. (1994) 'Effects of a polar stratospheric cloud parameterization on ozone depletion due to stratospheric aircraft in a two-dimensional model', *Journal of Geophysical Research*, 99(D9). Available at: <https://doi.org/10.1029/94jd01026>.

Crutzen, P.J. and Arnold, F. (1986) 'Nitric acid cloud formation in the cold Antarctic stratosphere: a major cause for the springtime "ozone hole"', *Nature*, 324(6098), pp. 651–655. Available at: <https://doi.org/10.1038/324651a0>.

Daniel, J.S. *et al.* (1996) 'On the age of stratospheric air and inorganic chlorine and bromine release', *Journal of Geophysical Research: Atmospheres*, 101(D11), pp. 16757–16770. Available at: <https://doi.org/10.1029/96JD01167>.

Daniel, J.S., *et al.* (2022) 'Chapter 7: Scenarios and Information for Policymakers' *Scientific Assessment of Ozone Depletion: 2022, GAW Report No. 278*,. Geneva.

Daniel, J.S., Solomon, S. and Albritton, D.L. (1995) 'On the evaluation of halocarbon radiative forcing and global warming potentials', *Journal of Geophysical Research: Atmospheres*, 100(D1), pp. 1271–1285. Available at: <https://doi.org/10.1029/94JD02516>.

Davis, M.E. *et al.* (2016) 'UV and infrared absorption spectra, atmospheric lifetimes, and ozone depletion and global warming potentials for CCl<sub>2</sub>FCCl<sub>2</sub>F (CFC-112), CCl<sub>3</sub>CClF<sub>2</sub> (CFC-112a), CCl<sub>3</sub>CF<sub>3</sub> (CFC-113a), and CCl<sub>2</sub>FCF<sub>3</sub> (CFC-114a)', *Atmospheric Chemistry and Physics*, 16(12), pp. 8043–8052. Available at: <https://doi.org/10.5194/acp-16-8043-2016>.

Dee, D.P. *et al.* (2011) 'The ERA-Interim reanalysis: Configuration and performance of the data assimilation system', *Quarterly Journal of the Royal Meteorological Society*, 137(656), pp. 553–597. Available at: <https://doi.org/10.1002/QJ.828>.

Diallo, M., Legras, B. and Chédin, A. (2012) 'Age of stratospheric air in the ERA-Interim', *Atmospheric Chemistry and Physics*, 12(24), pp. 12133–12154. Available at: <https://doi.org/10.5194/acp-12-12133-2012>.

Dobson, G. (1956) 'Origin and distribution of the polyatomic molecules in the atmosphere', *Proceedings of the Royal Society of London. Series A. Mathematical and Physical Sciences*, 236(1205), pp. 187–193. Available at: <https://doi.org/10.1098/rspa.1956.0127>.

Dobson, G.M.B., Harrison, D.N. and Lawrence, J. (1927) 'Measurements of the amount of ozone in the Earth's atmosphere and its relation to other geophysical conditions.— part II', *Proceedings of the Royal Society of London, Series A C*(122(790)), pp. 456–486.

Douglass, A.R. *et al.* (2008) 'Relationship of loss, mean age of air and the distribution of CFCs to stratospheric circulation and implications for atmospheric lifetimes', *Journal of Geophysical Research Atmospheres*, 113(14). Available at: <https://doi.org/10.1029/2007JD009575>.

Dubovik, O. *et al.* (2021) 'Grand Challenges in Satellite Remote Sensing', *Frontiers in Remote Sensing*, 2(February), pp. 1–10. Available at: <https://doi.org/10.3389/frsen.2021.619818>.

Engel, A. *et al.* (2002) 'Temporal development of total chlorine in the high-latitude stratosphere based on reference distributions of mean age derived from CO<sub>2</sub> and SF<sub>6</sub>', *Journal of Geophysical Research: Atmospheres*, 107(12). Available at: <https://doi.org/10.1029/2001jd000584>.

Engel, A. *et al.* (2006) 'Observation of mesospheric air inside the arctic stratospheric polar vortex in early 2003', *Atmospheric Chemistry and Physics*, 6(1), pp. 267–282. Available at: <https://doi.org/10.5194/ACP-6-267-2006>.

Engel, A. *et al.* (2009) 'Age of stratospheric air unchanged within uncertainties over the past 30 years', *Nature Geoscience*, 2(1), pp. 28–31. Available at: <https://doi.org/10.1038/ngeo388>.

Engel, A. *et al.* (2017) 'Mean age of stratospheric air derived from AirCore observations', *Atmospheric Chemistry and Physics*, 17(11), pp. 6825–6838. Available at: <https://doi.org/10.5194/acp-17-6825-2017>.

Engel, A. *et al.* (2018a) 'A refined method for calculating equivalent effective stratospheric chlorine', *Atmospheric Chemistry and Physics*, 18(2), pp. 601–619. Available at: <https://doi.org/10.5194/acp-18-601-2018>.

Engel, A., *et al.* (2018b) *Update on Ozone-Depleting Substances (ODSs) and Other Gases of Interest to the Montreal Protocol, Chapter 1 in Scientific Assessment of Ozone Depletion: 2018*. Geneva.

ESSenCe - Earth Online (no date). Available at: <https://earth.esa.int/eogateway/campaigns/essence> (Accessed: 13 July 2023).

Fang, X. *et al.* (2016) 'Hydrofluorocarbon (HFC) Emissions in China: An Inventory for 2005-2013 and Projections to 2050', *Environmental Science and Technology*, 50(4), pp. 2027–2034. Available at: <https://doi.org/10.1021/acs.est.5b04376>.

Farman, J.C., Gardiner, B.G. and Shanklin, J.D. (1985) 'Large losses of total ozone in Antarctica', *Nature*, 315, pp. 207–210.

Fisher, D.A. and Midgley, P.M. (1993) *THE PRODUCTION AND RELEASE TO THE ATMOSPHERE OF CFCs 113, 114 and 115*, *Atmospheric Environment*.

Fleming, E.L. *et al.* (1999) 'Simulation of stratospheric tracers using an improved empirically based two-dimensional model transport formulation', *Journal of Geophysical Research: Atmospheres*, 104(D19), pp. 23911–23934. Available at: <https://doi.org/10.1029/1999JD900332>.

Fleming, E.L. *et al.* (2001) 'Sensitivity of tracers and a stratospheric aircraft perturbation to two-dimensional model transport variations', *Journal of Geophysical Research Atmospheres*, 106(D13), pp. 14245–14263. Available at: <https://doi.org/10.1029/2000JD900732>.

Fleming, E.L. *et al.* (2002) 'Two-dimensional model simulations of the QBO in ozone and tracers in the tropical stratosphere', *Journal of Geophysical Research Atmospheres*, 107(23), p. ACL 1-1-ACL 1-17. Available at: <https://doi.org/10.1029/2001JD001146>.

Fleming, E.L. *et al.* (2007) 'The impact of interannual variability on multidecadal total ozone simulations', *Journal of Geophysical Research Atmospheres*, 112(10), pp. 1–21. Available at: <https://doi.org/10.1029/2006JD007953>.

Fleming, E.L. *et al.* (2011) 'A model study of the impact of source gas changes on the stratosphere for 1850-2100', *Atmospheric Chemistry and Physics*, 11(16), pp. 8515–8541. Available at: <https://doi.org/10.5194/ACP-11-8515-2011>.

Fleming, E.L. *et al.* (2015) 'The impact of current CH<sub>4</sub> and N<sub>2</sub>O atmospheric loss process uncertainties on calculated ozone abundances and trends', *Journal of Geophysical Research*, 120(10), pp. 5267–5293. Available at: <https://doi.org/10.1002/2014JD022067>.

Fleming, E.L. *et al.* (2020) 'The Impact of Continuing CFC-11 Emissions on Stratospheric Ozone', *Journal of Geophysical Research: Atmospheres*, 125(3), pp. 1–19. Available at: <https://doi.org/10.1029/2019JD031849>.

Fritsch, F. *et al.* (2020) 'Sensitivity of age of air trends to the derivation method for non-linear increasing inert SF<sub>6</sub>', *Atmospheric Chemistry and Physics*, 20(14), pp. 8709–8725. Available at: <https://doi.org/10.5194/acp-20-8709-2020>.

Fu, Q. *et al.* (2019) 'Observed changes in Brewer-Dobson circulation for 1980-2018', *Environmental Research Letters*, 14(11). Available at: <https://doi.org/10.1088/1748-9326/ab4de7>.

Garcia, R.R. and Randel, W.J. (2008) 'Acceleration of the brewer-dobson circulation due to increases in greenhouse gases', *Journal of the Atmospheric Sciences*, 65(8), pp. 2731–2739. Available at: <https://doi.org/10.1175/2008JAS2712.1>.

Garny, H. *et al.* (2024a) 'Age of Stratospheric Air: Progress on Processes, Observations, and Long-Term Trends', *Reviews of Geophysics*. John Wiley and Sons Inc. Available at: <https://doi.org/10.1029/2023RG000832>.

Garny, H. *et al.* (2024b) 'Correction of stratospheric age of air (AoA) derived from sulfur hexafluoride (SF<sub>6</sub>) for the effect of chemical sinks', *Atmospheric Chemistry and Physics*, 24(7), pp. 4193–4215. Available at: <https://doi.org/10.5194/acp-24-4193-2024>.

Gelaro, R. *et al.* (2017) 'The modern-era retrospective analysis for research and applications, version 2 (MERRA-2)', *Journal of Climate*, 30(14), pp. 5419–5454. Available at: <https://doi.org/10.1175/JCLI-D-16-0758.1>.

Gerken, T. *et al.* (2021) 'Examining CO<sub>2</sub> Model Observation Residuals Using ACT-America Data', *Journal of Geophysical Research: Atmospheres*, 126(18). Available at: <https://doi.org/10.1029/2020JD034481>.

Girschikofsky, M. *et al.* (2019) 'Optical sensor for real-time detection of trichlorofluoromethane', *Sensors (Switzerland)*, 19(3). Available at: <https://doi.org/10.3390/s19030632>.

Graziosi, F. *et al.* (2015) 'European emissions of HCFC-22 based on eleven years of high frequency atmospheric measurements and a Bayesian inversion method', *Atmospheric Environment*, 112, pp. 196–207. Available at: <https://doi.org/10.1016/j.atmosenv.2015.04.042>.

Grooß, J. -U. *et al.* (2002) 'Simulation of ozone depletion in spring 2000 with the Chemical Lagrangian Model of the Stratosphere (CLaMS)', *Journal of Geophysical Research: Atmospheres*, 107(D20). Available at: <https://doi.org/10.1029/2001JD000456>.

Hall, T.M. (2000) 'Path histories and timescales in stratospheric transport: Analysis of an idealized model', *Journal of Geophysical Research Atmospheres*, 105(D18), pp. 22811–22823. Available at: <https://doi.org/10.1029/2000JD900329>.

Hall, T.M. and Plumb, R.A. (1994) 'Age as a diagnostic of stratospheric transport', *Journal of Geophysical Research: Atmospheres*, 99(D1), pp. 1059–1070. Available at: <https://doi.org/10.1029/93JD03192>.

Hardiman, S.C., Butchart, N. and Calvo, N. (2014) 'The morphology of the Brewer-Dobson circulation and its response to climate change in CMIP5 simulations', *Quarterly Journal of the Royal Meteorological Society*, 140(683), pp. 1958–1965. Available at: <https://doi.org/10.1002/qj.2258>.

Harnisch, J. *et al.* (1996) 'Tropospheric trends for CF<sub>4</sub> and C<sub>2</sub>F<sub>6</sub> since 1982 derived from SF<sub>6</sub> dated stratospheric air', *Geophysical Research Letters*, 23(10), pp. 1099–1102. Available at: <https://doi.org/10.1029/96GL01198>.

Hartley, D. and Prinn, R. (1993) 'Feasibility of determining surface emissions of trace gases using an inverse method in a three-dimensional chemical transport model', *Journal of*

*Geophysical Research*, 98(D3), pp. 5183–5197. Available at:

<https://doi.org/10.1029/92JD02594>.

von Hobe, M. *et al.* (2013) 'Reconciliation of essential process parameters for an enhanced predictability of Arctic stratospheric ozone loss and its climate interactions (RECONCILE): activities and results', *Atmospheric Chemistry and Physics*, 13(18), pp. 9233–9268. Available at: <https://doi.org/10.5194/acp-13-9233-2013>.

Holton, JR. (1990) 'On the Global Exchange of Mass between the Stratosphere and Troposphere', *J. Atmos. Sci*, 47, pp. 392–395. Available at:

[https://doi.org/https://doi.org/10.1175/1520-0469\(1990\)047<0392:OTGEOM>2.0.CO;2](https://doi.org/https://doi.org/10.1175/1520-0469(1990)047<0392:OTGEOM>2.0.CO;2).

Holton, J.R. *et al.* (1995) 'Stratosphere-troposphere exchange', *Reviews of Geophysics*, 33(4), pp. 403–439. Available at: <https://doi.org/10.1029/95RG02097>.

Hottmann, B. *et al.* (2020) 'Impact of the South Asian monsoon outflow on atmospheric hydroperoxides in the upper troposphere', *Atmospheric Chemistry and Physics*, 20(21), pp. 12655–12673. Available at: <https://doi.org/10.5194/acp-20-12655-2020>.

Huang, X. *et al.* (2021) 'Constraining Emission Estimates of CFC-11 in Eastern China Based on Local Observations at Surface Stations and Mount Tai', *Environmental Science & Technology Letters*, 8(11), pp. 940–946. Available at:

<https://doi.org/10.1021/acs.estlett.1c00539>.

Jackman, C.H. *et al.* (1996) 'Past, present, and future modeled ozone trends with comparisons to observed trends', *Journal of Geophysical Research Atmospheres*, 101(22), pp. 28753–28767. Available at: <https://doi.org/10.1029/96jd03088>.

Jackman, C.H. *et al.* (2016) 'Atmospheric changes caused by galactic cosmic rays over the period 1960-2010', *Atmospheric Chemistry and Physics*, 16(9), pp. 5853–5866. Available at: <https://doi.org/10.5194/acp-16-5853-2016>.

Johansson, S. *et al.* (2020) 'Pollution trace gas distributions and their transport in the Asian monsoon upper troposphere and lowermost stratosphere during the StratoClim campaign 2017', *Atmospheric Chemistry and Physics*, 20(23), pp. 14695–14715. Available at: <https://doi.org/10.5194/acp-20-14695-2020>.

John, J.G. *et al.* (2012) 'Climate versus emission drivers of methane lifetime against loss by tropospheric OH from 1860-2100', *Atmospheric Chemistry and Physics*, 12(24), pp. 12021–12036. Available at: <https://doi.org/10.5194/acp-12-12021-2012>.

Karion, A. *et al.* (2010) 'AirCore: An innovative atmospheric sampling system', *Journal of Atmospheric and Oceanic Technology*, 27(11), pp. 1839–1853. Available at: <https://doi.org/10.1175/2010JTECHA1448.1>.

Kim, J.J.H. *et al.* (2020) 'New era of air quality monitoring from space: Geostationary environment monitoring spectrometer (GEMS)', *Bulletin of the American Meteorological Society*, 101(1), pp. E1–E22. Available at: <https://doi.org/10.1175/BAMS-D-18-0013.1>.

Kindler, T.P. *et al.* (1995) 'The fate of atmospheric phosgene and the stratospheric chlorine loadings of its parent compounds: CCl<sub>4</sub>, C<sub>2</sub>Cl<sub>4</sub>, C<sub>2</sub>HCl<sub>3</sub>, CH<sub>3</sub>CCl<sub>3</sub>, and CHCl<sub>3</sub>', *Journal of Geophysical Research: Atmospheres*, 100(D1), pp. 1235–1251. Available at: <https://doi.org/10.1029/94JD02518>.

Klonecki, A. *et al.* (2003) 'Seasonal changes in the transport of pollutants into the Arctic troposphere-model study', *Journal of Geophysical Research: Atmospheres*, 108(4). Available at: <https://doi.org/10.1029/2002jd002199>.

Kloss, C. *et al.* (2014) 'Atmospheric abundances, trends and emissions of CFC-216ba, CFC-216ca and HCFC-225ca', *Atmosphere*, 5(2), pp. 420–434. Available at: <https://doi.org/10.3390/atmos5020420>.

Ko, M.K.W. *et al.* (2013) 'SPARC Report N°6 (2013) Lifetimes of Stratospheric Ozone-Depleting Substances, Their Replacements, and Related Species', *SPARC Report*, No. 6, p. 256 pp. Available at: <http://www.sparc-climate.org/publications/sparc-reports/>.

Ko, M.K.W., Sze, N.D. and Weisenstein, D.K. (1991) 'Use of satellite data to constrain the model-calculated atmospheric lifetime for N<sub>2</sub>O: implications for other trace gases', *Journal of Geophysical Research*, 96(D4), pp. 7547–7552. Available at: <https://doi.org/10.1029/91JD00273>.

Konopka, P. *et al.* (2004) 'Mixing and ozone loss in the 1999-2000 Arctic vortex: Simulations with the three-dimensional Chemical Lagrangian Model of the Stratosphere (CLaMS)', *Journal of Geophysical Research: Atmospheres*, 109(2). Available at: <https://doi.org/10.1029/2003jd003792>.

Kouznetsov, R. *et al.* (2020) 'Simulating age of air and the distribution of SF<sub>6</sub> in the stratosphere with the SILAM model', *Atmospheric Chemistry and Physics*, 20(9), pp. 5837–5859. Available at: <https://doi.org/10.5194/acp-20-5837-2020>.

Kovács, T. *et al.* (2017) 'Determination of the atmospheric lifetime and global warming potential of sulfur hexafluoride using a three-dimensional model', *Atmospheric*

*Chemistry and Physics*, 17(2), pp. 883–898. Available at: <https://doi.org/10.5194/acp-17-883-2017>.

Lan, X. *et al.* (2017) 'Gradients of column CO<sub>2</sub> across North America from the NOAA Global Greenhouse Gas Reference Network', *Atmospheric Chemistry and Physics*, 17(24), pp. 15151–15165. Available at: <https://doi.org/10.5194/acp-17-15151-2017>.

Laube, J. *et al.* (2022) 'Chapter 1: Update On Ozone-Depleting Substances (ODSs) And Other Gases Of Interest To The Montreal Protocol', *Scientific Assessment of Ozone Depletion: 2022, GAW Report No. 278*. Geneva.

Laube, J.C. *et al.* (2008) 'Contribution of very short-lived organic substances to stratospheric chlorine and bromine in the tropics – a case study', *Atmospheric Chemistry and Physics*, 8(23), pp. 7325–7334. Available at: <https://doi.org/10.5194/acp-8-7325-2008>.

Laube, J.C. (2008) 'Determination of the distribution of halocarbons in the tropical upper troposphere and stratosphere', PhD.

Laube, J.C. *et al.* (2010) 'Fractional release factors of long-lived halogenated organic compounds in the tropical stratosphere', *Atmospheric Chemistry and Physics*, 10(3), pp. 1093–1103. Available at: <https://doi.org/10.5194/acp-10-1093-2010>.

Laube, J.C. *et al.* (2013) 'Observation-based assessment of stratospheric fractional release, lifetimes, and ozone depletion potentials of ten important source gases', *Atmospheric Chemistry and Physics*, 13(5), pp. 2779–2791. Available at: <https://doi.org/10.5194/acp-13-2779-2013>.

Laube, J.C. *et al.* (2014) 'Newly detected ozone-depleting substances in the atmosphere', *Nature Geoscience*, 7(4), pp. 266–269. Available at: <https://doi.org/10.1038/ngeo2109>.

Laube, J.C. *et al.* (2016) 'Tropospheric observations of CFC-114 and CFC-114a with a focus on long-term trends and emissions', *Atmospheric Chemistry and Physics*, 16(23), pp. 15347–15358. Available at: <https://doi.org/10.5194/acp-16-15347-2016>.

Laube, J.C. *et al.* (2020) 'Investigating stratospheric changes between 2009 and 2018 with halogenated trace gas data from aircraft, AirCores, and a global model focusing on CFC-11', *Atmospheric Chemistry and Physics*, 20(16), pp. 9771–9782. Available at: <https://doi.org/10.5194/acp-20-9771-2020>.

Laube, J.C. *et al.* (2025) 'Vertical distribution of halogenated trace gases in the summer Arctic stratosphere determined by two independent in situ methods'. Available at: <https://doi.org/10.5194/egusphere-2024-4034>.

Lawrence, Z.D. *et al.* (2020) 'The Remarkably Strong Arctic Stratospheric Polar Vortex of Winter 2020: Links to Record-Breaking Arctic Oscillation and Ozone Loss', *Journal of Geophysical Research: Atmospheres*, 125(22). Available at: <https://doi.org/10.1029/2020JD033271>.

Lee, C. *et al.* (2011) 'SO<sub>2</sub> emissions and lifetimes: Estimates from inverse modeling using in situ and global, space-based (SCIAMACHY and OMI) observations', *Journal of Geophysical Research Atmospheres*, 116(6). Available at: <https://doi.org/10.1029/2010JD014758>.

Lee, K.O. *et al.* (2021) 'Convective uplift of pollution from the Sichuan Basin into the Asian monsoon anticyclone during the StratoClim aircraft campaign', *Atmospheric Chemistry and Physics*, 21(5), pp. 3255–3274. Available at: <https://doi.org/10.5194/acp-21-3255-2021>.

Leedham-Elvidge, E. *et al.* (2018) 'Evaluation of stratospheric age of air from CF<sub>4</sub>, C<sub>2</sub>F<sub>6</sub>, C<sub>3</sub>F<sub>8</sub>, CHF<sub>3</sub>, HFC-125, HFC-227ea and SF<sub>6</sub>; Implications for the calculations of halocarbon lifetimes, fractional release factors and ozone depletion potentials', *Atmospheric Chemistry and Physics*, 18(5), pp. 3369–3385. Available at: <https://doi.org/10.5194/acp-18-3369-2018>.

Li, J. *et al.* (2023) 'A novel, cost-effective analytical method for measuring high-resolution vertical profiles of stratospheric trace gases using a gas chromatograph coupled with an electron capture detector', *Atmospheric Measurement Techniques*, 16(11), pp. 2851–2863. Available at: <https://doi.org/10.5194/amt-16-2851-2023>.

Li, S. *et al.* (2017) 'Emission estimates of methyl chloride from industrial sources in China based on high frequency atmospheric observations', *Journal of Atmospheric Chemistry*, 74(2), pp. 227–243. Available at: <https://doi.org/10.1007/s10874-016-9354-4>.

Liang, Q.; Newman, P.A.; and Reimann, S. (2016) 'SPARC Report on the Mystery of Carbon Tetrachloride'. Available at: <https://doi.org/10.3929/ethz-a-010690647>.

Lickley, M. *et al.* (2020) 'Quantifying contributions of chlorofluorocarbon banks to emissions and impacts on the ozone layer and climate', *Nature Communications*, 11(1). Available at: <https://doi.org/10.1038/s41467-020-15162-7>.

Lickley, M. *et al.* (2021) 'Joint inference of CFC lifetimes and banks suggests previously unidentified emissions', *Nature Communications*, 12(1). Available at: <https://doi.org/10.1038/s41467-021-23229-2>.

Lickley, M. *et al.* (2022) 'Bayesian assessment of chlorofluorocarbon (CFC), hydrochlorofluorocarbon (HCFC) and halon banks suggest large reservoirs still present in old equipment', (April), pp. 1–13.

Lickley, M.J. *et al.* (2024) 'The return to 1980 stratospheric halogen levels: A moving target in ozone assessments from 2006 to 2022', *EGUsphere [preprint]*, [Preprint]. Available at: <https://doi.org/10.5194/egusphere-2024-1289>.

Lin, P. and Fu, Q. (2013) 'Changes in various branches of the Brewer-Dobson circulation from an ensemble of chemistry climate models', *Journal of Geophysical Research Atmospheres*, 118(1), pp. 73–84. Available at: <https://doi.org/10.1029/2012JD018813>.

Lin, Y. *et al.* (2019) 'Observations of High Levels of Ozone-Depleting CFC-11 at a Remote Mountain-Top Site in Southern China', *Environmental Science & Technology Letters*, 6(3), pp. 114–118. Available at: <https://doi.org/10.1021/acs.estlett.9b00022>.

Loeffel, S. *et al.* (2022) 'The impact of sulfur hexafluoride (SF<sub>6</sub>) sinks on age of air climatologies and trends', *Atmospheric Chemistry and Physics*, 22(2), pp. 1175–1193. Available at: <https://doi.org/10.5194/acp-22-1175-2022>.

Long, D.A. *et al.* (2020) 'High-Accuracy Near-Infrared Carbon Dioxide Intensity Measurements to Support Remote Sensing', *Geophysical Research Letters*, 47(5). Available at: <https://doi.org/10.1029/2019GL086344>.

Lucas, R. *et al.* (2006) *Solar ultraviolet radiation : global burden of disease from solar ultraviolet radiation*. World Health Organization, Public Health and the Environment.

Luo, M. *et al.* (2013) 'Carbon monoxide (CO) vertical profiles derived from joined TES and MLS measurements', *Journal of Geophysical Research Atmospheres*, 118(18), pp. 10,601–10,613. Available at: <https://doi.org/10.1002/jgrd.50800>.

Mäder, J.A. *et al.* (2010) 'Evidence for the effectiveness of the Montreal Protocol to protect the ozone layer', *Atmospheric Chemistry and Physics*, 10(24), pp. 12161–12171. Available at: <https://doi.org/10.5194/acp-10-12161-2010>.

Martin Kaufmann *et al.* (2013) *ESSenCe-Final-Report*.

McCulloch, A. *et al.* (1999) 'Global emissions of hydrogen chloride and chloromethane from coal combustion, incineration and industrial activities: Reactive

Chlorine Emissions Inventory', *Journal of Geophysical Research Atmospheres*, 104(D7), pp. 8391–8403. Available at: <https://doi.org/10.1029/1999JD900025>.

McElroy, M.B., Salawitch, R.J. and Wofsy, S.C. (1986) 'Antarctic O3: Chemical mechanisms for the spring decrease', *Geophysical Research Letters*, 13(12), pp. 1296–1299. Available at: <https://doi.org/10.1029/GL013i012p01296>.

McKenna, D.S. *et al.* (2002a) 'A new Chemical Lagrangian Model of the Stratosphere (CLaMS) 1. Formulation of advection and mixing', *Journal of Geophysical Research: Atmospheres*, 107(D16). Available at: <https://doi.org/10.1029/2000JD000114>.

McKenna, D.S. *et al.* (2002b) 'A new Chemical Lagrangian Model of the Stratosphere (CLaMS) 2. Formulation of chemistry scheme and initialization', *Journal of Geophysical Research Atmospheres*, 107(15), p. ACH 4-1-ACH 4-14. Available at: <https://doi.org/10.1029/2000JD000113>.

McLandress, C. and Shepherd, T.G. (2009) 'Simulated anthropogenic changes in the Brewer-Dobson circulation, including its extension to high latitudes', *Journal of Climate*, 22(6), pp. 1516–1540. Available at: <https://doi.org/10.1175/2008JCLI2679.1>.

Mead, M.I. *et al.* (2008) 'Methyl halide emission estimates from domestic biomass burning in Africa', *Atmospheric Environment*, 42(21), pp. 5241–5250. Available at: <https://doi.org/10.1016/j.atmosenv.2008.02.066>.

Membrive, O. *et al.* (2017) 'AirCore-HR: A high-resolution column sampling to enhance the vertical description of CH<sub>4</sub> and CO<sub>2</sub>', *Atmospheric Measurement Techniques*, 10(6), pp. 2163–2181. Available at: <https://doi.org/10.5194/amt-10-2163-2017>.

Minschwaner, K. *et al.* (2012) 'Stratospheric loss and atmospheric lifetimes of CFC-11 Atmospheric Chemistry and Physics Discussions Stratospheric loss and atmospheric lifetimes of CFC-11 and CFC-12 derived from satellite observations Stratospheric loss and atmospheric lifetimes of CFC-11', *Atmos. Chem. Phys. Discuss*, 12, pp. 28733–28764. Available at: <https://doi.org/10.5194/acpd-12-28733-2012>.

Minschwaner, K., Salawitch, R.J. and McElroy, M.B. (1993) 'Absorption of solar radiation by O<sub>2</sub>: implications for O<sub>3</sub> and lifetimes of N<sub>2</sub>O, CFC13, and CF<sub>2</sub>Cl<sub>2</sub>', *Journal of Geophysical Research*, 98(D6). Available at: <https://doi.org/10.1029/93JD00223>.

Montzka, S.A. *et al.* (1999) 'Present and future trends in the atmospheric burden of ozone-depleting halogens', *Nature* 1999 398:6729, 398(6729), pp. 690–694. Available at: <https://doi.org/10.1038/19499>.

Montzka, S.A. *et al.* (2011) 'Small interannual variability of global atmospheric hydroxyl', *Science*, 331(6013), pp. 67–69. Available at: [https://doi.org/10.1126/SCIENCE.1197640/SUPPL\\_FILE/MONTZKA.SOM.PDF](https://doi.org/10.1126/SCIENCE.1197640/SUPPL_FILE/MONTZKA.SOM.PDF).

Montzka, S.A. *et al.* (2018) 'An unexpected and persistent increase in global emissions of ozone-depleting CFC-11', *Nature*, 557(7705), pp. 413–417. Available at: <https://doi.org/10.1038/s41586-018-0106-2>.

Montzka, S.A. *et al.* (2021) 'A decline in global CFC-11 emissions during 2018–2019', *Nature*, 590(7846), pp. 428–432. Available at: <https://doi.org/10.1038/s41586-021-03260-5>.

Moore, F.L. *et al.* (2003) 'Balloonborne in situ gas chromatograph for measurements in the troposphere and stratosphere', *Journal of Geophysical Research: Atmospheres*, 108(5). Available at: <https://doi.org/10.1029/2001jd000891>.

Moore, F.L. *et al.* (2014) 'A cost-effective trace gas measurement program for long-term monitoring of the stratospheric circulation', *Bulletin of the American Meteorological Society*, 95(1), pp. 147–155. Available at: <https://doi.org/10.1175/BAMS-D-12-00153.1>.

Morris, R.A. *et al.* (1995) *Effects of electron and ion reactions on atmospheric lifetimes of fully fluorinated compounds*, *JOURNAL OF GEOPHYSICAL RESEARCH*.

Mrozek, D.J. *et al.* (2016) 'Stratospheric Air Sub-sampler (SAS) and its application to analysis of I<sup>17</sup>O(CO<sub>2</sub>) from small air samples collected with an AirCore', *Atmospheric Measurement Techniques*, 9(11), pp. 5607–5620. Available at: <https://doi.org/10.5194/amt-9-5607-2016>.

Mühle, J. *et al.* (2010) 'Perfluorocarbons in the global atmosphere: Tetrafluoromethane, hexafluoroethane, and octafluoropropane', *Atmospheric Chemistry and Physics*, 10(11), pp. 5145–5164. Available at: <https://doi.org/10.5194/acp-10-5145-2010>.

Nakazawa, T. *et al.* (1995) 'Measurements of the stratospheric carbon dioxide concentration over Japan using a Balloon-borne cryogenic sampler', *Geophysical Research Letters*, 22(10), pp. 1229–1232. Available at: <https://doi.org/10.1029/95GL01188>.

National Oceanic and Atmospheric Administration (NOAA) Earth System Research Laboratory (ESRL) (2020) 'Combined Chlorofluorocarbon-113 data from # the NOAA/ESRL Global Monitoring Division'.

Neu, J.L. and Plumb, R.A. (1999) 'Age of air in a "leaky pipe" model of stratospheric transport', *Journal of Geophysical Research Atmospheres*, 104(D16), pp. 19243–19255. Available at: <https://doi.org/10.1029/1999JD900251>.

Newland, M.J. *et al.* (2013) 'Southern hemispheric halon trends and global halon emissions, 1978-2011', *Atmospheric Chemistry and Physics*, 13(11), pp. 5551–5565. Available at: <https://doi.org/10.5194/acp-13-5551-2013>.

Newman, P.A. *et al.* (2006) 'When will the Antarctic ozone hole recover?', *Geophysical Research Letters*, 33(12), pp. 1–5. Available at: <https://doi.org/10.1029/2005GL025232>.

Newman, P.A. *et al.* (2007) 'A new formulation of equivalent effective stratospheric chlorine (EESC)', *Atmospheric Chemistry and Physics*, 7(17), pp. 4537–4552. Available at: <https://doi.org/10.5194/ACP-7-4537-2007>.

NOAA (National Oceanic and Atmospheric Administration), NOAA/ESRL Global Monitoring Division. (2020). Available at: <https://gml.noaa.gov/hats/data.html>.

Oberländer, S., Langematz, U. and Meul, S. (2013) 'Unraveling impact factors for future changes in the Brewer-Dobson circulation', *Journal of Geophysical Research Atmospheres*, 118(18), pp. 10,296-10,312. Available at: <https://doi.org/10.1002/jgrd.50775>.

Oberländer-Hayn, S. *et al.* (2016) 'Is the Brewer-Dobson circulation increasing or moving upward?', *Geophysical Research Letters*, 43(4), pp. 1772–1779. Available at: <https://doi.org/10.1002/2015GL067545>.

Okamoto, K., Sato, K. and Akiyoshi, H. (2011) 'A study on the formation and trend of the Brewer-Dobson circulation', *Journal of Geophysical Research*, 116(D10), p. D10117. Available at: <https://doi.org/10.1029/2010JD014953>.

Olsen, M.A., Schoeberl, M.R. and Nielsen, J.E. (2007) 'Response of stratospheric circulation and stratosphere-troposphere exchange to changing sea surface temperatures', *Journal of Geophysical Research Atmospheres*, 112(16), pp. 1–8. Available at: <https://doi.org/10.1029/2006JD008012>.

Oman, L. *et al.* (2009) 'On the influence of anthropogenic forcings on changes in the stratospheric mean age', *Journal of Geophysical Research Atmospheres*, 114(3), pp. 1–15. Available at: <https://doi.org/10.1029/2008JD010378>.

Orkin, V.L., Kurylo, M.J. and Fleming, E.L. (2020) 'Atmospheric Lifetimes of Halogenated Hydrocarbons: Improved Estimations From an Analysis of Modeling Results',

*Journal of Geophysical Research: Atmospheres*, 125(16). Available at:

<https://doi.org/10.1029/2019JD032243>.

Ostermüller, J. *et al.* (2017) 'A new time-independent formulation of fractional release', *Atmospheric Chemistry and Physics*, 17(6), pp. 3788–3797. Available at:

<https://doi.org/10.5194/acp-17-3785-2017>.

Papanastasiou, D.K. *et al.* (2018) 'Global warming potential estimates for the C 1-C 3 hydrochlorofluorocarbons (HCFCs) included in the Kigali Amendment to the Montreal Protocol', *Atmos. Chem. Phys*, 18, pp. 6317–6330. Available at: <https://doi.org/10.5194/acp-18-6317-2018>.

Park, S. *et al.* (2021) 'A decline in emissions of CFC-11 and related chemicals from eastern China', *Nature*, 590(7846), pp. 433–437. Available at:

<https://doi.org/10.1038/s41586-021-03277-w>.

Patra, P.K. *et al.* (2011) 'TransCom model simulations of CH<sub>4</sub> and related species: linking transport, surface flux and chemical loss with CH<sub>4</sub> variability in the troposphere and lower stratosphere', *Atmospheric Chemistry and Physics*, 11(24), pp. 12813–12837. Available at: <https://doi.org/10.5194/ACP-11-12813-2011>.

Patten, K.O. and Wuebbles, D.J. (2010) 'Atmospheric lifetimes and Ozone Depletion Potentials of trans-1-chloro-3,3,3-trifluoropropylene and trans-1,2-dichloroethylene in a three-dimensional model', *Atmospheric Chemistry and Physics*, 10(22), pp. 10867–10874. Available at: <https://doi.org/10.5194/acp-10-10867-2010>.

Paul, D. *et al.* (2016) 'Radiocarbon analysis of stratospheric CO<sub>2</sub> retrieved from AirCore sampling', *Atmospheric Measurement Techniques*, 9(10), pp. 4997–5006. Available at: <https://doi.org/10.5194/amt-9-4997-2016>.

Ploeger, F. *et al.* (2019) 'How robust are stratospheric age of air trends from different reanalyses?', *Atmospheric chemistry and physics*, 19(January), pp. 1–32. Available at: <https://doi.org/10.5194/acp-2018-1281>.

Plumb, R.A. (1996) 'A "tropical pipe" model of stratospheric transport', *Journal of Geophysical Research Atmospheres*, 101(D2), pp. 3957–3972. Available at: <https://doi.org/10.1029/95JD03002>.

Plumb, R.A. (2002) 'Stratospheric transport', *Journal of the Meteorological Society of Japan*, 80(4 B), pp. 793–809. Available at: <https://doi.org/10.2151/jmsj.80.793>.

Plumb, R.A. (2007) 'Tracer interrelationships in the stratosphere', *Reviews of Geophysics*, 45(4). Available at: <https://doi.org/10.1029/2005RG000179>.

Plumb, R.A. and Ko, M.K.W. (1992) 'Interrelationships between mixing ratios of long-lived stratospheric constituents', *Journal of Geophysical Research*, 97(D9). Available at: <https://doi.org/10.1029/92JD00450>.

Prinn, R.G.; *et al.* (2020) *The ALE/GAGE/AGAGE Data Base*. Available at: <https://doi.org/10.3334/CDIAC/atg.db1001>.

Ravishankara, A.R. *et al.* (1993) 'Atmospheric lifetimes of long-lived halogenated species', *Science*, 259(5092), pp. 194–199. Available at: <https://doi.org/10.1126/SCIENCE.259.5092.194>.

Ray, E.A. *et al.* (2017) 'Quantification of the SF<sub>6</sub> lifetime based on mesospheric loss measured in the stratospheric polar vortex', *Journal of Geophysical Research*, 122(8), pp. 4626–4638. Available at: <https://doi.org/10.1002/2016JD026198>.

Ray, E.A. *et al.* (2024) 'Age of air from in situ trace gas measurements: Insights from a new technique', *EGUsphere Preprint repository* [Preprint]. Available at: <https://doi.org/10.5194/egusphere-2024-1887>.

Reithmeier, C., Sausen, R. and Grewe, V. (2008) 'Investigating lower stratospheric model transport: Lagrangian calculations of mean age and age spectra in the GCM ECHAM4', *Climate Dynamics*, 30(2–3), pp. 225–238. Available at: <https://doi.org/10.1007/s00382-007-0294-1>.

Reuter, M. *et al.* (2014) 'Decreasing emissions of NO<sub>x</sub> relative to CO<sub>2</sub> in East Asia inferred from satellite observations', *Nature Geoscience*, 7(11), pp. 792–795. Available at: <https://doi.org/10.1038/ngeo2257>.

Rhew, R.C., Miller, B.R. and Weiss, R.F. (2000) 'Natural methyl bromide and methyl chloride emissions from coastal salt marshes', *Nature*, 403(6767), pp. 292–295. Available at: <https://doi.org/10.1038/35002043>.

Richter, A. *et al.* (2004) 'Satellite measurements of NO<sub>2</sub> from international shipping emissions', *Geophysical Research Letters*, 31(23), pp. 1–4. Available at: <https://doi.org/10.1029/2004GL020822>.

Rigby, M. *et al.* (2013) 'Re-evaluation of the lifetimes of the major CFCs and CH<sub>3</sub>CCl<sub>3</sub> using atmospheric trends', *Atmospheric Chemistry and Physics*, 13(5), pp. 2691–2702. Available at: <https://doi.org/10.5194/ACP-13-2691-2013>.

Rigby, M. *et al.* (2019) 'Increase in CFC-11 emissions from eastern China based on atmospheric observations', *Nature*, 569(7757), pp. 546–550. Available at: <https://doi.org/10.1038/s41586-019-1193-4>.

Romualdez, L.J. *et al.* (2016) 'Precise Pointing and Stabilization Performance for the Balloon-borne Imaging Testbed (BIT): 2015 Test Flight'. Available at: <http://arxiv.org/abs/1603.01161>.

Rosenfield, J.E. *et al.* (1997) 'Stratospheric effects of Mount Pinatubo aerosol studied with a coupled two-dimensional model', *Journal of Geophysical Research Atmospheres*, 102(3), pp. 3649–3670. Available at: <https://doi.org/10.1029/96jd03820>.

Rosenfield, J.E., Douglas, A.R. and Considine, D.B. (2002) 'The impact of increasing carbon dioxide on ozone recovery', *Journal of Geophysical Research Atmospheres*, 107(5–6). Available at: <https://doi.org/10.1029/2001jd000824>.

Rosenlof, K.H. (1997) 'Hemispheric asymmetries in water vapor and inferences about transport in the lower stratosphere', *Journal of Geophysical Research Atmospheres*, 102(D11), pp. 13213–13234. Available at: <https://doi.org/10.1029/97JD00873>.

Salawitch, R.J. *et al.* (2023) *TWENTY QUESTIONS & ANSWERS ABOUT THE OZONE LAYER 2022 Update. Scientific Assessment of Ozone Depletion: 2022, 75 pp., World Meteorological Organization, Aura*. Available at: <https://ozone.unep.org/science/assessment/saphttps://www.csl.noaa.gov/assessments/ozone/2022>.

Sander, S.P. *et al.* (2006) *Chemical Kinetics and Photochemical Data for Use in Atmospheric Studies Evaluation Number 15 NASA Panel for Data Evaluation*. Available at: <http://jpldataeval.jpl.nasa.gov/>.

Sander, S.P. *et al.* (2011) *Chemical Kinetics and Photochemical Data for Use in Atmospheric Studies Evaluation Number 17 NASA Panel for Data Evaluation*. Available at: <http://jpldataeval.jpl.nasa.gov/>.

Say, D. *et al.* (2021) 'Global trends and European emissions of tetrafluoromethane (CF<sub>4</sub>), hexafluoroethane (C<sub>2</sub>F<sub>6</sub>) and octafluoropropane (C<sub>3</sub>F<sub>8</sub>)', *Atmospheric Chemistry and Physics*, 21(3), pp. 2149–2164. Available at: <https://doi.org/10.5194/acp-21-2149-2021>.

Schauffler, S.M. *et al.* (1999) 'Distributions of brominated organic compounds in the troposphere and lower stratosphere', *Journal of Geophysical Research Atmospheres*, 104(D17), pp. 21513–21535. Available at: <https://doi.org/10.1029/1999JD900197>.

Schauffler, S.M. (2003) 'Chlorine budget and partitioning during the Stratospheric Aerosol and Gas Experiment (SAGE) III Ozone Loss and Validation Experiment (SOLVE)', *Journal of Geophysical Research*, 108(D5), p. 4173. Available at: <https://doi.org/10.1029/2001JD002040>.

Schmidt, U. and Khedim, A. (1991) 'In situ measurements of carbon dioxide in the winter Arctic vortex and at midlatitudes: An indicator of the "age" of stratospheric air', *Geophysical Research Letters*, 18(4), pp. 763–766. Available at: <https://doi.org/10.1029/91GL00022>.

Seviour, W.J.M., Butchart, N. and Hardiman, S.C. (2012) 'The Brewer-Dobson circulation inferred from ERA-Interim', *Quarterly Journal of the Royal Meteorological Society*, 138(665), pp. 878–888. Available at: <https://doi.org/10.1002/qj.966>.

Shepherd, T.G. (2007) 'Transport in the Middle Atmosphere', *Journal of the Meteorological Society of Japan. Ser. II*, 85B(0), pp. 165–191. Available at: <https://doi.org/10.2151/jmsj.85B.165>.

Shepherd, T.G. *et al.* (2014) 'Reconciliation of halogen-induced ozone loss with the total-column ozone record', *Nature Geoscience*, 7(6), pp. 443–449. Available at: <https://doi.org/10.1038/ngeo2155>.

Simmonds, P.G. *et al.* (2017) 'Changing trends and emissions of hydrochlorofluorocarbons ( HCFCs ) and their hydrofluorocarbon ( HFCs ) replacements', pp. 4641–4655. Available at: <https://doi.org/10.5194/acp-17-4641-2017>.

Solomon, S. *et al.* (1986) 'On the depletion of Antarctic ozone', *Nature*, 321(6072), pp. 755–758. Available at: <https://doi.org/10.1038/321755a0>.

Solomon, S. (1988) 'The mystery of the Antarctic Ozone "Hole"', *Reviews of Geophysics*, 26(1), pp. 131–148. Available at: <https://doi.org/10.1029/RG026I001P00131>.

Solomon, S. *et al.* (1992a) 'On the evaluation of ozone depletion potentials', *Journal of Geophysical Research: Atmospheres*, 97(D1), pp. 825–842. Available at: <https://doi.org/10.1029/91JD02613>.

Solomon, S. and Albritton, D.L. (1992b) 'Time-dependent ozone depletion potentials for short- and long-term forecasts', *Nature*, 357(6373), pp. 33–37. Available at: <https://doi.org/10.1038/357033a0>.



Trudinger, C.M. *et al.* (2016) 'Atmospheric abundance and global emissions of perfluorocarbons CF<sub>4</sub>, C<sub>2</sub>F<sub>6</sub> and C<sub>3</sub>F<sub>8</sub> since 1800 inferred from ice core, firn, air archive and in situ measurements', *Atmospheric Chemistry and Physics*, 16(18), pp. 11733–11754. Available at: <https://doi.org/10.5194/acp-16-11733-2016>.

Tukiainen, S. *et al.* (2016) 'Retrieval of atmospheric CH<sub>4</sub> profiles from Fourier transform infrared data using dimension reduction and MCMC', *Journal of Geophysical Research*, 121(17), pp. 10312–10327. Available at: <https://doi.org/10.1002/2015JD024657>.

Umezawa, T. *et al.* (2014) 'Methyl chloride in the upper troposphere observed by the CARIBIC passenger aircraft observatory: Large-scale distributions and Asian summer monsoon outflow', *Journal of Geophysical Research*, 119(9), pp. 5542–5558. Available at: <https://doi.org/10.1002/2013JD021396>.

UNEP (2018) *United Nations Environment Programme Report of the Thirtieth Meeting of the Parties to the Montreal Protocol on Substances that Deplete the Ozone Layer Introduction*.

UNEP (2019) *Pre-session documents of the Executive Committee of the Multilateral Fund for the Implementation of the Montreal Protocol. Addendum: Reports on Projects with Specific Reporting Requirements*.

Velders, G.J.M. and Daniel, J.S. (2014) 'Uncertainty analysis of projections of ozone-depleting substances: Mixing ratios, EESC, ODPs, and GWPs', *Atmospheric Chemistry and Physics*, 14(6), pp. 2757–2776. Available at: <https://doi.org/10.5194/ACP-14-2757-2014>.

Volk, C.M. *et al.* (1996) *Quantifying Transport Between the Tropical and Mid-Latitude Lower Stratosphere*. Available at: <https://www.science.org>.

Volk, C.M. *et al.* (1997) 'Evaluation of source gas lifetimes from stratospheric observations', *Journal of Geophysical Research Atmospheres*. Blackwell Publishing Ltd, pp. 25543–25564. Available at: <https://doi.org/10.1029/97jd02215>.

Vollmer, M.K. *et al.* (2018) 'Atmospheric histories and emissions of chlorofluorocarbons CFC-13, ΣCFC-114, and CFC-115', *Atmospheric Chemistry and Physics*, 18(2), pp. 979–1002. Available at: <https://doi.org/10.5194/acp-18-979-2018>.

Waugh, D.W., Strahan, S.E. and Newman, P.A. (2007) 'Sensitivity of stratospheric inorganic chlorine to differences in transport', *Atmospheric Chemistry and Physics*, 7(18), pp. 4935–4941. Available at: <https://doi.org/10.5194/acp-7-4935-2007>.

Weatherhead, E.C. and Andersen, S.B. (2006) 'The search for signs of recovery of the ozone layer', *Nature*, 441(1), pp. 39–45. Available at: <https://doi.org/10.1038/nature04746>.

Weisenstein, D.K. *et al.* (2004) 'Separating chemistry and transport effects in two-dimensional models', *Journal of Geophysical Research Atmospheres*, 109(18). Available at: <https://doi.org/10.1029/2004JD004744>.

Western, L.M. *et al.* (2022) 'A renewed rise in global HCFC-141b emissions between 2017-2021', *Atmospheric Chemistry and Physics*, 22(14), pp. 9601–9616. Available at: <https://doi.org/10.5194/acp-22-9601-2022>.

Western, L.M. *et al.* (2023) 'Global increase of ozone-depleting chlorofluorocarbons from 2010 to 2020', *Nature Geoscience* [Preprint]. Available at: <https://doi.org/10.1038/s41561-023-01147-w>.

Wilmouth, D.M. *et al.* (2006) 'Evolution of inorganic chlorine partitioning in the Arctic polar vortex', *Journal of Geophysical Research Atmospheres*, 111(16). Available at: <https://doi.org/10.1029/2005JD006951>.

WMO (2003) *World Meteorological Organization Global Ozone Research and Monitoring Project—Report No. 47 SCIENTIFIC ASSESSMENT OF OZONE DEPLETION: 2002*.

World Meteorological Organization (2010) *Scientific Assessment of Ozone Depletion: 2010 World Meteorological Organization Global Ozone Research and Monitoring Project—Report No. 52*. Available at: <http://ozone.unep.org/science/assessment/sap>.

Wunch, D. *et al.* (2010) 'Calibration of the total carbon column observing network using aircraft profile data', *Atmospheric Measurement Techniques*, 3(5), pp. 1351–1362. Available at: <https://doi.org/10.5194/amt-3-1351-2010>.

Yang, M. *et al.* (2021) 'CFCs measurements at high altitudes in northern China during 2017–2018: Concentrations and potential emission source regions', *Science of the Total Environment*, 754. Available at: <https://doi.org/10.1016/j.scitotenv.2020.142290>.

Yazici, B., Can, Z.S. and Calli, B. (2014) 'Prediction of future disposal of end-of-life refrigerators containing CFC-11', *Waste Management*, 34(1), pp. 162–166. Available at: <https://doi.org/10.1016/j.wasman.2013.09.008>.

Yokouchi, Y. *et al.* (2000) 'A strong source of methyl chloride to the atmosphere from tropical coastal land', *Nature*. Edited by D. Helmig and M. Val Martin, 403(6767), pp. 295–298. Available at: <https://doi.org/10.1038/35002049>.

Young, P.J. *et al.* (2011) 'The seasonal cycle and interannual variability in stratospheric temperatures and links to the Brewer-Dobson circulation: An analysis of MSU and SSU data', *Journal of Climate*, 24(23), pp. 6243–6258. Available at: <https://doi.org/10.1175/JCLI-D-10-05028.1>.

Young, P.J. *et al.* (2012) 'Changes in stratospheric temperatures and their implications for changes: In the brewer-dobson circulation, 1979-2005', *Journal of Climate*, 25(5), pp. 1759–1772. Available at: <https://doi.org/10.1175/2011JCLI4048.1>.

Zeng, L. *et al.* (2020) 'Long-term temporal variations and source changes of halocarbons in the Greater Pearl River Delta region, China', *Atmospheric Environment*, 234. Available at: <https://doi.org/10.1016/j.atmosenv.2020.117550>.

Zheng, C. *et al.* (2024) 'Influence of atmospheric circulation on the interannual variability of transport from global and regional emissions into the Arctic', *Atmospheric Chemistry and Physics*, 24(12), pp. 6965–6985. Available at: <https://doi.org/10.5194/acp-24-6965-2024>.